Quantum Theory of the Optical and Electronic Properties of Semiconductors

Fourth Edition

Hartmut Haug
Stephan W. Koch

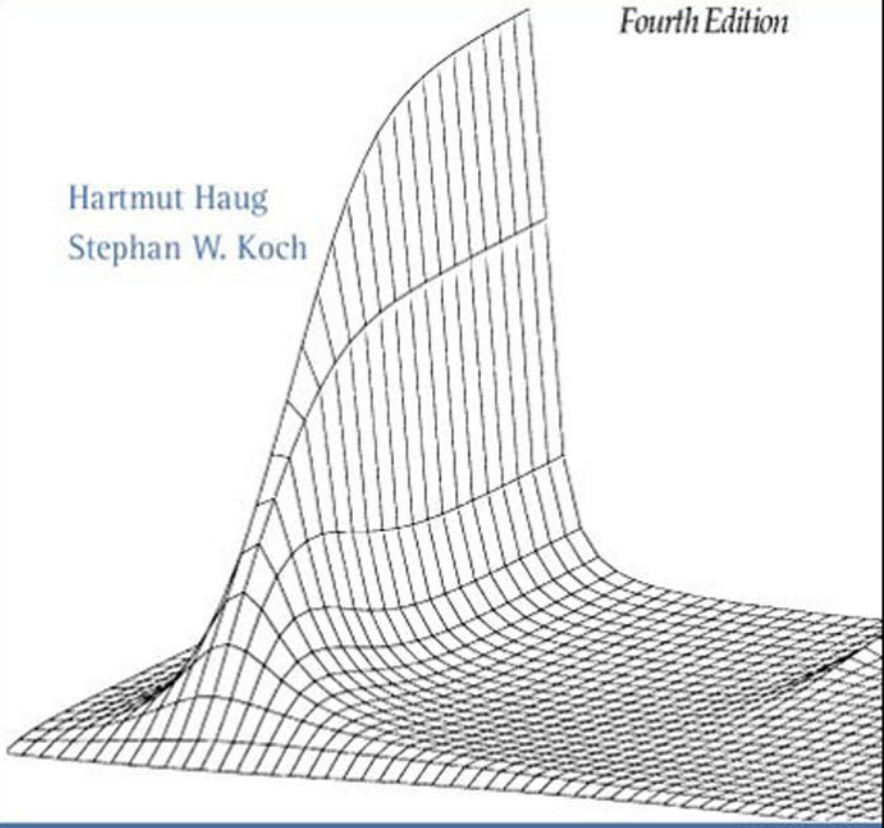

World Scientific

Published by

World Scientific Publishing Co. Pte. Ltd.

5 Toh Tuck Link, Singapore 596224

USA office: Suite 202, 1060 Main Street, River Edge, NJ 07661

UK office: 57 Shelton Street, Covent Garden, London WC2H 9HE

British Library Cataloguing-in-Publication Data
A catalogue record for this book is available from the British Library.

QUANTUM THEORY OF THE OPTICAL AND ELECTRONIC PROPERTIES OF SEMICONDUCTORS

ISBN 981-238-609-2
ISBN 981-238-756-0 (pbk)

Printed in Singapore.

Preface

The electronic properties of semiconductors form the basis of the latest and current technological revolution, the development of ever smaller and more powerful computing devices, which affect not only the potential of modern science but practically all aspects of our daily life. This dramatic development is based on the ability to engineer the electronic properties of semiconductors and to miniaturize devices down to the limits set by quantum mechanics, thereby allowing a large scale integration of many devices on a single semiconductor chip.

Parallel to the development of electronic semiconductor devices, and no less spectacular, has been the technological use of the optical properties of semiconductors. The fluorescent screens of television tubes are based on the optical properties of semiconductor powders, the red light of GaAs light emitting diodes is known to all of us from the displays of domestic appliances, and semiconductor lasers are used to read optical discs and to write in laser printers. Furthermore, fiber-optic communications, whose light sources, amplifiers and detectors are again semiconductor electro-optical devices, are expanding the capacity of the communication networks dramatically.

Semiconductors are very sensitive to the addition of carriers, which can be introduced into the system by doping the crystal with atoms from another group in the periodic system, electronic injection, or optical excitation. The electronic properties of a semiconductor are primarily determined by transitions within one energy band, i.e., by *intraband transitions*, which describe the transport of carriers in real space. Optical properties, on the other hand, are connected with transitions between the valence and conduction bands, i.e., with *interband transitions*. However, a strict separation is impossible. Electronic devices such as a p-n diode can only be under-

stood if one considers also interband transitions, and many optical devices cannot be understood if one does not take into account the effects of intraband scattering, carrier transport and diffusion. Hence, the optical and electronic semiconductor properties are intimately related and should be discussed jointly.

Modern crystal growth techniques make it possible to grow layers of semiconductor material which are narrow enough to confine the electron motion in one dimension. In such *quantum-well* structures, the electron wave functions are quantized like the standing waves of a particle in a square well potential. Since the electron motion perpendicular to the quantum-well layer is suppressed, the semiconductor is *quasi-two-dimensional*. In this sense, it is possible to talk about low-dimensional systems such as quantum wells, quantum wires, and quantum dots which are effectively two, one and zero dimensional.

These few examples suffice to illustrate the need for a modern textbook on the electronic and optical properties of semiconductors and semiconductor devices. There is a growing demand for solid-state physicists, electrical and optical engineers who understand enough of the basic microscopic theory of semiconductors to be able to use effectively the possibilities to engineer, design and optimize optical and electronic devices with certain desired characteristics.

In this fourth edition, we streamlined the presentation of the material and added several new aspects. Many results in the different chapters are developed in parallel first for bulk material, and then for quasi-two-dimensional quantum wells and for quasi-one-dimensional quantum wires, respectively. Semiconductor quantum dots are treated in a separate chapter. The semiconductor Bloch equations have been given a central position. They have been formulated not only for free particles in various dimensions, but have been given, e.g., also in the Landau basis for low-dimensional electrons in strong magnetic fields or in the basis of quantum dot eigenfunctions. The Bloch equations are extended to include correlation and scattering effects at different levels of approximation. Particularly, the relaxation and the dephasing in the Bloch equations are treated not only within the semiclassical Boltzmann kinetics, but also within quantum kinetics, which is needed for ultrafast semiconductor spectroscopy. The applications of these equations to time-dependent and coherent phenomena in semiconductors have been extended considerably, e.g., by including separate chapters for the excitonic optical Stark effect and various nonlinear wave-mixing configurations. The presentation of the nonequilibrium Green's function theory

has been modified to present both introductory material as well as applications to Coulomb carrier scattering and time-dependent screening. In several chapters, direct comparisons of theoretical results with experiments have been included.

This book is written for graduate-level students or researchers with general background in quantum mechanics as an introduction to the quantum theory of semiconductors. The necessary many-particle techniques, such as field quantization and Green's functions are developed explicitly. Wherever possible, we emphasize the motivation of a certain derivation and the physical meaning of the results, avoiding the discussion of formal mathematical aspects of the theory. The book, or parts of it, can serve as textbook for use in solid state physics courses, or for more specialized courses on electronic and optical properties of semiconductors and semiconductor devices. Especially the later chapters establish a direct link to current research in semicoductor physics. The material added in the fourth edition should make the book as a whole more complete and comprehensive.

Many of our colleagues and students have helped in different ways to complete this book and to reduce the errors and misprints. We especially wish to thank L. Banyai, R. Binder, C. Ell, I. Galbraith, Y.Z. Hu, M. Kira, M. Lindberg, T. Meier, and D.B. Tran-Thoai for many scientific discussions and help in several calculations. We appreciate helpful suggestions and assistance from our present and former students S. Benner, K. El-Sayed, W. Hoyer, J. Müller, M. Pereira, E. Reitsamer, D. Richardson, C. Schlichenmaier, S. Schuster, Q.T. Vu, and T. Wicht. Last but not least we thank R. Schmid, Marburg, for converting the manuscript to Latex and for her excellent work on the figures.

Frankfurt and Marburg — Hartmut Haug
August 2003 — Stephan W. Koch

About the authors

Hartmut Haug obtained his Ph.D (Dr. rer. nat., 1966) in Physics at the University of Stuttgart. From 1967 to 1969, he was a faculty member at the Department of Electrical Engineering, University of Wisconsin in Madison. After working as a member of the scientific staff at the Philips Research Laboratories in Eindhoven from 1969 to 1973, he joined the Institute of Theoretical Physics of the University of Frankfurt, where he was a full professor from 1975 to 2001 and currently is an emeritus. He has been a visiting scientist at many international research centers and universities.

Stephan W. Koch obtained his Ph. D. (Dr. phil. nat., 1979) in Physics at the University of Frankfurt. Until 1993 he was a full professor both at the Department of Physics and at the Optical Sciences Center of the University of Arizona, Tucson (USA). In the fall of 1993, he joined the Philipps-University of Marburg where he is a full professor of Theoretical Physics. He is a Fellow of the Optical Society of America. He received the Leibniz prize of the Deutsche Physikalische Gesellschaft (1997) and the Max-Planck Research Prize of the Humboldt Foundation and the Max-Planck Society (1999).

Contents

This page intentionally left blank

Chapter 1

Oscillator Model

The valence electrons, which are responsible for the binding of the atoms in a crystal can either be tightly bound to the ions or can be free to move through the periodic lattice. Correspondingly, we speak about insulators and metals. Semiconductors are intermediate between these two limiting cases. This situation makes semiconductors extremely sensitive to imperfections and impurities, but also to excitation with light. Before techniques were developed allowing well controlled crystal growth, research in semiconductors was considered by many physicists a highly suspect enterprise.

Starting with the research on Ge and Si in the 1940's, physicists learned to exploit the sensitivity of semiconductors to the content of foreign atoms in the host lattice. They learned to dope materials with specific impurities which act as donors or acceptors of electrons. Thus, they opened the field for developing basic elements of semiconductor electronics, such as diodes and transistors. Simultaneously, semiconductors were found to have a rich spectrum of optical properties based on the specific properties of the electrons in these materials.

Electrons in the ground state of a semiconductor are bound to the ions and cannot move freely. In this state, a semiconductor is an insulator. In the excited states, however, the electrons are free, and become similar to the conduction electrons of a metal. The ground state and the lowest excited state are separated by an energy gap. In the spectral range around the energy gap, pure semiconductors exhibit interesting linear and nonlinear optical properties. Before we discuss the quantum theory of these optical properties, we first present a classical description of a dielectric medium in which the electrons are assumed to be bound by harmonic forces to the positively charged ions. If we excite such a medium with the periodic transverse electric field of a light beam, we induce an electrical polarization due

to microscopic displacement of bound charges. This *oscillator model* for the electric polarization was introduced in the pioneering work of Lorentz, Planck, and Einstein. We expect the model to yield reasonably realistic results as long as the light frequency does not exceed the frequency corresponding to the energy gap, so that the electron stays in its bound state.

We show in this chapter that the analysis of this simple model already provides a qualitative understanding of many basic aspects of light–matter interaction. Furthermore, it is useful to introduce such general concepts as optical susceptibility, dielectric function, absorption and refraction, as well as Green's function.

1.1 Optical Susceptibility

The electric field, which is assumed to be polarized in the x-direction, causes a displacement x of an electron with a charge $e \simeq -1.6\ 10^{-16}$ C $\simeq -4.8\ 10^{-10}$ esu from its equilibrium position. The resulting polarization, defined as dipole moment per unit volume, is

$$\mathcal{P} = \frac{P}{L^3} = n_0 e x = n_0 d \ , \tag{1.1}$$

where $L^3 = V$ is the volume, $d = ex$ is the electric dipole moment, and n_0 is the mean electron density per unit volume. Describing the electron under the influence of the electric field $\mathcal{E}(t)$ (parallel to x) as a damped driven oscillator, we can write Newton's equation as

$$m_0 \frac{d^2x}{dt^2} = -2m_0\gamma\frac{dx}{dt} - m_0\omega_0^2 x + e\mathcal{E}(t) \ , \tag{1.2}$$

where γ is the damping constant, and m_0 and ω_0 are the mass and resonance frequency of the oscillator, respectively. The electric field is assumed to be monochromatic with a frequency ω, i.e., $\mathcal{E}(t) = \mathcal{E}_0 \cos(\omega t)$. Often it is convenient to consider a complex field

$$\mathcal{E}(t) = \mathcal{E}(\omega) e^{-i\omega t} \tag{1.3}$$

and take the real part of it whenever a final physical result is calculated. With the ansatz

$$x(t) = x(\omega) e^{-i\omega t} \tag{1.4}$$

we get from Eq. (1.2)

$$m_0(\omega^2 + i2\gamma\omega - \omega_0^2)x(\omega) = -e\mathcal{E}(\omega) \tag{1.5}$$

and from Eq. (1.1)

$$\mathcal{P}(\omega) = -\frac{n_0 e^2}{m_0}\frac{1}{\omega^2 + i2\gamma\omega - \omega_0^2}\mathcal{E}(\omega) \ . \tag{1.6}$$

The complex coefficient between $\mathcal{P}(\omega)$ and $\mathcal{E}(\omega)$ is defined as the optical susceptibility $\chi(\omega)$. For the damped driven oscillator, this optical susceptibility is

$$\boldsymbol{\chi(\omega) = -\frac{n_0 e^2}{2m_0\omega_0'}\left(\frac{1}{\omega - \omega_0' + i\gamma} - \frac{1}{\omega + \omega_0' + i\gamma}\right)} \ . \tag{1.7}$$

optical susceptibility

Here,

$$\omega_0' = \sqrt{\omega_0^2 - \gamma^2} \tag{1.8}$$

is the resonance frequency that is renormalized (shifted) due to the damping. In general, the optical susceptibility is a tensor relating different vector components of the polarization $\mathcal{P}_i$ and the electric field $\mathcal{E}_i$. An important feature of $\chi(\omega)$ is that it becomes singular at

$$\omega = -i\gamma \pm \omega_0' \ . \tag{1.9}$$

This relation can only be satisfied if we formally consider complex frequencies $\omega = \omega' + i\omega''$. We see from Eq. (1.7) that $\chi(\omega)$ has poles in the lower half of the complex frequency plane, i.e. for $\omega'' < 0$, but it is an analytic function on the real frequency axis and in the whole upper half plane. This property of the susceptibility can be related to causality, i.e., to the fact that the polarization $\mathcal{P}(t)$ at time t can only be influenced by fields $\mathcal{E}(t-\tau)$ acting at earlier times, i.e., $\tau \geq 0$. Let us consider the most general linear relation between the field and the polarization

$$\mathcal{P}(t) = \int_{-\infty}^{t} dt' \chi(t, t')\mathcal{E}(t') \ . \tag{1.10}$$

Here, we take both $\mathcal{P}(t)$ and $\mathcal{E}(t)$ as real quantities so that $\chi(t)$ is a real quantity as well. The response function $\chi(t,t')$ describes the memory of the system for the action of fields at earlier times. Causality requires that fields $\mathcal{E}(t')$ which act in the future, $t' > t$, cannot influence the polarization of the system at time t. We now make a transformation to new time arguments T and τ defined as

$$T = \frac{t+t'}{2} \text{ and } \tau = t - t' \ . \tag{1.11}$$

If the system is in equilibrium, the memory function $\chi(T,\tau)$ depends only on the time difference τ and not on T, which leads to

$$\begin{aligned} \mathcal{P}(t) &= \int_{-\infty}^{t} dt' \chi(t-t')\mathcal{E}(t') \\ &= \int_{0}^{\infty} d\tau \chi(\tau)\mathcal{E}(t-\tau). \end{aligned} \tag{1.12}$$

Next, we use a Fourier transformation to convert Eq. (1.12) into frequency space. For this purpose, we define the Fourier transformation $f(\omega)$ of a function $f(t)$ through the relations

$$\begin{aligned} f(\omega) &= \int_{-\infty}^{\infty} dt f(t) e^{i\omega t} \\ f(t) &= \int_{-\infty}^{\infty} \frac{d\omega}{2\pi} f(\omega) e^{-i\omega t} \ . \end{aligned} \tag{1.13}$$

Using this Fourier representation for $x(t)$ and $\mathcal{E}(t)$ in Eq. (1.2), we find for $x(\omega)$ and $\mathcal{E}(\omega)$ again the relation (1.5) and thus the resulting susceptibility (1.7), showing that the ansatz (1.3) – (1.4) is just a shortcut for a solution using the Fourier transformation.

Multiplying Eq. (1.12) by $e^{i\omega t}$ and integrating over t , we get

$$\mathcal{P}(\omega) = \int_{0}^{\infty} d\tau \chi(\tau) e^{i\omega\tau} \int_{-\infty}^{+\infty} dt \mathcal{E}(t-\tau) e^{i\omega(t-\tau)} = \chi(\omega)\mathcal{E}(\omega) \ , \tag{1.14}$$

where

$$\chi(\omega) = \int_{0}^{\infty} d\tau \chi(\tau) e^{i\omega\tau} \ . \tag{1.15}$$

The convolution integral in time, Eq. (1.12), becomes a product in Fourier space, Eq. (1.14). The time-dependent response function $\chi(t)$ relates two real quantities, $\mathcal{E}(t)$ and $\mathcal{P}(t)$, and therefore has to be a real function itself. Hence, Eq. (1.15) implies directly that $\chi^*(\omega) = \chi(-\omega)$ or $\chi'(\omega) = \chi'(-\omega)$ and $\chi''(\omega) = -\chi''(-\omega)$. Moreover, it also follows that $\chi(\omega)$ is analytic for $\omega'' \geq 0$, because the factor $e^{-\omega'' \tau}$ forces the integrand to zero at the upper boundary, where $\tau \to \infty$.

Since $\chi(\omega)$ is an analytic function for real frequencies we can use the Cauchy relation to write

$$\chi(\omega) = \int_{-\infty}^{+\infty} \frac{d\nu}{2\pi i} \frac{\chi(\nu)}{\nu - \omega - i\delta} \ , \tag{1.16}$$

where δ is a positive infinitesimal number. The integral can be evaluated using the Dirac identity (see problem (1.1))

$$\lim_{\delta \to 0} \frac{1}{\omega - i\delta} = P\frac{1}{\omega} + i\pi\delta(\omega) \ , \tag{1.17}$$

where P denotes the principal value of an integral under which this relation is used. We find

$$\chi(\omega) = P \int_{-\infty}^{+\infty} \frac{d\nu}{2\pi i} \frac{\chi(\nu)}{\nu - \omega} + \frac{1}{2} \int_{-\infty}^{+\infty} d\nu \chi(\nu) \delta(\nu - \omega) \ . \tag{1.18}$$

For the real and imaginary parts of the susceptibility, we obtain separately

$$\chi'(\omega) = P \int_{-\infty}^{+\infty} \frac{d\nu}{\pi} \frac{\chi''(\nu)}{\nu - \omega} \tag{1.19}$$

$$\chi''(\omega) = -P \int_{-\infty}^{+\infty} \frac{d\nu}{\pi} \frac{\chi'(\nu)}{\nu - \omega} \ . \tag{1.20}$$

Splitting the integral into two parts

$$\chi'(\omega) = P \int_{-\infty}^{0} \frac{d\nu}{\pi} \frac{\chi''(\nu)}{\nu - \omega} + P \int_{0}^{+\infty} \frac{d\nu}{\pi} \frac{\chi''(\nu)}{\nu - \omega} \tag{1.21}$$

and using the relation $\chi''(\omega) = -\chi''(-\omega)$, we find

$$\chi'(\omega) = P \int_{0}^{+\infty} \frac{d\nu}{\pi} \chi''(\nu) \left(\frac{1}{\nu + \omega} + \frac{1}{\nu - \omega} \right) \ . \tag{1.22}$$

Combining the two terms yields

$$\boldsymbol{\chi'(\omega) = P \int_0^{+\infty} \frac{d\nu}{\pi} \chi''(\nu) \frac{2\nu}{\nu^2 - \omega^2}} \ . \tag{1.23}$$

Kramers–Kronig relation

This is the Kramers–Kronig relation, which allows us to calculate the real part of $\chi(\omega)$ if the imaginary part is known for all positive frequencies. In realistic situations, one has to be careful with the use of Eq. (1.23), because $\chi''(\omega)$ is often known only in a finite frequency range. A relation similar to Eq. (1.23) can be derived for χ'' using (1.20) and $\chi'(\omega) = \chi'(-\omega)$, see problem (1.3).

1.2 Absorption and Refraction

Before we give any physical interpretation of the susceptibility obtained with the oscillator model we will establish some relations to other important optical coefficients. The displacement field $D(\omega)$ can be expressed in terms of the polarization $\mathcal{P}(\omega)$ and the electric field[1]

$$D(\omega) = \mathcal{E}(\omega) + 4\pi\mathcal{P}(\omega) = [1 + 4\pi\chi(\omega)]\mathcal{E}(\omega) = \epsilon(\omega)\mathcal{E}(\omega) \ , \tag{1.24}$$

where the optical (or transverse) dielectric function $\epsilon(\omega)$ is obtained from the optical susceptibility (1.7) as

$$\boldsymbol{\epsilon(\omega) = 1 + 4\pi\chi(\omega) = 1 - \frac{\omega_{pl}^2}{2\omega_0'} \left(\frac{1}{\omega - \omega_0' + i\gamma} - \frac{1}{\omega + \omega_0' + i\gamma} \right)} \ . \tag{1.25}$$

optical dielectric function

Here, ω_{pl} denotes the plasma frequency of an electron plasma with the mean density n_0 :

[1] We use cgs units in most parts of this book.

$$\boldsymbol{\omega_{pl} = \sqrt{\frac{4\pi n_0 e^2}{m_0}}} \ . \tag{1.26}$$

plasma frequency

The plasma frequency is the eigenfrequency of the electron plasma density oscillations around the position of the ions. To illustrate this fact, let us consider an electron plasma of density $n(\mathbf{r}, t)$ close to equilibrium. The equation of continuity is

$$e\frac{\partial n}{\partial t} + \text{div}\ \mathbf{j} = 0 \tag{1.27}$$

with the current density

$$\mathbf{j}(\mathbf{r}, t) = en(\mathbf{r}, t)\mathbf{v}(\mathbf{r}, t) \ . \tag{1.28}$$

The source equation for the electric field is

$$\text{div}\mathcal{E} = 4\pi e(n - n_0) \tag{1.29}$$

and Newton's equation for free carriers can be written as

$$m_0\frac{\partial \mathbf{v}}{\partial t} = e\mathcal{E} \ . \tag{1.30}$$

We now linearize Eqs. (1.27) – (1.29) around the equilibrium state where the velocity is zero and no fields exist. Inserting

$$\begin{aligned} n &= n_0 + \delta n_1 + \mathcal{O}(\delta^2) \\ \mathbf{v} &= \delta\mathbf{v}_1 + \mathcal{O}(\delta^2) \\ \mathcal{E} &= \delta\mathcal{E}_1 + \mathcal{O}(\delta^2) \end{aligned} \tag{1.31}$$

into Eqs. (1.27) – (1.30) and keeping only terms linear in δ, we obtain

$$\frac{\partial n_1}{\partial t} + n_0\text{div}\mathbf{v}_1 = 0 \ , \tag{1.32}$$

$$\text{div}\mathcal{E}_1 = 4\pi e n_1 \ , \tag{1.33}$$

and

$$m_0 \frac{\partial \mathbf{v}_1}{\partial t} = e\mathcal{E}_1. \tag{1.34}$$

The equation of motion for n_1 can be derived by taking the time derivative of Eq. (1.32) and using Eqs. (1.33) and (1.34) to get

$$\frac{\partial^2 n_1}{\partial t^2} = -n_0 \mathrm{div} \frac{\partial \mathbf{v}_1}{\partial t} = -\frac{n_0 e}{m_0} \mathrm{div} \mathcal{E}_1 = -\omega_{pl}^2 n_1 \ . \tag{1.35}$$

This simple harmonic oscillator equation is the classical equation for charge density oscillations with the eigenfrequency ω_{pl} around the equilibrium density n_0.

Returning to the discussion of the optical dielectric function (1.25), we note that $\epsilon(\omega)$ has poles at $\omega = \pm\omega_0' - i\gamma$, describing the resonant and the nonresonant part, respectively. If we are interested in the optical response in the spectral region around ω_0 and if ω_0 is sufficiently large, the nonresonant part gives only a small contribution and it is often a good approximation to neglect it completely.

In order to simplify the resulting expressions, we now consider only the resonant part of the dielectric function and assume $\omega_0 >> \gamma$, so that $\omega_0 \simeq \omega_0'$ and

$$\epsilon(\omega) = 1 - \frac{\omega_{pl}^2}{2\omega_0} \frac{1}{\omega - \omega_0 + i\gamma} \ . \tag{1.36}$$

For the real part of the dielectric function, we thus get the relation

$$\epsilon'(\omega) - 1 = -\frac{\omega_{pl}^2}{2\omega_0} \frac{\omega - \omega_0}{(\omega - \omega_0)^2 + \gamma^2} \ , \tag{1.37}$$

while the imaginary part has the following resonance structure

$$\epsilon''(\omega) = \frac{\omega_{pl}^2}{4\omega_0} \frac{2\gamma}{(\omega - \omega_0)^2 + \gamma^2} \ . \tag{1.38}$$

Examples of the spectral variations described by Eqs. (1.37) and (1.38) are shown in Fig. 1.1. The spectral shape of the imaginary part is determined by the Lorentzian line-shape function $2\gamma/[(\omega - \omega_0)^2 + \gamma^2]$. It decreases asymptomatically like $1/(\omega - \omega_0)^2$, while the real part of $\epsilon(\omega)$ decreases like $1/(\omega - \omega_0)$ far away from the resonance.

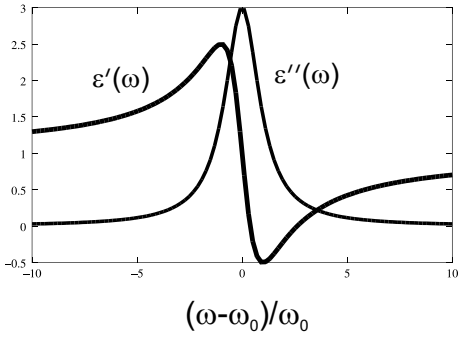

Fig. 1.1 Dispersion of the real and imaginary part of the dielectric function, Eq. (1.37) and (1.38), respectively. The broadening is taken as $\gamma/\omega_0 = 0.1$ and $\epsilon''_{max} = \omega_{pl}^2/2\gamma\omega_o$.

In order to understand the physical information contained in $\epsilon'(\omega)$ and $\epsilon''(\omega)$, we consider how a light beam propagates in the dielectric medium. From Maxwell's equations

$$\mathrm{curl}\,\mathbf{H}(\mathbf{r},t) = \frac{1}{c}\frac{\partial}{\partial t}\mathbf{D}(\mathbf{r},t) \tag{1.39}$$

$$\mathrm{curl}\,\mathcal{E}(\mathbf{r},t) = -\frac{1}{c}\frac{\partial}{\partial t}\mathbf{B}(\mathbf{r},t) \tag{1.40}$$

we find with $\mathbf{B}(\mathbf{r},t) = \mathbf{H}(\mathbf{r},t)$, which holds at optical frequencies,

$$\mathrm{curl}\,\mathrm{curl}\,\mathcal{E}(\mathbf{r},t) = -\frac{1}{c}\frac{\partial}{\partial t}\mathrm{curl}\,\mathbf{H}(\mathbf{r},t) = -\frac{1}{c^2}\frac{\partial^2}{\partial t^2}\mathbf{D}(\mathbf{r},t)\ . \tag{1.41}$$

Using curl curl = grad div $-\,\Delta$, we get for a transverse electric field with $\mathrm{div}\mathcal{E}(\mathbf{r},\mathrm{t}) = 0$, the wave equation

$$\Delta\mathcal{E}(\mathbf{r},t) - \frac{1}{c^2}\frac{\partial^2}{\partial t^2}\mathbf{D}(\mathbf{r},t) = 0\ . \tag{1.42}$$

Here, $\Delta \equiv \nabla^2$ is the Laplace operator. A Fourier transformation of Eq. (1.42) with respect to time yields

$$\Delta\mathcal{E}(\mathbf{r},\omega) + \frac{\omega^2}{c^2}\epsilon'(\omega)\mathcal{E}(\mathbf{r},\omega) + i\frac{\omega^2}{c^2}\epsilon''(\omega)\mathcal{E}(\mathbf{r},\omega) = 0\ . \tag{1.43}$$

For a plane wave propagating with wave number $k(\omega)$ and extinction coefficient $\kappa(\omega)$ in the z direction,

$$\mathcal{E}(\mathbf{r},\omega) = \mathcal{E}_0(\omega)e^{i[k(\omega)+i\kappa(\omega)]z} \ , \tag{1.44}$$

we get from Eq. (1.43)

$$[k(\omega) + i\kappa(\omega)]^2 = \frac{\omega^2}{c^2}[\epsilon'(\omega) + i\epsilon''(\omega)] \ . \tag{1.45}$$

Separating real and imaginary part of this equation yields

$$k^2(\omega) - \kappa^2(\omega) = \frac{\omega^2}{c^2}\epsilon'(\omega) \ , \tag{1.46}$$

$$2\kappa(\omega)k(\omega) = \frac{\omega^2}{c^2}\epsilon''(\omega) \ . \tag{1.47}$$

Next, we introduce the index of refraction $n(\omega)$ as the ratio between the wave number $k(\omega)$ in the medium and the vacuum wave number $k_0 = \omega/c$

$$k(\omega) = n(\omega)\frac{\omega}{c} \tag{1.48}$$

and the absorption coefficient $\alpha(\omega)$ as

$$\alpha(\omega) = 2\kappa(\omega) \ . \tag{1.49}$$

The absorption coefficient determines the decay of the intensity $I \propto |\mathcal{E}|^2$ in real space. $1/\alpha$ is the length, over which the intensity decreases by a factor

$1/e$. From Eqs. (1.46) – (1.49) we obtain the relations

$$\boldsymbol{n(\omega) = \sqrt{\frac{1}{2}\left[\epsilon'(\omega) + \sqrt{\epsilon'^2(\omega) + \epsilon''^2(\omega)}\right]}} \tag{1.50}$$

index of refraction

and

$$\boldsymbol{\alpha(\omega) = \frac{\omega}{n(\omega)c}\epsilon''(\omega)} \ . \tag{1.51}$$

absorption coefficient

Hence, Eqs. (1.38) and (1.51) yield a Lorentzian absorption line, and Eqs. (1.37) and (1.50) describe the corresponding frequency-dependent index of refraction. Note that for $\epsilon''(\omega) << \epsilon'(\omega)$, which is often true in semiconductors, Eq. (1.50) simplifies to

$$n(\omega) \simeq \sqrt{\epsilon'(\omega)} \ . \tag{1.52}$$

Furthermore, if the refractive index $n(\omega)$ is only weakly frequency-dependent for the ω-values of interest, one may approximate Eq. (1.51) as

$$\alpha(\omega) \simeq \frac{\omega}{n_b c}\epsilon''(\omega) = \frac{4\pi\omega}{n_b c}\chi''(\omega) \ , \tag{1.53}$$

where n_b is the background refractive index.

For the case $\gamma \to 0$, i.e., vanishing absorption line width, the line-shape function approaches a delta function (see problem 1.3)

$$\lim_{\gamma\to 0} \frac{2\gamma}{(\omega-\omega_0)^2 + \gamma^2} = 2\pi\delta(\omega - \omega_0) \ . \tag{1.54}$$

In this case, we get

$$\epsilon''(\omega) = \pi\frac{\omega_{pl}^2}{2\omega_0}\delta(\omega - \omega_0) \tag{1.55}$$

and the real part becomes

$$\epsilon'(\omega) = 1 - \frac{\omega_{pl}^2}{2\omega_0} \frac{1}{\omega - \omega_0} \quad . \tag{1.56}$$

1.3 Retarded Green's Function

An alternative way of solving the inhomogeneous differential equation

$$m_0 \left(\frac{\partial^2}{\partial t^2} + 2\gamma \frac{\partial}{\partial t} + \omega_0^2 \right) x(t) = e\mathcal{E}(t) \tag{1.57}$$

is obtained by using the Green's function of Eq. (1.57). The so-called *retarded Green's function* $G(t-t')$ is defined as the solution of Eq. (1.57), where the inhomogeneous term $e\mathcal{E}(t)$ is replaced by a delta function

$$m_0 \left(\frac{\partial^2}{\partial t^2} + 2\gamma \frac{\partial}{\partial t} + \omega_0^2 \right) G(t-t') = \delta(t-t') \quad . \tag{1.58}$$

Fourier transformation yields

$$\begin{aligned} G(\omega) &= -\frac{1}{m_0} \frac{1}{\omega^2 + i2\gamma\omega - \omega_0^2} \\ &= -\frac{1}{2m_0\omega_0'} \left(\frac{1}{\omega - \omega_0' + i\gamma} - \frac{1}{\omega + \omega_0' + i\gamma} \right) \quad , \end{aligned} \tag{1.59}$$

retarded Green's function of an oscillator

where ω_0' is defined in Eq. (1.8). In terms of $G(t-t')$, the solution of Eq. (1.57) is then

$$x(t) = \int_{-\infty}^{+\infty} dt' G(t-t') e\mathcal{E}(t') \quad , \tag{1.60}$$

as can be verified by inserting (1.60) into (1.57). Note, that the general solution of an inhomogeneous linear differential equation is obtained by adding the solution (1.60) of the inhomogeneous equation to the general solution of the homogeneous equation. However, since we are only interested in the induced polarization, we just keep the solution (1.60).

In general, the retarded Green's function $G(t-t')$ has the properties

$$G(t-t') = \begin{bmatrix} finite \\ 0 \end{bmatrix} \text{ for } \begin{bmatrix} t \geq t' \\ t < t' \end{bmatrix} \tag{1.61}$$

or

$$G(\tau) \propto \theta(\tau) \ ,$$

where $\theta(\tau)$ is the unit-step or Heavyside function

$$\theta(\tau) = \begin{bmatrix} 1 \\ 0 \end{bmatrix} \text{ for } \begin{bmatrix} \tau \geq 0 \\ \tau < 0 \end{bmatrix} \ . \tag{1.62}$$

For $\tau < 0$ we can close in (1.60) the integral by a circle with an infinite radius in the upper half of the complex frequency plane since

$$\lim_{|\omega|\to\infty} \quad e^{i(\omega'+i\omega'')|\tau|} = \lim_{|\omega|\to\infty} \quad e^{i\omega'\tau} e^{-\omega''|\tau|} = 0 \ . \tag{1.63}$$

As can be seen from (1.59), $G(\omega)$ has no poles in the upper half plane making the integral zero for $\tau < 0$. For $\tau \geq 0$ we have to close the contour integral in the lower half plane, denoted by C_ℓ, and get

$$\begin{aligned} G(\tau) &= -\frac{1}{2m_0\omega_0'}\theta(\tau) \int_{C_\ell} \frac{d\omega}{2\pi} e^{-i\omega\tau} \left(\frac{1}{\omega - \omega_0' + i\gamma} - \frac{1}{\omega + \omega_0' + i\gamma} \right) \\ &= i\theta(\tau) \frac{1}{2m_0\omega_0'} [e^{-(i\omega_0'+\gamma)\tau} - e^{(i\omega_0'-\gamma)\tau}] \ . \end{aligned} \tag{1.64}$$

The property that $G(\tau) = 0$ for $\tau < 0$ is the reason for the name *retarded Green's function* which is often indicated by a superscript r, i.e.,

$$G^r(\tau) = 0 \text{ for } \tau < 0 \longleftrightarrow G^r(\omega) = \text{ analytic for } \omega'' \geq 0 \ . \tag{1.65}$$

The Fourier transform of Eq. (1.60) is

$$\begin{aligned} x(\omega) &= \int_{-\infty}^{+\infty} dt \int_{-\infty}^{+\infty} dt' e^{i\omega(t-t')} G(t-t') e^{i\omega t'} e\mathcal{E}(t') \\ &= e\, G(\omega)\mathcal{E}(\omega) \ . \end{aligned} \tag{1.66}$$

With $\mathcal{P}(\omega) = en_0 x(\omega) = \chi(\omega)\mathcal{E}(\omega)$ we obtain

$$\chi(\omega) = n_0 e^2 G(\omega) \tag{1.67}$$

$$\chi(\omega) = -\frac{n_0 e^2}{2m\omega_0'}\left(\frac{1}{\omega - \omega_0' + i\gamma} - \frac{1}{\omega + \omega_0' + i\gamma}\right) \tag{1.68}$$

in agreement with Eq. (1.7).

This concludes the introductory chapter. In summary, we have discussed the most important optical coefficients, their interrelations, analytic properties, and explicit forms in the oscillator model. It turns out that this model is often sufficient for a qualitatively correct description of isolated optical resonances. However, as we progress to describe the optical properties of semiconductors, we will see the necessity to modify and extend this simple model in many respects.

REFERENCES

For further reading we recommend:

J.D. Jackson, *Classical Electrodynamics*, 2nd *ed.*, Wiley, New York, (1975)
L.D. Landau and E.M. Lifshitz, *The Classical Theory of Fields*, 3rd *ed.*, Addison–Wesley, Reading, Mass. (1971)
L.D. Landau and E.M. Lifshitz, *Electrodynamics of Continuous Media*, Addison–Wesley, Reading, Mass. (1960)

PROBLEMS

Problem 1.1: Prove the Dirac identity

$$\frac{1}{r \mp i\epsilon} = P\frac{1}{r} \pm i\pi\delta(r) \ , \tag{1.69}$$

where $\epsilon \to 0$ and use of the formula under an integral is implied.
Hint: Write Eq. (1.69) under the integral from $-\infty$ to $+\infty$ and integrate in pieces from $-\infty$ to $-\epsilon$, from $-\epsilon$ to $+\epsilon$ and from $+\epsilon$ to $+\infty$.

Problem 1.2: Derive the Kramers–Kronig relation relating $\chi''(\omega)$ to the integral over $\chi'(\omega)$.

Problem 1.3: Show that the Lorentzian

$$f(\omega) = \frac{1}{\pi}\frac{\gamma}{(\omega - \omega_0)^2 + \gamma^2} \tag{1.70}$$

approaches the delta function $\delta(\omega - \omega_0)$ for $\gamma \to 0$.

Problem 1.4: Verify Eq. (1.56) by evaluating the Kramers–Kronig transformation of Eq. (1.55). Note, that only the resonant part of Eq. (1.22) should be used in order to be consistent with the resonant term approximation in Eq. (1.36).

Problem 1.5: Use Eq. (1.13) to show that

$$\int_{-\infty}^{\infty} d\omega \, e^{i\omega t} = 2\pi\delta(t).$$

This page intentionally left blank

Chapter 2

Atoms in a Classical Light Field

Semiconductors like all crystals are periodic arrays of one or more types of atoms. A prototype of a semiconductor is a lattice of group IV atoms, e.g. Si or Ge, which have four electrons in the outer electronic shell. These electrons participate in the covalent binding of a given atom to its four nearest neighbors which sit in the corners of a tetrahedron around the given atom. The bonding states form the valence bands which are separated by an energy gap from the energetically next higher states forming the conduction band.

In order to understand the similarities and the differences between optical transitions in a semiconductor and in an atom, we will first give an elementary treatment of the optical transitions in an atom. This chapter also serves to illustrate the difference between a quantum mechanical derivation of the polarization and the classical theory of Chap. 1.

2.1 Atomic Optical Susceptibility

The stationary Schrödinger equation of a single electron in an atom is

$$\mathcal{H}_0\psi_n(\mathbf{r}) = \hbar\epsilon_n\psi_n(\mathbf{r}) \ , \tag{2.1}$$

where $\hbar\epsilon_n$ and ψ_n are the energy eigenvalues and the corresponding eigenfunctions, respectively. For simplicity, we discuss the example of the hydrogen atom which has only a single electron. The Hamiltonian $\mathcal{H}_0$ is then given by the sum of the kinetic energy operator and the Coulomb potential in the form

$$\mathcal{H}_0 = -\frac{\hbar^2\nabla^2}{2m_0} - \frac{e^2}{r} \ . \tag{2.2}$$

An optical field couples to the dipole moment of the atom and introduces time-dependent changes of the wave function

$$i\hbar\frac{\partial\psi(\mathbf{r},t)}{\partial t} = [\mathcal{H}_0 + \mathcal{H}_I(t)]\psi(\mathbf{r},t) \tag{2.3}$$

with

$$\mathcal{H}_I(t) = -ex\mathcal{E}(t) = -d\mathcal{E}(t) \ . \tag{2.4}$$

Here, d is the operator for the electric dipole moment and we assumed that the homogeneous electromagnetic field is polarized in x-direction. Expanding the time-dependent wave functions into the stationary eigenfunctions of Eq. (2.1)

$$\psi(\mathbf{r},t) = \sum_m a_m(t)e^{-i\epsilon_m t}\psi_m(\mathbf{r}) \ , \tag{2.5}$$

inserting into Eq. (2.3), multiplying from the left by $\psi_n^*(\mathbf{r})$ and integrating over space, we find for the coefficients a_n the equation

$$i\hbar\frac{da_n}{dt} = -\mathcal{E}(t)\sum_m e^{-i\epsilon_{mn}t}\langle n|d|m\rangle a_m \ , \tag{2.6}$$

where

$$\epsilon_{mn} = \epsilon_m - \epsilon_n \tag{2.7}$$

is the frequency difference and

$$\langle n|d|m\rangle = \int d^3r\psi_n^*(\mathbf{r})d\psi_m(\mathbf{r}) \equiv d_{nm} \tag{2.8}$$

is the electric dipole matrix element. We assume that the electron was initially at $t \to -\infty$ in the state $|l\rangle$, i.e.,

$$a_n(t \to -\infty) = \delta_{n,l} \ . \tag{2.9}$$

Now we solve Eq. (2.6) iteratively taking the field as perturbation. For this purpose, we introduce the smallness parameter Δ and expand

$$a_n = a_n^{(0)} + \Delta a_n^{(1)} + \ldots \tag{2.10}$$

and

$$\mathcal{E}(t) \to \Delta\mathcal{E}(t) \ . \tag{2.11}$$

Inserting (2.10) and (2.11) into Eq. (2.6), we obtain in order Δ^0

$$\frac{da_n^{(0)}}{dt} = 0 \ , \tag{2.12}$$

which is satisfied by

$$a_n^{(0)} = \delta_{n,l} \ . \tag{2.13}$$

In first order of Δ, we have

$$i\hbar \frac{da_n^{(1)}}{dt} = -\mathcal{E}(t) d_{nl} e^{-i\epsilon_{ln}t} \ . \tag{2.14}$$

For $n = l$ there is no field-dependent contribution, i.e., $a_l^{(i)} \equiv 0$ for $i \geq 1$, since $d_{ll} = 0$. Integrating Eq. (2.14) for $n \neq l$ from $-\infty$ to t yields

$$a_n^{(1)}(t) = -\frac{1}{i\hbar} \int_{-\infty}^{t} dt' \mathcal{E}(t') d_{nl} e^{-i\epsilon_{ln}t'} \ , \tag{2.15}$$

where $a_n^{(1)}(t = -\infty) = 0$ has been used. This condition is valid since we assumed that the electron is in state l without the field, Eq. (2.9).

To solve the integral in Eq. (2.15), we express the field through its Fourier transform

$$\mathcal{E}(t) = \lim_{\gamma \to 0} \int \frac{d\omega}{2\pi} \mathcal{E}(\omega) e^{-i\omega t} e^{\gamma t} \ . \tag{2.16}$$

Here, we introduced the adiabatic switch-on factor $\exp(\gamma t)$, to assure that $\mathcal{E}(t) \to 0$ when $t \to -\infty$. We will see below that the switch-on parameter γ plays the same role as the infinitesimal damping parameter of Chap. 1. The existence of γ makes sure that the resulting optical susceptibility has poles only in the lower half of the complex plane, i.e., causality is obeyed. For notational simplicity, we will drop the $\lim_{\gamma \to 0}$ in front of the expressions, but it is understood that this limit is always implied. Inserting Eq. (2.16) into Eq. (2.15) we obtain

$$a_n^{(1)}(t) = -\frac{d_{nl}}{\hbar} \int \frac{d\omega}{2\pi} \mathcal{E}(\omega) \frac{e^{-i(\omega + \epsilon_{ln})t}}{\omega + \epsilon_{ln} + i\gamma} \ , \tag{2.17}$$

where we let $\gamma \to 0$ in the exponent after the integration.

If we want to generate results in higher-order perturbation theory, we have to continue the iteration by inserting the first-order result into the RHS of (2.6) and calculate this way $a^{(2)}$ etc. These higher-order terms

contain quadratic and higher powers of the electric field. However, we are limiting ourselves to the terms linear in the field, i.e. we employ *linear response theory*.

The total wave function (2.5) is now

$$\psi(\mathbf{r},t) = e^{-i\epsilon_l t}\Bigg[\psi_l(\mathbf{r}) - \sum_{m\neq l}\frac{d_{lm}}{\hbar}\psi_m(\mathbf{r})\int\frac{d\omega}{2\pi}\mathcal{E}(\omega)\frac{e^{-i\omega t}}{\omega+\epsilon_{lm}+i\gamma}\Bigg] + \mathcal{O}(\mathcal{E}^2) \ . \tag{2.18}$$

The field-induced polarization is given as the expectation value of the dipole operator

$$\mathcal{P}(t) = n_0\int d^3r\psi^*(\mathbf{r},t)d\psi(\mathbf{r},t) \ , \tag{2.19}$$

where n_0 is the density of the mutually independent (not interacting) atoms in the system. Inserting the wave function (2.18) into Eq. (2.19), and keeping only terms which are first order in the field, we obtain the polarization as

$$\mathcal{P}(t) = -n_0\sum_m\frac{|d_{lm}|^2}{\hbar}\int\frac{d\omega}{2\pi}\left[\mathcal{E}(\omega)\frac{e^{-i\omega t}}{\omega+\epsilon_{lm}+i\gamma} + \mathcal{E}^*(\omega)\frac{e^{i\omega t}}{\omega+\epsilon_{lm}-i\gamma}\right]. \tag{2.20}$$

In the integral over the last term, we substitute $\omega\to-\omega$ and use $\mathcal{E}^*(-\omega) = \mathcal{E}(\omega)$, which is valid since $\mathcal{E}(t)$ is real. This way we get

$$\begin{aligned}\mathcal{P}(t) &= -n_0\sum_m\frac{|d_{lm}|^2}{\hbar}\int\frac{d\omega}{2\pi}\mathcal{E}(\omega)e^{-i\omega t}\left[\frac{1}{\omega+\epsilon_{lm}+i\gamma} - \frac{1}{\omega-\epsilon_{lm}+i\gamma}\right] \\ &= \int\frac{d\omega}{2\pi}\mathcal{P}(\omega)e^{-i\omega t} \ .\end{aligned} \tag{2.21}$$

This equation yields $\mathcal{P}(\omega) = \chi(\omega)\mathcal{E}(\omega)$ with the optical susceptibility

$$\boldsymbol{\chi(\omega) = -\frac{n_0}{\hbar} \sum_{m} |d_{lm}|^2 \left(\frac{1}{\omega + \epsilon_{lm} + i\gamma} - \frac{1}{\omega - \epsilon_{lm} + i\gamma} \right)} \ . \quad (2.22)$$

atomic optical susceptibility

2.2 Oscillator Strength

If we compare the atomic optical susceptibility, Eq. (2.22), with the result of the oscillator model, Eq. (1.7), we see that both expressions have similar structures. However, in comparison with the oscillator model the atom is represented not by one but by many oscillators with different transition frequencies ϵ_{ln}. To see this, we rewrite the expression (2.22), pulling out the same factors which appear in the oscillator result, Eq. (1.7),

$$\chi(\omega) = \frac{n_0 e^2}{2m_0} \sum_{n} \frac{f_{nl}}{\epsilon_{nl}} \left(\frac{1}{\omega - \epsilon_{ln} + i\gamma} - \frac{1}{\omega + \epsilon_{ln} + i\gamma} \right) \ . \quad (2.23)$$

Hence, each partial oscillator has the strength of

$$\boldsymbol{f_{nl} = \frac{2m_0}{\hbar} |x_{nl}|^2 \epsilon_{nl}} \ . \quad (2.24)$$

oscillator strength

Here, we used $|d_{nl}|^2 = e^2 |x_{nl}|^2$. Adding the strengths of all oscillators by summing over all the final states n, we find

$$\sum_{n} f_{nl} = \frac{2m_0}{\hbar} \sum_{n} \langle n|x|l\rangle\langle l|x|n\rangle(\epsilon_n - \epsilon_l) \ . \quad (2.25)$$

Using the Schrödinger equation $\mathcal{H}_0|n\rangle = \hbar\epsilon_n|n\rangle$, we can write

$$\langle l|x|n\rangle(\epsilon_n - \epsilon_l) = \frac{1}{\hbar}\langle l|[x, \mathcal{H}_0]|n\rangle = -\frac{1}{\hbar}\langle l|[\mathcal{H}_0, x]|n\rangle \ , \quad (2.26)$$

where $[\mathcal{H}_0, x] = x\mathcal{H}_0 - \mathcal{H}_0 x$ is the commutator of x and $\mathcal{H}_0$. Inserting (2.26) into (2.25) and using the completeness relation $\sum_n |n\rangle\langle n| = 1$ we get

$$\sum_n f_{nl} = -\frac{2m_0}{\hbar^2}\langle l|[\mathcal{H}_0, x]x|l\rangle \ . \tag{2.27}$$

Alternatively to (2.26), we can also manipulate the first term in Eq. (2.25) by writing

$$\langle n|x|l\rangle(\epsilon_n - \epsilon_l) = \langle n|[\mathcal{H}_0, x]|l\rangle \ , \tag{2.28}$$

so that

$$\sum_n f_{nl} = \frac{2m_0}{\hbar^2}\langle l|x[\mathcal{H}_0, x]|l\rangle \ . \tag{2.29}$$

Adding Eqs. (2.27) and (2.29) and dividing by two shows that the sum over the oscillator strength is given by a double commutator

$$\sum_n f_{nl} = \frac{m_0}{\hbar^2}\langle l|[x, [\mathcal{H}_0, x]]|l\rangle = \frac{m_0}{\hbar^2}\langle l|[[x, \mathcal{H}_0], x]|l\rangle \ . \tag{2.30}$$

The double commutator can be evaluated easily using

$$[x, \mathcal{H}_0] = -\frac{\hbar^2}{2m_0}\left(x\frac{d^2}{dx^2} - \frac{d^2}{dx^2}x\right) = \frac{\hbar^2}{m_0}\frac{d}{dx} = \frac{i\hbar}{m_0}p_x \tag{2.31}$$

and

$$[p_x, x] = -i\hbar \tag{2.32}$$

to get

$$\boldsymbol{\sum_n f_{nl} = 1} \ . \tag{2.33}$$

oscillator strength sum rule

Eq. (2.33) is the oscillator strength sum rule showing that the total transition strength in an atom can be viewed as that of one oscillator which is distributed over many partial oscillators, each having the strength f_{nl}.

Writing the imaginary part of the dielectric function of the atom as $\epsilon''(\omega) = 4\pi\chi''(\omega)$, using $\chi(\omega)$ from Eq. (2.23) and employing the Dirac identity, Eq. (1.69), we obtain

$$\epsilon''(\omega) = \omega_{pl}^2 \frac{\pi}{2} \sum_n \frac{f_{nl}}{\epsilon_{nl}} [\delta(\omega - \epsilon_{nl}) - \delta(\omega - \epsilon_{ln})] \ , \tag{2.34}$$

with $\omega_{pl}^2 = 4\pi n_0 e^2/m_0$. Since $|l\rangle$ is the occupied initial state and $|n\rangle$ are the final states, we see that the first term in Eq. (2.34) describes light absorption. Energy conservation requires

$$\hbar\epsilon_n = \hbar\omega + \hbar\epsilon_l \ , \tag{2.35}$$

i.e., an optical transition from the lower state $|l\rangle$ to the energetically higher state $|n\rangle$ takes place if the energy difference $\hbar\epsilon_{nl}$ is equal to the energy $\hbar\omega$ of a light quantum, called a photon. In other words, a photon is absorbed and the atom is excited from the initial state $|l\rangle$ to the final state $|n\rangle$. This interpretation of our result is the correct one, but to be fully appreciated it actually requires also the quantum mechanical treatment of the light field.

The second term on the RHS of Eq. (2.34) describes negative absorption causing amplification of the light field, i.e., optical gain. This is the basis of laser action. In order to produce optical gain, the system has to be prepared in a state $|l\rangle$ which has a higher energy than the final state $|n\rangle$, because the energy conservation expressed by the delta function in the second term on the RHS of (2.34) requires

$$\hbar\epsilon_l = \hbar\omega + \hbar\epsilon_n \ . \tag{2.36}$$

If the energy of a light quantum equals the energy difference $\hbar\epsilon_{ln}$, stimulated emission occurs. In order to obtain stimulated emission in a real system, one has to invert the system so that it is initially in an excited state rather than in the ground state.

2.3 Optical Stark Shift

Until now we have only calculated and discussed the linear response of an atom to a weak light field. For the case of two atomic levels interacting with the light field, we will now determine the response at arbitrary field intensities. Calling these two levels $n = 1, 2$ with

$$\epsilon_2 > \epsilon_1 \ , \tag{2.37}$$

we get from Eq. (2.6) the following two coupled differential equations:

$$i\hbar\frac{da_1}{dt} = -\mathcal{E}(t)e^{-i\epsilon_{21}t}d_{12}a_2 \ , \tag{2.38}$$

$$i\hbar\frac{da_2}{dt} = -\mathcal{E}(t)e^{-i\epsilon_{21}t}d_{21}a_1 \ , \tag{2.39}$$

where we used $d_{ii} = 0$. Assuming a simple monochromatic field of the form

$$\mathcal{E}(t) = \frac{1}{2}\mathcal{E}(\omega)(e^{-i\omega t} + c.c.) \tag{2.40}$$

yields

$$i\hbar\frac{da_1}{dt} = -d_{12}\frac{\mathcal{E}(\omega)}{2}\left[e^{-i(\omega+\epsilon_{21})t} + e^{i(\omega-\epsilon_{21})t}\right]a_2 \ , \tag{2.41}$$

$$i\hbar\frac{da_2}{dt} = -d_{21}\frac{\mathcal{E}(\omega)}{2}\left[e^{-i(\omega-\epsilon_{21})t} + e^{i(\omega+\epsilon_{21})t}\right]a_1 \ , \tag{2.42}$$

where $\epsilon_{12} = -\epsilon_{21}$ has been employed. These two coupled differential equations are often called the *optical Bloch equations*. If we are interested only in the light-induced changes around the resonance,

$$\omega \simeq \epsilon_2 - \epsilon_1 \ , \tag{2.43}$$

we see that the exponential factor $\exp[i(\omega - \epsilon_{21})t]$ is almost time-independent, whereas the second exponential $\exp[i(\omega+\epsilon_{21})t]$ oscillates very rapidly. If we keep both terms, we would find that $\exp[i(\omega-\epsilon_{21})t]$ leads to the resonant term proportional to

$$\frac{1}{(\omega-\epsilon_{21})+i\gamma} \to P\frac{1}{\omega-\epsilon_{21}} - i\pi\delta(\omega-\epsilon_{21}) \tag{2.44}$$

in the susceptibility, whereas $\exp[i(\omega+\epsilon_{21})t]$ leads to the nonresonant term proportional to

$$\frac{1}{(\omega+\epsilon_{21})+i\gamma} \to P\frac{1}{\omega+\epsilon_{21}} - i\pi\delta(\omega+\epsilon_{21}) \ . \tag{2.45}$$

For optical frequencies satisfying (2.43), the δ-function in (2.45) cannot be satisfied since $\epsilon_2 > \epsilon_1$, and the principal value gives only a weak contribution

to the real part. Hence, one often completely ignores the nonresonant parts so that Eqs. (2.41) and (2.42) simplify to

$$i\hbar\frac{da_1}{dt} = -\frac{d_{12}\mathcal{E}(\omega)}{2}e^{i(\omega-\epsilon_{21})t}a_2 \ , \tag{2.46}$$

$$i\hbar\frac{da_2}{dt} = -\frac{d_{21}\mathcal{E}(\omega)}{2}e^{-i(\omega-\epsilon_{21})t}a_1 \ . \tag{2.47}$$

This approximation is also called the *rotating wave approximation* (RWA). This name originates from the fact that the periodic time development in Eqs. (2.46) and (2.47) can be represented as a rotation of the Bloch vector (see Chap. 5). If one transforms these simplified Bloch equations into a time frame which rotates with the frequency difference $\omega - \epsilon_{21}$, the neglected term would be ω out of phase and more or less average to zero for longer times.

To solve Eqs. (2.46) and (2.47), we first treat the case of exact resonance, $\omega = \epsilon_{21}$. Differentiating Eq. (2.47) and inserting (2.46) we get

$$\frac{d^2a_2}{dt^2} = i\frac{d_{21}\mathcal{E}(\omega)}{2\hbar}\frac{da_1}{dt} = -\left|\frac{d_{12}\mathcal{E}(\omega)}{2\hbar}\right|^2 a_2 = -\frac{\omega_R^2}{4}a_2 \ , \tag{2.48}$$

where we used $d_{21} = d_{12}^*$ and introduced the *Rabi frequency* as

$$\boldsymbol{\omega_R = \frac{|d_{21}\mathcal{E}|}{\hbar}} \ . \tag{2.49}$$

Rabi frequency

The solution of (2.48) is of the form

$$a_2(t) = a_2(0)e^{\pm i\omega_R t/2} \ . \tag{2.50}$$

For $a_1(t)$ we get the equivalent result. Inserting the solutions for a_1 and a_2 back into Eq. (2.5) yields

$$\psi(\mathbf{r},t) = a_1(0)e^{-i(\epsilon_1\pm\omega_R/2)t}\psi_1(\mathbf{r}) + a_2(0)e^{-i(\epsilon_2\pm\omega_R/2)t}\psi_2(\mathbf{r}) \ , \tag{2.51}$$

showing that the original frequencies ϵ_1 and ϵ_2 have been changed to $\epsilon_1 \pm \omega_R/2$ and $\epsilon_2 \pm \omega_R/2$, respectively. Hence, as indicated in Fig. 2.1 one has not just one but three optical transitions with the frequencies ϵ_{21}, and $\epsilon_{21} \pm \omega_R$, respectively. In other words, under the influence of the light

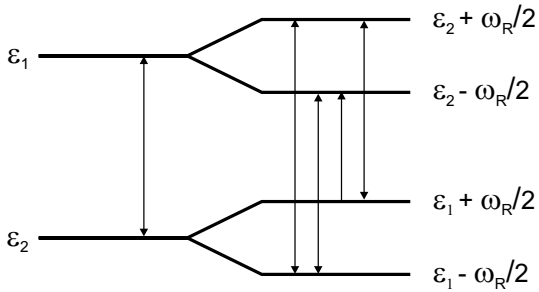

Fig. 2.1 Schematic drawing of the frequency scheme of a two-level system without the light field (left part of Figure) and light-field induced level splitting (right part of Figure) for the case of a resonant field, i.e., zero detuning. The vertical arrows indicate the possible optical transitions between the levels.

field the single transition possible in two-level atom splits into a triplet, the main transition at ϵ_{21} and the *Rabi sidebands* at $\epsilon_{21} \pm \omega_R$. Eq. (2.49) shows that the splitting is proportional to the product of field strength and electric dipole moment. Therefore, Rabi sidebands can only be observed for reasonably strong fields, where the Rabi frequency is larger than the line broadening, which is always present in real systems.

The two-level model can be solved also for the case of a finite detuning $\nu = \epsilon_{21} - \omega$. In this situation, Eqs. (2.46) and (2.47) can be written as

$$\frac{da_1}{dt} = ie^{-i\nu t}\frac{d_{12}\mathcal{E}(\omega)}{2\hbar}a_2 \tag{2.52}$$

$$\frac{da_2}{dt} = ie^{i\nu t}\frac{d_{21}\mathcal{E}(\omega)}{2\hbar}a_1 \ . \tag{2.53}$$

Taking the time derivative of Eq. (2.52)

$$\frac{d^2a_1}{dt^2} = e^{-i\nu t}\frac{d_{21}\mathcal{E}(\omega)}{2\hbar}\left(a_2\nu + i\frac{da_2}{dt}\right) \ , \tag{2.54}$$

and expressing a_2 and da_2/dt in terms of a_1 we get

$$\frac{d^2a_1}{dt^2} = -i\nu\frac{da_1}{dt} - \frac{\omega_R^2 a_1}{4} \tag{2.55}$$

with the solution

$$a_1(t) = a_1(0)e^{i\Omega t} \text{ (or } a_1(t) = a_1(0)e^{-i\Omega t}) \ , \tag{2.56}$$

where

$$\Omega = -\frac{\nu}{2} \pm \frac{1}{2}\sqrt{\nu^2 + \omega_R^2} \ . \tag{2.57}$$

Similarly, we obtain

$$a_2(t) = a_2(0)e^{-i\Omega t} \ (\text{or } a_2(t) = a_2(0)e^{i\Omega t}) \ . \tag{2.58}$$

Hence, we again get split and shifted levels

$$\epsilon_2 \to \Omega_2 \equiv \epsilon_2 + \Omega = \epsilon_2 - \frac{\nu}{2} \pm \frac{1}{2}\sqrt{\nu^2 + \omega_R^2} \tag{2.59}$$

$$\epsilon_1 \to \Omega_1 \equiv \epsilon_1 - \Omega = \epsilon_1 + \frac{\nu}{2} \pm \frac{1}{2}\sqrt{\nu^2 + \omega_R^2} \ . \tag{2.60}$$

The coherent modification of the atomic spectrum in the electric field of a light field resembles the Stark splitting and shifting in a static electric field. It is therefore called *optical Stark effect*. The modified or, as one also says, the renormalized states of the atom in the intense light field are those of a *dressed atom*. While the optical Stark effect has been well-known for a long time in atoms, it has been seen relatively recently in semiconductors, where the dephasing times are normally much shorter than in atoms, as will be discussed in more detail in later chapters of this book.

REFERENCES

For the basic quantum mechanical theory used in this chapter we recommend:

A.S. Davydov, *Quantum Mechanics*, Pergamon, New York (1965)
L.I. Schiff, *Quantum Mechanics*, 3rd *ed.*, McGraw–Hill, New York (1968)

The optical properties of two-level atoms are treated extensively in:

L. Allen and J.H. Eberly, *Optical Resonance and Two-Level Atoms*, Wiley and Sons, New York (1975)
P. Meystre and M. Sargent III, *Elements of Quantum Optics*, Springer, Berlin (1990)

M. Sargent III, M.O. Scully, and W.E. Lamb, Jr., *Laser Physics*, Addison–Wesley, Reading, MA (1974)

PROBLEMS

Problem 2.1: To describe the dielectric relaxation in a dielectric medium, one often uses the *Debye model* where the polarization obeys the equation

$$\frac{d\mathcal{P}}{dt} = -\frac{1}{\tau}[\mathcal{P}(t) - \chi_0 \mathcal{E}(t)] \ . \tag{2.61}$$

Here, τ is the relaxation time and χ_0 is the static dielectric susceptibility. The initial condition is

$$\mathcal{P}(t = -\infty) = 0 \ .$$

Compute the optical susceptibility.

Problem 2.2: Compute the oscillator strength for the transitions between the states of a quantum mechanical harmonic oscillator. Verify the sum rule, Eq. (2.33).

Chapter 3

Periodic Lattice of Atoms

After our discussion of the basic optical properties of a single atom in Chap. 2, we now analyze how the atomic energy spectrum is modified in a solid. As our model solid, we take a perfect crystal, where the ions are arranged in a periodic lattice. In the spirit of a Hartree–Fock or mean field theory, we assume that the influence of this periodic arrangement of ions on a given crystal electron can be expressed in the form of an effective periodic *lattice potential* which contains the mean field of the nuclei and all the other electrons.

For simplicity, we consider only ideal crystals, which consist of a perfect ionic lattice and some electrons which experience the lattice periodic potential. We are interested in the wave functions and allowed energy states of a single electron moving in the effective lattice potential $V_0(\mathbf{r})$. Many-electron effects will be discussed in later chapters of this book.

3.1 Reciprocal Lattice, Bloch Theorem

For the valence electrons in a crystal, the lattice potential $V_0(\mathbf{r})$ is an attractive potential due to the superposition of the Coulomb potentials of the nuclei and the inner electrons of the ions. However, for our considerations we never need the explicit form of $V_0(\mathbf{r})$. We only utilize some general features, such as the symmetry and periodicity properties of the potential which reflect the structure of the crystal lattice.

The periodicity of the effective lattice potential is expressed by the translational symmetry

$$V_0(\mathbf{r}) = V_0(\mathbf{r} + \mathbf{R}_n) \ , \tag{3.1}$$

where $\mathbf{R}_n$ is a lattice vector, i.e., a vector which connects two identical sites in an infinite lattice, which are n lattice cells apart. It is convenient to expand the lattice vectors

$$\mathbf{R}_n = \sum_i n_i \mathbf{a}_i \ , \tag{3.2}$$

where n_i are integers and $\mathbf{a}_i$ are the basis vectors which span the unit cells. Note, that the basis vectors are not unit vectors and they are generally not even orthogonal. They point into the directions of the three axes of the unit cell, which may have e.g. a rhombic or more complicated shape. The basis vectors are parallel to the usual Cartesian unit vectors only in the case of orthogonal lattices such as the cubic one.

To make use of the fact that the potential acting on the electron has the periodicity of the lattice, we introduce a translation operator T_n

$$T_n f(\mathbf{r}) = f(\mathbf{r} + \mathbf{R}_n) \ , \tag{3.3}$$

where f is an arbitrary function. Applying T_n to the wave function ψ of an electron in the periodic potential $V_0(\mathbf{r})$, we obtain

$$T_n \psi(\mathbf{r}) = \psi(\mathbf{r} + \mathbf{R}_n) = t_n \psi(\mathbf{r}) \ , \tag{3.4}$$

where t_n is a phase factor, because the electron probability distributions $|\psi(\mathbf{r})|^2$ and $|\psi(\mathbf{r} + \mathbf{R}_n)|^2$ have to be identical. Since the Hamiltonian

$$\mathcal{H} = \frac{p^2}{2m_0} + V_0(\mathbf{r}) \tag{3.5}$$

has the full lattice symmetry, the commutator of $\mathcal{H}$ and T_n vanishes:

$$[\mathcal{H}, T_n] = 0 \ . \tag{3.6}$$

Under this condition a complete set of functions exists which are simultaneously eigenfunctions to $\mathcal{H}$ and T_n:

$$\mathcal{H}\psi_\lambda(\mathbf{k}, \mathbf{r}) = E_\lambda \psi_\lambda(\mathbf{k}, \mathbf{r}) \tag{3.7}$$

and

$$T_n \psi_\lambda(\mathbf{k}, \mathbf{r}) = \psi_\lambda(\mathbf{k}, \mathbf{r} + \mathbf{R}_n) = t_n \psi_\lambda(\mathbf{k}, \mathbf{r}) \ . \tag{3.8}$$

Here, we introduced $\mathbf{k}$ as the quantum number associated with the translation operator. As discussed above, t_n can only be a phase factor with the properties

$$|t_n| = 1 \ , \tag{3.9}$$

and

$$t_n t_m = t_{n+m} \tag{3.10}$$

since

$$T_{n+m} = T_n T_m \ , \tag{3.11}$$

stating the obvious fact that a translation by $\mathbf{R}_n + \mathbf{R}_m$ is identical to a translation by $\mathbf{R}_m$ followed by another translation by $\mathbf{R}_n$. A possible choice to satisfy Eqs. (3.8) – (3.11) is

$$t_n = e^{i(\mathbf{k}\cdot\mathbf{R}_n + 2\pi N)} \ , \tag{3.12}$$

where $2\pi N$ is an allowed addition because

$$e^{i2\pi N} = 1 \ , \text{ for } N = \text{integer} \ . \tag{3.13}$$

We now define a *reciprocal lattice vector* $\mathbf{g}$ through the relation

$$e^{i\mathbf{k}\cdot\mathbf{R}_n} \equiv e^{i(\mathbf{k}+\mathbf{g})\cdot\mathbf{R}_n} \tag{3.14}$$

so that $\mathbf{g}\cdot\mathbf{R}_n = 2\pi N$. Expanding $\mathbf{g}$ in the basis vectors $\mathbf{b}_i$ of the reciprocal lattice

$$\mathbf{g} = \sum_{i=1}^{3} m_i \mathbf{b}_i, \quad m_i = \text{ integer} \ , \tag{3.15}$$

we find

$$\mathbf{g}\cdot\mathbf{R}_n = \sum_{ij} m_i n_j \mathbf{b}_i \cdot \mathbf{a}_j = 2\pi N \ , \tag{3.16}$$

if

$$\mathbf{b}_i \cdot \mathbf{a}_j = 2\pi\delta_{ij} \ , \quad i,j = 1,2,3 \ . \tag{3.17}$$

Consequently, $\mathbf{b}_i$ is perpendicular to both $\mathbf{a}_j$ and $\mathbf{a}_k$ with $i \neq k, j$ and can be written as the vector product

$$\mathbf{b}_i = c\,\mathbf{a}_j \times \mathbf{a}_k \quad . \tag{3.18}$$

To determine the proportionality constant c, we use

$$\mathbf{a}_i \cdot \mathbf{b}_i = c\,\mathbf{a}_i \cdot (\mathbf{a}_j \times \mathbf{a}_k) = 2\pi \quad , \tag{3.19}$$

which yields

$$c = \frac{2\pi}{\mathbf{a}_i \cdot (\mathbf{a}_j \times \mathbf{a}_k)} \quad . \tag{3.20}$$

Hence,

$$\mathbf{b}_i = 2\pi \frac{\mathbf{a}_j \times \mathbf{a}_k}{\mathbf{a}_i \cdot (\mathbf{a}_j \times \mathbf{a}_k)} \quad . \tag{3.21}$$

Similarly, we can express the $\mathbf{a}_i$ in terms of the $\mathbf{b}_i$.

In summary, we have introduced two lattices characterized by the unit vectors $\mathbf{a}_i$ and $\mathbf{b}_i$, respectively, which are reciprocal to one another. Since the $\mathbf{a}_i$ are the vectors of the real crystal lattice, the lattice defined by the $\mathbf{b}_i$ is called the *reciprocal lattice*. The unit cells spanned by the $\mathbf{a}_i$ are called the *Wigner–Seitz cells*, while the unit cells spanned by the $\mathbf{b}_i$ are the *Brillouin zones*. One can think of a transformation between the real and reciprocal lattice spaces as a discrete three-dimensional Fourier transform.

For the example of a cubic lattice, we have

$$|\mathbf{b}_i| = \frac{2\pi}{|\mathbf{a}_i|} \quad . \tag{3.22}$$

Consequently, the smallest reciprocal lattice vector in this case has the magnitude

$$g_i = \frac{2\pi}{a_i} \quad . \tag{3.23}$$

Going back to Eq. (3.14), it is clear that we can restrict the range of k values to the region

$$-\frac{g_i}{2} \leq k_i \leq \frac{g_i}{2} \quad , \tag{3.24}$$

since all other values of k can be realized by adding (or subtracting) multiple reciprocal lattice vectors. This range of k-values is called the first Brillouin zone.

Considerations along the lines of Eqs. (3.1) – (3.14) led F. Bloch to formulate the following theorem, which has to be fulfilled by the electronic wave functions in the lattice:

$$\boldsymbol{e^{i\mathbf{k}\cdot\mathbf{R}_n}\psi_\lambda(\mathbf{k},\mathbf{r}) = \psi_\lambda(\mathbf{k},\mathbf{r}+\mathbf{R}_n)} \ . \tag{3.25}$$

Bloch theorem

To satisfy this relation, we make the ansatz

$$\boldsymbol{\psi_\lambda(\mathbf{k},\mathbf{r}) = \frac{e^{i\mathbf{k}\cdot\mathbf{r}}}{L^{3/2}} u_\lambda(\mathbf{k},\mathbf{r})} \ , \tag{3.26}$$

Bloch wave function

where L^3 is the volume of the crystal and λ is the energy eigenvalue. $\mathbf{k}$ is the eigenvalue for the periodicity (crystal momentum). The function $u_\lambda(\mathbf{k},\mathbf{r})$ is often called *Bloch function*. The ansatz (3.26) fulfills the Bloch theorem (3.25), if the Bloch function u_λ is periodic in real space

$$u_\lambda(\mathbf{k},\mathbf{r}) = u_\lambda(\mathbf{k},\mathbf{r}+\mathbf{R}_n) \ , \tag{3.27}$$

i.e. the Bloch function $u_\lambda(\mathbf{k},\mathbf{r})$ has the lattice periodicity.

The Schrödinger equation for a crystal electron is

$$\mathcal{H}\psi_\lambda(\mathbf{k},\mathbf{r}) = \left[\frac{p^2}{2m_0} + V_0(r)\right]\psi_\lambda(\mathbf{k},\mathbf{r}) = E_\lambda(\mathbf{k})\psi_\lambda(\mathbf{k},\mathbf{r}) \ , \tag{3.28}$$

where m_0 is the free electron mass. Inserting Eq. (3.26) into (3.28) and using the relation

$$\begin{aligned}\sum_j \frac{\partial^2}{\partial x_j^2}\psi_\lambda &= -k^2\psi_\lambda + 2i\sum_j k_j \frac{e^{i\mathbf{k}\cdot\mathbf{r}}}{L^{3/2}}\frac{\partial u_\lambda}{\partial x_j} + \frac{e^{i\mathbf{k}\cdot\mathbf{r}}}{L^{3/2}}\sum_j \frac{\partial^2 u_\lambda}{\partial x_j^2} \\ &= \frac{e^{i\mathbf{k}\cdot\mathbf{r}}}{L^{3/2}}(\nabla + i\mathbf{k})^2 u_\lambda \ ,\end{aligned} \tag{3.29}$$

we obtain

$$\left[-\frac{\hbar^2}{2m_0}(\nabla + i\mathbf{k})^2 + V_0(\mathbf{r})\right] u_\lambda(\mathbf{k},\mathbf{r}) = E_\lambda(\mathbf{k}) u_\lambda(\mathbf{k},\mathbf{r}) \ . \tag{3.30}$$

With $\mathbf{p} = -i\hbar\nabla$ Eq. (3.30) can be written in the form

$$\left[-\frac{\hbar^2}{2m_0}\nabla^2 + \frac{\hbar}{m_0}\mathbf{k}\cdot\mathbf{p} + V_0(\mathbf{r})\right] u_\lambda(\mathbf{k},\mathbf{r}) = \left[E_\lambda(\mathbf{k}) - \frac{\hbar^2 k^2}{2m_0}\right] u_\lambda(\mathbf{k},\mathbf{r}), \tag{3.31}$$

which will be the starting point for the $\mathbf{k}\cdot\mathbf{p}$ analysis in Sec. 3.3.

Before we describe some approximate solutions of Eq. (3.31), we first discuss in the remainder of this section further general properties of the Bloch wave function. The wave functions (3.26) are complete and orthonormal,

$$\int_{L^3} d^3r \psi^*_\lambda(\mathbf{k},\mathbf{r})\psi_{\lambda'}(\mathbf{k}',\mathbf{r}) = \delta_{\lambda,\lambda'}\delta_{\mathbf{k},\mathbf{k}'} \ , \tag{3.32}$$

since they are eigenfunctions of the crystal Hamiltonian, Eq. (3.5). In Eq. (3.32), we normalized the Bloch functions to the crystal volume L^3, so that

$$\int_{L^3} d^3r |\psi_\lambda(\mathbf{k},\mathbf{r})|^2 = 1 = \frac{1}{L^3}\int_{L^3} d^3r |u_\lambda(\mathbf{k},\mathbf{r})|^2 \ . \tag{3.33}$$

The convenient normalization of the wave functions to the volume L^3 needs some comments, since all real crystals with finite volume have surfaces and thus they do not have the full translational symmetry which we assumed above. However, the problems related to the surfaces can be avoided through a trick, i.e., the introduction of *periodic boundary conditions*. Let us assume the crystal has an end face in z direction at $z = L = N_3|\mathbf{a}_3|$. Periodic boundary conditions imply that one assumes the crystal end face to be connected with the front face at $z = 0$. Generalizing this concept to all space dimensions, the electron wave functions have to satisfy the condition

$$\psi_\lambda(\mathbf{k},\mathbf{r} + N_i\mathbf{a}_i) = \psi_\lambda(\mathbf{k},\mathbf{r}) \ , \tag{3.34}$$

where N_i is the total number of unit vectors in the direction i. These periodic boundary conditions are convenient since they eliminate the surface but keep the crystal volume finite.

Using the periodic boundary conditions in the plane wave factor of Eq. (3.26) implies

$$e^{i\mathbf{k}\cdot(\mathbf{R}_m + N_i\mathbf{a}_i)} = e^{i\mathbf{k}\cdot\mathbf{R}_m} \ , \tag{3.35}$$

which is satisfied if $N_i\,\mathbf{k}\cdot\mathbf{a}_i = 2\pi M$, where M is an integer. In a cubic lattice,

$$-\frac{\pi}{a_i} \le k \le \frac{\pi}{a_i} \tag{3.36}$$

and M is therefore restricted:

$$|M| = |\mathbf{k}\cdot\mathbf{a}_i|\frac{N_i}{2\pi} \le \frac{N_i}{2} \quad \text{or} \quad -\frac{N_i}{2} \le M \le \frac{N_i}{2}\ . \tag{3.37}$$

The Bloch form of the electron wave function in a crystal, Eq. (3.26), consists of an envelope function and a Bloch function u_λ. The envelope function for an infinite crystal, or a crystal with periodic boundary conditions, has the form of a plane wave, $\exp(\mathrm{i}\mathbf{k}\cdot\mathbf{r})$. While the Bloch function varies spatially on an atomic scale, the envelope function varies for small k-values only on a much longer, *mesoscopic* scale. Here we say mesoscopic scale rather than macroscopic scale, because in a real crystal the quantum mechanical coherence is usually not maintained over macroscopic distances.

Coming back to the normalization integral in Eq. (3.33), we notice that since the Bloch functions u_λ have the periodicity of the lattice, the integral over the crystal volume can be evaluated as

$$\int_{L^3} \to \sum_N \int_{l^3}\ , \tag{3.38}$$

where l^3 is the volume of an elementary cell, so that $L^3 = Nl^3$ when N is the number of elementary cells. Substituting Eq. (3.27) into Eq. (3.33) we obtain

$$\sum_{n=1}^{N} \frac{1}{N}\int_{l^3}\frac{d^3r}{l^3}|u_\lambda(\mathbf{k},\mathbf{r})|^2 = \frac{1}{l^3}\int_{l^3} d^3r|u_\lambda(\mathbf{k},\mathbf{r})|^2 = 1\ , \tag{3.39}$$

showing that the Bloch functions are normalized within an elementary cell. Furthermore one can show that the Bloch functions are a complete set for any fixed momentum value

$$\sum_\lambda u^*_\lambda(\mathbf{k},\mathbf{r})u_\lambda(\mathbf{k},\mathbf{r}') = l^3\delta(\mathbf{r}-\mathbf{r}')\ . \tag{3.40}$$

Sometimes it is useful to introduce localized functions as expansion set instead of the delocalized Bloch functions u_λ. An example of such localized

functions are the *Wannier functions* $w_\lambda(\mathbf{r}-\mathbf{R}_n)$. The Wannier functions are related to the Bloch functions via

$$w_\lambda(\mathbf{r}-\mathbf{R}_n) = \frac{1}{\sqrt{L^3 N}} \sum_{\mathbf{k}} e^{i\mathbf{k}\cdot(\mathbf{r}-\mathbf{R}_n)} u_\lambda(\mathbf{k},\mathbf{r}) \tag{3.41}$$

and

$$u_\lambda(\mathbf{k},\mathbf{r}) = \sqrt{\frac{L^3}{N}} \sum_{n} e^{-i\mathbf{k}\cdot(\mathbf{r}-\mathbf{R}_n)} w_\lambda(\mathbf{r}-\mathbf{R}_n) \ . \tag{3.42}$$

It may be shown that the Wannier functions are concentrated around a lattice point $\mathbf{R}$. They are orthogonal for different lattice points

$$\int d^3 r w^*_\lambda(\mathbf{r}) w_{\lambda'}(\mathbf{r}-\mathbf{R}_n) = \delta_{\lambda,\lambda'}\delta_{n,0} \ , \tag{3.43}$$

see problem 3.2. Particularly in spatially inhomogeneous situations it is often advantageous to use Wannier functions as the expansion set. The full electron wave function expressed in terms of Wannier functions is

$$\psi_\lambda(\mathbf{k},\mathbf{r}) = \frac{1}{\sqrt{N}} \sum_{n} e^{i\mathbf{k}\cdot\mathbf{R}_n} w_\lambda(\mathbf{r}-\mathbf{R}_n) \ . \tag{3.44}$$

3.2 Tight-Binding Approximation

After these symmetry considerations, we discuss simple approximations for calculating the allowed energies and eigenfunctions of an electron in the crystal lattice. First we treat the so-called *tight-binding approximation* which may serve as elementary introduction into the wide field of band structure calculations. In Sec. 3-3 and 3-4, we then introduce more quantitative approximations which are useful to compute the band structure in a limited region of k-space.

In the tight-binding approximation, we start from the electron wave functions of the isolated atoms which form the crystal. We assume that the electrons stay close to the atomic sites and that the electronic wave functions centered around neighboring sites have little overlap. Consequently, there is almost no overlap between wave functions for electrons that are separated by two or more atoms (next-nearest neighbors, next-next nearest neighbors, etc). The relevant overlap integrals decrease rapidly with increasing distance between the atoms at sites m and l, so that only a few terms have to be taken into account.

The Schrödinger equation for a single atom located at the lattice point l is

$$\mathcal{H}_0\phi_\lambda(\mathbf{r}-\mathbf{R}_l)=\mathcal{E}_\lambda\phi_\lambda(\mathbf{r}-\mathbf{R}_l) \tag{3.45}$$

with the Hamiltonian

$$\mathcal{H}_0=-\frac{\hbar^2\nabla^2}{2m_0}+V_0(\mathbf{r}-\mathbf{R}_l)\ , \tag{3.46}$$

where $V_0(\mathbf{r}-\mathbf{R}_l)$ is the potential of the l-th atom. The full problem of the periodic solid is then

$$\left[-\frac{\hbar^2\nabla^2}{2m_0}+\sum_l V_0(\mathbf{r}-\mathbf{R}_l)-E_\lambda(\mathbf{k})\right]\psi_\lambda(\mathbf{k},\mathbf{r})=0\ . \tag{3.47}$$

The total potential is the sum of the single-atom potentials. To solve Eq. (3.47), we make the ansatz

$$\boldsymbol{\psi_\lambda(\mathbf{k},\mathbf{r})=\sum_n \frac{e^{i\mathbf{k}\cdot\mathbf{R}_n}}{L^{3/2}}\phi_\lambda(\mathbf{r}-\mathbf{R}_n)}\ , \tag{3.48}$$

tight-binding wave function

which obviously fulfills the Bloch theorem, Eq. (3.25). With the periodic boundary conditions (3.34) we obtain

$$\begin{aligned}\psi(\mathbf{k},\mathbf{r})&=\frac{1}{L^{3/2}}\sum_n e^{i\mathbf{k}\cdot\mathbf{R}_n}\phi_\lambda(\mathbf{r}-\mathbf{R}_n)\\&=\frac{1}{L^{3/2}}\sum_n e^{i\mathbf{k}\cdot\mathbf{R}_n}\phi_\lambda(\mathbf{r}+N_i\mathbf{a}_i-\mathbf{R}_n)\ .\end{aligned} \tag{3.49}$$

Denoting $\mathbf{R}_n-N_i\mathbf{a}_i=\mathbf{R}_m$, we can write the last line as

$$\psi(\mathbf{k},\mathbf{r})=\frac{1}{L^{3/2}}\sum_m e^{i\mathbf{k}\cdot(\mathbf{R}_m+N_i\mathbf{a}_i)}\phi_\lambda(\mathbf{r}-\mathbf{R}_m)\ . \tag{3.50}$$

In order to compute the energy, we have to evaluate

$$E_\lambda(\mathbf{k})=\frac{\int d^3r\psi^*_\lambda(\mathbf{k},\mathbf{r})\mathcal{H}\psi_\lambda(\mathbf{k},\mathbf{r})}{\int d^3r\psi^*_\lambda(\mathbf{k},\mathbf{r})\psi_\lambda(\mathbf{k},\mathbf{r})}=\frac{\mathcal{N}}{\mathcal{D}}\ , \tag{3.51}$$

where the numerator can be written as

$$\mathcal{N} = \frac{1}{L^3} \sum_{n,m} e^{i\mathbf{k}\cdot(\mathbf{R}_n - \mathbf{R}_m)} \int d^3r \phi_\lambda^*(\mathbf{r} - \mathbf{R}_m) \mathcal{H} \phi_\lambda(\mathbf{r} - \mathbf{R}_n) \tag{3.52}$$

and the denominator is

$$\mathcal{D} = \frac{1}{L^3} \sum_{n,m} e^{i\mathbf{k}\cdot(\mathbf{R}_n - \mathbf{R}_m)} \int d^3r \phi_\lambda^*(\mathbf{r} - \mathbf{R}_m) \phi_\lambda(\mathbf{r} - \mathbf{R}_n) \ . \tag{3.53}$$

Since we assume strongly localized electrons, the integrals decrease rapidly with increasing distance between site n and m. The leading contribution is $n = m$, then $n = m \pm 1$, etc. In our final result, we only want to keep the leading order of the complete expression (3.51). Therefore, it is sufficient to approximate in the denominator:

$$\int d^3r \phi_\lambda^*(\mathbf{r} - \mathbf{R}_m) \phi_\lambda(\mathbf{r} - \mathbf{R}_n) \simeq \delta_{n,m} \ , \tag{3.54}$$

so that

$$\mathcal{D} = \sum_{n,m} \frac{\delta_{n,m}}{L^3} = \sum_n \frac{1}{L^3} = \frac{N}{L^3} \ . \tag{3.55}$$

We denote the integral in the numerator as

$$\mathcal{I} = \int d^3r \phi_\lambda^*(\mathbf{r} - \mathbf{R}_m) \left[-\frac{\hbar^2 \nabla^2}{2m_0} + \sum_l \mathbf{V}_0(\mathbf{r} - \mathbf{R}_l) \right] \phi_\lambda(\mathbf{r} - \mathbf{R}_n) \ .$$

It can be approximated as follows

$$\begin{aligned} \mathcal{I} &= \delta_{n,m} \left[\sum_l \delta_{l,n} \mathcal{E}_\lambda + \sum_{l \neq n} \int d^3r \phi_\lambda^*(\mathbf{r} - \mathbf{R}_n) V_0(\mathbf{r} - \mathbf{R}_l) \phi_\lambda(\mathbf{r} - \mathbf{R}_n) \right] \\ &\quad + \delta_{n\pm1,m} \sum_l \int d^3r \phi_\lambda^*(\mathbf{r} + \mathbf{R}_{n\pm1}) V_0(\mathbf{r} - \mathbf{R}_l) \phi_\lambda(\mathbf{r} + \mathbf{R}_n) + \dots \\ &\equiv \delta_{n,m} \mathcal{E}'_\lambda + \delta_{n\pm1,m} B_\lambda + \dots \ , \end{aligned} \tag{3.56}$$

where $\mathcal{E}'_\lambda$ is the renormalized (shifted) atomic energy level and B_λ is the overlap integral. Energy shift and overlap integral for the states λ usually have to be determined numerically by evaluating the integral expressions

in Eq. (3.56). The resulting numerical values and signs depend on details of the functions ϕ_λ and the lattice periodic potential V_0.

If we neglect the contributions of the next nearest neighbors in Eq. (3.56), we can write the total numerator as

$$\mathcal{N} \simeq \frac{1}{L^3} \sum_{n,m} e^{i\mathbf{k}\cdot(\mathbf{R}_n - \mathbf{R}_m)} (\delta_{n,m} \mathcal{E}'_\lambda + \delta_{n\pm1,m} B_\lambda) \ . \tag{3.57}$$

Inserting Eqs. (3.55) and (3.57) into Eq. (3.51), we obtain

$$E_\lambda(\mathbf{k}) = \mathcal{E}'_\lambda + \frac{B_\lambda}{N} \sum_{n,m} \delta_{m,n\pm1} e^{i\mathbf{k}\cdot(\mathbf{R}_n - \mathbf{R}_m)} \ . \tag{3.58}$$

To analyze this result and to gain some insight into the formation of energy bands, we now restrict the discussion to the case of an ideal cubic lattice with lattice vector $\mathbf{a}$, so that

$$\mathbf{R}_{n\pm1} = \mathbf{R}_n \pm \mathbf{a} \ . \tag{3.59}$$

Using Eq. (3.59) to evaluate the m summation in (3.58), we see that the exponentials combine as

$$e^{i\mathbf{k}\cdot\mathbf{a}} + e^{-i\mathbf{k}\cdot\mathbf{a}} = 2\cos(\mathbf{k}\cdot\mathbf{a})$$

so that the n-summation simply yields a factor N and the final result for the energy is

$$E_\lambda(\mathbf{k}) = \mathcal{E}'_\lambda + 2B_\lambda \cos(\mathbf{k}\cdot\mathbf{a}) \ . \tag{3.60}$$

Eq. (3.60) describes the tight-binding cosine bands. Schematically two such bands are shown in Fig. 3.1, one for $B_\lambda > 0$ (lower band) and one for $B_\lambda < 0$ (upper band).

To evaluate the detailed band structure, we need the values of $\mathcal{E}_\lambda$ and B_λ. Without proof, we just want to mention at this point that for an attractive potential V_0 (as in the case of electrons and ions) and p-type atomic functions ϕ, $B_\lambda > 0$, whereas for s-type atomic functions, $B_\lambda < 0$. Between the allowed energy levels, we have energy gaps, i.e., forbidden energy regions.

In summary, we have the following general results:

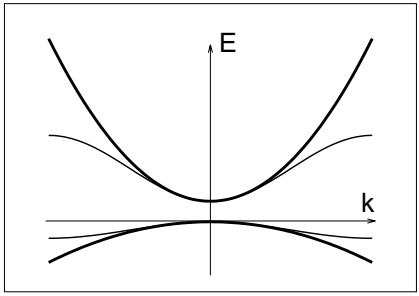

Fig. 3.1 Schematic drawing of the energy dispersion resulting from Eq. (3.60) for the cases of $B_\lambda > 0$ (lower band) and $B_\lambda < 0$ (upper band). The effective mass approximation results, Eq. (3.61), are shown as the thick lines.

(i) The discrete atomic energy levels become quasi-continuous energy regions, called energy bands, with a certain band width.

(ii) There may be energy gaps between different bands.

(iii) Depending on the corresponding atomic functions, the bands $E_\lambda(\mathbf{k})$ may have positive or negative curvature around the band extrema.

(iv) In the vicinity of the band extrema, one can often make a parabolic approximation

$$E_\lambda(\mathbf{k}) \simeq E_{\lambda,0} + \frac{\hbar^2 k^2}{2m_{\lambda,eff}}, \quad m_{\lambda,eff} = \frac{\hbar^2}{\left.\frac{\partial^2 E_\lambda(\mathbf{k})}{\partial k^2}\right|_{k=0}} \ . \tag{3.61}$$

In the regimes where the parabolic approximation is valid, the electrons can be considered quasi-free electrons but with an effective mass m_{eff}, which may be positive or negative, as indicated in Fig. 3.1. A large value of the overlap integral B_λ results in a wide band and corresponding small effective mass $m_{\lambda,eff}$.

(v) Ignoring possible electronic correlation effects and other band structure subtleties, i.e., at the mean field level, one can assume that the states in the bands are filled according to the Pauli principle, beginning with the lowest states. The last completely filled band is called *valence band*.

The next higher band is the *conduction band*.

There are three basic cases realized in nature:

(i) The conduction band is empty and separated by a large band gap from the valence band. This defines an *insulator*. The electrons cannot be accelerated in an electric field since no empty states with slightly different E_k are available. Therefore, we have no electrical conductivity.

(ii) An insulator with a relatively small band gap is called a *semiconductor*. The definition of *small band gap* is somewhat arbitrary, but a good operational definition is to say that the band gap should be on the order of or less than an optical photon energy. In semiconductors, electrons can be moved relatively easily from the valence band into the conduction band, e.g., by absorption of visible or infrared light.

(iii) If the conduction band is partly filled, we have a finite electrical conductivity and hence a *metal*.

3.3 k·p Theory

In this section, we describe two approximate methods, the $\mathbf{k} \cdot \mathbf{p}$ perturbation theory and Kane's $\mathbf{k} \cdot \mathbf{p}$ theory. This $\mathbf{k} \cdot \mathbf{p}$ approximation forms the basis for relatively simple, phenomenological band structure calculations (Sec. 3-4), which yield a quantitative description for states in the vicinity of the band gap.

The basic idea behind $\mathbf{k} \cdot \mathbf{p}$ approximations is to assume that one has solved the band structure problem at some point $\mathbf{k}_0$ with high symmetry. Here, we will take this point as $\mathbf{k}_0 = 0$, which is called the Γ-point of the Brillouin zone. In particular, we assume that we know all energy eigenvalues $E_\lambda(0)$ and the corresponding Bloch functions $u_\lambda(\mathbf{k}_0 = 0, \mathbf{r}) = u_\lambda(0, \mathbf{r})$. In order to compute the Bloch functions $u_\lambda(\mathbf{k}, \mathbf{r})$ and the corresponding energy eigenvalues $E_\lambda(\mathbf{k})$ for $\mathbf{k}$ in the vicinity of the Γ-point, we expand the lattice periodic function $u_\lambda(\mathbf{k}, \mathbf{r})$ in terms of the function $u_{\lambda'}(0, \mathbf{r})$, which form a complete set.

We write Eq. (3.31) in the form of

$$\left[\mathcal{H}_0 + \frac{\hbar}{m_0}\mathbf{k} \cdot \mathbf{p}\right] u_\lambda(\mathbf{k}, \mathbf{r}) = \overline{E}_\lambda(\mathbf{k}) u_\lambda(\mathbf{k}, \mathbf{r}) \ , \tag{3.62}$$

where

$$\mathcal{H}_0 = \frac{p^2}{2m_0} + V_0(\mathbf{r}) \tag{3.63}$$

and

$$\overline{E}_\lambda(\mathbf{k}) = E_\lambda(\mathbf{k}) - \frac{\hbar^2 k^2}{2m_0} \ . \tag{3.64}$$

In second-order nondegenerate perturbation theory, we get

$$\overline{E}_\lambda(\mathbf{k}) = E_\lambda(0) + \sum_{\eta \neq \lambda} \frac{\hbar^2}{m_0^2} \frac{(\mathbf{k} \cdot \langle \lambda | \mathbf{p} | \eta \rangle)(\mathbf{k} \cdot \langle \eta | \mathbf{p} | \lambda \rangle)}{E_\lambda(0) - E_\eta(0)} \tag{3.65}$$

and

$$|\mathbf{k}, \lambda\rangle = |\lambda\rangle + \frac{\hbar}{m_0} \sum_{\eta \neq \lambda} \frac{|\eta\rangle \mathbf{k} \cdot \langle \eta | \mathbf{p} | \lambda \rangle}{E_\lambda(0) - E_\eta(0)} \ . \tag{3.66}$$

There is no first-order energy correction in Eq. (3.65), since by parity

$$\langle \lambda | \mathbf{p} | \lambda \rangle = 0 \ . \tag{3.67}$$

We use here the Dirac notation with the state vectors $|\mathbf{k}, \lambda\rangle$ and $|\mathbf{k} = 0, \lambda\rangle \equiv |\lambda\rangle$. The corresponding Bloch functions are the real space representations of these vectors, i.e., $u_\lambda(\mathbf{k}, \mathbf{r}) = \langle \mathbf{r} | \mathbf{k}, \lambda \rangle$. We consider as the simplest example two states called $|0\rangle$ and $|1\rangle$ with the energies $E_0 = E_g$ and $E_1 = 0$. With $\langle 0 | p_i | 1 \rangle = \mathsf{p}_i$ we find

$$E_{0,1}(k) = E_{0,1} + \frac{\hbar^2 k^2}{2m_0} \pm \sum_{i,j} \frac{\hbar^2 k_i k_j}{2m_0} \frac{2\mathsf{p}_i^* \mathsf{p}_j}{m_0 E_g} \ , \tag{3.68}$$

where the + (−) sign is for $E_0(E_1)$. The energy has a quadratic $\mathbf{k}$-dependence, so that it is meaningful to introduce the effective mass tensor

$$\left(\frac{1}{m_{eff}} \right)_{ij} = \frac{1}{m_0} \left(\delta_{ij} \pm \frac{2\mathsf{p}_i^* \mathsf{p}_j}{m_0 E_g} \right) \ . \tag{3.69}$$

In isotropic cases, such as in cubic symmetry, the effective masses are scalar quantities

$$m_i = \frac{m_0}{1 \pm \frac{2\mathsf{p}^2}{m_0 E_g}} \text{ with } i = c, v \ . \tag{3.70}$$

For a sufficiently large momentum matrix element, the effective mass of the lower (valence) band can become negative, as is the case for the example shown in Fig. 3.1, while the effective mass of the conduction band becomes much smaller than the free electron mass.

Eq. (3.70) shows that the effective masses are determined by the interband matrix element of the momentum operator and by the energy gap. Because the effective masses can be measured experimentally, one frequently uses this relation to express the interband momentum matrix element in terms of the effective electron mass $m_e = m_c$ and the hole mass $m_h = -m_v$. Eq. (3.70) allows one to express p^2 in terms of the reduced electron–hole mass m_r:

$$\frac{1}{m_r} = \frac{1}{m_e} + \frac{1}{m_h} = \frac{4\mathsf{p}^2}{m_0^2 E_g} \ . \tag{3.71}$$

This result is often used to estimate the value of p^2.

Next, we have to consider the case that some of the bands are degenerate. In the element semiconductors of group IV, the four electrons in the outer shell of the atoms populate the sp^3 orbitals. The same is true for the isoelectronic compound semiconductors of the groups III–V and II–VI. In a cubic symmetry, the valence band states at $k = 0$ are made up of three degenerate p-like states. The conduction band at $k = 0$ consists of an s-like state. Thus, at the center of the Brillouin zone we can approximate the cubic symmetry, which is the only case we consider here, by a spherical one and use in the following the eigenfunctions of the angular momentum operator as basis states. These four states are $|l = 0, m_l = 0\rangle = |0, 0\rangle$, $|l = 1, m_l = \pm 1\rangle = |1, \pm 1\rangle$ and $|l = 1, m_l = 0\rangle = |1, 0\rangle$. Following Kane, we diagonalize the Hamiltonian $\mathcal{H} = \mathcal{H}_0 + \hbar\mathbf{k} \cdot \mathbf{p}/m_0$ in the basis of these four states. A linear combination of these states at a finite wave vector $\mathbf{k}$ is

$$|\psi(\mathbf{k})\rangle = \sum_{l'=0,1,|m'_{l'}|\leq l'} c_{l',m'_{l'}}(\mathbf{k})|l', m'_{l'}\rangle \ . \tag{3.72}$$

From the stationary Schrödinger equation (3.62) we get

$$\langle l, m_l|\mathcal{H}_0 + \frac{\hbar}{m_0}(\mathbf{k} \cdot \mathbf{p}) - \overline{E}(k)|\psi(\mathbf{k})\rangle = 0 \ . \tag{3.73}$$

With the selection rules (see problem 3.4)

$$\langle l, m_l|\mathbf{k} \cdot \mathbf{p}|l', m'_{l'}\rangle = k\mathsf{p}\delta_{l,l'\pm 1}\delta_{m_l,m'_{l'}} \tag{3.74}$$

we find the secular equation

$$\begin{pmatrix} E_0 - \overline{E} & 0 & Ak & 0 \\ 0 & E_1 - \overline{E} & 0 & 0 \\ Ak & 0 & E_1 - \overline{E} & 0 \\ 0 & 0 & 0 & E_1 - \overline{E} \end{pmatrix} = 0 \tag{3.75}$$

with $A = \hbar p/m_0$. Rows one through four of (3.75) correspond to the angular momentum quantum numbers (l, m_l) in the order (0,0), (1,1), (1,0), and (1,-1), respectively.

Evaluation of the determinant (3.75) yields the fourth-order equation

$$(E_1 - \overline{E})(E_1 - \overline{E}) \left[(E_0 - \overline{E})(E_1 - \overline{E}) - A^2 k^2 \right] = 0 \ , \tag{3.76}$$

which has the two unchanged solutions

$$E = E_1 + \frac{\hbar^2 k^2}{2m_0} \ , \tag{3.77}$$

and the two modified solutions

$$E = \frac{\hbar^2 k^2}{2m_0} + \frac{E_g}{2} \left(1 \pm \sqrt{1 + \frac{4A^2 k^2}{E_g^2}} \right) \ , \tag{3.78}$$

where $E_0 = E_g$ and $E_1 = 0$ has been used. Expanding the nonparabolic dispersion (3.78) up to second order, we find again the effective masses of Eq. (3.70).

Eq. (3.77) shows that two degenerate valence bands still have a positive curvature with effective masses equal to the free-electron mass. Hence, this result cannot describe the situation found in direct-gap semiconductors where all valence bands have a negative effective mass around the Γ-point. This failure is due to the omission of all states other than the sp^3 states.

Furthermore, in crystals with cubic symmetry only two bands are degenerate at $k = 0$, while the third band is shifted to lower energies. It turns out that the spin–orbit interaction, which has not been considered so far, is responsible for this split-off. To fix these shortcomings, we introduce in the next section a method which takes into account the spin and the spin–orbit interaction and, at least phenomenologically, the influence of other bands.

3.4 Degenerate Valence Bands

For a more realistic treatment of the semiconductor valence bands around the Γ-point, we now take also the spin into account. In the presence of spin–orbit interaction, only the total angular momentum, i.e. the sum of the orbital and spin angular momentum, is a conserved quantity. From the three valence band states $|l = 1, m_l = \pm 1\rangle = 1/\sqrt{2}|X \pm iY\rangle$ and $|l = 1, m_l = 0\rangle = |Z\rangle$ and the spin states $|\uparrow\rangle$ and $|\downarrow\rangle$ one can form the eigenstates of the total angular momentum operator

$$\mathbf{J} = \mathbf{L} + \mathbf{s} \ . \tag{3.79}$$

Since $|l - s| \leq j \leq l + s$, the six eigenstates of $\mathbf{J}$, which result from the states with $l = 1$ and $s = 1/2$, have the quantum numbers $j = 3/2, m_j = \pm 3/2, \pm 1/2$ and $j = 1/2$, $m_j = \pm 1/2$. The state with $j = 3/2$ and $m_j = \pm 3/2$ can be expressed in terms of the product states

$$|3/2, \pm 3/2\rangle = |m_l = \pm 1, \begin{pmatrix}\uparrow\\ \downarrow\end{pmatrix}\rangle \ , \tag{3.80}$$

where the upper (lower) sign and the upper (lower) spin orientation belong together. From these states, one gets by applying the flip-flop operators (see problem 3.5) the states with $m_J = \pm 1/2$:

$$|3/2, \pm 1/2\rangle = \frac{1}{\sqrt{3}}\left(\sqrt{2}|m_l = 0, \begin{pmatrix}\uparrow\\ \downarrow\end{pmatrix}\rangle + |m_l = \pm 1, \begin{pmatrix}\downarrow\\ \uparrow\end{pmatrix}\rangle\right) \ . \tag{3.81}$$

The states with $j = 1/2$ and $m_j = \pm 1/2$ are the antisymmetric combinations of the two states in Eq. (3.81), so that an orthogonal state results

$$|1/2, \pm 1/2\rangle = \frac{1}{\sqrt{3}}\left(-|m_l = 0, \begin{pmatrix}\uparrow\\ \downarrow\end{pmatrix}\rangle + \sqrt{2}|m_l = \pm 1, \begin{pmatrix}\downarrow\\ \uparrow\end{pmatrix}\rangle\right) \ . \tag{3.82}$$

The spin–orbit interaction, which can be obtained from relativistic quantum mechanics, splits the two $j = 1/2$ states off to lower energies. For simplicity, we neglect these two split-off states in the following.

The remaining task is to diagonalize the Hamiltonian by forming a linear combination of the four $j = 3/2$ states. If we simply apply Kane's diagonalization concept to these four states coupled to an s state, we would still get a valence band with positive curvature, because the influence of the other bands has not yet been incorporated. To overcome this difficulty, one often uses a phenomenological Hamiltonian for the four $j = 3/2$ states

which are degenerate at the Γ-point with $E(0) = 0$. The general form of a Hamiltonian which is quadratic in k, invariant under rotations, and which can be constructed with the two vectors $\mathbf{k}$ and $\mathbf{J}$ is

$$\boldsymbol{\mathcal{H}} = \frac{\hbar^2}{2m_0}\left[\left(\gamma_1 + \frac{5}{2}\gamma_2\right)k^2 - 2\gamma_2(\mathbf{k}\cdot\mathbf{J})^2\right] \ . \tag{3.83}$$

Hamiltonian for heavy- and light-hole bands in spherical approximation

Here, the energy is counted as hole energy ($E_h = -E_v$) with the origin at the top of the valence bands. For later comparison, the constants which appear in front of the invariant scalars k^2 and $\mathbf{k}\cdot\mathbf{J}^2$ in (3.83) have been expressed in terms of the phenomenological Luttinger parameters γ_i,

$$\alpha = \gamma_1 + \frac{5\gamma_2}{2} \text{ and } \beta = 2\gamma_2 \ . \tag{3.84}$$

Because of the spherical symmetry, the result has to be independent of the direction of the k-vector.

If we take the wave vector as $\mathbf{k}= k\mathbf{e}_z$, the Hamiltonian (3.83) is already diagonal for the four $J = 3/2$ states and has the two twofold degenerate energy eigenvalues

$$E = \frac{\hbar^2 k^2}{2m_0}\left(\gamma_1 + \frac{5}{2}\gamma_2 - 2\gamma_2 m_j^2\right) \ , \tag{3.85}$$

where m_j is the eigenvalue of J_z. The two resulting energy eigenvalues are

$$E_{hh} = (\gamma_1 - 2\gamma_2)\frac{\hbar^2 k^2}{2m_0} \text{ for } m_j = \pm\frac{3}{2}$$

and

$$E_{lh} = (\gamma_1 + 2\gamma_2)\frac{\hbar^2 k^2}{2m_0} \text{ for } m_j = \pm\frac{1}{2} \ . \tag{3.86}$$

E_{hh} and E_{lh} are the energies of the *heavy-hole* and *light-hole* valence bands, respectively. These two bands are still degenerate at the Γ-point, but the degeneracy is lifted at finite k-values due to the different effective hole masses

$$\frac{1}{m_{hh}} = \frac{1}{m_0}(\gamma_1 - 2\gamma_2) \tag{3.87}$$

and

$$\frac{1}{m_{lh}} = \frac{1}{m_0}(\gamma_1 + 2\gamma_2) \ . \tag{3.88}$$

The two Luttinger parameters, γ_1 and γ_2, can be adjusted so that Eqs. (3.87) and (3.88) yield the heavy and light-hole mass which are measured experimentally.

Luttinger considered a more general Hamiltonian acting on the four $j = 3/2$ states, which is invariant only under the symmetry operations of the cubic symmetry group:

$$\boldsymbol{\mathcal{H} = \frac{\gamma_1}{2m_0}\hbar^2 k^2 - \frac{\hbar^2}{9m_0}\sum_{i,j}\left[\gamma_3 - (\gamma_3 - \gamma_2)\delta_{ij}\right] K_{ij} J_{ij}} \ , \tag{3.89}$$

Luttinger's hole band Hamiltonian for cubic symmetry

where

$$K_{ij} = 3k_i k_j - \delta_{ij} k^2 \tag{3.90}$$

and

$$J_{ij} = \frac{3}{2}(J_i J_j + J_j J_i) - \delta_{ij} J^2. \tag{3.91}$$

The traces of the two tensors $\overline{\mathrm{K}}$ and $\overline{\mathrm{J}}$ vanish. If the two Luttinger parameters γ_3 and γ_2 are equal, the Luttinger Hamiltonian reduces again to the form (3.83) with the only difference that $\mathbf{k}$ cannot be oriented arbitrarily in cubic symmetry. The x and y components of the total angular momentum operators are $J_x = (J_+ + J_-)/2$ and $J_y = (J_+ - J_-)/2i$. J_+ and J_- are the flip-flop operators which raise or lower the quantum number m_j of J_z by one, see also problem 3.5. Note, that the eigenvalue of the operator $\langle J^2 \rangle = j(j+1)$. Therefore, in general, the operators J_i connect the four $j = 3/2$ states, and the Luttinger Hamiltonian has to be diagonalized by a linear combination of the four states. After some algebraic work one gets the energy eigenvalues

$$E(k) = E(0) + \frac{1}{2m_0}\left[Ak^2 \pm \sqrt{B^2 k^4 + C^2(k_x^2 k_y^2 + k_y^2 k_z^2 + k_z^2 k_x^2)}\right]. \tag{3.92}$$

The constants are given in terms of the Luttinger parameters γ_i by

$$A = \gamma_1 \, , \ \ B = 2\gamma_2 \, , \ \ C^2 = 12(\gamma_3^2 - \gamma_2^2) \ . \tag{3.93}$$

The Luttinger parameters for many semiconductor materials can, e.g., be found in Landolt–Börnstein. Typical values for some III–V semiconductors are

	γ_1	γ_2	γ_3
$GaAs$	6.85	2.1	2.9
$InAs$	19.67	8.37	9.29
InP	6.35	2.08	2.76 .

(3.94)

It is almost always true that

$$\gamma_1 > \gamma_2 \simeq \gamma_3 \ . \tag{3.95}$$

So one sees again that the assumption of spherical symmetry is a good approximation.

REFERENCES

Extended introductions to and treatments of band structure theory can be found in the following literature:

N.W. Ashcroft and N.D. Mermin, *Solid State Physics*, Saunders College (HRW), Philadelphia (1976)
J. Callaway, *Quantum Theory of the Solid State*, Part *A*, Academic Press, New York (1974)
M.L. Cohen and J.R. Chelikowsky, *Electronic Structure and Optical Properties of Semiconductors*, Springer Solid State Sciences Vol. 75, Springer, Berlin (1988)
E.O. Kane, *p.* 75 in *Semiconductors and Semimetals*, edited by R.K. Willardson and A.C. Beer, Academic, New York (1966)
C. Kittel, *Introduction to Solid State Physics*, Wiley and Sons, New York (1971)
J.M. Luttinger and M. Kohn, Phys. Rev. **97**, 869 (1955)

J.M. Luttinger, Phys. Rev. **102**, 1030 (1956)

PROBLEMS

Problem 3.1: Energy bands in a solid may be discussed in the framework of a one-dimensional model with the potential

$$V(x) = -V_0 \sum_{n=-\infty}^{\infty} \delta(x + na) \ , \tag{3.96}$$

where $V_0 > 0\,, n$ is an integer, and a is the lattice constant.

a) Determine the most general electron wave function ψ first in the region $0 < x < a$ and then, using Bloch's theorem, also in the region $a < x < 2a$.

b) Derive the relation between $d\psi/dx$ at $x_1 = a+\epsilon$ and $d\psi/dx$ at $x_2 = a-\epsilon$ for $\epsilon \to 0$ by integrating the Schrödinger equation from x_1 to x_2.

c) Use the result of *b*) and $\lim_{\epsilon\to 0}\psi(x_1) = \lim_{\epsilon\to 0}\psi(x_2)$ to show that the energy eigenvalue $E(k)$ of an electron in the potential (3.96) satisfies the equation

$$\cos(ka) = \cos(\kappa a) - \frac{maV_0}{\hbar^2}\frac{\sin(\kappa a)}{\kappa a} \ , \tag{3.97}$$

where $\kappa = \sqrt{2mE/\hbar^2}$.

d) Expand

$$f(\kappa a) = \cos(\kappa a) - \frac{maV_0}{\hbar^2}\frac{\sin(\kappa a)}{\kappa a} \tag{3.98}$$

around $\kappa a = n\pi - \delta, \delta > 0$, up to second order in δ assuming $maV_0/\hbar^2 << 1$ and determine the regimes in which Eq. (3.97) has no solutions (energy gaps).

e) Solve Eq. (3.97) graphically and discuss the qualitative features of the electron dispersion $E(k)$.

Problem 3.2: *a*) Prove the orthogonality relation, Eq. (3.43), for the Wannier functions.

b) Show that the Wannier function $w_\lambda(\mathbf{r}-\mathbf{R})$ is localized around the lattice point $\mathbf{R}$.
Hint: Use the Bloch form Eq. (3.26) around the band edge,

$$\psi_\lambda(\mathbf{k},\mathbf{r}) \simeq \frac{e^{i\mathbf{k}\cdot\mathbf{r}}}{L^{3/2}} u_\lambda(\mathbf{k}=0,\mathbf{r}) \ , \tag{3.99}$$

to expand w_λ.

Problem 3.3: In the so-called *nearly free electron* model, the free-electron wave function is used as

$$\phi(\mathbf{k},\mathbf{r}) = \frac{1}{L^{3/2}} e^{i\mathbf{k}\cdot\mathbf{r}} \tag{3.100}$$

and the unperturbed energies are

$$E(\mathbf{k}) = \frac{\hbar^2 k^2}{2m_0} \ . \tag{3.101}$$

Changing $\mathbf{k}$ to $\mathbf{k}+\mathbf{g}$ where $\mathbf{g}$ is a reciprocal lattice vector, one arrives at an identical situation. Hence

$$E(\mathbf{k}+\mathbf{g}) = \frac{\hbar^2(\mathbf{k}+\mathbf{g})^2}{2m_0} \tag{3.102}$$

is another allowed unperturbed energy dispersion, as is $E(\mathbf{k}+2\mathbf{g})$, etc. The resulting total energy dispersion has many crossing points, indicating energy degeneracy. This degeneracy is lifted due to the presence of the ionic potential $V(\mathbf{r})$, which has the full lattice periodicity. Expanding $V(\mathbf{r})$ as the Fourier series

$$V(\mathbf{r}) = \sum_n V_n e^{i\mathbf{g}_n\cdot\mathbf{r}} \ , \tag{3.103}$$

allows one to write the Hamiltonian

$$\mathcal{H} = \frac{p^2}{2m_0} + V_0 + \sum_{m\neq 0} V_m e^{i\mathbf{g}_m\mathbf{r}} \equiv \mathcal{H}_0 + W \ . \tag{3.104}$$

To investigate the effect of the ionic potential on a degenerate state near the boundary of the Brillouin zone, one may use the wave functions of the unperturbed problem

$$\mathcal{H}_0\phi(\mathbf{k},\mathbf{r}) = \left(\frac{p^2}{2m_0} + V_0\right)\phi(\mathbf{k},\mathbf{r}) = E_0(k)\phi(\mathbf{k},\mathbf{r}) \ , \tag{3.105}$$

with

$$E_0(k) = E(k) + V_0 \ .$$

a) Take two nearly degenerate states k, k' at the zone boundary as basis states and write the total wave function as

$$\Phi(\mathbf{r}) = a_{\mathbf{k}}\phi(\mathbf{k},\mathbf{r}) + a_{\mathbf{k}'}\phi(\mathbf{k}',\mathbf{r}) \ . \tag{3.106}$$

Insert (3.106) into the Schrödinger equation with the Hamiltonian (3.102) and derive coupled equations for $a_{\mathbf{k}}$ and $a_{\mathbf{k}'}$.

b) The coupled equations for $a_{\mathbf{k}}$ and $a_{\mathbf{k}'}$ have a solution only if the coefficient determinant vanishes. Use this condition to derive the new energy dispersion relation showing that the degeneracy at $k = k'$ is lifted through the finite interaction matrix element.

d) Discuss the resulting dispersion curve and the development of energy bands and band gaps.

Problem 3.4: Verify the selection rule (3.74)

$$\langle l, m_l|\mathbf{k}\cdot\mathbf{p}|l', m_{l'}'\rangle = k\mathsf{p}\delta_{l,l'\pm1}\delta_{m_l,m_{l'}'} \ .$$

Hint: The operator $\mathbf{p}$ transforms like $\mathbf{r}$. The scalar product is $\mathbf{k}\cdot\mathbf{p} = \mathrm{kp}\cos\theta$, and $\cos\theta \propto Y_{1,0}(\theta,\phi)$. Derive the selection rule using the addition theorem for the spherical harmonics $Y_{l,m_l}(\theta,\phi)$:

$$Y_{1,0}Y_{l,m_l} = A\,Y_{l+1,m_l} + B\,Y_{l-1,m_l} \ . \tag{3.107}$$

Problem 3.5: Calculate the states (3.81) by applying the flip-flop operators $J_\mp = L_\mp + s_\mp$ to the left- and right hand side of the states (3.80).

The action of $J_\pm = J_x \pm iJ_y$ on $|J, m_J\rangle$ is defined by the relation

$$J_\pm|j, m_j\rangle = \sqrt{j(j+1) - m_j(m_j \pm 1)}|j, m_j \pm 1\rangle \ . \tag{3.108}$$

Equivalent relations hold for the action of $L_\pm$ on $|l, m_l\rangle$ and $s_\pm$ on $|s, m_s\rangle$.

Chapter 4

Mesoscopic Semiconductor Structures

In recent years, advances in crystal growth techniques made it possible to realize semiconductor microstructures, which are so small that their electronic and optical properties deviate substantially from those of bulk materials. In these microstructures, the energetically low-lying electron and hole states are confined in one or more directions to a region of length L_c, which is still considerably larger than the lattice constant but so small that the electron envelope wave functions become quantized. Structures of this size are called *mesoscopic* because the confinement length L_c is intermediate between the microscopic lattice constant and the macroscopic extension of a bulk crystal.

The best known examples of such mesoscopic semiconductor structures are *quantum wells*, where the electrons are confined in one space dimension. The translational motion in the plane perpendicular to the confinement direction is unrestricted. Such a quantum well, e.g. of the III–V compound semiconductor GaAs, can be realized by using molecular beam epitaxy to deposit several GaAs layers in between layers of a material with a wider band gap, such as Ga_xAl_{1-x} As, with $0 < x < 0.4$. For substantially larger Al concentrations, the barrier material becomes an indirect-gap semiconductor.

In most cases, the quantum-well structures are designed in such a way that the lowest electron and hole states are confined in the well material. These *type-I* structures will be discussed in more detail in this and later chapters of this book. To complete this classification, we mention here also the *type-II* quantum wells, where electrons and holes are confined in different parts of the structure, e.g. holes in the wells and electrons in the barriers, as in GaAs/AlAs. Type-II quantum wells will not be covered in this book.

If the free electronic motion is confined in two dimensions, the structure is called a *quantum wire*, and if the confinement exists in all three space dimensions, we speak of a *quantum dot*. The electronic and optical properties of these mesoscopic semiconductor microstructures will be analyzed throughout this book. After a general discussion of some basic quantum confinement effects, we discuss in this chapter the confinement-induced modifications of the electronic band structure in semiconductor quantum wells, which are currently the best studied quantum confined structures and can serve as a paradigm for others.

In later chapters, where we discuss elementary excitations and optical properties of semiconductors, we present the derivations and results as much as possible in parallel for three-, two- and one-dimensional systems in order to gain some insight into the dimensional dependence of the various effects. Because in quantum dots the translational motion is completely suppressed, a separate chapter is devoted to the optical properties of quantum dots.

4.1 Envelope Function Approximation

In this section, we discuss the situation of a perfect and symmetric quantum well, where the optically excited electrons are completely confined inside the well material. In this idealized case, the envelope wave function of these electrons has to vanish at the interface between well and barrier. In the Bloch wave function, Eq. (3.26), the slowly varying plane-wave envelope for the motion perpendicular to the well has to be replaced by a quantized standing wave $\zeta_n(z)$:

$$\psi(\mathbf{r}) = \zeta_n(z)\frac{e^{i(k_x x+k_y y)}}{L}u_\lambda(\mathbf{k}\simeq 0,\mathbf{r}) \ . \tag{4.1}$$

In terms of the localized Wannier functions (3.44), the envelope approximation is

$$\psi(\mathbf{r}) = \sum_{\mathbf{m}} \zeta_n(R_{z,m_z})\frac{e^{i(k_x R_{x,m_x}+k_y R_{y,m_y})}}{L}w_\lambda(\mathbf{r}-\mathbf{R_m}) \ . \tag{4.2}$$

The energies of these quantized envelope states are very similar to those of a particle in a box. These energies are proportional to n/L_c^2, where $n = 1, 2, \ldots$ and L_c is the width of the well. A reduction of the size of the microstructure shifts all energies to higher values, showing clearly that the

electron levels and thus the optical properties can be changed through the design of the structure.

Because of the additional translational motion within the layer, each of the energy levels forms a subband. If the electrons populate only the lowest subband, the translational degree of freedom perpendicular to the well is completely quantized. As far as the translational electron motion is concerned, the quantum well can be approximated as a two-dimensional system under these conditions. However, in these mesoscopic structures the Bloch functions and the band structure are in first approximation still those of a bulk semiconductor. Refinements of this statement with respect to the degenerate valence bands will be given later in this chapter.

It is important to note that the Coulomb interaction in most mesoscopic systems remains essentially three-dimensional. Because the dielectric properties of the materials of the microstructure and of the barrier are normally very similar, the Coulomb field lines between two charged particles also penetrate the barrier material. This situation of a kinetically two-dimensional structure where, however, the interaction potential is basically three-dimensional, is often denoted as *quasi-two-dimensional*.

If one creates an additional lateral confinement in a quantum well, e.g. by etching, one can obtain a quasi-one-dimensional quantum wire. In a rectangular quantum wire, e.g., the plane-wave envelopes for the translational motion in the two directions perpendicular to the wire axis have to be replaced by quantized standing waves, leaving only a plane-wave factor for the motion along the wire axis. Therefore, the quantum wire is a quasi-one-dimensional system, and

$$\psi(\mathbf{r}) = \zeta_n(x)\zeta_m(y)\frac{e^{ik_z z}}{\sqrt{L}}u_\lambda(\mathbf{k} \simeq 0, \mathbf{r}) \ . \tag{4.3}$$

Finally, in a mesoscopic quantum dot the electronic quantum confinement suppresses the translational motion completely, so that

$$\psi(\mathbf{r}) = \zeta_n(x)\zeta_m(y)\zeta_p(z)u_\lambda(\mathbf{k} \simeq 0, \mathbf{r}) \ . \tag{4.4}$$

It is obvious from the wave functions (4.1) – (4.4), that the free translational motion in these microstructures is described by a D-dimensional wave vector $\mathbf{k}$. The sum over this wave vector is thus

$$\sum_{\mathbf{k}} = \sum_{\mathbf{k}} \frac{(\Delta k)^D}{(\Delta k)^D} \ \rightarrow \ \left(\frac{L}{2\pi}\right)^D \int dk^D \ . \tag{4.5}$$

If we evaluate the integral in polar coordinates we get

$$\sum_{\mathbf{k}} = \left(\frac{L}{2\pi}\right)^D \int d\Omega_D \int_0^\infty dk\, k^{D-1} \ , \tag{4.6}$$

where Ω_D is the space angle in D dimensions. If the integrand is isotropic the space angle integral yields Ω_D which equals 4π in $3D$, 2π in $2D$, and 2 in $1D$, respectively. The k integral is usually transformed in an energy integral with $\frac{\hbar^2 k^2}{2m} = E$ and $\frac{\hbar^2}{2m} 2k\, dk = dE$ so that

$$\sum_{\mathbf{k}} = \left(\frac{L}{2\pi}\right)^D \frac{1}{2} \int d\Omega_D \left(\frac{2m}{\hbar^2}\right)^{\frac{D}{2}} \int_0^\infty dE\, E^{\frac{D}{2}-1} \ . \tag{4.7}$$

The integrand in Eq. (4.7) is called the *density of states*, $\rho_D(E) \propto E^{\frac{D}{2}-1}$. Eq. (4.7) shows that $\rho_D(E)$ differs strongly in various dimensions $\rho_3(E) \propto \sqrt{E}$, $\rho_2(E) = \theta(E)$, and $\rho_1(E) = 1/\sqrt{E}$. Because the absorption in the free-carrier model follows the density of states (see Chap. 5), this is a further source for the strong modifications of the optical properties resulting from the reduction of the dimensionality. To summarize, the optical properties can be changed strongly by quantum confinement which introduces an extra localization energy and changes of the density of states. Later in the book we will see that also the effects due to many-body interactions are strongly dependent on the dimensionality.

4.2 Conduction Band Electrons in Quantum Wells

In this section, we extend the discussion of elementary properties of electrons in a semiconductor quantum well, whose thickness in the z direction we denote as L_c. In a type I quantum well, the energy difference ΔE_g between the larger band gap of the barrier and the smaller band gap of the well material causes a confinement potential both for the electrons in the conduction band and for the holes in the valence band. In a GaAs-GaAlAs quantum well, e.g., the resulting well depths are $\Delta V^e \simeq 2\Delta E_g/3$ and $\Delta V^h \simeq \Delta E_g/3$, respectively. The potential jump occurs within one atomic layer so that one can model the quantum well as a one-dimensional potential well with infinitely steep walls. Simple analytic results are obtained if one assumes that the well is infinitely deep, so that the confinement

potential can be written as

$$V_{con}(z) = \begin{cases} 0 \quad \text{for } -L_c/2 < z < L_c/2 \\ \infty \text{ for } |z| > L_c/2 \end{cases} \quad . \tag{4.8}$$

For the $x-y$ plane there is no quantum confinement and the carriers can move freely. For the electrons in the nondegenerate conduction band, one can easily calculate the envelope function using the effective mass approximation for the low lying states. We shift the treatment of holes to the next section, because the symmetry reduction in a quantum well causes a mixing of the degenerate valence bands.

The Schrödinger equation for the electron in the idealized quantum well is

$$[\mathcal{H}_e(\mathbf{r}) + V_{con}(z)]\psi(\mathbf{r}) = E\,\psi(\mathbf{r}) \ . \tag{4.9}$$

Following the arguments of the preceding section, we write

$$\psi(\mathbf{r}) = \frac{1}{L}\zeta(z)e^{ik_x x + k_y y}u_c(\mathbf{k} \simeq 0, \mathbf{r}) \ , \tag{4.10}$$

where $\zeta(z)$ is the mesoscopically slowly varying envelope function. We assume that the electron Hamiltonian without the confinement potential leads to the energies $E_e(k) = E_g + \hbar^2(k_\perp^2 + k_z^2)/2m_e$, where m_e is the effective mass of the electrons in the conduction band. Replacing $\hbar k_z \to -i\hbar\partial/\partial z$ we find the following equation for the standing-wave envelope $\zeta(z)$:

$$\left[-\frac{\hbar^2}{2m_e}\frac{\partial^2}{\partial z^2} + V_{con}(z)\right]\zeta(z) = E_z\zeta(z) \ . \tag{4.11}$$

This one-dimensional Schrödinger equation is that of a particle in a box with the eigenfunctions

$$\zeta(z) = A\,\sin(k_z z) + B\,\cos(k_z z) \ , \tag{4.12}$$

where A and B are constants, which still have to be determined, and

$$k_z^2 = 2m_e\frac{E_z}{\hbar^2} \ . \tag{4.13}$$

The boundary conditions for the wave functions are

$$\zeta(L_c/2) = \zeta(-L_c/2) = 0 \ . \tag{4.14}$$

Because of the inversion symmetry of the confinement potential around $z = 0$, the wave functions (4.12) can be classified into even and odd states. For the even states, $A = 0$, and the odd states, $B = 0$, one gets the normalized envelope functions

$$\begin{aligned} \zeta_{even}(z) &= \sqrt{\frac{2}{L_c}} \cos(k_z z) \\ \zeta_{odd}(z) &= \sqrt{\frac{2}{L_c}} \sin(k_z z) \ . \end{aligned} \tag{4.15}$$

The boundary condition (4.14) yields

$$\begin{aligned} k_{z,even} &= \frac{\pi}{L_c}(2n-1) \\ k_{z,odd} &= \frac{\pi}{L_c} 2n \qquad \text{for } n = 1, 2, 3, \ldots, \end{aligned} \tag{4.16}$$

so that

$$\begin{aligned} E_{z,even} &= \frac{\pi^2 \hbar^2}{2 m_e L_c^2}(2n-1)^2 \\ E_{z,odd} &= \frac{\pi^2 \hbar^2}{2 m_e L_c^2}(2n)^2 \qquad \text{for } n = 1, 2, 3 \ldots, \end{aligned}$$

or

$$E_z = \frac{\pi^2 \hbar^2}{2 m_e L_c^2} \bar{n}^2 \ , \tag{4.17}$$

with $\bar{n} = 2n - 1$ (for even states) and $\bar{n} = 2n$(for odd states). Equations (4.15) – (4.17) show that the quantum confinement inhibits the free electron motion in z-direction. Only discrete k_z values are allowed, leading to a series of *quantized* states. We see that the lowest energy state (ground state) is even, $\bar{n} = 1$ in Eq. (4.17), followed by states with alternating odd and even symmetry. The energy of the ground state is nothing but the zero-point energy $(\Delta p_z)^2/2m_e$ which arises because of Heisenberg's uncertainty relation between the localization length $\Delta z = L_c$ and the corresponding momentum uncertainty Δp_z.

Adding the energies of the motion in plane and in z-direction we find the total energy of the electron subject to one-dimensional quantum con-

finement as

$$E = \frac{\hbar^2}{2m_e}\left(\frac{n^2\pi^2}{L_c^2} + k_\perp^2\right), \quad n = 1, 2, 3, \ldots \tag{4.18}$$

indicating a succession of energy *subbands*, i.e., energy parabola $\hbar^2 k_\perp^2/2m_e$ separated by $\hbar^2\pi^2/2m_e L_c^2$. The different subbands are labeled by the quantum numbers n.

In order to have a more realistic description, one has to use a finite confinement potential

$$V_{con}(z) = \begin{cases} 0 & \text{for } -L_c/2 < z < L_c/2 \\ V_c & \text{for } |z| > L_c/2 \end{cases} . \tag{4.19}$$

The analysis closely follows that of the infinite potential case, however, the energies can no longer be determined analytically. The Schrödinger equation for the $x-y$ motion is unchanged but the equation for the z-motion now has to be solved separately in the three regions: i) $|z| < L_c/2$, ii) $z > L_c/2$, and iii) $z < -L_c/2$. In region i), the solution is given by (4.13) and in regions ii) and iii) by

$$\zeta(z) = C_\pm e^{\pm K_z z} \tag{4.20}$$

with

$$K_z^2 = \frac{2m_e}{\hbar^2}(V_c - E_z) \ . \tag{4.21}$$

The normalization of the wave functions requires that we have to choose the exponentially decaying solutions in (4.20). Furthermore, we have to match the wave functions and their derivatives at the interfaces $\pm z_c/2$. This yields for the even states

$$\zeta_{even}(z) = \begin{cases} B\,\cos k_z z & \text{for } -L_c/2 < z < L_c/2 \\ C\,e^{-K_z z} & \text{for } z > L_c/2 \\ C\,e^{K_z z} & \text{for } z < -L_c/2 \end{cases} \tag{4.22}$$

with the condition (see problem 4.2)

$$\sqrt{E_z}\tan\left(\sqrt{m_e\frac{E_z}{2\hbar^2}}L_c\right) = \sqrt{V_c - E_z} \ . \tag{4.23}$$

The solution of this equation gives the energy eigenvalues E_z for the even states.

The same procedure for the odd states yields

$$\zeta_{odd}(z) = \begin{cases} A \sin k_z z & \text{for } -L_c/2 < z < L_c/2 \\ C\, e^{-K_z z} & \text{for } z > L_c/2 \\ -C\, e^{K_z z} & \text{for } z < -L_c/2 \end{cases} \tag{4.24}$$

with

$$-\sqrt{E_z}\cot\left(\sqrt{m_e \frac{E_z}{2\hbar^2}}\right) L_c = \sqrt{V_c - E_z}\ . \tag{4.25}$$

The roots of the transcendental equations (4.23) and (4.25) have to be determined numerically. The number of bound states in the well depends on the depth of the potential well V_c. As long as V_c is positive, there is always at least one bound even state, the ground state. If more than one bound quantum confined state exists, the symmetry between the successive higher states alternates, until one reaches the highest bound state. The energetically still higher states are unbound and not confined to the quantum wells.

4.3 Degenerate Hole Bands in Quantum Wells

We have seen in the previous section, that multiple subbands occur due to the quantization of the electron motion in z-direction. For degenerate bands, one has to expect modifications of the band structure for the in-plane motion of the carriers, since the quantum confinement generally leads to a reduction of the original spherical or cubic symmetry, and thus to a removal of band degeneracies and to band mixing. We assume here — as implicitly done before — perfectly *lattice matched conditions* between the barrier and the well material. Generally, however, perfect lattice matching is not a necessary requirement for the epitaxial growth of heterostructures. A small mismatch of the lattice constants can often be accommodated by elastically straining one or both of the components leading to *strained layer structures*.

As for the electrons, we assume that an effective bulk Hamiltonian for the holes can be used for the determination of the envelope functions if one replaces $\hbar k_z \rightarrow p_z = -i\hbar\partial/\partial z$. The matrix of the hole-band Hamiltonian (3.83) for the four degenerate eigenstates $J = 3/2$ states with

$m_J = 3/2, 1/2, -1/2, -3/2$ is given by (see problem 4.3)

$$\langle m'_J|\mathcal{H}|m_J\rangle = \mathcal{H}_{m'm} = \begin{pmatrix} \mathcal{H}_{lh} & b & c & 0 \\ b^* & \mathcal{H}_{hh} & 0 & c \\ c^* & 0 & \mathcal{H}_{hh} & -b \\ 0 & c^* & -b^* & \mathcal{H}_{lh} \end{pmatrix} = 0 \ , \tag{4.26}$$

with

$$\mathcal{H}_{hh} = \frac{1}{2m_0}\langle p_z^2\rangle(\gamma_1 - 2\gamma_2) + \frac{\hbar^2(k_x^2 + k_y^2)}{2m_0}(\gamma_1 + \gamma_2) \ , \tag{4.27}$$

$$\mathcal{H}_{lh} = \frac{1}{2m_0}\langle p_z^2\rangle(\gamma_1 + 2\gamma_2) + \frac{\hbar^2(k_x^2 + k_y^2)}{2m_0}(\gamma_1 - \gamma_2) \ , \tag{4.28}$$

$$b = -\sqrt{3}\frac{\hbar}{m_0}\gamma_2\langle p_z\rangle(k_x - ik_y) \ , \tag{4.29}$$

$$c = -\frac{\hbar^2}{m_0}\frac{\sqrt{3}}{2}\gamma_2(k_x - ik_y)^2 \ . \tag{4.30}$$

Here, we introduced

$$\langle p_z\rangle = \int_{-L_c/2}^{+L_c/2} dz\zeta(z)^* \left(-i\hbar\frac{\partial}{\partial z}\right)\zeta(z) \tag{4.31}$$

and

$$\langle p_z^2\rangle = \int_{-L_c/2}^{+L_c/2} dz\zeta(z)^* \left(-i\hbar\frac{\partial}{\partial z}\right)^2\zeta(z) \tag{4.32}$$

as expectation values with the envelope functions ζ. For a symmetric well, $\langle p_z\rangle$ vanishes between states of equal symmetry. Thus, if we neglect intersubband mixing, $b = 0$.

Note, that the light-hole Hamiltonian $\mathcal{H}_{lh}$ has, due to the finite localization energy $\langle p_z^2\rangle/2m_0$, a higher energy than the heavy-hole Hamiltonian. Consequently, the degeneracy at $\mathbf{k}_\perp = 0$ of the bulk semiconductor material is lifted. However, according to these simple arguments, the unperturbed bands in the quantum well would cross at a finite $\mathbf{k}_\perp$ value. Interchanging the first and last row and successively the first and last column in (4.26)

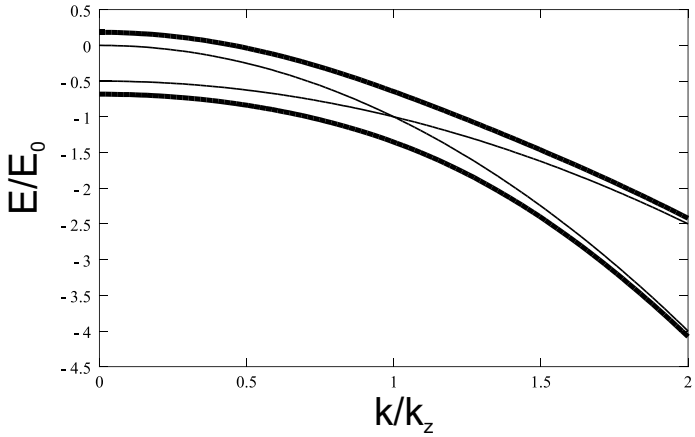

Fig. 4.1 The full lines show the mixing of the heavy and light-hole valence bands in a GaAs quantum well according to Eq. (4.36). The thin lines show the bands without band mixing.

yields the following eigenvalue problem

$$\det \begin{pmatrix} \mathcal{H}_{lh} - E & c^* & 0 & 0 \\ c & \mathcal{H}_{hh} - E & 0 & 0 \\ 0 & 0 & \mathcal{H}_{hh} - E & c^* \\ 0 & 0 & c & \mathcal{H}_{lh} - E \end{pmatrix} = 0 \ . \tag{4.33}$$

Since the matrix is block diagonal, one is left with the diagonalization of a two-by-two matrix

$$\det \begin{pmatrix} \mathcal{H}_{lh} - E & c^* \\ c & \mathcal{H}_{hh} - E \end{pmatrix} = 0 \ . \tag{4.34}$$

The corresponding eigenvalues are given by

$$(\mathcal{H}_{lh} - E)(\mathcal{H}_{hh} - E) - |c|^2 = 0 \ . \tag{4.35}$$

The solutions are

$$E_{1,2} = \frac{1}{2} \left[(\mathcal{H}_{hh} + \mathcal{H}_{lh}) \pm \sqrt{(\mathcal{H}_{hh} - \mathcal{H}_{lh})^2 + 4|c|^2} \right] \ . \tag{4.36}$$

The resulting dispersion is shown in Fig. 4.1 for $c = 0$ and $c \neq 0$. We see the typical level repulsion and the state mixing in the momentum region where the dispersion cross for $c = 0$.

REFERENCES

Many of the references to Chap. 3 are also relevant for this chapter. For the discussion of electronic states and band structures in quantum-wells and heterostructures in particular see

M. Altarelli, *p.*12 in *Heterojunctions and Semiconductor Superlattices*, Eds. G. Allan, G. Bastard, N. Boccara, M. Lannoo and M. Voos, Springer Verlag, Berlin (1985)
G. Bastard, *Wave Mechanics Applied to Semiconductor Heterostructures*, Les Editions de Physique, Paris (1988)
C. Weisbuch, in *Semiconductors and Semimetals*, Vol. 24, *p.* 1, *ed.* R. Dingle, Academic, New York (1987)

PROBLEMS

Problem 4.1: Use the effective mass approximation to calculate the electron energies.
a) for a square quantum wire with finite barrier height in two dimensions,

b) for a square quantum dot (quantum box), in which the electrons are confined in all three dimensions.

Show that increasing quantum confinement causes an increasing zero-point energy due to the Heisenberg uncertainty principle.

Problem 4.2: Solve the Schrödinger equation for the motion of an electron in a finite potential well. Derive the transcendental equations (4.23) and (4.25) for the energy eigenvalues using the conditions of continuity of the wave function and its derivative at the boundary of the confinement potential.

Problem 4.3: Calculate the matrix $\langle m'_J|\mathcal{H}|m_J\rangle$ for the $J = 3/2$ states

using the Hamiltonian (3.83).

a) Show that $J^2 - J_z^2 = \frac{1}{2}(J_+J_- + J_-J_+)$.
b) Express the Hamiltonian (3.83) in terms of the operators $J_\pm = J_x \pm iJ_y$, J_z, and J^2. Derive the form

$$\frac{2m_0}{\hbar^2}\mathcal{H} = \left[\gamma_1 + \frac{5}{2}\gamma_2 - \gamma_2(J^2 - J_z^2)\right](k_x^2 + k_y^2) + \left(\gamma_1 + \frac{5}{2}\gamma_2 - 2\gamma_2 J_z^2\right)k_z^2$$
$$-2\gamma_2 k_z\left[\{J_+, J_z\}(k_x - ik_y) + \text{h.c}\right] - \frac{\gamma_2}{2}\left[J_+^2(k_x - ik_y)^2 + \text{h.c.}\right] \quad , \tag{4.37}$$

where $\{J_z, J_+\} = \frac{1}{2}(J_xJ_+ + J_+J_z)$ and h.c. means the hermitian conjugate of the preceding term, and $\hbar k_z = \langle p_z \rangle$.

c) Calculate the matrix elements (4.26) – (4.31) using Eq. (3.108) for the action of $J_\pm$ on the states $|J, m_J\rangle$. Note, that $\langle J^2 \rangle = J(J+1)$.

Chapter 5

Free Carrier Transitions

In a typical semiconductor, the gap between the valence band and the conduction band corresponds to the energy $\hbar\omega$ of infrared or visible light. A photon with an energy $\hbar\omega > E_g$ can excite an electron from the valence band into the conduction band, leaving behind a hole in the valence band. The excited conduction-band electron and the valence-band hole carry opposite charges and interact via the mutually attractive Coulomb potential. This electron–hole Coulomb interaction will naturally influence the optical spectrum of a semiconductor. However, in order to obtain some qualitative insight, in a first approximation we disregard all the Coulomb effects and treat the electrons and holes as quasi-free particles.

5.1 Optical Dipole Transitions

Generally, electrons in the bands of a semiconductor are not in pure states but in so-called mixed states. Therefore, we have to extend the quantum mechanical method used to calculate the optical polarization in comparison to the treatment presented in Chap. 2. While pure states are described by wave functions, mixed states are described by a density matrix. In this chapter, we again use the technique of Dirac state vectors $|\lambda\mathbf{k}\rangle$ with the orthogonality relation

$$\langle\lambda'\mathbf{k}'|\lambda\mathbf{k}\rangle = \delta_{\lambda',\lambda}\delta_{\mathbf{k}',\mathbf{k}} \tag{5.1}$$

and the completeness relation

$$\sum_{\lambda\mathbf{k}} |\lambda\mathbf{k}\rangle\langle\lambda\mathbf{k}| = 1 \ . \tag{5.2}$$

The state vectors $|\lambda\mathbf{k}\rangle$ are eigenstates of the crystal Hamiltonian (3.5), which we now denote by $\mathcal{H}_0$:

$$\mathcal{H}_0|\lambda\mathbf{k}\rangle = E_\lambda(\mathbf{k})|\lambda\mathbf{k}\rangle = \hbar\epsilon_{\lambda,\mathbf{k}}|\lambda\mathbf{k}\rangle \ . \tag{5.3}$$

As usual, Eq. (5.3) is transformed into the Schrödinger equation in real-space representation by multiplying (5.3) from the left with the vector $\langle\mathbf{r}|$. The Schrödinger wave function $\psi_\lambda(\mathbf{k},\mathbf{r})$ for the state $|\lambda\mathbf{k}\rangle$ is just the scalar product

$$\psi_\lambda(\mathbf{k},\mathbf{r}) = \langle\mathbf{r}|\lambda\mathbf{k}\rangle \ , \tag{5.4}$$

i.e., the Bloch wave function (3.26) for the band λ.

The Hamiltonian of electrons in a crystal can be obtained in this representation by multiplying $\mathcal{H}_o$ from the left and right with the completeness relation (5.2)

$$\mathcal{H}_0 = \sum_{\lambda'\mathbf{k}'} |\lambda'\mathbf{k}'\rangle\langle\lambda'\mathbf{k}'|\mathcal{H}_0 \sum_{\lambda\mathbf{k}} |\lambda\mathbf{k}\rangle\langle\lambda\mathbf{k}| \ . \tag{5.5}$$

Using Eqs. (5.3) and (5.1), we find the diagonal representation

$$\mathcal{H}_0 = \hbar \sum_{\lambda\mathbf{k}} \epsilon_{\lambda,\mathbf{k}}|\lambda\mathbf{k}\rangle\langle\lambda\mathbf{k}| \ . \tag{5.6}$$

The action of the Hamiltonian (5.6) on an arbitrary state vector can easily be understood. The "bra-vector" $\langle\lambda\mathbf{k}|$ projects out that part which contains the state with the quantum numbers $\lambda,\mathbf{k}$ represented by the "ket-vector" $|\lambda\mathbf{k}\rangle$.

As discussed in Chap. 2, the dipole interaction with the light is described by

$$\mathcal{H}_I = -er\,\mathcal{E}(t) = -d\,\mathcal{E}(t) \ , \tag{5.7}$$

where $er = d$ is the projection of the dipole moment in the direction of the electromagnetic field. Using the completeness relation twice yields

$$\mathcal{H}_I = -e\,\mathcal{E}(t) \sum_{\mathbf{k},\mathbf{k}',\lambda,\lambda'} r_{\lambda\lambda'}(\mathbf{k}',\mathbf{k})|\lambda'\mathbf{k}'\rangle\langle\lambda\mathbf{k}| \ , \tag{5.8}$$

with

$$r_{\lambda'\lambda}(\mathbf{k}',\mathbf{k}) = \langle\lambda'\mathbf{k}'|r|\lambda\mathbf{k}\rangle \ . \tag{5.9}$$

To compute the dipole matrix element, we assume only *interband transitions*, $\lambda \neq \lambda'$, and use the same trick as in Eqs. (2.26) and (2.31) to get

$$\begin{aligned}\mathbf{r}_{\lambda'\lambda}(\mathbf{k}',\mathbf{k}) &= \frac{1}{E_\lambda(\mathbf{k}) - E_{\lambda'}(\mathbf{k}')}\langle\lambda'\mathbf{k}'|[\mathbf{r},\mathcal{H}_0]|\lambda\mathbf{k}\rangle \\ &= \frac{i}{m_0(\epsilon_{\lambda,\mathbf{k}} - \epsilon_{\lambda',\mathbf{k}'})}\langle\lambda'\mathbf{k}'|\mathbf{p}|\lambda\mathbf{k}\rangle \ . \end{aligned} \tag{5.10}$$

Inserting

$$1 = \int_{L^3} d^3r|\mathbf{r}\rangle\langle\mathbf{r}|$$

and using the fact that the momentum operator is diagonal in the $\mathbf{r}$-representation, we get

$$\langle\lambda'\mathbf{k}'|\mathbf{p}|\lambda\mathbf{k}\rangle = \int_{L^3} d^3r\, \psi^*_{\lambda'}(\mathbf{k}',\mathbf{r})\mathbf{p}\psi_\lambda(\mathbf{k},\mathbf{r}) \ . \tag{5.11}$$

As in Sec. 3.3, we expand the Bloch functions $u_\lambda(\mathbf{k},\mathbf{r})$ into the complete set $u_\eta(0,\mathbf{r})$. Using only the leading term of the $\mathbf{k}\cdot\mathbf{p}$-result, Eq. (3.66), we get

$$\psi_\lambda(\mathbf{k},\mathbf{r}) \simeq e^{i\mathbf{k}\cdot\mathbf{r}}\frac{u_\lambda(0,\mathbf{r})}{L^{3/2}} \ . \tag{5.12}$$

Inserting (5.12) into (5.11) yields

$$\langle\lambda'\mathbf{k}'|\mathbf{p}|\lambda\mathbf{k}\rangle \simeq \frac{1}{L^3}\int_{L^3} d^3r\, e^{-i(\mathbf{k}'-\mathbf{k})\cdot\mathbf{r}}u^*_{\lambda'}(0,\mathbf{r})(\hbar\mathbf{k}+\mathbf{p})u_\lambda(0,\mathbf{r}) \ , \tag{5.13}$$

where the additive $\hbar\mathbf{k}$ results from commuting $\mathbf{p}$ and $\exp(\mathrm{i}\mathbf{k}\cdot\mathbf{r})$. Now we split the integral over the entire crystal into the unit-cell integral and the sum over all unit cells, Eq. (3.38), replace $\mathbf{r} \to \mathbf{r} + \mathbf{R}_n$, and use Eq. (3.27), to get

$$\langle\lambda'\mathbf{k}'|\mathbf{p}|\lambda\mathbf{k}\rangle \simeq \sum_{n=1}^{N}\frac{e^{-i(\mathbf{k}'-\mathbf{k})\cdot\mathbf{R}_n}}{N}\int_{l^3} d^3r\frac{e^{-i(\mathbf{k}'-\mathbf{k})\cdot\mathbf{r}}}{l^3}u^*_{\lambda'}(0,\mathbf{r})(\hbar\mathbf{k}+\mathbf{p})u_\lambda(0,\mathbf{r}) \ . \tag{5.14}$$

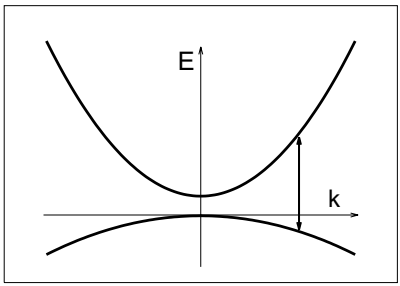

Fig. 5.1 Schematic drawing of conduction and valence bands and an optical dipole transition connecting identical **k**-points in both bands.

Since the unit-cell integral yields the same result for all unit cells, we can take it out of the summation over the unit cells, which then yields $\delta_{\mathbf{k},\mathbf{k}'}$, and Eq. (5.14) becomes

$$\langle \lambda' \mathbf{k}' | \mathbf{p} | \lambda \mathbf{k} \rangle = \frac{\delta_{\mathbf{k},\mathbf{k}'}}{l^3} \int_{l^3} d^3 r \, u^*_{\lambda'}(0, \mathbf{r}) \mathbf{p} \, u_\lambda(0, \mathbf{r}) \equiv \delta_{\mathbf{k},\mathbf{k}'} \mathbf{p}_{\lambda'\lambda}(0) \ , \qquad (5.15)$$

where the term $\propto \hbar\mathbf{k}$ disappeared because of the orthogonality of the lattice periodic functions and our $\lambda \neq \lambda'$ requirement.

The δ-function in Eq. (5.15) shows that the optical dipole matrix element couples identical **k**-states in different bands, so that optical transitions are "perpendicular" if plotted in an energy–wave–number diagram, as in Fig. 5.1. The *dipole approximation* is equivalent to ignoring the photon momentum in comparison to a typical electron momentum in the Brillouin zone.

Collecting all contributions to the dipole matrix element, we get

$$e\mathbf{r}_{\lambda'\lambda}(\mathbf{k}', \mathbf{k}) = \frac{ie}{m_0(\epsilon_{\lambda',\mathbf{k}} - \epsilon_{\lambda,\mathbf{k}})} \delta_{\mathbf{k},\mathbf{k}'} \mathbf{p}_{\lambda'\lambda}(0) \qquad (5.16)$$

or

$$\boldsymbol{e r_{\lambda'\lambda}(k', k) = d_{\lambda'\lambda}(k', k) = \delta_{k,k'} d_{\lambda'\lambda}(0) \frac{\epsilon_{\lambda',0} - \epsilon_{\lambda,0}}{\epsilon_{\lambda',k} - \epsilon_{\lambda,k}}} \ , \qquad (5.17)$$

optical dipole matrix element

where we used Eq. (5.16) for $k = k' = 0$ to lump all parameters into

$$\mathbf{d}_{\lambda'\lambda}(0) = \frac{ie\mathbf{p}_{\lambda'\lambda}(0)}{m_0(\epsilon_{\lambda',0} - \epsilon_{\lambda,0})} \ . \qquad (5.18)$$

For the cases of two parabolic bands with effective masses m_λ and $m_{\lambda'}$ and dispersions

$$\hbar\epsilon_{\lambda',\mathbf{k}} = E_g + \frac{\hbar^2 k^2}{2m_{\lambda'}} \quad \text{and} \quad \hbar\epsilon_{\lambda,\mathbf{k}} = \frac{\hbar^2 k^2}{2m_\lambda} \ , \qquad (5.19)$$

the optical dipole matrix element is

$$\mathbf{d}_{\lambda'\lambda}(\mathbf{k}', \mathbf{k}) = \delta_{\mathbf{k},\mathbf{k}'} \mathbf{d}_{\lambda'\lambda}(0) \frac{E_g}{E_g + \frac{\hbar^2 k^2}{2}\left(\frac{1}{m_\lambda} + \frac{1}{m_{\lambda'}}\right)} \ . \qquad (5.20)$$

Except for the δ-function the $\mathbf{k}$-dependence of the dipole matrix element can often be neglected in the spectral region around the semiconductor band edge. The $\mathbf{k}$-dependence is usually important only if the variation over the whole first Brillouin zone is needed, as in Kramers–Kronig transformations or computations of refractive index contributions.

5.2 Kinetics of Optical Interband Transitions

In order to keep the following treatment as simple as possible, we now make a *two-band approximation* by restricting our treatment to one valence band v and one conduction band c out of the many bands of a real semiconductor, i.e., $\lambda = c, v$. This two-band model is a reasonable first approximation to calculate the optical response of a real material if all the other possible transitions are sufficiently detuned with regard to the frequency region of interest. We will treat first quasi-D-dimensional semiconductors, followed by an extension to quantum confined semiconductors with several subbands.

5.2.1 *Quasi-D-Dimensional Semiconductors*

To simplify our analysis even further, we ignore the k-dependence of the dipole matrix element and write the interaction Hamiltonian in the form

$$\mathcal{H}_I = -\mathcal{E}(t) \sum_{\mathbf{k},\{\lambda\neq\lambda'\}=\{c,v\}} d_{\lambda'\lambda} |\lambda'\mathbf{k}\rangle\langle\lambda\mathbf{k}| \equiv \sum_{\mathbf{k}} \mathcal{H}_{I,\mathbf{k}} \ , \tag{5.21}$$

showing that different k-states are not mixed as long as we ignore the Coulomb interaction between the carriers.

Evaluating the summation over the band indices yields

$$\mathcal{H}_{I,\mathbf{k}} = -\mathcal{E}(t)(\, d_{cv}\, |c\mathbf{k}\rangle\langle v\mathbf{k}| + d^*_{cv} |v\mathbf{k}\rangle\langle c\mathbf{k}|) \ , \tag{5.22}$$

where $d^*_{cv} = d_{vc}$ has been used. For our subsequent calculations it is advantageous to transform the Hamiltonian into the interaction representation

$$\begin{aligned} \mathcal{H}^{int}_{I,\mathbf{k}}(t) &= \exp\left(\frac{i}{\hbar}\mathcal{H}_0 t\right) \mathcal{H}_{I,\mathbf{k}} \exp\left(-\frac{i}{\hbar}\mathcal{H}_0 t\right) \\ &= -\mathcal{E}(t)\left[e^{i(\epsilon_{c,\mathbf{k}}-\epsilon_{v,\mathbf{k}})t} d_{cv} |c\mathbf{k}\rangle\langle v\mathbf{k}| + h.c.\right] \ , \end{aligned} \tag{5.23}$$

where $h.c.$ denotes the Hermitian conjugate of the preceding term.

The single-particle density matrix $\rho_{\mathbf{k}}(t)$ of the state $\mathbf{k}$ can be expanded into the eigenstates $|\lambda\mathbf{k}\rangle$

$$\boldsymbol{\rho_{\mathbf{k}}} = \sum_{\boldsymbol{\lambda',\lambda}} \boldsymbol{\rho_{\lambda',\lambda}(\mathbf{k},t)} |\boldsymbol{\lambda'\mathbf{k}}\rangle\langle\boldsymbol{\lambda\mathbf{k}}| \ . \tag{5.24}$$

single-particle density matrix for the state k

The equation of motion for the density matrix is the Liouville equation

$$\frac{d}{dt}\rho_{\mathbf{k}}(t) = -\frac{i}{\hbar}[\mathcal{H}_{\mathbf{k}} \ , \ \rho_{\mathbf{k}}(t)] \tag{5.25}$$

which is written in the interaction representation as

$$\frac{d}{dt}\rho^{int}_{\mathbf{k}}(t) = -\frac{i}{\hbar}[\mathcal{H}^{int}_{I,\mathbf{k}} \ , \ \rho^{int}_{\mathbf{k}}(t)] \tag{5.26}$$

with

$$\rho_{\mathbf{k}}^{int}(t) = \exp\left(\frac{i}{\hbar}\mathcal{H}_0 t\right)\rho_{\mathbf{k}}(t)\exp\left(-\frac{i}{\hbar}\mathcal{H}_0 t\right) \ . \tag{5.27}$$

Inserting Eqs. (5.23) and (5.27) into (5.26), we get

$$\begin{aligned}\frac{d}{dt}\rho_{\mathbf{k}}^{int}(t) =& \frac{i}{\hbar}\mathcal{E}(t)\sum_{\lambda',\lambda}\rho_{\lambda'\lambda}^{int}(\mathbf{k},t) \\ &\times\Big[e^{i(\epsilon_{c,\mathbf{k}}-\epsilon_{v,\mathbf{k}})t}d_{cv}\left(|c\mathbf{k}\rangle\langle v\mathbf{k}|\lambda'\mathbf{k}\rangle\langle\lambda\mathbf{k}| - |\lambda'\mathbf{k}\rangle\langle\lambda\mathbf{k}|c\mathbf{k}\rangle\langle v\mathbf{k}|\right) \\ &+e^{-i(\epsilon_{c,\mathbf{k}}-\epsilon_{v,\mathbf{k}})t}d_{cv}^{*}\left(|v\mathbf{k}\rangle\langle c\mathbf{k}|\lambda'\mathbf{k}\rangle\langle\lambda\mathbf{k}| - |\lambda'\mathbf{k}\rangle\langle\lambda\mathbf{k}|v\mathbf{k}\rangle\langle c\mathbf{k}|\right)\Big] \ .\end{aligned} \tag{5.28}$$

Taking the matrix element

$$\rho_{cv}^{int}(\mathbf{k},t) = \langle c\mathbf{k}|\rho_{\mathbf{k}}^{int}(t)|v\mathbf{k}\rangle \tag{5.29}$$

of Eq. (5.28) yields

$$\frac{d}{dt}\rho_{cv}^{int}(\mathbf{k},t) = \frac{i}{\hbar}d_{cv}\mathcal{E}(t)e^{i(\epsilon_{c,\mathbf{k}}-\epsilon_{v,\mathbf{k}})t}[\rho_{vv}(\mathbf{k},t) - \rho_{cc}(\mathbf{k},t)] \ , \tag{5.30}$$

where we used

$$\rho_{\lambda\lambda}^{int} = \rho_{\lambda\lambda} \ .$$

Eq. (5.30) shows that the off-diagonal elements ρ_{cv} of the density matrix for the momentum state $\mathbf{k}$ couple to the diagonal elements ρ_{cc}, ρ_{vv}, of the same state. The coupling between different $\mathbf{k}$-values is introduced when we also include the Coulomb interaction among the carriers.

The diagonal elements of the density matrix $\rho_{\lambda\lambda}$ give the probability to find an electron in the state $|\lambda\mathbf{k}\rangle$, i.e., $\rho_{\lambda\lambda}$ is the population distribution of the electrons in band λ. From Eq. (5.28) we obtain

$$\frac{d}{dt}\rho_{cc}(\mathbf{k},t) = \frac{i}{\hbar}\mathcal{E}(t)\left[d_{cv}e^{i(\epsilon_{c,\mathbf{k}}-\epsilon_{v,\mathbf{k}})t}\rho_{vc}^{int}(\mathbf{k},t) - c.c.\right] \ , \tag{5.31}$$

$$\begin{aligned}\frac{d}{dt}\rho_{vv}(\mathbf{k},t) &= \frac{i}{\hbar}\mathcal{E}(t)\left[d_{cv}^{*}e^{i(\epsilon_{v,\mathbf{k}}-\epsilon_{c,\mathbf{k}})t}\rho_{cv}^{int}(\mathbf{k},t) - c.c.\right] \\ &= -\frac{d}{dt}\rho_{cc}(\mathbf{k},t) \ .\end{aligned} \tag{5.32}$$

In Eqs. (5.31) and (5.32), we used $\rho_{cv} = \rho^*_{vc}$, which follows from Eq. (5.30).

5.2.2 *Quantum Confined Semiconductors with Subband Structure*

In the Wannier function representation (4.2), the electron state is characterized by a band index i and by an envelope index ν in which we collect the quantum number n of the confined part of the envelope, and the D-dimensional wave vector $\mathbf{k}$ of the plane wave part of the envelope. For a quantum well, e.g., the envelope $\zeta_\mu(\mathbf{r})$ would stand for $\zeta_\mu(z)\exp(i\mathbf{k}_\parallel \cdot \mathbf{r}_\parallel)/L$. The optical matrix element is

$$\begin{aligned}\mathbf{d}_{i,\nu;j,\mu} &= \langle i,\nu|e\mathbf{r}|j,\mu\rangle \\ &= \frac{1}{N}\sum_{n,m}\zeta^*_{i,\nu}(\mathbf{R}_n)\zeta_{j,\mu}(\mathbf{R}_m)\int d^3r w^*_i(\mathbf{r}-\mathbf{R}_n)e\mathbf{r}w_j(\mathbf{r}-\mathbf{R}_m)\,. \end{aligned} \tag{5.33}$$

With the substitution $\mathbf{r} \to (\mathbf{r}-\mathbf{R}_n)+\mathbf{R}_n$ the integral over the Wannier functions yields approximately

$$\delta_{n,m}\Big(\mathbf{r}_{ij} + \mathbf{R}_n\delta_{i,j}\Big)\ ,$$

where $\mathbf{r}_{ij} = \int d^3r w^*_i(\mathbf{r})\mathbf{r}w_j(\mathbf{r})$ is the matrix element between Wannier functions localized at the same lattice site. Approximating the sum over all lattice sites by an integral $\frac{1}{NV_0}\sum_{\mathbf{n}} V_0 \to \frac{1}{V}\int d^3r$, where V_0 is the volume of a unit cell, we finally get

$$\mathbf{d}_{i,\nu;j,\mu} = \frac{e\mathbf{r}_{ij}}{V}\int d^3r\zeta^*_{i,\nu}(\mathbf{r})\zeta_{j,\mu}(\mathbf{r}) + \frac{1}{V}\int d^3r\zeta^*_{i,\nu}(\mathbf{r})e\mathbf{r}\zeta_{i,\mu}(\mathbf{r})\delta_{i,j}\ . \tag{5.34}$$

This result holds if the envelope function is much more extended than the Wannier function. The first term represents the optical matrix element of the interband transitions $i \neq j$, usually for transitions between states of one of the valence bands and the conduction band. For a quantum well, the integral over the envelope functions would yield the momentum selection rule $\mathbf{k}_\parallel = \mathbf{k}'_\parallel$ and the subband selection rule. Often the equal subband contributions $n = m$ are dominant. The second term describes the matrix element of the infrared intersubband transitions.

The density matrix for a mesoscopic semiconductor structure with several subbands is

$$\rho(t) = \sum_{i,j,\nu,\mu} \rho_{i,\nu;j,\mu}(t)|i\nu\rangle\langle j\mu| \ . \tag{5.35}$$

From the Liouville equation we obtain the equation of motion as

$$\left[\frac{d}{dt} + i(\epsilon_{i,\nu} - \epsilon_{j,\mu})\right] \rho_{i,\nu;j,\mu} = \frac{i\mathcal{E}(t)}{\hbar} \sum_{l,\sigma} (d_{i,\nu;l,\sigma}\rho_{l,\sigma;j,\mu} - \rho_{i,\nu;l,\sigma}d_{l,\sigma;j,\mu}) \ , \tag{5.36}$$

where $d_{i,\nu;j,\mu}$ is the projection of the dipole matrix element in field direction. In order to study a specific system, one has to insert the appropriate dipole matrix element, Eq. (5.34), for the optical transitions of interest.

Equations (5.30) – (5.32) for the two-band system, and Eq. (5.36) for the multi-band system, describe the interband kinetics of the free carrier model. In later chapters of this book, many-body effects due to the interaction between the excited carriers will be incorporated into these equations. However, before we discuss the interaction processes in detail, we analyze two important limiting cases of the noninteracting system in this chapter: i) coherent optical interband transitions and ii) the case of a quasi-equilibrium electron–hole plasma.

Coherent optical interband transitions are realized at least approximately in experiments using ultra-short optical pulses. Here, the carriers follow the laser field coherently, i.e., without significant dephasing. Examples of such coherent optical processes are the optical Stark effect, ultrafast adiabatic following, photon echo, and the observation of quantum beats.

A quasi-equilibrium situation is typically reached in experiments which use stationary excitation, or at least excitation with optical pulses which are long in comparison to the carrier scattering times. Under these conditions the excited carriers have sufficient time to reach thermal quasi-equilibrium distributions within their bands. "Quasi-equilibrium" means that the carriers are in equilibrium among themselves, but the total crystal is out of total thermodynamic equilibrium. In total equilibrium, there would be no carriers in the conduction band of the semiconductor.

5.3 Coherent Regime: Optical Bloch Equations

In this section, we discuss the interband kinetics for semiconductor systems for the coherent regime assuming a two-band system. The extensions to microstructures with several subbands is straightforward, using the results of the last subsection.

We simplify the free-carrier interband kinetic equations (5.30) – (5.32) by assuming an electromagnetic field in the form

$$\mathcal{E}(t) = \frac{E_0}{2}(e^{i\omega t} + e^{-i\omega t}) \ , \tag{5.37}$$

where E_0 is a slowly varying amplitude. Using

$$\rho_{cv}(\mathbf{k}, t) = \rho_{cv}^{int}(\mathbf{k}, t) e^{-i(\epsilon_{c,\mathbf{k}} - \epsilon_{v,\mathbf{k}})t} \tag{5.38}$$

and taking into account only the resonant terms (rotating wave approximation, RWA) proportional to $\exp[\pm i(\omega - \epsilon_{c,\mathbf{k}} + \epsilon_{v,\mathbf{k}})t]$, we can write the interband equations as

$$\left(\frac{d}{dt} + i\nu_{\mathbf{k}}\right) \rho_{cv}(\mathbf{k}, t) e^{i\omega t} = -\frac{i\omega_R}{2}[\rho_{cc}(\mathbf{k}, t) - \rho_{vv}(\mathbf{k}, t)] \ , \tag{5.39}$$

and

$$\begin{aligned} \frac{d}{dt}\rho_{cc}(\mathbf{k}, t) &= -\frac{i}{2}\omega_R[\rho_{cv}(\mathbf{k}, t)e^{i\omega t} - \rho_{vc}(\mathbf{k}, t)e^{-i\omega t}] \\ &= -\frac{d}{dt}\rho_{vv}(\mathbf{k}, t) \ . \end{aligned} \tag{5.40}$$

Here, we introduced the detuning

$$\nu_{\mathbf{k}} = \epsilon_{c,\mathbf{k}} - \epsilon_{v,\mathbf{k}} - \omega \tag{5.41}$$

and the Rabi frequency

$$\omega_R = \frac{d_{cv} E_0}{\hbar} \ . \tag{5.42}$$

With the assumption $d_{cv} = d_{vc}$ the Rabi frequency is real.

A helpful geometrical visualization of the kinetics described by Eqs. (5.39) and (5.40) is obtained if we introduce the *Bloch vector*, whose

real components are

$$\begin{aligned} U_1(\mathbf{k},t) &= 2\ \mathrm{Re}[\rho_{cv}(\mathbf{k},t)e^{i\omega t}] \\ U_2(\mathbf{k},t) &= 2\ \mathrm{Im}[\rho_{cv}(\mathbf{k},t)e^{i\omega t}] \\ U_3(\mathbf{k},t) &= [\rho_{cc}(\mathbf{k},t) - \rho_{vv}(\mathbf{k},t)]\ . \end{aligned} \tag{5.43}$$

From Eqs. (5.39) and (5.40) we obtain the following equations of motion for the Bloch-vector components

$$\begin{aligned} \frac{\boldsymbol{d}}{\boldsymbol{dt}}\boldsymbol{U_1(\mathbf{k},t)} &= \boldsymbol{\nu_\mathbf{k}\, U_2(\mathbf{k},t)} \\ \frac{\boldsymbol{d}}{\boldsymbol{dt}}\boldsymbol{U_2(\mathbf{k},t)} &= \boldsymbol{-\nu_\mathbf{k}\, U_1(\mathbf{k},t) - \omega_R\, U_3(\mathbf{k},t)} \\ \frac{\boldsymbol{d}}{\boldsymbol{dt}}\boldsymbol{U_3(\mathbf{k},t)} &= \boldsymbol{\omega_R\, U_2(\mathbf{k},t)}\ . \end{aligned} \tag{5.44}$$

coherent optical Bloch equations

These coherent Bloch equations can be written as single vector equation

$$\frac{d}{dt}\mathbf{U}(\mathbf{k},t) = \boldsymbol{\Omega} \times \mathbf{U}(\mathbf{k},t)\ , \tag{5.45}$$

where

$$\boldsymbol{\Omega} = \omega_R\, \mathbf{e}_1 - \nu_\mathbf{k}\, \mathbf{e}_3 \tag{5.46}$$

is the vector of the rotation frequency, and the $\mathbf{e}_i$ are Cartesian unit vectors.

It is well known from elementary mechanics that

$$\frac{d\mathbf{r}}{dt} = \boldsymbol{\omega} \times \mathbf{r} \tag{5.47}$$

describes the rotation of the vector $\mathbf{r}$ around $\boldsymbol{\omega}$, where the direction of $\boldsymbol{\omega}$ is the rotation axis and ω is the angular velocity. Using the analogy of Eqs. (5.45) and (5.47) one can thus describe the optical interband kinetics as a rotation of the Bloch vector. The length of the vector remains constant, and since in the absence of a field

$$\mathbf{U}(\mathbf{k},t) = U_3(\mathbf{k},t)\ \mathbf{e}_3 = -\mathbf{e}_3\ , \tag{5.48}$$

the Bloch vector for coherent motion is a unit vector with length one.

If the system is excited at resonance, $\nu_{\mathbf{k}} = 0$, then $\mathbf{U}$ rotates under the influence of a coherent field around the $\mathbf{e}_1$ axis in the $z-y$ plane. Starting in the ground state, $U_3(t=0) = -1$, a light field rotates the Bloch vector with the Rabi frequency around the -$\mathbf{e}_1$ axis. After the time $\omega_R t = \pi/2$ the inversion U_3 is zero, and the polarization reaches its maximum $U_2 = 1$. After $\omega_R t = \pi$ the system is in a completely inverted state, $U_3 = 1$, and it returns after $\omega_R t = 2\pi$ to the initial state, $U_3 = -1$. Such a rotation is called *Rabi flopping*. A light pulse of given duration turns the Bloch vector a certain angle. This is the basic idea for the phenomenon of *photon echo*. With a finite detuning $\nu > 0$, e.g., a z-component is added to the rotation axis, so that the rotations no longer connect the points $U_3 = 1$ and $U_3 = -1$.

For a more realistic description, we have to add dissipative terms to the Bloch equations. Here, we simply introduce a phenomenological damping of the polarization, i.e., we assume a decay of the transverse vector components U_1 and U_2 with a *transverse relaxation time* T_2. Additionally, we take into account that the inversion U_3 decays, e.g., by spontaneous emission, to the ground state $U_3 = -1$. This population decay time is the *longitudinal relaxation time* T_1. It is an important task of the many-body theory to derive the relaxation times from the system interactions. Including these relaxation times, the Bloch equations take the form

$$\begin{aligned}
\frac{d}{dt}U_1(\mathbf{k},t) &= -\frac{U_1(\mathbf{k},t)}{T_2} + \nu_{\mathbf{k}}\, U_2(\mathbf{k},t) \\
\frac{d}{dt}U_2(\mathbf{k},t) &= -\frac{U_2(\mathbf{k},t)}{T_2} - \nu_{\mathbf{k}}\, U_1(\mathbf{k},t) - \omega_R\, U_3(\mathbf{k},t) \\
\frac{d}{dt}U_3(\mathbf{k},t) &= -\frac{U_3(\mathbf{k},t)+1}{T_1} + \omega_R\, U_2(\mathbf{k},t)\ . \qquad (5.49)
\end{aligned}$$

optical Bloch equations with relaxation

To get a feeling for the decay processes described by the relaxation rates in Eqs. (5.49), let us assume that a short pulse with the area $\pi/4$ has induced an initial maximum polarization

$$\mathbf{U}(\mathbf{k}, t=0) = U_1(\mathbf{k}, t=0)\ \mathbf{e}_1 + U_2(\mathbf{k}, t=0)\ \mathbf{e}_2\ . \qquad (5.50)$$

To study the *free induction decay*, i.e., the decay in the absence of the field,

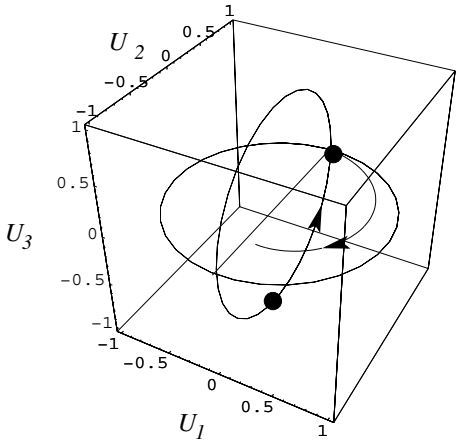

Fig. 5.2 Schematic drawing of the rotation of the Bloch vector for excitation with a rectangular pulse of area $\pi/2$ pulse and a finite detuning for $T_2 \ll T_1$.

we take $\omega_R = 0$ in (5.49) and obtain

$$\begin{aligned}\frac{d}{dt}U_1(\mathbf{k},t) &= -\frac{U_1(\mathbf{k},t)}{T_2} + \nu_{\mathbf{k}}\, U_2(\mathbf{k},t)\\ \frac{d}{dt}U_2(\mathbf{k},t) &= -\frac{U_2(\mathbf{k},t)}{T_2} - \nu_{\mathbf{k}}\, U_1(\mathbf{k},t)\end{aligned} \tag{5.51}$$

with the solution

$$\begin{pmatrix} U_1(\mathbf{k},t)\\ U_2(\mathbf{k},t)\end{pmatrix} = \begin{pmatrix} \cos(\nu_{\mathbf{k}}t) & \sin(\nu_{\mathbf{k}}t)\\ -\sin(\nu_{\mathbf{k}}t) & \cos(\nu_{\mathbf{k}}t)\end{pmatrix}\begin{pmatrix} U_1(\mathbf{k},t)\\ U_2(\mathbf{k},t)\end{pmatrix} e^{-t/T_2} \quad . \tag{5.52}$$

Eq. (5.52) shows how T_2 causes a decay of the polarization while it rotates with the detuning frequency $\nu_{\mathbf{k}}$ around the z-axis. The polarization spirals from the initial value to the stable fix point $U_1 = U_2 = 0$, if we disregard the inversion decay. Because of the band dispersion included in $\nu_{\mathbf{k}}$, the polarization of electron–hole pairs with different $\mathbf{k}$-values rotates with different rotation frequencies. If one applies after a time τ a second light pulse, which causes a rotation of the Bloch vector by π around the $\mathbf{e}_1$ axis, one keeps the Bloch vector in the $x-y$ plane (Fig. 5.2). A polarization component which

had rotated at time τ by an angle α will find itself again separated from the origin after the π pulse, this time by $-\alpha$. Since all polarization components continue to rotate around $\mathbf{e}_3$ with $\nu_{\mathbf{k}}$, they all return to the origin after the time 2τ. The coherent superposition of all polarization components causes the emission of a light pulse, the *photon echo* pulse. Naturally, the intensity of the photon echo depends on the dephasing time and decreases as

$$[e^{-2\tau/T_2}]^2 = e^{-4\tau/T_2} \ . \tag{5.53}$$

By varying the time delay τ between the two pulses, one can thus use a photon echo experiment to measure the dephasing time T_2.

5.4 Quasi-Equilibrium Regime: Free Carrier Absorption

The assumption of quasi-thermal distributions of the electrons in the conduction band and of the holes in the valence band provides a significant shortcut for the analysis of the optical response, since the diagonal elements of the density matrix do not have to be computed, but are given by thermal distribution functions. We discuss some aspects of carrier–carrier scattering and the mechanisms leading to a quasi-equilibrium situation in later chapters of this book. Here, in the framework of the free carrier model we simply postulate this situation. As is well known, the thermal equilibrium distribution for electrons is the Fermi distribution

$$\rho^0_{\lambda\lambda} = \frac{1}{e^{(\epsilon_{\lambda,\mathbf{k}}-\mu_\lambda)\beta}+1} \equiv f_{\lambda,k} \ , \tag{5.54}$$

where $\beta = 1/(k_B T)$ is the inverse thermal energy and k_B is the Boltzmann constant. The Fermi distribution and its properties are discussed in more detail in the following Chap. 6. For the present purposes, it is sufficient to note that the chemical potential μ_λ is determined by the condition that the sum $\sum_{\mathbf{k}} f_{\lambda,k}$ yields the total number of electrons N_λ in a band λ, i.e.,

$$\sum_{\mathbf{k}} f_{\lambda,k} = N_\lambda \rightarrow \mu_\lambda = \mu_\lambda(N_\lambda, T) \ , \tag{5.55}$$

where we assume that the summation over the two spin directions is included with the $\mathbf{k}$-summation. In total equilibrium and for thermal energies, which are small in comparison to the band gap, the valence band is

completely filled and the conduction band is empty, i.e.,

$$N_v = N, N_c = 0 \text{ for } 1/\beta << E_g \ ,$$

where N is the number of atoms.

The quasi-equilibrium approximation is a significant simplification in comparison to the full set of Bloch equations, since we do not have to solve Eqs. (5.31) and (5.32) for the diagonal terms. Inserting the distribution functions (5.54) into the RHS of Eq. (5.30), expressing the field through its Fourier transform, Eq. (2.16), and integrating over time yields

$$\rho_{cv}^{int}(\mathbf{k},t) = \int \frac{d\omega}{2\pi} \frac{d_{cv}\mathcal{E}(\omega)e^{i(\epsilon_{c,\mathbf{k}}-\epsilon_{v,\mathbf{k}}-\omega)t}}{\hbar(\epsilon_{c,\mathbf{k}}-\epsilon_{v,\mathbf{k}}-\omega-i\gamma)}(f_{v,k}-f_{c,k}) \ . \tag{5.56}$$

The optical polarization is given by

$$\mathcal{P}(t) = \mathrm{tr}[\rho(t)d] = \mathrm{tr}[\rho^{int}(t)d^{int}(t)] \ , \tag{5.57}$$

where tr stands for trace, i.e., the sum over all diagonal matrix elements:

$$\begin{aligned}\mathcal{P}(t) &= \frac{1}{L^3}\sum_{\mathbf{k}}[\rho_{cv}^{int}(\mathbf{k},t)d_{vc}^{int}(\mathbf{k},t) + \rho_{vc}^{int}(\mathbf{k},t)d_{cv}^{int}(\mathbf{k},t)] \\ &= \frac{1}{L^3}\sum_{\mathbf{k}}\int\frac{d\omega}{2\pi}\frac{|d_{cv}|^2(f_{v,k}-f_{c,k})}{\hbar(\epsilon_{c,\mathbf{k}}-\epsilon_{v,\mathbf{k}}-\omega-i\gamma)}\mathcal{E}(\omega)e^{-i\omega t} + \text{c.c.} \ ,\end{aligned} \tag{5.58}$$

and

$$d_{vc}^{int}(\mathbf{k},t) = d_{vc}e^{i(\epsilon_{v,\mathbf{k}}-\epsilon_{c,\mathbf{k}})t} \ . \tag{5.59}$$

Since

$$\chi(\omega) = \mathcal{P}(\omega)/\mathcal{E}(\omega) \tag{5.60}$$

and

$$\mathcal{P}(t) = \int\frac{d\omega}{2\pi}\mathcal{P}(\omega)e^{-i\omega t} \ , \tag{5.61}$$

we obtain the optical susceptibility as

$$\chi(\omega) = -\sum_{\mathbf{k}} \frac{|d_{cv}|^2}{L^3}(f_{v,k} - f_{c,k}) \left[\frac{1}{\hbar(\epsilon_{v,\mathbf{k}} - \epsilon_{c,\mathbf{k}} + \omega + i\gamma)} - \frac{1}{\hbar(\epsilon_{c,\mathbf{k}} - \epsilon_{v,\mathbf{k}} + \omega + i\gamma)} \right] . \tag{5.62}$$

optical susceptibility for free carriers

According to Eq. (1.53), the absorption spectrum is determined by the imaginary part of $\chi(\omega)$

$$\begin{aligned} \alpha(\omega) &= \frac{4\pi\omega}{n_b c}\chi''(\omega) \\ &= \frac{4\pi^2\omega}{L^3 n_b c} \sum_{\mathbf{k}} |d_{cv}|^2 (f_{v,k} - f_{c,k})\, \delta\big[\hbar(\epsilon_{v,\mathbf{k}} - \epsilon_{c,\mathbf{k}} + \omega)\big] . \end{aligned} \tag{5.63}$$

Since it is possible to evaluate Eq. (5.63) for different dimensionalities D of the electron system, we will give the result for the general case. As discussed in Chap. 3, it is often possible to approximate the band energies $\epsilon_{c,\mathbf{k}}$ and $\epsilon_{v,\mathbf{k}}$ by quadratic functions around the band extrema. Unless noted otherwise, we always assume that the extrema of both bands occur at the center of the Brillouin zone, i.e., at $k = 0$. Such semiconductors are called direct-gap semiconductors. Introducing the effective masses m_c and m_v for electrons in the conduction band and valence band, respectively, we write the energy difference as

$$\hbar(\epsilon_{c,\mathbf{k}} - \epsilon_{v,\mathbf{k}}) = \frac{\hbar^2 k^2}{2m_c} - \frac{\hbar^2 k^2}{2m_v} + E_g . \tag{5.64}$$

Since the valence-band curvature is negative, we have a negative mass for the electrons in the valence band, $m_v < 0$. To avoid dealing with negative masses, one often prefers to introduce *holes* as new quasi-particles with a positive effective mass

$$m_h = -m_v . \tag{5.65}$$

In the *electron–hole representation*, one discusses electrons in the conduction band and holes in the valence band. The probability $f_{h,k}$ to have a

hole at state k is given as

$$f_{h,k} = 1 - f_{v,k} \ . \tag{5.66}$$

The charge of the hole is opposite to that of the electron, i.e., $+e$. Eq. (5.65) implies that the energy of a hole is counted in the opposite way of the electron energy, i.e., the hole has minimum energy when it is at the top of the valence band. To emphasize the symmetry in our results, we rename the conduction-band mass $m_c \to m_e$, $f_c \to f_e$, and understand from now on that the term electron is used for conduction-band electrons and hole for valence-band holes, respectively. In the electron–hole notation, the free carrier absorption (5.63) is

$$\alpha(\omega) = \frac{4\pi^2\omega}{L^3 n_b c} \sum_{\mathbf{k}} |d_{cv}|^2 (1 - f_{e,k} - f_{h,k})\, \delta\big[\hbar(\epsilon_{v,\mathbf{k}} - \epsilon_{c,\mathbf{k}} + \omega)\big] \ . \tag{5.67}$$

Furthermore, we write the energy difference as

$$\hbar(\epsilon_{c,k} - \epsilon_{v,k}) = \hbar(\epsilon_{e,k} + \epsilon_{h,k}) = \frac{\hbar^2 k^2}{2m_r} + E_g \ , \tag{5.68}$$

where

$$\frac{1}{m_r} = \frac{1}{m_e} + \frac{1}{m_h} \quad \text{or} \quad m_r = \frac{m_e m_h}{m_e + m_h} \tag{5.69}$$

is the reduced electron–hole mass.

In order to proceed with our evaluation of the absorption coefficient for electrons with D translational degrees of freedom, it is useful to convert the sum over $\mathbf{k}$ into an integral. Following the steps in Eqs. (4.5) – (4.7) we evaluate the $\mathbf{k}$-summation in Eq. (5.67) to obtain

$$\alpha(\omega) = \frac{8\pi^2\omega |d_{cv}|^2}{n_b c L_c^{3-D}} \frac{1}{(2\pi)^D} \Omega_D S_D(\omega) \ . \tag{5.70}$$

In Eq. (5.70), we have replaced the ratio L^D/L^3 by $1/L_c^{3-D}$, where L_c denotes again the length of the system in the confined space dimensions, see Chap. 4. Furthermore, we introduced

$$S_D(\omega) = \int_0^\infty dk\, k^{D-1} \delta\left(\tfrac{\hbar^2 k^2}{2m_r} + E_g + E_0^{(D)} - \hbar\omega\right) (1 - f_{e,k} - f_{h,k}) \ . \tag{5.71}$$

In the energy-conserving δ-function, we included also the zero-point energy, which for ideal confinement (infinite potential) is

$$E_0^{(D)} = \frac{\hbar^2}{2m_r}\left(\frac{\pi}{L_c}\right)^2 (3-D) \tag{5.72}$$

for the $(3-D)$ confined directions (see problem 5.2). Taking the electron–hole–pair reduced-mass energy

$$\frac{\hbar^2 k^2}{2m_r} = x \tag{5.73}$$

as the integration variable, we can evaluate the integral in Eq. (5.71) with

$$k = \left(\frac{2m_r}{\hbar^2}\right)^{1/2} x^{1/2} \quad \text{and} \quad dk = \frac{1}{2}\left(\frac{2m_r}{\hbar^2}\right)^{1/2} \frac{dx}{x^{1/2}} \tag{5.74}$$

as

$$S_D(\omega) = \frac{1}{2}\left(\frac{2m_r}{\hbar^2}\right)^{D/2} \int_0^\infty dx\, x^{(D-2)/2}\, \delta(x + E_g + E_0^{(D)} - \hbar\omega) \times [1 - f_e(x) - f_h(x)] \ , \tag{5.75}$$

where

$$f_i(x) = \frac{1}{e^{\beta(xm_r/m_i - \mu_i)} + 1} \quad \text{for} \quad i = e, h \ . \tag{5.76}$$

The final integral in Eq. (5.75) is easily evaluated yielding

$$S_D(\omega) = \tfrac{1}{2}\left(\tfrac{2m_r}{\hbar^2}\right)^{D/2} (\hbar\omega - E_g - E_0^{(D)})^{(D-2)/2} \Theta(\hbar\omega - E_g - E_0^{(D)}) A(\omega) \ , \tag{5.77}$$

where $\Theta(x)$ is again the Heavyside unit-step function and

$$A(\omega) = 1 - f_e(\omega) - f_h(\omega) \tag{5.78}$$

with

$$f_i(\omega) = \frac{1}{e^{\beta[(\hbar\omega - E_g - E_0^{(D)})m_r/m_i - \mu_i]} + 1} \quad \text{for} \quad i = e, h \ . \tag{5.79}$$

The factor $A(\omega)$ in (5.77) is often referred to as *band-filling factor*. Inserting the result for $S(\omega)$ into Eq. (5.70), we obtain for the absorption coefficient

$$\boldsymbol{\alpha(\omega) = \alpha_0^D \frac{\hbar\omega}{E_0} \left(\frac{\hbar\omega - E_g - E_0^{(D)}}{E_0} \right)^{\frac{D-2}{2}} \Theta(\hbar\omega - E_g - E_0^{(D)}) A(\omega)} \ , \tag{5.80}$$

absorption coefficient for free carriers

where we introduced the energy $E_0 = \hbar^2/(2m_r a_0^2)$ and the length $a_0 = \hbar^2\epsilon_0/(e^2 m_r)$ as scaling parameters, and

$$\alpha_0^D = \frac{4\pi^2 |d_{cv}|^2}{\hbar n_b c} \frac{1}{(2\pi a_0)^D} \Omega_D \frac{1}{L_c^{3-D}} \tag{5.81}$$

To discuss the resulting semiconductor absorption, we first consider the case of unexcited material, where $f_e(\omega) = f_h(\omega) = 0$, i.e., $A(\omega) = 1$. The absorption spectra obtained from Eq. (5.80) for this case are plotted in Fig. 5.3. The figure shows that in two-dimensional materials the absorption sets in at $E_g + E_0^{(2)}$ like a step function, while it starts like a square root $\sqrt{\hbar\omega - E_g}$ in bulk material with $D = 3$, and it diverges like

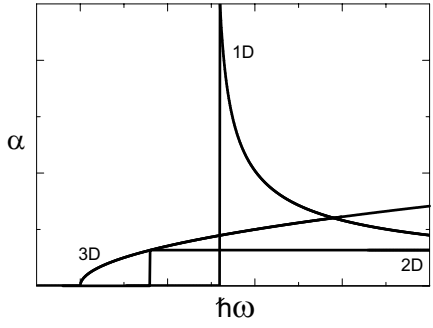

Fig. 5.3 Free electron absorption spectra for semiconductors, where the electrons can move freely in one, two, or three space dimensions.

$1/\sqrt{\hbar\omega - E_g - E_0^{(1)}}$ for $D = 1$. The function $S(\omega)$ is just the density of states. If we considered not strictly two- or one-dimensional conditions, but a quantum well or quantum wire with a finite thickness, the density of states would exhibit steps corresponding to the quantization of the electron motion in the confined space dimensions. The first step, which is all that we have taken into account, belongs to the lowest eigenvalue. Further steps corresponding to higher energy eigenvalues in the confined direction would belong to higher subbands.

As mentioned earlier, through optical pumping or injection of carriers, one may realize a situation with a finite number of electrons and holes. In this case, one speaks about an excited semiconductor, where the band-filling factor $A(\omega)$, Eq. (5.78), differs from one. Using the properties of the Fermi functions, one can rewrite $A(\omega)$ as (see problem 5.1)

$$A(\omega) = \Big[(1 - f_e(\omega))(1 - f_h(\omega)) + f_e(\omega) f_h(\omega)\Big] \tanh\left[\frac{\beta}{2}(\hbar\omega - E_g - \mu)\right] \ , \tag{5.82}$$

where we introduced the total chemical potential μ as

$$\mu = \mu_e + \mu_h \ . \tag{5.83}$$

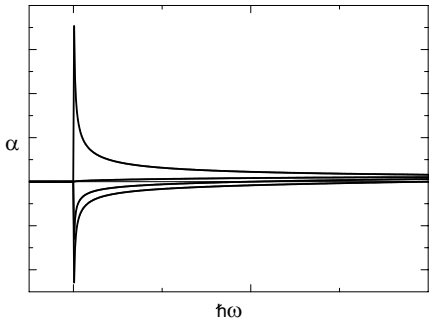

Fig. 5.4 Absorption/gain spectra for a one-dimensional free carrier system using the carrier densities $N = 0, 3.5, 5.4, 7.4 \times 10^5 \mathrm{cm}^{-1}$, from top to bottom.

Since

$$0 \leq f_{e/h} \leq 1 \ , \tag{5.84}$$

we see that the prefactor of the tanh term in Eq. (5.82) is strictly positive, varying between 0.5 and 1. However, $\tanh(x)$ changes its sign at $x = 0$. The band-filling factor, and therefore the optical absorption, can become negative if $\mu > 0$ and

$$E_g < \hbar\omega < E_g + \mu \ . \tag{5.85}$$

Examples of the density-dependent absorption spectra for one-, two-, and three-dimensional free carrier systems are plotted in Figs. 5.4, 5.5, and 5.6, respectively.

As the electron–hole densities are increased, the carrier distributions gradually become more and more degenerate with positive chemical potential μ/k_BT. In most semiconductor systems, the effective mass of the holes is more than three times larger than that of the electrons. Consequently, the valence band density of states is very large and the holes remain non degenerate up to rather large densities. For the highest densities in Figs. 5.4 – 5.6, the absorption becomes negative in the spectral region above the band gap, i.e., light with these frequencies is amplified, it experiences gain rather than loss (absorption).

The appearance of optical gain in the electron–hole system is the basis of semiconductor lasers, whose basic operational principles are discussed later

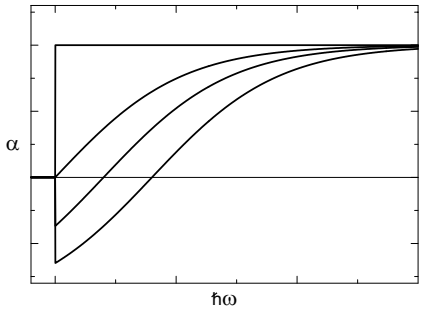

Fig. 5.5 Absorption/gain spectra for a two-dimensional free carrier system using the carrier densities $N = 0, 5, 8.3, 12 \times 10^{11}\mathrm{cm}^{-2}$, from top to bottom.

in this book. It is interesting to compare the spectral properties of the gain for the different effective dimensionalities of the carrier system. Due to the vanishing density of states at the band gap, in a three-dimensional system (Fig. 5.6), the gain gradually increases with increasing energy and peaks at an energy between the band gap and the total chemical potential of the carrier system. Due to the step-like density of states in a two dimensional system (Fig. 5.5) we always have the gain maximum directly at the band gap, only the spectral region of optical gain increases with increasing carrier density. In the one-dimensional carrier system of Fig. 5.4, we see a very sharply peaked gain right at the band gap whose amplitude increases with increasing carrier density.

For many applications one would often prefer the gain properties of the one-dimensional system unless a broad spectral gain band width is needed, e.g., for short-pulse generation. Anyway, the strong gain modifications caused by changing the effective dimensionality of the carrier system are one of the main motives of the ongoing research and development efforts in the area of low-dimensional semiconductor structures.

The density-dependent absorption spectra shown in Figs. 5.4 – 5.6 are the first example of optical nonlinearities which we discuss. The effects included in our present treatment are usually referred to as *band-filling nonlinearities*. Throughout this book we will encounter a variety of different sources for optical semiconductor nonlinearities.

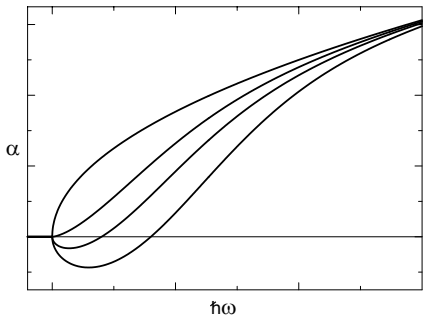

Fig. 5.6 Absorption/gain spectra for a three-dimensional free carrier system using the carrier densities $N = 0, 3.3, 5.8, 9.5 \times 10^{17}\mathrm{cm}^{-3}$, from top to bottom.

REFERENCES

The optical Bloch equations for two-level atoms are treated extensively in:

L. Allen and J.H. Eberly, *Optical Resonance and Two-Level Atoms*, Wiley and Sons, New York (1975)
M. Sargent III, M.O. Scully, And W.E. Lamb, *Laser Physics*, Addison Wesley, New York (1974)

For further reading on the material presented in this chapter see e.g.:

M. Balkanski, *ed., Optical Properties of Solids*, Handbook of Semiconductors Vol. 2, *ed.* T.S. Moss, North Holland, Amsterdam (1980)
J.L. Pankove, *Optical Processes in Semiconductors*, Dover Publ., New York (1971)

PROBLEMS

Problem 5.1: Solve the coherent Bloch equations (5.44) for the resonant case, $\nu_{\mathbf{k}} = 0$, in the form

$$U_i(t) = \sum_{i,j} A_{ij}(t) U_j(0).$$

Problem 5.2: Show that

$$1 - f_e(\omega) - f_h(\omega) = \Big\{ \big[1 - f_e(\omega)\big]\big[1 - f_h(\omega)\big] + f_e(\omega) f_h(\omega) \Big\} \times \tanh\left[\frac{\beta}{2} (\hbar\omega - E_g - \mu) \right] .$$

Hint: Use $\tanh(x) = (e^x - e^{-x})/(e^x + e^{-x})$.

Problem 5.3: Calculate the onset of the absorption due to the second subband in a quasi-two-dimensional semiconductor well.

Problem 5.4: Use the Liouville equation to derive Eq. (5.36) for the multi-subband quantum-well structure.

This page intentionally left blank

Chapter 6

Ideal Quantum Gases

As an introduction to the quantum mechanical analysis of many particle systems, we discuss in this chapter some properties of ideal quantum gases. An ideal gas is a system of noninteracting particles that is nevertheless in thermodynamic equilibrium. We analyze these systems in some detail to get experience in working with creation and destruction operators and also because we need several of the results obtained in later parts of this book.

An elementary particle with spin $s = \hbar(n + 1/2)$, $n = 0, 1, 2, \ldots$, is called a *Fermion*, while a particle with $s = \hbar n$ is called a *Boson*, see also Appendix A. The *Pauli exclusion principle* states that for Fermions it is forbidden to populate a single-particle state more than once. This feature is incorporated into the Fermi creation and destruction operators. For example, if the same Fermi destruction operator acts on the same state more than once, it always yields zero. Bosons, on the other hand, do not obey the exclusion principle, so that no limitation of the occupation of any quantum state exists. We discuss in this chapter, how these differences result in completely different statistical properties of a gas of Bosons or Fermions.

The general method of field quantization, the so-called *second quantization*, is summarized in Appendix A both for Fermion and Boson systems. In this and the following chapter, we put a hat on top of operators in second quantized form, such as $\hat{n}$ for the particle number operator, to distinguish them from the corresponding c-numbers.

In order to describe quantum mechanical systems at finite temperatures, we need the concept of *ensemble averages*. Such averages are computed

using the statistical operator $\hat{\rho}$ which is defined as

$$\hat{\boldsymbol{\rho}} = \frac{\mathbf{exp}[-\boldsymbol{\beta}(\hat{\boldsymbol{\mathcal{H}}} - \boldsymbol{\mu}\hat{\boldsymbol{N}})]}{\mathrm{tr}\ \mathbf{exp}[-\boldsymbol{\beta}(\hat{\boldsymbol{\mathcal{H}}} - \boldsymbol{\mu}\hat{\boldsymbol{N}})]} \ . \tag{6.1}$$

statistical operator for grand-canonical ensemble

Equation (6.1) defines the statistical operator for a *grand-canonical ensemble* with a variable number of particles. The expectation value $\langle\hat{Q}\rangle$ of an arbitrary operator $\hat{Q}$ in that ensemble is computed as

$$\langle\hat{Q}\rangle = \mathrm{tr}\ \hat{\rho}\,\hat{Q} \ . \tag{6.2}$$

The trace of an operator $\hat{Q}$ can be evaluated using any complete orthonormal set of functions $|n\rangle$ or $|l\rangle$, since

$$\mathrm{tr}\ \hat{Q} = \sum_l \langle l|\hat{Q}|l\rangle = \sum_{l,n} \langle l|n\rangle\langle n|\hat{Q}|l\rangle = \sum_n \langle n|\hat{Q}|n\rangle \ . \tag{6.3}$$

For practical calculations, it is most convenient to choose the functions as eigenfunctions to the operator $\hat{Q}$. If this is not possible we want to choose the functions at least as eigenfunctions of some dominant part of $\hat{Q}$, so that the remainder is *small* in some sense. The precise meaning of *small* and how to choose the most appropriate functions to evaluate the respective traces will be discussed for special cases in later chapters of this book.

6.1 Ideal Fermi Gas

For didactic purposes, we write the spin index explicitly in this chapter. The Hamiltonian for a system of noninteracting Fermions is

$$\hat{\mathcal{H}} = \sum_{\mathbf{k},s} E_k \hat{a}^\dagger_{\mathbf{k},s}\hat{a}_{\mathbf{k},s} = \sum_{\mathbf{k},s} E_k \hat{n}_{\mathbf{k},s} \ , \tag{6.4}$$

where $E_k = \hbar^2k^2/2m$ is the kinetic energy. The operators $\hat{a}^\dagger_{\mathbf{k},s}$ and $\hat{a}_{\mathbf{k},s}$ are, respectively, the creation and annihilation operators of a Fermion in the quantum state $(\mathbf{k}, s)$. They obey anti-commutation rules

$$[\hat{a}_{\mathbf{k},s}\ ,\ \hat{a}^\dagger_{\mathbf{k}',s'}]_+ = \hat{a}_{\mathbf{k},s}\hat{a}^\dagger_{\mathbf{k}',s'} + \hat{a}^\dagger_{\mathbf{k}',s'}\hat{a}_{\mathbf{k},s} = \delta_{\mathbf{k},\mathbf{k}'}\delta_{s,s'} \ , \tag{6.5}$$

and

$$[\hat{a}_{\mathbf{k},s}\,,\,\hat{a}_{\mathbf{k}',s'}]_+ = [\hat{a}^\dagger_{\mathbf{k},s}\,,\,\hat{a}^\dagger_{\mathbf{k}',s'}]_+ = 0 \ , \tag{6.6}$$

see Appendix A. The combination

$$\hat{n}_{\mathbf{k},s} = \hat{a}^\dagger_{\mathbf{k},s}\hat{a}_{\mathbf{k},s} \tag{6.7}$$

is the particle number operator with the eigenstates $|n_{\mathbf{k},s}\rangle$:

$$\hat{n}_{\mathbf{k},s}|n_{\mathbf{k},s}\rangle = n_{\mathbf{k},s}|n_{\mathbf{k},s}\rangle \text{ with } n_{\mathbf{k},s} = 0, 1 \ , \tag{6.8}$$

since each quantum state can be occupied by at most one Fermion.

To obtain the probability distribution function for Fermions, we compute the expectation value of the particle number operator in the state $(\mathbf{k}, s)$, i.e., we compute the mean occupation number

$$f_{\mathbf{k},s} = \langle\hat{n}_{\mathbf{k},s}\rangle = \frac{\text{tr } e^{[-\beta\sum_{\mathbf{k}',s'}(E_{k'}-\mu)\hat{n}_{\mathbf{k}',s'}]}\hat{n}_{\mathbf{k},s}}{\text{tr } e^{[-\beta\sum_{\mathbf{k}',s'}(E_{k'}-\mu)\hat{n}_{\mathbf{k}',s'}]}} \ . \tag{6.9}$$

To evaluate these expressions, we use

$$e^{[-\beta\sum_{\mathbf{k}',s'}(E_{k'}-\mu)\hat{n}_{\mathbf{k}',s'}]} = \prod_{\mathbf{k}',s'} e^{-\beta(E_{k'}-\mu)\hat{n}_{\mathbf{k}',s'}} \ . \tag{6.10}$$

This equation holds since the exponential operators on the LHS of Eq. (6.10) all commute, which directly follows from the commutation of the number operators for different states $(\mathbf{k}, s)$. Hence, Eq. (6.9) can be written as

$$f_{\mathbf{k},s} = \frac{\text{tr}\prod_{\mathbf{k}'s'} e^{-\beta(E_{k'}-\mu)\hat{n}_{\mathbf{k}',s'}}\hat{n}_{\mathbf{k},s}}{\text{tr}\prod_{\mathbf{k}'s'} e^{-\beta(E_{k'}-\mu)\hat{n}_{\mathbf{k}',s'}}} \ . \tag{6.11}$$

Since the particle number operator is diagonal in the $|n_{\mathbf{k},s}\rangle$ basis, we can use

$$\text{tr } \prod_{\mathbf{k}'s'} \cdots = \prod_{\mathbf{k}'s'} \text{tr} \ldots ,$$

in Eq. (6.11). It is most convenient to evaluate the trace with the eigenfunctions (6.8) of the particle number operator, so that

$$\text{tr } e^{-\beta(E_k-\mu)\hat{n}_{\mathbf{k},s}} = \sum_{n_{\mathbf{k},s}=0}^{1} e^{-\beta(E_k-\mu)n_{\mathbf{k},s}} \ . \tag{6.12}$$

All factors $(\mathbf{k}', s')$ in the numerator and denominator of Eq. (6.11) cancel, except for the term with $\mathbf{k}' = \mathbf{k}$ and $s' = s$. Therefore, Eq. (6.11) simplifies to

$$f_{\mathbf{k},s} = \frac{\sum_{n_{\mathbf{k},s}=0}^{1} e^{-\beta(E_k-\mu)n_{\mathbf{k},s}} n_{\mathbf{k},s}}{\sum_{n_{\mathbf{k},s}=0}^{1} e^{-\beta(E_k-\mu)n_{\mathbf{k},s}}} \quad . \tag{6.13}$$

Evaluating the sums and rearranging the terms yields the Fermi–Dirac distribution

$$\boldsymbol{f_{\mathbf{k},s} = \frac{1}{e^{\beta(E_k-\mu)}+1}} \quad . \tag{6.14}$$

Fermi–Dirac distribution

Eq. (6.14) shows that the distribution function depends only on the magnitude of $\mathbf{k}$ and not on the spin. Therefore, we often denote the Fermi–Dirac distribution simply by f_k. Examples for the Fermi–Dirac distribution function are plotted in Fig. 6.1 for three different temperatures.

We obtain the total number of particles N by summing the distribution function f_k over all quantum states $\mathbf{k}, s$:

$$N = \sum_{\mathbf{k},s} f_k = 2 \sum_{\mathbf{k}} f_k \quad . \tag{6.15}$$

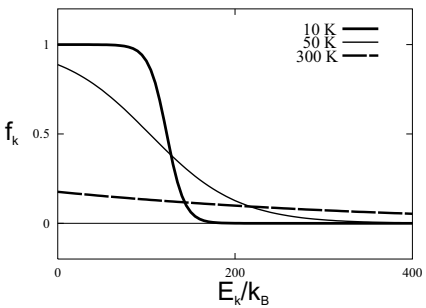

Fig. 6.1 Fermi–Dirac distribution function f_k as function of E_k/k_B for the particle density $n = 1 \cdot 10^{18}\mathrm{cm}^{-3}$ and three temperatures.

This relation determines the chemical potential $\mu = \mu(n, T)$ as a function of particle density n and temperature T. In order to evaluate Eq. (6.15), it is again useful to convert the sum over $\mathbf{k}$ into an integral over the energy ϵ

$$\sum_{\mathbf{k}} \to \int_0^\infty d\epsilon\, \rho^{(D)}(\epsilon) \ , \tag{6.16}$$

where, comparing to Eq. (4.7), the D-dimensional density of states is identified as

$$\rho^{(D)}(\epsilon) = \Omega_D \left(\frac{L}{2\pi}\right)^D \frac{1}{2} \left(\frac{2m}{\hbar^2}\right)^{D/2} \epsilon^{(D-2)/2} \ . \tag{6.17}$$

6.1.1 *Ideal Fermi Gas in Three Dimensions*

For a system with three dimensions, Eq. (6.15) yields

$$N = \frac{L^3}{2\pi^2} \left(\frac{2m}{\hbar^2}\right)^{3/2} \int_0^\infty d\epsilon \sqrt{\epsilon} \frac{1}{e^{\beta(\epsilon-\mu)}+1} \ . \tag{6.18}$$

Unfortunately, this integral cannot be evaluated analytically. We will therefore consider first the low-temperature limit $T \to 0$ or $\beta \to \infty$. If $\beta \to \infty$

$$f_k = \begin{pmatrix} 1 \\ 0 \end{pmatrix} \text{ for } \begin{pmatrix} \epsilon < \mu \\ \epsilon > \mu \end{pmatrix} \text{ or } f_k = \theta(\mu - \epsilon) \ , \tag{6.19}$$

showing that the Fermi function degenerates into the unit-step function. The chemical potential of this *degenerate Fermi distribution* is often denoted as the *Fermi energy* E_F

$$\mu(n, T = 0) = E_F = \frac{\hbar^2 k_F^2}{2m} \ , \tag{6.20}$$

where we have introduced k_F as the Fermi wave number. This is the wave number of the energetically highest state occupied at $T = 0$. In this degenerate limit, Eq. (6.18) yields

$$n = \frac{N}{L^3} = \frac{1}{2\pi^2} \left(\frac{2m}{\hbar^2}\right)^{3/2} \frac{2}{3} E_F^{3/2} = \frac{1}{3\pi^2} k_F^3 \tag{6.21}$$

and thus

$$k_F = (3\pi^2 n)^{1/3} \ . \tag{6.22}$$

Inserting this into Eq. (6.20), we get

$$E_F = \frac{\hbar^2}{2m}(3\pi^2 n)^{2/3} \quad . \tag{6.23}$$

In the high-temperature limit, where $\beta \to 0$, the chemical potential must grow fast to large negative values

$$\lim_{\beta \to 0}(-\mu\beta) = \infty \tag{6.24}$$

in order to keep the integral in Eq. (6.18) finite. The quantity $\exp(\beta\mu)$, called the *virial*, is thus a small quantity for $\beta E_F << 1$ and can be used as an expansion parameter. In lowest approximation, the Fermi function can be approximated by

$$f_k = \frac{e^{\beta(\mu - E_k)}}{1 + e^{\beta(\mu - E_k)}} \simeq e^{\beta\mu} e^{-\beta E_k} \quad . \tag{6.25}$$

In this case, Eq. (6.18) yields

$$n = \frac{e^{\beta\mu}}{2\pi^2}\left(\frac{2m}{\hbar^2\beta}\right)^{3/2} \int_0^\infty dx\sqrt{x}\, e^{-x} \quad . \tag{6.26}$$

The integral is $\sqrt{\pi}/2$, so that

$$n = n_0\, e^{\beta\mu} \quad , \tag{6.27}$$

where

$$n_0 = \frac{1}{4}\left(\frac{2m}{\hbar^2\pi\beta}\right)^{3/2} \quad , \tag{6.28}$$

or, using Eqs. (6.26) and (6.27),

$$e^{\beta\mu} = 4n\left(\frac{\hbar^2\pi\beta}{2m}\right)^{3/2} \quad . \tag{6.29}$$

Inserting this result into Eq. (6.25) yields the classical nondegenerate, or *Boltzmann distribution*

$$\boldsymbol{f_k = 4n\left(\frac{\hbar^2\pi\beta}{2m}\right)^{3/2} e^{-\beta E_k}\ .} \tag{6.30}$$

Boltzmann distribution

For the parameters used in Fig. 6.1, the distribution function at $T = 300$K is practically indistinguishable from the Boltzmann distribution function (6.30) for the same conditions.

At this point, we will briefly describe how one can obtain an analytic approximation for $\mu(n, T)$, which is good for all except very strongly degenerate situations. Here, we follow the work of Joyce and Dixon (1977) and Aguilera–Navaro *et al.* (1988). According to Eq. (6.18), the normalized density $\nu = n/n_0$ can be written as

$$\nu = \frac{n}{n_0} = \frac{2}{\sqrt{\pi}} \int_0^\infty dx\, \sqrt{x} \frac{z\, e^{-x}}{1 + ze^{-x}}\ , \tag{6.31}$$

where $z = \exp(\beta\mu)$. The integral can be evaluated using the series representation

$$\begin{aligned} \nu &= \frac{2}{\sqrt{\pi}} \int_0^\infty dx\, \sqrt{x} \sum_{n=0}^{\infty} (-1)^n z^{n+1} e^{-x(n+1)} \\ &= \sum_{n=1}^{\infty} (-1)^{n+1} \frac{z^n}{n^{3/2}}\ . \end{aligned} \tag{6.32}$$

Clearly, this expansion converges only for $\mu < 0$ or $z < 1$. However, the convergence range can be extended using the following resummation. First we invert Eq. (6.32) to express z in terms of ν

$$z = \sum_{n=1}^{\infty} b_n \nu^n \tag{6.33}$$

where the comparison with Eq. (6.32) shows that $b_1 = 1$. Taking the logarithm of Eq. (6.33), we can write $\beta\mu$ as

$$\beta\mu = \ln\nu + \sum_{n=1}^{\infty} B_n \nu^n \quad . \tag{6.34}$$

The logarithmic derivative of Eq. (6.34) yields

$$\nu \frac{d\beta\mu}{d\nu} = 1 + \sum_{n=1}^{\infty} B_n n \nu^n \quad . \tag{6.35}$$

Now, we make a Padé approximation by writing the infinite sum on the RHS of Eq. (6.34) as the ratio of two polynomials of order L and M

$$\nu \frac{d\beta\mu}{d\nu} \simeq \frac{\sum_{i=0}^{L} p_i \nu^i}{\sum_{i=0}^{M} q_i \nu^i} = [L/M](\nu) \quad . \tag{6.36}$$

This approximation is called the L/M-Padé approximation. Comparison with the fully numerical result shows that the approximation with $L = 2$ and $M = 1$ already gives quite accurate estimates. A final integration yields

$$\beta\mu \simeq \ln(\nu) + K_1 \ln(K_2\nu + 1) + K_3\nu \quad , \tag{6.37}$$

with $K_1 = 4.897$, $K_2 = 0.045$, and $K_3 = 0.133$.

The comparison of Eqs. (6.37) and (6.29) shows that the logarithmic term in Eq. (6.37) is exactly the classical result. The chemical potential

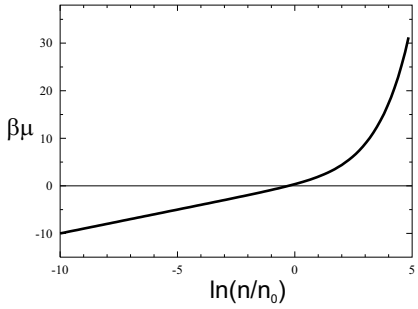

Fig. 6.2 Chemical potential μ for a three-dimensional Fermi gas as function of n/n_0 where n_0 is defined in Eq. (6.28).

according to Eq. (6.37) is plotted in Fig. 6.2. Within drawing accuracy, the result is indistinguishable from the exact chemical potential obtained as numerical solution of Eq. (6.18). Hence, Eq. (6.37) yields a good approximation for the range $-\infty < \mu\beta \leq 30$.

6.1.2 *Ideal Fermi Gas in Two Dimensions*

For a two-dimensional system, Eq. (6.15) yields

$$n = \frac{N}{L^2} = \frac{1}{2\pi}\left(\frac{2m}{\hbar^2\beta}\right)\int_0^\infty dx \frac{1}{e^x e^{-\beta\mu}+1} \ , \tag{6.38}$$

where $n = N/L^2$ now is the two-dimensional particle density and L^2 is the area. Using $\exp(x) = t$ as a new integration variable, the integral in Eq. (6.38) becomes

$$\int_1^\infty dt \frac{1}{t(te^{-\mu\beta}+1)} = \int_1^\infty dt \left(\frac{1}{t} - \frac{1}{t+e^{\mu\beta}}\right) = \ln(1+e^{\mu\beta}) \ . \tag{6.39}$$

Hence, we find the analytical result

$$n = \frac{m}{\hbar^2\beta\pi}\ln(1+e^{\beta\mu}) \tag{6.40}$$

or

$$\boldsymbol{\beta\mu(n,T) = \ln\left(e^{\hbar^2\beta\pi n/m}-1\right)} \ . \tag{6.41}$$

2*D* Fermion chemical potential

6.2 Ideal Bose Gas

Our discussion of the ideal Bose gas with spin $s = 0$ proceeds similar to the analysis of the ideal Fermi gas. The Hamiltonian is

$$\hat{\mathcal{H}} = \sum_{\mathbf{k}} E_k \hat{b}^\dagger_{\mathbf{k}} \hat{b}_{\mathbf{k}} = \sum_{\mathbf{k}} E_k \hat{n}_{\mathbf{k}} \ , \tag{6.42}$$

and the Bose commutation relations are

$$[\hat{b}_{\mathbf{k}}\,,\,\hat{b}^{\dagger}_{\mathbf{k}'}] = \hat{b}_{\mathbf{k}}\hat{b}^{\dagger}_{\mathbf{k}'} - \hat{b}^{\dagger}_{\mathbf{k}'}\hat{b}_{\mathbf{k}} = \delta_{\mathbf{k},\mathbf{k}'}\ , \tag{6.43}$$

and

$$[\hat{b}_{\mathbf{k}}\,,\,\hat{b}_{\mathbf{k}'}] = [\hat{b}^{\dagger}_{\mathbf{k}}\,,\,\hat{b}^{\dagger}_{\mathbf{k}'}] = 0\ , \tag{6.44}$$

see Appendix A. The expectation value of the particle number operator is

$$g_k \equiv \langle \hat{n}_{\mathbf{k}} \rangle = \frac{\mathrm{tr}\ e^{-\beta(E_k-\mu)\hat{n}_{\mathbf{k}}}\hat{n}_{\mathbf{k}}}{\mathrm{tr}\ e^{-\beta(E_k-\mu)\hat{n}_{\mathbf{k}}}}\ . \tag{6.45}$$

As in the Fermi case, the traces in Eq. (6.45) are evaluated choosing the eigenfunctions $|n_{\mathbf{k}}\rangle$ of the particle number operator

$$\hat{n}_{\mathbf{k}}|n_{\mathbf{k}}\rangle = n_{\mathbf{k}}|n_{\mathbf{k}}\rangle\,,\ \text{where } n_{\mathbf{k}} = 0, 1, 2, \ldots,\ N, \ldots \infty\ . \tag{6.46}$$

In contrast to the Fermi gas, where the Pauli principle allows all quantum states to be occupied only once, each state can be populated arbitrarily often in the Bose system. We obtain

$$\begin{aligned} \mathrm{tr}\ e^{-\beta(E_k-\mu)\hat{n}_{\mathbf{k}}} &= \sum_{n_{\mathbf{k}}=0}^{\infty} e^{-\beta(E_k-\mu)n_{\mathbf{k}}} \\ &= \sum_{n=0}^{\infty} a^n = \frac{1}{1-a}\ , \end{aligned} \tag{6.47}$$

where $a = \exp[-\beta(E_k-\mu)]$. It is straightforward to evaluate the numerator in Eq. (6.45) as derivative of the denominator, showing that Eq. (6.45) yields the Bose–Einstein distribution function

$$\boldsymbol{g_k = \frac{1}{e^{\beta(E_k-\mu)} - 1}\ .} \tag{6.48}$$

Bose–Einstein distribution

Generally, for Bosons we have two possible cases:

i) Particle number not conserved, i.e. $N = \sum_{\mathbf{k}} g_k \neq$ constant. In this case, μ cannot be determined from this relation, it has to be equal to zero: $\mu = 0$.

Examples for this class of Bosons are thermal photons and phonons.

ii) Particle number conserved, i.e., $N = \sum_{\mathbf{k}} g_k$ = constant. Then $\mu = \mu(N,T)$ is determined from Eq. (6.15) as in the Fermi system. Due to the minus sign in the denominator of the Bose–Einstein distribution, the sum in Eq. (6.47) converges only for $\mu \leq 0$ since the smallest value of E_k is zero. Examples of this class of Bosons are He atoms.

In the remainder of this chapter, we discuss some properties of the Bose system with conserved particle number, case ii). As in the Fermi case, $\beta\mu$ takes on large negative values for high temperatures. Thus, for $T \to \infty$, we can neglect the -1 in the denominator of Eq. (6.48) as compared to $e^{-\beta\mu}$ showing that the Bose–Einstein distribution also converges toward the Boltzmann distribution for high temperatures.

6.2.1 *Ideal Bose Gas in Three Dimensions*

If we study the chemical potential of the ideal Bose gas for decreasing temperatures, we find that μ is negative and that its absolute value decreases toward zero. We denote the critical temperature at which μ becomes zero as T_c :

$$\mu(n, T = T_c) = 0 \ . \tag{6.49}$$

To determine the value of T_c, we use Eq. (6.48) with $\mu = 0$ and compute the total number of Bosons first for the three-dimensional system :

$$\begin{aligned} N &= \sum_{\mathbf{k}} g_k = \int_0^\infty d\epsilon \rho^{(3)}(\epsilon) \frac{1}{e^{\beta\epsilon} - 1} \\ &= \frac{L^3}{4\pi^2} \left(\frac{2m}{\hbar^2} \right)^{3/2} \int_0^\infty d\epsilon \sqrt{\epsilon} \frac{1}{e^{\beta\epsilon} - 1} \ . \end{aligned} \tag{6.50}$$

The series representation

$$\frac{1}{e^x - 1} = \sum_{n=1}^{\infty} e^{-nx} \tag{6.51}$$

allows us to rewrite Eq. (6.50) as

$$N = \frac{L^3}{(2\pi)^2}\left(\frac{2m}{\beta\hbar^2}\right)^{3/2}\sum_{n=1}^{\infty}\int_0^{\infty} dx\, e^{-nx}x^{1/2} \ , \tag{6.52}$$

and the substitution $nx = t$ yields

$$N = \frac{L^3}{(2\pi)^2}\left(\frac{2m}{\beta\hbar^2}\right)^{3/2}\left(\sum_{n=1}^{\infty}\frac{1}{n^{3/2}}\right)\int_0^{\infty} dt\, e^{-t}t^{1/2} \ , \tag{6.53}$$

where the sum is the ζ function and the integral is the Γ function, both with the argument $3/2$. Hence, we obtain for the density

$$\frac{N}{L^3} = n = \frac{1}{(2\pi)^2}\left(\frac{2m}{\beta\hbar^2}\right)^{3/2}\zeta(3/2)\Gamma(3/2) \ , \tag{6.54}$$

showing that $n \propto T^{3/2}$ for $\mu = 0$. Setting $T = T_c$, i.e., $\beta = \beta_c$, we find from Eq. (6.54) that

$$k_B T_c = \frac{\hbar^2}{2m}n^{2/3}\left[\frac{2\pi^2}{\Gamma(3/2)\zeta(3/2)}\right]^{2/3} \ . \tag{6.55}$$

The result (6.55) implies that T_c is a finite temperature ≥ 0. Now we know that $\mu = 0$ at $T = T_c$, but what happens if T falls below T_c? The chemical potential has to remain zero, since otherwise the Bose–Einstein distribution function would diverge. All the calculations (6.50) – (6.54) assumed $\mu = 0$ and are therefore also valid for $T < T_c$. However, from the result (6.54) we see that N decreases with decreasing temperature yielding the apparent contradiction

$$N(T < T_c) < N(T = T_c) = N \ . \tag{6.56}$$

The solution of this problem came from the famous physicist *Albert Einstein*. He realized that the apparently missing particles in (6.56) are in fact condensed into the state $k = 0$, which has zero weight in the transformation from the sum to the integral in Eq. (6.16). Therefore, the term with $k = 0$ has to be treated separately for Bose systems at $T < T_c$. This can be done by writing

$$N = \sum_{k \neq 0} n_k + N_0$$
$$= \frac{L^3}{(2\pi)^2} \left(\frac{2mk_BT}{\hbar^2} \right)^{3/2} \zeta(3/2)\Gamma(3/2) + N_0 \ . \tag{6.57}$$

This equation shows that all particles are condensed into the state $k = 0$ at $T = 0$. This condensation in k-space is called the *Bose–Einstein condensation*. It corresponds to a real-space correlation effect in the Bosonic system leading to superconductivity and superfluidity. For temperatures between $T = 0$ K and T_c, the three-dimensional Bose system consists of a mixture of condensed and normal particles.

6.2.2 *Ideal Bose Gas in Two Dimensions*

Using the two-dimensional density of states, we get for the total number of Bosons

$$N = \frac{L^2}{4\pi} \left(\frac{2m}{\hbar^2\beta} \right) \int_0^\infty dx \, \frac{1}{e^{x-\beta\mu} - 1} \ . \tag{6.58}$$

The resulting expression for the two-dimensional particle density, $n = N/L^2$, can be evaluated in the same way as the corresponding expression for Fermions, yielding

$$n = -\frac{1}{4\pi} \left(\frac{2m}{\hbar^2\beta} \right) \ln(1 - e^{\beta\mu}) \ . \tag{6.59}$$

The argument of the logarithmic term has to be larger than 0, i.e., $e^{\beta\mu} < 1$ and $\mu < 0$ for any finite β value. Therefore, the chemical potential approaches zero only asymptotically as $T \to 0$ and there is no Bose–Einstein condensation in an ideal two-dimensional Bose system.

6.3 Ideal Quantum Gases in *D* Dimensions

In this section, we summarize some universal results for the temperature and density dependence of the chemical potential for Fermi, Bose, and Boltzmann statistics in a D-dimensional ideal quantum gas. In the previous sections, we have already considered the three- and two-dimensional cases.

Here, however, we also include the one-dimensional case and formalize the previous considerations.

As discussed preceding Eq. (6.15), the chemical potential μ is determined from the relation

$$n = \frac{2s+1}{L^D} \sum_{\mathbf{k}} f_k^{\pm} \quad , \tag{6.60}$$

where $n = N/L^D$ is the D-dimensional particle density, $2s+1$ is the spin degeneracy, with $s = 0$ or 1 for Bosons and $s = 1/2$ for Fermions, and $\mathbf{k}$ is the D-dimensional wave vector. The thermal distributions $f_k^{\pm}$ are defined as

$$f_k^{\pm} = \frac{1}{e^{\beta(E_k - \mu)} \pm 1} \quad , \tag{6.61}$$

with + for Fermions and − for Bosons. As before, we reformulate Eq. (6.60) with the virial $z = e^{\beta\mu}$ and get

$$n = (2s+1) z I_D(0) \left(\frac{I_D^{\pm}(z)}{I_D(0)} \right) \quad , \tag{6.62}$$

where

$$I_D^{\pm}(z) = L^{-D} \sum_{\mathbf{k}} \frac{1}{e^{\beta E_k} \pm z} \quad . \tag{6.63}$$

The first factor $I_D(0)$ in Eq. (6.62) can be evaluated most easily in Cartesian coordinates:

$$\begin{aligned} I_D(0) &= L^{-D} \sum_{\mathbf{k}} e^{-\beta E_k} = \prod_{i=1}^{D} \int_{-\infty}^{+\infty} \frac{dk_i}{2\pi} e^{-\beta \hbar^2 k_i^2 / 2m} \\ &= \left(\frac{m}{2\pi\hbar^2 \beta} \right)^{D/2} = n \left(\frac{k_B T}{E_{0D}} \right)^{D/2} \quad , \end{aligned} \tag{6.64}$$

where the D-dimensional zero-point energy is

$$E_{0D} = \frac{2\pi\hbar^2}{m} n^{2/D} \quad . \tag{6.65}$$

The D-dimensional integrals of the final normalized expression $I_D^{\pm}(z)/I_D(0)$ in Eq. (6.62) are now evaluated in polar coordinates. Because the integrands

do not depend on angles, the space angle as well as other normalization constants drop out and we obtain from Eq. (6.62) :

$$1 = (2s+1)z \left(\frac{k_B T}{E_{0D}}\right)^{D/2} \left(\frac{J_D^{\pm}(z)}{J_D(0)}\right) \quad , \tag{6.66}$$

where

$$J_D^{\pm}(z) = \int_0^{\infty} dk\, k^{D-1} \frac{1}{e^{k^2} \pm z} \quad \text{and} \quad J_D(0) = \Gamma(D/2). \tag{6.67}$$

The gamma function is given for $D = 3, 2$, and 1 by the values $\Gamma(3/2) = \sqrt{\pi/2}$, $\Gamma(1) = 1, \Gamma(1/2) = \sqrt{\pi}$, respectively. In general, the integral $J_D^{\pm}(z)$ has to be evaluated numerically for the three- and one-dimensional cases. We obtain an analytical result only in two dimensions (see Sec. 6-1.2 and 6-2.2):

$$J_2^{\pm}(z) = \mp \frac{1}{z} \ln(1 \pm z) \ . \tag{6.68}$$

As before, the limiting case of Boltzmann distributions is obtained from Eq. (6.66) if we approximate the factor $J_D^{\pm}(z)/J_D(0) \simeq 1$.

In order to compare the particle statistics with each other for different dimensionalities, we rewrite Eq. (6.66) as

$$\frac{k_B T}{E_{0D}} = \left[(2s+1)z \frac{J_D^{\pm}(z)}{J_D(0)}\right]^{-2/D} \quad . \tag{6.69}$$

The ratio of the thermal energy $k_B T$ to the zero-point energy E_{0D} is a measure of the degeneracy of the ideal quantum gas. For ratios larger than one, quantum effects can be neglected. On the other hand, quantum effects dominate over thermal ones if $k_B T/E_{0D}$ is smaller than one. In Fig. 6.3, we plot $k_B T/E_{0D}$ logarithmically versus the ratio of the chemical potential to the thermal energy $\mu\beta$. For better comparison, we have put $s = 0$ for all cases. In such a plot, we obtain a straight line with a slope of $-2/D$ for the Boltzmann limit, as can be seen by taking the logarithm of the RHS of Eq. (6.69). For Bosons, the figure shows clearly that for $D = 3$ the chemical potential becomes zero in the vicinity of $k_B T \simeq E_{0D}$, whereas it approaches zero only asymptotically for $D = 2, 1$. This shows again the absence of a Bose–Einstein condensation in dimensions lower than three. For Fermions, the chemical potential becomes positive and converges to the Fermi energy as the degeneracy parameter $k_B T/E_{0D} \to 0$.

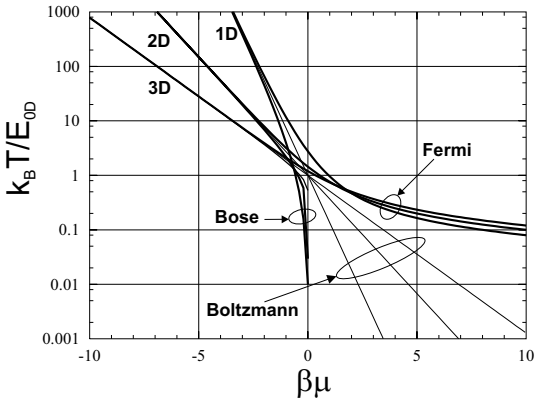

Fig. 6.3 Comparison of $k_B T/E_{0D}$ plotted logarithmically versus $\mu\beta$ for the Bose, Fermi and Boltzmann statistics of a $3D$, $2D$ and $1D$ quantum gas.

REFERENCES

The Padé approximation for the Fermion chemical potential is discussed in:

J.B. Joyce and R.W. Dixon, Appl. Phys. Lett. **31**, 354 (1977)
V.C. Aguilera–Navaro, G.A. Esterez, and A. Kostecki, J. Appl. Phys. **63**, 2848 (1988)
C. Ell, R. Blank, S. Benner, and H. Haug. Journ. Opt. Soc. Am. **B6**, 2006 (1989)

PROBLEMS

Problem 6.1: Consider a linear chain of atoms with masses M and interatomic distance a. The coupling between the atoms is given by a harmonic force with the force constant K.

a) Show that the Lagrange function is

$$\mathcal{L} = \frac{1}{2}M\sum_{r=1}^{N}\left(\frac{dq_r}{dt}\right)^2 - \frac{1}{2}K\sum_{r=1}^{N}(q_r - q_{r+1})^2$$

where q_r is the displacement of the r-th atom from its equilibrium position.

b) Compute the canonical momentum p_r.

c) The displacements can be expanded into *normal coordinates* Q_k

$$q_r(t) = \frac{1}{\sqrt{N}} \sum_k Q_k(t) e^{ikar} \quad .$$

Use

$$\sum_k e^{iar(k-k')} = N\delta_{kk'}$$

and the periodic boundary conditions $q_{r+N} = q_r$ to determine the allowed k-values.

d) The displacements are quantized by introducing the commutation relations

$$[\hat{p}_r, \hat{q}_s] = \frac{\hbar}{i}\delta_{rs}$$

$$[\hat{p}_r, \hat{p}_s] = 0 = [\hat{q}_r, \hat{q}_s] \quad .$$

Use the fact that the displacement is a Hermitian operator

$$\hat{q}_r^\dagger = \hat{q}_r$$

to show the relations

$$\hat{Q}_k^\dagger = \hat{Q}_{-k} \quad ;$$

$$\hat{P}_k \equiv \frac{\partial \hat{\mathcal{L}}}{\partial(\partial \hat{Q}_k/\partial t)} = \hat{P}_{-k}^\dagger \quad ;$$

$$[\hat{Q}_k, \hat{P}_{k'}] = -\frac{\hbar}{i}\delta_{kk'} \quad ;$$

and

$$\begin{aligned}\hat{\mathcal{H}} &= \frac{1}{2M}\sum_k \hat{P}_k\hat{P}_{-k} + K\sum_k [1-\cos(ak)]\hat{Q}_k\hat{Q}_{-k} \\ &= \sum_k \hbar\omega_k \left(\frac{1}{2M\hbar\omega_k}\hat{P}_k\hat{P}_{-k} + \frac{M\omega_k}{2\hbar}\hat{Q}_k\hat{Q}_{-k}\right) \quad ,\end{aligned}$$

where $\omega_k^2 = 2\frac{K}{M}[1 - \cos(ak)]$.

e) Introduce the phonon operators $\hat{a}_k$ and $\hat{a}_k^\dagger$ through the linear transformations

$$\hat{a}_k^\dagger = \sqrt{\frac{M\omega_k}{2\hbar}}\hat{Q}_{-k} - i\sqrt{\frac{1}{2\hbar M\omega_k}}\hat{P}_k$$

$$\hat{a}_k = \sqrt{\frac{M\omega_k}{2\hbar}}\hat{Q}_k + i\sqrt{\frac{1}{2\hbar M\omega_k}}\hat{P}_{-k} \quad .$$

Verify the phonon commutation relation

$$[\hat{a}_k, \hat{a}_{k'}^\dagger] = \delta_{kk'}$$

and show that the Hamiltonian becomes

$$\hat{\mathcal{H}} = \sum_k \hbar\omega_k \left(\hat{a}_k^\dagger \hat{a}_k + \frac{1}{2}\right) \quad .$$

Hint: Follow the discussion in Appendix A.

Problem 6.2: The Fourier expansion of $\hat{\mathbf{A}}$ is given by

$$\hat{\mathbf{A}}(\mathbf{r}, t) = \sum_{\mathbf{k}} e^{i\mathbf{k}\cdot\mathbf{r}}\hat{\mathbf{A}}(\mathbf{k}, t) \quad ,$$

and correspondingly for $\hat{\Pi}(\mathbf{r}, t)$. Prove, that in the Coulomb gauge the commutator of $\hat{\mathbf{A}}(\mathbf{k}, t)$ and $\hat{\Pi}(\mathbf{k}, t)$ is

$$[\hat{A}_l(\mathbf{k}, t), \hat{\Pi}_j(\mathbf{k}, t)] = i\hbar\left(\delta_{lj} - \frac{k_l k_j}{k^2}\right) \quad .$$

Problem 6.3: Expand the chemical potential of a nearly degenerate $3D$ Fermion system for low temperatures (Sommerfeld expansion).

Problem 6.4: Determine the temperature at which a $2D$ Fermion system of a given density has zero chemical potential.

Problem 6.5: Calculate the energy and specific heat of a nearly degenerate $2D$ Fermion system.

Chapter 7

Interacting Electron Gas

In this chapter, we discuss a model for the interacting electron gas in a solid. To keep the analysis as simple as possible, we neglect the discrete lattice structure of the ions in the solid and treat the positive charges as a smooth background, called jellium-like jelly.

This jellium model was originally designed to describe the conduction characteristics of simple metals. However, as we will see in later chapters of this book, this model is also useful to compute some of the intraband properties of an excited semiconductor. In such a system, we have to deal with an electron–hole gas, which consists of the excited electrons in the conduction band and the corresponding holes, i.e., missing electrons, in the valence band. In this case, one again has total charge neutrality, since the negative charges of the electrons are compensated by the positive charges of the holes.

In the following sections, we discuss the jellium model in such a way that only very minor changes are required when we want to apply the results to the case of an excited semiconductor.

7.1 The Electron Gas Hamiltonian

The Hamiltonian of a three-dimensional electron system is the sum of kinetic and interaction energy. In the previous chapter on ideal quantum gases, we discussed the kinetic energy part in great detail. Now we add the Coulomb interaction part in the jellium model approximation. For this purpose, we write the Coulomb Hamiltonian in first quantization as

$$\mathcal{H}_C = \frac{1}{2} \sum_{\alpha,\alpha'} \int d^3r \, d^3r' \, \rho_\alpha(\mathbf{r}) \, \rho_{\alpha'}(\mathbf{r}') \, W(\mathbf{r} - \mathbf{r}') \ , \tag{7.1}$$

where W is the interaction potential. Since the detailed form of W is not needed for our initial considerations, we defer this discussion until the end of this section. The term $\mathbf{r} = \mathbf{r}'$ has to be excluded from the integration in (7.1) since this is the infinite interaction energy of charges at the same position (self-energy). For notational simplicity, we keep the unrestricted integration and subtract the self-energy at the end.

The index α in Eq. (7.1) runs over electrons, $\alpha = e$, and ions, $\alpha = i$. The charge density ρ_α is

$$\rho_e(\mathbf{r}) = -|e| \sum_{i=1}^{N} \delta(\mathbf{r} - \mathbf{r}_i) \tag{7.2}$$

for the electrons and

$$\rho_i(\mathbf{r}) = |e| \frac{N}{L^3} \tag{7.3}$$

for the ions, reflecting our assumption that the ions form a uniform positive charge background.

Now, we take the Fourier transformation of the charge density and the interaction potential. For the spatial $3D$ Fourier transformation, we use the following conventions

$$f_{\mathbf{q}} = \int \frac{d^3r}{L^3} f(\mathbf{r}) e^{-i\mathbf{q}\cdot\mathbf{r}} \tag{7.4}$$

$$f(\mathbf{r}) = \sum_{\mathbf{q}} f_{\mathbf{q}} e^{i\mathbf{q}\cdot\mathbf{r}} \tag{7.5}$$

and

$$\sum_{\mathbf{q}} e^{i\mathbf{q}\cdot(\mathbf{r}-\mathbf{r}')} = L^3 \delta(\mathbf{r} - \mathbf{r}') \tag{7.6}$$

$$\int \frac{d^3r}{L^3} e^{i(\mathbf{q}-\mathbf{q}')\cdot\mathbf{r}} = \delta_{\mathbf{q},\mathbf{q}'} \ . \tag{7.7}$$

With these definitions we obtain the Coulomb interaction Hamiltonian (7.1) as

$$\mathcal{H}_C = \frac{L^6}{2} \sum_{\alpha,\alpha',\mathbf{q}} W_{\mathbf{q}} \rho_{\alpha,-\mathbf{q}} \rho_{\alpha',\mathbf{q}} \ , \tag{7.8}$$

where

$$\rho_{e,\mathbf{q}} = -\frac{|e|}{L^3}\sum_{i=1}^{N} e^{-i\mathbf{q}\cdot\mathbf{r}_i} \tag{7.9}$$

and

$$\rho_{i,\mathbf{q}} = \frac{|e|N}{L^3}\delta_{\mathbf{q},0} \ . \tag{7.10}$$

Evaluating the sum over electron and ion contributions allows us to write the total Coulomb Hamiltonian as the sum of three terms:

$$\mathcal{H}_C = \mathcal{H}_C^{e-e} + \mathcal{H}_C^{e-i} + \mathcal{H}_C^{i-i} \ . \tag{7.11}$$

The electron–electron interaction is

$$\begin{aligned}\mathcal{H}_C^{e-e} &= \frac{e^2}{2}\sum_{i,j,\mathbf{q}} W_{\mathbf{q}} e^{i\mathbf{q}\cdot(\mathbf{r}_i-\mathbf{r}_j)} \\ &= \frac{e^2}{2}\left(\sum_{i,j,\mathbf{q}\neq 0} W_{\mathbf{q}} e^{i\mathbf{q}\cdot(\mathbf{r}_i-\mathbf{r}_j)} + W_{\mathbf{q}=0}N^2\right) \ ,\end{aligned} \tag{7.12}$$

where we separated the contribution with $\mathbf{q} = 0$ in the second line. For the electron–ion interaction, we get

$$\mathcal{H}_C^{e-i} = -\frac{e^2}{2}\sum_{j,\mathbf{q}} W_{\mathbf{q}} N\delta_{\mathbf{q},0}(e^{i\mathbf{q}\cdot\mathbf{r}_j} + e^{-i\mathbf{q}\cdot\mathbf{r}_j}) = -e^2 W_{\mathbf{q}=0}N^2 \ , \tag{7.13}$$

and the ion–ion interaction yields

$$\mathcal{H}_C^{i-i} = \frac{e^2}{2}W_{\mathbf{q}=0}N^2 \ . \tag{7.14}$$

Adding all the contributions (7.12) – (7.14), we obtain for the Coulomb Hamiltonian in the jellium model

$$\mathcal{H}_C = \frac{e^2}{2}\sum_{i,j\neq i,\mathbf{q}\neq 0} W_{\mathbf{q}} e^{i\mathbf{q}\cdot(\mathbf{r}_i-\mathbf{r}_j)} \ . \tag{7.15}$$

In the double summation, we now exclude the term with $i = j$, which is just the electron self-interaction mentioned in the discussion after Eq. (7.1). Writing

$$\sum_{\substack{i,j\neq i\\ \mathbf{q}\neq 0}} W_{\mathbf{q}} e^{i\mathbf{q}\cdot(\mathbf{r}_i-\mathbf{r}_j)} = \sum_{i,\mathbf{q}\neq 0} W_{\mathbf{q}} e^{i\mathbf{q}\cdot\mathbf{r}_i} \sum_{j\neq i} e^{-i\mathbf{q}\cdot\mathbf{r}_j}$$
$$= \sum_{i,\mathbf{q}\neq 0} W_{\mathbf{q}} e^{i\mathbf{q}\cdot\mathbf{r}_i} \left(\sum_j e^{-i\mathbf{q}\cdot\mathbf{r}_j} - e^{-i\mathbf{q}\cdot\mathbf{r}_i} \right)$$
$$= \sum_{i,j,\mathbf{q}\neq 0} W_{\mathbf{q}} e^{i\mathbf{q}\cdot(\mathbf{r}_i-\mathbf{r}_j)} - N \sum_{\mathbf{q}\neq 0} W_{\mathbf{q}} \ , \tag{7.16}$$

and using (7.9), the Coulomb Hamiltonian becomes

$$\boldsymbol{\mathcal{H}_C = \frac{1}{2} \sum_{\mathbf{q}\neq 0} W_{\mathbf{q}} (L^6 \rho_{e,-\mathbf{q}} \rho_{e,\mathbf{q}} - e^2 N)} \ . \tag{7.17}$$

Coulomb Hamiltonian for jellium model

The calculations leading to the Hamiltonian (7.17) show that the only, but extremely important effect resulting from the attractive interaction of the electrons with the homogeneous positive charge background is to eliminate the term $q = 0$ from the sum in the electron–electron interaction Hamiltonian.

In order to obtain the Coulomb Hamiltonian in second quantization, we replace the charge density $\rho_{e,\mathbf{q}}$ in (7.17) by the charge density operator

$$\rho_{e,-\mathbf{q}} \rightarrow \hat{\rho}_{e,-\mathbf{q}} \ , \tag{7.18}$$

and

$$N \rightarrow \hat{N} \ , \tag{7.19}$$

where $\hat{N}$ is the operator for the total number of electrons, so that

$$\hat{\mathcal{H}}_C = \frac{1}{2} \sum_{\mathbf{q}\neq 0} W_{\mathbf{q}} (L^6 \hat{\rho}_{e,-\mathbf{q}} \hat{\rho}_{e,\mathbf{q}} - e^2 \hat{N}) \ . \tag{7.20}$$

As the next step, we now want to introduce the electron creation and destruction operators $\hat{a}^\dagger_{\mathbf{k},s}$ and $\hat{a}_{\mathbf{k},s}$, which we used already in Chap. 6. For

this purpose, we write the charge density operator in real space as

$$\hat{\rho}_e(\mathbf{r}) = -|e|\ \hat{n}(\mathbf{r}) = -|e| \sum_s \hat{\psi}_s^\dagger(\mathbf{r})\hat{\psi}_s(\mathbf{r}) \ , \tag{7.21}$$

where the field operators $\hat{\psi}_s^\dagger(\mathbf{r})$, $\hat{\psi}_s(\mathbf{r})$ describe creation and destruction of an electron at position $\mathbf{r}$ with spin s (see Appendix A). Using the plane-wave expansion

$$\hat{\psi}_s(\mathbf{r}) = \frac{1}{L^{3/2}} \sum_{\mathbf{k}} \hat{a}_{\mathbf{k},s} e^{i\mathbf{k}\cdot\mathbf{r}} \ , \tag{7.22}$$

we obtain

$$\hat{\rho}_e(\mathbf{r}) = -\frac{|e|}{L^3} \sum_{\mathbf{k},\mathbf{k}',s} \hat{a}_{\mathbf{k}',s}^\dagger \hat{a}_{\mathbf{k},s} e^{i(\mathbf{k}-\mathbf{k}')\cdot\mathbf{r}} \ . \tag{7.23}$$

Taking the Fourier transformation of (7.23) yields

$$\hat{\rho}_{e,\mathbf{q}} = -\frac{|e|}{L^3} \sum_{\mathbf{k},s} \hat{a}_{\mathbf{k}-\mathbf{q},s}^\dagger \hat{a}_{\mathbf{k},s} \ . \tag{7.24}$$

After inserting (7.24) into the Hamiltonian (7.20), we obtain

$$\hat{\mathcal{H}}_C = \frac{1}{2} \sum_{\substack{\mathbf{k},\mathbf{k}' \\ \mathbf{q}\neq 0,s,s'}} \hat{a}_{\mathbf{k}+\mathbf{q},s}^\dagger \hat{a}_{\mathbf{k},s} \hat{a}_{\mathbf{k}'-\mathbf{q},s'}^\dagger \hat{a}_{\mathbf{k}',s'} V_{\mathbf{q}} - \frac{1}{2} \sum_{\mathbf{q}\neq 0} \hat{N} V_{\mathbf{q}} \ , \tag{7.25}$$

where we abbreviated

$$V_{\mathbf{q}} = e^2 W_{\mathbf{q}} \ . \tag{7.26}$$

Reordering the creation and destruction operators using the anti-commutation relations (6.5) – (6.6) yields

$$\begin{aligned} \hat{\mathcal{H}}_C = {} & \frac{1}{2} \sum_{\substack{\mathbf{k},\mathbf{k}' \\ \mathbf{q}\neq 0 \\ s,s'}} \hat{a}_{\mathbf{k}+\mathbf{q},s}^\dagger \hat{a}_{\mathbf{k}'-\mathbf{q},s'}^\dagger \hat{a}_{\mathbf{k}',s'} \hat{a}_{\mathbf{k},s} V_{\mathbf{q}} \\ & + \frac{1}{2} \sum_{\mathbf{k},s} \hat{a}_{\mathbf{k},s}^\dagger \hat{a}_{\mathbf{k},s} \sum_{\mathbf{q}\neq 0} V_{\mathbf{q}} - \frac{1}{2} \sum_{\mathbf{q}\neq 0} \hat{N} V_{\mathbf{q}} \ . \end{aligned} \tag{7.27}$$

The last two terms cancel since

$$\hat{N} = \sum_{\mathbf{k},s} \hat{a}^{\dagger}_{\mathbf{k},s} \hat{a}_{\mathbf{k},s} \ . \tag{7.28}$$

Adding the kinetic energy part, Eq. (6.4), we obtain the total electron gas Hamiltonian

$$\hat{\mathcal{H}} = \sum \boldsymbol{E_k} \hat{\boldsymbol{a}}^{\dagger}_{\mathbf{k},s} \hat{\boldsymbol{a}}_{\mathbf{k},s} + \frac{\mathbf{1}}{\mathbf{2}} \sum_{\substack{\mathbf{k},\mathbf{k'} \\ \mathbf{q}\neq 0 \\ s,s'}} \boldsymbol{V_{\mathbf{q}}} \hat{\boldsymbol{a}}^{\dagger}_{\mathbf{k}+\mathbf{q},s} \hat{\boldsymbol{a}}^{\dagger}_{\mathbf{k'}-\mathbf{q},s'} \hat{\boldsymbol{a}}_{\mathbf{k'},s'} \hat{\boldsymbol{a}}_{\mathbf{k},s} \ . \tag{7.29}$$

electron gas Hamiltonian

The only missing ingredient is now the detailed form of the interaction potential $V_{\mathbf{q}}$. We start from the Coulomb interaction potential in real space

$$V(r) = \frac{e^2}{\epsilon_0 r} \ , \tag{7.30}$$

where we include the background dielectric constant ϵ_0 to take into account the polarizability of the valence electrons and of the lattice. Using Eq. (7.4), we have

$$\begin{aligned} V_{\mathbf{q}} &= \int \frac{d^3r}{L^3} V(r) e^{-i\mathbf{q}\cdot\mathbf{r}} \\ &= \frac{e^2}{L^3\epsilon_0} \int d^3r \, e^{i\mathbf{q}\cdot\mathbf{r}} \frac{1}{r} = \frac{2\pi e^2}{L^3\epsilon_0} \int_0^{\infty} dr \, r \int_{-1}^{1} d\cos\theta \, e^{iqr\,\cos\theta} \\ &= -i\frac{2\pi e^2}{L^3\epsilon_0 q} \int_0^{\infty} dr \, (e^{iqr} - e^{-iqr}) \ . \end{aligned} \tag{7.31}$$

To evaluate the remaining integral in Eq. (7.31), we introduce the convergence generating factor $\exp(-\gamma r)$ under the integral and take the limit of $\gamma \to 0$ after the evaluation. This yields

$$\begin{aligned} V_{\mathbf{q}} &= -i\frac{2\pi e^2}{\epsilon_0 L^3 q} \lim_{\gamma\to 0} \int_0^{\infty} dr (e^{iqr} - e^{-iqr}) e^{-\gamma r} \\ &= \lim_{\gamma\to 0} \frac{4\pi e^2}{\epsilon_0 L^3 (q^2+\gamma^2)} \ , \end{aligned} \tag{7.32}$$

so that

$$\boldsymbol{V_{\mathbf{q}} = V_q^{3D} = \frac{4\pi e^2}{\epsilon_0 L^3}\frac{1}{q^2}} \ . \tag{7.33}$$

3*D* Coulomb potential

7.2 Three-Dimensional Electron Gas

Now we use the electron gas Hamiltonian to compute the ground-state energy ($T = 0$) in Hartree–Fock approximation. Since we know that at $T = 0$ all particles are in states with $|\mathbf{k}| \leq k_F$, the Hartree–Fock ground-state wave function is

$$|0\rangle_{HF} = \hat{a}^\dagger_{\mathbf{k}_1,s_1}\hat{a}^\dagger_{\mathbf{k}_2,s_2}\ldots\hat{a}^\dagger_{\mathbf{k}_N,s_N}|0\rangle = \prod_{k_i\leq k_F}\hat{a}^\dagger_{\mathbf{k}_i,s_i}|0\rangle \ . \tag{7.34}$$

Due to the anti-commutation relations between the Fermi operators, Eq. (7.34) automatically has the correct symmetry. The Hartree–Fock ground state energy is

$$E_0^{HF} = {}_{HF}\langle 0|\hat{H}|0\rangle_{HF} = E_{kin}^{HF} + E_{pot}^{HF} \ . \tag{7.35}$$

First we evaluate the kinetic energy

$$E_{kin}^{HF} = \sum_{\mathbf{k},s} E_k \ {}_{HF}\langle 0|\hat{a}^\dagger_{\mathbf{k},s}\hat{a}_{\mathbf{k},s}|0\rangle_{HF} \ . \tag{7.36}$$

We simply get

$${}_{HF}\langle 0|\hat{a}^\dagger_{\mathbf{k},s}\hat{a}_{\mathbf{k},s}|0\rangle_{HF} = \Theta(k_F - k) \ , \tag{7.37}$$

since in the Hartree–Fock ground state all states below the Fermi wave number are occupied and all states above k_F are empty. The Θ-function can also be written as

$$\Theta(k_F - k) = \Theta(E_F - E_k) = f_k(T = 0) \ , \tag{7.38}$$

which is just the Fermi distribution at $T = 0$. Therefore,

$$E_{kin}^{HF} = 2\sum_{\mathbf{k}} E_k \Theta(E_F - E_k) = \frac{L^3}{\pi^2}\frac{\hbar^2}{2m}\int_0^{k_F} dk\, k^4 = \frac{L^3}{\pi^2}\frac{\hbar^2}{2m}\frac{k_F^5}{5} \quad , \tag{7.39}$$

where Eq. (4.6) for $D = 3$ has been used. With the Fermi wave number $k_F = (3\pi^2 n)^{1/3}$, Eq. (6.22), we find

$$E_{kin}^{HF} = \frac{\hbar^2 L^3}{10m\pi^2}(3\pi^2 n)^{5/3} \quad . \tag{7.40}$$

For the potential energy, we obtain

$$E_{pot}^{HF} = \frac{1}{2}\sum_{\substack{\mathbf{q}\neq 0 \\ \mathbf{k},\mathbf{k}',s,s'}} V_q\, {}_{HF}\langle 0|\hat{a}^\dagger_{\mathbf{k}+\mathbf{q},s}\hat{a}^\dagger_{\mathbf{k}'-\mathbf{q},s'}\hat{a}_{\mathbf{k}',s'}\hat{a}_{\mathbf{k},s}|0\rangle_{HF} \quad . \tag{7.41}$$

This term is nonzero only if

$$|\mathbf{k}|, |\mathbf{k}'| \leq k_F \quad \text{and} \quad |\mathbf{k}+\mathbf{q}|, |\mathbf{k}'-\mathbf{q}| \leq k_F \quad , \tag{7.42}$$

as can be seen by acting with the destruction operators on the Hartree–Fock ground state to the right, and with the h.c. of the creation operators on the Hartree–Fock ground state to the left, respectively. To evaluate (7.41), we now commute $\hat{a}^\dagger_{\mathbf{k}'-\mathbf{q},s'}$ to the right, using the Fermi commutation relations repeatedly. We obtain

$$\begin{aligned}
&{}_{HF}\langle 0|\hat{a}^\dagger_{\mathbf{k}+\mathbf{q},s}\hat{a}^\dagger_{\mathbf{k}'-\mathbf{q},s'}\hat{a}_{\mathbf{k}',s'}\hat{a}_{\mathbf{k},s}|0\rangle_{HF} = \\
&-{}_{HF}\langle 0|\hat{a}^\dagger_{\mathbf{k}+\mathbf{q},s}\hat{a}_{\mathbf{k}',s'}(-\hat{a}_{\mathbf{k},s}\hat{a}^\dagger_{\mathbf{k}'-\mathbf{q},s'} + \delta_{\mathbf{k},\mathbf{k}'-\mathbf{q}}\delta_{s,s'})|0\rangle_{HF} = \\
&-{}_{HF}\langle 0|\hat{a}^\dagger_{\mathbf{k}+\mathbf{q},s}\hat{a}_{\mathbf{k}+\mathbf{q},s}|0\rangle_{HF}\delta_{\mathbf{k},\mathbf{k}'-\mathbf{q}}\delta_{s,s'} \quad ,
\end{aligned} \tag{7.43}$$

where $\mathbf{q} \neq 0$ and

$$\hat{a}^\dagger_{\mathbf{k}'-\mathbf{q},s'}|0\rangle_{HF} = 0 \text{ for } |\mathbf{k}'-\mathbf{q}| \leq k_F \tag{7.44}$$

has been used. Furthermore,

$${}_{HF}\langle 0|\hat{a}^\dagger_{\mathbf{k}+\mathbf{q},s}\hat{a}_{\mathbf{k}+\mathbf{q},s}|0\rangle_{HF} = 1 \tag{7.45}$$

since all states $|\mathbf{k}+\mathbf{q}| < k_F$ are occupied. Using (7.42) – (7.45) and inserting into (7.41) yields

$$E_{pot}^{HF} = -\frac{1}{2} \sum_{\substack{\mathbf{q}\neq 0 \\ \mathbf{k},\mathbf{k}',s}} V_q \, \delta_{\mathbf{k}+\mathbf{q},\mathbf{k}'} \Theta(E_F - E_k) \, \Theta(E_F - E_{k'})$$

$$= -\frac{1}{2} \sum_{\mathbf{k},\mathbf{k}'\neq\mathbf{k},s} V_{|\mathbf{k}-\mathbf{k}'|} f_k(T=0) f_{k'}(T=0) \ . \tag{7.46}$$

Explicit evaluation of the sum in the last line and use of Eq. (6.22) gives (see problem 7.1)

$$E_{pot}^{HF} \equiv E_{exc} = -\frac{e^2 L^3}{4\pi^3 \epsilon_0} (3\pi^2 n)^{4/3} \ . \tag{7.47}$$

The Hartree–Fock result for the potential energy due to electron–electron repulsion is just the *exchange energy*, which increases with density with a slightly smaller power than the kinetic energy. The exchange energy is an energy reduction, since the term with $\mathbf{q} = 0$ is omitted from the Hamiltonian as a consequence of the Coulomb attraction between electrons and positive jellium background. Adding Eqs. (7.40) and (7.47) we obtain the total Hartree–Fock energy as

$$\frac{E_{HF}}{L^3} = \frac{\hbar^2}{10 m \pi^2} (3\pi^2 n)^{5/3} - \frac{e^2}{4\pi^3 \epsilon_0} (3\pi^2 n)^{4/3} \ . \tag{7.48}$$

For low densities, the negative exchange energy dominates, while the kinetic energy is larger at high densities, see Fig. 7.1. For intermediate densities, there is actually an energy minimum, indicative of the existence of a stable phase which is the electron–hole–liquid phase. Hence, already at the level of this relatively simple Hartree–Fock theory, we find signatures of a stable electron–hole liquid. This famous prediction of Keldysh has been verified experimentally by the observation of electron–hole liquid droplets, mostly in indirect gap semiconductors. The density within these droplets is the stable liquid density. They condense and coexist with the electron–hole gas, as soon as a critical density is exceeded and the temperature is below the critical condensation temperature.

In order to gain more physical insight into electron gas properties and to understand the energy reduction due to the exchange effects, we now calculate for the Hartree–Fock ground state the conditional probability to simultaneously find electrons at the position $\mathbf{r}$ with spin s and at $\mathbf{r}'$ with

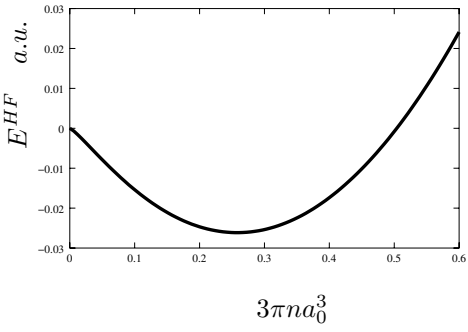

Fig. 7.1 Hartree–Fock energy versus density scaled by the Bohr radius $a_0 = \hbar\epsilon_0/(me^2)$

spin s'. This conditional probability is just the correlation function

$$R_{ss'}(\mathbf{r},\mathbf{r}') = {}_{HF}\langle 0|\hat{\psi}_s^\dagger(\mathbf{r})\hat{\psi}_{s'}^\dagger(\mathbf{r}')\hat{\psi}_{s'}(\mathbf{r}')\hat{\psi}_s(\mathbf{r})|0\rangle_{HF} \ . \tag{7.49}$$

Obviously, this correlation function is only finite if the annihilation operators simultaneously find an electron in $(\mathbf{r}, s)$ and $(\mathbf{r}', s')$. The creation operators simply put the annihilated electrons back into their previous states.

Using (7.22) to express the field operators in terms of the electron creation and destruction operators allows us to write the electron correlation function as

$$R_{ss'}(\mathbf{r},\mathbf{r}') = \tfrac{1}{L^6}\sum e^{i(\mathbf{l}'-\mathbf{k}')\cdot\mathbf{r}'+i(\mathbf{l}-\mathbf{k})\cdot\mathbf{r}}\, {}_{HF}\langle 0|\hat{a}_{\mathbf{k},s}^\dagger\hat{a}_{\mathbf{k}',s'}^\dagger\hat{a}_{\mathbf{l}',s'}\hat{a}_{\mathbf{l},s}|0\rangle_{HF} \ . \tag{7.50}$$

The sum runs over $(\mathbf{l},\mathbf{l}',\mathbf{k},\mathbf{k}')$ with $(|\mathbf{l}|,|\mathbf{l}'|,|\mathbf{k}|,|\mathbf{k}'|) < k_F$. As in our calculation of E_{pot}^{HF}, we again commute all creation operators to the right and use Eq. (7.44). As intermediate step, we obtain

$${}_{HF}\langle 0|\hat{a}_{\mathbf{k},s}^\dagger\hat{a}_{\mathbf{k}',s'}^\dagger\hat{a}_{\mathbf{l}',s'}\hat{a}_{\mathbf{l},s}|0\rangle_{HF} = {}_{HF}\langle 0|\hat{a}_{\mathbf{k},s}^\dagger\hat{a}_{\mathbf{l},s}\delta_{\mathbf{k}',\mathbf{l}'} - \hat{a}_{\mathbf{k},s}^\dagger\hat{a}_{\mathbf{l}',s'}\delta_{\mathbf{k}',\mathbf{l}}\delta_{s,s'}|0\rangle_{HF}, \tag{7.51}$$

where the first term is the so-called *direct term* and the second term is the *exchange term*. Using the Fermi anti-commutation relations and Eq. (7.44) one more time yields

$$R_{ss'}(\mathbf{r},\mathbf{r}') = \frac{1}{L^6}\sum e^{i(\mathbf{l}'-\mathbf{k}')\cdot\mathbf{r}'+i(\mathbf{l}-\mathbf{k})\cdot\mathbf{r}}(\delta_{\mathbf{k},\mathbf{l}}\delta_{\mathbf{k}',\mathbf{l}'} - \delta_{\mathbf{k}',\mathbf{l}}\delta_{\mathbf{k},\mathbf{l}'}\delta_{s,s'})$$
$$= \frac{1}{L^6}[(N/2)^2 - \delta_{ss'}|F(\mathbf{r}-\mathbf{r}')|^2] \ . \tag{7.52}$$

The first term in (7.52) results from

$$\sum_{\mathbf{k}}^{k_F}\sum_{\mathbf{k}'}^{k_F} 1 = (N/2)^2 \ ,$$

where we have to divide the total electron number N by two since no spin summations are included, and in the second term we defined

$$F(\rho) = \sum_{\mathbf{k}}^{k_F} e^{i\mathbf{k}\cdot\rho} = n\frac{3}{2}\frac{\sin k_F\rho - \rho k_F\cos k_F\rho}{(k_F\rho)^3} \ . \tag{7.53}$$

Here, we used Eq. (6.22) to introduce the factor k_F^3 in terms of the density n. Inserting Eq. (7.53) into Eq. (7.52), we obtain

$$R_{ss'}(\mathbf{r},\mathbf{r}') = \frac{n^2}{4}\left\{1 - 9\delta_{ss'}\left[\frac{\sin(k_F|\mathbf{r}-\mathbf{r}'|) - |\mathbf{r}-\mathbf{r}'|k_F\cos(k_F|\mathbf{r}-\mathbf{r}'|)}{(k_F|\mathbf{r}-\mathbf{r}'|)^3}\right]^2\right\} . \tag{7.54}$$

This result is plotted in Fig. 7.2. It shows that the conditional probability to find an electron at $\mathbf{r}'$ with spin s', given that there is an electron at $\mathbf{r}$ with spin s, depends only on the separation $|\mathbf{r}-\mathbf{r}'|$ between the two electrons. Furthermore, if s and s' are different, the second term on the RHS of Eq. (7.54) vanishes, and we find that the correlation function is constant. However, for electrons with equal spin, $s = s'$, we can convince ourselves by a Taylor expansion that $R_{ss}(\rho \to 0) \to 0$. This result shows that the electrons with equal spin avoid each other as a consequence of the Pauli exclusion principle (exchange repulsion). Each electron is surrounded by an *exchange hole*, i.e., by a net positive charge distribution.

The existence of the exchange hole expresses the fact that the mean separation between electrons with equal spin is larger than it would be without the Pauli principle. This result is correct also for the ideal Fermi gas, where actually the Hartree–Fock ground state is the exact ground state of the system. For the interacting electron gas treated in this chapter, the increased separation between repulsive charges *reduces the overall Coulomb*

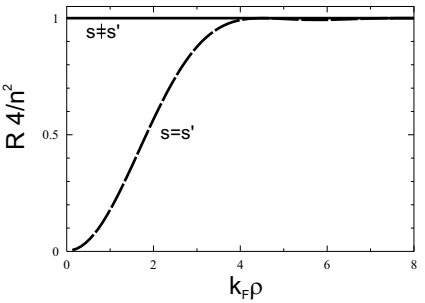

Fig. 7.2 Pair correlation function $R_{ss'}$ for the three-dimensional electron plasma, Eq. (7.54), as function of the dimensionless particle distance $k_F\rho$, where $\rho = |\mathbf{r} - \mathbf{r}'|$ and k_F is given by Eq. (6.22).

repulsion. One can say that the electron interacts with its own exchange hole. Since this is an attractive interaction, the total energy is reduced, as we found in Eq. (7.47).

According to the Hartree–Fock theory, electrons with different spin do not avoid each other, since the states are chosen to satisfy the exchange principle but they do not include Coulomb correlations. The exchange principle is satisfied as long as one quantum number, here the spin, is different. However, in reality there will be an additional correlation, which leads to the so-called *Coulomb hole*. To treat these correlation effects, one has to go beyond Hartree–Fock theory, e.g., using screened Hartree–Fock (RPA), see Chap. 9. Generally, one can write the exact ground state energy E_0 as

$$E_0 = E_0^{HF} + E_{cor} = E_{kin}^{HF} + E_{exc} + E_{cor} \ , \tag{7.55}$$

where the correlation energy is defined as

$$E_{cor} = E_0 - E_0^{HF} \ . \tag{7.56}$$

An exact calculation of E_{cor} is generally not possible. To obtain good estimates for E_{cor} is one of the tasks of many-body theory.

7.3 Two-Dimensional Electron Gas

Even in those semiconductor structures which we consider as low-dimensional, such as quantum wells, quantum wires, or quantum dots, the Coulomb potential varies as $1/r$. The reason is that the electric field lines between two charges are not confined within these structures. The field lines also pass through the surrounding material, which is often another semiconductor material with a very similar dielectric constant.

In this section, we discuss the situation of idealized semiconductor quantum wells, where the electron motion is confined to two dimensions, but the Coulomb interaction has its three-dimensional space dependence. For simplicity, we disregard here all modifications which occur for different dielectric constants in the confinement layer and the embedding material. As introduced in Chap. 4, we assume that the carriers are confined to the x, y layer and put the transverse coordinate $z = 0$. For this case, we need only the two dimensional Fourier transform of the Coulomb potential:

$$V_q = \int \frac{d^2r}{L^2} V(r) e^{i\mathbf{q}\cdot\mathbf{r}} \tag{7.57}$$

with $V(r)$ given by Eq. (7.30). Eq. (7.57) yields

$$V_q = \frac{e^2}{\epsilon_0 L^2} \int_0^\infty dr \int_0^{2\pi} d\phi \, e^{iqr cos\phi} = \frac{2\pi e^2}{\epsilon_0 L^2 q} \int_0^\infty d(qr) J_0(qr) \ , \tag{7.58}$$

where $J_0(x)$ is the zero-order Bessel function of the first kind. Since

$$\int_0^\infty dx \, J_0(x) = 1$$

we obtain

$$\boldsymbol{V_{\mathbf{q}} = V_q^{2D} = \frac{2\pi e^2}{\epsilon_0 L^2} \frac{1}{q}} \ . \tag{7.59}$$

quasi-2D Coulomb potential

Eq. (7.59) shows that the Coulomb potential in two dimensions exhibits a $1/q$ dependence instead of the $1/q^2$ dependence in $3D$.

Using Eq. (7.59) in Eq. (7.46), we obtain the exchange energy as (see problem 7.1)

$$E_{exc}^{2D} = -\frac{L^2 e^2 C}{3\pi\epsilon_0}(2\pi n)^{3/2} \ , \tag{7.60}$$

where

$$C = \sum_{l=0,2,\ldots,\infty} \frac{2}{l+2}\left[\frac{1}{2^l}\binom{l}{l/2}\right]^2 \ . \tag{7.61}$$

is a numerical constant and $n = N/L^2$.

In order to compare the exchange energy in $2D$ and $3D$, we introduce the normalized distance r_s between particles through the relation

$$\frac{4\pi}{3}r_s^3 = \frac{1}{na_0^3} = \frac{L^3}{Na_0^3} \tag{7.62}$$

in $3D$. Here, a_0 is the characteristic length scale given by the Bohr radius of the bound electron–hole pairs, i.e., excitons (see Chap. 10 for details). At this point we use the definition of a_0 as

$$a_0 = \frac{\hbar^2\epsilon_0}{me^2} \tag{7.63}$$

in three dimensions. In two dimensions, we have

$$\pi r_s^2 = \frac{1}{na_0^2} = \frac{L^2}{N\,a_0^2} \ , \tag{7.64}$$

where a_0 now is the $2D$ Bohr radius, which is half of the $3D$ Bohr radius. The $3D$ exchange energy is seen to vary with the particle distance r_s as

$$E_{exc}^{3D} \propto -r_s^{-4} \ , \tag{7.65}$$

whereas

$$E_{exc}^{2D} \propto -r_s^{-3} \ , \tag{7.66}$$

i.e., in three dimensions the exchange energy falls off more rapidly for larger distances than in two dimensions. This is a consequence of the larger phase space volume for $D = 3$ compared to the $D = 2$ case.

In the evaluation of the pair correlation function $R_{ss'}(\mathbf{r}, \mathbf{r}')$ for the $2D$ electron gas, we obtain formally the same result as in Eq. (7.52), except now

$$F(\mathbf{r} - \mathbf{r}') = n \frac{J_1(k_F|\mathbf{r} - \mathbf{r}'|)}{k_F|\mathbf{r} - \mathbf{r}'|} \tag{7.67}$$

with J_1 being the first-order Bessel function of the first kind. Here we have introduced the two-dimensional Fermi wave number k_F through the relation

$$N = 2 \sum_{\mathbf{k}} f_k = \frac{L^2}{\pi} \int_0^{k_F} dk\, k \ . \tag{7.68}$$

Evaluating Eq. (7.68) yields

$$k_F = \sqrt{2\pi n} \ . \tag{7.69}$$

The resulting pair correlation function for $2D$ is plotted in Fig. 7.3. Schematically, the variations of the correlation function in two-dimensions resemble those of the three-dimensional result shown in Fig. 7.2. A more detailed comparison between Figs. 7.2 and 7.3, however, shows that the oscillatory structures are somewhat more pronounced in the $2D$ system, indicating that the exchange correlations of the electrons are stronger in two than in three dimensions.

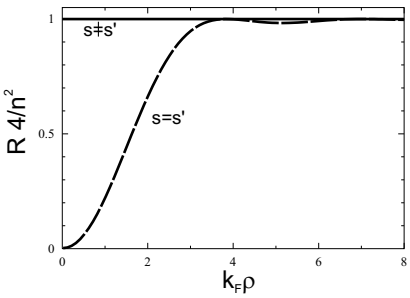

Fig. 7.3 Pair correlation function $R_{ss'}$ for the quasi-two-dimensional electron plasma, Eqs. (7.52) and (7.67), as function of the dimensionless particle distance $k_F\rho$, where $\rho = |\mathbf{r} - \mathbf{r}'|$ and k_F is given by Eq. (7.69).

7.4 Multi-Subband Quantum Wells

In order to calculate the properties of electron gases in quantum wells with several subbands, we have to evaluate the matrix elements of the Coulomb potential between the various envelope eigenfunctions of the quantum well. It is convenient to start with the $3D$ Fourier transform of the Coulomb potential V_q^{3D} of Eq. (7.33), where L^3 has to be replaced by $L^2 L_z$ with L_z being the thickness of the quantum well. With this modification, we obtain the Coulomb potential $V_{q\|}(z)$, where z is the coordinate perpendicular to the layer, by a $1D$ Fourier transform of Eq. (7.33) with respect to the perpendicular momentum component $q_\perp$:

$$\begin{aligned} V_{q\|}(z) &= \sum_{q_\perp} V_q^{3D} e^{iq_\perp z} \\ &= \frac{4\pi e^2}{\epsilon_0 L^2 L_z} \int_{-\infty}^{+\infty} \frac{dq_\perp}{\Delta q_\perp} \frac{e^{iq_\perp z}}{q_\|^2 + q_\perp^2} \ , \end{aligned} \tag{7.70}$$

where we have split the momentum vector into its components parallel and perpendicular to the plane. With $\Delta q_\perp = 2\pi/L_z$ we get

$$V_{q\|}(z) = \frac{2e^2}{\epsilon_0 L^2} \int_{-\infty}^{+\infty} dq_\perp \frac{e^{iq_\perp z}}{q_\|^2 + q_\perp^2} = \frac{2\pi e^2}{\epsilon_0 L^2 q_\|} e^{-q_\| |z|} = V_{q_\|}^{2D} e^{-q_\| |z|} \ . \tag{7.71}$$

The Coulomb potential of a quasi-$2D$ structure, Eq. (7.59), follows from this general result in the limit $q_\| |z| \ll 1$.

The matrix elements of the Coulomb interaction $V_{q_\|}(z_1 - z_2)$ between two electrons at the perpendicular positions z_1 and z_2 described by the

envelope functions $\zeta_n(z_i)$ are

$$\boldsymbol{V_{n',m';m,n}(q_\parallel) =}$$
$$\boldsymbol{V^{2D}_{q_\parallel}} \int \boldsymbol{dz_1} \int \boldsymbol{dz_2 \zeta_{n'}(z_2) \zeta_{m'}(z_1) e^{q_\parallel |z_2 - z_1|} \zeta_m(z_1) \zeta_n(z_2)} \; . \quad (7.72)$$

Coulomb potential for multi-band quantum wells

The interaction Hamiltonian in the multi-subband situation is

$$\hat{\mathcal{H}}_C = \frac{1}{2} \sum_{\substack{n',m';n,m \\ \mathbf{k},\mathbf{k}',\mathbf{q},s,s'}} V_{n',m';m,n}(q) \hat{a}^\dagger_{n',\mathbf{k}'-\mathbf{q},s'} \hat{a}^\dagger_{m',\mathbf{k}+\mathbf{q},s} \hat{a}_{m,\mathbf{k},s} \hat{a}_{n,\mathbf{k}',s'} \; . \quad (7.73)$$

Here, the vectors $\mathbf{k}, \mathbf{k}', \mathbf{q}$ are all momentum wave vectors in the plane of the quantum well. The resulting exchange energy is

$$E_{exc} = -\frac{1}{2} \sum_{m,n,\mathbf{k},\mathbf{q},s} V_{m,n;m,n}(q) f_{m,\mathbf{k}-\mathbf{q}} f_{n,\mathbf{k}} \; , \quad (7.74)$$

where $f_{m,\mathbf{k}}$ is the occupation probability of state $m, \mathbf{k}$ and the term $q = 0$ has to be excluded.

7.5 Quasi-One-Dimensional Electron Gas

Motivated by the success of semiconductor quantum-well structures in permitting the study of quasi-two-dimensional phenomena, there is strong interest in structures with even more pronounced quantum confinement effects. Examples are the quantum wires where electrons and holes are free to move in one space dimension, and the quantum dots where the carriers are confined in all three space dimensions. Quantum dots will be discussed separately later in this book. In this section, we analyze some of the basic physical properties of electrons in quantum wires. Quantum wires have been made in different sophisticated ways, always adding quantum confinement to restrict the free carrier motion to one dimension. The additional confinement potentials have been generated through various techniques, such as growth of structures on specially prepared substrates, using grooves, etching of quantum wells, ion implantation, or with the help of induced stresses

in the material below a quantum well.

The analysis of the confinement effects in quantum wires has to be done carefully. If we simply put the transverse coordinates $x = y = 0$, we would find that the resulting one-dimensional Coulomb potential has several pathological features. Loudon showed already in the year 1959 that the ground-state energy of an electron–hole pair is infinite in one dimension.

In order to obtain a regularized Coulomb potential, we consider a quasi-one-dimensional quantum wire with a finite but small extension in the quantum-confined directions. We use the envelope function approximation for the carrier wave functions and average the Coulomb potential with the transverse quantized envelope functions. This way, we obtain a mathematically well-defined, nonsingular interaction potential. The simplest example is a cylindrical quantum wire of radius R with infinite lateral boundaries. For this case, the envelope wave function corresponding to the lowest confinement energy level is

$$\phi(\rho) = \frac{J_0(\alpha_0 \rho / R)}{\sqrt{\pi} R J_1(\alpha_0)} \ , \tag{7.75}$$

where $J_n(\rho)$ is the radial Bessel function of order n. The corresponding confinement energy is

$$E_e = \frac{\alpha_0^2 \hbar^2}{2 m_e R^2} \ , \tag{7.76}$$

and $\alpha_0 = 2.405$ is the first zero of $J_0(x) = 0$. The denominator in Eq. (7.75) results from the normalization of the wave function (see problem 7.3).

The quasi-one-dimensional ($q1D$) Coulomb potential between two electrons is obtained by averaging the three-dimensional Coulomb potential with the radial envelope functions :

$$\boldsymbol{V^{q1D}(z_1, z_2) = \frac{e^2}{\epsilon_0 \pi^2 R^4 J_1^4(\alpha_0)} \int_0^R d\rho_1 \rho_1 \int_0^R d\rho_2 \rho_2 \int_0^{2\pi} d\theta_1 \int_0^{2\pi} d\theta_2}$$
$$\boldsymbol{\times \frac{J_0^2(\alpha_0 \rho_1 / R) J_0^2(\alpha_0 \rho_2 / R)}{\sqrt{(z_1 - z_2)^2 + (\rho_1 \cos\theta_1 - \rho_2 \cos\theta_2)^2 + (\rho_1 \sin\theta_1 - \rho_2 \sin\theta_2)^2}}} \ . \tag{7.77}$$

quasi-1D Coulomb potential

This quasi-one-dimensional Coulomb potential is finite at $z \equiv z_1 - z_2 = 0$

and can be approximated quite well by the simple regularized potential

$$V^{q1D}(z) = \frac{e^2}{\epsilon_0} \frac{1}{|z| + \gamma R} \ , \tag{7.78}$$

where γ is a fitting parameter which has the value $\gamma \simeq 0.3$. As shown in Fig. 7.4, the potential (7.78) is finite at $z = 0$, and varies as $1/z$ for large distances.

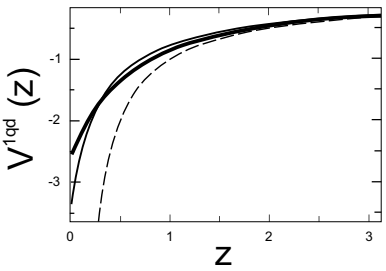

Fig. 7.4 The quasi-one-dimensional Coulomb potential according to Eq. (7.77) as function of particle separation z (thick solid line). The dashed curve is a Coulomb potential, and the thin solid line is the regularized Coulomb potential, Eq. (7.78), for $\gamma = 0.3$.

From Eq. (7.46) we see that the quasi-one-dimensional exchange energy for a thermal electron gas is

$$E^{q1D}_{exc} = -\frac{1}{2} \sum_{\mathbf{k},\mathbf{k}',s} V^{q1D}_{|\mathbf{k}-\mathbf{k}'|} f_k \, f_{k'} \ , \tag{7.79}$$

where V^{q1D}_k is the Fourier transform with respect to z of (7.77) or its approximation (7.78). At $T = 0$, Eq. (7.79) yields

$$E^{q1D}_{exc} = -\frac{1}{2} \sum_{\mathbf{k},\mathbf{k}',s} V^{q1D}_{|\mathbf{k}-\mathbf{k}'|} \theta(E_F - E_k) \, \theta(E_F - E_{k'}) \ , \tag{7.80}$$

and the one-dimensional density is

$$n = \frac{k_F}{\pi} \ . \tag{7.81}$$

REFERENCES

C. Kittel, *Quantum Theory of Solids*, Wiley and Sons, New York (1967)
R. Loudon, Am. J. Phys. **27**, 649 (1959)
D. Pines, *Elementary Excitations in Solids*, Benjamin, New York, (1966)

For the Coulomb interaction in quantum wires see e.g.:

R. Loudon, Am. J. Phys. **44**, 1064 (1976)
L. Banyai, I. Galbraith, C. Ell, and H. Haug, Phys. Rev. **B36**, 6099 (1987)

PROBLEMS

Problem 7.1: Use the Hamiltonian (7.29) and the Hartree–Fock wave function (7.34) to compute the ground-state energy with the $3D$ and the $2D$ Coulomb interaction potentials, respectively. Hint: Use the expansion in terms of Legendre polynomials

$$\begin{aligned}
\frac{1}{|\mathbf{k}-\mathbf{k}'|^2} &= \frac{1}{k^2}\sum_{n,n'}\left(\frac{k'}{k}\right)^{\mathrm{n+n'}} P_n(\cos\theta)P_{n'}(\cos\theta) \text{ for } k' < k \\
&= \frac{1}{k'^2}\sum_{n,n'}\left(\frac{k}{k'}\right)^{\mathrm{n+n'}} P_n(\cos\theta)P_{n'}(\cos\theta) \text{ for } k < k' \\
\frac{1}{|\mathbf{k}-\mathbf{k}'|} &= \frac{1}{k}\sum_{n}\left(\frac{k'}{k}\right)^{n} P_n(\cos\theta) \text{ for } k' < k \\
&= \frac{1}{k'}\sum_{n}\left(\frac{k}{k'}\right)^{n} P_n(\cos\theta) \text{ for } k < k'
\end{aligned}$$

and the integrals

$$\int_{-1}^{1} d\cos\theta\, P_n(\cos\theta) P_{n'}(\cos\theta) = \frac{2}{2n+1}\delta_{n,n'}$$

$$\int_0^{2\pi} d\theta\, P_n(\cos\theta) = 2\pi \left[\frac{1}{2^n}\begin{pmatrix} n \\ n/2 \end{pmatrix}\right]^2 \text{ for } n \text{ even}$$

$$= 0 \text{ for } n \text{ odd } .$$

Problem 7.2: Compute the pair correlation function (7.50) for the $3D$ and $2D$ case. Prove that $R_{ss}(\mathbf{r}-\mathbf{r}') \to 0$ for $r \to \mathrm{r}'$.

Problem 7.3: Evaluate the Coulomb matrix elements for the two lowest subbands of a infinitely high quantum well confinement potential.

Problem 7.4: Compute the properly normalized envelope wave function corresponding to the lowest eigenvalue for a quantum wire of radius R and infinite confinement barriers.

This page intentionally left blank

Chapter 8

Plasmons and Plasma Screening

In this chapter, we discuss collective excitations in the electron gas. As mentioned earlier, *collective excitations* are excitations that belong to the entire system. The collective excitations of the electron gas (= plasma) are called *plasmons*. These excitations and their effect on the dielectric constant are discussed in Chap. 1 in the framework of classical electrodynamics. In this chapter, we now develop the corresponding second-quantized formalism, which reveals that electron–electron pair excitations occur which influence the dielectric constant and other properties in fundamental ways. The excitations in the electron plasma are responsible for screening of the Coulomb potential, effectively reducing it to a potential whose interaction range is reduced with increasing plasma density. A simplified description of the screening is developed in terms of an effective collective excitation, and this is referred to as the plasmon pole approximation.

8.1 Plasmons and Pair Excitations

In order to analyze elementary excitations of the electron plasma, we compute the dynamical evolution of a charge density fluctuation. In the formalism of second quantization, we evaluate the equation of motion for the expectation value of the electron charge density operator

$$\langle \hat{\rho}_{e,\mathbf{q}} \rangle = -\frac{|e|}{L^3} \sum_{\mathbf{k},s} \langle \hat{a}^\dagger_{\mathbf{k}-\mathbf{q},s} \hat{a}_{\mathbf{k},s} \rangle \tag{8.1}$$

defined in Eq. (7.24). In a spatially homogeneous equilibrium system, this expectation value would vanish for $q \neq 0$, however, we assume here a spatially inhomogeneous charge density distribution.

To simplify the notation in the remainder of this book, we suppress from now on the superscript ˆ for operators, unless this is needed to avoid misunderstandings. Furthermore, the spin index is only given where necessary. In all other cases, it can be assumed to be included in the quasi-momentum subscript.

In the following, we can also drop the subscript e of the charge density operator, since we discuss only electrons in this chapter. With this simplified notation Eq. (8.1) becomes

$$\langle \rho_{\mathbf{q}} \rangle = -\frac{|e|}{L^3} \sum_{\mathbf{k}} \langle a^\dagger_{\mathbf{k}-\mathbf{q}} a_{\mathbf{k}} \rangle \ . \tag{8.2}$$

To obtain the equation of motion for $\langle \rho_{\mathbf{q}} \rangle$, we use the Heisenberg equation for $a^\dagger_{\mathbf{k}-\mathbf{q}} a_{\mathbf{k}}$

$$\frac{d}{dt} a^\dagger_{\mathbf{k}-\mathbf{q}} a_{\mathbf{k}} = \frac{i}{\hbar} [\mathcal{H},\, a^\dagger_{\mathbf{k}-\mathbf{q}} a_{\mathbf{k}}] \tag{8.3}$$

with the electron gas Hamiltonian

$$\mathcal{H} = \sum_{\mathbf{k}} E_k a^\dagger_{\mathbf{k}} a_{\mathbf{k}} + \frac{1}{2} \sum_{\substack{\mathbf{k},\mathbf{k}' \\ \mathbf{q}\neq 0}} V_q a^\dagger_{\mathbf{k}-\mathbf{q}} a^\dagger_{\mathbf{k}'+\mathbf{q}} a_{\mathbf{k}'} a_{\mathbf{k}} \ . \tag{8.4}$$

Evaluating the commutators on the RHS of Eq. (8.3), we get for the kinetic term

$$\frac{i}{\hbar} \sum_{\mathbf{k}'} E_{k'} [a^\dagger_{\mathbf{k}'} a_{\mathbf{k}'}, a^\dagger_{\mathbf{k}-\mathbf{q}} a_{\mathbf{k}}] = i(\epsilon_{k-q} - \epsilon_k) a^\dagger_{\mathbf{k}-\mathbf{q}} a_{\mathbf{k}} \ , \tag{8.5}$$

where we have again introduced the frequencies

$$\epsilon_k = E_k/\hbar \quad \text{and} \quad \epsilon_{k-q} = \epsilon_{|\mathbf{k}-\mathbf{q}|} = E_{|\mathbf{k}-\mathbf{q}|}/\hbar \ . \tag{8.6}$$

For the Coulomb term, we obtain

$$\begin{aligned} &\sum \frac{iV_p}{2\hbar} \ [a^\dagger_{\mathbf{k}'-\mathbf{p}} a^\dagger_{\mathbf{p}'+\mathbf{p}} a_{\mathbf{p}'} a_{\mathbf{k}'} \ , \ a^\dagger_{\mathbf{k}-\mathbf{q}} a_{\mathbf{k}}] = \\ &= \sum \frac{iV_p}{2\hbar} \Big(a^\dagger_{\mathbf{k}-\mathbf{q}-\mathbf{p}} a^\dagger_{\mathbf{p}'+\mathbf{p}} a_{\mathbf{p}'} a_{\mathbf{k}} - a^\dagger_{\mathbf{k}'-\mathbf{p}} a^\dagger_{\mathbf{k}-\mathbf{q}+\mathbf{p}} a_{\mathbf{k}'} a_{\mathbf{k}} \\ &\qquad + a^\dagger_{\mathbf{k}-\mathbf{q}} a^\dagger_{\mathbf{k}'-\mathbf{p}} a_{\mathbf{k}-\mathbf{p}} a_{\mathbf{k}'} - a^\dagger_{\mathbf{k}-\mathbf{q}} a^\dagger_{\mathbf{p}'+\mathbf{p}} a_{\mathbf{p}'} a_{\mathbf{k}+\mathbf{p}} \Big) \ . \end{aligned} \tag{8.7}$$

After renaming $\mathbf{p}$ to **-** $\mathbf{p}$, using $V_{-p} = V_p$, and rearranging some operators, we see that the first and second term and the third and fourth term become identical.

Collecting all contributions of the commutator in (8.3), and taking the expectation value, we obtain

$$\frac{d}{dt}\langle a^\dagger_{\mathbf{k-q}} a_{\mathbf{k}}\rangle = i(\epsilon_{k-q} - \epsilon_k)\langle a^\dagger_{\mathbf{k-q}} a_{\mathbf{k}}\rangle + \frac{i}{\hbar}\sum_{\mathbf{p}',\mathbf{p}} V_p \left(\langle a^\dagger_{\mathbf{k-q-p}} a^\dagger_{\mathbf{p}'+\mathbf{p}} a_{\mathbf{p}'} a_{\mathbf{k}}\rangle + \langle a^\dagger_{\mathbf{k-q}} a^\dagger_{\mathbf{p}'-\mathbf{p}} a_{\mathbf{k-p}} a_{\mathbf{p}'}\rangle\right). \quad (8.8)$$

Since we are interested in $\langle \rho_{\mathbf{q}}\rangle$, we have to solve Eq. (8.8) and sum over $\mathbf{k}$. However, we see from Eq. (8.8) that the two-operator dynamics is coupled to four-operator terms. One way to proceed therefore would be to compute the equation of motion for the four-operator term. Doing this we find that the four-operator equation couples to six-operator terms, which in turn couple to eight-operator terms, etc. Hence, if we follow this approach we obtain an infinite hierarchy of equations, which we have to truncate at some stage in order to get a closed set of coupled differential equations.

Instead of deriving such a hierarchy of equations, we make a factorization approximation directly in Eq. (8.8), splitting the four-operator expectation values into products of the relevant two-operator expectation values. For the one-component plasma under consideration, we choose the combinations

$$\langle a^\dagger_{\mathbf{k-q}} a_{\mathbf{k}}\rangle \text{ and } \langle a^\dagger_{\mathbf{k}} a_{\mathbf{k}}\rangle = f_k \quad (8.9)$$

as relevant, assuming that these terms dominate the properties of our system. This approximation scheme is often called *random phase approximation* (RPA). In (8.9), $f_{\mathbf{k}}$ denotes the carrier distribution function which is the Fermi–Dirac distribution function for electrons in thermodynamic equilibrium. However, our approximations are also valid for nonequilibrium distributions.

A hand-waving argument for the random phase approximation is to say that an expectation value $\langle a^\dagger_{\mathbf{k}} a_{\mathbf{k}'}\rangle$ has a dominant time dependence

$$\langle a^\dagger_{\mathbf{k}} a_{\mathbf{k}'}\rangle \propto e^{i(\omega_{\mathbf{k}} - \omega_{\mathbf{k}'})t} \quad . \quad (8.10)$$

These expectation values occur under sums, so that expressions like

$$\sum_{\mathbf{k},\mathbf{k}'} e^{i(\omega_{\mathbf{k}}-\omega_{\mathbf{k}'})t}$$

have to be evaluated. Since terms with $\mathbf{k} \neq \mathbf{k}'$ oscillate rapidly they more or less average to zero, whereas the term with $\mathbf{k} = \mathbf{k}'$ gives the dominant contribution.

Technically, when we make the RPA approximation, we pick specific combinations of wave numbers from the sums on the RHS of Eq. (8.8), factorize the four-operator expectation values into the expressions (8.9), and ignore all other contributions. For example, in the term

$$T_1 = \frac{i}{\hbar} \sum_{\mathbf{p}',\mathbf{p}\neq 0} V_p \langle a^\dagger_{\mathbf{k}-\mathbf{q}-\mathbf{p}} a^\dagger_{\mathbf{p}'+\mathbf{p}} a_{\mathbf{p}'} a_{\mathbf{k}} \rangle \tag{8.11}$$

we choose $\mathbf{p} = -\mathbf{q}$ and obtain

$$T_1 \simeq \frac{iV_q}{\hbar} \sum_{\mathbf{p}'} \langle a^\dagger_{\mathbf{k}} a^\dagger_{\mathbf{p}'-\mathbf{q}} a_{\mathbf{p}'} a_{\mathbf{k}} \rangle \ , \tag{8.12}$$

where $V_q = V_{-q}$ since the Coulomb potential depends only on the absolute value of $\mathbf{q}$. Now we commute $a_{\mathbf{k}}$ in (8.12) to the left:

$$T_1 \simeq \frac{iV_q}{\hbar} \sum_{\mathbf{p}'} \left(-\langle a^\dagger_{\mathbf{k}} a_{\mathbf{p}'} \rangle \delta_{\mathbf{p}'-\mathbf{q},\mathbf{k}} + \langle a^\dagger_{\mathbf{k}} a_{\mathbf{k}} a^\dagger_{\mathbf{p}'-\mathbf{q}} a_{\mathbf{p}'} \rangle \right) \ . \tag{8.13}$$

Factorizing the four-operator expectation value and using (8.9) yields

$$T_1 \simeq \frac{iV_q}{\hbar} \left(-\langle a^\dagger_{\mathbf{k}} a_{\mathbf{k}+\mathbf{q}} \rangle + f_{\mathbf{k}} \sum_{\mathbf{p}'} \langle a^\dagger_{\mathbf{p}'-\mathbf{q}} a_{\mathbf{p}'} \rangle \right) \ . \tag{8.14}$$

Similarly, for the second Coulomb term in Eq. (8.8),

$$T_2 = \frac{i}{\hbar} \sum_{\mathbf{p}',\mathbf{p}\neq 0} V_p \langle a^\dagger_{\mathbf{k}-\mathbf{q}} a^\dagger_{\mathbf{p}'-\mathbf{p}} a_{\mathbf{k}-\mathbf{p}} a_{\mathbf{p}'} \rangle \ , \tag{8.15}$$

we select $\mathbf{p} = \mathbf{q}$ and commute the first destruction operator to the left to get

$$T_2 \simeq \frac{iV_q}{\hbar} \sum_{\mathbf{p}'} \left(\langle a^\dagger_{\mathbf{k}-\mathbf{q}} a_{\mathbf{p}'} \rangle \delta_{\mathbf{p}',\mathbf{k}} - \langle a^\dagger_{\mathbf{k}-\mathbf{q}} a_{\mathbf{k}-\mathbf{q}} a^\dagger_{\mathbf{p}'-\mathbf{q}} a_{\mathbf{p}'} \rangle \right) \ , \tag{8.16}$$

or, after factorization,

$$T_2 \simeq \frac{iV_q}{\hbar}\left(\langle a^\dagger_{\mathbf{k}-\mathbf{q}} a_{\mathbf{k}}\rangle - f_{\mathbf{k}-\mathbf{q}} \sum_{\mathbf{p}'} \langle a^\dagger_{\mathbf{p}'-\mathbf{q}} a_{\mathbf{p}'}\rangle\right) . \tag{8.17}$$

Inserting the approximation (8.14) and (8.17) into Eq. (8.8) yields

$$\frac{d}{dt}\langle a^\dagger_{\mathbf{k}-\mathbf{q}} a_{\mathbf{k}}\rangle \simeq i(\epsilon_{k-q} - \epsilon_k)\langle a^\dagger_{\mathbf{k}-\mathbf{q}} a_{\mathbf{k}}\rangle + \frac{iV_q}{\hbar}(f_{\mathbf{k}} - f_{\mathbf{k}-\mathbf{q}}) \sum_{\mathbf{p}'} \langle a^\dagger_{\mathbf{p}'-\mathbf{q}} a_{\mathbf{p}'}\rangle . \tag{8.18}$$

In order to find the eigenfrequencies of the charge density, we use the ansatz

$$\langle a^\dagger_{\mathbf{k}-\mathbf{q}} a_{\mathbf{k}}\rangle(t) = e^{-i(\omega + i\delta)t}\langle a^\dagger_{\mathbf{k}-\mathbf{q}} a_{\mathbf{k}}\rangle(0) \ , \tag{8.19}$$

in Eq. (8.18) to obtain

$$\hbar(\omega + i\delta + \epsilon_{k-q} - \epsilon_k)\langle a^\dagger_{\mathbf{k}-\mathbf{q}} a_{\mathbf{k}}\rangle = V_q(f_{\mathbf{k}-\mathbf{q}} - f_{\mathbf{k}}) \sum_{\mathbf{p}'} \langle a^\dagger_{\mathbf{p}'-\mathbf{q}} a_{\mathbf{p}'}\rangle \ . \tag{8.20}$$

Dividing both sides by $\hbar(\omega + i\delta + \epsilon_{k-q} - \epsilon_k)$, summing the resulting equation over $\mathbf{k}$, and multiplying by $-e/L^3$, we find

$$\langle \rho_{\mathbf{q}}\rangle = V_q \langle \rho_{\mathbf{q}}\rangle \sum_{\mathbf{k}} \frac{f_{\mathbf{k}-\mathbf{q}} - f_{\mathbf{k}}}{\hbar(\omega + i\delta + \epsilon_{k-q} - \epsilon_k)} \ . \tag{8.21}$$

We see that $\langle \rho_{\mathbf{q}}\rangle$ cancels, so that

$$V_q \sum_{\mathbf{k}} \frac{f_{\mathbf{k}-\mathbf{q}} - f_{\mathbf{k}}}{\hbar(\omega + i\delta + \epsilon_{k-q} - \epsilon_k)} = 1 \ . \tag{8.22}$$

Introducing the first-order approximation $P^1(q,\omega)$ to the *polarization function* $P(q,\omega)$ as

$$P^1(q,\omega) = \sum_{\mathbf{k}} \frac{f_{\mathbf{k}-\mathbf{q}} - f_{\mathbf{k}}}{\hbar(\omega + i\delta + \epsilon_{k-q} - \epsilon_k)} \ , \tag{8.23}$$

we can write Eq. (8.22) as

$$V_q \, P^1(q,\omega) = 1 \ . \tag{8.24}$$

The real part of this equation determines the eigenfrequencies $\omega = \omega_q$:

$$V_q \sum_{\mathbf{k}} \frac{f_{\mathbf{k}-\mathbf{q}} - f_{\mathbf{k}}}{\hbar(\omega_q + \epsilon_{k-q} - \epsilon_k)} = 1 \ , \tag{8.25}$$

where we let $\delta \to 0$.

To analyze the solutions of Eq. (8.25), we first discuss the long wavelength limit for a three dimensional plasma. Long wave length means $\lambda \to \infty$, and hence $q \propto 1/\lambda \to 0$. We expand Eq. (8.25) in terms of q and drop higher-order corrections. Using

$$E_{k-q} - E_k = \frac{\hbar^2}{2m}(k^2 - 2\mathbf{k}\cdot\mathbf{q} + q^2) - \frac{\hbar^2 k^2}{2m} \simeq -\frac{\hbar^2 \mathbf{k}\cdot\mathbf{q}}{m} \tag{8.26}$$

and

$$f_{\mathbf{k}-\mathbf{q}} - f_{\mathbf{k}} = f_{\mathbf{k}} - \mathbf{q}\cdot\nabla_{\mathbf{k}} f_{\mathbf{k}} + \cdots - f_{\mathbf{k}} \simeq -\mathbf{q}\cdot\nabla_{\mathbf{k}} f_{\mathbf{k}} \tag{8.27}$$

in Eq. (8.25) yields

$$\begin{aligned} 1 &\simeq -V_q \sum_{\mathbf{k},i} \frac{q_i \frac{\partial f}{\partial k_i}}{\hbar\omega_0 - \hbar^2 \mathbf{k}\cdot\mathbf{q}/m} \\ &\simeq -\frac{V_q}{\hbar\omega_0} \sum_{\mathbf{k},i} q_i \frac{\partial f}{\partial k_i} \left(1 + \frac{\hbar\mathbf{k}\cdot\mathbf{q}}{m\omega_0}\right) \ , \end{aligned} \tag{8.28}$$

where we have set $\omega_{q\to 0} = \omega_0$. The first term vanishes since, after evaluation of the sum, it is proportional to the distribution function for $k \to \infty$. So we are left with

$$1 = -\frac{V_q}{\hbar\omega_0} \sum_{\mathbf{k},i} q_i \frac{\partial f}{\partial k_i} \frac{\hbar\mathbf{k}\cdot\mathbf{q}}{m\omega_0} \ . \tag{8.29}$$

Partial integration gives

$$1 = V_q \frac{q^2}{m\omega_0^2} \sum_{\mathbf{k}} f_{\mathbf{k}} = V_q \frac{q^2 N}{m\omega_0^2} = \frac{4\pi e^2}{\epsilon_0 q^2 L^3} \frac{q^2 N}{m\omega_0^2} \ , \tag{8.30}$$

or

$$\omega_0^2 = \frac{4\pi e^2 n}{\epsilon_0 m} = \omega_{pl}^2 \ , \tag{8.31}$$

showing that in the long wave-length limit, $q \to 0$, $\omega_{q\to 0} = \omega_{pl}$, i.e., we recover the classical result for the eigenfrequency of the electron plasma. The only difference to the plasma frequency defined in Eq. (1.26) is the factor of $1/\epsilon_0$ which results from the fact that we include the background dielectric constant in the present chapter.

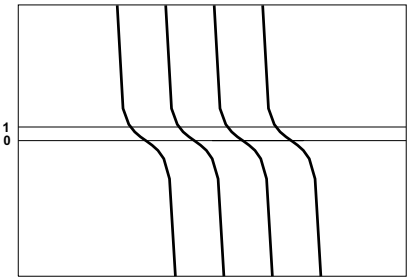

Fig. 8.1 Graphical solution of Eq. (8.25). The full lines are a schematic drawing of part of the LHS of Eq. (8.25) and the line "1" is the RHS of Eq. (8.25).

Next, we discuss the solution of Eq. (8.25) for general wave lengths. First we write the LHS of Eq. (8.25) in the form

$$V_q \sum_{\mathbf{k}} \frac{f_{\mathbf{k}-\mathbf{q}} - f_{\mathbf{k}}}{\hbar(\omega_q + \epsilon_{k-q} - \epsilon_k)} = V_q \sum_{\mathbf{k}} \frac{f_{\mathbf{k}}}{\hbar} \left(\frac{1}{\omega_q + \epsilon_k - \epsilon_{k+q}} - \frac{1}{\omega_q + \epsilon_{k-q} - \epsilon_k} \right) . \tag{8.32}$$

This expression shows that poles occur at

$$\omega_q = \epsilon_{k+q} - \epsilon_k = \frac{\hbar k q}{m} \cos\theta + \frac{\hbar q^2}{2m} \tag{8.33}$$

and

$$\omega_q = \epsilon_k - \epsilon_{k-q} = \frac{\hbar q k}{m} \cos\theta - \frac{\hbar q^2}{2m} \ , \tag{8.34}$$

where θ is the angle between $\mathbf{k}$ and $\mathbf{q}$. As schematically shown in Fig. 8.1, we can find the solutions of Eq. (8.25) as the intersections of the LHS of Eq. (8.25) with the straight line "1", which is the RHS of Eq. (8.25). From Fig. 8.1 we see that these intersection points are close to the poles of the LHS.

For illustration, we discuss in the following the situation of a thermalized electron plasma at low-temperatures. Here, we know that the extrema of

the allowed k values are $k' = \pm k_F$. Considering only $\omega_q > 0$, we obtain from Eq. (8.33)

$$\omega_q^{max} = \frac{\hbar q k_F}{m} + \frac{\hbar q^2}{2m} \ , \tag{8.35}$$

for $\cos(\theta) = 1$ and

$$\omega_q^{min} = -\frac{\hbar q k_F}{m} + \frac{\hbar q^2}{2m} \ , \tag{8.36}$$

for $\cos\theta = -1$. From Eq. (8.34) we get no solution for $\cos\theta = -1$ and for $\cos\theta = 1$ we obtain

$$\omega_q^{ext} = \frac{\hbar q k_F}{m} - \frac{\hbar q^2}{2m} \ . \tag{8.37}$$

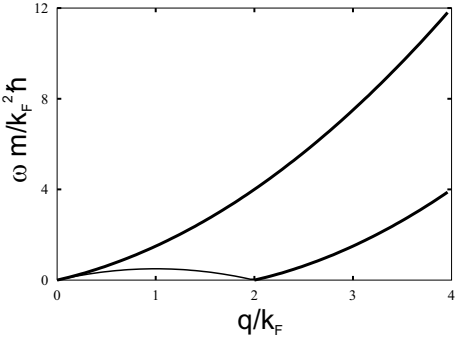

Fig. 8.2 The thick lines show the boundary of the continuum of pair excitations at $T = 0\,K$, according to Eqs. (8.35) and (8.36), respectively. The thin line is the result of Eq. (8.37).

As shown in Fig. 8.2, Eqs. (8.35) and (8.36) define two parabolas that are displaced from the origin by $\pm k_F$. The region between these parabolas for $\omega_q > 0$ is the region where we find the poles. Physically these solutions represent the transition of an electron form $\mathbf{k}$ to $\mathbf{k} \pm \mathbf{q}$, i.e., these are *pair excitations*. They are called pair excitations because the pair of states $\mathbf{k}$ and $\mathbf{k} \pm \mathbf{q}$ is involved in the transition. The region between the parabolas is therefore called the *continuum of electron–pair excitations*. These pair

excitations are not to be confused with electron–hole pairs, which we discuss in later chapters of this book. Note, that the pair excitations need an empty final state to occur, and at low temperatures typically involve scattering from slightly below the Fermi surface to slightly above.

The lack of empty final states for scattering with small momentum transfer prevents conduction in an insulator, although there is no lack of electrons. When a plasma mode hits the continuum of pair excitations, it gets damped heavily (Landau damping), causing the collective plasmon excitation to decay into pair excitations. At finite temperatures the boundaries of the pair-excitation spectrum are not sharp, but qualitatively the picture remains similar to the $T = 0$ result.

8.2 Plasma Screening

One of the most important effects of the many-body interactions in an electron plasma is the phenomenon of plasma screening. To discuss plasma screening quantum mechanically, we start with the effective single particle Hamiltonian

$$\mathcal{H} = \int d^3r\, \psi^\dagger(\mathbf{r}) \left(-\frac{\hbar^2 \nabla^2}{2m} \right) \psi(\mathbf{r}) + \int d^3r\, V_{eff}(r) \psi^\dagger(\mathbf{r}) \psi(\mathbf{r}) \ , \tag{8.38}$$

where

$$V_{eff}(r) = V(r) + V_{ind}(r) \tag{8.39}$$

is the sum of the Coulomb potential $V(r)$ of a test charge and the induced potential $V_{ind}(r)$ of the screening particles. The effective potential V_{eff} has to be determined self-consistently. The Fourier transform of Eq. (8.38) is

$$\mathcal{H} = \sum_{\mathbf{k}} E_k a^\dagger_{\mathbf{k}} a_{\mathbf{k}} + \sum_{\mathbf{p}} V_{eff}(p) \sum_{\mathbf{k}} a^\dagger_{\mathbf{k}+\mathbf{p}} a_{\mathbf{k}} \ , \tag{8.40}$$

and the equation of motion for $a^\dagger_{\mathbf{k}-\mathbf{q}} a_{\mathbf{k}}$ is

$$\begin{aligned} \frac{d}{dt} a^\dagger_{\mathbf{k}-\mathbf{q}} a_{\mathbf{k}} &= \frac{i}{\hbar} [\mathcal{H}, a^\dagger_{\mathbf{k}-\mathbf{q}} a_{\mathbf{k}}] \\ &= i(\epsilon_{k-q} - \epsilon_k) a^\dagger_{\mathbf{k}-\mathbf{q}} a_{\mathbf{k}} \\ &\quad - \frac{i}{\hbar} \sum_{\mathbf{p}} V_{eff}(p) (a^\dagger_{\mathbf{k}-\mathbf{q}} a_{\mathbf{k}-\mathbf{p}} - a^\dagger_{\mathbf{k}+\mathbf{p}-\mathbf{q}} a_{\mathbf{k}}) \ . \end{aligned} \tag{8.41}$$

Using the random phase approximation in the last two terms and taking the expectation value yields

$$\frac{d}{dt}\langle a^\dagger_{\mathbf{k-q}} a_{\mathbf{k}}\rangle = i(\epsilon_{k-q} - \epsilon_k)\langle a^\dagger_{\mathbf{k-q}} a_{\mathbf{k}}\rangle - \frac{iV_{eff}(q)}{\hbar}(f_{\mathbf{k-q}} - f_{\mathbf{k}}) \ . \tag{8.42}$$

We assume that the test charge varies in time as $\exp(-i(\omega+i\delta)t)$, where $\omega+i\delta$ establishes an adiabatic switch-on of the test charge potential. Making the ansatz that the driven density has the same time dependence

$$\langle a^\dagger_{\mathbf{k-q}} a_{\mathbf{k}}\rangle \propto e^{-i(\omega+i\delta)t} \ , \tag{8.43}$$

Eq. (8.42) yields

$$\hbar(\omega + i\delta + \epsilon_{k-q} - \epsilon_k)\langle a^\dagger_{\mathbf{k-q}} a_{\mathbf{k}}\rangle = V_{eff}(q)(f_{\mathbf{k-q}} - f_{\mathbf{k}}) \ , \tag{8.44}$$

and therefore

$$\langle a^\dagger_{\mathbf{k-q}} a_{\mathbf{k}}\rangle = V_{eff}(q)\frac{f_{\mathbf{k-q}} - f_{\mathbf{k}}}{\hbar(\omega + i\delta + \epsilon_{k-q} - \epsilon_k)} \ , \tag{8.45}$$

or, after multiplication by $-|e|/L^3$ and summation over $\mathbf{k}$,

$$\langle \rho_q\rangle = -\frac{|e|}{L^3}V_{eff}(q)P^1(q,\omega) \ , \tag{8.46}$$

where P^1 again is the polarization function defined in Eq. (8.23) and ρ_q is defined in Eq. (8.2).

The potential of the screening particles obeys Poisson's equation in the form

$$\nabla^2 V_{ind}(r) = \frac{4\pi|e|\rho(r)}{\epsilon_0} \ . \tag{8.47}$$

Taking the Fourier transform and using (8.46), Poisson's equation becomes

$$\begin{aligned} V_{ind}(q) &= -\frac{4\pi|e|}{\epsilon_0 q^2}\rho_q = \frac{4\pi e^2}{\epsilon_0 q^2 L^3}V_{eff}(q)P^1(q,\omega) \\ &= V_q\, V_{eff}(q)P^1(q,\omega) \ . \end{aligned} \tag{8.48}$$

Inserting (8.48) into the Fourier-transform of Eq. (8.39):

$$V_{eff}(q) = V_q + V_{ind}(q) \ , \tag{8.49}$$

yields

$$V_{eff}(q) = V_q[1 + V_{eff}(q)P^1(q,\omega)] \tag{8.50}$$

or

$$V_{eff}(q) = \frac{V_q}{1 - V_q P^1(q,\omega)} = \frac{V_q}{\epsilon(q,\omega)} \equiv V_s(q,\omega) \ . \tag{8.51}$$

Here, we introduced $V_s(q,\omega)$ as the *dynamically screened Coulomb potential*. The dynamic dielectric function $\epsilon(q,\omega)$ is given by

$$\epsilon(q,\omega) = 1 - V_q P^1(q,\omega) \ , \tag{8.52}$$

or, using Eq. (8.23)

$$\boldsymbol{\epsilon(q,\omega) = 1 - V_q \sum_{\mathbf{k}} \frac{f_{\mathbf{k-q}} - f_{\mathbf{k}}}{\hbar(\omega + i\delta + \epsilon_{k-q} - \epsilon_k)}} \ . \tag{8.53}$$

Lindhard formula for the longitudinal dielectric function

The Lindhard formula describes a complex retarded dielectric function, i.e., the poles are in the lower complex frequency plane, and it includes spatial dispersion (q dependence) and temporal dispersion (ω dependence). Eq. (8.53) is valid both in 3 and 2 dimensions. In the derivation, we sometimes used the $3D$ expressions, but that could have been avoided without changing the final result. Note, that the expectation value $f_{\mathbf{k}}$ of the particle density operator is equal to the Fermi–Dirac distribution function f_k for a thermal plasma. However, Eq. (8.53) is valid also for nonequilibrium distribution functions.

The longitudinal plasma eigenmodes are obtained from

$$\mathbf{Re}[\boldsymbol{\epsilon(q,\omega)}] = \mathbf{0} \quad \text{or} \quad \mathbf{1 = V_q Re}[\boldsymbol{P^1(q,\omega)}] \ . \tag{8.54}$$

longitudinal eigenmodes

This equation is identical to the plasma eigenmode equation (8.25). Hence, our discussion of plasma screening of the Coulomb potential and of the col-

lective plasma oscillations obtained from $\epsilon(q,\omega)=0$, shows that screening and plasmons are intimately related phenomena.

8.3 Analysis of the Lindhard Formula

To appreciate the Lindhard (or RPA) result, we discuss some important limiting cases in $3D$ and $2D$ systems.

8.3.1 *Three Dimensions*

In the long wave-length limit, $q \to 0$, we repeat the steps described by Eqs. (8.26) – (8.31) to obtain

$$\epsilon(0,\omega) = 1 - \frac{\omega_{pl}^2}{\omega^2} \ , \tag{8.55}$$

the classical (or Drude) dielectric function, which is the same as the result obtained for the oscillator model in Chap. 1.

In the static limit, $\omega + i\delta \to 0$, Eq. (8.53) yields

$$\epsilon(q,0) = 1 - V_q \sum_{\mathbf{k}} \frac{f_{k-q} - f_k}{E_{k-q} - E_k} \ . \tag{8.56}$$

Using the expansions (8.26) and (8.27) again and assuming a thermal equilibrium Fermi–Dirac carrier distribution, we can write

$$\sum_i q_i \frac{\partial f_k}{\partial k_i} = -\sum_i q_i \frac{\partial f_k}{\partial \mu}\frac{\partial \epsilon_k}{\partial k_i} = -\sum_i q_i \, k_i \frac{\hbar^2}{m}\frac{\partial f_k}{\partial \mu} \ . \tag{8.57}$$

This way we find

$$\begin{aligned}\epsilon(q,0) &= 1 + \frac{4\pi e^2}{\epsilon_0 q^2}\frac{\partial}{\partial \mu}\frac{1}{L^3}\sum_{\mathbf{k}} f_k \\ &= 1 + \frac{4\pi e^2}{\epsilon_0 q^2}\frac{\partial n}{\partial \mu} \equiv 1 + \frac{\kappa^2}{q^2} \ .\end{aligned} \tag{8.58}$$

Here, we introduced

$$\boldsymbol{\kappa = \sqrt{\frac{4\pi e^2}{\epsilon_0}\frac{\partial n}{\partial \mu}}} \tag{8.59}$$

3*D* screening wave number

as the inverse *screening length*, i.e., the *screening wave number*. Using (8.58) in (8.51) we find the statically screened potential

$$\boldsymbol{V_s(q) = \frac{4\pi e^2}{\epsilon_0 L^3}\frac{1}{q^2+\kappa^2} = \frac{V_q}{\epsilon(q,0)}} \ . \tag{8.60}$$

3*D* statically screened Coulomb potential

This result shows nicely how the plasma screening removes the divergence at $q \to 0$ from the Coulomb potential. Taking the Fourier transformation of Eq. (8.60) yields

$$V_s(r) = \sum_{\mathbf{q}} \frac{4\pi e^2}{\epsilon_0 L^3 (q^2+\kappa^2)} e^{i\mathbf{q}\cdot\mathbf{r}} = \frac{e^2}{\epsilon_0 r} e^{-\kappa r} \ , \tag{8.61}$$

compare Eqs. (7.31) – (7.32) without the limit $\gamma \to 0$. The statically screened Coulomb potential is plotted in Fig. 8.3 together with the bare potential. The comparison shows that the long-ranged bare Coulomb potential is screened to a distance $1/\kappa$. The statically Coulomb potential, Eq. (8.61) is often called Yukawa potential.

The inverse screening length given by Eq. (8.59) can be evaluated analytically for the two limiting cases of i) a degenerate electron gas where the Fermi function is the unit-step function and ii) for the nondegenerate case where the distribution function is approximated as Boltzmann distribution. In the literature, the theory of screening in the degenerate ($T = 0$) electron gas is often referred to as *Thomas–Fermi screening*. In Chap. 6, where we discussed some properties of the degenerate electron gas, we found that the

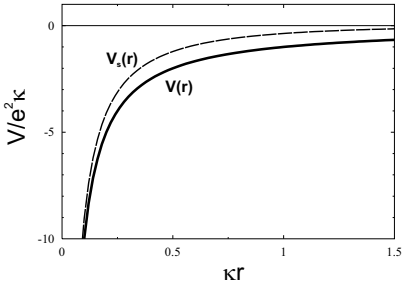

Fig. 8.3 Statically screened (thin line) and unscreened (thick line) Coulomb potential for a three-dimensional system.

density can be written as

$$n = \frac{1}{2\pi^2}\left(\frac{2m}{\hbar^2}\right)^{3/2}\frac{2}{3}E_F^{3/2} \ , \tag{8.62}$$

where the Fermi energy $E_F \equiv \mu(T=0)$. From Eq. (8.62) we obtain

$$\frac{\partial n}{\partial \mu} = \frac{3}{2}\frac{n}{E_F} \ , \tag{8.63}$$

so that the screening wave number (8.59) in this case becomes

$$\boldsymbol{\kappa = \sqrt{\frac{6\pi e^2 n}{\epsilon_0 E_F}}} \ . \tag{8.64}$$

3*D* Thomas–Fermi screening wave number

The theory of screening in the nondegenerate limit is known as *Debye–Hückel screening*. For this case, we approximate the Fermi distribution by the Boltzmann distribution and use Eq. (6.27) to obtain the derivative of the chemical potential as

$$\frac{\partial \mu}{\partial n} = \frac{1}{\beta n} \ . \tag{8.65}$$

Inserting this into Eq. (8.59) yields

$$\boldsymbol{\kappa = \sqrt{\frac{4\pi e^2 n\beta}{\epsilon_0}}} \ . \tag{8.66}$$

3*D* Debye–Hückel screening wave number

8.3.2 *Two Dimensions*

To investigate the long wave-length limit of the Lindhard formula for a two-dimensional system, we again insert the expansions (8.26) – (8.28) into Eq. (8.53) to obtain

$$\epsilon(q \to 0, \omega) - 1 = V_q \frac{L^2}{m\omega^2} 2 \int \frac{d^2k}{(2\pi)^2} \sum_{i,j} q_i q_j k_j \frac{\partial f_k}{\partial k_i} \ , \tag{8.67}$$

where the factor 2 comes from the spin summation implicitly included in $\sum_{\mathbf{k}}$. Partial integration on the RHS of Eq. (8.67) yields with

$$2 \int \frac{d^2k}{(2\pi)^2} k_j \frac{\partial f_k}{\partial k_i} = -2 \int \frac{d^2k}{(2\pi)^2} f_k \frac{\partial k_j}{\partial k_i} = -n\, \delta_{ij}$$

the Drude result

$$\epsilon(q \to 0, \omega) = 1 - \frac{\omega_{pl}^2(q)}{\omega^2} \ , \tag{8.68}$$

where n is the $2D$ particle density N/L^2. In Eq. (8.68), we introduced the $2D$ plasma frequency

$$\boldsymbol{\omega_{pl}(q) = \sqrt{\frac{2\pi e^2 n}{\epsilon_0 m}} q} \ . \tag{8.69}$$

2*D* plasma frequency

To study the static limit, $\omega = 0$, of the Lindhard formula, we use the $2D$ Coulomb potential, Eq. (7.59), and obtain

$$\epsilon(q, 0) = 1 + V_q \frac{\partial n}{\partial \mu}$$

so that

$$\boldsymbol{\epsilon(q,0) = 1 + \frac{\kappa}{q}}\,, \tag{8.70}$$

$2D$ static dielectric function

where the inverse screening length in quasi-two dimensions is

$$\kappa = \frac{2\pi e^2}{\epsilon_0}\frac{\partial n}{\partial \mu} \ . \tag{8.71}$$

Hence, the statically screened $2D$ Coulomb potential is

$$V_s(q) = \frac{2\pi e^2}{\epsilon_0 L^2}\frac{1}{q+\kappa} \ . \tag{8.72}$$

For the chemical potential of the two-dimensional Fermi gas, we have the explicit result given in Eq. (6.41):

$$\beta\mu(n,T) = \ln\left(e^{\hbar^2\beta\pi n/m} - 1\right) \ . \tag{8.73}$$

Hence, we obtain

$$\frac{\partial \mu}{\partial n} = \frac{\hbar^2\pi}{m}\frac{1}{1 - e^{-\hbar^2\beta\pi n/m}} \tag{8.74}$$

and thus

$$\kappa = \frac{2me^2}{\epsilon_0\hbar^2}(1 - e^{-\hbar^2\beta\pi n/m}) \ . \tag{8.75}$$

Using the explicit expression for the $2D$ chemical potential, it is easy to verify that

$$1 - e^{-\hbar^2\beta\pi n/m} = f_{k=0} \ , \tag{8.76}$$

where f_k is the Fermi–Dirac distribution of the carriers. Combining (8.75) and (8.76), the $2D$ screening wave number assumes the simple form

$$\boldsymbol{\kappa = \frac{2me^2}{\epsilon_0 \hbar^2} f_{k=0}} \ . \tag{8.77}$$

$2D$ screening wave number

This expression is correct for all densities and temperatures. It is interesting to note that the screening wave number in $2D$ becomes independent of the density for low temperature and high densities, whereas the corresponding $3D$ result always remains density-dependent.

8.3.3 *One Dimension*

One could continue along the lines of the three- and two-dimensional analysis and discuss the RPA screening also for quantum wires. However, we prefer not to describe these developments, but rather point out a general trend of the dimensionality dependence of screening. Let us consider for example two electrons. In a bulk material, all field lines between these two charges can be screened by other optically excited charged particles. In quantum wells, already some of the field lines pass through the barrier material. Since the optically excited electrons of holes are confined to the quantum well, the lines in the barrier material cannot be screened. Simultaneously, the density of states is reduced in $2D$ as compared to $3D$. Correspondingly, the influence of screening in $2D$ is considerably weaker than in $3D$, whereas the effects of state filling become more pronounced. This trend continues if one passes from $2D$ quantum wells to quasi-one-dimensional quantum wires as illustrated in Fig. 8.4.

Obviously, only the field lines very close to the wire axis can be screened. Considering at the same time the further reduced density of states, one can conclude that screening effects may often be neglected in comparison with the dominating state filling effects. In Chap. 13, we present an example where we compute the nonlinear optical properties of quantum wires, clearly showing that the results are influenced only weakly by screening.

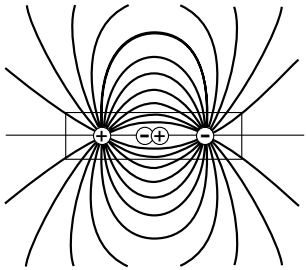

Fig. 8.4 Schematic drawing of the field lines in a quantum wire.

8.4 Plasmon–Pole Approximation

Equations (8.55) and (8.68) show that in the long wave-length limit, both in $3D$ and $2D$, the inverse dielectric function

$$\frac{1}{\epsilon(q \to 0, \omega)} = \frac{\omega^2}{(\omega + i\delta)^2 - \omega_{pl}^2} = 1 + \frac{\omega_{pl}^2}{(\omega + i\delta)^2 - \omega_{pl}^2} \tag{8.78}$$

has just one pole. We use this observation to construct an approximation for the full dielectric function $\epsilon(q, \omega)$, which tries to replace the continuum of poles contained in the Lindhard formula by one effective plasmon pole at ω_q :

$$\boldsymbol{\frac{1}{\epsilon(q,\omega)} = 1 + \frac{\omega_{pl}^2}{(\omega + i\delta)^2 - \omega_q^2}} \ . \tag{8.79}$$

plasmon–pole approximation

The effective plasmon frequency ω_q is chosen to fulfill certain sum rules (Mahan, 1981) which can be derived from the Kramers–Kronig relation, Eq. (1.23),

$$\epsilon'(q,\omega) - 1 = \frac{2}{\pi} P \int_0^\infty d\omega' \frac{\omega' \epsilon''(q,\omega')}{\omega'^2 - \omega^2} \ . \tag{8.80}$$

We make use of the static long wave-length limit, which for $3D$ is given by Eq. (8.58),

$$\epsilon'(q,0) - 1 = \frac{\kappa^2}{q^2} = \frac{2}{\pi} \lim_{q\to 0} P \int_0^\infty d\omega' \frac{\epsilon''(q,\omega')}{\omega'} \quad . \tag{8.81}$$

This is the so-called conductivity sum rule. According to Eq. (8.79), we have

$$\epsilon(q,\omega) = \frac{\omega^2 - \omega_q^2}{(\omega + i\delta - \Omega_q)(\omega + i\delta + \Omega_q)} \tag{8.82}$$

where

$$\Omega_q^2 = \omega_q^2 - \omega_{pl}^2 \quad . \tag{8.83}$$

Using the Dirac identity in Eq. (8.82) and inserting the result into the RHS of Eq. (8.81), we find

$$\frac{\kappa^2}{q^2} = \frac{\omega_{pl}^2}{\Omega_q^2} \quad , \tag{8.84}$$

where $\lim_{q\to 0}$ is implied. Eq. (8.84) yields

$$\lim_{q\to 0} \omega_q^2 = \omega_{pl}^2 \left(1 + \frac{q^2}{\kappa^2}\right) \quad . \tag{8.85}$$

Following Lundquist (1967), we therefore choose the form

$$\boldsymbol{\omega_q^2 = \omega_{pl}^2 \left(1 + \frac{q^2}{\kappa^2}\right) + \nu_q^2} \quad . \tag{8.86}$$

$3D$ effective plasmon frequency

The last term ν_q^2 in this equation is added in order to simulate the contribution of the pair continuum. Usually we take

$$\nu_q^2 = C\, q^4 \quad , \tag{8.87}$$

where C is a numerical constant. Practical applications show that it is often sufficient to use the much simpler plasmon–pole approximation instead of

the full RPA dielectric function to obtain reasonable qualitative results for the effects of screening.

Similarly, one gets for two-dimensional systems (see problem 8.2)

$$\omega_q^2 = \omega_{pl}^2(q)\left(1 + \frac{q}{\kappa}\right) + \nu_q^2 \tag{8.88}$$

as the effective $2D$ plasmon frequency.

REFERENCES

G.D. Mahan, *Many Particle Physics*, Plenum Press, New York (1981)
B.I. Lundquist, Phys. Konden. Mat. **6**, 193 and 206 (1967)
D. Pines and P. Nozieres, *The Theory of Quantum Liquids*, Benjamin, Reading, Mass. (1966)

For the modifications of the plasmon–pole approximation in an electron–hole plasma see, e.g.:

R. Zimmermann, *Many-Particle Theory of Highly Excited Semiconductors*, Teubner, Berlin (1988)
H. Haug and S. Schmitt–Rink, Prog. Quantum Electron. **9**, 3 (1984)

PROBLEMS

Problem 8.1: Use the quasi-$2D$ Coulomb potential

$$V_k = \frac{2\pi e^2}{L^2 \epsilon_0 k}$$

and apply the classical theory outlined in Chap. 1 to verify that the $2D$ plasma frequency is given by Eq. (8.69).

Problem 8.2: Derive the effective plasmon frequency, Eq. (8.88), of the $2D$ plasmon–pole approximation.

Chapter 9

Retarded Green's Function for Electrons

In the treatment of the classical oscillator model in Chap. 1, we have seen how a retarded Green's function determines the response of the oscillator to a driving field. In this chapter, we will now discuss how a retarded Green's function can also be introduced for quantum-mechanical many-body systems, such as the electron gas of Chap. 7. The retarded Green's function contains information about the spectral properties of the system, i.e., about the changes of the single-particle energies which occur due to the interactions with other particles of fields. Furthermore, retarded Green's functions of many-body systems determine the linear response to external fields in the same way as for the classical oscillator.

9.1 Definitions

We define the retarded Green's function for electrons as

$$G^r_{ss'}(\mathbf{r}t,\mathbf{r}'t') = -\frac{i}{\hbar}\theta(t-t')\langle[\psi_s(\mathbf{r},t)\,,\,\psi^\dagger_{s'}(\mathbf{r}',t')]_+\rangle \ . \tag{9.1}$$

The average $\langle\dots\rangle$ stands for tr $(\rho\dots)$, the statistical operator ρ being taken at some fixed initial time, e.g., $t=-\infty$. Due to the step function $\theta(t-t')$, G^r is retarded with $G^r(t,t')=0$ for $t'>t$.

Let us express the retarded Green's function in terms of its two operator products

$$\begin{aligned} G^r_{ss'}(\mathbf{r}t,\mathbf{r}'t') &= \theta(t-t')\Big[-\frac{i}{\hbar}\langle\psi_s(\mathbf{r},t)\psi^\dagger_{s'}(\mathbf{r}',t')\rangle - \frac{i}{\hbar}\langle\psi^\dagger_{s'}(\mathbf{r}',t')\psi_s(\mathbf{r},t)\rangle\Big] \\ &\equiv \theta(t-t')\Big[G^>_{ss'}(\mathbf{r}t,\mathbf{r}'t') - G^<_{ss'}(\mathbf{r}t,\mathbf{r}'t')\Big] \ . \end{aligned} \tag{9.2}$$

Here, we have defined two new Green's functions $G^>$ (speak G greater) and $G^<$ (speak G lesser). They can be considered as generalizations of the reduced density matrix for a two-time-dependent correlation function. In particular $G^<$ is called the particle propagator. Its equal time limit is up to the factor $i/\hbar$ identical to the single-particle reduced density matrix. It describes the kinetics in nonequilibrium systems, where one has to calculate not only the spectral properties contained in (9.1), but also the evolution of the particle distribution over these renormalized states, as will be outlined further in the appendix.

The following manipulations show that, as its classical counterpart, the quantum mechanical Green's function G^r also obeys a differential equation with an inhomogeneity given by delta functions in space and time. The equation of motion for the retarded Green's function is

$$\begin{aligned} i\hbar\frac{\partial}{\partial t}G^r_{ss'}(\mathbf{r}t,\mathbf{r}'t') &= \frac{\partial\theta(t-t')}{\partial t}\langle[\psi_s(\mathbf{r},t),\psi^\dagger_{s'}(\mathbf{r}',t')]_+\rangle \\ &\quad -\frac{i}{\hbar}\theta(t-t')\langle\left[i\hbar\frac{\partial\psi_s(\mathbf{r},t)}{\partial t},\psi^\dagger_{s'}(\mathbf{r}',t')\right]_+\rangle \\ &= \delta(t-t')\langle[\psi_s(\mathbf{r},t),\psi^\dagger_{s'}(\mathbf{r}',t)]_+\rangle \\ &\quad -\frac{i}{\hbar}\theta(t-t')\langle[[\psi_s(\mathbf{r},t),\mathcal{H}(t)],\psi^\dagger_{s'}(\mathbf{r}',t')]_+\rangle \ , \end{aligned} \tag{9.3}$$

where the Heisenberg equation $i\hbar\,\partial\psi/\partial t = [\psi,\mathcal{H}]$ has been used. The equal time anti-commutator in the first term of Eq. (9.3) is

$$[\psi_s(\mathbf{r},t),\psi^\dagger_{s'}(\mathbf{r}'t)]_+ = \delta(\mathbf{r}-\mathbf{r}')\delta_{s,s'} \ , \tag{9.4}$$

so that a differential equation for the Green's function results which has a singular inhomogeneity in space and time:

$$i\hbar\frac{\partial}{\partial t}G^r_{ss'}(\mathbf{r}t,\mathbf{r}'t') = \delta(t-t')\delta(\mathbf{r}-\mathbf{r}')\delta_{s,s'}$$
$$-\frac{i}{\hbar}\theta(t-t')\langle\left[[\psi_s(\mathbf{r},t),\mathcal{H}(t)],\psi^\dagger_{s'}(\mathbf{r}',t')\right]_+\rangle\,. \tag{9.5}$$

equation of motion for retarded Green's function

Let us first consider the ideal Fermi gas with the Hamiltonian (6.4). Evaluating the commutator in the second term on the RHS of Eq. (9.5) we obtain the equation of motion for this simple case as

$$\left(i\hbar\frac{\partial}{\partial t}+\frac{\hbar^2\nabla^2}{2m}\right)G^r_{0,ss'}(\mathbf{r}t,\mathbf{r}'t') = \delta(t-t')\delta(\mathbf{r}-\mathbf{r}')\delta_{s,s'}\ . \tag{9.6}$$

Here, we introduced the subscript 0 to indicate that we are dealing with the noninteracting situation. Eq. (9.6) shows that G^r_0 is diagonal in the spin indices and depends only on the relative coordinates $\boldsymbol{\rho}=\mathbf{r}-\mathbf{r}'$ and $\tau=t-t'$. Taking the Fourier transform of Eq. (9.6) with respect to $\boldsymbol{\rho}$ and τ and introducing the notation

$$G^r_{0,ss'}(\boldsymbol{\rho},\tau) = \sum_{\mathbf{k}}\int\frac{d\omega}{2\pi}e^{i(\mathbf{k}\cdot\boldsymbol{\rho}-\omega\tau)}G^r_{0,ss'}(\mathbf{k},\omega)\ , \tag{9.7}$$

the Green's function equation for the ideal Fermi gas becomes

$$\left(\hbar\omega-\frac{\hbar^2k^2}{2m}\right)G^r_{0,ss'}(\mathbf{k},\omega) = \delta_{s,s'}\ , \tag{9.8}$$

or

$$G^r_{0,ss'}(\mathbf{k},\omega) = \delta_{s,s'}\frac{1}{\hbar(\omega-\epsilon_k+i\delta)}\ , \tag{9.9}$$

with $\hbar\epsilon_k=\hbar^2k^2/2m$. In Eq. (9.9), we included the infinitesimal imaginary part $+i\delta$ which shifts the poles to the lower half of the complex frequency plane. As discussed in Chap. 1, this shift guarantees the correct retardation, i.e., $G^r(\tau<0)=0$. It is seen from Eq. (9.9) that the poles of the retarded Green's function give the single-particle energies $\hbar\epsilon_k$.

It is worthwhile to look at the time variation of the free particle retarded Green function by taking the Fourier transform of (9.9)

$$\begin{aligned} G^r_{0,ss'}(\mathbf{k}, t-t') &= \int \frac{d\omega}{2\pi} G^r_{0,ss'}(\mathbf{k},\omega) e^{-i\omega(t-t')} \\ &= \int \frac{d\omega}{2\pi} \delta_{s,s'} \frac{e^{-i\omega(t-t')}}{\hbar(\omega - \epsilon_k + i\delta)} \\ &= -i\delta_{s,s'}\theta(t-t') e^{-i\epsilon_k(t-t')} \ . \end{aligned} \tag{9.10}$$

Here, we used the same complex integration arguments as discussed in the context of Eq. (1.63). From the resulting expression in Eq. (9.10) we see that the retarded free-electron Green's function oscillates in time simply with the kinetic energy of the electron.

9.2 Interacting Electron Gas

Writing the electron gas Hamiltonian of Chap. 7 in terms of field creation and destruction operators, we obtain

$$\begin{aligned} \mathcal{H} = &\sum_s \int d^3r \psi^\dagger_s(\mathbf{r}) \left(-\frac{\hbar^2\nabla^2}{2m} \right) \psi_s(\mathbf{r}) \\ &+ \frac{1}{2} \sum_{s,s'} \int d^3r\, d^3r' \psi^\dagger_s(\mathbf{r}) \psi^\dagger_{s'}(\mathbf{r}') \frac{e^2}{\epsilon_0 |\mathbf{r}-\mathbf{r}'|} \psi_{s'}(\mathbf{r}') \psi_s(\mathbf{r}) \\ &- \sum_s \int d^3r\, d^3r' \psi^\dagger_s(\mathbf{r}) \frac{e^2 n(\mathbf{r}')}{\epsilon_0 |\mathbf{r}-\mathbf{r}'|} \psi_s(\mathbf{r}) + \frac{e^2}{2} \int d^3r\, d^3r' \frac{n(\mathbf{r}) n(\mathbf{r}')}{\epsilon_0 |\mathbf{r}-\mathbf{r}'|} \ , \end{aligned} \tag{9.11}$$

where $n(\mathbf{r})$ is the background charge distribution, which is not treated as an operator in the jellium approximation. With the Hamiltonian (9.11), we evaluate the commutator in Eq. (9.5):

$$\begin{aligned} [\psi_s(\mathbf{r},t), \mathcal{H}(t)] = &-\frac{\hbar^2\nabla^2}{2m} \psi_s(\mathbf{r},t) \\ &+ \sum_{s''} \int d^3r'' V(\mathbf{r}-\mathbf{r}'') \psi^\dagger_{s''}(\mathbf{r}'',t) \psi_{s''}(\mathbf{r}'',t) \psi_s(\mathbf{r},t) \\ &- \int d^3r'' V(\mathbf{r}-\mathbf{r}'')\, n(\mathbf{r}'')\, \psi_s(\mathbf{r},t) \ . \end{aligned} \tag{9.12}$$

Inserting Eq. (9.12) into Eq. (9.5), we see that the Coulomb interaction gives rise to two additional terms in the equation of motion:

$$-\frac{i}{\hbar}\theta(t-t')\int d^3r'' V(\mathbf{r}-\mathbf{r}'')\Big\{\sum_{s''}\langle[\psi^\dagger_{s''}(\mathbf{r}'',t)\psi_{s''}(\mathbf{r}'',t)\psi_s(\mathbf{r},t)\,,\,\psi^\dagger_{s'}(\mathbf{r}',t')]_+\rangle$$
$$-n(\mathbf{r}'')\langle[\psi_s(\mathbf{r},t),\psi^\dagger_{s'}(\mathbf{r}',t')]_+\rangle\Big\}\ . \tag{9.13}$$

Hence, as a consequence of the interaction, higher order Green's functions with more than two electron operators also appear. The simplest possible approximation is to factorize the four-operator expectation values in the first term of Eq. (9.13) into products of two-operator expectation values. These can be arranged into two terms, each containing a retarded Green's function:

$$-\frac{i}{\hbar}\theta(t-t')\langle[\psi^\dagger_{s''}(\mathbf{r}'',t)\psi_{s''}(\mathbf{r}'',t)\psi_s(\mathbf{r},t)\,,\,\psi^\dagger_{s'}(\mathbf{r}',t')]_+\rangle \tag{9.14}$$
$$\simeq \langle\psi^\dagger_{s''}(\mathbf{r}'',t)\psi_{s''}(\mathbf{r}'',t)\rangle G^r_{ss'}(\mathbf{r}t,\mathbf{r}'t') - \langle\psi^\dagger_{s''}(\mathbf{r}'',t)\psi_s(\mathbf{r},t)\rangle G^r_{s''s}(\mathbf{r}''t,\mathbf{r}'t')\ .$$

The minus sign in the second term arises because we had to commute two electron annihilation operators before taking the expectation values. Inserting Eq. (9.14) into Eq. (9.13) yields

$$\int d^3r''\,V(\mathbf{r}-\mathbf{r}'')\left\{\left[\sum_{s''}\langle\psi^\dagger_{s''}(\mathbf{r}'',t)\psi_{s''}(\mathbf{r}'',t)\rangle - n(\mathbf{r}'')\right]G^r_{ss'}(\mathbf{r}t,\mathbf{r}'t')\right.$$
$$\left.-\sum_{s''}\langle\psi^\dagger_{s''}(\mathbf{r}'',t)\psi_s(\mathbf{r},t)\rangle G^r_{s''s'}(\mathbf{r}''t,\mathbf{r}'t')\right\}\ . \tag{9.15}$$

The first term, also called the *Hartree term*, contributes only if charge neutrality is locally disturbed, i.e., if

$$\sum_{s''}\langle\psi^\dagger_{s''}(\mathbf{r}'',t)\psi_{s''}(\mathbf{r}'',t)\rangle \neq n(\mathbf{r}'')\ . \tag{9.16}$$

However, the second term, also called *Fock* or *exchange term*, always yields an energy reduction due to the exchange-hole around each Fermion, as discussed in Chap. 7.

Generally, the Green's function equation of motion for an interacting system can be written in the form of a *Dyson equation*:

$$\left(i\hbar\frac{\partial}{\partial t} - \frac{\hbar^2\nabla^2}{2m}\right) G^r_{ss'}(\mathbf{r}t, \mathbf{r}'t') = \delta(t-t')\delta(\mathbf{r}-\mathbf{r}')\delta_{s,s'}$$
$$+ \sum_{s''} \int d^3r''\, dt''\hbar\Sigma^r_{ss''}(\mathbf{r}t, \mathbf{r}''t'')G^r_{s''s'}(\mathbf{r}''t'', \mathbf{r}'t') \ . \tag{9.17}$$

Dyson equation for retarded Green's function

Here, we have introduced Σ^r as the *retarded self-energy* which combines all those terms appearing as a consequence of the many-body interaction. In order to reproduce the results of our factorization approximation, we have to choose the Hartree–Fock self-energy as

$$\hbar\Sigma^r_{ss''}(\mathbf{r}t, \mathbf{r}''t'') = \delta(t-t'')\Big\{\delta(\mathbf{r}-\mathbf{r}'')\delta_{s,s''}$$
$$\times \int d^3r_1\, V(\mathbf{r}-\mathbf{r}_1)\Big[\sum_{s_1}\langle\psi^\dagger_{s_1}(\mathbf{r}_1,t)\psi_{s_1}(\mathbf{r}_1,t)\rangle - n(\mathbf{r_1})\Big]$$
$$- V(\mathbf{r}-\mathbf{r}'')\langle\psi^\dagger_{s''}(\mathbf{r}'',t)\psi_s(\mathbf{r},t)\rangle\Big\} \ , \tag{9.18}$$

where the second term is the *exchange self-energy*. The Hartree–Fock self-energy approximation is instantaneous, i.e., not retarded.

For homogeneous stationary systems, G^r and Σ^r depend only on the relative coordinates $\mathbf{r}-\mathbf{r}' = \boldsymbol{\rho}$ and $t-t' = \tau$, and not on the center-of-mass coordinates $(\mathbf{r}+\mathbf{r}')/2$ and $(t+t')/2$. Furthermore, we assume for simplicity that the Green's function and the self-energy are both diagonal in the spin index. Taking the Fourier transform with respect to $\boldsymbol{\rho}$ and τ, as defined in Eq. (9.7), the Dyson equation (9.17) takes the form

$$\left(\hbar\omega - \frac{\hbar^2k^2}{2m}\right) G^r_{ss}(\mathbf{k},\omega) = 1 + \hbar\Sigma^r_{ss}(\mathbf{k},\omega)G^r_{ss}(\mathbf{k},\omega) \tag{9.19}$$

or

$$\boldsymbol{G^r_{ss}(\mathbf{k},\omega) = \frac{1}{\hbar[\omega + i\delta - \epsilon_k - \Sigma^r_{ss}(\mathbf{k},\omega)]}} \ . \tag{9.20}$$

retarded electron Green's function

Equation (9.20) shows that the free-particle energy ϵ_k is replaced by $\epsilon_k + \Sigma^r(\mathbf{k},\omega)$ as a consequence of the interactions, thus explaining the origin of the name *self-energy*. Usually, the self-energy is a complex frequency-dependent function. In the static limit ($\omega = 0$), the real part of Σ^r yields a shift of the single-particle energies due to the many-body interactions, and the imaginary part describes the corresponding broadening (inverse damping time).

As illustrative example, we now evaluate the self-energy, Eq. (9.18), for spatially and temporally homogeneous systems. As mentioned earlier, the Hartree term vanishes in this case as a consequence of charge neutrality. For the exchange term, we get

$$\hbar\Sigma^r_{exc,ss}(\mathbf{k},\omega) = -\sum_{\mathbf{q}} V_{|\mathbf{k}-\mathbf{q}|} n_{\mathbf{q}} \ , \tag{9.21}$$

where $\psi(\mathbf{r},t) = \sum_{\mathbf{k}} e^{i\mathbf{k}\cdot\mathbf{r}} a_{\mathbf{k}}(t)$ (with $L^3 \equiv 1$ for simplicity) and

$$\begin{aligned} \langle \psi^\dagger(\mathbf{r}'',t)\psi(\mathbf{r},t)\rangle &= \sum_{\mathbf{k},\mathbf{k}'} \langle a^\dagger_{\mathbf{k}'}(t) a_{\mathbf{k}}(t)\rangle e^{i(\mathbf{k}\cdot\mathbf{r} - \mathbf{k}'\cdot\mathbf{r}'')} \\ &= \sum_{\mathbf{k}} n_{\mathbf{k}}\, e^{i\mathbf{k}\cdot(\mathbf{r}-\mathbf{r}'')} \end{aligned} \tag{9.22}$$

have been used. For a thermal electron distribution, $n_{\mathbf{k}}$ is given by the Fermi distribution f_k, and the exchange self-energy is

$$\hbar\Sigma^r_{exc,ss}(\mathbf{k},\omega) = -\sum_{\mathbf{q}} V_{|\mathbf{k}-\mathbf{q}|} f_q \ . \tag{9.23}$$

Hence, as a consequence of the exchange interaction, all single-particle energies $\hbar\epsilon_k$ are replaced by the renormalized energies

$$\hbar e_k = \hbar\epsilon_k + \hbar\Sigma^r_{exc}(k) \ . \tag{9.24}$$

In order to estimate the numerical value of the energy shift for the case of a degenerate electron plasma, we approximate the relevant momentum

transfer by the Fermi wave number

$$|\mathbf{k}-\mathbf{q}| \simeq k_F \ . \tag{9.25}$$

Then Eq. (9.23) yields

$$\hbar\Sigma^r_{exc,ss} \simeq -\sum_{\mathbf{q}} V_{k_F} f_q = -\frac{1}{2} V_{k_F} n \ , \tag{9.26}$$

where the factor $1/2$ appears since we do not sum over the spin. Using the expression for the Fermi wave number, Eq. (6.22), and the three-dimensional Coulomb potential, Eq. (7.33), we see that the exchange energy varies with the plasma density as

$$\hbar\Sigma^r_{exc,ss} \simeq -\frac{2}{3^{2/3}\pi^{1/3}} \frac{e^2}{\epsilon_0} n^{1/3} \ . \tag{9.27}$$

Eq. (9.27) shows that the energy reduction per particle increases with increasing plasma density n. This increase is proportional to $n^{1/3}$, i.e., proportional to the inverse mean inter-particle distance. Basically the same result has already been obtained in Eq. (7.47), where we analyzed the total exchange energy of the system. All these results are a consequence of the net energy gain (reduced Coulomb repulsion) resulting from the Pauli exclusion principle causing particles with equal spin to avoid each other. Qualitatively, we can estimate this energy gain as the Coulomb energy $e^2/\epsilon_0 r$ evaluated for $r = n^{-1/3}$.

For a quasi-two dimensional system, we have to evaluate Eq. (9.26) with V_q and k_F given by Eqs. (7.59) and (7.69), respectively. The resulting exchange self-energy varies as $-n^{1/2}$. In two dimensions, the energy gain due to the exchange hole is $(e^2/\epsilon_0)n^{-1/2}$, where $n^{-1/2}$ measures the distance between particles.

9.3 Screened Hartree–Fock Approximation

Semiconductors under optical excitation or with an injected current are ideally suited to study the density-dependent renormalizations of the single-particle energies, because one can vary the plasma density in these systems over many orders of magnitude. To obtain a realistic estimate for the single-particle energy renormalization, we now make use of the plasmon–pole approximation. Basically, we extend the Hartree–Fock approximation of the previous section by replacing the bare Coulomb potential V_q with the

screened one, $V_s(q,\omega) = V_q/\epsilon(q,\omega)$. However, we will see that we have to include a correlation self-energy at the same time, the so-called Coulomb-hole self-energy, which describes the energy reduction due to the depletion shell around a given charged particle.

As a consequence of the frequency dependence of $V_s(q,\omega)$, the resulting retarded self-energy is also frequency-dependent and cannot simply be interpreted as single-particle energy shift. In order to avoid this complication, we restrict our treatment to the static approximation

$$V_s(q) = \frac{V_q}{\epsilon(q,0)} \ . \tag{9.28}$$

Replacing V_q by $V_s(q)$ in the exchange self-energy, Eq. (9.23), we obtain

$$\hbar\boldsymbol{\Sigma}^{\boldsymbol{r}}_{\boldsymbol{exc,ss}}(\boldsymbol{k}) = -\sum_{\mathbf{k'}} \boldsymbol{V_s}(|\mathbf{k}-\mathbf{k'}|)\boldsymbol{f_{k'}} \equiv \hbar\boldsymbol{\Sigma}^{\boldsymbol{r}}_{\boldsymbol{SX}}(\boldsymbol{k}) \ . \tag{9.29}$$

screened exchange self-energy

In Sec. 9.2, we discuss that the momentum transfer in a degenerate plasma is of the order of k_F, allowing us to approximate Eq. (9.29) as

$$\hbar\Sigma^r_{SX}(k \simeq 0) \simeq -\frac{1}{2} n\, V_s(k_F) \ . \tag{9.30}$$

This expression can be evaluated using the plasmon–pole approximation. We obtain for the three-dimensional system

$$\hbar\Sigma^r_{SX} \simeq -\frac{1}{2} n \frac{4\pi e^2}{\epsilon_0 k_F^2} \left(1 - \frac{\omega_{pl}^2}{\omega_{k_F}^2}\right) \ , \tag{9.31}$$

where ω_q^2 and ω_{pl}^2 are given by Eqs. (8.86) and (8.31), respectively. In the two dimensional case, we get

$$\hbar\Sigma^r_{SX} \simeq -\frac{1}{2}\, n\, \frac{2\pi e^2}{\epsilon_0 k_F} \left(1 - \frac{\omega_{pl}^2(k_F)}{\omega_{k_F}^2}\right) \ , \tag{9.32}$$

where Eqs. (8.88) and (8.69)have been used.

A comparison of these results with the experiment and with a detailed derivation shows that the screened exchange self-energy underestimates the true single-particle energy shifts. This is not astonishing since, as we have mentioned before, there has to be an additional contribution due to the

Coulomb correlation effects not included in the Hartree–Fock theory. The corresponding term which appears in addition to the screened exchange self-energy, is called the *Coulomb hole self-energy*, $\sum_{CH}$. The origin of this name is due to the strong reduction of the pair correlation function $R_{ss'}(|\mathbf{r}-\mathbf{r}'|=0)$ also for electrons with different spin, $s \neq s'$, when the proper Coulomb correlations are included in the many-electron wave function. In analogy to the "exchange hole" discussed in Chap. 7, this correlation effect is referred to as "Coulomb hole". Hence, the Coulomb-hole self-energy describes the reduction of the total energy due to the fact that the electrons avoid each other because of their mutual Coulomb repulsion. The renormalized single-particle energy is instead of Eq. (9.24)

$$e_k = \epsilon_k + \Sigma_{SX}(k) + \Sigma_{CH} \quad . \tag{9.24a}$$

The derivation of the Coulomb-hole contribution to the self-energy is presented in later chapters of this book. There, we also discuss the corresponding change of the effective semiconductor band gap. Here, we only want to mention that this contribution can be calculated as the change of the self-interaction of a particle with and without the presence of a plasma, i.e.,

$$\hbar\Sigma_{CH} = \frac{1}{2}\lim_{r\to 0}\left[V_s(r) - V(r)\right] \quad . \tag{9.33}$$

Ignoring for the moment the term $\propto q^4$ in the effective plasmon frequency ω_q of the single-plasmon-pole approximation, one obtains for $V_s(r)$ the Yukawa potential, Eq. (8.61), both in $2d$ and $3d$. Using the Yukawa potential in Eq. (9.33) we obtain the Coulomb-hole self-energy as

$$\Sigma_{CH} = -\frac{e^2}{2\epsilon_0}\kappa \quad , \tag{9.34}$$

where we have included static screening through ϵ_0 and κ is the screening wave number in $2d$ or $3d$, respectively.

For the three-dimensional system, it is possible to improve the result (9.34) by analytically evaluating $V_s(r)$ using the full static plasmon–pole approximation,

$$V_s(r) = \frac{L^3}{(2\pi)^3}\int d^3q V_s(q) e^{-i\mathbf{q}\cdot\mathbf{r}} \quad , \tag{9.35}$$

where

$$V_s(q) = \frac{4\pi e^2}{\epsilon_0 q^2}\left[1 + \frac{1}{1 + \frac{q^2}{\kappa^2} + \left(\frac{\nu_q}{\omega_{pl}}\right)^2}\right] \quad . \tag{9.36}$$

The resulting expression is

$$\begin{aligned} V_s(r) &= \frac{e^2}{\epsilon_0 r} e^{-ra_+}\left[\cos(ra_-) + (4/u^2 - 1)^{-1/2}\sin(ra_-)\right] \quad \text{for} \quad u \le 2 \\ &= \frac{e^2}{2\epsilon_0 r}\left[b_- e^{-rc_+} + b_+ e^{-rc_-}\right] \quad \text{for} \quad u > 2 \ , \end{aligned} \tag{9.37}$$

where

$$u = \frac{\omega_{pl}}{\kappa^2 C^{1/2}} \quad , \quad a_\pm = \frac{\kappa u}{2}\sqrt{\frac{2}{u} \pm 1} \quad , \quad b_\pm = 1 \pm \left(1 - \frac{4}{u^2}\right)^{-1/2} \quad ,$$

and

$$c_\pm = \frac{\kappa u}{\sqrt{2}}\left[1 \pm \left(1 - \frac{4}{u^2}\right)^{1/2}\right]^{1/2} \quad .$$

The screened Coulomb interaction potential according to Eq. (9.37) is plotted in Fig. 9.1 for low and high plasma density and compared to the Yukawa potential, Eq. (8.61), for the same parameter values. A prominent feature that we note is the more effective screening with increasing plasma density causing the strong reduction of the effective Coulomb potential. Whereas the Yukawa potential is always negative, indicating electron–electron repulsion, the plasmon–pole approximation yields an effective Coulomb potential, which becomes attractive at large distances and sufficiently high plasma densities.

Evaluating the Coulomb hole self-energy, Eq. (9.33), for the potential given by Eq. (9.37) we obtain

$$\begin{aligned} \Sigma_{CH} &= -a_0\kappa E_0\left(\tfrac{2}{1-4/u^2}\right)^{1/2}(b_+ - b_-) \qquad \text{for} \quad u \ge 2 \\ &= -a_0\kappa E_0 u\left[(1+\tfrac{2}{u})^{1/2} - (1+\tfrac{2}{u})^{-1/2}\right] \quad \text{for} \quad u < 2 \end{aligned} \tag{9.38}$$

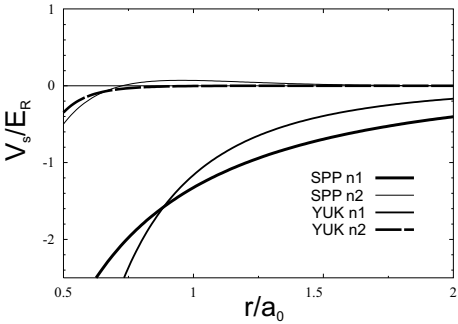

Fig. 9.1 Comparison of the screened Coulomb potential $V_s(r)$ using the single-plasmon-pole approximation (SPP), Eq. (9.37) and the Yukawa potential (YUK), Eq. (8.61), for the plasma densities $n_1 = 10^{-3}\, a_0^{-3}$ and $n_2 = a_0^{-3}$, respectively. Here, a_0 is the $3d$ Bohr radius, and $E_R = E_0$ is given by Eq. (9.39).

where

$$E_0 = \frac{e^2}{2a_0\epsilon_0} = E_R \ . \tag{9.39}$$

An evaluation of Eq. (9.38) is shown in Fig. 9.2 for parameter values which are typical for bulk GaAs. We see that Σ_{CH} varies almost linearly with $1/r_s$ over a wide range of density values.

At the end of this chapter, we want to mention that the retarded Green's function is by no means the only Green's function which obeys a differential equation with a singular inhomogeneity. There exists, e.g., a time-ordered Green's function which is uniquely related to the retarded Green's function in equilibrium systems, but for which one has strict diagrammatic rules for developing perturbative approximations. As already mentioned, the situation is different in nonequilibrium systems, such as optically excited semiconductors. Here, a general nonequilibrium Green's function theory exists, which allows us to calculate not only the spectral properties of the system (contained in the retarded Green's function) but also the kinetic evolution of the distribution of the excitations in the system described by the particle propagator. Furthermore, this general nonequilibrium Green's function theory provides also strict diagrammatic rules for the retarded Green's function. An introduction to the theory of nonequilibrium Green's functions is given in Chap. 21 and Appendix B of this book.

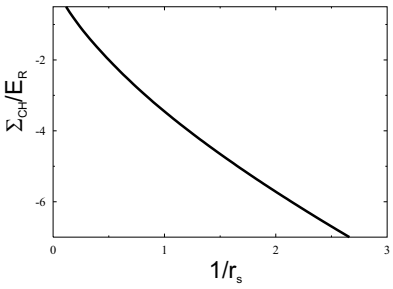

Fig. 9.2 Coulomb hole self-energy, Eq. (9.38), as function of particles density expressed in terms of $1/r_s$, Eq. (7.62). The used parameter values are $a_0 = 1.096 \cdot 10^{-6}$cm, $T = 10$K, $E_0 = 5.32$meV, $m_e/m = 1.12$, $m_h/m = 9.1$, where m is the reduced electron–hole mass.

REFERENCES

S. Doniach and E.H. Sondheimer, *Green's Functions for Solid State Physicists*, Benjamin, Reading, Mass. (1974)
A.L. Fetter and J.D. Walecka, *Quantum Theory of Many-Particle Physics*, McGraw–Hill, New York (1971)
G.D. Mahan, *Many Particle Physics*, Plenum Press, New York (1981)
D. Pines and P. Nozieres, *The Theory of Quantum Liquids*, Benjamin, Reading, Mass. (1966)

PROBLEMS

Problem 9.1: Follow the steps discussed in this chapter to prove Eq. (9.18).

Problem 9.2: Evaluate Eq. (9.18) for a quasi-2d system. Use the approximations discussed for the 3d case to obtain an estimate for the exchange self-energy.

Problem 9.3: Perform the Fourier transform in (9.10) by closing the frequency integration in the upper or lower complex frequency plane depending on the sequence of t and t'.

This page intentionally left blank

Chapter 10

Excitons

In the preceding chapters, we discussed the quantum statistics and the many-body Coulomb effects in an electron plasma with positive background (jellium). The results obtained are clearly relevant for a metal since it has a partially filled conduction band. Moreover, these results are also important for a dielectric medium such as a semiconductor, since they describe the carrier–carrier interactions within the same band, i.e., the *intraband interactions*. However, as already discussed in Chap. 5, the optical properties of semiconductors are mostly related to *interband transitions* between the valence and conduction bands.

As it turns out, one can separate the many-body treatment of the electron–hole system in excited semiconductors quite naturally into the determination of *spectral properties* and *kinetic properties*. As spectral, we denote energy shifts and the broadening due to interactions, i.e., the renormalizations of the states due to the many-body interactions. The kinetics, on the other hand, deals with the development of the particle distributions in the renormalized states. The optical properties are mainly linked with the *interband kinetics*, whereas the transport properties are connected with the *intraband kinetics* of electrons and/or holes, depending on the kind of free carriers in the semiconductor.

The analysis of the semiconductor interband transitions for variable excitation conditions is discussed in the following chapter. In the present chapter, we consider only the low-excitation regime, where an extremely small density of electrons and holes exist. We therefore concentrate on the analysis of one-electron-hole pair effects.

10.1 The Interband Polarization

In Chap. 5, we discussed the optical susceptibility due to free-carrier transitions in semiconductors. In the present chapter, we now generalize this treatment to include also the Coulomb effects. Again, we first compute the optical susceptibility from which we then get the absorption coefficient and the refractive index.

We start by analyzing the macroscopic interband polarization induced by the coherent monochromatic classical light field $\mathbf{E}(\mathbf{r},t)$. The polarization $\mathbf{P}(t)$ is defined as the expectation value of the electric dipole $e\mathbf{r}$ as

$$\begin{aligned}\mathbf{P}(\mathbf{t}) &= \sum_s \int d^3r \, \langle \hat{\psi}_s^\dagger(\mathbf{r},t)\, e\mathbf{r}\, \hat{\psi}_s(\mathbf{r},t)\rangle \\ &= \sum_s \int d^3r \mathrm{tr}[\rho_0 \hat{\psi}_s^\dagger(\mathbf{r},t)\, e\mathbf{r}\, \hat{\psi}_s(\mathbf{r},t)] \ . \end{aligned} \tag{10.1}$$

In Eq. (10.1), the average is taken with the equilibrium statistical operator ρ_0 describing the system at the initial time before the field was switched on. If one introduces the reduced one-particle density matrix $\rho(\mathbf{r},\mathbf{r}',t)$ as the single-time correlation function

$$\rho_{ss'}(\mathbf{r},\mathbf{r}',t) = \langle \hat{\psi}_s^\dagger(\mathbf{r},t)\hat{\psi}_{s'}(\mathbf{r}',t)\rangle \ , \tag{10.2}$$

one can rewrite Eq. (10.1) as

$$\mathbf{P}(t) = \sum_s \int d^3r \, \rho_{ss'}(\mathbf{r},\mathbf{r}',t)|_{r=r',s=s'} e\mathbf{r} \ . \tag{10.3}$$

These general definitions now have to be adapted to a semiconductor by expanding the electron field operators into an appropriate basis.

In the case of a spatially homogeneous system, one is dealing with completely delocalized electrons. Then the Bloch functions $\psi_\lambda(\mathbf{k},\mathbf{r})$ are the appropriate set for expanding the field operators

$$\hat{\psi}_s(\mathbf{r},t) = \sum_{\lambda,\mathbf{k}} a_{\lambda,\mathbf{k},s}(t)\psi_\lambda(\mathbf{k},\mathbf{r}) \ . \tag{10.4}$$

Inserting this expansion into Eq. (10.1) yields

$$\mathbf{P}(t) = \sum_{s,\lambda,\lambda',\mathbf{k},\mathbf{k}'} \langle a^\dagger_{\lambda,\mathbf{k},s} a_{\lambda',\mathbf{k}',s}\rangle \int d^3r \, \psi^*_{\lambda,\mathbf{k}}(\mathbf{r})\, e\mathbf{r}\, \psi_{\lambda',\mathbf{k}'}(\mathbf{r}) \ . \tag{10.5}$$

The integral has been evaluated in Chap. 5, Eqs. (5.11) – (5.20). We use the result (5.20) in the form

$$\int d^3r\, \psi^*_{\lambda,\mathbf{k}}(\mathbf{r})\, e\mathbf{r}\, \psi_{\lambda',\mathbf{k}'}(\mathbf{r}) \simeq \delta_{\mathbf{k},\mathbf{k}'}\mathbf{d}_{\lambda\lambda'} \ , \tag{10.6}$$

where $\lambda \neq \lambda'$. Inserting Eq. (10.6) into Eq. (10.5), we obtain the polarization in a spatially homogeneous system as

$$\mathbf{P}(t) = \sum_{\mathbf{k},s,\lambda,\lambda'} \langle a^\dagger_{\lambda,\mathbf{k},s} a_{\lambda',\mathbf{k},s}(t)\rangle \mathbf{d}_{\lambda\lambda'} = \sum_{\mathbf{k},s,\lambda,\lambda'} P_{\lambda\lambda',\mathbf{k},s}(t)\mathbf{d}_{\lambda\lambda'} \ , \tag{10.7}$$

where we introduced the pair function

$$P_{\lambda\lambda',\mathbf{k},s}(t) = \langle a^\dagger_{\lambda,\mathbf{k},s} a_{\lambda',\mathbf{k},s}(t)\rangle \ . \tag{10.8}$$

As in Chap. 5, we restrict the treatment to the optical transitions between the valence and conduction bands of the semiconductor (two-band approximation). Furthermore, we suppress the spin index s from now on, assuming that it is included in $\mathbf{k}$. The following calculations will not depend on s, only the spin summation in the definition of the polarization (10.1) will lead to an extra prefactor of 2 in the final result. Choosing $\lambda = v$ and $\lambda' = c$, the pair function, Eq. (10.8) becomes

$$P_{vc,\mathbf{k}}(t) = \langle a^\dagger_{v,\mathbf{k}} a_{c,\mathbf{k}}(t)\rangle \ . \tag{10.9}$$

This quantity is a representation of the off-diagonal elements of the reduced density matrix. In an equilibrium system without permanent dipole moment, these off-diagonal matrix elements vanish. However, the presence of the light induces optical transitions between the bands. Therefore, the interband polarization P_{vc} in such an externally driven system is finite.

In second quantization, we write the interaction Hamiltonian, Eq. (2.4), between the electric field and the semiconductor electrons as

$$\mathcal{H}_I = \int d^3r\, \hat{\psi}^\dagger(\mathbf{r})(-e\mathbf{r}) \cdot \mathcal{E}(\mathbf{r},t)\hat{\psi}(\mathbf{r}) \ . \tag{10.10}$$

Assuming that the electric field has a simple exponential space dependence,

$$\mathcal{E}(\mathbf{r},t) = \mathcal{E}(t)\frac{1}{2}\left(e^{i\mathbf{q}\cdot\mathbf{r}} + \text{c.c.}\right) \ , \tag{10.11}$$

and using the expansion (10.4) for spatially homogeneous systems, we obtain

$$\mathcal{H}_I \simeq -\sum_{\mathbf{k}} \mathcal{E}(t)(a^\dagger_{c,\mathbf{k}} a_{v,\mathbf{k}} d_{cv} + h.c.) \ , \tag{10.12}$$

where we took the limit $q \to 0$ (dipole approximation) and defined d_{cv} as the projection of the dipole $\mathbf{d}_{cv}$ in the direction of the field $\mathcal{E}$. The interaction Hamiltonian, (10.12), shows how the applied field causes transitions of electrons between valence and conduction band.

Besides the interaction with the external field, we also have to consider the kinetic and Coulomb contributions from the electrons. These effects are described by the Hamiltonian (7.29). For our present purposes, we have to extend the treatment of Chap. 7 by including also the band index λ:

$$\mathcal{H}_{el} = \sum_{\lambda,\mathbf{k}} E_{\lambda,k} a^\dagger_{\lambda,\mathbf{k}} a_{\lambda,\mathbf{k}} + \frac{1}{2} \sum_{\substack{\mathbf{k},\mathbf{k}' \\ \mathbf{q}\neq\mathbf{0} \\ \lambda,\lambda'}} V_q a^\dagger_{\lambda,\mathbf{k}+\mathbf{q}} a^\dagger_{\lambda',\mathbf{k}'-\mathbf{q}} a_{\lambda',\mathbf{k}'} a_{\lambda,\mathbf{k}} \ . \tag{10.13}$$

This Hamiltonian is obtained from Eq. (7.29) by including the summation over the band indices λ, λ'. Furthermore, we have omitted all those Coulomb terms which do not conserve the number of electrons in each band. Such terms are neglected because they would describe interband scattering, i.e., promotion of an electron from valence to conduction band or vice versa due to the Coulomb interaction, which is energetically very unfavorable.

For the two-band model, we restrict the band summation to $\lambda, \lambda' = c, v$ and obtain

$$\begin{aligned} \mathcal{H}_{el} = & \sum_{\mathbf{k}} \left(E_{c,k} a^\dagger_{c,\mathbf{k}} a_{c,\mathbf{k}} + E_{v,k} a^\dagger_{v,\mathbf{k}} a_{v,\mathbf{k}}\right) \\ & + \frac{1}{2} \sum_{\mathbf{k},\mathbf{k}',\mathbf{q}\neq\mathbf{0}} V_q \Big(a^\dagger_{c,\mathbf{k}+\mathbf{q}} a^\dagger_{c,\mathbf{k}'-\mathbf{q}} a_{c,\mathbf{k}'} a_{c,\mathbf{k}} + a^\dagger_{v,\mathbf{k}+\mathbf{q}} a^\dagger_{v,\mathbf{k}'-\mathbf{q}} a_{v,\mathbf{k}'} a_{v,\mathbf{k}} \\ & + 2 a^\dagger_{c,\mathbf{k}+\mathbf{q}} a^\dagger_{v,\mathbf{k}'-\mathbf{q}} a_{v,\mathbf{k}'} a_{c,\mathbf{k}} \Big) \ . \end{aligned} \tag{10.14}$$

For simplicity, we use the single particle energies in effective mass approximation and write the conduction and valence band energies as

$$E_{c,k} = \hbar\epsilon_{c,k} = E_g + \hbar^2 k^2 / 2m_c \ , \tag{10.15}$$

and

$$E_{v,k} = \hbar\epsilon_{v,k} = \hbar^2 k^2/2m_v \ . \tag{10.16}$$

The full Hamiltonian of the electrons in the valence and conduction bands interacting with the light field is now given by

$$\mathcal{H} = \mathcal{H}_I + \mathcal{H}_{el} \ . \tag{10.17}$$

To derive the equation of motion of the polarization, we use the Heisenberg equation for the individual operators. An elementary but lengthy calculation for the isotropic, homogeneous case yields

$$\begin{aligned}
&\hbar\left[i\frac{d}{dt} - (\epsilon_{c,k} - \epsilon_{v,k})\right] P_{vc,\mathbf{k}}(t) = \big[n_{c,\mathbf{k}}(t) - n_{v,\mathbf{k}}(t)\big] d_{cv}\mathcal{E}(t) \\
&+ \sum_{\mathbf{k}',\mathbf{q}\neq\mathbf{0}} V_q \Big(\langle a^\dagger_{c,\mathbf{k}'+\mathbf{q}} a^\dagger_{v,\mathbf{k}-\mathbf{q}} a_{c,\mathbf{k}'} a_{c,\mathbf{k}} \rangle + \langle a^\dagger_{v,\mathbf{k}'+\mathbf{q}} a^\dagger_{v,\mathbf{k}-\mathbf{q}} a_{v,\mathbf{k}'} a_{c,\mathbf{k}} \rangle \\
&+ \langle a^\dagger_{v,\mathbf{k}} a^\dagger_{c,\mathbf{k}'-\mathbf{q}} a_{c,\mathbf{k}'} a_{c,\mathbf{k}-\mathbf{q}} \rangle + \langle a^\dagger_{v,\mathbf{k}} a^\dagger_{v,\mathbf{k}'-\mathbf{q}} a_{v,\mathbf{k}'} a_{c,\mathbf{k}-\mathbf{q}} \rangle \Big) \ ,
\end{aligned} \tag{10.18}$$

where, as usual,

$$n_{\lambda,\mathbf{k}} = \langle a^\dagger_{\lambda,\mathbf{k}} a_{\lambda,\mathbf{k}} \rangle \ . \tag{10.19}$$

The first line of Eq. (10.18) is basically the same as Eq. (5.30) of the free-carrier theory. The four-operator terms appear as a consequence of the Coulomb part of the electron Hamiltonian (10.14).

To proceed with our calculations, we again make a random phase approximation to split the four-operator terms in Eq. (10.18) into products of densities and interband polarizations. For example, we approximate

$$\langle a^\dagger_{c,\mathbf{k}'+\mathbf{q}} a^\dagger_{v,\mathbf{k}-\mathbf{q}} a_{c\mathbf{k}'} a_{c,\mathbf{k}} \rangle \simeq P_{vc,\mathbf{k}'} n_{c,\mathbf{k}} \delta_{\mathbf{k}-\mathbf{q},\mathbf{k}'} \ , \tag{10.20}$$

because the term $\propto \delta_{\mathbf{q},\mathbf{0}}$ does not contribute. As result, we obtain

$$\hbar\left[i\frac{\boldsymbol{d}}{\boldsymbol{dt}} - (\boldsymbol{e_{c,k}} - \boldsymbol{e_{v,k}})\right]\boldsymbol{P_{vc,k}(t)}$$
$$= \left[\boldsymbol{n_{c,k}(t)} - \boldsymbol{n_{v,k}(t)}\right]\left[\boldsymbol{d_{cv}\mathcal{E}(t)} + \sum_{\mathbf{q}\neq\mathbf{k}} \boldsymbol{V_{|k-q|}P_{vc,q}}\right] \quad . \qquad (10.21)$$

dynamics of interband polarization (pair) function

In Eq. (10.21), we introduced the renormalized frequencies

$$e_{\lambda,k} = e_{\lambda,k} + \Sigma_{exc,\lambda}(k) \qquad (10.22)$$

with the exchange self-energy

$$\hbar\Sigma_{exc,\lambda}(k) = -\sum_{\mathbf{q}\neq\mathbf{k}} V_{|\mathbf{k}-\mathbf{q}|} n_{\lambda,\mathbf{q}} \ , \qquad (10.23)$$

compare Eq. (9.21).

As in the case of free carriers, Eq. (5.30), we see that Eq. (10.21) couples the dynamics of the interband polarization to the evolution of the carrier distribution functions. Consequently, we need additional equations for $\partial n_{c,\mathbf{k}}(t)/\partial t$ and $\partial n_{v,\mathbf{k}}(t)/\partial t$. The resulting coupled equations would then be the optical Bloch equations (5.30) – (5.32) with the additional Coulomb effects included. We will discuss these *semiconductor Bloch equations* in Chap. 12. For the purposes of the present chapter, we eliminate the population dynamics by making the quasi-equilibrium assumption discussed in Chap. 5. In quasi equilibrium, we assume that the time scales of interest are sufficiently long so that the rapid scattering processes have already driven the carrier distributions to equilibrium in the form of quasi-stationary Fermi–Dirac distributions. We can then make the replacements

$$n_{c,\mathbf{k}}(t) \to f_{c,k} \quad \text{and} \quad n_{v,\mathbf{k}}(t) \to f_{v,k} \ ,$$

and Eq. (10.21) simplifies to

$$\hbar\left[i\frac{d}{dt}-(e_{c,k}-e_{v,k})\right]P_{vc,\mathbf{k}}(t)$$
$$=\left(f_{c,\mathbf{k}}-f_{v,\mathbf{k}}\right)\left[d_{cv}\mathcal{E}(t)+\sum_{\mathbf{q}\neq\mathbf{k}}V_{|\mathbf{k}-\mathbf{q}|}P_{vc,\mathbf{q}}\right] \quad . \tag{10.24}$$

To gain some insight and to recover the results of Chap. 5, we solve Eq. (10.24) first for $V_q = 0$, i.e., for noninteracting particles. The free-carrier polarization equation

$$\hbar\left[i\frac{d}{dt}-(e_{c,k}-\epsilon_{v,k})\right]P^0_{vc,k}(t)=(f_{c,k}-f_{v,k})d_{cv}\mathcal{E}(t) \ , \tag{10.25}$$

can simply be solved by Fourier transformation

$$P^0_{vc,k}(\omega)=(f_{c,k}-f_{v,k})\frac{d_{cv}}{\hbar\left[\omega+i\delta-(\epsilon_{c,k}-\epsilon_{v,k})\right]}\mathcal{E}(\omega) \ , \tag{10.26}$$

so that

$$P^0_{vc,k}(t)=\int\frac{d\omega}{2\pi}(f_{c,k}-f_{v,k})\frac{d_{cv}}{\hbar\left[\omega+i\delta-(\epsilon_{c,k}-\epsilon_{v,k})\right]}\mathcal{E}(\omega)e^{-i\omega t} \ . \tag{10.27}$$

From Eq. (10.7) in two-band approximation we obtain the optical polarization as

$$P(t)=\sum_{\mathbf{k}}P_{cv,\mathbf{k}}(t)d_{vc}+\text{c.c.} \ , \tag{10.28}$$

which for our special case yields

$$P^0(t)=\sum_{\mathbf{k}}\int\frac{d\omega}{2\pi}|d_{cv}|^2\frac{f_{c,k}-f_{v,k}}{\hbar\left[\omega+i\delta-(\epsilon_{c,k}-\epsilon_{v,k})\right]}\mathcal{E}(\omega)e^{-i\omega t}+\text{c.c.} \ , \tag{10.29}$$

i.e., the free-particle result of Chap. 5.

10.2 Wannier Equation

The solution of Eq. (10.24) for finite carrier densities will be addressed in Chap. 15, where we discuss quasi-equilibrium optical nonlinearities of semiconductors. In the remainder of the present chapter, we concentrate

on the linear optical properties, i.e., the situation of an unexcited crystal where

$$f_{c,k} \equiv 0 \quad \text{and} \quad f_{v,k} \equiv 1 \ . \tag{10.30}$$

Inserting (10.30) into Eq. (10.24) and taking the Fourier transform yields

$$\left[\hbar(\omega+i\delta)-E_g-\frac{\hbar^2k^2}{2m_r}\right] P_{vc,\mathbf{k}}(\omega)=-\left[d_{cv}\mathcal{E}(\omega)+\sum_{\mathbf{q}\neq\mathbf{k}} V_{|\mathbf{k}-\mathbf{q}|}P_{vc,\mathbf{q}}(\omega)\right] \ , \tag{10.31}$$

where

$$\frac{1}{m_r} = \frac{1}{m_c} - \frac{1}{m_v} \tag{10.32}$$

is the inverse reduced mass. As a reminder, we note again at this point that $m_v < 0$.

The solution of Eq. (10.31) is facilitated by transforming into real space. Multiplying Eq. (10.31) from the left by

$$\frac{L^3}{(2\pi)^3}\int d^3k \ldots$$

and using the Fourier transform in the form

$$\begin{aligned} f(\mathbf{r}) &= \frac{L^3}{(2\pi)^3}\int d^3q f_{\mathbf{q}} e^{-i\mathbf{q}\cdot\mathbf{r}} \\ f_{\mathbf{q}} &= \frac{1}{L^3}\int d^3r f(\mathbf{r}) e^{i\mathbf{q}\cdot\mathbf{r}} \end{aligned} \tag{10.33}$$

we obtain

$$\left[\hbar(\omega+i\delta) - E_g + \frac{\hbar^2\nabla^2_{\mathbf{r}}}{2m_r} + V(r)\right] P_{vc}(\mathbf{r},\omega) = -d_{cv}\mathcal{E}(\omega)\,\delta(\mathbf{r})L^3 \ . \tag{10.34}$$

One way to solve this inhomogeneous equation is to expand P_{vc} into the solution of the corresponding homogeneous equation :

$$-\left[\frac{\hbar^2\nabla_{\mathbf{r}}^2}{2m_r}+V(r)\right]\psi_\nu(\mathbf{r})=E_\nu\psi_\nu(\mathbf{r})\ . \tag{10.35}$$

Wannier equation

Eq. (10.35) has exactly the form of a two-particle Schrödinger equation for the relative motion of an electron and a hole interacting via the attractive Coulomb potential $V(r)$. This equation is known as the *Wannier equation*.

The pair equation (10.21) and the related Wannier equation have been derived under the assumption that the Coulomb potential varies little within one unit cell. This assumption is valid only if the resulting electron–hole–pair Bohr radius a_0 which determines the extension of the ground state wave function is considerably larger than a lattice constant.

The Wannier equation (10.35) is correct in this form for two- and three-dimensional systems. For a quasi-one-dimensional (q1D) quantum wire, we have to replace the Coulomb potential by the envelope averaged potential $V^{q1D}(z)$, e.g., in the approximation of Eq. (7.78) for cylindrical wires

$$V^{q1D}(z)=\frac{e^2}{\epsilon_0}\frac{1}{|z|+\gamma R}\ .$$

Since there is a one-to-one correspondence with the hydrogen atom, if we replace the proton by the valence-band hole, we can solve the Wannier equation in analogy to the hydrogen problem, which is discussed in many quantum mechanics textbooks, such as Landau and Lifshitz (1958) or Schiff (1968). Introducing the scaled radius

$$\rho=r\alpha \tag{10.36}$$

Eq. (10.35) becomes

$$\left(-\nabla_\rho^2-\frac{\lambda}{\rho}\right)\psi(\rho)=\frac{2m_rE_\nu}{\hbar^2\alpha^2}\psi(\rho)\ , \tag{10.37}$$

where

$$\lambda=\frac{e^2 2m_r}{\epsilon_0\hbar^2\alpha}=\frac{2}{\alpha a_0}\ , \tag{10.38}$$

and

$$a_0 = \frac{\hbar^2 \epsilon_0}{e^2 m_r} \ . \tag{10.39}$$

As in the hydrogen-atom case, the energy E_ν is negative for bound states ($E_{bound} < E_g$) and positive for the ionization continuum. We define

$$a_0^2 \alpha^2 = -\frac{8 m_r E_\nu a_0^2}{\hbar^2} = -4 \frac{E_\nu}{E_0} \tag{10.40}$$

with the energy unit

$$E_0 = \frac{\hbar^2}{2 m_r a_0^2} = \frac{e^2}{2 \epsilon_0 a_0} = \frac{e^4 m_r}{2 \epsilon_0^2 \hbar^2} \tag{10.41}$$

to rewrite Eq. (10.37) as

$$\left(-\nabla_\rho^2 - \frac{\lambda}{\rho} \right) \psi(\rho) = -\frac{1}{4} \psi(\rho) \ , \tag{10.42}$$

and

$$\lambda = \frac{e^2}{\hbar \epsilon_0} \sqrt{-\frac{m_r}{2 E_\nu}} \ . \tag{10.43}$$

With this choice of α^2 the parameter λ will be real for bound states and imaginary for the ionization continuum.

The treatment of the q1D case proceeds similarly. Here one sets

$$\zeta = \alpha(|z| + \gamma R) \tag{10.44}$$

which again yields Eq. (10.42) with ρ replaced by ζ and α and λ unchanged.

We now proceed to solve Eq. (10.42) for the cases of three- and two-dimensional semiconductors. For this purpose, we write the Laplace operator in spherical/polar coordinates as

$$\begin{aligned}
\nabla_\rho^2 &= \frac{1}{\rho^2} \frac{\partial}{\partial \rho} \rho^2 \frac{\partial}{\partial \rho} - \frac{\mathcal{L}^2}{\rho^2} && \text{in } 3D \\
\nabla_\rho^2 &= \frac{1}{\rho} \frac{\partial}{\partial \rho} \rho \frac{\partial}{\partial \rho} - \frac{\mathcal{L}_z^2}{\rho^2} && \text{in } 2D \\
\nabla_\rho^2 &= \frac{\partial^2}{\partial \zeta^2} && \text{in } q1D \ ,
\end{aligned} \tag{10.45}$$

where $\mathcal{L}$ and $\mathcal{L}_z$ are the operators of the total angular momentum and its z component,

$$\mathcal{L}^2 = -\left(\frac{1}{\sin^2\theta}\frac{\partial^2}{\partial\phi^2} + \frac{1}{\sin\theta}\frac{\partial}{\partial\theta}\sin\theta\frac{\partial}{\partial\theta}\right) \tag{10.46}$$

and

$$\mathcal{L}_z^2 = -\frac{\partial^2}{\partial\phi^2} \ . \tag{10.47}$$

These operators obey the following eigenvalue equations

$$\mathcal{L}^2 Y_{l,m}(\theta,\phi) = l(l+1)Y_{l,m}(\theta,\phi) \quad \text{with} \quad |m| \le l \tag{10.48}$$

and

$$\mathcal{L}_z \frac{1}{\sqrt{2\pi}} e^{im\phi} = m\frac{1}{\sqrt{2\pi}} e^{im\phi} \ , \tag{10.49}$$

where the functions $Y_{l,m}(\theta,\phi)$ are the spherical harmonics with $m = 0, \pm1, \pm2, \ldots$ and $l = 0, 1, 2 \ldots$. With the ansatz

$$\psi(\rho) = f_l(\rho)Y_{l,m}(\theta,\phi) \qquad \text{in } 3D \tag{10.50}$$

$$= f_m(\rho)\frac{1}{\sqrt{2\pi}} e^{im\phi} \qquad \text{in } 2D \tag{10.51}$$

$$= f(\zeta) \qquad \text{in } q1D \tag{10.52}$$

we find the equation for the radial part of the wave function as

$$\left(\frac{1}{\rho^2}\frac{\partial}{\partial\rho}\rho^2\frac{\partial}{\partial\rho} + \frac{\lambda}{\rho} - \frac{1}{4} - \frac{l(l+1)}{\rho^2}\right) f_l(\rho) = 0 \quad \text{in} \quad 3D$$

$$\left(\frac{1}{\rho}\frac{\partial}{\partial\rho}\rho\frac{\partial}{\partial\rho} + \frac{\lambda}{\rho} - \frac{1}{4} - \frac{m^2}{\rho^2}\right) f_m(\rho) = 0 \quad \text{in} \quad 2D$$

$$\left(\frac{\partial^2}{\partial\zeta^2} + \frac{\lambda}{\zeta} - \frac{1}{4}\right) f(\zeta) = 0 \quad \text{in} \quad q1D \ . \tag{10.53}$$

10.3 Excitons

We now discuss the bound-state solutions which are commonly referred to as *Wannier excitons*. In order to solve Eq. (10.53) for this case, we first

determine the asymptotic form of the wave functions for large radii. For $\rho \to \infty$, the leading terms in Eq. (10.53) are

$$\left(\frac{d^2}{d\rho^2} - \frac{1}{4}\right) f_\infty(\rho) = 0 \tag{10.54}$$

and the convergent solution is therefore of the form

$$f_\infty(\rho) = e^{-\rho/2} \ . \tag{10.55}$$

Writing $f(\rho) = f_0(\rho) f_\infty(\rho)$ and studying the asymptotic behavior for small ρ suggests that for $\rho \to 0$ the function $f_0(\rho)$ should vary like ρ^l $(3D)$ or $\rho^{|m|}$ $(2D)$, respectively. Thus we make the ansatz for the total wave functions

$$\begin{aligned} f_l(\rho) &= \rho^l e^{-\frac{\rho}{2}} R(\rho) \qquad \text{in } 3D \\ f_m(\rho) &= \rho^{|m|} e^{-\frac{\rho}{2}} R(\rho) \text{ in } 2D \\ f(\zeta) &= e^{-\frac{\zeta}{2}} R(\zeta) \qquad \text{in } q1D \ . \end{aligned} \tag{10.56}$$

Inserting (10.56) into Eq. (10.53) yields

$$\begin{aligned} &\rho \frac{\partial^2 R}{\partial \rho^2} + \big[2(l+1) - \rho\big] \frac{\partial R}{\partial \rho} + (\lambda - l - 1) R = 0 && \text{in} \quad 3D \\ &\rho \frac{\partial^2 R}{\partial \rho^2} + (2|m| + 1 - \rho) \frac{\partial R}{\partial \rho} + \left(\lambda - |m| - \frac{1}{2}\right) R = 0 && \text{in} \quad 2D \\ &\left(\frac{\partial^2}{\partial \zeta^2} + \frac{\partial}{\partial \zeta} + \frac{\lambda}{\zeta}\right) R = 0 && \text{in} \quad q1D \ . \end{aligned} \tag{10.57}$$

Because the three- and two-dimensional equations are of the same type, we proceed first with these two cases and turn to the discussion of the quasi-one-dimensional case later.

10.3.1 *Three- and Two-Dimensional Cases*

Both the $3D$ and $2D$ equations in Eq. (10.57) are of the form

$$\rho \frac{\partial^2 R}{\partial \rho^2} + (p + 1 - \rho) \frac{\partial R}{\partial \rho} + qR = 0 \tag{10.58}$$

with

$$\begin{aligned} &p = 2l + 1 \quad , \quad q = \lambda - l - 1 \quad \text{in } 3D \\ &p = 2|m| \quad , \quad q = \lambda - |m| - \tfrac{1}{2} \text{ in } 2D \end{aligned} \tag{10.59}$$

The solution of Eq. (10.58) can be obtained by a power series expansion

$$R(\rho) = \sum_{\nu=0} \beta_\nu \rho^\nu \quad . \tag{10.60}$$

Inserting (10.60) into (10.58) and comparing the coefficients of the different powers of ρ yields the recursive relation

$$\beta_{\nu+1} = \beta_\nu \frac{\nu - q}{(\nu+1)(\nu+p+1)} \quad . \tag{10.61}$$

In order to get a result which can be normalized, the series must terminate for $\nu = \nu_{max}$, so that all $\beta_{\nu \geq \nu_{max}} = 0$. Thus $\nu_{max} - q = 0$, or, using (10.59) for the $3D$ case,

$$\nu_{max} + l + 1 = \lambda \equiv n \quad , \tag{10.62}$$

where the main quantum number n can assume the values $n = 1, 2, \ldots$, respectively, for $l = \nu_{max} = 0$; $l = 1$ and $\nu_{max} = 0$, or $l = 0$, $\nu_{max} = 1$, etc.

Correspondingly, we have in $2D$,

$$\nu_{max} + |m| + \frac{1}{2} = \lambda \equiv n + \frac{1}{2} \quad . \tag{10.63}$$

Here, the allowed values of the main quantum number are $n = 0, 1, 2, \ldots$. The bound-state energies follow from Eqs. (10.43), (10.62) and (10.63) as

$$\boldsymbol{E_n = -E_0 \frac{1}{n^2}} \quad \text{with } \boldsymbol{n = 1, 2, \ldots} \tag{10.64}$$

$3D$ exciton bound-state energies

and

$$\boldsymbol{E_n = -E_0 \frac{1}{(n+1/2)^2}} \quad \text{with } \boldsymbol{n = 0, 1, \ldots}, \tag{10.65}$$

$2D$ exciton bound-state energies

where we identify E_0, Eq. (10.41), as the exciton Rydberg energy and a_0, Eq. (10.39), as the exciton Bohr radius which we used already in earlier chapters as a characteristic length scale.

The binding energy of the exciton ground state is E_0 in $3D$ and $4E_0$ in $2D$, respectively. The larger binding energy in $2D$ can be understood by considering quantum well structures with decreasing width. The wave function tries to conserve its spherical symmetry as much as possible since the admixture of p-wave functions is energetically unfavorable. Confinement parallel to the quantum wells is therefore accompanied by a decrease in the Bohr radius perpendicular to the wells. In fact, the exciton radius is obtained from the exponential term

$$e^{-\rho/2} = e^{-\alpha r/2}$$

with $\alpha = 2/a_0 n$ in $3D$ and $\alpha = 2/a_0(n + 1/2)$ in $2D$. In the ground state, the $3D$ exciton radius is thus simply the exciton Bohr radius a_0, but it is only $a_0/2$ in $2D$.

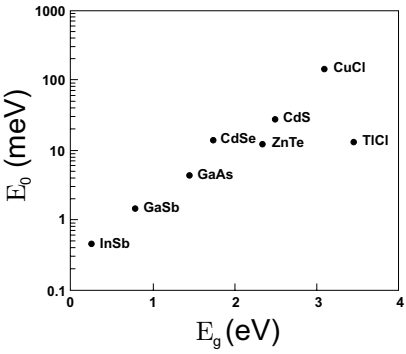

Fig. 10.1 Experimental values for the exciton binding energy E_0 versus band gap energy E_g.

Eq. (10.41) shows that the exciton Rydberg energy E_0 is inversely proportional to the square of the background dielectric constant. The background dielectric constant describes the screening of the Coulomb interaction in an unexcited crystal. This screening requires virtual interband transitions which become more and more unlikely for materials with larger band gap energy E_g. As a result, the exciton Rydberg is large for wide-gap materials such as I–VII compound semiconductors, where one element is from the first group of the periodic table and the other one from the seventh. As shown in Fig. 10.1, for direct-gap materials, E_0 generally decreases when one goes through the series of I–VII, II–VI, and III–V compound semiconductors.

From Eq. (10.56) and (10.60) we can now obtain the complete radial exciton wave functions. These functions still have to be normalized so that

$$\int_0^\infty dr\, r^{D-1} |f(r)|^2 = 1 \ . \tag{10.66}$$

The resulting first few normalized functions in $3D$ are

ν_{max}	n	l	$f_{n,l}(\rho) = C\rho^l e^{-\frac{\rho}{2}} \sum_\nu \beta_\nu \rho^\nu$	E_n
0	**1**	**0**	$f_{1,0}(r) = \frac{1}{a_0^{3/2}} 2\, e^{-r/a_0}$	$E_1 = -E_0$
1	**2**	**0**	$f_{2,0}(r) = \frac{1}{(2a_0)^{3/2}}(2 - \frac{r}{a_0}) e^{-r/2a_0}$	$E_2 = -\frac{E_0}{4}$
0	**2**	**1**	$f_{2,1}(r) = \frac{1}{(2a_0)^{3/2}} \frac{r}{\sqrt{3}a_0} e^{-r/2a_0}$	$E_2 = -\frac{E_0}{4}$.

(10.67)

$3D$ radial exciton wave functions

The first few normalized eigenfunctions in $2D$ are

ν_{max}	n	m	$f_{n,m}(\rho) = C\rho^{\lvert m\rvert}e^{-\frac{\rho}{2}}\sum_\nu \beta_\nu \rho^\nu$	E_n
0	0	0	$f_{0,0}(r) = \frac{1}{a_0}4e^{-2r/a_0}$	$E_{n=0} = -4E_0$
1	1	0	$f_{1,0}(r) = \frac{4}{a_0 3\sqrt{3}}\left(1 - \frac{4r}{3a_0}\right)e^{-\frac{2r}{3a_0}}$	$E_1 = -\frac{4E_0}{9}$
0	1	± 1	$f_{1,\pm 1}(r) = \frac{16}{a_0 9\sqrt{6}}\frac{r}{a_0}e^{-2r/3a_0}$	$E_1 = -\frac{4E_0}{9}$.

(10.68)

2*D* radial exciton wave functions

The solution of the differential equation (10.58) with integer p and q can be written in terms of the associate Laguerre polynomials

$$L_q^p(\rho) = \sum_{\nu=0}^{q-p}(-1)^{\nu+p}\frac{(q!)^2\rho^\nu}{(q-p-\nu)!(p+\nu)!\nu!} \ . \tag{10.69}$$

Thus, the normalized exciton wave functions can be expressed in general by these orthogonal Laguerre polynomials as

$$\psi_{n,l,m}(\mathbf{r}) = -\sqrt{\left(\frac{2}{na_0}\right)^3\frac{(n-l-1)!}{2n[(n+l)!]^3}}\rho^l e^{-\frac{\rho}{2}}L_{n+l}^{2l+1}(\rho)\,Y_{l,m}(\theta,\phi)\,, \tag{10.70}$$

3*D* exciton wave function

where $\rho = 2r/na_0$ and

$$\psi_{n,m}(\mathrm{r}) = \sqrt{\frac{1}{\pi a_0^2 (n+\frac{1}{2})^3} \frac{(n-|m|)!}{[(n+|m|)!]^3}} \rho^{|m|} e^{-\frac{\rho}{2}} L_{n+|m|}^{2|m|}(\rho)\, e^{im\phi} \tag{10.71}$$

$2D$ exciton wave function

with $\rho = 2r/[(n+1/2)a_0]$.

10.3.2 *Quasi-One-Dimensional Case*

The Wannier equation (10.53) for quantum wires is a Whittaker equation

$$\left(\frac{\partial^2}{\partial \zeta^2} + \frac{\lambda}{\zeta} - \frac{1}{4} + \frac{1/4 - \mu^2}{\zeta^2} \right) W_{\lambda,\mu}(\zeta) = 0 \tag{10.72}$$

with $\mu = \pm 1/2$. $W_{\lambda,1/2}(\zeta)$ are Whittaker functions, the quantum numbers λ have to be determined from the boundary conditions. From Eqs. (10.38) and (10.40) we obtain the energy eigenvalues as

$$E_\lambda = -E_0 \frac{1}{\lambda^2} \ , \tag{10.73}$$

$q1D$ exciton bound-state energies

where E_0 is the $3D$ exciton Rydberg energy, Eq. (10.41).

The eigenfunctions can be classified according to their parity as even and odd functions with $df(\zeta)/dz\,|_{z=0} = 0$ and $f(\zeta)\,|_{z=0} = 0$, respectively. For dipole allowed transitions, the odd functions do not couple to the light field, which allows us to limit our discussion to the even eigenfunctions

$$f_\lambda(|z|) = \mathcal{N}_\lambda W_{\lambda,1/2}\left(\frac{2(|z| + \gamma R)}{\lambda a_0} \right) \ . \tag{10.74}$$

$q1D$ exciton wave functions

The normalization constant $\mathcal{N}_\lambda$ is given by

$$\mathcal{N}_\lambda = \frac{1}{\lambda a_0}\left(\int_{R_\lambda}^{\infty} dx\,|W_{\lambda,1/2}(x)|^2\right)^{-1/2} \quad ,$$

with $R_\lambda = 2\gamma R/(\lambda a_0)$. The Whittaker functions have the following useful integral representation

$$W_{\lambda,1/2}(\zeta) = \frac{e^{-\zeta/2}}{\Gamma(1-\lambda)}\int_0^\infty dt\, e^{-t}\left(1+\frac{\zeta}{t}\right)^{\lambda} \quad . \tag{10.75}$$

The derivative with respect to ζ is

$$\frac{dW_{\lambda,1/2}(\zeta)}{d\zeta} = \frac{e^{-\zeta/2}}{\Gamma(1-\lambda)}\int_0^\infty dt\, e^{-t}\left(1+\frac{\zeta}{t}\right)^{\lambda}\left(-\frac{1}{2}+\frac{\lambda}{\zeta+t}\right) \quad . \tag{10.76}$$

At the origin, $\zeta = \alpha\gamma R = 2\gamma R/(\lambda a_0)$, Eq. (10.76) has to vanish for the even functions. For the ground state, λ_0 is very small, $\lambda_0 << 1$. Also, for thin wires $\alpha\gamma R << 1$. It then follows from Eq. (10.76) that

$$\int_0^\infty dt\, e^{-t}\left(-\frac{1}{2}+\frac{\lambda_0}{\zeta+t}\right) \simeq 0 \quad . \tag{10.77}$$

The first term can be integrated directly. The second term is proportional to the exponential integral, which gives the leading contribution $\lambda_0\,\ln(\zeta)$ for small ζ. Thus the approximate ground state eigenvalue for thin wires is determined by

$$\frac{1}{2} + \lambda_0\,\ln\left(\frac{2\gamma R}{\lambda_0 a_0}\right) = 0 \quad . \tag{10.78}$$

Because $\lambda_0 << 1$ for $\gamma R < a_0$, the corresponding exciton binding energy $|E_{\lambda_0}| = E_0/\lambda_0^2$ is much larger than the $3D$ exciton Rydberg energy for a thin quantum wire, at least for an infinite confinement potential. For more realistic confinement potentials as in a GaAs/GaAlAs wire, E_{λ_0} may be as much as $5E_0$. In still thinner wires, the electrons and holes are no longer confined inside the wire well.

For the higher excited states, the eigenvalue λ_n rapidly approaches the integer n with increasing n, i.e., $\lambda_n \to n$ according to

$$\lambda_n - n = -\frac{1}{\ln(2\alpha R/na_0)} \quad . \tag{10.79}$$

As a consequence, the usual Balmer series is obtained for the energies of the higher bound states. At the same time the Whittaker eigenfunctions of these higher states can be expressed, as Loudon showed, by Laguerre polynomials

$$f_{\lambda_n}(|z|) \to \left(\frac{2}{a_0^3 n^5 (n!)^2}\right)^{1/2} e^{-|z|/na_0} |z| L_n^1(2|z|/na_0) \ . \tag{10.80}$$

The wave function of these higher states vanishes at the origin $f_{\lambda_n}(0) \to 0$.

10.4 The Ionization Continuum

For the continuous spectrum of the ionized states with $E_\nu \geq 0$, we put

$$E_\nu \equiv E_k = \frac{\hbar^2 k^2}{2m_r} \tag{10.81}$$

so that Eqs. (10.38) and (10.43) yield

$$\alpha = 2ik \quad , \quad \lambda = -i\frac{e^2 m_r}{\epsilon_0 \hbar^2 k} = -\frac{i}{a_0 k} \ . \tag{10.82}$$

10.4.1 *Three- and Two-Dimensional Cases*

Following the same argumentation as in the case of the bound-state solution, we obtain from an asymptotic analysis for small and large ρ the prefactors $\rho^l \exp(-\rho/2)$ and $\rho^{|m|} \exp(-\rho/2)$ for $3D$ and $2D$, respectively. Making an ansatz as in Eq. (10.56) we then obtain the equations

$$\begin{aligned} &\rho\frac{\partial^2 R}{\partial \rho^2} + (2(l+1) - \rho)\frac{\partial R}{\partial \rho} - (i|\lambda| + l + 1)R = 0 \qquad \text{in } 3D \\ &\rho\frac{\partial^2 R}{\partial \rho^2} + (2|m| + 1 - \rho)\frac{\partial R}{\partial \rho} - \left(i|\lambda| + |m| + \frac{1}{2}\right) R = 0 \quad \text{in } 2D \ . \end{aligned} \tag{10.83}$$

These equations are solved by the confluent hypergeometric functions

$$F\big[l + 1 + i|\lambda|;\, 2(l+1);\, \rho\big] \text{ and } F\left(|m| + \frac{1}{2} + i|\lambda|;\, 2|m| + 1;\, \rho\right) \ , \tag{10.84}$$

where $F(a;b;z)$ is defined as

$$F(a;b;z) = 1 + \frac{a}{b\cdot 1}z + \frac{a(a+1)}{b(b+1)\cdot 1\cdot 2}z^2 + \dots \quad . \tag{10.85}$$

The normalization of the continuum states has to be chosen in such a way that it connects continuously with the normalization of the higher bound states, as discussed for the $3D$ exciton problem by Elliott (1963) and by Shinada and Sugano (1966) for $2D$. Therefore, we normalize the wave functions in a sphere/circle of radius $\mathcal{R}$, where eventually $\mathcal{R}\to\infty$. The respective normalization integrals in $3D$ and $2D$ are

$$\begin{aligned} |A_{3D}| \quad & \int_0^{\mathcal{R}} dr\, r^2\,(2kr)^{2l}\Big|F\big[l+1+i|\lambda|;\,2(l+1);\,2ikr\big]\Big|^2 = 1 \\ |A_{2D}| & \int_0^{\mathcal{R}} dr\, r\,(2kr)^{2|m|}\Big|F(|m|+\tfrac{1}{2}+i|\lambda|;\,2|m|+1;\,2ikr)\Big|^2 = 1 \quad . \end{aligned} \tag{10.86}$$

Since these integrals do not converge for $\mathcal{R}\to\infty$, we can use the asymptotic expressions for $z\to\infty$ for the confluent hypergeometric functions

$$F(a;b;z) = \frac{\Gamma(b)e^{i\pi a}z^{-a}}{\Gamma(b-a)}\left[1+\mathcal{O}\left(\frac{1}{|z|}\right)\right] + \frac{\Gamma(b)e^{z}z^{a-b}}{\Gamma(a)}\left[1+\mathcal{O}\left(\frac{1}{|z|}\right)\right] \quad , \tag{10.87}$$

where $\Gamma(n) = (n-1)!$, n integer, is the Gamma function. Using (10.87) in (10.86) we compute the normalization factors A_{3D} and A_{2D} and finally obtain the normalized wave function as

$$\begin{aligned} \psi_{k,l,m}(\mathbf{r}) = {} & \tfrac{(i2kr)^l}{(2l+1)!}e^{\frac{\pi|\lambda|}{2}}\sqrt{\tfrac{2\pi k^2}{\mathcal{R}|\lambda|\sinh(\pi|\lambda|)}\prod_{j=0}^{l}(j^2+|\lambda|^2)} \\ & \times\; e^{-ikr}F(l+1+i|\lambda|;\,2l+2;\,2ikr)\,Y_{l,m}(\theta\phi) \end{aligned} \tag{10.88}$$

in $3D$ and

$$\begin{aligned} \psi_{k,m}(\mathbf{r}) = {} & \tfrac{(i2kr)^{|m|}}{(2|m|)!}\sqrt{\tfrac{\pi k}{\mathcal{R}(1/4+|\lambda|^2)\cosh(\pi|\lambda|)}\prod_{j=0}^{|m|}\left[\left(j-\tfrac{1}{2}\right)^2+|\lambda|^2\right]} \\ & \times\quad e^{\frac{\pi|\lambda|}{2}}e^{-ikr}F\left(|m|+\tfrac{1}{2}+i|\lambda|;\,2|m|+1;\,2ikr\right)\tfrac{e^{im\phi}}{\sqrt{2\pi}} \end{aligned} \tag{10.89}$$

in $2D$. For later reference, it is important to note that the allowed k-values are defined by

$$k\mathcal{R} = \pi n \quad \text{and} \quad \Delta k = \frac{\pi}{\mathcal{R}} \ .$$

Therefore, we have in this case

$$\sum_k = \frac{\mathcal{R}}{\pi} \sum_k \Delta k \to \frac{\mathcal{R}}{\pi} \int dk \ .$$

10.4.2 *Quasi-One-Dimensional Case*

With the scaling of Eqs. (10.81) and (10.83), Eq. (10.53) becomes for the continuum states

$$\left[\frac{d^2}{d\zeta^2} - \left(\frac{1}{4} + i \frac{|\lambda|}{\zeta} \right) \right] f(\zeta) = 0 \ . \tag{10.90}$$

The two independent solutions of Eq. (10.90) are the Whittaker functions

$$\begin{aligned} W^{(1)}_{-i|\lambda|,1/2}(\zeta) &= \Gamma(1+i|\lambda|)\zeta e^{-\zeta/2}[F(1+i|\lambda|,2;\zeta) + G(1+i|\lambda|,2;\zeta)] \ , \\ W^{(2)}_{-i|\lambda|,1/2}(\zeta) &= \Gamma(1-i|\lambda|)\zeta e^{-\zeta/2}[F(1+i|\lambda|,2;\zeta) - G(1+i|\lambda|,2;\zeta)] \ , \end{aligned} \tag{10.91}$$

where $F(a,b;x)$ is the confluent hypergeometric function defined in Eq. (10.85) and $G(1+i|\lambda|,2;\zeta)$ is given by

$$\begin{aligned} G(1+i|\lambda|,2;\zeta) = \frac{e^{-2\pi|\lambda|}-1}{2\pi i} \Bigg\{ & \Big[2\ln\zeta + \pi \cot(\pi + i\pi|\lambda|) - i\pi \Big] \\ & \times F(1+i|\lambda|,2;\zeta) \\ & - 2\sum_{n=0}^{\infty} \Big[\psi(1+n) + \psi(2+n) - \psi(1+n+i|\lambda|) \Big] \\ & \times \frac{\Gamma(1+i|\lambda|+n)\Gamma(2)\zeta^n}{\Gamma(1+i|\lambda|)\Gamma(2+n)n!} + \frac{2e^{-\pi|\lambda|}}{\zeta|\Gamma(1+i|\lambda|)|^2} \Bigg\}. \end{aligned} \tag{10.92}$$

Here $\psi(x) = d\ln\Gamma(x)/dx$ is the digamma function. The two solutions (10.91) will be denoted $W^{(1)}$ and $W^{(2)}$. The even wave functions have

again a vanishing derivative at the origin. Employing a similar normalization procedure as above one finds for the even functions the result

$$f_k(\zeta) = \left(\frac{e^{\pi|\lambda|}}{2\pi}\right)^{1/2} \frac{D_0^{(2)} W^{(1)}(\zeta) - D_0^{(1)} W^{(2)}(\zeta)}{(|D_0^{(1)}|^2 + |D_0^{(2)}|^2)^{1/2}} \ , \tag{10.93}$$

where

$$D_0^{(j)} = \frac{dW^{(j)}(\zeta)}{d\zeta}|_{\zeta=2ik\gamma R} \ .$$

10.5 Optical Spectra

With the knowledge of the exciton and continuum wave functions and the energy eigenvalues, we can now solve the inhomogeneous equation (10.34) to obtain the interband polarization and thus calculate the optical spectrum of a semiconductor in the band edge region. We limit our treatment to the discussion of optically allowed transitions in direct-gap semiconductors, because these semiconductors are particularly interesting with regards to their use for electro-optical devices. Optical transitions across an indirect gap, where the extrema of the valence and conduction band are at different points in the Brillouin zone, need the simultaneous participation of a photon and a phonon in order to satisfy total momentum conservation. Here, the phonon provides the necessary wave vector for the transition. Such two-quantum processes have a much smaller transition probability than the direct transitions.

To solve Eq. (10.34), we expand the polarization into the solutions of the Wannier equation

$$P_{vc}(\mathbf{r}, \omega) = \sum_\nu b_\nu \, \psi_\nu(\mathbf{r}) \ . \tag{10.94}$$

Inserting (10.94) into (10.34), multiplying by $\psi_\mu^*(\mathbf{r})$ and integrating over $\mathbf{r}$, we find

$$\sum_\nu b_\nu \big[\hbar(\omega + i\delta) - E_g - E_\nu\big] \int d^3r \, \psi_\mu^*(\mathbf{r}) \psi_\nu(\mathbf{r}) = -d_{cv} \, \mathcal{E}(\omega) \, L^3 \psi_\mu^*(\mathbf{r} = 0) \ , \tag{10.95}$$

or

$$b_\mu = -\frac{d_{cv} L^3 \psi_\mu^*(\mathbf{r}=0)}{\hbar(\omega+i\delta) - E_g - E_\mu} \mathcal{E}(\omega) \ . \tag{10.96}$$

From Eq. (10.94), we see that

$$P_{vc}(\mathbf{r},\omega) = -\sum_\nu \mathcal{E}(\omega) \frac{d_{cv}\, L^3\, \psi_\nu^*(\mathbf{r}=0)}{\hbar(\omega+i\delta) - E_g - E_\nu} \psi_\nu(\mathbf{r}) \ , \tag{10.97}$$

and therefore

$$P_{vc,\mathbf{k}}(\omega) = -\sum_\nu \mathcal{E}(\omega) \frac{d_{cv} \psi_\nu^*(\mathbf{r}=0)}{\hbar(\omega+i\delta) - E_g - E_\nu} \int d^3r\, \psi_\nu(\mathbf{r}) e^{i\mathbf{k}\cdot\mathbf{r}} \ . \tag{10.98}$$

To compute the optical susceptibility from Eq. (10.98), we write the temporal Fourier transform of Eq. (10.28) as

$$\begin{aligned} P(\omega) &= \sum_{\mathbf{k}} \int dt\, (P_{cv,\mathbf{k}}(t) d_{vc} + P_{cv,\mathbf{k}}^*(t) d_{vc}) e^{i\omega t} \\ &= \sum_{\mathbf{k}} (P_{cv,\mathbf{k}}(\omega) d_{vc} + P_{cv,\mathbf{k}}^*(-\omega) d_{vc}) \ . \end{aligned} \tag{10.99}$$

Inserting Eq. (10.98), using $\mathcal{E}^*(-\omega) = \mathcal{E}(\omega)$, and

$$\sum_{\mathbf{k}} \int d^3r\, \psi_\nu(\mathbf{r}) e^{i\mathbf{k}\cdot\mathbf{r}} = 2L^3\, \psi_\nu(\mathbf{r}=0) \ , \tag{10.100}$$

we get

$$\begin{aligned} P(\omega) = &-2L^3 \sum_\nu |d_{cv}|^2 |\psi_\nu(\mathbf{r}=0)|^2 \mathcal{E}(\omega) \\ &\times \left[\frac{1}{\hbar(\omega+i\delta) - E_g - E_\nu} - \frac{1}{\hbar(\omega+i\delta) + E_g + E_\nu} \right] \ , \end{aligned} \tag{10.101}$$

where the factor 2 comes from the spin summation implicitly included in the $\mathbf{k}$-summation. From the relation

$$\chi(\omega) = \frac{\mathcal{P}(\omega)}{\mathcal{E}(\omega)} = \frac{P(\omega)}{L^3 \mathcal{E}(\omega)} \ , \tag{10.102}$$

we finally obtain the electron-hole-pair susceptibility as

$$\boldsymbol{\chi(\omega) = -2|d_{cv}|^2 \sum_{\mu} |\psi_{\mu}(\mathbf{r}=\mathbf{0})|^2}$$

$$\boldsymbol{\times \left[\frac{1}{\hbar(\omega + i\delta) - E_g - E_{\mu}} - \frac{1}{\hbar(\omega + i\delta) + E_g + E_{\mu}} \right]} \ . \qquad (10.103)$$

electron–hole–pair susceptibility

The first term in (10.103) is the resonant contribution and the second term is the nonresonant part, respectively. One often leaves out the nonresonant part since it does not contribute to the absorption, as can be verified using the Dirac identity, Eq. (1.69), and noting that the δ-function cannot be satisfied for $\omega > 0$.

Eq. (10.103) shows that the optical susceptibility is the sum over all states μ, where the oscillator strength of each transition is determined by the probability to find the conduction-band electron and the valence-band hole at the origin, i.e., within the same lattice unit cell.

10.5.1 *Three- and Two-Dimensional Cases*

The wave functions which are finite in the origin are those with $l = 0$ and $m = 0$ in $3D$ and those with $m = 0$ in $2D$. Using the wave functions (10.70), (10.71) and (10.89) and

$$Y_{0,0} = \frac{1}{\sqrt{4\pi}} \ ,$$

the resonant part of the optical susceptibility for a three-dimensional semiconductor becomes

$$\chi(\omega) = -\frac{2|d_{cv}|^2}{\pi E_0 a_0^3} \Big[\sum_n \frac{1}{n^3} \frac{E_0}{\hbar(\omega + i\delta) - E_g - E_n} + \frac{1}{2} \int dx \frac{x e^{\pi/x}}{\sinh(\pi/x)} \frac{E_0}{\hbar(\omega + i\delta) - E_g - E_0 x^2} \Big] \ . \qquad (10.104)$$

Inserting (10.104) into Eq. (1.53) and using the Dirac identity, we obtain the band edge absorption spectrum as

$$\boldsymbol{\alpha(\omega) = \alpha_0^{3D} \frac{\hbar\omega}{E_0} \left[\sum_{n=1}^{\infty} \frac{4\pi}{n^3} \delta(\Delta + \frac{1}{n^2}) + \Theta(\Delta) \frac{\pi e^{\frac{\pi}{\sqrt{\Delta}}}}{\sinh(\frac{\pi}{\sqrt{\Delta}})} \right]} \,,$$

3*D* Elliott formula (10.105)

where

$$\Delta = (\hbar\omega - E_g)/E_0 \tag{10.106}$$

and α_0^D has been defined in Eq. (5.81).

Eq. (10.105) is often called the Elliott formula. The $3D$ exciton absorption spectrum consists of a series of sharp lines with a rapidly decreasing oscillator strength $\propto n^{-3}$ and a continuum absorption due to the ionized states. A comparison of the continuum part α_{cont} of (10.105) with Eq. (5.80) describing the free-carrier absorption spectrum α_{free}, shows that one can write

$$\alpha_{cont} = \alpha_{free}\, C(\omega) \tag{10.107}$$

where

$$C(\omega) = \frac{\frac{\pi}{\sqrt{\Delta}} e^{\pi/\sqrt{\Delta}}}{\sinh(\pi/\sqrt{\Delta})} \tag{10.108}$$

is the so-called Sommerfeld or Coulomb enhancement factor. For $\Delta \to 0$, $C(\omega) \to 2\pi/\sqrt{\Delta}$ so that the continuum absorption assumes a constant value at the band gap, in striking difference to the square-root law of the free-carrier absorption. This shows that the attractive Coulomb interaction not only creates the bound states but has also a pronounced influence on the ionization continuum. If one takes into account a realistic broadening of the single particle-energy eigenstates, e.g., caused by scattering of electron–hole pairs with phonons, only a few bound states can be spectrally resolved. The energetically higher bound states merge continuously with the absorption of the ionized states. Fig. 10.2 shows a schematic and a computed absorption spectrum for a bulk semiconductor. The dominant feature is the $1s$-exciton absorption peak. The $2s$-exciton is also resolved, but its height is only $1/8$ of the $1s$- resonance. The higher exciton states appear only as a small peak just below the band gap and the continuum absorption is almost constant

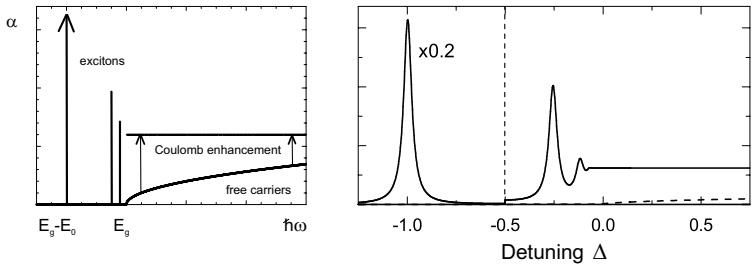

Fig. 10.2 Schematic (left figure) and calculated (right figure) band edge absorption spectrum for a $3D$ semiconductor. Shown are the results obtained with and without including the Coulomb interaction. The $1s$-exciton part of the computed absorption spectra has been scaled by a factor of 0.2 .

in the shown spectral region. Such spectra are indeed observed at very low temperatures in extremely good-quality semiconductors.

For the two-dimensional limit, we obtain the resonant part of the optical susceptibility as

$$\chi(\omega) = -\frac{|d_{cv}|^2}{L_c \pi a_0^2 E_0} \left[\sum_{n=0}^{\infty} \frac{2}{(n+1/2)^3} \frac{E_0}{\hbar(\omega + i\delta) - E_g - E_n} + \int dx \frac{x e^{\pi/x}}{\cosh(\pi/x)} \frac{E_0}{\hbar(\omega + i\delta) - E_g - E_0 x^2} \right] , \tag{10.109}$$

and the resulting absorption spectrum is

$$\boldsymbol{\alpha(\omega) = \alpha_0^{2D} \frac{\hbar\omega}{E_0} \left[\sum_{n=0}^{\infty} \frac{4}{(n+\frac{1}{2})^3} \delta\left(\Delta + \frac{1}{(n+\frac{1}{2})^2} \right) + \Theta(\Delta) \frac{e^{\frac{\pi}{\sqrt{\Delta}}}}{\cosh(\frac{\pi}{\sqrt{\Delta}})} \right].} \tag{10.110}$$

$2D$ Elliott formula

The $2D$ Coulomb enhancement factor

$$C(\omega) = \frac{e^{\pi/\sqrt{\Delta}}}{\cosh(\pi/\sqrt{\Delta})} \tag{10.111}$$

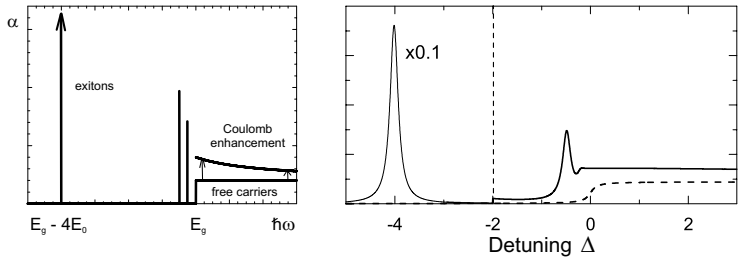

Fig. 10.3 Schematic (left figure) and calculated (right figure) band edge absorption spectrum for a $2D$ semiconductor. Shown are the results obtained with and without including the Coulomb interaction. The $1s$-exciton part of the computed absorption spectra has been scaled by a factor of 0.1 .

approaches 2 for $\Delta \to 0$. The absorption at the band edge is thus twice the free-carrier continuum absorption. For a finite damping, the absorption of the ionized states and the absorption in the higher bound states again join continuously. Fig. 10.3 shows both, the schematic and the computed absorption spectrum using Eq. (10.110). In comparison to the $3D$-case, the $2D$ $1s$-exciton is spectrally far better resolved as a consequence of the four-fold increase in binding energy in $2D$.

10.5.2 *Quasi-One-Dimensional Case*

In the final subsection of this exciton chapter, we discuss the optical spectra of quantum wires. Because of the cut-off in the Coulomb potential we have for the optical susceptibility

$$\chi(\omega) = -2|d_{cv}|^2 \sum_{\lambda} |f_\lambda(\alpha\gamma R)|^2 \times \left[\frac{1}{\hbar(\omega + i\delta) - E_g - E_\lambda} - \frac{1}{\hbar(\omega + i\delta) + E_g + E_\lambda} \right] . \qquad (10.112)$$

With the q1D eigenfunctions of the bound and ionized pair states, Eqs. (10.75) and (10.97), respectively, we get the following resonant contributions to the spectrum

$$\chi(\omega) = -\frac{2}{E_0}|d_{cv}|^2 \left[\sum_\lambda |N_\lambda W^2_{\lambda,1/2}(2\gamma R/\lambda a_0)|^2 \frac{E_0}{\hbar(\omega + i\delta) - E_g - E_\lambda} \right.$$
$$\left. + \frac{2}{a_0} \int_0^\infty dx \, \frac{e^{\pi/x}}{2\pi} \frac{|D_0^{(2)} W^{(1)} - D_0^{(1)} W^{(2)}|^2}{|D_0^{(1)}|^2 + |D_0^{(2)}|^2} \frac{E_0}{\hbar(\omega + i\delta) - E_g - E_0 x^2} \right] , \tag{10.113}$$

where $x = a_0 k$ is used again as the integration variable in the contribution of the continuum states. The functions $D_0^{(i)}$ and $W^{(i)}$ defined in Eqs. (10.93) and (10.91), respectively, are all evaluated at $\zeta = 2ik\gamma R$. The absorption spectrum is finally given by

$$\alpha(\omega) = \frac{4\pi\omega}{nc} \frac{2}{E_0} |d_{cv}|^2 \left[\sum_\lambda |N_\lambda W^2_{\lambda,1/2}(2\gamma R/\lambda a_0)|^2 \pi \delta(\Delta - E_\lambda/E_0) \right.$$
$$\left. + \frac{1}{\pi a_0} \frac{|D_0^{(2)} W^{(1)} - D_0^{(1)} W^{(2)}|^2}{|D_0^{(1)}|^2 + |D_0^{(2)}|^2} \frac{e^{\pi/\sqrt{\Delta}}}{2\sqrt{\Delta}} \right] , \tag{10.114}$$

where $\Delta = (\hbar\omega - E_g)/E_0$ is again the normalized energy detuning from the band gap. The Sommerfeld factor which describes the deviations of the

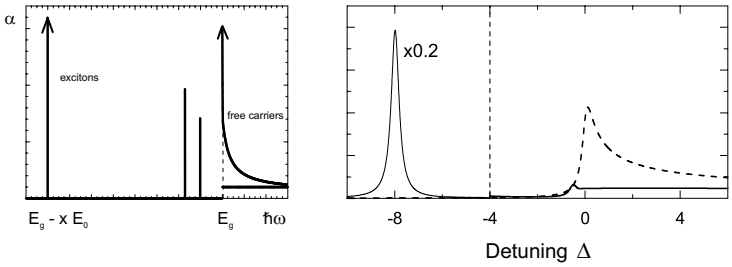

Fig. 10.4 Schematic (left figure) and calculated (right figure) band edge absorption spectrum for a *quasi*-1*D* semiconductor. Shown are the results obtained with and without including the Coulomb interaction. The 1*s*-exciton part of the computed absorption spectra has been scaled by a factor of 0.2 .

continuum spectrum from the free-carrier spectrum in Chap. 5 is given by

$$C(\omega) = \frac{e^{\pi/\sqrt{\Delta}}}{8} \frac{|D_0^{(2)} W^{(1)} - D_0^{(1)} W^{(2)}|^2}{|D_0^{(1)}|^2 + |D_0^{(2)}|^2} \quad . \tag{10.115}$$

In striking contrast to the $3D$ and $2D$ cases, the q1D Sommerfeld factor $C(\omega) < 1$ for all $\hbar\omega > E_g$. Due to this fact, the singular $1D$-density of states does not show up at all in the absorption spectrum (see Fig. 10.4). In fact, the band gap in a quantum wire cannot be determined directly from the low-intensity optical spectra, so that other techniques, such as two-photon absorption, have to be used for such a measurement. The absences of any structure at the band gap is by no means a consequence of a finite broadening but solely a Coulomb effect. A very large part of the total oscillator strength is accumulated in the exciton ground state. Note, that the first excited state has odd parity, only the second excited state contributes to the absorption spectrum. The approximate vanishing of the higher bound states (10.80) shows that they have indeed very small oscillator strengths.

REFERENCES

R.J. Elliott, in *Polarons and Excitons*, eds. C.G. Kuper and G.D. Whitefield, Oliver and Boyd, (1963), *p.* 269
L.D. Landau and E.M. Lifshitz, *Quantum Mechanics*, Pergamon, New York (1958)
L.I. Schiff, *Quantum Mechanics*, 3rd *ed.*, McGraw Hill, New York (1968)
M. Shinada and S. Sugano, J. Phys. Soc. Japan **21**, 1936 (1966)

For further discussion of the theory of excitons see:

Polarons and Excitons, eds. C.G. Kuper and G.D. Whitefield, Oliver and Boyd, (1963)
R.S. Knox, *Theory of Excitons*, Academic, New York (1963)

For the theory of excitons in quantum wires see:

R. Loudon, Am. J. Phys. **27**, 649 (1959)
L. Banyai, I. Galbraith, C. Ell, and H. Haug, Phys. Rev. **B36**, 6099 (1987)

T. Ogawa and T. Takagahara, Phys. Rev. **B43**, 14325 (1991)

PROBLEMS

Problem 10.1: Derive the Hamiltonian (10.14) from Eq. (7.29) by including the band index λ with all the operators and by summing over $\lambda = c, v$. Discuss the terms which have been omitted in (10.14).

Problem 10.2: Use the Heisenberg equation with the Hamiltonian (10.14) to compute the equation of motion (10.18) for the interband polarization. Make the Hartree–Fock approximation in the four-operator terms to obtain Eq. (10.21).

Problem 10.3: Verify that Eqs. (10.105) and (10.110) correctly reduce to the respective free-particle result without Coulomb interaction. Hint: Formally one can let the Bohr radius $a_0 \to \infty$ to obtain the free-particle limit.

Chapter 11

Polaritons

In direct-gap semiconductors, excitons and photons are strongly coupled. To account for this coupling, it can be useful, especially in the linear regime, to introduce new quasi-particles, the *polaritons*, which combine exciton and photon properties. This polariton concept has been very helpful for explaining optical measurements in $3D$- semiconductors with a large direct gap at low excitation densities.

11.1 Dielectric Theory of Polaritons

In Chap. 10, we derived the Wannier equation, Eq. (10.35), for the relative motion of an electron–hole pair. If we include also the center-of-mass motion, this equation becomes

$$-\left[\frac{\hbar^2\nabla^2_{\mathbf{R}}}{2M}+\frac{\hbar^2\nabla^2_{\mathbf{r}}}{2m_r}+V(r)\right]\psi(\mathbf{R},\mathbf{r})=E_{tot}\psi(\mathbf{R},\mathbf{r}) \ , \tag{11.1}$$

where $M=m_e+m_h$. As in the case of the hydrogen atom, the center-of-mass motion is described by a plane wave

$$\psi(\mathbf{R},\mathbf{r})=\frac{e^{i\mathbf{k}\cdot\mathbf{R}}}{L^{3/2}}\psi(\mathbf{r}) \ . \tag{11.2}$$

Correspondingly, the total energy eigenvalue of Wannier excitons is

$$E_{tot}=E_g+E_n+\frac{\hbar^2K^2}{2M} \ . \tag{11.3}$$

As in the case of an hydrogen atom, the center-of-mass wave function of the exciton is a plane wave $\propto \exp(i\mathbf{k}\cdot\mathbf{R})$.

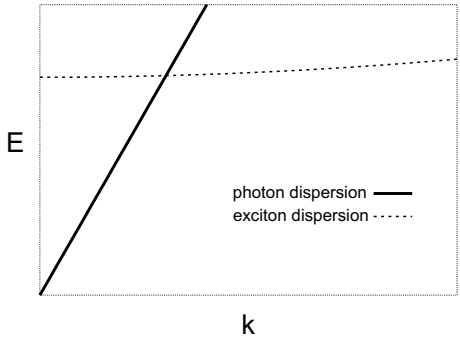

Fig. 11.1 Schematic drawing of photon and 1*s*-exciton dispersion.

In Fig. 11.1, we plot the dispersion of the 1*s*-exciton together with the dispersion of the light

$$\hbar\omega_k = \frac{\hbar c k}{n_0} \ , \tag{11.4}$$

where n_0 is the background refractive index of the medium. The figure shows that both dispersions intersect, i.e., there is a degeneracy at the intersection point. The exciton–photon interaction removes that degeneracy introducing a modified joint dispersion. The quasi-particles associated with this new dispersion are the exciton–polaritons. In general, polaritons are also formed by transverse optical phonons and the light, called phonon–polaritons. Since we do not discuss phonon–polaritons in this book, we refer to the exciton–polaritons simply as polaritons.

The optical dielectric function for the excitons, i.e., without the ionization continuum, is

$$\begin{aligned} \epsilon(\omega) &= \epsilon_0[1 + 4\pi\chi(\omega)] \\ &= \epsilon_0 \left[1 - 8\pi |d_{cv}|^2 \sum_n \frac{|\psi_n(\mathbf{r}=0)|^2}{\hbar(\omega + i\delta) - E_g - E_n} \right] \ , \end{aligned} \tag{11.5}$$

where $\epsilon_0 = n_0^2$ and Eq. (10.103) have been used. In this form, only resonant terms are contained and the momentum of the emitted or absorbed photon has been neglected. In order to find the propagating electromagnetic modes

in a dielectric medium, we have to insert $\epsilon(\omega)$ into the wave equation (1.43) for the transverse electric field of a light beam. For a plane wave, we get

$$\left[-k^2 + \frac{\omega^2}{c^2}\epsilon(\omega)\right] \mathcal{E}_\omega e^{i(\mathbf{k}\cdot\mathbf{r}-\omega t)} = 0 \ . \tag{11.6}$$

The transverse eigenmodes of the medium are obtained from the requirement that $\mathcal{E}_\omega \neq 0$, so that

$$\boldsymbol{c^2k^2 = \omega^2\epsilon(\omega)} \ . \tag{11.7}$$

transverse eigenmodes

11.1.1 *Polaritons without Spatial Dispersion and Damping*

Let us analyze Eq. (11.7) considering only the contribution of the lowest exciton level,

$$\epsilon(\omega) \simeq \epsilon_0 \left[1 - 8\pi|d_{cv}|^2 \frac{|\psi_1(\mathbf{r}=0)|^2}{\hbar(\omega + i\delta) - E_g + E_0}\right] \ , \tag{11.8}$$

or

$$\epsilon(\omega) = \epsilon_0 \left(1 - \frac{\Delta}{\omega - \omega_0 + i\delta}\right) \ , \tag{11.9}$$

where

$$\hbar\Delta = 8\pi|d_{cv}|^2|\psi_1(\mathbf{r}=0)|^2 \quad \text{and} \quad \hbar\omega_0 = E_g - E_0 \ . \tag{11.10}$$

In order to satisfy Eq. (11.7), the wave number k has to be chosen complex

$$k = k' + ik'' \ . \tag{11.11}$$

Then we can write the real and imaginary part of Eq. (11.7) as

$$\frac{\omega^2\epsilon_0}{c^2}\left(1 - \frac{\Delta}{\omega - \omega_0}\right) = k'^2 - k''^2 \tag{11.12}$$

and

$$\pi\delta(\omega - \omega_0)\frac{\omega_0^2\epsilon_0}{c^2} = 2k'k'' \ , \tag{11.13}$$

respectively, where the Dirac identity, Eq. (1.17), has been used. The imaginary part of the wave number is proportional to $\delta(\omega - \omega_0)$ describing absorption at the exciton resonance. Outside the resonance ($\omega \neq \omega_0$) we obtain the undamped polariton modes

$$\omega\sqrt{\frac{\omega - \omega_0 - \Delta}{\omega - \omega_0}} = \frac{ck'}{\sqrt{\epsilon_0}} \ . \tag{11.14}$$

The resulting dispersion is plotted in Fig. 11.2.

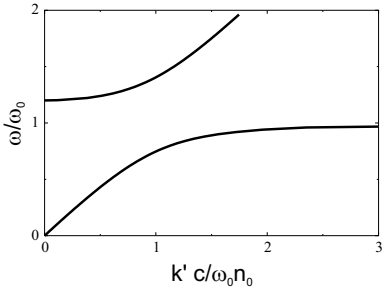

Fig. 11.2 Polariton dispersion without spatial dispersion for $\Delta/\omega_0 = 0.2$.

From Eq. (11.14) one obtains for low frequencies, $\omega << \omega_0$, a photon-like dispersion

$$\omega \simeq \frac{ck'}{\sqrt{\epsilon_0(1 + \Delta/\omega_0)}} \tag{11.15}$$

with a light velocity slightly smaller than c/n_0. For $\omega \to \omega_0$, the wave number diverges, $k' \to \infty$. No solution of Eq. (11.14) exists for frequencies between ω_0 and $\omega_0 + \Delta$. In other words, there is a *stop band* between ω_0 and $\omega_0 + \Delta$ separating the lower and upper polariton branch. At $\omega_0 + \Delta$, k' is zero and for $\omega >> \omega_0$ one again obtains a photon-like dispersion with the light velocity c/n_0.

The longitudinal eigenmodes of a dielectric medium are determined by

$$\boldsymbol{\epsilon(\omega) = 0} \ , \tag{11.16}$$

longitudinal eigenmodes

which yields the eigenfrequencies of the longitudinal exciton $\omega_l = \omega_0 + \Delta$, while the transverse exciton frequency $\omega_t = \omega_0$. Therefore, Δ is called the longitudinal-transverse (LT) splitting.

For the longitudinal excitons, the polarization is parallel to the wave vector $\mathbf{k}$. Eq. (11.10) shows that the longitudinal-transverse splitting is proportional to the so-called optical matrix element

$$|d_{cv}|^2 |\psi_1(\mathbf{r} = 0)|^2 \propto \frac{|d_{cv}|^2}{a_0^d} \ , \tag{11.17}$$

where Eqs. (10.70) and (10.71) have been used. The region in which no transverse waves propagate is thus particularly large for crystals with small exciton Bohr radii, i.e., in wide-gap semiconductors such as CuCl. Whether the LT-splitting can be observed experimentally depends on the ratio of Δ to the exciton damping δ, which is finite in real crystals, e.g., as a consequence of the exciton–phonon interaction. For $\Delta >> \delta$, the stop band is physically important, but not for $\Delta << \delta$.

In general, the dielectric functions for longitudinal and transverse excitations are not the same. However, they become degenerate in the long wave-length limit, which we have considered so far. For more details see Haug and Schmitt–Rink (1984).

11.1.2 *Polaritons with Spatial Dispersion and Damping*

If the momentum of the photon is not disregarded, the momentum conservation requires that the created or annihilated exciton has the same finite wave vector as the photon. The energy of an exciton with a finite translational momentum $\hbar k$ is given by Eq. (11.3). Then the transverse dielectric function becomes wave-number-dependent, yielding for the $1s$-exciton state

$$\epsilon(\mathbf{k}, \omega) = \epsilon_0 \left(1 - \frac{\Delta}{\omega - \omega_0 - \frac{\hbar k^2}{2M} + i\gamma} \right) \ . \tag{11.18}$$

Here, we treat the damping γ as a generally nonvanishing constant. However, we note that a realistic description of an exciton absorption line often

requires a frequency-dependent damping $\gamma(\omega)$. A constant γ results in a Lorentzian absorption line, but in reality one observes at elevated temperatures nearly universally an exponential decrease of the exciton absorption $\alpha(\omega)$ for frequencies below the exciton resonance, i.e.,

$$\boldsymbol{\alpha(\omega) = \alpha_0 e^{-(\omega_0-\omega)/\sigma}} \quad \text{for } \boldsymbol{\omega < \omega_0} \ . \tag{11.19}$$

Urbach rule

The derivation of the Urbach rule needs a damping $\gamma(\omega)$ which decreases with increasing detuning $\omega_0 - \omega$. The physical origin of the dynamical or frequency-dependent damping is the following: the absorption of a photon with insufficient energy $\hbar\omega < \hbar\omega_0$ requires the scattering of the virtually created exciton with energy $\hbar\omega$ into a state $E_k = \hbar\omega_0 + \hbar^2 k^2/2M$ under the absorption or scattering of an already present excitation in the crystal. In polar semiconductors, the relevant excitation will be a longitudinal optical (LO) phonon. Now it is evident that $\gamma(\omega)$ decreases rapidly with decreasing frequency because the probability to absorb n LO phonons decreases rapidly with increasing n. From a microscopic point of view, the damping is the imaginary part of the exciton self-energy $\Sigma(\mathbf{k}, \omega)$, which in general is both frequency- and momentum-dependent.

Now let us return to the simple form of Eq. (11.18) to discuss the transverse eigenmodes. Because a momentum-dependent dielectric function means a nonlocal response in real space, one speaks in this case also of a dielectric function with spatial dispersion. Inserting Eq. (11.18) into the eigenmode equation (11.7) yields

$$\frac{c^2 k^2}{\epsilon_0} = \omega^2 \left(1 - \frac{\Delta}{\omega - \omega_0 - \frac{\hbar k^2}{2M} + i\gamma} \right) \ . \tag{11.20}$$

The solution of this equation for the real and imaginary part of the wave number is shown in Fig. 11.3.

With spatial dispersion and finite damping one finds for all frequencies two branches, ω_1 and ω_2. At high frequencies, $\omega/\omega_0 > 1$, Fig. 11.3 again shows a photon-like and an exciton-like branch. In the range of the LT-split, $\omega_2(k')$ has some structure which results in a negative group velocity [negative slope of $\omega_2(k')$]. One sees, however, that in this range the damping of this mode increases strongly. In a region with damping, the group velocity loses its

meaning. Instead, the Poynting vector has to be calculated, from which one gets an energy velocity. At still lower frequency the branch ω_2 continues as a Tscherenkov mode with $c_T > c/n_0$. But again this has no physical significance due to the very large damping. The mode ω_1 is damped in the range of the LT-splitting and becomes photon-like with little damping below the exciton resonance, $\omega/\omega_0 = 1$.

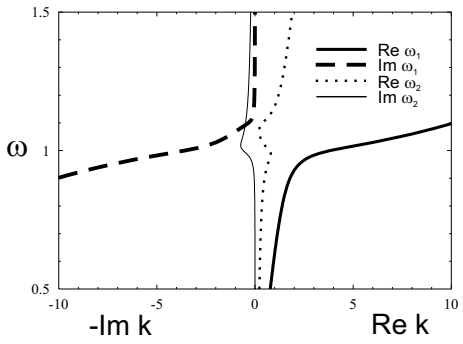

Fig. 11.3 Polariton dispersion with spatial dispersion and damping for $\Delta/\omega_0 = 0.1$, $\gamma/\omega_0 = 0.01$, $\hbar\omega_0\epsilon_0/2Mc^2 = 0.001$. The frequency ω is in units of ω_0 and k is in units of c/ω_0, respectively.

If one considers the influence of the interface between the crystal and, e.g., vacuum, the presence of two propagating modes requires an additional boundary condition (ABC). Often Pekar's additional boundary condition is chosen which states that the normal component of the polarization has to be zero at the interface. The need for the additional boundary condition stems from the fact that one has used a three dimensional spatial Fourier transform, which is not allowed for a crystal with a surface. To avoid this problem, one has to calculate the two-point polarization function $P_{cv}(\mathbf{r}, \mathbf{r}', t)$ for a spatially inhomogeneous system.

11.2 Hamiltonian Theory of Polaritons

Polaritons can also be discussed directly as mixed exciton–photon excitations in a semiconductor. For this end, we will introduce exciton creation and destruction operators, which, as we will show, obey Bose commutation relations in the linear regime. For the subsequent calculations, it is

convenient to introduce a hole operator

$$\beta^{\dagger}_{-\mathbf{k},-s} \equiv a_{v,\mathbf{k},s} \tag{11.21}$$

indicating that the annihilation of an electron with ($\mathbf{k}$, s) in the valence band corresponds to the creation of a hole with the opposite momentum and spin. To keep the notation symmetrical, we define

$$\alpha^{\dagger}_{\mathbf{k},s} \equiv a^{\dagger}_{c,\mathbf{k},s} \ , \tag{11.22}$$

where the electron operators α, $\alpha^{\dagger}$ operate exclusively in the conduction band and the hole operators β, $\beta^{\dagger}$ operate in the valence band, respectively.

Suppressing the spin index, and using the electron–hole pair operator

$$\alpha^{\dagger}_{\mathbf{k}}\beta^{\dagger}_{-\mathbf{k}'} \ , \tag{11.23}$$

the operator describing generation of an exciton in the state ν with total momentum $\mathbf{K}$ can be written as

$$\begin{aligned} B^{\dagger}_{\nu,\mathbf{K}} &= \sum_{\mathbf{k},\mathbf{k}'} \delta\big[\mathbf{K} - (\mathbf{k} - \mathbf{k}')\big]\psi_{\nu}\left(\frac{\mathbf{k}+\mathbf{k}'}{2}\right)\alpha^{\dagger}_{\mathbf{k}}\beta^{\dagger}_{-\mathbf{k}'} \\ &= \sum_{\mathbf{k}} \psi_{\nu}(\mathbf{k} - \mathbf{K}/2)\alpha^{\dagger}_{\mathbf{k}}\beta^{\dagger}_{\mathbf{K}-\mathbf{k}} \ . \end{aligned} \tag{11.24}$$

The derivation of this relation is best obtained in the Dirac representation, where

$$B^{\dagger}_{\nu,\mathbf{K}} = |\nu\mathbf{K}\rangle\langle 0| \ . \tag{11.25}$$

Multiplying Eq. (11.25) with the completeness relation in terms of the electron–hole pairs

$$\sum_{\mathbf{k},\mathbf{k}'} |\mathbf{k},-\mathbf{k}'\rangle\langle\mathbf{k},-\mathbf{k}'| = 1 \ , \tag{11.26}$$

one gets

$$
\begin{aligned}
B^\dagger_{\nu,\mathbf{K}} &= \sum_{\mathbf{k},\mathbf{k}'} |\mathbf{k},-\mathbf{k}'\rangle\langle\mathbf{k},-\mathbf{k}'|\nu\mathbf{K}\rangle\langle 0| \\
&= \sum_{\mathbf{k},\mathbf{k}'} \langle\mathbf{k},-\mathbf{k}'|\nu\mathbf{K}\rangle|\mathbf{k},-\mathbf{k}'\rangle\langle 0| \\
&= \sum_{\mathbf{k},\mathbf{k}'} \langle\mathbf{k},-\mathbf{k}'|\nu\mathbf{K}\rangle\alpha^\dagger_{\mathbf{k}}\beta^\dagger_{-\mathbf{k}'} \ . \qquad (11.27)
\end{aligned}
$$

Furthermore,

$$
\begin{aligned}
\langle\mathbf{k},-\mathbf{k}'|\nu\mathbf{K}\rangle &= \int d^3r\, d^3r' \langle\mathbf{k},-\mathbf{k}'|\mathbf{r},\mathbf{r}'\rangle\langle\mathbf{r},\mathbf{r}'|\nu\mathbf{K}\rangle \\
&= \int d^3r\, d^3r' e^{-i\mathbf{k}\cdot\mathbf{r}}\, e^{i\mathbf{k}'\cdot\mathbf{r}'} e^{i\mathbf{K}\cdot(\mathbf{r}+\mathbf{r}')/2}\psi_\nu(\mathbf{r}-\mathbf{r}') \\
&= \delta[\mathbf{K}-(\mathbf{k}-\mathbf{k}')]\psi_\nu\left(\frac{\mathbf{k}+\mathbf{k}'}{2}\right) \ , \qquad (11.28)
\end{aligned}
$$

where $\psi_\nu(\mathbf{k})$ is the Fourier transform of the exciton wave function for the relative motion. Explicitly, the Fourier transforms for the ground-state wave functions are

$$
\psi_0(k) = 8\sqrt{\pi a_0^3}\frac{1}{[1+(ka_0)^2]^2} \qquad \text{in } 3D \qquad (11.29)
$$

and

$$
\psi_0(k) = \sqrt{2\pi}a_0\frac{1}{[1+(ka_0/2)^2]^{3/2}} \qquad \text{in } 2D \ . \qquad (11.30)
$$

We see that $\psi_0(k)$ is roughly constant for $0 < k < 1/a_0$ or $2/a_0$, and falls off rapidly for large k values.

The commutator for the exciton operators is

$$
\begin{aligned}
[B_{0,0}, B^\dagger_{0,0}] &= \sum_{\mathbf{k},\mathbf{k}'} \psi_0(k)\psi_0^*(k')\left[\beta_{-\mathbf{k}}\alpha_{\mathbf{k}}\,,\,\alpha^\dagger_{\mathbf{k}'}\beta^\dagger_{-\mathbf{k}'}\right] \\
&= \sum_{\mathbf{k}} |\psi_0(k)|^2(1-\alpha^\dagger_{\mathbf{k}}\alpha_{\mathbf{k}}-\beta^\dagger_{-\mathbf{k}}\beta_{-\mathbf{k}}) \qquad (11.31)
\end{aligned}
$$

so that

$$
\langle[B_{0,0}, B^\dagger_{0,0}]\rangle = 1 - \mathcal{O}(na_0^d). \qquad (11.32)
$$

This is a Bosonic commutator relation for a vanishing number of electrons and holes, i.e. in the linear regime. At elevated densities, however, one has to take the deviations from the Bosonic nature into account.

The Hamiltonian for free excitons can be written as

$$\mathcal{H}_0 = \sum_{\mathbf{k}} \hbar e_{\nu k} B^\dagger_{\nu,\mathbf{k}} B_{\nu,\mathbf{k}}. \tag{11.33}$$

In order to express the interaction Hamiltonian $\mathcal{H}_I$ of the electron system with the light field in terms of exciton operators, we multiply Eq. (11.24) with $\psi^*_\nu(\boldsymbol{\kappa})$ and sum over ν to get

$$\begin{aligned}\sum_\nu \psi^*_\nu(\boldsymbol{\kappa}) B^\dagger_{\nu,\mathbf{K}} &= \sum_{\nu\mathbf{k}} \psi^*_\nu(\boldsymbol{\kappa})\psi_\nu(\mathbf{k}-\mathbf{K}/2)\alpha^\dagger_{\mathbf{k}}\beta^\dagger_{\mathbf{K}-\mathbf{k}} \\ &= \sum_{\mathbf{k}} \delta_{\boldsymbol{\kappa},\mathbf{k}-\mathbf{K}/2}\alpha^\dagger_{\mathbf{k}}\beta^\dagger_{\mathbf{K}-\mathbf{k}} = \alpha^\dagger_{\frac{1}{2}\mathbf{K}+\boldsymbol{\kappa}}\beta^\dagger_{\frac{1}{2}\mathbf{K}-\boldsymbol{\kappa}} \ . \end{aligned} \tag{11.34}$$

Taking the finite wave number q of the light explicitly into account, $\mathcal{H}_I$ can then be written as

$$\begin{aligned}\mathcal{H}_I &= -\sum_{\mathbf{k},\mathbf{q}} d_{cv}\left[\alpha^\dagger_{\frac{1}{2}\mathbf{q}+\mathbf{k}}\beta^\dagger_{\frac{1}{2}\mathbf{q}-\mathbf{k}}\mathcal{E}(\mathbf{q})e^{-i\omega_q t} + \text{h.c.}\right] \\ &= -\sum_{\mathbf{k},\mathbf{q},\nu} d_{cv}\left[\psi_\nu(k)B^\dagger_{\nu,\mathbf{q}}\mathcal{E}(\mathbf{q})e^{-i\omega_q t} + \text{h.c.}\right] \ . \end{aligned} \tag{11.35}$$

Using

$$\mathcal{E}(\mathbf{q},t) = -\frac{1}{c}\frac{\partial}{\partial t}A(\mathbf{q},t) \ , \tag{11.36}$$

we obtain

$$\mathcal{E}(\mathbf{q},t) = \mathcal{E}(\mathbf{q})e^{-i\omega_q t} = i\sqrt{2\pi\hbar\omega_q}(b_{\mathbf{q}} - \text{h.c.}) \ , \tag{11.37}$$

where we denote the photon annihilation operator by $b_{\mathbf{q}}$ (see Appendix A), and

$$\omega_q = \frac{cq}{\sqrt{\epsilon_0}} \ . \tag{11.38}$$

The exciton–photon interaction Hamiltonian in the resonant approximation is thus

$$\mathcal{H}_I = -i\hbar \sum_{\mathbf{q},\nu} g_{\nu\mathbf{q}} (B^\dagger_{\nu\mathbf{q}} b_{\mathbf{q}} - \text{h.c.}) \tag{11.39}$$

with the optical matrix element

$$\hbar g_{\nu\mathbf{q}} = d_{cv} \psi^*_\nu(\mathbf{r}=0) \sqrt{\pi\hbar\omega_q/2} \ . \tag{11.40}$$

The total exciton–photon Hamiltonian is now

$$\mathcal{H} = \hbar \sum_{\mathbf{q}} \left[\sum_\nu e_{\nu q} B^\dagger_{\nu\mathbf{q}} B_{\nu\mathbf{q}} + \omega_q b^\dagger_{\mathbf{q}} b_{\mathbf{q}} - i \sum_\nu g_{\nu\mathbf{q}} (B^\dagger_{\nu\mathbf{q}} b_{\mathbf{q}} - \text{h.c.}) \right] \ . \tag{11.41}$$

In the following, we consider only the lowest exciton level. The bilinear Hamiltonian (11.41) can be diagonalized by introducing *polariton operators* $p_{\mathbf{q}}$ as linear combination of exciton and photon operators :

$$p_{\mathbf{q}} = u_{\mathbf{q}} B_{\mathbf{q}} + v_{\mathbf{q}} b_{\mathbf{q}} \ . \tag{11.42}$$

We demand that the polariton operators obey the Bose commutation relations

$$[p_{\mathbf{q}} \, , \, p^\dagger_{\mathbf{q}}] = |u_{\mathbf{q}}|^2 + |v_{\mathbf{q}}|^2 = 1 \ . \tag{11.43}$$

We now choose the unknown coefficients $u_{\mathbf{q}}$ and $v_{\mathbf{q}}$ so that the Hamiltonian (11.41) becomes diagonal in the polariton operators

$$\mathcal{H} = \hbar \sum_{\mathbf{q}} \Omega_q p^\dagger_{\mathbf{q}} p_{\mathbf{q}} \ . \tag{11.44}$$

It turns out that the transformation coefficients $u_{\mathbf{q}}$ and $v_{\mathbf{q}}$ and the polariton spectrum $\Omega_{\mathbf{q}}$ can best be found by evaluating the commutator $[p, H]/\hbar$ once directly using the polariton Hamiltonian (11.44) and once using Eq. (11.42) together with the exciton–photon Hamiltonian. We obtain

$$\begin{aligned} \Omega_{\mathbf{q}} p_{\mathbf{q}} &= \Omega_{\mathbf{q}} (u_{\mathbf{q}} B_{\mathbf{q}} + v_{\mathbf{q}} b_{\mathbf{q}}) \\ &= u_{\mathbf{q}} (e_{\mathbf{q}} B_{\mathbf{q}} - i g_{\mathbf{q}} b_{\mathbf{q}}) + v_{\mathbf{q}} (\omega_{\mathbf{q}} b_{\mathbf{q}} + i g_{\mathbf{q}} B_{\mathbf{q}}) \ . \end{aligned} \tag{11.45}$$

Comparing the coefficients of $B_{\mathbf{q}}$ and $b_{\mathbf{q}}$ we find

$$0 = (\Omega_{\mathbf{q}} - e_{\mathbf{q}}) u_{\mathbf{q}} + i g_{\mathbf{q}} v_{\mathbf{q}}$$

and

$$0 = -ig_{\mathbf{q}}u_{\mathbf{q}} + (\Omega_{\mathbf{q}} - \omega_{\mathbf{q}})v_{\mathbf{q}} \ , \tag{11.46}$$

respectively. The determinant of the coefficients of $u_{\mathbf{q}}$ and $v_{\mathbf{q}}$ has to vanish, i.e,

$$(\Omega_{\mathbf{q}} - e_{\mathbf{q}})(\Omega_{\mathbf{q}} - \omega_{\mathbf{q}}) - g_{\mathbf{q}}^2 = 0 \ ,$$

or

$$\boldsymbol{\Omega_{\mathbf{q},1,2} = \frac{1}{2}(e_{\mathbf{q}} + \omega_{\mathbf{q}}) \pm \frac{1}{2}\sqrt{(e_{\mathbf{q}} - \omega_{\mathbf{q}})^2 + 4g_{\mathbf{q}}^2}} \ . \tag{11.47}$$

polariton spectrum

We see immediately that $\Omega_{1,2}$ are the frequencies of the upper and lower polariton branches which we found already in Sec. 11.1. For $q \to 0$, the upper branch approaches $e_0 + g^2/e_0$ showing that the LT splitting in this formulation is given by g^2/e_0, which vanishes for g from Eq. (11.40).

Using Eqs. (11.43) and (11.46), we find for the upper polariton branch

$$u_{\mathbf{q},1} = \sqrt{\frac{\Omega_{\mathbf{q},1} - \omega_{\mathbf{q}}}{2\Omega_{\mathbf{q},1} - e_{\mathbf{q}} - \omega_{\mathbf{q}}}} \quad \text{and } v_{\mathbf{q},1} = i\sqrt{\frac{\Omega_{\mathbf{q},1} - e_{\mathbf{q}}}{2\Omega_{\mathbf{q},1} - e_{\mathbf{q}} - \omega_{\mathbf{q}}}} \tag{11.48}$$

and for the lower polariton branch with $\Omega_2 < e, \omega$ the coefficients

$$u_{\mathbf{q},2} = \sqrt{\frac{\Omega_{\mathbf{q},2} - \omega_{\mathbf{q}}}{2\Omega_{\mathbf{q},2} - e_{\mathbf{q}} - \omega_{\mathbf{q}}}} \quad \text{and } v_{\mathbf{q},2} = -i\sqrt{\frac{\Omega_{\mathbf{q},2} - e_{\mathbf{q}}}{2\Omega_{\mathbf{q},2} - e_{\mathbf{q}} - \omega_{\mathbf{q}}}} \ . \tag{11.49}$$

Fig. (11.4) shows the wave number dependence of $|u_1|^2$ and $|v_1|^2$ for the upper polariton branch according to Eq. (11.48), for simplicity without spatial dispersion, i.e., with $e_q = e_0$. The upper branch polariton is exciton-like for small q-values, ($|u_1|^2 \simeq 1$), and changes around the exciton resonance successively into a photon-like excitation ($|v_1|^2 \simeq 1$). The lower branch polariton shows the reverse properties.

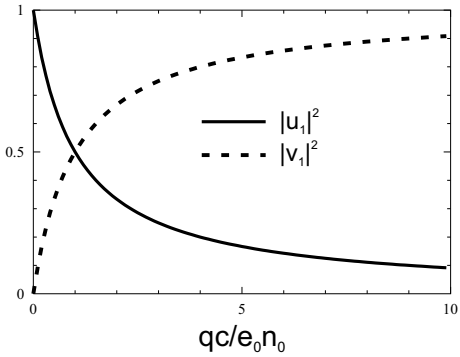

Fig. 11.4 Dispersion of $|u_i|^2$ and $|v_i|^2$ for the upper polariton branch.

The resulting polariton Hamiltonian is

$$\mathcal{H} = \hbar \sum_{\mathbf{q},i=1,2} \Omega_{i,q} p^\dagger_{i,\mathbf{q}} p_{i,\mathbf{q}} \ . \tag{11.50}$$

All formulas derived in this chapter hold only if the nonresonant interaction terms are small. The full interaction Hamiltonian with nonresonant terms has the form

$$\mathcal{H}_I = i\hbar \sum g_q (B_\mathbf{q} + B^\dagger_{-\mathbf{q}})(b_{-\mathbf{q}} - b^\dagger_\mathbf{q}) \ . \tag{11.51}$$

The total Hamiltonian can still be diagonalized by a transformation which mixes $B_\mathbf{q}$, $b_\mathbf{q}$ and $B^\dagger_{-\mathbf{q}}$, $b^\dagger_{-\mathbf{q}}$ operators linearly :

$$p_{i,\mathbf{q}} = u_{i,1,\mathbf{q}} B_\mathbf{q} + u_{i,2,\mathbf{q}} b_\mathbf{q} + u_{i,3,\mathbf{q}} B^\dagger_{-\mathbf{q}} + u_{i,4,\mathbf{q}} b^\dagger_{-\mathbf{q}} \ . \tag{11.52}$$

This slightly more general transformation is called the Hopfield (1958) polariton transformation.

If we compare the dielectric formalism used at the beginning of this chapter with the diagonalization procedure of this section, we see that an advantage of the first approach is that it allows us quite naturally to include the damping of the modes.

11.3 Microcavity Polaritons

Even though we did not specify it explicitly, the polariton properties discussed so far are valid for infinitely extended bulk materials. Modifications are necessary when we deal with quantum confined systems, such as quantum wells and wires. In these cases, free propagation is possible only in the unconfined directions, leading to two- or one-dimensional polariton modes.

More interesting are configurations with quantum confinement not only for the electrons but also for the photons. Here, the confinement for the photons can be provided by converting two parallel end faces of a semiconductor crystal into mirrors of very high reflectivity. This generates an optical resonator, i.e., a Fabry Perot cavity, which has eigenmodes determined by the length L of the cavity and the quality of the mirrors. In the simplest case, these mirrors could be made with metallic films, but often one uses so-called distributed Bragg reflectors (DBR mirrors) that are made of alternating layers of low and high refractive index material with a layer thickness of a quarter of the wave length of light.

If L equals half a wave length of light, one has a one-dimensional microcavity where only one longitudinal optical mode is allowed. This mode is just a standing wave with nodes at both mirrors and a single maximum in the middle of the sample, while parallel to the mirrors one has still a continuum of transverse running modes with a wave vector $\mathbf{k}_{\|}$.

To determine the microcavity mode, we start with the wave equation (1.43) in the form

$$\Delta\mathbf{E}(\mathbf{r},\omega) + \frac{\omega^2}{c^2}\epsilon(\omega)\mathbf{E}(\mathbf{r},\omega) = 0 \ , \tag{11.53}$$

where we assume a situation without any resonances in the spectral range of interest, so that the dielectric function is purely real, $\epsilon = n^2$. The solution for the lowest mode of the microresonator is

$$\mathbf{E}(\mathbf{r},\omega) = \mathbf{E}_0 \sin(\frac{\pi z}{L}) e^{i\mathbf{k}_{\|}\cdot\mathbf{r}} \ . \tag{11.54}$$

Inserting (11.54) into the wave equation (11.53), we find the eigenfrequencies

$$\omega_{0,k_{\|}} = \frac{c}{n}\sqrt{\frac{\pi^2}{L^2} + k_{\|}^2} \ . \tag{11.55}$$

Note, that in contrast to the dispersion of bulk photons, the dispersion of

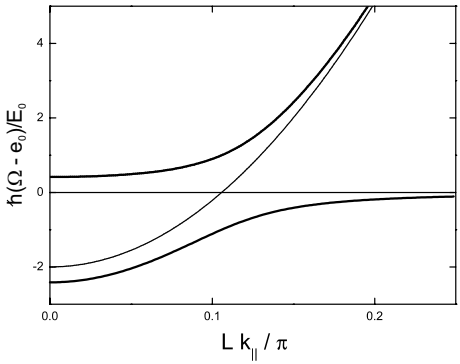

Fig. 11.5 Exciton polariton dispersion of a planar microcavity versus parallel momentum $k_\parallel$. The thin lines show the bare caving photon and exciton dispersions.

the microcavity polaritons (11.55) approaches a finite frequency in the long wave-length limit $k_\parallel \to 0$.

Next, we consider the interaction of this light mode with a $2D$ quantum well placed in the middle of the microcavity, i.e. at $z = L/2$, where the optical mode has its maximum. If one couples the $1s$-excitons of this quantum well to the photons of the microcavity mode, one gets in analogy with (11.41) the following resonant exciton–photon Hamiltonian

$$\mathcal{H} = \hbar \sum_{\mathbf{k}_\parallel} \left[e_{0,k_\parallel} B^\dagger_{0,\mathbf{k}_\parallel} B_{0,\mathbf{k}_\parallel} + \omega_{0,k_\parallel} b^\dagger_{0,\mathbf{k}_\parallel} b_{0,\mathbf{k}_\parallel} - i g_{k_\parallel} \left(B^\dagger_{0,\mathbf{k}_\parallel} b_{0,\mathbf{k}_\parallel} - h.c. \right) \right] . \tag{11.56}$$

Here, in analogy with (11.40), the interaction matrix element is given by

$$\hbar g_{k_\parallel} = d_{cv} \psi_0^{2D}(r=0) \sqrt{\pi \hbar \omega_{0,k_\parallel}} \ . \tag{11.57}$$

Applying the same diagonalization procedure as discussed in the last section, we get the following microcavity polariton spectrum

$$\Omega_{\mathbf{k}_\parallel,1,2} = \frac{1}{2}(e_{0,\mathbf{k}_\parallel} + \omega_{0,\mathbf{k}_\parallel}) \pm \frac{1}{2} \sqrt{(e_{0,\mathbf{k}_\parallel} - \omega_{0,\mathbf{k}_\parallel})^2 + 4 g^2_{k_\parallel}} \ . \tag{11.58}$$

A sketch of the resulting microcavity polariton is given in Fig. 11.5 for a cavity mode which is degenerate at $k_\parallel = 0$ with the $1s$-exciton. One sees

that in contrast to the bulk polariton both branches of the microresonator polariton tend to a finite frequency at $k_{\|} \to 0$ which gives these structures unique optical properties.

REFERENCES

The polariton concept has been introduced by:

J.J. Hopfield, Phys. Rev. **112**, 1555 (1958)

For a discussion of the ABC problem see:

V.M. Agranovich and V.L. Ginzburg, *Crystal Optics with Spatial Dispersion and Excitons*, Springer Verlag, Berlin (1984)
K. Cho, *Excitons*, Topics in Current Physics, Vol. 14, Springer Verlag, Berlin (1979)
A. Stahl and I. Balslev, *Electrodynamics of the Semiconductor Band Edge*, Springer Tracts in Modern Physics 110, Springer Verlag, Berlin (1987)

For a full numerical solution of the ABC problem and detailed comparisons to experiments see:

H.C. Schneider, F. Jahnke, S.W. Koch, J. Tignon, T. Hasche, and D.S. Chemla, "Polariton Propagation in High-Quality Semiconductors — Microscopic Theory and Experiment versus Additional Boundary Conditions", Phys. Rev. **B63**, 045202 (2001)

For a discussion of many aspects of semiconductor microcavity systems and a detailed list of references see:

G. Khitrova, H.M. Gibbs, F. Jahnke, M. Kira, and S.W. Koch, "Semiconductor Physics of Quantum Wells and Normal-Mode Coupling Microcavities", Rev. Mod. Phys. **71**, 1591 (1999)

PROBLEMS

Problem 11.1: Generalize Eq. (11.20) to include the energetically higher ($n = 2, 3, \dots$) exciton levels.

Problem 11.2: Compute the Fourier transform of the 1s-exciton wave

function in $2D$ and $3D$.

Problem 11.3: Compute the polariton transformation coefficients $u_{\mathbf{q}}$ and $v_{\mathbf{q}}$ and the polariton spectrum $\Omega_{\mathbf{q}}$ by evaluating the commutator $[p, \mathcal{H}]$ once using the polariton Hamiltonian, Eq. (11.44), and once using Eq. (11.42) together with the exciton–photon Hamiltonian.

Problem 11.4: Show that the operators for the lower and upper polariton branches commute, e.g., $[p_1, p_2^\dagger] = 0$.

Problem 11.5: Diagonalize the microcavity exciton–photon Hamiltonian (11.56) and derive the dispersion relation, Eq. (11.58), by applying the polariton transformation according to Eqs. (11.42) – (11.47).

This page intentionally left blank

Chapter 12

Semiconductor Bloch Equations

The previous two chapters analyze the interband transitions in semiconductors in the linear regime focusing on the correct treatment of the all important Coulomb attraction between the conduction-band electron and the valence-band hole. In this and the following chapters, we will now extend that treatment into the nonlinear regime where several electron–hole pairs are excited and the interactions between these pairs have to be considered. In situations with elevated electron–hole–pair densities, we have to deal with finite numbers of electrons and holes in the conduction and valence band which are coupled dynamically to the interband polarization. In this chapter, we derive the set of coupled differential equations which governs the coupled dynamics of electrons, holes and the optical polarization in the spectral vicinity of the semiconductor band gap. We call these equations the *semiconductor Bloch equations* since they are the direct generalization of the equations for the free-carrier transitions, which can be put into the form of Bloch equations, as has been shown in Chap. 5.

12.1 Hamiltonian Equations

We start from the Hamiltonian

$$\mathcal{H} = \mathcal{H}_{el} + \mathcal{H}_l \ , \tag{12.1}$$

where

$$\begin{aligned}\mathcal{H}_{el} = &\sum_{\mathbf{k}} \left(E_{c,k} a^{\dagger}_{c,\mathbf{k}} a_{c,\mathbf{k}} + E_{v,k} a^{\dagger}_{v,\mathbf{k}} a_{v,\mathbf{k}}\right) \\ &+ \frac{1}{2} \sum_{\mathbf{k},\mathbf{k}',\mathbf{q}\neq\mathbf{0}} V_q \left(a^{\dagger}_{c,\mathbf{k}+\mathbf{q}} a^{\dagger}_{c,\mathbf{k}'-\mathbf{q}} a_{c,\mathbf{k}'} a_{c,\mathbf{k}} + a^{\dagger}_{v,\mathbf{k}+\mathbf{q}} a^{\dagger}_{v,\mathbf{k}'-\mathbf{q}} a_{v,\mathbf{k}'} a_{v,\mathbf{k}}\right. \\ &\left. + 2 a^{\dagger}_{c,\mathbf{k}+\mathbf{q}} a^{\dagger}_{v,\mathbf{k}'-\mathbf{q}} a_{v,\mathbf{k}'} a_{c,\mathbf{k}}\right) \end{aligned} \tag{12.2}$$

is the electron part of the Hamiltonian in two-band approximation. Here, we include only those Coulomb interaction processes that conserve the particle number in each band. In other words, interband Coulomb processes in which, e.g., one electron and one hole are annihilated and two electrons are created are not taken into account due to the relatively large energy gap between both bands.

$$\mathcal{H}_I = -\sum_{\mathbf{k}} \mathcal{E}(t) (a^{\dagger}_{c,\mathbf{k}} a_{v,\mathbf{k}} d_{cv} + h.c.) \ , \tag{12.3}$$

describes the interband dipole coupling to the light field.

For the subsequent calculations, it is convenient to transform the total Hamiltonian into the electron–hole representation (see Chap. 11). Inserting the definitions (11.21) and (11.22),

$$\beta^{\dagger}_{-\mathbf{k}} = a_{v,\mathbf{k}} \tag{12.4}$$

and

$$\alpha^{\dagger}_{\mathbf{k}} = a^{\dagger}_{c,\mathbf{k}} \ , \tag{12.5}$$

into the Hamiltonian (12.1) and restoring normal ordering of the electron and hole operators, we obtain

$$\begin{aligned}\mathcal{H} = &\sum_{\mathbf{k}} \left(E_{e,k}\alpha^\dagger_{\mathbf{k}}\alpha_{\mathbf{k}} + E_{h,k}\beta^\dagger_{-\mathbf{k}}\beta_{-\mathbf{k}}\right) \\ &+ \frac{1}{2}\sum_{\mathbf{k},\mathbf{k}',\mathbf{q}\neq 0} V_q\left(\alpha^\dagger_{\mathbf{k}+\mathbf{q}}\alpha^\dagger_{\mathbf{k}'-\mathbf{q}}\alpha_{\mathbf{k}'}\alpha_{\mathbf{k}} + \beta^\dagger_{\mathbf{k}+\mathbf{q}}\beta^\dagger_{\mathbf{k}'-\mathbf{q}}\beta_{\mathbf{k}'}\beta_{\mathbf{k}} - 2\alpha^\dagger_{\mathbf{k}+\mathbf{q}}\beta^\dagger_{\mathbf{k}'-\mathbf{q}}\beta_{\mathbf{k}'}\alpha_{\mathbf{k}}\right) \\ &- \sum_{\mathbf{k}} \mathcal{E}(t)\left(d_{cv}\alpha^\dagger_{\mathbf{k}}\beta^\dagger_{-\mathbf{k}} + \text{h.c.}\right) \ , \end{aligned} \tag{12.6}$$

electron–hole Hamiltonian

where constant terms have been left out. The single particle energies in (12.6) are

$$E_{e,k} = E_{c,k} = \hbar\epsilon_{e,k}$$

and

$$E_{h,k} = -E_{v,k} + \sum_{\mathbf{q}\neq 0} V_q = \hbar\epsilon_{h,k} \ , \tag{12.7}$$

showing that the kinetic energy of the holes includes the Coulomb exchange energy $-\sum V_q n_{v,|\mathbf{k}-\mathbf{q}|}$ with $n_{v,|\mathbf{k}-\mathbf{q}|} = 1$ for the full valence band. The low-intensity interband transition energy is therefore

$$\Delta E_k = E_{c,k} - E_{v,k} + \sum_{\mathbf{q}\neq 0} V_q \ . \tag{12.8}$$

In extension of the analysis in Chap. 10, we now want to derive the coupled equations of motion for the following elements of the reduced density matrix

$$\begin{aligned} \langle\alpha^\dagger_{\mathbf{k}}\alpha_{\mathbf{k}}\rangle &= n_{e,\mathbf{k}}(t) \\ \langle\beta^\dagger_{-\mathbf{k}}\beta_{-\mathbf{k}}\rangle &= n_{h,\mathbf{k}}(t) \\ \langle\beta_{-\mathbf{k}}\alpha_{\mathbf{k}}\rangle &= P_{he}(\mathbf{k},t) \equiv P_{\mathbf{k}}(t) \ . \end{aligned} \tag{12.9}$$

We proceed as in Chap. 10 and compute the Hamiltonian equations of motion, but this time for all the expectation values (12.9). Straightforward operator algebra yields

$$\hbar \left[i\frac{d}{dt} - (\epsilon_{e,k} + \epsilon_{h,k}) \right] P_{\mathbf{k}} = (n_{e,\mathbf{k}} + n_{h,\mathbf{k}} - 1) d_{vc} \mathcal{E}(t)$$
$$+ \sum_{\mathbf{k}',\mathbf{q}\neq 0} V_q \Big(\langle \alpha^\dagger_{\mathbf{k}'+\mathbf{q}} \beta_{-\mathbf{k}+\mathbf{q}} \alpha_{\mathbf{k}'} \alpha_{\mathbf{k}} \rangle - \langle \beta^\dagger_{\mathbf{k}'+\mathbf{q}} \beta_{-\mathbf{k}+\mathbf{q}} \beta_{\mathbf{k}'} \alpha_{\mathbf{k}} \rangle$$
$$+ \langle \beta_{-\mathbf{k}} \alpha^\dagger_{\mathbf{k}'-\mathbf{q}} \alpha_{\mathbf{k}'} \alpha_{\mathbf{k}-\mathbf{q}} \rangle - \langle \beta_{-\mathbf{k}} \beta^\dagger_{\mathbf{k}'-\mathbf{q}} \beta_{\mathbf{k}'} \alpha_{\mathbf{k}-\mathbf{q}} \rangle \Big) \ , \tag{12.10}$$

$$\hbar \frac{\partial}{\partial t} n_{e,\mathbf{k}} = -2 \, \mathrm{Im} \Big[d_{cv} \, \mathcal{E}(t) \, P^*_{\mathbf{k}} \Big]$$
$$+ i \sum_{\mathbf{k}',\mathbf{q}\neq 0} V_q \Big(\langle \alpha^\dagger_{\mathbf{k}} \alpha^\dagger_{\mathbf{k}'-\mathbf{q}} \alpha_{\mathbf{k}-\mathbf{q}} \alpha_{\mathbf{k}'} \rangle - \langle \alpha^\dagger_{\mathbf{k}+\mathbf{q}} \alpha^\dagger_{\mathbf{k}'-\mathbf{q}} \alpha_{\mathbf{k}} \alpha_{\mathbf{k}'} \rangle$$
$$+ \langle \alpha^\dagger_{\mathbf{k}} \alpha_{\mathbf{k}-\mathbf{q}} \beta^\dagger_{\mathbf{k}'-\mathbf{q}} \beta_{\mathbf{k}'} \rangle - \langle \alpha^\dagger_{\mathbf{k}+\mathbf{q}} \alpha_{\mathbf{k}} \beta^\dagger_{\mathbf{k}'-\mathbf{q}} \beta_{\mathbf{k}'} \rangle \Big) \ , \tag{12.11}$$

$$\hbar \frac{\partial}{\partial t} n_{h,\mathbf{k}} = -2 \, \mathrm{Im} \Big[d_{cv} \, \mathcal{E}(t) \, P^*_{\mathbf{k}} \Big]$$
$$+ i \sum_{\mathbf{k}',\mathbf{q}\neq \mathbf{0}} V_q \Big(\langle \beta^\dagger_{-\mathbf{k}} \beta^\dagger_{\mathbf{k}'-\mathbf{q}} \beta_{-\mathbf{k}-\mathbf{q}} \beta_{\mathbf{k}'} \rangle - \langle \beta^\dagger_{-\mathbf{k}+\mathbf{q}} \beta^\dagger_{\mathbf{k}'-\mathbf{q}} \beta_{-\mathbf{k}} \beta_{\mathbf{k}'} \rangle$$
$$+ \langle \alpha^\dagger_{\mathbf{k}'+\mathbf{q}} \alpha_{\mathbf{k}'} \beta^\dagger_{-\mathbf{k}} \beta_{-\mathbf{k}+\mathbf{q}} \rangle - \langle \alpha^\dagger_{\mathbf{k}'+\mathbf{q}} \alpha_{\mathbf{k}'} \beta^\dagger_{-\mathbf{k}-\mathbf{q}} \beta_{-\mathbf{k}} \rangle \Big) \ . \tag{12.12}$$

As in our derivation of the polarization equation in Chap. 10, we now again split the four-operator terms into products of densities and interband polarizations plus the unfactorized rest. This way we separate the equations of motion into the *Hartree–Fock* and *scattering* parts

$$\frac{\partial}{\partial t} \langle A \rangle = \frac{\partial}{\partial t} \langle A \rangle_{HF} + \frac{\partial}{\partial t} \langle A \rangle \Big|_{scatt} \ . \tag{12.13}$$

Here, the scattering terms are simply defined as the differences between the full and the Hartree–Fock terms so that the decomposition is formally exact. However, at later stages we will have to make approximations to obtain manageable expressions for the scattering terms.

Using the decomposition (12.13) for all the four-operator terms in Eq. (12.10) – (12.12), one can write the resulting equations as

$$\frac{\partial P_{\mathbf{k}}}{\partial t} = -i(e_{e,k} + e_{h,k})P_{\mathbf{k}} \tag{12.14}$$
$$- \frac{i}{\hbar}\big(n_{e,\mathbf{k}} + n_{h,\mathbf{k}} - 1\big)\left[d_{cv}\mathcal{E}(t) + \sum_{\mathbf{q}\neq\mathbf{k}} V_{|\mathbf{k}-\mathbf{q}|}P_{\mathbf{q}}\right] + \left.\frac{\partial P_{\mathbf{k}}}{\partial t}\right|_{scatt} ,$$

$$\frac{\partial n_{e,\mathbf{k}}}{\partial t} = -\frac{2}{\hbar}\mathrm{Im}\left\{\left[d_{cv}\mathcal{E}(t) + \sum_{\mathbf{q}\neq\mathbf{k}} V_{|\mathbf{k}-\mathbf{q}|}P_{\mathbf{q}}\right]P^*_{\mathbf{k}}\right\} + \left.\frac{\partial n_{e,\mathbf{k}}}{\partial t}\right|_{scatt} , \tag{12.15}$$

$$\frac{\partial n_{h,\mathbf{k}}}{\partial t} = -\frac{2}{\hbar}\mathrm{Im}\left\{\left[d_{cv}\mathcal{E}(t) + \sum_{\mathbf{q}\neq\mathbf{k}} V_{|\mathbf{k}-\mathbf{q}|}P_{\mathbf{q}}\right]P^*_{\mathbf{k}}\right\} + \left.\frac{\partial n_{h,\mathbf{k}}}{\partial t}\right|_{scatt} , \tag{12.16}$$

where again the renormalized single-particle energies

$$\hbar e_{i,k} = \hbar\epsilon_{i,k} + \Sigma_{exc,i}(k) = \hbar\epsilon_{i,k} - \sum_{\mathbf{q}} V_{|\mathbf{k}-\mathbf{q}|}n_{i,q} \ , \ i = e,h \tag{12.17}$$

have been introduced.

Approximations for the scattering terms of Eqs. (12.14) – (12.16) will be discussed in Sec. 12.3 and in later chapters of this book. Here, we note that in all three equations the combination

$$\frac{1}{\hbar}\left[d_{cv}\mathcal{E}(t) + \sum_{\mathbf{q}\neq\mathbf{k}} V_{|\mathbf{k}-\mathbf{q}|}P_{\mathbf{q}}\right]$$

appears. In generalization of the Rabi frequency (2.49) for an atomic system, we therefore introduce the *generalized Rabi frequency*

$$\boldsymbol{\omega_{R,\mathbf{k}}} = \frac{\mathbf{1}}{\hbar}\left(\boldsymbol{d_{cv}\mathcal{E}} + \sum_{\mathbf{q}\neq\mathbf{k}} \boldsymbol{V_{|\mathbf{k}-\mathbf{q}|}P_{\mathbf{q}}}\right) , \tag{12.18}$$

generalized Rabi frequency

emphasizing the fact, that the electron–hole system does not react to the applied field $\mathcal{E}(t)$ alone, but to the effective field which is the sum of the

applied field and the internal dipole field of all generated electron–hole excitations.

With the definition (12.18), Eqs. (12.14) – (12.16) can be written in the very compact form

$$\begin{aligned}
\frac{\partial P_{\mathbf{k}}}{\partial t} &= -i(e_{e,k} + e_{h,k})P_{\mathbf{k}} - i(n_{e,\mathbf{k}} + n_{h,\mathbf{k}} - 1)\omega_{R,\mathbf{k}} + \left.\frac{\partial P_{\mathbf{k}}}{\partial t}\right|_{scatt} \\
\frac{\partial n_{e,\mathbf{k}}}{\partial t} &= -2\,\mathrm{Im}(\omega_{R,\mathbf{k}} P^*_{\mathbf{k}}) + \left.\frac{\partial n_{e,\mathbf{k}}}{\partial t}\right|_{scatt} \\
\frac{\partial n_{h,\mathbf{k}}}{\partial t} &= -2\,\mathrm{Im}(\omega_{R,\mathbf{k}} P^*_{\mathbf{k}}) + \left.\frac{\partial n_{h,\mathbf{k}}}{\partial t}\right|_{scatt} \quad .
\end{aligned} \tag{12.19}$$

semiconductor Bloch equations

Since Eqs. (12.19) are the generalization of the optical Bloch equations (5.30) – (5.32), we call them the *semiconductor Bloch equations*.

These semiconductor Bloch equations constitute the basis for most of our understanding of the optical properties of semiconductors and semiconductor microstructures. Depending on the strength and time dynamics of the applied laser light field contained in the generalized Rabi frequency (12.18), one can distinguish several relevant regimes:

- the *low excitation regime* in which the exciton resonances — sometimes accompanied by exciton molecule (biexciton) resonances — dominate the optical properties. The interaction with phonons provides the most important relaxation and dephasing mechanism. As the density increases gradually, scattering between electron–hole excitations also becomes important.
- the *high excitation regime* in which an electron–hole plasma is excited. Here, the screening of the Coulomb interaction by the optically excited carriers and the collective plasma oscillations are the relevant physical phenomena. The main dissipative mechanism is the carrier–carrier Coulomb scattering.
- the *quasi-equilibrium regime* which can be realized on relatively long time scales. Here, the excitations have relaxed into a quasi-equilibrium and can be described by thermal distributions. The relatively slow approach to equilibrium can be described by a semi-classical relaxation

and dephasing kinetics.
- the *ultrafast regime* in which quantum coherence and the beginning dissipation determine the optical response. The process of decoherence, of the beginning relaxation and the build-up of correlations, e.g., by a time-dependent screening are governed by the quantum kinetics with memory structure of the carrier–carrier and carrier–phonon scattering.

The optical light field can consist of two or more light pulses propagating in equal or different directions with the same or different carrier frequencies, pulse envelopes, and intensities, respectively. The semiconductor Bloch equations are excellently suited to analyze such multi-pulse experiments and the wide variety of physical phenomena, such as relaxation, dephasing, and build-up of correlations. Among the many different possible configurations in nonlinear spectroscopy, there are two basic experimental set-ups that we will analyze in the following chapters of this book:

- As *four-wave mixing* (FWM) spectroscopy, we denote a typical experimental configuration where two or three pulsed laser beams hit the sample under different angles of incidence and variable time delays. The pulses induce polarizations in the crystal. These polarizations interfere, forming a lattice (grating), from which one obtains refracted signals in various orders. The decay of the FWM signal is often studied to analyze dephasing processes in detail.

- Time resolved *differential transmission spectroscopy* (DTS) refers to experiments where two more or less co-linearly propagating pulsed laser beams with equal or different carrier frequencies hit the sample with variable time delay. The carriers excited by the first, often stronger pulse (the pump pulse) modify the absorption of the second, usually weak pulse (the probe pulse). Such DTS-experiments give direct information about build-up and decay of nonlinearities induced by the pump, especially about the relaxation kinetics of the electron–hole excitations.

The analysis of such experiments under various conditions in terms of the semiconductor Bloch equations will be a major issue in some of the following chapters of this book.

Generally, the scattering terms in the semiconductor Bloch equations (12.19) describe all the couplings of the polarizations and populations, i.e., of the single-particle density matrix elements to higher-order correlations,

such as two-particle and phonon- or photon-assisted density matrices. However, in many cases one can identify specific physical mechanisms that dominate the scattering terms in some of the excitation regimes listed above. For example, in the low excitation regime often the coupling of the excited carriers to phonons determines relaxation and dephasing, whereas at high carrier densities carrier–carrier scattering dominates. For relatively long pulses, Markov approximations for the scattering processes are often justified, and the scattering terms can be described by Boltzmann-like scattering rates due to carrier–phonon or carrier–carrier scattering, respectively.

For ultra-short pulses, the Markov approximations may break down. Here, quantum kinetics with its memory structure has to be used to describe the effects of scattering processes which are often not completed during the action of a light pulse. In this regime, the quantum coherence of the electron states influence the scattering kinetics in an important way and give rise to a mixture of coherent and dissipative effects.

In all situations, the semiconductor Bloch equations are a very suitable theoretical framework which, however, has to be supplemented with an appropriate treatment of the scattering terms in order to describe the various aspects of the rich physics which one encounters in pulse excited semiconductors. In general, the semiconductor Bloch equations have to be treated together with the Maxwell equations for the light field in order to determine the optical response. This self consistent coupling of Maxwell and semiconductor Bloch equations (for shortness also called Maxwell–semiconductor–Bloch equations) is needed as soon as spatially extended structures are analyzed where light propagation effects become important. Relevant examples are the polariton effects analyzed in the previous chapter, as well as semiconductor lasers or the phenomenon of optical bistability discussed later in this book. In optically thin samples, however, where propagation effects are unimportant, the transmitted light field is proportional to the calculated polarization field. Under these conditions one can treat the semiconductor Bloch equations separately from Maxwell's equations to calculate the optical response.

Superficially, the semiconductor Bloch equations seem to be diagonal in the momentum index $\mathbf{k}$, but in reality already the Coulomb terms in the generalized Rabi frequency (12.18) and in the exchange energy (12.17) and even more the scattering terms lead to strong couplings of all momentum states. As simple limiting cases, the semiconductor Bloch equations reproduce both the optical Bloch equations for free-carrier transitions (see Chap. 5) and the Wannier equation for electron–hole pairs.

The first equation of Eq. (12.19) is nothing but the polarization equation (10.21) supplemented by the scattering term. The factor

$$1 - n_{e,\mathbf{k}} - n_{h,\mathbf{k}} = n_{v,\mathbf{k}} - n_{c,\mathbf{k}}$$

is again the population inversion of the state $\mathbf{k}$. Its effects on the optical absorption spectra are often denoted as *Pauli blocking*, *state filling*, or more generally as *phase space filling*.

If one ignores all the Coulomb potential terms, $V(q) \to 0$, Eqs. (12.19) reduce to the free-carrier optical Bloch equations of Chap. 5. As shown in Chap. 10, the homogeneous part of Eq. (12.19) becomes the generalized Wannier equation for electron–hole pairs with the effective Coulomb interaction being renormalized by the phase-space filling factor. The term

$$-2\,\mathrm{Im}\big(\omega_{R,\mathbf{k}} P^*_{\mathbf{k}}\big)$$

in the last two equations of (12.19) describes the generation of electrons and holes pairs by the absorption of light. As long as the scattering terms are ignored, the rate of change of the hole population (last equation of (12.19)) is identical to the rate of change of the electron population, second equation of (12.19).

12.2 Multi-Subband Microstructures

Before we proceed with the discussion of the semiconductor Bloch equations, we will give their formulation for microstructures with several subbands. For free carriers, the density matrix equations have already been derived in Chap. 5, Eq. (5.36). In terms of the creation and annihilation operators, we write the reduced density matrix as

$$\rho_{i,\mu;j,\nu}(\mathbf{k},t) = \langle a^\dagger_{j,\nu,\mathbf{k}}(t) a_{i,\mu,\mathbf{k}}(t)\rangle \quad . \tag{12.20}$$

Note the inversion of the indices between left and right hand side of this definition. For quantum dots with confinement in all directions, the wave vector has to be dropped, and the index ν represents the whole set of quantum numbers for the discrete energy levels.

For the optical transitions between subband μ in the valence band $j = v$ and subband ν in the conduction band $i = c$ induced by a coherent light field, the optical polarization components are given by the off-diagonal

matrix elements

$$P_{\nu;\mu}(\mathbf{k}) = \rho_{c,\mu;v,\nu}(\mathbf{k}) = \langle a^{\dagger}_{v,\nu,\mathbf{k}} a_{c,\mu,\mathbf{k}} \rangle \ . \tag{12.21}$$

The other relevant matrix elements are the electron occupation probability for state $\mathbf{k}$ in subband ν

$$n_{e,\nu,\mathbf{k}} = \rho_{c,\nu;c,\nu}(\mathbf{k}) = \langle a^{\dagger}_{c,\nu,\mathbf{k}} a_{c,\nu,\mathbf{k}} \rangle \tag{12.22}$$

and the hole occupation probability in subband μ which is given by

$$n_{h,\mu,\mathbf{k}} = 1 - \rho_{v,\mu;v,\mu}(\mathbf{k}) = 1 - \langle a^{\dagger}_{v,\mu,\mathbf{k}} a_{v,\mu,\mathbf{k}} \rangle \ . \tag{12.23}$$

The equation of motion for the density matrix follows from the Heisenberg equation $\frac{dA}{dt} = \frac{i}{\hbar}[H, A]$ in the form

$$\frac{da^{\dagger}_{j,\nu,\mathbf{k}} a_{i,\mu,\mathbf{k}}}{dt} = \frac{da^{\dagger}_{j,\nu,\mathbf{k}}}{dt} a_{i,\mu,\mathbf{k}} + a^{\dagger}_{j,\nu,\mathbf{k}} \frac{da_{i,\mu,\mathbf{k}}}{dt} \ . \tag{12.24}$$

Since we only want to explicitly compute the Hartree–Fock parts of the multiband semiconductor Bloch equations, we do not have to use the full interaction Hamiltonian. It is sufficient to work with the Hartree–Fock Hamiltonian which includes the interaction with the light field

$$\mathcal{H}_{HF} = \sum \hbar \epsilon_{i',\mu',\mathbf{k}} a^{\dagger}_{i',\mu',\mathbf{k}} a_{i',\mu',\mathbf{k}} - \mathcal{E}(t) \sum d_{i',\mu';j',\nu'}(\mathbf{k}) a^{\dagger}_{i',\mu',\mathbf{k}} a_{j',\nu',\mathbf{k}}$$
$$- \sum V_{i',\mu',j',\nu';j',\nu'',i',\mu''}(q) \big[\rho_{j',\nu'';i',\mu'}(\mathbf{k}-\mathbf{q}) - \delta_{j',v}\delta_{i',v}\delta_{\nu'',\mu'} \big] a^{\dagger}_{j',\nu',\mathbf{k}} a_{i',\mu'',\mathbf{k}} \, . \tag{12.25}$$

This Hamiltonian is obtained by making the Hartree–Fock approximation in the full many-body multi-subband Hamiltonian. Here, the Coulomb interaction potential is

$$V_{i',\mu',j',\nu';j',\nu'',i',\mu''}(q) = \frac{2\pi e^2}{\epsilon_0 L^2} \int dz dz' \zeta^{*}_{i',\mu'}(z) \zeta^{*}_{j',\nu'}(z') \times \frac{e^{-q|z-z'|}}{q} \zeta_{j',\nu''}(z') \zeta_{i',\mu''}(z) \ , \tag{12.26}$$

compare problem 12.2. In deriving Eq. (12.26), we again excluded the interband Coulomb scattering processes but allowed for intersubband scattering.

In the Hartree–Fock Hamiltonian (12.25), we have subtracted the exchange energy with the full valence band, because this Hartree–Fock exchange energy is already included in the band structure calculations. Thus for the terms with $j' = i' = v$ and $\nu'' = \mu'$ the contributions of the valence band subbands to the energy renormalizations are determined by the hole distribution functions, $1 - \rho_{v,\mu';v,\mu'}(-\mathbf{k}) = n_{h,\mu'}(\mathbf{k})$, in analogy to the situation in bulk semiconductors.

With the HF Hamiltonian (12.25) one finds the multi-subband Bloch equations

$$\begin{aligned}
&\left[\frac{d}{dt} + i\big(\epsilon_{i,\mu,\mathbf{k}} - \epsilon_{j,\nu,\mathbf{k}}\big)\right] \rho_{i,\mu;j,\nu}(\mathbf{k}) \\
&= -\frac{i}{\hbar}\mathcal{E}(t) \sum \Big[\rho_{i,\mu;i',\mu'}(\mathbf{k}) d_{i',\mu';j,\nu}(\mathbf{k}) - d_{i,\mu;j',\nu'}(\mathbf{k}) \rho_{j',\nu';j,\nu}(\mathbf{k})\Big] \\
&- \frac{i}{\hbar} \sum \Big\{ \rho_{i,\mu;j',\nu'}(\mathbf{k}) \big[\rho_{j',\nu'';j,\mu'}(\mathbf{k}-\mathbf{q}) - \delta_{j',v}\delta_{j,v}\delta_{\nu'',\mu'}\big] V_{j,\mu',j',\nu';j',\nu'',j,\nu}(q) \\
&- V_{i',\mu',i,\mu;i,\nu'',i',\mu''}(q) \big[\rho_{i,\nu'';i',\mu'}(\mathbf{k}-\mathbf{q}) - \delta_{i,v}\delta_{i',v}\delta_{\nu'',\mu'}\big] \rho_{i',\mu'';j,\nu}(\mathbf{k}) \Big\} \\
&+ \left.\frac{d}{dt}\rho_{i,\mu;j,\nu}(\mathbf{k})\right|_{scatt} . \qquad (12.27)
\end{aligned}$$

Here, we have added the scattering terms which describe higher correlation and dissipative collision rates.

Without subband structure the multi-subband equation (12.27) reduces to the two-band semiconductor Bloch equations (12.19). For compactness of notation, we do not split Eq. (12.27) into separate equations for the off-diagonal polarization components and the diagonal components ($i = j, \mu = \nu$), which describe the density kinetics in the various subbands. Depending on the selection rules and the spectral width of the exciting laser pulse, finite polarization components can be induced for more than one pair of subbands. As in the two-band semiconductor Bloch equations, the Coulomb exchange terms generate nonlinear terms in the multi-subband equations.

12.3 Scattering Terms

All interaction effects beyond the mean field approximation are contained in the scattering terms. In particular, these terms introduce dissipative behavior in the form of dephasing rates for the interband polarization and collision rates describing the relaxation of the electron and hole distributions. The relaxation kinetics drives the particle distribution toward ther-

mal distributions often in times much shorter than the radiative lifetime of the carriers.

A simple phenomenological description of the relaxation needs at least two relaxation times, called T_1' and T_1:

$$\left.\frac{dn_{e,\mathbf{k}}}{dt}\right|_{scatt} = \frac{f_{e,\mathbf{k}} - n_{e,\mathbf{k}}(t)}{T_1'} - \frac{n_{e,\mathbf{k}}(t)}{T_1} \quad , \tag{12.28}$$

where $f_{e,\mathbf{k}} = 1/(e^{(e_k-\mu)\beta}+1)$ is the Fermi function of Chap. 6. Here, the second term describes recombination of carriers whereas the first term models the intraband relaxation, i.e., the relaxation of the general nonequilibrium distribution $n_{e,\mathbf{k}}$ towards a quasi-equilibrium Fermi distribution $f_{e,\mathbf{k}}$, leaving the total number of electrons in the conduction band unchanged. Thus

$$\sum f_{e,\mathbf{k}} = \sum n_{e,\mathbf{k}}(t) = N_e(t) \quad . \tag{12.29}$$

This relation allows us to calculate the chemical potential $\mu_e(T, N_e(t))$. A refined treatment would take into account that $f_{e,\mathbf{k}}$ does not yet describe the total equilibrium distribution, but only a local equilibrium $f_{e,\mathbf{k}}(t)$ with slowly varying chemical potential and temperature, and — more generally — also with a slowly changing drift velocity. We will, however, not dwell further on these phenomenological treatments, but ask how such a dissipative kinetics can be derived microscopically by coupling the electron system to a bath with a continuous energy spectrum.

Before doing that, let us also briefly consider the dephasing kinetics of the interband polarization which describes the decay of quantum coherence in a coherently excited system. The simplest description of dephasing uses a dephasing time, also called a transverse relaxation time T_2. This simple phenomenological description of dephasing works surprisingly often reasonably well, given the complex underlying scattering kinetics. However, also here, nonlinear and non-Markovian effects set a limit to the simple phenomenological ansatz.

In the low excitation regime, the dissipative kinetics is determined by impurity scattering or in pure, polar III–V and II–VI compound semiconductors by the scattering of the excited carriers with phonons. Of the various different phonon branches, the carrier scattering with longitudinal optical (LO) phonons usually leads to the most rapid dynamics. At high excitation levels, where a dense electron–hole plasma is generated, the carrier–carrier collisions are the fastest dissipative processes. We treat here the simpler case of LO-phonon scattering first. In contrast to acoustic

phonons with their linear dispersion, optical phonons have little dispersion and can often simply be described by one energy $\hbar\omega_0$. Typical LO-phonon energies in III–V and II–VI semiconductors are of the order of 20 to 40 meV.

The carriers are scattered within their bands by the absorption or emission of one LO phonon. The corresponding intraband scattering Hamiltonian, the so-called Fröhlich Hamiltonian, is given by:

$$\mathcal{H}_{e-LO} = \sum_{i,\mathbf{k},\mathbf{q}} \hbar g_{\mathbf{q}} a^{\dagger}_{i,\mathbf{k}+\mathbf{q}} a_{i,\mathbf{k}} \left(b_{\mathbf{q}} + b^{\dagger}_{-\mathbf{q}} \right) \ , \tag{12.30}$$

where $b_{\mathbf{q}}$ and $b^{\dagger}_{-\mathbf{q}}$ are the bosonic phonon annihilation and creation operators, respectively. Note, that the momentum conservation is built into the Fröhlich Hamiltonian. The analysis shows that as long as the energy spectrum of the electrons is continuous, the coupling to a bath of dispersionless optical phonons will give rise to dissipation. Only in quantum dots, where the carriers are confined in all space dimensions so that no momentum can be defined, one has to take the dispersion of the LO-phonons into account in order to get dephasing.

If the momentum transfer is neglected by setting $q = 0$ in the Fröhlich interaction Hamiltonian, an exactly treatable model results because different electron momentum states are no longer coupled. Even though it is based on additional assumptions, such an exactly treatable model is of considerable interest to study carrier relaxation and dephasing for arbitrary strengths of the coupling.

The interaction matrix element $g_{\mathbf{q}}$ is given by

$$|g_{\mathbf{q}}|^2 = \frac{\omega_0 V_{\mathbf{q}}}{2\hbar} \left(\frac{1}{\epsilon_\infty} - \frac{1}{\epsilon_0} \right) \ , \tag{12.31}$$

where $V_{\mathbf{q}}$ is again the bare Coulomb matrix element and ϵ_0 and ϵ_∞, respectively, are the low and high frequency dielectric constants of the unexcited crystal. The Coulomb matrix element in (12.31) shows that effective carrier–carrier interaction mediated by the exchange of an LO phonon is also of Coulombic nature. The screening of $V_{\mathbf{q}}$ due to optical phonons with the frequency ω_0 occurs between the low and high frequency limit. This is the reason why the difference between $1/\epsilon_\infty$ and $1/\epsilon_0$ determines the interaction potential (see also problem 12.5).

It is usual, to define the strength of the LO-phonon coupling as the ratio of phonon-induced electron energy shift to phonon energy in terms of the

dimensionless Fröhlich coupling parameter

$$\alpha_i = e^2 \sqrt{\frac{m_i}{2\hbar^3 \omega_0}} \left(\frac{1}{\epsilon_\infty} - \frac{1}{\epsilon_0} \right) \ . \tag{12.32}$$

In the weakly polar III–V compounds, $\alpha_i \ll 1$, which justifies the use of perturbation theory in these materials. In the more polar II–VI compounds, $\alpha_i \simeq 1$, which defines the intermediate polaron coupling regime. Here, nonperturbative methods are needed.

We limit our discussion here to the weak coupling regime. The collision term due to LO-phonon scattering is given by

$$\begin{aligned} \left. \frac{\partial \rho_{i,j}(\mathbf{k})}{\partial t} \right|_{scatt} &= \frac{i}{\hbar} \langle \Big([\mathcal{H}_{e-LO}, a^\dagger_{j,\mathbf{k}}] a_{i,\mathbf{k}} + a^\dagger_{j,\mathbf{k}} [\mathcal{H}_{e-LO}, a_{i,\mathbf{k}}] \Big) \rangle \\ &= i \sum_{\mathbf{q}} g_{\mathbf{q}} \Big(\langle a^\dagger_{j,\mathbf{k}+\mathbf{q}} a_{i,\mathbf{k}} \big(b_{\mathbf{q}} + b^\dagger_{-\mathbf{q}} \big) \rangle - \langle a^\dagger_{j,\mathbf{k}} a_{i,\mathbf{k}-\mathbf{q}} \big(b_{\mathbf{q}} + b^\dagger_{-\mathbf{q}} \big) \rangle \Big) \\ &= i \sum_{\mathbf{q}} g_{\mathbf{q}} \Big(F^-_{ij,\mathbf{k},\mathbf{q}} + F^+_{ij,\mathbf{k},\mathbf{q}} - G^-_{ij,\mathbf{k},\mathbf{q}} - G^+_{ij,\mathbf{k},\mathbf{q}} \Big) \ . \end{aligned} \tag{12.33}$$

We see, that the scattering term couples the two-operator dynamics to expectation values of two electron and one phonon operator. These quantities are called phonon-assisted density matrices. In detail, the phonon-assisted density matrices are

$$\begin{aligned} F^-_{ij,\mathbf{k},\mathbf{q}} &= \langle a^\dagger_{j,\mathbf{k}+\mathbf{q}} a_{i,\mathbf{k}} b_{\mathbf{q}} \rangle \\ F^+_{ij,\mathbf{k},\mathbf{q}} &= \langle a^\dagger_{j,\mathbf{k}+\mathbf{q}} a_{i,\mathbf{k}} b^\dagger_{-\mathbf{q}} \rangle \\ G^-_{ij,\mathbf{k},\mathbf{q}} &= \langle a^\dagger_{j,\mathbf{k}} a_{i,\mathbf{k}-\mathbf{q}} b_{\mathbf{q}} \rangle \\ G^+_{ij,\mathbf{k},\mathbf{q}} &= \langle a^\dagger_{j,\mathbf{k}} a_{i,\mathbf{k}-\mathbf{q}} b^\dagger_{-\mathbf{q}} \rangle \ . \end{aligned} \tag{12.34}$$

There are relations between the four phonon-assisted density matrices. F^- and F^+, and similarly G^- and G^+ differ only by the exchange of the phonon annihilation and creation operators. Consequently, the phonon absorption and emission processes in the $-$ and $+$ functions are interchanged, which can simply be accomplished by a reversal of the phonon frequency and momentum, as will be discussed later. Furthermore,

$$G^-_{ij,\mathbf{k},\mathbf{q}} = F^-_{ij,\mathbf{k},\mathbf{q}} \Big|_{\mathbf{k} \to \mathbf{k}-\mathbf{q}} \quad \text{and} \quad G^+_{ij,\mathbf{k},\mathbf{q}} = F^+_{ij,\mathbf{k},\mathbf{q}} \Big|_{\mathbf{k} \to \mathbf{k}-\mathbf{q}} \ , \tag{12.35}$$

so only one phonon-assisted density matrix has to be evaluated explicitly.

Because we do not know the phonon-assisted density matrices, we write down their equations of motion under the full Hamiltonian $\mathcal{H} = \mathcal{H}_{HF} +$

$\mathcal{H}_{LO} + \mathcal{H}_{e-LO}$, where $\mathcal{H}_{LO} = \sum_{\mathbf{q}} \hbar\omega_0 b^\dagger_{\mathbf{q}} b_{\mathbf{q}}$ is the free phonon Hamiltonian. The electron Hartree–Fock Hamiltonian can be written as

$$\mathcal{H}_{HF} = \sum_{ij,\mathbf{k}} H_{ij,\mathbf{k}} a^\dagger_{i,\mathbf{k}} a_{j,\mathbf{k}} \ , \tag{12.36}$$

where the Hamilton matrix is given by

$$H_{ij,\mathbf{k}} = \epsilon_{i,\mathbf{k}}\delta_{ij} - \sum_{\mathbf{q}} V(q)(\rho_{ij,\mathbf{k}-\mathbf{q}} - \delta_{iv}\delta_{jv}) - \mathcal{E}(t) d_{ij}(\mathbf{k}) \ , \tag{12.37}$$

which includes the coupling to the coherent light field. We will call $\mathcal{H}_{HF} + \mathcal{H}_{LO} = \mathcal{H}_{mf}$ the mean-field Hamiltonian.

The resulting equation of motion is

$$\frac{\partial F^-_{ij,\mathbf{k},\mathbf{q}}}{\partial t} = \left.\frac{\partial F^-_{ij,\mathbf{k},\mathbf{q}}}{\partial t}\right|_{mf} + \frac{i}{\hbar}\langle\big[\mathcal{H}_{e-LO}\,,\, a^\dagger_{j,\mathbf{k}+\mathbf{q}} a_{i,\mathbf{k}} b_{\mathbf{q}}\big]\rangle \ . \tag{12.38}$$

The homogeneous mean-field time development is given by

$$\left.\frac{\partial F^-_{ij,\mathbf{k},\mathbf{q}}}{\partial t}\right|_{mf} = \frac{i}{\hbar}\sum_l \Big(F^-_{il,\mathbf{k},\mathbf{q}} H_{lj,\mathbf{k}+\mathbf{q}} - H_{il,\mathbf{k}} F^-_{lj,\mathbf{k},\mathbf{q}}\Big) - \big(i\omega_0 + \gamma_{ij,\mathbf{k},\mathbf{q}}\big) F^-_{ij,\mathbf{k},\mathbf{q}} \ , \tag{12.39}$$

or explicitly

$$\begin{aligned}\left.\frac{\partial F^-_{ij,\mathbf{k},\mathbf{q}}}{\partial t}\right|_{mf} &= i\big(\epsilon_{j,\mathbf{k}+\mathbf{q}} - \epsilon_{i,\mathbf{k}} - \omega_0 + i\gamma_{ij,\mathbf{k},\mathbf{q}}\big) F^-_{ij,\mathbf{k},\mathbf{q}} \\ &\quad - \frac{i}{\hbar}\mathcal{E}(t)\sum\Big[F^-_{il,\mathbf{k},\mathbf{q}} d_{lj}(\mathbf{k}+\mathbf{q}) - d_{il}(\mathbf{k}) F^-_{lj,\mathbf{k},\mathbf{q}}\Big] \\ &\quad - \frac{i}{\hbar}\sum\Big\{F^-_{il,\mathbf{k},\mathbf{q}} V(q')\big[\rho_{lj}(\mathbf{k}+\mathbf{q}-\mathbf{q}') - \delta_{l,v}\delta_{j,v}\big] \\ &\quad - V(q')\big[\rho_{il}(\mathbf{k}-\mathbf{q}') - \delta_{iv}\delta_{lv}\big] F^-_{lj,\mathbf{k},\mathbf{q}}\Big\} \ .\end{aligned} \tag{12.40}$$

The first line of (12.40) describes the free evolution of the phonon-assisted density matrix F^-. We have added an infinitesimal damping $\gamma_{ij,\mathbf{k},\mathbf{q}}$ to insure an adiabatic switching on. The second line describes the Stark shifts of the energy levels due to the laser light pulse, while the next two lines describe the Hartree–Fock corrections. In total, Eq. (12.40) gives a homogeneous equation for the mean-field development of F^-. The second term in Eq. (12.38), which has not been evaluated so far, gives rise to inhomogeneous terms in the form of new higher order density matrices. We decouple

the resulting hierarchy of an infinite series of equations of larger and larger density matrices by factorization into single particle reduced density matrices. Best insight in the physical nature of the resulting terms is obtained, if we do not evaluate the commutator in (12.38) at all, but factorize the products of four electron and two phonon operators directly:

$$\begin{aligned}&\frac{i}{\hbar}\langle\big[\mathcal{H}_{e-LO}\,,\,a^{\dagger}_{j,\mathbf{k}+\mathbf{q}}a_{i,\mathbf{k}}b_{\mathbf{q}}\big]\rangle \\ &= ig_{\mathbf{q}}\sum\Big\{N_{\mathbf{q}}\rho_{ii'}(\mathbf{k})\big[\delta_{i'j}-\rho_{i'j}(\mathbf{k}+\mathbf{q})\big] \\ &-(N_{\mathbf{q}}+1)\rho_{ii'}(\mathbf{k}+\mathbf{q})\big[\delta_{i'j}-\rho_{i'j}(\mathbf{k})\big]\Big\}\ ,\end{aligned} \tag{12.41}$$

where $N_{\mathbf{q}} = 1/(e^{\beta\hbar\omega_0}-1) = N(\omega_0)$ is the number of thermal LO phonons. For simplicity, we consider the phonons as a thermal bath. Similar equations hold for the other three phonon-assisted density matrices.

12.3.1 *Intraband Relaxation*

Let us consider for the moment only diagonal density matrices

$$\rho_{i,i}(\mathbf{k}) = n_i(\mathbf{k}) \tag{12.42}$$

and neglect corrections of the energy spectrum (i.e. lines 2 to 4 in (12.39)). Under these simplifying conditions, Eq. (12.38) reduces to

$$\begin{aligned}&\frac{\partial F^{-}_{ii,\mathbf{k},\mathbf{q}}}{\partial t} = i\big(\epsilon_{i,\mathbf{k}+\mathbf{q}}-\epsilon_{i,\mathbf{k}}-\omega_0+i\gamma_{ii,\mathbf{k},\mathbf{q}}\big)F^{-}_{ii,\mathbf{k},\mathbf{q}}+ \\ &ig_{\mathbf{q}}\Big\{N(\omega_0)n_i(\mathbf{k},t)\big[1-n_i(\mathbf{k}+\mathbf{q},t)\big]-\big[N(\omega_0)+1\big]n_i(\mathbf{k}+\mathbf{q},t)\big[1-n_i(\mathbf{k},t)\big]\Big\}\ .\end{aligned} \tag{12.43}$$

A formal integration yields

$$\begin{aligned}&F^{-}_{ii,\mathbf{k},\mathbf{q}}(t) = ig_{\mathbf{q}}\int_{-\infty}^{t}dt'e^{i\left(\epsilon_{i,\mathbf{k}+\mathbf{q}}-\epsilon_{i,\mathbf{k}}-\omega_0+i\gamma_{ii,\mathbf{k},\mathbf{q}}\right)(t-t')} \\ &\times\Big\{N(\omega_0)n_i(\mathbf{k},t')\big[1-n_i(\mathbf{k}+\mathbf{q},t')\big] \\ &-\big[N(\omega_0)+1\big]n_i(\mathbf{k}+\mathbf{q},t')\big[1-n_i(\mathbf{k},t')\big]\Big\}\ .\end{aligned} \tag{12.44}$$

As already mentioned, the phonon-assisted density matrix F^{+} can be obtained from F^{-} by interchanging phonon absorption and emission and reversing the phonon momentum. We introduce for this purpose the sign

function $\sigma = \pm 1$ and replace $\omega_0 \to \sigma\omega_0$ and note that the following relations are valid:

$$\sigma N(\sigma\omega_0)|_{\sigma=-1} = -\frac{1}{e^{-\beta\hbar\omega_0}-1} = \frac{e^{\beta\hbar\omega_0}-1+1}{e^{\beta\hbar\omega_0}-1} = N(\omega_0)+1 \ , \quad (12.45)$$

and

$$\sigma\big[N(\sigma\omega_0)+1\big]\big|_{\sigma=-1} = N(\omega_0) \ . \quad (12.46)$$

Using these relations, we formally introduce into the scattering rate (12.33) a sum over σ:

$$\begin{aligned}\frac{\partial n_i(\mathbf{k})}{\partial t}\bigg|_{scatt} &= -\sum_{q,\sigma=\pm1} \sigma g_{\mathbf{q}}^2 \int_{-\infty}^{t} dt' e^{i\left(\epsilon_{i,\mathbf{k}+\sigma\mathbf{q}}-\epsilon_{i,\mathbf{k}}-\sigma\omega_0+i\gamma_{ii,\mathbf{k},\mathbf{q}}\right)(t-t')} \\ &\times \Big\{ N(\sigma\omega_0) n_i(\mathbf{k},t')\big[1-n_i(\mathbf{k}+\sigma\mathbf{q},t')\big] \\ &- \big[N(\sigma\omega_0)+1\big] n_i(\mathbf{k}+\sigma\mathbf{q},t')\big[1-n_i(\mathbf{k},t')\big]\Big\} \\ &- \Big\{\mathbf{k}\to\mathbf{k}-\sigma\mathbf{q}\Big\} \ . \end{aligned} \quad (12.47)$$

The last term generates from the preceding ones the contributions of the G functions.

The appearance of the time integral on the RHS of Eq. (12.47) shows that in general the scattering rate depends on the history of the system. In particular, the distribution functions enter into the scattering rate with their values at earlier times $t' \le t$. Processes with such a memory structure are called non-Markovian. They arise from the elimination of the dynamics of the phonons and the higher correlations. Such non-Markovian scattering integrals are typical for the short-time regime in which quantum mechanical coherence of the electron and phonon states (here in the form of the coherent exponential wave factors) is still present. Therefore, the non-Markovian short-time dynamics is called *quantum kinetics*. Only for long times, the non-Markovian quantum kinetics reduces to the Markovian scattering kinetics of Boltzmann.

Suppose that the particles are excited by a pulse around $t = 0$. If the time t is long enough so that $t\omega_0 \gg 1$, the exponentials oscillate rapidly. The distribution functions vary slowly compared to the exponentials and can be taken out of the integral with their value at the upper boundary. This is the so-called *Markov approximation*. The integrals over the remaining exponentials then yield the energy conserving Dirac delta function times

a factor of π. In detail, the time integral has the structure

$$\int_{-\infty}^{t} dt' e^{i(\Delta\epsilon+i\gamma)(t-t')} = \left.\frac{e^{i(\Delta\epsilon+i\gamma)(t-t')}}{-i(\Delta\epsilon+i\gamma)}\right|_{-\infty}^{t} = \frac{i}{\Delta\epsilon+i\gamma} \ . \tag{12.48}$$

With Dirac's identity we get

$$\frac{i}{\Delta\epsilon+i\gamma} = i\left[\mathrm{P}\frac{1}{\Delta\epsilon} - i\pi\delta(\Delta\epsilon)\right] = i\mathrm{P}\frac{1}{\Delta\epsilon} + \pi\delta(\Delta\epsilon) \ , \tag{12.49}$$

where P denotes the principal value of the integral. Using this result in Eq. (12.47), taking the real part, and evaluating the σ summation, we obtain in this long-time limit the result:

$$\begin{aligned}
&\left.\frac{\partial n_i(\mathbf{k})}{\partial t}\right|_{scatt} = -\sum_{\mathbf{q}} 2\pi g_{\mathbf{q}}^2 \delta\left(\epsilon_{i,\mathbf{k}+\mathbf{q}} - \epsilon_{i,\mathbf{k}} - \omega_0\right) \\
&\times\Big\{N_{\mathbf{q}} n_i(\mathbf{k},t)\left[1-n_i(\mathbf{k}+\mathbf{q},t)\right] - (N_{\mathbf{q}}+1) n_i(\mathbf{k}+\mathbf{q},t)\left[1-n_i(\mathbf{k},t)\right]\Big\} \\
&-\sum_{\mathbf{q}} 2\pi g_{\mathbf{q}}^2 \delta\left(\epsilon_{i,\mathbf{k}-\mathbf{q}} - \epsilon_{i,\mathbf{k}} + \omega_0\right) \\
&\times\Big\{(N_{\mathbf{q}}+1) n_i(\mathbf{k},t)\left[1-n_i(\mathbf{k}-\mathbf{q},t)\right] - N_{\mathbf{q}} n_i(\mathbf{k}-\mathbf{q},t)\left[1-n_i(\mathbf{k},t)\right]\Big\} \ .
\end{aligned} \tag{12.50}$$

electron–phonon Boltzmann scattering rate

This is the famous Boltzmann scattering rate. It contains the transition probabilities per unit time as determined by Fermi's golden rule, compare Fig. 12.1. The first scattering rate describes an intraband electron transition from state $i, \mathbf{k}$ to state $i, \mathbf{k}+\mathbf{q}$ by absorption of a phonon. For this transition, one needs a phonon (the probability is given by $N_{\mathbf{q}}$), the initial electron state has to be occupied (probability $n_i(\mathbf{k}, t)$) and the final state has to be empty (probability $1 - n_i(\mathbf{k}+\mathbf{q}, t)$). Due to this transition rate the electron distribution at state $i, \mathbf{k}$ decreases (- sign). The next term describes the back-scattering from the initial state $i, \mathbf{k}+\mathbf{q}$ with $N_{\mathbf{q}}$ phonons to the final state $i, \mathbf{k}$ with $N_{\mathbf{q}}+1$ phonons. This phonon emission process takes place as stimulated and spontaneous emission. Thus one gets a factor $N_{\mathbf{q}}+1$. For both described scattering processes, the energy before and after the collision has to be conserved $\epsilon_{i,\mathbf{k}+\mathbf{q}} = \epsilon_{i,\mathbf{k}} + \omega_0$. In the following

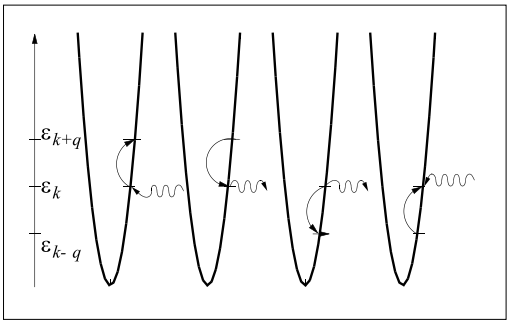

Fig. 12.1 Sketch of the four electron–phonon scattering processes. The solid lines symbolize the electrons scattering from their initial to final states and the curled lines represent the phonon absorption or emission, respectively.

terms, emission and absorption is interchanged and the phonon momentum $\mathbf{q}$ is reversed. These rates stem from the + functions. As a consequence of the Markov approximation, the Boltzmann scattering rate depends only on the distributions at time t and not on the values of the distributions at earlier times. The Boltzmann scattering rates drive the system toward thermal equilibrium, which is characterized by a maximum of the entropy. In our case, the electrons will relax to thermal distributions with the lattice temperature.

If one drops the assumption that only diagonal elements of the density matrix exist, one gets for the scattering rate of the density $n_i(\mathbf{k})$ extra terms arising from the population factors in the equations for $F^{-}_{ii,\mathbf{k},\mathbf{q}}$:

$$ig_{\mathbf{q}}\Big[N_{\mathbf{q}}\rho_{i,j\neq i}(\mathbf{k})\rho_{j\neq i,i}(\mathbf{k}+\mathbf{q})-(N_{\mathbf{q}}+1)\rho_{ij\neq i}(\mathbf{k}+\mathbf{q})\rho_{j\neq i,i}(\mathbf{k})\Big] \ . \quad (12.51)$$

These terms contain products of the interband polarization components, showing that there is also scattering into and out of the coherently excited interband polarization. For shortness, these terms are often called P^2 terms. Before we discuss the influence of the other mean-field terms in the equation for the phonon-assisted density matrix, we first analyze the basic mechanisms of dephasing.

12.3.2 *Dephasing of the Interband Polarization*

In order to analyze how the intraband phonon scattering destroys the coherent interband polarization, we now consider the off-diagonal elements of the phonon-assisted density matrix equation (12.38), e.g., with $i = c$ and $j = v$ again without the optical Stark effect terms and without the Coulomb exchange terms:

$$\begin{aligned}\frac{\partial F^-_{cv,\mathbf{k},\mathbf{q}}}{\partial t} &= i\big(\epsilon_{v,\mathbf{k}+\mathbf{q}} - \epsilon_{c,\mathbf{k}} - \omega_0 + i\gamma_{cv,\mathbf{k},\mathbf{q}}\big)F^-_{cv,\mathbf{k},\mathbf{q}} \\ &+ ig_{\mathbf{q}}\Big\{-N(\omega_0)\rho_{cc}(\mathbf{k})\rho_{cv}(\mathbf{k}+\mathbf{q}) + N(\omega_0)\rho_{cv}(\mathbf{k})\big[1-\rho_{vv}(\mathbf{k}+\mathbf{q})\big] \\ &+ \big[N(\omega_0)+1\big]\rho_{cc}(\mathbf{k}+\mathbf{q})\rho_{cv}(\mathbf{k}) - \big[N(\omega_0)+1\big]\rho_{cv}(\mathbf{k}+\mathbf{q})\big[1-\rho_{vv}(\mathbf{k})\big]\Big\} \ . \end{aligned} \tag{12.52}$$

Next, we note that the optically induced off-diagonal matrix elements are rapidly oscillating functions. In order to insulate the slowly varying parts, we split off the oscillations with the carrier frequency ω of the exciting light field:

$$\rho_{cv}(\mathbf{k},t) = e^{-i\omega t}p_{cv}(\mathbf{k},t) \ . \tag{12.53}$$

A formal integration yields

$$\begin{aligned}F^-_{cv,\mathbf{k},\mathbf{q}}(t) &= ig_{\mathbf{q}}e^{-i\omega t}\int_{-\infty}^{t} dt' e^{i\left(\epsilon_{v,\mathbf{k}+\mathbf{q}} - \epsilon_{c,\mathbf{k}} + \omega - \omega_0 + i\gamma_{cv,\mathbf{k},\mathbf{q}}\right)(t-t')} \\ &\times \Big\{-N(\omega_0)\rho_{cc}(\mathbf{k},t')p_{cv}(\mathbf{k}+\mathbf{q},t') + N(\omega_0)p_{cv}(\mathbf{k},t')\big[1-\rho_{vv}(\mathbf{k}+\mathbf{q},t')\big] \\ &+ \big[N(\omega_0)+1\big]\rho_{cc}(\mathbf{k}+\mathbf{q},t')p_{cv}(\mathbf{k},t') \\ &- \big[N(\omega_0)+1\big]p_{cv}(\mathbf{k}+\mathbf{q},t')\big[1-\rho_{vv}(\mathbf{k},t')\big]\Big\} \ . \end{aligned} \tag{12.54}$$

This result shows that, due to the action of the light field in the off-diagonal matrix elements, an electron state $c, \mathbf{k}$ is mixed with a valence band state $v, \mathbf{k}$, which in turn is scattered via phonon interaction into the state $v, \mathbf{k}+\mathbf{q}$. In the long-time limit, this second-order process, which constitutes the basic dephasing mechanism, is possible under energy conservation because $\epsilon_{c,\mathbf{k}} - \omega \simeq \epsilon_{v,\mathbf{k}}$.

Inserting all phonon-assisted density matrices into the scattering rate of the off-diagonal density matrix element, we obtain

$$
\begin{aligned}
&\left.\frac{\partial \rho_{cv}(\mathbf{k},t)}{\partial t}\right|_{scatt} = \\
&-\sum_{q,\sigma} \sigma g_{\mathbf{q}}^2 e^{-i\omega t} \int_{-\infty}^{t} dt' e^{i\left(\epsilon_{v,\mathbf{k}+\mathbf{q}}-\epsilon_{c,\mathbf{k}}+\omega-\sigma\omega_0+i\gamma_{cv,\mathbf{k},\mathbf{q}}\right)(t-t')} \\
&\times \Big\{ N(\sigma\omega_0)\big[p_{cv}(\mathbf{k},t')n_h(\mathbf{k}+\sigma\mathbf{q},t') - p_{cv}(\mathbf{k}+\sigma\mathbf{q},t')n_e(\mathbf{k},t')\big] \\
&+ \big[N(\sigma\omega_0)+1\big]\big[p_{cv}(\mathbf{k},t')n_e(\mathbf{k}+\sigma\mathbf{q},t') - p_{cv}(\mathbf{k}+\sigma\mathbf{q},t')n_h(\mathbf{k},t')\big] \Big\} \\
&- \Big\{ \mathbf{k} \to \mathbf{k}+\sigma\mathbf{q} \Big\} \ . \qquad (12.55)
\end{aligned}
$$

The integral has a real part which describes the dephasing and an imaginary part which describes the self-energy corrections due to the coupling to LO phonons. These self-energies are called the polaron shifts. In the long-time limit, we can again make the Markov approximation by pulling the distribution functions out of the integral taking their values at the upper time t. The integral over the remaining exponential yields a complex energy denominator which can be decomposed into its real and imaginary part using Dirac's identity as explicitly shown above.

12.3.3 *Full Mean-Field Evolution of the Phonon-Assisted Density Matrices*

Let us return to the equation (12.39) for the phonon-assisted density matrix, which contains the full mean-field time development under the coherent light field and the Coulomb Hartree–Fock terms. These terms introduce into the scattering integrals the particle spectra renormalized by the optical Stark effect and by the Coulomb exchange process. These spectral renormalizations are time-dependent, i.e., they give the information which particle spectra are realized at a given time. In order to include these effects, we write (12.38) in the form

$$
\frac{\partial F^{-}_{ij,\mathbf{k},\mathbf{q}}}{\partial t} = \left.\frac{\partial F^{-}_{ij,\mathbf{k},\mathbf{q}}}{\partial t}\right|_{mf} + R_{ij,\mathbf{k},\mathbf{q}} \ , \qquad (12.56)
$$

where

$$
R_{ij,\mathbf{k},\mathbf{q}} = \frac{i}{\hbar}\langle [H_{e-LO}\ ,\ a^{\dagger}_{j,\mathbf{k}+\mathbf{q}} a_{i,\mathbf{k}} b_{\mathbf{q}}] \rangle \qquad (12.57)
$$

is the inhomogeneous scattering term. The mean-field terms are defined in Eq. (12.39). The solution of the inhomogeneous equation can be written as

$$F^{-}_{ij,\mathbf{k},\mathbf{q}}(t) = \sum_{l} \int_{-\infty}^{t} dt' T^{-}_{il}(t,t') R_{lj,\mathbf{k},\mathbf{q}}(t') \ . \tag{12.58}$$

Here, $T^{-}_{il}(t,t')$ is the time evolution matrix which develops according to the mean-field Hamiltonian

$$\begin{aligned} \frac{\partial T^{-}_{ij,\mathbf{k},\mathbf{q}}}{\partial t} &= \left.\frac{\partial T^{-}_{ij,\mathbf{k},\mathbf{q}}}{\partial t}\right|_{mf} \\ &= \frac{i}{\hbar} \sum_{l} \Big(T^{-}_{il,\mathbf{k},\mathbf{q}} H_{lj,\mathbf{k}+\mathbf{q}} - H_{il,\mathbf{k}} T^{-}_{lj,\mathbf{k},\mathbf{q}} \Big) - \big(i\omega_0 + \gamma_{ij,\mathbf{k},\mathbf{q}} \big) T^{-}_{ij,\mathbf{k},\mathbf{q}} \ , \end{aligned} \tag{12.59}$$

from the initial value $T_{ij,\mathbf{k},\mathbf{q}}(t,t) = \delta_{ij}$. The validity of the ansatz (12.58) can be checked by direct insertion into (12.38). Note, that the time evolution matrix reduces simply to the free-particle exponential time evolution

$$T_{ij,\mathbf{k},\mathbf{q}}(t,t') \rightarrow e^{i\left(\epsilon_{j,\mathbf{k}+\mathbf{q}} - \epsilon_{i,\mathbf{k}} - \omega_0 + i\gamma_{ij,\mathbf{k},\mathbf{q}}\right)(t-t')} \ , \tag{12.60}$$

if only the free-particle terms are considered. In the full solution for the scattering term, the exponentials have simply to be replaced by the time evolution operator $T(t,t')$.

So far the damping constants $\gamma_{ij,\mathbf{k},\mathbf{q}}$ have been considered as infinitesimal quantities. A detailed numerical inspection of the equations shows, however, that, particularly for larger coupling constants, one needs finite damping constants in order to obtain numerically stable solutions. It turns out, that a self-consistent approach in which the damping constants are also evaluated for the electron–LO phonon interaction yields the required stability.

REFERENCES

For further reading on the material presented in this chapter see:

N. Peyghambarian, S.W. Koch, and A. Mysyrowicz, *Introduction to Semiconductor Optics*, Prentice Hall, Englewood Cliffs (1993)
H. Haug and S. Schmitt–Rink, Progr. Quantum Electron. **9**, 3 (1984)

H. Haug ed., *Optical Nonlinearities and Instabilities in Semiconductors*, Academic Press, New York (1988)
A. Stahl and I. Balslev, *Electrodynamics of the Semiconductor Band Edge*, Springer Tracts in Modern Physics 110, Springer, Berlin (1987)
R. Zimmermann, *Many-Particle Theory of Highly Excited Semiconductors*, Teubner, Leipzig (1988)
H. Haug and A.P. Jauho, *Quantum Kinetics for Transport and Optics of Semiconductors*, Springer, Berlin (1996)
S. Mukamel, *Principles of Nonlinear Optical Spectroscopy*, Oxford University Press, Oxford (1995)
T. Kuhn, *Density matrix theory of coherent ultrafast dynamics*, in *Theory of Transport Properties of Semiconductor Nanostructures*, ed. E. Schöll, Chapmann and Hill, London (1998), pp. 173
W. Schäfer and M. Wegener, *Semiconductor Optics and Transport Phenomena* Springer, Berlin (2002)

PROBLEMS

Problem 12.1: Derive the electron–hole Hamiltonian, Eq. (12.6).

Problem 12.2: Derive the multi-subband Coulomb interaction potential (12.26). Hint: Use the envelope wave functions discussed in Sec. 5.2.2 and perform the two-dimensional Fourier transform of Sec. 7.3 over the in-plane coordinate $\mathbf{r}_{\parallel}$.

Problem 12.3: Generalize the two-band many-body Hamiltonian, Eq. (10.14), to the multi-band situation. Make the Hartree–Fock approximation to derive Eq. (12.25).

Problem 12.4: Show that the entropy density defined as

$$s(t) = -k_B \sum_{\mathbf{k}} \Big\{ n_{\mathbf{k}}(t) \ln\big[n_{\mathbf{k}}(t)\big] + (1 - n_{\mathbf{k}}(t)) \ln\big[1 - n_{\mathbf{k}}(t)\big] \Big\}$$

of an electron gas increases monotonously for the Boltzmann scattering rate for electron–phonon interaction.

Problem 12.5: Derive the electron–LO phonon interaction constant $g_{\mathbf{q}}$ (12.31) by considering the low- and high-frequency limit of the Coulomb interaction in a polar medium. At low frequencies both the ion displacement

and the orbital polarization are present, while at high frequencies the inertia

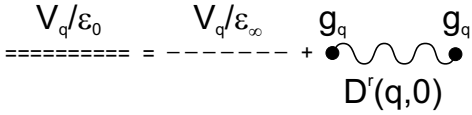

Fig. 12.2 Diagrams of the Coulomb and phonon-mediated interaction

of the ions is too large so that their oscillations cannot follow. Therefore,

$$\frac{V_{\mathbf{q}}}{\epsilon_0} = \frac{V_{\mathbf{q}}}{\epsilon_\infty} + g_{\mathbf{q}}^2 D^r(q, \omega \simeq 0) \ ,$$

with $\epsilon(\omega = 0) = \epsilon_0$ and $\epsilon(\omega \to \infty) = \epsilon_\infty$, see Fig. 12.2. $D^r(q, \omega)$ is the retarded phonon Green's function. The last term is the electron–electron interaction caused by an exchange of a phonon. Calculate the free phonon Green's function from its definition in time with $t' = 0$ for $t \geq 0$

$$D^r(q,t) = -\frac{i}{\hbar}\langle[(b_{\mathbf{q}}^\dagger(t) + b_{-\mathbf{q}}(t)), (b_{\mathbf{q}} + b_{-\mathbf{q}}^\dagger)]\rangle \ ,$$

and by using $b_{\mathbf{q}}(t) = e^{-i\omega_0 t} b_{\mathbf{q}}$. Apply the Fourier transform into frequency space and take the low-frequency limit.

Chapter 13

Excitonic Optical Stark Effect

Very efficient experimental methods to study the optical properties of semiconductors are those that use two successive laser pulses, one to prepare the system in a certain way and one to test it after a variable time delay. The simplest geometry of such an experiment is schematically shown in Fig. 13.1.

Because the characteristic times for optical dephasing and relaxation of band electrons in semiconductors are rather short, one has to use femtosecond laser pulses if one wants to study the quantum coherence and initial relaxation stages of the excited states. Generally speaking, the dephasing times become larger as the phase space of the excited electrons is reduced by quantum confinement, particularly, if one eliminates all translational degrees of freedom as in quantum dots. It is also true that the dephasing times are longer in the low-density regime where one excites primarily neutral complexes such as excitons or biexcitons (two electron–hole–pair states),

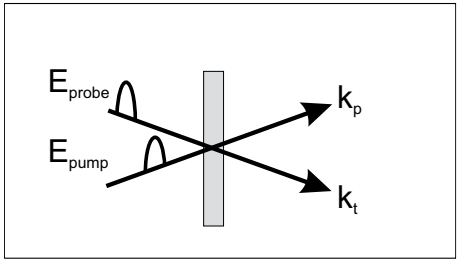

Fig. 13.1 Geometry of a pump-probe experiment.

particularly, in systems where their binding energies are large. Similarly, if one excites spin-polarized states, one finds relatively slow spin dephasing because spin–flip processes are relatively rare. In these cases, one can use picosecond pulses instead of the femtosecond pulses mentioned before. For the analysis of such time-resolved two-pulse experiments, the semiconductor Bloch equations form the appropriate theoretical framework. The coherent laser light field in these equations has to describe naturally both pulses.

A very important example of a "coherent" semiconductor response is the *excitonic optical Stark effect*, where a strong pump pulse excites the material energetically below the exciton resonance and the probe pulse monitors the transmission change at the exciton resonance. The optical Stark effect in a two-level system has already been discussed in Chap. 2. Here, the coherent light field mixes the wave functions of the two states leading to the dressed states. Even though the Stark effect is well-known in atomic systems, it was only observed in semiconductors in the mid 1980's because of the above mentioned short dephasing times.

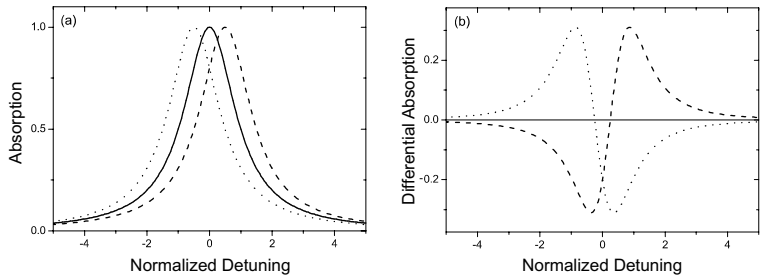

Fig. 13.2 (a) Redshift (shift to lower energies, dotted line) and blueshift (dashed line) of an excitonic resonance α_0 (solid line) and (b) the resulting absorption change (differential absorption) $\alpha - \alpha_0$.

In our discussion of the optical Stark effect in semiconductors, we concentrate on the case of nonresonant excitation of the exciton, where it is a good approximation to ignore absorption and generation of real carriers. In this case, the optical Stark effect manifests itself as a light-induced shift of the excitonic resonance. Depending on the selection rules of the optical transitions this shift can be a blueshift, i.e. shift of the resonance to higher energies, or a redshift (see Fig. 13.2).

We discuss different features of the excitonic optical Stark effect in three steps. First, we present analytic results of a two-band model for a quasi-stationary situation and then we discuss dynamic excitation conditions. In the third step, we include the selection rules for the transitions and also consider biexcitonic correlations, which allows us to discuss pump–probe configurations for different polarizations of the pump and probe pulses.

13.1 Quasi-Stationary Results

In this section, we present the analysis of the quasi-stationary optical Stark effect. This condition applies only when the amplitude variations of the light field are so slow, that we can make an adiabatic approximation. For femtosecond experiments, this procedure is generally not valid. Nevertheless, we start our discussion with that stationary case in order to understand the similarities and differences of this coherent phenomenon in atomic and semiconductor systems. Particularly, we analyze analytically the modifications due to the semiconductor many-body effects. Dynamical solutions for pulsed excitation are then discussed in the following section.

As an introduction, we first reformulate the treatment of Chap. 2 of the optical Stark shift of a two-level atom in terms of the Bloch equations for the polarization and the population. In second quantization, the Hamiltonian for the two-level system is

$$\mathcal{H} = \sum_{j=1,2} \hbar\epsilon_j \, a_j^\dagger \, a_j - \Big[d_{21} \, \mathcal{E}(t) a_2^\dagger \, a_1 + \text{h.c.} \Big] \tag{13.1}$$

with the coherent pump field $\mathcal{E}(t) = \mathcal{E}_p e^{-i\omega_p t}$. Via the Heisenberg equation for the operators, we get the following equations for the polarization $P = \langle a_1^\dagger a_2 \rangle$ and the density in the upper state $n = n_2 = \langle a_2^\dagger a_2 \rangle = 1 - n_1$:

$$i\frac{dP}{dt} = \epsilon P - (1-2n)\frac{d_{21}}{\hbar}\mathcal{E}_p \tag{13.2}$$

and

$$\frac{dn}{dt} = \frac{i}{\hbar}(d_{21} \, \mathcal{E}_p \, P^* - \text{h.c.}) \tag{13.3}$$

with $\epsilon = \epsilon_2 - \epsilon_1$. These two completely coherent equations (no damping terms) have a conserved quantity (see problem 13.1)

$$K = (1-2n)^2 + 4|P|^2 \ . \tag{13.4}$$

With the initial condition $n = 0$ and $P = 0$ we have $K = 1$, or

$$n = \frac{1}{2}(1 \pm \sqrt{1 - 4|P|^2}) \ . \tag{13.5}$$

Eq. (13.5) shows that the density is completely determined by the polarization. This is only true for a fully coherent process, or in the language of quantum mechanics, for *virtual excitations*. These excitations of the atom vanish if the field is switched off, whereas real excitations would stay in the system and would decay on a much longer time scale determined by the carrier lifetime. From Eqs. (13.2) - (13.5) one can again derive the results of Chap. 2 (see problem 13.2).

Next, we turn to the coherent Bloch equations of the semiconductor which have been derived in Chap. 12, see Eqs. (12.19). Here, we omit all damping and collision terms, an approximation which is clearly not valid for resonant excitation, where real absorption occurs. With $n_k = n_{c,k} = 1 - n_{v,k}$, we can write Eqs. (12.19) as

$$i\frac{dP_k}{dt} = e_k\, P_k - (1 - 2n_k)\omega_{R,k} \tag{13.6}$$

$$\frac{dn_k}{dt} = i(\omega_{R,k}P_k^* - \omega_{R,k}^* P_k) \ , \tag{13.7}$$

where $\hbar e_k$ is the pair energy renormalized by the exchange energy

$$\hbar e_k = \hbar(e_{e,k} + e_{h,k}) = E_g + \frac{\hbar^2 k^2}{2m} - 2\sum_{k'} V_{k-k'} n_{k'} \tag{13.8}$$

and $\omega_{R,k}$ is the effective Rabi frequency, Eq. (12.18).

Note, that there is a complete formal analogy between the two-level atom equations (13.2) – (13.3) and the semiconductor equations (13.6) – (13.7) for each k-state, except for the renormalizations of the pair energy and of the Rabi frequency, which mix the k-states in a complicated way. From this analogy, we get immediately the conservation law

$$n_k = \frac{1}{2}(1 \pm \sqrt{1 - 4|P_k|^2}) \ . \tag{13.9}$$

If the fields are switched on adiabatically only the minus sign in Eq. (13.9) can be realized and the relations $0 \le n_k \le 1/2$ and $0 \le |P_k|^2 \le 1/2$ hold.

Solving Eqs. (13.6) and (13.9) adiabatically, i.e., neglecting all possible slow amplitude variations, we find for $\mathcal{E}(t) = \mathcal{E}_p \exp(-i\omega_p t)$

$$P_k = \frac{(1-2n_k)\omega_{R,k}}{e_k - \omega_p} \quad . \tag{13.10}$$

Eq. (13.10) together with Eqs. (13.7) - (13.9) form a complicated system of nonlinear integral equations, which can be solved numerically or which has to be simplified by further approximations.

In experiments, one usually applies a weak test beam to measure the effects which the strong pump beam introduces in the semiconductor. To study this situation, we add to the pump beam a weak test beam $\mathcal{E}_t \exp(-i\omega_t t)$ which induces an additional small polarization δP_k. Linearizing Eqs. (13.6) - (13.9) yields

$$i\frac{d}{dt}\delta P_k = \delta e_k\, P_k + e_k\, \delta P_k + 2\delta n_k\, \omega_{R,k} - (1-2n_k)\, \delta\omega_{R,k} \quad , \tag{13.11}$$

where

$$\delta e_k = -\frac{2}{\hbar}\sum_{k'} V_{k-k'}\, \delta n_{k'} \quad , \tag{13.12}$$

$$\delta n_k = \frac{P_k\, \delta P_k^* + P_k^*\, \delta P_k}{1-2n_k} \quad , \tag{13.13}$$

and

$$\hbar\, \delta\omega_{R,k} = d_{cv}\, \mathcal{E}_t\, e^{-i\omega_t t} + \sum_{k'} V_{k-k'}\, \delta P_{k'} \quad . \tag{13.14}$$

We now eliminate the time dependence of the pump field by splitting off a factor $\exp(-i\omega_p t)$ of P_k, δP_k and $\omega_{R,k}$, e.g., $P_k = p_k \exp(-i\omega_p t)$. This way we obtain

$$i\frac{d}{dt}\delta p_k = \delta e_k\, p_k + (e_k - \omega_p)\delta p_k + 2\delta n_k\, \omega_{R,k} - (1-2n_k)\delta\omega_{R,k} \quad , \tag{13.15}$$

where we redefined the change in the Rabi frequency as

$$\hbar\, \delta\omega_{R,k} \rightarrow \hbar\, \delta\omega_{R,k} = d_{cv}\, \mathcal{E}_t\, e^{i\Delta t} + \sum_{k'} V_{k-k'}\delta p_{k'} \quad , \tag{13.16}$$

and $\Delta = \omega_p - \omega_t$ is the frequency difference of the pump and test beam. This system of equations can be solved if the solutions of P_k and n_k under

the influence of the strong pump beam alone are known. For a stationary problem, we have to choose the form

$$\delta p_k = \delta p_k^+ \; e^{+i\Delta t} + \delta p_k^- \, e^{-i\Delta t} \quad . \tag{13.17}$$

Once δp_k^+ is known, we get the susceptibility and the absorption spectrum of the test beam in the usual way. In particular, one is interested to see how the exciton absorption spectrum is influenced by a pump beam which is detuned far below the lowest exciton resonance. In order to get a realistic absorption spectrum, one takes a finite damping for polarization δP_k induced by the test beam into account. Note again, that a purely coherent equation for the P_k induced by the pump-beam, and a dissipative equation for δP_k are a physically justified model, because of the rapidly decreasing damping with increasing detuning, i.e., the frequency-dependent dephasing. In Fig. 13.3, we show the results of a numerical evaluation of the stationary equation for a quasi-two-dimensional GaAs quantum-well structure. The detuning of the pump beam with respect to the 1s-exciton was chosen as ten exciton Rydberg energies. Fig. 13.3 clearly shows a large blueshift of the exciton resonance with increasing pump intensity. Simultaneously also a blueshift of the band edge occurs and the exciton oscillator strength does not decrease.

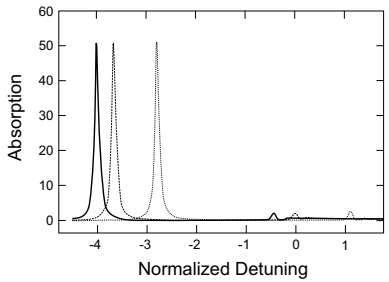

Fig. 13.3 Calculated $2D$ absorption spectrum versus normalized detuning $(\hbar\omega - E_G)/E_0$ according to Ell *et al.* for $(E_g - \hbar\omega_p)/E_0 = 10$ and the pump intensities $I_p = 0$, 7.5, and 30 MW/cm^2 from left to right.

In order to analyze these numerical results, we analytically solve the equations in first order of the pump intensity. Thus $\mathcal{E}_p$, P_k, and n_k can be

considered as small expansion parameters. From Eq. (13.9) we find

$$n_k = |P_k|^2 + \mathcal{O}(|P_k|^4) \ . \tag{13.18}$$

The quasi-stationary equation for the polarization induced by the test beam reduces with $\delta p_k^+ >> \delta p_k^-$ to (see problem 13.3)

$$\sum_{k'} \Big[H^0_{kk'} + \Delta H_{kk'} - \hbar(\omega_t + i\delta)\delta_{kk'} \Big] \delta p^+_{k'} = (1 - 2|p_k|^2) d_{cv}\, \mathcal{E}_t \ , \tag{13.19}$$

where H^0 is the unperturbed pair Hamiltonian

$$H^0_{kk'} = \left(E_g + \frac{\hbar^2 k^2}{2m} \right) \delta_{kk'} - V_{k-k'} \ , \tag{13.20}$$

and

$$\begin{aligned} \Delta H_{kk'} &= 2\delta_{kk'} d_{cv} \mathcal{E}_p p_k^* + 2|p_k|^2 V_{k-k'} - 2\delta_{kk'} \sum_{k''} V_{k-k''} |p_{k''}|^2 \\ &\quad + 2\delta_{kk'} p_k^* \sum_{k''} V_{k-k''} p_{k''} - 2 p_k V_{k-k'} p^*_{k'} \ . \end{aligned} \tag{13.21}$$

We now expand the polarization induced by the test field in terms of the unperturbed exciton eigenfunctions, i.e., in terms of the eigenfunctions of the Hamiltonian (13.20):

$$\delta p_k^+ = \sum_\lambda \delta p_\lambda^+ \, \psi_{\lambda,k} \ . \tag{13.22}$$

Inserting this expansion into Eq. (13.19), multiplying with $\psi^*_{\lambda,k}$ from the left, and summing over all k yields

$$\sum_{\lambda'} \Big[\hbar(\omega_\lambda - \omega_t - i\delta)\delta_{\lambda\lambda'} + \Delta H_{\lambda\lambda'} \Big] \delta p^+_{\lambda'} = \sum_k \psi^*_{\lambda,k} (1 - 2|p_k|^2)\, d_{cv}\, \mathcal{E}_t \ . \tag{13.23}$$

Here, we introduced the perturbation Hamiltonian

$$\Delta H_{\lambda\lambda'} = \Pi_{\lambda\lambda'} + \Delta_{\lambda\lambda'} \ , \tag{13.24}$$

where $\Pi_{\lambda\lambda'}$ is the anharmonic interaction between the exciton and the pump field,

$$\Pi_{\lambda\lambda'} = 2\, \mathcal{E}_p \sum_k \psi^*_{\lambda,k} d_{cv}\, p_k^*\, \psi_{\lambda',k} \ , \tag{13.25}$$

and $\Delta_{\lambda\lambda'}$ is the exciton–exciton interaction

$$\Delta_{\lambda\lambda'} = 2\sum_{kk'} V_{k-k'}\psi^*_{\lambda,k}(p^*_k - p^*_{k'})(p_k\,\psi_{\lambda',k'} + p_{k'}\psi_{\lambda',k}) \ . \tag{13.26}$$

We can rewrite Eq. (13.23) as

$$\hbar\delta p^+_\lambda = \frac{\sum_k \psi^*_{\lambda,k}(1-2|p_k|^2)d_{cv}\,\mathcal{E}_t - \sum_{\lambda'\neq\lambda}\Delta H_{\lambda\lambda'}\,\delta p^+_{\lambda'}}{\bar\omega_\lambda - \omega_t - i\delta} \ , \tag{13.27}$$

where $\bar\omega_\lambda$ is the renormalized exciton frequency

$$\bar\omega_\lambda = \omega_\lambda + \Delta H_{\lambda\lambda}/\hbar \ . \tag{13.28}$$

Eq. (13.27) can be solved iteratively with

$$\hbar\delta p^{+(1)}_\lambda = \frac{\sum_k \psi^*_{\lambda,k}(1-2|p_k|^2)d_{cv}\,\mathcal{E}_p}{\bar\omega_\lambda - \omega_t - i\delta} \ . \tag{13.29}$$

Note, that in this procedure even the first-order result contains the shifted exciton energies $\hbar\omega_\lambda$ i.e., the Stark shift as well as the phase-space filling. In the next order, one finds

$$\hbar\delta p^{+(2)}_\lambda = \hbar\delta p^{+(1)}_\lambda - \frac{\sum_{\lambda'\neq\lambda}\Delta H_{\lambda\lambda'}\delta p^{+(1)}_{\lambda'}}{\bar\omega_\lambda - \omega_t - i\delta} \ . \tag{13.30}$$

The linear optical susceptibility of the test beam is finally obtained as

$$\chi_t(\omega_t) = 2\sum_\lambda \frac{d^*_\lambda\,\delta p^+_\lambda}{\mathcal{E}_t} \ , \tag{13.31}$$

where

$$d_\lambda = \sum_k d_{cv}\,\psi^*_{\lambda,k} \ . \tag{13.32}$$

The resulting susceptibility has the form (see problem 13.4)

$$\chi_t(\omega_t) = \frac{2}{\hbar}\sum_\lambda \frac{\bar f_\lambda}{\bar\omega_\lambda - \omega_t - i\delta} \ , \tag{13.33}$$

where $\bar f_\lambda$ is the renormalized exciton oscillator strength:

$$\bar f_\lambda = |d_\lambda|^2 - 2d^*_\lambda\sum_k \psi^*_{\lambda,k}|p_k|^2 d_{cv} + \sum_{\lambda'\neq\lambda}\frac{d^*_\lambda\Delta H_{\lambda\lambda'}d_{\lambda'} + (\lambda \rightleftharpoons \lambda')}{\hbar(\omega_\lambda - \omega_{\lambda'})} \ . \tag{13.34}$$

Note, that the result (13.33) is put into the usual form of the exciton susceptibility, but it contains renormalized exciton energies $\bar{\omega}_\lambda$ and renormalized oscillator strengths $\bar{f}_\lambda$. In this low-intensity regime, the quasi-stationary optical Stark effect can be described completely in terms of shifts of the exciton levels and in terms of changes of the exciton oscillator strengths. The first correction term of the oscillator strength in Eq. (13.34) describes the reduction due to phase-space filling, while the terms due to the perturbation ΔH describe the corrections caused by the anharmonic exciton–photon and the exciton–exciton interaction.

In the linear approximation in the pump field, the polarization p_k can be written in terms of an exciton Green's function

$$p_k(\omega_p) = -d_{cv}\,\mathcal{E}_p\,G^r(k,\omega_p) \ , \tag{13.35}$$

with

$$G^r(k,\omega_p) = -\sum_\lambda \frac{\psi^*_{\lambda,k}\psi_\lambda(r=0)}{\hbar(\omega_\lambda - \omega_p - i\delta)} \ . \tag{13.36}$$

For small detuning $\omega_p - \omega_{1s} << E_0$, the Green's function simplifies to

$$G^r(k,\omega_p) = -\frac{\psi^*_{1s,k}\psi_{1s}(r=0)}{\hbar(\omega_{1s} - \omega_p - i\delta)} \ , \tag{13.37}$$

so that

$$\Pi_{\lambda\lambda} = \psi^*_{1s}(r=0)\sum_k \psi_{1s,k}|\psi_{\lambda,k}|^2 \frac{2|d\,\mathcal{E}_p|^2}{\hbar(\omega_{1s}-\omega_p)} \ . \tag{13.38}$$

The Stark shift due to the anharmonic exciton–photon interaction is equal to the usual two-level Stark shift $(2|d\,\mathcal{E}_p|^2)/\hbar(\omega_{1s}-\omega_p)$ times an enhancement factor due to the electron–hole correlation

$$\rho_\lambda = \psi^*_{1s}(r=0)\sum_k \psi_{1s,k}|\psi_{\lambda,k}|^2 \ . \tag{13.39}$$

For the band edge, we find with $|\psi_{\lambda=\infty,k}|^2 = \delta_{k,0}$

$$\rho_\infty = \psi^*_{1s}(r=0)\,\psi_{1s,k=0} \ . \tag{13.40}$$

Using the two- and three-dimenisonal exciton wave functions (see Chap. 10)

$$\psi_{1s,k} = \frac{\sqrt{2\pi}\, a_0}{\left[1 + (ka_0/2)^2\right]^{3/2}}$$
$$\psi_{1s,k} = \frac{8\sqrt{\pi a_0^3}}{\left[1 + (ka_0)^2\right]^2} \ ,$$

we find (see problem 13.4)

$$\rho_{1s} = \begin{pmatrix} 16/7 \\ 7/2 \end{pmatrix} ; \quad \rho_\infty = \begin{pmatrix} 4 \\ 8 \end{pmatrix} \quad \text{for} \quad \begin{pmatrix} 2D \\ 3D \end{pmatrix} . \tag{13.41}$$

For small detuning, we obtain the surprising result that the contribution of the anharmonic exciton–photon interaction to the Stark shifts is larger for the continuum states than for the exciton.
Similarly, the polarization–polarization interaction $\Delta_{\lambda\lambda}$ can be written for small detuning as

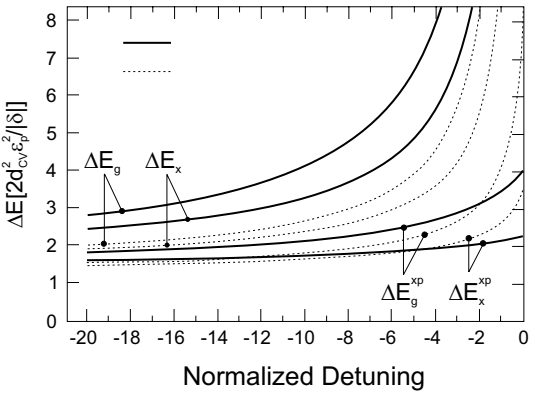

Fig. 13.4 Calculated shifts of the exciton ΔE_x and of the band gap ΔE_g versus normalized detuning $(\hbar\omega_p - E_{1s})/E_0$; as well as shifts due to the anharmonic exciton–photon interaction alone, ΔE_x^{xp} and ΔE_g^{xp} respectively.

$$\begin{aligned}\Delta_{\lambda\lambda} &= 2|\psi^*_{1s}(r=0)d\mathcal{E}_p|^2 \\ &\quad\times \sum_{kk'} \frac{V_{k-k'}\psi^*_{\lambda,k}(\psi^*_{1s,k}-\psi^*_{1s,k'})(\psi_{1s,k}\psi_{\lambda,k'}-\psi_{1s,k'}\psi_{\lambda,k})}{\hbar^2(\omega_{1s}-\omega_p)^2} \\ &= \nu_\lambda \frac{2|d\mathcal{E}_p|^2}{\hbar(\omega_{1s}-\omega_p)} \ . \end{aligned} \tag{13.42}$$

The enhancement factor ν_λ diverges as $1/(\omega_{1s}-\omega_p)$ for $\omega_p \to \omega_{1s}$. Again, the integrals can be evaluated analytically and yield

$$\nu_{1s} = \frac{E_0}{\hbar(\omega_{1s}-\omega_p)} a_{1s} \ , \tag{13.43}$$

where

$$a_{1s} = \begin{pmatrix} 64(1-315\pi^2/2^{12}) \\ 26/3 \end{pmatrix} \simeq \begin{pmatrix} 15.4 \\ 8.66 \end{pmatrix} \quad \text{for} \quad \begin{pmatrix} 2D \\ 3D \end{pmatrix} \ , \tag{13.44}$$

and

$$\nu_\infty = \frac{E_0}{\hbar(\omega_{1s}-\omega_p)} a_\infty \ , \tag{13.45}$$

where

$$a_\infty = \begin{pmatrix} 64(1-3\pi/16) \\ 24 \end{pmatrix} \simeq \begin{pmatrix} 26.3 \\ 24 \end{pmatrix} \quad \text{for} \quad \begin{pmatrix} 2D \\ 3D \end{pmatrix} \ . \tag{13.46}$$

Again, we see that these contributions to the Stark shifts are larger for the continuum states than for the exciton ground state. For general values of the detuning, the shifts have to be evaluated numerically. Fig. 13.4 shows the resulting shifts of the exciton and the continuum states for varying detuning. For all values of the detuning, the blueshift of the continuum states is larger than that of the exciton ground state, i.e., the exciton binding energy increases.

Now, we are in a position to understand the numerical results for the quasi-stationary Stark effect shown in Fig. 13.3. The phase-space filling due to the action of the pump beam, which would result in a reduction of the oscillator strength of the exciton, is overcompensated by the anharmonic exciton–photon and exciton–exciton interaction, which increase the binding energy and thus the oscillator strength. These conclusions can indeed be verified by evaluating the oscillator strength (13.34) explicitly.

13.2 Dynamic Results

In our investigation of dynamical aspects of the optical Stark effect, we again start from the coherent semiconductor Bloch equations, Eqs. (13.6) and (13.7). We write the total field $\mathcal{E}$ as sum of pump $\mathcal{E}_p$ and test field $\mathcal{E}_t$

$$\begin{aligned}\mathcal{E}(\mathbf{r},t) &= \mathcal{E}_p(\mathbf{r},t) + \mathcal{E}_t(\mathbf{r},t) \\ &= \mathcal{E}_p(t)e^{-i(\mathbf{k}_p\cdot\mathbf{r}+\Omega t)} + \mathcal{E}_t(t)e^{-i(\mathbf{k}_t\cdot\mathbf{r}+\Omega t)}\end{aligned} \tag{13.47}$$

with $\mathbf{k}_p \neq \mathbf{k}_t$.

In order to obtain analytical results, we ignore the nonlinear terms, i.e., the terms involving products of polarizations and densities, i.e., we treat only the linear coherent part

$$\hbar\left[i\frac{\partial}{\partial t} - (\epsilon_{e,k} + \epsilon_{h,k})\right] P_{\mathbf{k}} = (2n_{\mathbf{k}} - 1)d_{cv}\mathcal{E}(t) - \sum_{\mathbf{q}\neq\mathbf{k}} V_{|\mathbf{k}-\mathbf{q}|}P_{\mathbf{q}} \ , \tag{13.48}$$

$$\hbar\frac{\partial}{\partial t}n_{\mathbf{k}} = i\big[d_{cv}\mathcal{E}(t)P^*_{\mathbf{k}} - \text{c.c.}\big] \ , \tag{13.49}$$

where we again assumed

$$n_{h,\mathbf{k}} = n_{e,\mathbf{k}} = n_{\mathbf{k}} \ . \tag{13.50}$$

As initial conditions, we assume an unexcited system,

$$n_{\mathbf{k}} = P_{cv,\mathbf{k}} = 0 \ .$$

As in Eqs. (10.31) - (10.35), we now transform the equations to real space:

$$i\hbar\frac{\partial}{\partial t}P(\mathbf{r}) = \mathcal{H}_{eh}P(\mathbf{r}) + d_{cv}\mathcal{E}(t)\big[2n(\mathbf{r}) - \delta(\mathbf{r})\big] \tag{13.51}$$

and

$$\hbar\frac{\partial}{\partial t}n(\mathbf{r}) = i\big[d_{cv}\mathcal{E}(t)P^*(-\mathbf{r}) - \text{c.c.}\big] \ , \tag{13.52}$$

Here,

$$\mathcal{H}_{eh} = E_g - \frac{\hbar^2\nabla^2}{2m_r} - V(r) \tag{13.53}$$

is the Wannier Hamiltonian, compare Eq. (10.35). Note, that under the present conditions the equations yield local charge neutrality,

$$n_e(\mathbf{r}) = n_h(-\mathbf{r}) \equiv n(\mathbf{r}) \ .$$

Now, we multiply Eqs. (13.51) and (13.52) by $\psi_\lambda(\mathbf{r})$, where $\psi_\lambda(\mathbf{r})$ is the eigenfunction of the Wannier equation (10.35). Then we integrate over $\mathbf{r}$ to obtain

$$i\hbar\frac{\partial}{\partial t}P_\lambda = \hbar\epsilon_\lambda P_\lambda + d_{cv}\mathcal{E}(t)\big[2n_\lambda - \psi_\lambda(r=0)\big] \ , \tag{13.54}$$

and

$$\hbar\frac{\partial}{\partial t}n_\lambda = i\, d_{cv}\mathcal{E}(t)P^*_\lambda - id^*_{cv}\mathcal{E}(t)P_\lambda \ , \tag{13.55}$$

where we used the notation

$$\begin{aligned}\int d^3r\psi_\lambda(\mathbf{r})P(\mathbf{r}) &= P_\lambda \ , \\ \int d^3r\psi_\lambda(\mathbf{r})n(\mathbf{r}) &= n_\lambda \ .\end{aligned} \tag{13.56}$$

The set of Eqs. (13.54) – (13.55) is closed for each λ. The source term in Eq. (13.54) is proportional to the electron–hole–pair wave function in the origin and therefore only the s-functions contribute. Hence, $\psi_\lambda(\mathbf{r})$ is a real function that depends only on $|\mathbf{r}|$.

Introducing now

$$P_\lambda = \psi_\lambda(r=0)\mathcal{P}_\lambda \text{ and } n_\lambda = \psi_\lambda(r=0)N_\lambda \ , \tag{13.57}$$

we obtain the simplified equations of motion

$$\begin{aligned}\frac{\partial}{\partial t}\mathcal{P}_\lambda &= -(i\epsilon_\lambda + \gamma)\mathcal{P}_\lambda - \frac{id_{cv}}{\hbar}\mathcal{E}(t)(2N_\lambda - 1) \\ \frac{\partial}{\partial t}N_\lambda &= -\Gamma n_\lambda + i\frac{d_{cv}}{\hbar}\mathcal{E}(t)\mathcal{P}^*_\lambda - i\frac{d^*_{cv}}{\hbar}\mathcal{E}^*(t)\mathcal{P}_\lambda \ ,\end{aligned} \tag{13.58}$$

where we added the appropriate phenomenological damping terms. We use the total field in the form of Eq. (13.47). In order to eliminate the optical frequencies, we introduce the notation

$$\mathcal{P}_\lambda \equiv e^{-i\Omega t}p_\lambda \quad \text{and} \quad w_\lambda \equiv (1 - 2N_\lambda) \ . \tag{13.59}$$

Inserting these definitions into Eqs. (13.58) yields

$$\frac{\partial}{\partial t}p_\lambda = [i(\epsilon_\lambda - \Omega) + \gamma]p_\lambda + i\frac{d_{cv}}{\hbar}\left[\mathcal{E}_p(t)\, e^{-i\mathbf{k}_p\cdot\mathbf{r}} + \mathcal{E}_t(t)\, e^{-i\mathbf{k}_t\cdot\mathbf{r}}\right] w_\lambda \tag{13.60}$$

and

$$\frac{\partial}{\partial t}w_\lambda = -\Gamma(w_\lambda - 1) - i\,\frac{2d_{cv}}{\hbar}\left[\mathcal{E}_p(t)\, e^{-i\mathbf{k}_p\cdot\mathbf{r}} + \mathcal{E}_t(t)\, e^{-i\mathbf{k}_t\cdot\mathbf{r}}\right] p_\lambda^* + i\frac{2d_{cv}^*}{\hbar}\left[\mathcal{E}_p^*(t)\, e^{i\mathbf{k}_p\cdot\mathbf{r}} + \mathcal{E}_t^*(t) e^{i\mathbf{k}_t\cdot\mathbf{r}}\right] p_\lambda \ . \tag{13.61}$$

In order to keep the theory as simple as possible, we assume that $\mathcal{E}_t(t)$ is short on all the relevant time scales, so we can approximate

$$\mathcal{E}_t(t) = \mathcal{E}_t\, \delta(t - t_t) \ . \tag{13.62}$$

This corresponds to a broad frequency spectrum. The experiment measures only that part of the signal which propagates in probe direction. Therefore, we are interested only in that component of the solution for p_λ which has the spatial factor

$$\propto e^{i\mathbf{k}_t\cdot\mathbf{r}} \ . \tag{13.63}$$

Since we consider the case of an arbitrarily weak probe, we include only terms which are linear in $\mathcal{E}_t$. To obtain analytic results, we ignore all terms which are higher than second order in $\mathcal{E}_p(t)$.

Clearly, for $t < t_t$, we have no signal in the direction of the probe. The only contribution is

$$p_\lambda(t < t_t) = i\frac{d_{cv}}{\hbar} e^{-i\mathbf{k}_p\cdot\mathbf{r}} \int_{-\infty}^{t} dt' e^{-\left[i(\epsilon_\lambda - \Omega) + \gamma\right](t - t')} \mathcal{E}_p(t') w_\lambda(t') \ . \tag{13.64}$$

For that period of time during which the probe is incident on the sample, we can solve Eq. (13.61) as

$$\int_{t_{t_-}}^{t_{t_+}} dt \frac{\partial w_\lambda}{\partial t} = w_\lambda(t_{t_+}) - w_\lambda(t_{t_-})$$
$$\simeq -i\,\frac{2d_{cv}}{\hbar}\,e^{-i\mathbf{k}_t\cdot\mathbf{r}}\mathcal{E}_t\,p^*_\lambda(t_{t_-}) + i\frac{2d^*_{cv}}{\hbar}e^{i\mathbf{k}_t\cdot\mathbf{r}}\mathcal{E}^*_t p_\lambda(t_{t_-}) + \dots \quad , \tag{13.65}$$

where we denote by t_{t_-} and t_{t_+} the times just before and after the probe pulse, respectively. In Eq. (13.65), we used

$$p_\lambda(t_t) = p_\lambda(t_{t_-}) + \mathcal{O}(\mathcal{E}_t) \quad , \tag{13.66}$$

where the correction term of order $\mathcal{E}_t$ has been neglected, since we are interested only in terms linear in $\mathcal{E}_t$. The expression for $p_\lambda(t_{t_-})$ is given by Eq. (13.64). Inserting Eq. (13.65) into Eq. (13.64) shows that a grating

$$\propto e^{i(\mathbf{k}_t - \mathbf{k}_p)\cdot\mathbf{r}} \tag{13.67}$$

is formed in the sample. Light from the pump pulse can scatter from the grating into the direction of the probe and can therefore be seen by the detector. In addition, the probe transmission is also modified through the saturation of the transitions.

To include all effects systematically, we now solve Eqs. (13.60) and (13.61) for the polarization and density variables by expanding them in powers of the fields

$$\begin{aligned} p_\lambda(t) =& i\frac{d_{cv}}{\hbar}\int_{-\infty}^{t} dt' e^{-\left[i(\epsilon_\lambda-\Omega)+\gamma\right](t-t')}\left[\mathcal{E}_p(t')e^{-i\mathbf{k}_p\cdot\mathbf{r}} + \mathcal{E}_t(t')e^{-i\mathbf{k}_t\cdot\mathbf{r}}\right] w_\lambda(t') \\ \simeq& \; i\frac{d_{cv}}{\hbar}\mathcal{E}_t\,e^{-i\mathbf{k}_t\cdot\mathbf{r}}\,e^{-\left[i(\epsilon_\lambda-\Omega)+\gamma\right](t-t_t)} w_\lambda(t_{t_-})\Theta(t-t_t) \\ &+ i\frac{d_{cv}}{\hbar}\int_{-\infty}^{t} dt'\,e^{-\left[i(\epsilon_\lambda-\Omega)+\gamma\right](t-t')}\mathcal{E}_p(t')w_\lambda(t')e^{-i\mathbf{k}_p\cdot\mathbf{r}} \end{aligned} \tag{13.68}$$

and

$$
\begin{aligned}
w_\lambda(t) = 1 &- \frac{i2d_{cv}}{\hbar}\int_{-\infty}^{t} dt' e^{-\Gamma(t-t')}\Big[\mathcal{E}_p(t')e^{-i\mathbf{k}_p\cdot\mathbf{r}} + \mathcal{E}_t(t')e^{-i\mathbf{k}_t\cdot\mathbf{r}}\Big]p^*_\lambda(t') \\
&+ i\frac{2d^*_{cv}}{\hbar}\int_{-\infty}^{t} dt'\, e^{-\Gamma(t-t')}\Big[\mathcal{E}^*_p(t')e^{i\mathbf{k}_p\cdot\mathbf{r}} + \mathcal{E}^*_t(t')e^{i\mathbf{k}_t\cdot\mathbf{r}}\Big]p_\lambda(t') \\
&\simeq 1 - i\frac{2d_{cv}}{\hbar}e^{-\Gamma(t-t_t)}\mathcal{E}_t\, e^{-i\mathbf{k}_t\cdot\mathbf{r}}p^*_\lambda(t_{t_-})\Theta(t-t_t) \\
&+ i\frac{2d^*_{cv}}{\hbar}e^{-\Gamma(t-t_t)}\mathcal{E}^*_t\, e^{i\mathbf{k}_t\cdot\mathbf{r}}p_\lambda(t_{t_-})\Theta(t-t_t) \\
&- i\frac{2d_{cv}}{\hbar}\int_{-\infty}^{t} dt'\, e^{-\Gamma(t-t')}\mathcal{E}_p(t')p^*_\lambda(t')e^{-i\mathbf{k}_p\cdot\mathbf{r}} \\
&+ i\frac{2d^*_{cv}}{\hbar}\int_{-\infty}^{t} dt'\, e^{-\Gamma(t-t')}\mathcal{E}^*_p(t')p_\lambda(t')e^{i\mathbf{k}_p\cdot\mathbf{r}}\ , \qquad (13.69)
\end{aligned}
$$

where we used Eq. (13.62) for the probe pulse. Now, we insert Eq. (13.69) into Eq. (13.68) and solve the resulting integral equation iteratively. This way, we obtain many terms, most of which do not contribute to our final result. In order to keep our equations as short as possible, we write only those terms which lead to a contribution in the final result that influences the probe transmission. We obtain

$$
\begin{aligned}
p_\lambda(t) &= \frac{id_{cv}}{\hbar}\mathcal{E}_t e^{-i\mathbf{k}_t\cdot\mathbf{r}}\, e^{-[i(\epsilon_\lambda-\Omega)+\gamma](t-t_t)}w_\lambda(t_{t_-})\,\Theta(t-t_t) \\
&+2\frac{d^2_{cv}}{\hbar^2}\mathcal{E}_t e^{-i(\mathbf{k}_t+\mathbf{k}_p)\cdot\mathbf{r}}p^*_\lambda(t_{t_-})\int_{t_t}^{t} dt'\, e^{-[i(\epsilon_\lambda-\Omega)+\gamma](t-t')}e^{-\Gamma(t'-t_t)}\mathcal{E}_p(t')\Theta(t-t_t) \\
&-2\frac{|d_{cv}|^2}{\hbar^2}\int_{-\infty}^{t} dt' e^{-[i(\epsilon_\lambda-\Omega)+\gamma](t-t')}\mathcal{E}_p(t')\int_{-\infty}^{t'} dt'' e^{-\Gamma(t'-t'')}\mathcal{E}^*_p(t'')p_\lambda(t'') \\
&+\dots\ . \qquad (13.70)
\end{aligned}
$$

The third line of this expression is of the order $(\mathcal{E}_p)^2$ and contains an integral over p_λ. Since we keep only terms up to the order $\mathcal{E}_t(\mathcal{E}_p)^2$ in our analysis, it is sufficient to solve this integral by inserting the first line of Eq. (13.70) and the first term of Eq. (13.69) to get

$$
\begin{aligned}
p_\lambda(t) &= i\frac{d_{cv}}{\hbar}\mathcal{E}_t\, e^{-i\mathbf{k}_t\cdot\mathbf{r}}\, e^{-[i(\epsilon_\lambda-\Omega)+\gamma](t-t_t)} w_\lambda(t_{t_-})\,\Theta(t-t_t) \\
&+ 2\frac{d_{cv}^2}{\hbar^2}\mathcal{E}_t e^{-i(\mathbf{k}_t+\mathbf{k}_p)\cdot\mathbf{r}} p_\lambda^*(t_{t_-}) \\
&\times \int_{t_t}^{t} dt'\, e^{-[i(\epsilon_\lambda-\Omega)+\gamma](t-t')} e^{-\Gamma(t'-t_t)}\mathcal{E}_p(t')\Theta(t-t_t) \\
&- i\frac{2d_{cv}}{\hbar}\frac{|d_{cv}|^2}{\hbar^2}\mathcal{E}_t\, e^{-i\mathbf{k}_t\cdot\mathbf{r}} \int_{t_t}^{t} dt'\, e^{-[i(\epsilon_\lambda-\Omega)+\gamma](t-t')}\mathcal{E}_p(t') \\
&\times \int_{t_t}^{t'} dt''\, e^{-\Gamma(t'-t'')}\mathcal{E}_p^*(t'')\, e^{-[i(\epsilon_\lambda-\Omega)+\gamma](t''-t_t)}\,\Theta(t-t_t) \\
&+ \dots \quad . \qquad (13.71)
\end{aligned}
$$

At the end of our calculations, we are interested in the optical susceptibility $\chi_\lambda(\omega)$ for the probe pulse. Therefore, we study the Fourier transform of the polarization

$$
\begin{aligned}
\mathcal{P}_\lambda(\omega) &= \int_{-\infty}^{\infty} dt\, e^{i\omega t}\,\mathcal{P}_\lambda(t) = \int_{-\infty}^{\infty} dt\, e^{i(\omega-\Omega)t} p_\lambda(t) \\
&= \int_{t_t}^{\infty} dt\, e^{i(\omega-\Omega)t} p_\lambda(t) = \int_0^{\infty} dt\, e^{i(\omega-\Omega)t} p_\lambda(t+t_t)\, e^{-i(\omega-\Omega)t_t} \quad . \qquad (13.72)
\end{aligned}
$$

Here, we used the result of Eq. (13.71), that $p_\lambda(t)$ has a component proportional to $e^{(i\mathbf{k}_t\cdot\mathbf{r})}$, (13.63), only for $t > t_t$, i.e., after the probe hit the sample. For the spectrum of the probe (test) pulse, we can write

$$
\begin{aligned}
\mathcal{E}_t(\omega) &= \int_{-\infty}^{\infty} dt\,\mathcal{E}_t(t)\, e^{i\omega t} = \int_{-\infty}^{\infty} dt\,\mathcal{E}_t(t)\, e^{i(\omega-\Omega)t}\, e^{-i\mathbf{k}_t\cdot\mathbf{r}} \\
&\simeq \mathcal{E}_t\, e^{i(\omega-\Omega)t_t}\, e^{-i\mathbf{k}_t\cdot\mathbf{r}} \qquad (13.73)
\end{aligned}
$$

Using Eqs. (13.66) and (13.71) – (13.73), we obtain

$$\begin{aligned}\mathcal{P}_\lambda(\omega) &= i\frac{d_{cv}}{\hbar}\frac{\mathcal{E}_t(\omega)}{\gamma - i(\omega-\epsilon_\lambda)}\Bigg\{ w_\lambda(t_{t_-}) \\ &- i\frac{2d_{cv}}{\hbar}e^{-i\mathbf{k}_p\cdot\mathbf{r}}\, p^*_\lambda(t_{t_-}) \int_0^\infty dt'\, e^{[i(\omega-\Omega)-\Gamma]t'}\, \mathcal{E}_p(t'+t_t) \\ &- 2\frac{|d_{cv}|^2}{\hbar^2}\int_0^\infty dt\, e^{i(\omega-\Omega)t}\, \mathcal{E}_p(t+t_t) \\ &\times \int_0^t dt'\, e^{-\Gamma(t-t')}\, e^{-[i(\epsilon_\lambda-\Omega)+\gamma]t'}\, \mathcal{E}^*_p(t'+t_t)\Bigg\} \\ &\equiv \chi_\lambda(\omega)\mathcal{E}_t(\omega)\ . \end{aligned} \tag{13.74}$$

Extracting the probe susceptibility, we find

$$\begin{aligned}\chi_\lambda(\omega) &= i\frac{d_{cv}}{\hbar}\frac{1}{\gamma - i(\omega-\epsilon_\lambda)}\Bigg\{ w_\lambda(t_{t_-}) \\ &-2\frac{|d_{cv}|^2}{\hbar^2}\int_{-\infty}^{t_t} dt'\, e^{\left[i(\epsilon_\lambda-\Omega)-\gamma\right](t_t-t')}\mathcal{E}^*_p(t')\int_0^\infty dt\, e^{\left[i(\omega-\Omega)-\Gamma\right]t}\mathcal{E}_p(t+t_t) \\ &-2\frac{|d_{cv}|^2}{\hbar^2}\int_0^\infty dt\, e^{i(\omega-\Omega)t}\mathcal{E}_p(t+t_t)\int_0^t dt' e^{-\Gamma(t-t')}e^{-\left[i(\epsilon_\lambda-\Omega)+\gamma\right]t'}\, \mathcal{E}^*_p(t'+t_t)\Bigg\} \end{aligned} \tag{13.75}$$

where Eq. (13.64) has been used for $p^*_\lambda(t_{t_-})$. The last term in Eq. (13.75) can also be written in the form

$$\begin{aligned}&-2\frac{|d_{cv}|^2}{\hbar^2}\int_0^\infty dt'\int_{t'}^\infty dt\, e^{i(\omega-\Omega)t}\mathcal{E}_p(t+t_t)\, e^{-\Gamma(t-t')}\, e^{-\left[i(\epsilon_\lambda-\Omega)+\gamma\right]t'}\mathcal{E}^*_p(t'+t_t) \\ &= -2\frac{|d_{cv}|^2}{\hbar^2}\int_0^\infty dt'\int_0^\infty dt e^{i(\omega-\Omega)t}\, e^{-\Gamma t}\, e^{-\left[i(\epsilon_\lambda-\omega)+\gamma\right]t'}\mathcal{E}_p(t+t'+t_t)\mathcal{E}^*_p(t'+t_t) \\ &\simeq -2\frac{|d_{cv}|^2}{\hbar^2}\frac{1}{\Gamma - i(\omega-\Omega)}\int_0^\infty dt\, e^{-\left[i(\epsilon_\lambda-\omega)\gamma\right]t}|\, \mathcal{E}_p(t+t_t)|^2 \\ &\simeq -i\, 2\frac{|d_{cv}|^2}{\hbar^2}\frac{1}{\omega-\Omega}\int_0^\infty dt\, e^{-\left[i(\epsilon_\lambda-\omega)+\gamma\right]t}|\, \mathcal{E}_p(t+t_t)|^2\ . \end{aligned} \tag{13.76}$$

Taking $\epsilon_\lambda = \omega_x$, with ω_x denoting the exciton resonance frequency, we can use Eq. (13.76) to discuss the excitonic optical Stark effect. In order to see the light-induced shift more clearly, we consider the large detuning case,

$$|\omega - \Omega| >> \gamma \, , \, |\omega - \epsilon_\lambda| \ .$$

Inserting Eq. (13.76) into Eq. (13.75), we obtain the asymptotic behavior as

$$\delta\chi_\lambda(\omega) \simeq 2\frac{d_{cv}}{\hbar}\frac{|d_{cv}|^2}{\hbar^2}\frac{1}{\omega - \Omega}\int_0^\infty dt \frac{e^{-[i(\epsilon_\lambda - \omega)+\gamma]t}}{\gamma - i(\omega - \epsilon_\lambda)} |\, \mathcal{E}_p(t + t_t)|^2 \qquad (13.77)$$

and for the pump-induced absorption change we get

$$\begin{aligned} \delta\alpha(\omega) &= -\mathrm{Im}\left[\frac{d_{cv}^*}{\hbar}\delta\chi_\lambda(\omega)\right] = \\ &\simeq \frac{|d_{cv}|^4}{\hbar^4}\frac{2}{\Omega - \epsilon_\lambda}\mathrm{Im}\left[\int_0^\infty dt \frac{e^{-\left[i(\epsilon_\lambda - \omega)+\gamma\right]t}}{\gamma - i(\omega - \epsilon_\lambda)} |\, \mathcal{E}_p(t + t_t)|^2\right] \ . \end{aligned} \qquad (13.78)$$

To analyze Eq. (13.78), let us assume for a moment that we excite the sample by a *cw*-beam, i.e., $\mathcal{E}_p(t) = \mathcal{E}_p = \text{const}$. Then we obtain from Eq. (13.78)

$$\delta\alpha(\omega) \propto -\frac{|\mathcal{E}_p|^2}{e - \Omega_p}\frac{2\gamma(\epsilon_\lambda - \omega)}{\left[(\epsilon_\lambda - \omega)^2 + \gamma^2\right]^2} \qquad (13.79)$$

which describes the absorption change caused by the shift of a Lorentzian resonance. This can be seen by looking at

$$\frac{\gamma}{\gamma^2 + (\epsilon_\lambda - \omega - \delta)^2} - \frac{\gamma}{\gamma^2 + (\epsilon_\lambda - \omega)^2} \simeq -\frac{2\delta\gamma(\epsilon_\lambda - \omega)}{\left[\gamma^2 + (\epsilon_\lambda - \omega)^2\right]^2} \ , \qquad (13.80)$$

where we assumed $\delta << |\epsilon_\lambda - \omega|$. Hence, Eq. (13.79) yields a dispersive shape around the resonance, $\omega = \epsilon_\lambda$, which describes decreasing and increasing absorption below and above the resonance, respectively.

For the case of pulsed excitation, the sample response is much more complex. Inserting the full Eq. (13.75) into the first line of Eq. (13.78), we obtain the results in Fig. 13.5 for different pump–probe delays. Fig. 13.5 shows, that for negative time delays, $t_t < 0$, i.e., when the probe pulse comes before the pump pulse maximum, the probe-transmission change

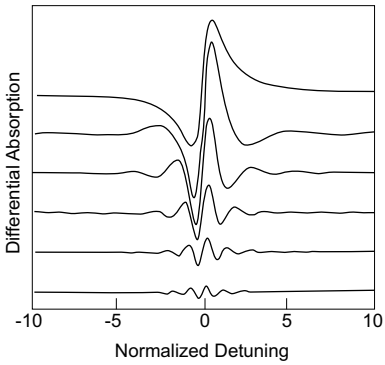

Fig. 13.5 Differential absorption spectra calculated in the spectral vicinity of the exciton resonance $\epsilon_\lambda = \omega_x$. The detuning is defined as $(\omega - \omega_x)/\sigma$, where σ^{-1} is the temporal width of the pump pulse. The FWHM of the pump pulse was assumed to be 120 fs, and the central pump frequency was detuned -10 below the resonance. The different curves are for different pump–probe delays t_t with 100 fs intervals, starting from the bottom at -500 fs (probe before pump) to the top curve which is for 0 fs (pump–probe overlap). [After Koch *et al.* (1988).]

shows oscillatory structures which evolve into the dispersive shape of the optical Stark effect.

Similar oscillations are obtained for the case of resonant interband excitation (Koch *et al.*, 1988). In this situation, the pump laser is tuned into the spectral regime of interband absorption, coupling an entire region of electron–hole transitions. The spectral extent of this region is given by the spectral width of the pump pulse. For negative pump–probe delays, the femtosecond experiments also show transient transmission oscillations. In contrast to the optical Stark effect, however, these oscillations then develop into a symmetric feature, called the *spectral hole*, which describes the saturation of the pump-laser coupled electron–hole transition.

The general origin of the transient transmission oscillations is found in the grating, Eq. (13.67), which scatters parts of the pump pulse into the direction of the probe pulse. For $t < t_t$, the scattered pump interferes with the probe and causes the oscillations. Alternatively, one can also view the transient oscillations as perturbed free induction decay. The probe pulse excites the polarization, which decays on the time scale of the coherence decay time. The pump pulse then modifies the medium and perturbs (shifts) the resonances, thus leading to the interference oscillations. For more de-

tails, see the review article by Koch *et al.* (1988) and the given references.

13.3 Correlation Effects

In this section, we go beyond the limit of extremely low intensities. This makes it necessary to include in the semiconductor Bloch equations not only the pure Hartree–Fock terms but also the leading contributions of the correlation terms. In order to have a systematic approach, we go back to the Coulomb part of the many-body Hamiltonian, Eq. (12.6), where we now add extra summations over different electron (e, e') and hole (h, h') states

$$\begin{aligned}\mathcal{H}_C = & \frac{1}{2} \sum_{\mathbf{k},\mathbf{k}',\mathbf{q}\neq 0,e,e'} V_q \alpha^\dagger_{e,\mathbf{k}+\mathbf{q}} \alpha^\dagger_{e',\mathbf{k}'-\mathbf{q}} \alpha_{e',\mathbf{k}'} \alpha_{e,\mathbf{k}} \\ & + \frac{1}{2} \sum_{\mathbf{k},\mathbf{k}',\mathbf{q}\neq 0,h,h'} V_q \beta^\dagger_{h,\mathbf{k}+\mathbf{q}} \beta^\dagger_{h',\mathbf{k}'-\mathbf{q}} \beta_{h',\mathbf{k}'} \beta_{h,\mathbf{k}} \\ & - \sum_{\mathbf{k},\mathbf{k}',\mathbf{q}\neq 0,e,h} V_q \alpha^\dagger_{e,\mathbf{k}+\mathbf{q}} \beta^\dagger_{h,\mathbf{k}'-\mathbf{q}} \beta_{h,\mathbf{k}'} \alpha_{e,\mathbf{k}} \ . \end{aligned} \tag{13.81}$$

Similarly, the interaction between the carriers and the classical electromagnetic field, $\mathcal{H}_I$, is generalized to

$$\mathcal{H}_I = -\mathbf{E}(t) \cdot \sum_{\mathbf{k},e,h} \left[\mathbf{d}^{eh} \alpha^\dagger_{e,\mathbf{k}} \beta^\dagger_{h,-\mathbf{k}} + (\mathbf{d}^{eh})^* \beta_{h,-\mathbf{k}} \alpha_{e,\mathbf{k}} \right] \ , \tag{13.82}$$

with the electron–hole interband dipole matrix element $\mathbf{d}^{eh}$. In our analysis, we explicitly include the heavy-hole valence band and the lowest conduction band, both of which are twofold spin-degenerate. The two heavy-hole bands $(h = 1, 2)$ are characterized by the states $|-3/2, h>$ and $|3/2, h>$, and the conduction bands $(e = 1, 2)$ by $|-1/2, e>$ and $|1/2, e>$, respectively. For light propagating in the z-direction, i.e., perpendicular to the plane of the quantum well, we use the usual circularly polarized dipole matrix elements

$$\begin{aligned} \mathbf{d}^{11} &= d_0 \, \boldsymbol{\sigma}^+ = \frac{d_0}{\sqrt{2}} \begin{pmatrix} 1 \\ i \end{pmatrix} \ , \\ \mathbf{d}^{12} &= \mathbf{d}^{21} = 0 \ , \\ \mathbf{d}^{22} &= d_0 \, \boldsymbol{\sigma}^- = \frac{d_0}{\sqrt{2}} \begin{pmatrix} 1 \\ -i \end{pmatrix} \ , \end{aligned} \tag{13.83}$$

where d_0 is the modulus of $\mathbf{d}^{11}$ and $\mathbf{d}^{22}$. Due to these selection rules, i.e., $\mathbf{d}^{eh} \propto \delta_{eh}$, we have two separate subspaces of optical excitations, that are optically isolated. They are, however, coupled by the many-body Coulomb-interaction, since it is independent of the band indices (spin).

As in Chap. 12, we evaluate the Heisenberg equation for the different operator combinations to obtain

$$\begin{aligned} i\hbar\frac{\partial}{\partial t}P^{eh}_{\mathbf{k}} \;=\; & -\left(E^{e}_{\mathbf{k}}+E^{h}_{\mathbf{k}}\right)P^{eh}_{\mathbf{k}}+\sum_{\mathbf{q}\neq 0}V_q P^{eh}_{\mathbf{k}-\mathbf{q}} \\ & +\left(\mathbf{d}^{eh}-\sum_{e'}f^{ee'}_{\mathbf{k}}\mathbf{d}^{e'h}-\sum_{h'}\mathbf{d}^{eh'}f^{h'h}_{\mathbf{k}}\right)\cdot\mathbf{E} \\ & -\sum_{\mathbf{q}\neq 0,\mathbf{k}',e'}V_q\Big(\left\langle\alpha^{\dagger}_{e,\mathbf{k}}\alpha^{\dagger}_{e',\mathbf{k}'}\beta^{\dagger}_{h,\mathbf{k}+\mathbf{q}}\alpha_{e',\mathbf{k}'-\mathbf{q}}\right\rangle \\ & \qquad -\left\langle\alpha^{\dagger}_{e,\mathbf{k}+\mathbf{q}}\alpha^{\dagger}_{e',\mathbf{k}'}\beta^{\dagger}_{h,\mathbf{k}}\alpha_{e',\mathbf{k}'+\mathbf{q}}\right\rangle\Big) \\ & +\sum_{\mathbf{q}\neq 0,\mathbf{k}',h'}V_q\Big(\left\langle\alpha^{\dagger}_{e,\mathbf{k}+\mathbf{q}}\beta^{\dagger}_{h',\mathbf{k}'+\mathbf{q}}\beta^{\dagger}_{h,\mathbf{k}}\beta_{h',\mathbf{k}'}\right\rangle \\ & \qquad -\left\langle\alpha^{\dagger}_{e,\mathbf{k}}\beta^{\dagger}_{h',\mathbf{k}'+\mathbf{q}}\beta^{\dagger}_{h,\mathbf{k}-\mathbf{q}}\beta_{h',\mathbf{k}'}\right\rangle\Big)\;. \end{aligned} \tag{13.84}$$

In the two-band case, i.e., if only a single conduction and a single valence band is considered, we have $e = e' = 1$ and $h = h' = 1$ in Eq. (13.84). In the more general multiband configuration, summations over all the respective bands have to be considered. Since we restrict the analysis in this section to transitions from heavy-holes to the lowest conduction band, $P^{eh}_{\mathbf{k}}$ is non-vanishing only for $e = h = 1$ and $e = h = 2$, i.e., concerning the subband indices it is proportional to δ_{eh}, since the terms with $e \neq h$ have no sources. For similar reasons, also $f^{ee'}_{\mathbf{k}}$ and $f^{h'h}_{\mathbf{k}}$ are diagonal, i.e., proportional to $\delta_{ee'}$ and $\delta_{hh'}$, respectively.

In order to deal with the four-operator correlations that appear in Eq. (13.84), we follow an approach where the nonlinear optical response is classified according to an expansion in powers of the applied field. Stahl and coworkers (1994) were the first who recognized that this traditional nonlinear optics expansion establishes a systematic truncation scheme of the Coulombic many-body correlations for purely coherent optical excitation configurations. In the following, we outline the basic steps that are involved in this procedure.

Studying the structure of the coupled equations for the correlation functions, one finds that the four-operator terms which appear in the equation

of motion for the microscopic polarization can be decomposed into

$$\left\langle \alpha^\dagger_{e,\mathbf{k}}\alpha^\dagger_{e',\mathbf{k}'}\beta^\dagger_{h'',\mathbf{k}''}\alpha_{e''',\mathbf{k}'''}\right\rangle = \sum_{\hat{\mathbf{k}},\hat{h}}\left\langle \alpha^\dagger_{e,\mathbf{k}}\alpha^\dagger_{e',\mathbf{k}'}\beta^\dagger_{h'',\mathbf{k}''}\beta^\dagger_{\hat{h},\hat{\mathbf{k}}}\right\rangle\left\langle \beta_{\hat{h},\hat{\mathbf{k}}}\alpha_{e''',\mathbf{k}'''}\right\rangle + \mathcal{O}(E^5)\ , \tag{13.85}$$

where $\left\langle \alpha^\dagger_{e,\mathbf{k}}\alpha^\dagger_{e',\mathbf{k}'}\beta^\dagger_{h'',\mathbf{k}''}\beta^\dagger_{\hat{h},\hat{\mathbf{k}}}\right\rangle$ can be considered as an unfactorized product of polarization operators that is of second order in the field, $\propto \mathcal{O}(E^2)$ since two electron–hole pairs are created, whereas $\left\langle \beta_{\hat{h},\hat{\mathbf{k}}}\alpha_{e''',\mathbf{k}'''}\right\rangle$ is linear in the field, $\propto \mathcal{O}(E)$ since a single electron–hole pair is destroyed. Hence, the right hand side of Eq. (13.85) is at least of third order in the field.

The correctness of this decoupling scheme can be verified quite easily, whereas one needs more general considerations to obtain the explicit expressions. In the most straightforward way, one first notes that Eq. (13.85) is valid when the semiconductor is in its ground state, since in this case both sides vanish. Then one can take the time derivative of the lowest (third) order contributions of Eq. (13.85) which are given by

$$\begin{aligned}\left\langle \frac{\partial}{\partial t}(\alpha^\dagger_{e,\mathbf{k}}\alpha^\dagger_{e',\mathbf{k}'}\beta^\dagger_{h'',\mathbf{k}''}\alpha_{e''',\mathbf{k}'''})\right\rangle = &\\ \sum_{\hat{\mathbf{k}},\hat{h}}\left\langle \frac{\partial}{\partial t}(\alpha^\dagger_{e,\mathbf{k}}\alpha^\dagger_{e',\mathbf{k}'}\beta^\dagger_{h'',\mathbf{k}''}\beta^\dagger_{\hat{h},\hat{\mathbf{k}}})\right\rangle\left\langle \beta_{\hat{h},\hat{\mathbf{k}}}\alpha_{e''',\mathbf{k}'''}\right\rangle &\\ + \sum_{\hat{\mathbf{k}},\hat{h}}\left\langle \alpha^\dagger_{e,\mathbf{k}}\alpha^\dagger_{e',\mathbf{k}'}\beta^\dagger_{h'',\mathbf{k}''}\beta^\dagger_{\hat{h},\hat{\mathbf{k}}}\right\rangle\left\langle \frac{\partial}{\partial t}(\beta_{\hat{h},\hat{\mathbf{k}}}\alpha_{e''',\mathbf{k}'''})\right\rangle\ .&\end{aligned} \tag{13.86}$$

Computing the time derivatives by evaluating the commutators with the Hamiltonian according to the Heisenberg equation, inserting the obtained equations of motion up to the required order in the field, and performing the summations, Eq. (13.86) and thus Eq. (13.85) are readily verified.

Another, even simpler example for such a decoupling in a fully coherent situation is the expression for the occupation probabilities in terms of the microscopic polarizations up to second order in the field

$$\begin{aligned} f^{ee'}_{\mathbf{k}} &= \sum_{h'}(P^{eh'}_{\mathbf{k}})^* P^{e'h'}_{\mathbf{k}} + \mathcal{O}(E^4)\ ,\\ f^{hh'}_{\mathbf{k}} &= \sum_{e'}(P^{e'h}_{\mathbf{k}})^* P^{e'h'}_{\mathbf{k}} + \mathcal{O}(E^4)\ . \end{aligned} \tag{13.87}$$

Analogous to what has been said above, also this conservation law, which is nothing but the expansion of Eq. (13.9), can be verified by computing

the time derivative and inserting the expressions up to the required order.

Instead of just merely verifying the decouplings in Eqs. (13.85) and (13.87), we address the coherent dynamics of a many-body system on the level of a general analysis. Let us start by defining a normally ordered operator product as

$$\{N, M\} \equiv c^\dagger(\varphi_N)\, c^\dagger(\varphi_{N-1}) \ldots c^\dagger(\varphi_1)\, c(\psi_1) \ldots c(\psi_{M-1})\, c(\psi_M) \ , \quad (13.88)$$

where depending on φ_i and ψ_j the operators $c^\dagger$ and c are electron or hole creation or annihilation operators for certain $\mathbf{k}_i$ and $\mathbf{k}_j$, respectively. The quantities $\{N, M\}$ contain the full information about the dynamics of the photoexcited system. E.g., the microscopic polarization $P^{eh}_{\mathbf{k}}$ corresponds to $\{0, 2\}$, its complex conjugate $(P^{eh}_{\mathbf{k}})^*$ corresponds to $\{2, 0\}$, and the occupation probabilities $f^{aa}_{\mathbf{k}}$ to $\{1, 1\}$.
Next, we consider the time derivative of the normally ordered operator products, which is given by

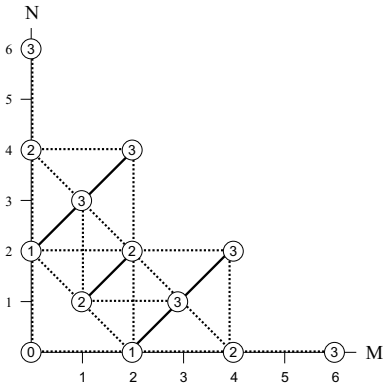

Fig. 13.6 Sketch of the coupling between dynamical variables, ($\{N, M\}$). The numbers in the circles denote the minimum order of the corresponding expectation value $< \{N, M\} >$ in the external field amplitude. The dotted (solid) lines symbolize the optical (Coulomb) coupling. [After Lindberg *et al.* (1994).]

$$\frac{\partial}{\partial t}\{N+1,M+1\} = \left(\frac{\partial c^\dagger(\varphi_{N+1})}{\partial t}\right)\{N,M\}\,c(\psi_{M+1}) + c^\dagger(\varphi_{N+1})\left(\frac{\partial\{N,M\}}{\partial t}\right)c(\psi_{M+1}) + c^\dagger(\varphi_{N+1})\,\{N,M\}\left(\frac{\partial c(\psi_{M+1})}{\partial t}\right) \quad . \tag{13.89}$$

To analyze to which correlations functions $\{N,M\}$ are coupled, one can evaluate the equations of motion for the operators, i.e., $\frac{\partial c^\dagger(\varphi_i)}{\partial t}$ and $\frac{\partial c(\varphi_j)}{\partial t}$. Using Heisenberg's equation, one finds that $\{1,0\}$ ($\{0,1\}$) is coupled to itself by the single-particle (band structure) part, coupled to $\{0,1\}$ ($\{1,0\}$) by the light-matter interaction, and coupled to $\{2,1\}$ ($\{1,2\}$) by the many-body Coulomb interaction.

Inserting these results into Eq. (13.89) and restoring normal ordering, i.e., commuting all creation operators to the left of the destruction operators, one can see that the light-matter interaction couples $\{N,M\}$ to $\{N-1,M+1\}$, $\{N+1,M-1\}$, $\{N-2,M\}$, and $\{N,M-2\}$, since it is given by pairs of creation and destruction operators. The many-body Coulomb interaction, however, couples $\{N,M\}$ to $\{N,M\}$ and $\{N+1,M+1\}$. Therefore, the four-operator part of the Hamiltonian generates the coupling to products that contain more operators, i.e., the many-body hierarchy. Clearly, for both parts of the Hamiltonian, operators with $N-M$ being odd are only coupled to other operators where $N-M$ is odd, and operators with $N-M$ being even are only coupled to other operators where $N-M$ is even. Thus, if we start from the ground state as the initial condition, i.e., $\langle\{0,0\}\rangle = 1$ and all other expectation values are zero, the operators $\{N,M\}$ with $N-M$ being odd vanish at all times, since they contain no sources. These considerations are visualized in Fig. 13.6. This, furthermore, clearly shows that in any finite order in the external field, only a finite number of expectation values contribute to the optical response. To find the lowest order in the light field of any term $\{N,M\}$, one only needs to evaluate the minimum number of dotted lines in Fig. 13.6, which are needed to connect it to $\{0,0\}$.

As can be seen from Fig. 13.6 and can be proven rigorously, see Lindberg *et al.* (1994), the minimum order in the field in which $\langle\{N,M\}\rangle$ is finite is $(N+M)/2$ if N and M are both even and $(N+M)/2+1$ if N and M are both odd, i.e.,

$$\langle\, c^\dagger(\varphi_{2N})\,\ldots\,c^\dagger(\varphi_1)\,c(\psi_1)\,\ldots\,c(\psi_{2M})\,\rangle = O(E^{N+M}) \quad , \tag{13.90}$$

and

$$\langle\, c^\dagger(\varphi_{2N+1}) \,\ldots\, c^\dagger(\varphi_1)\, c(\psi_1) \,\ldots\, c(\psi_{2M+1}) \,\rangle \;=\; O(E^{N+M+2}) \;. \tag{13.91}$$

If one starts initially from the ground state of the semiconductor and the dynamics is fully coherent, one can factorize expectation values containing a mix of creation and destruction operators to lowest order into products of expectation values which contain either only creation or only destruction operators. For our case, we can write

$$\begin{aligned}&\langle\, c^\dagger(\varphi_{2N}) \ldots c^\dagger(\varphi_1)\, c(\psi_1) \ldots c(\psi_{2M}) \,\rangle = \\ &\quad \langle\, c^\dagger(\varphi_{2N}) \ldots c^\dagger(\varphi_1) \,\rangle\, \langle\, c(\psi_1) \ldots c(\psi_{2M}) \,\rangle \;+\; O(E^{N+M+2}) \;,\end{aligned} \tag{13.92}$$

and

$$\begin{aligned}&\langle\, c^\dagger(\varphi_{2N+1}) \ldots c^\dagger(\varphi_1)\, c(\psi_1) \ldots c(\psi_{2M+1}) \,\rangle = \\ &\quad \langle\, c^\dagger(\varphi_{2N+1}) \ldots c^\dagger(\varphi_1) \,\rangle\, \langle\, c(\psi_1) \ldots c(\psi_{2M+1}) \,\rangle \;+\; O(E^{N+M+4}) \;.\end{aligned} \tag{13.93}$$

To prove Eqs. (13.92) and (13.93), it is important to note that in the Heisenberg picture, where the operators are time-dependent, all expectation values are taken with respect to the initial state, which is the ground state $|\,0\,\rangle$ of the semiconductor, i.e.,

$$\begin{aligned}&\langle\, c^\dagger(\varphi_N)\, c^\dagger(\varphi_{N-1}) \ldots c^\dagger(\varphi_1)\, c(\psi_1) \ldots c(\psi_M) \,\rangle \;= \\ &\quad \langle\, 0 \,|\, c_H^\dagger(\varphi_N, t) \ldots c_H^\dagger(\varphi_1, t)\, c_H(\psi_1, t) \ldots c_H(\psi_M, t) \,|\, 0 \,\rangle \;.\end{aligned} \tag{13.94}$$

Now, one can define an interaction picture by decomposing the Hamiltonian into $\mathcal{H} = \mathcal{H}_0 + \mathcal{H}_I$, where H_0 contains the free-particle and the Coulomb interaction parts. As is well known, in the interaction picture an operator O becomes time-dependent according to

$$O_I(t) \;=\; e^{i\mathcal{H}_0 t}\; O\; e^{-i\mathcal{H}_0 t} \;. \tag{13.95}$$

Inserting the interaction representation of the identity operator in between the creation and destruction operators of a ground state expectation value of Heisenberg operators, i.e., in between $c_H^\dagger(\varphi_1, t)$ and $c_H(\psi_1, t)$ of

Eq. (13.94), one finds by iterating the exponentials $e^{\pm iH_0 t}$ of Eq. (13.95)

$$\begin{aligned}
\langle\, 0 \,|\, c_H^\dagger(\varphi_N,t) \ldots c_H^\dagger(\varphi_1,t)\, c_H(\psi_1,t) \ldots c_H(\psi_M,t) \,|\, 0 \,\rangle = \\
&\langle\, 0 \,|\, c_H^\dagger(\varphi_N,t) \ldots c_H^\dagger(\varphi_1,t) \,|\, 0 \,\rangle \, \langle\, 0 \,|\, c_H(\psi_1,t) \ldots c_H(\psi_M,t) \,|\, 0 \,\rangle \\
&+ \sum_{\delta_1} \langle\, 0 \,|\, c_H^\dagger(\varphi_N,t) \ldots c_H^\dagger(\varphi_1,t)\, c_I^\dagger(\delta_1,t) \,|\, 0 \,\rangle \\
&\qquad\qquad \times \langle\, 0 \,|\, c_I(\delta_1,t)\, c_H(\psi_1,t) \ldots c_H(\psi_M,t) \,|\, 0 \,\rangle \\
&+ \frac{1}{2} \sum_{\delta_1,\delta_2} \langle\, 0 \,|\, c_H^\dagger(\varphi_N,t) \ldots c_H^\dagger(\varphi_1,t)\, c_I^\dagger(\delta_2,t)\, c_I^\dagger(\delta_1,t) \,|\, 0 \,\rangle \\
&\qquad\qquad \times \langle\, 0 \,|\, c_I(\delta_1,t)\, c_I(\delta_2,t)\, c_H(\psi_1,t) \ldots c_H(\psi_M,t) \,|\, 0 \,\rangle \\
&+ \cdots \,. \qquad (13.96)
\end{aligned}$$

This general result can be used to expand all correlation functions into their contributions up to any defined order in the field.

We now apply this scheme to obtain the equations of motion which describe the optical semiconductor response in the coherent $\chi^{(3)}$-limit. In order to be able to distinguish between the uncorrelated Hartree-Fock part and the correlation contributions, it is convenient to define a pure four-particle correlation function via

$$\begin{aligned}
\bar{B}^{eh'e'h}_{\mathbf{k},\mathbf{k}',\mathbf{k}'',\mathbf{k}'''} &= \left\langle \alpha^\dagger_{e,\mathbf{k}} \beta^\dagger_{h',\mathbf{k}'} \alpha^\dagger_{e',\mathbf{k}''} \beta^\dagger_{h,\mathbf{k}'''} \right\rangle \\
&\quad - \left\langle \alpha^\dagger_{e,\mathbf{k}} \beta^\dagger_{h',\mathbf{k}'} \right\rangle \left\langle \alpha^\dagger_{e',\mathbf{k}''} \beta^\dagger_{e,\mathbf{k}'''} \right\rangle - \left\langle \alpha^\dagger_{e,\mathbf{k}} \beta^\dagger_{h,\mathbf{k}'''} \right\rangle \left\langle \alpha^\dagger_{e',\mathbf{k}''} \beta^\dagger_{h',\mathbf{k}'} \right\rangle \\
&= B^{eh'e'h}_{\mathbf{k},\mathbf{k}',\mathbf{k}'',\mathbf{k}'''} \\
&\quad - \left\langle \alpha^\dagger_{e,\mathbf{k}} \beta^\dagger_{h',\mathbf{k}'} \right\rangle \left\langle \alpha^\dagger_{e',\mathbf{k}''} \beta^\dagger_{e,\mathbf{k}'''} \right\rangle - \left\langle \alpha^\dagger_{e,\mathbf{k}} \beta^\dagger_{h,\mathbf{k}'''} \right\rangle \left\langle \alpha^\dagger_{e',\mathbf{k}''} \beta^\dagger_{h',\mathbf{k}'} \right\rangle . \qquad (13.97)
\end{aligned}$$

Using the above introduced expansions up to third order in the field, the polarization equation can be written as

$$\frac{\partial}{\partial t} P^{eh}_{\mathbf{k}} = \frac{\partial}{\partial t} P^{eh}_{\mathbf{k}} |_{hom} + \sum_{n=1}^{3} \frac{\partial}{\partial t} P^{eh}_{\mathbf{k}} |_{inhom,n} \;, \qquad (13.98)$$

with

$$i\hbar\frac{\partial}{\partial t}P_{\mathbf{k}}^{eh}|_{hom} = -\left(E_{\mathbf{k}}^{e}+E_{\mathbf{k}}^{h}\right)P_{\mathbf{k}}^{eh}+\sum_{\mathbf{q}}V_{q}P_{\mathbf{k}-\mathbf{q}}^{eh}\,, \tag{13.99}$$

$$\begin{aligned} i\hbar\frac{\partial}{\partial t}P_{\mathbf{k}}^{eh}|_{inhom,1} = &\left[\mathbf{d}^{eh}-\sum_{e',h'}(P_{\mathbf{k}}^{eh'})^{*}P_{\mathbf{k}}^{e'h'}\mathbf{d}^{e'h}\right.\\ &\left.-\sum_{h',e'}\mathbf{d}^{eh'}\sum_{e'}(P_{\mathbf{k}}^{e'h'})^{*}P_{\mathbf{k}}^{e'h}\right]\cdot\mathbf{E}\ , \end{aligned} \tag{13.100}$$

$$\begin{aligned} i\hbar\frac{\partial}{\partial t}P_{\mathbf{k}}^{eh}|_{inhom,2} = &-\sum_{\mathbf{q},e',h'}V_{q}\Big[P_{\mathbf{k}}^{eh'}\Big(P_{\mathbf{k}}^{e'h'}\Big)^{*}P_{\mathbf{k}-\mathbf{q}}^{e'h}-P_{\mathbf{k}+\mathbf{q}}^{eh'}\Big(P_{\mathbf{k}+\mathbf{q}}^{e'h'}\Big)^{*}P_{\mathbf{k}}^{e'h}\\ &+P_{\mathbf{k}+\mathbf{q}}^{eh'}\Big(P_{\mathbf{k}}^{e'h'}\Big)^{*}P_{\mathbf{k}}^{e'h}-P_{\mathbf{k}}^{eh'}\Big(P_{\mathbf{k}-\mathbf{q}}^{e'h'}\Big)^{*}P_{\mathbf{k}-\mathbf{q}}^{e'h}\Big]\ , \end{aligned} \tag{13.101}$$

$$\begin{aligned} i\hbar\frac{\partial}{\partial t}P_{\mathbf{k}}^{eh}|_{inhom,3} = &\sum_{\mathbf{q},\mathbf{k}',e',h'}V_{q}\Big(P_{\mathbf{k}'}^{e'h'}\Big)^{*}\Big(\bar{B}_{\mathbf{k},\mathbf{k}',\mathbf{k}'-\mathbf{q},\mathbf{k}-\mathbf{q}}^{eh'e'h}-\bar{B}_{\mathbf{k}+\mathbf{q},\mathbf{k}',\mathbf{k}'-\mathbf{q},\mathbf{k}}^{eh'e'h}\\ &+\bar{B}_{\mathbf{k}+\mathbf{q},\mathbf{k}'+\mathbf{q},\mathbf{k}',\mathbf{k}}^{eh'e'h}-\bar{B}_{\mathbf{k},\mathbf{k}'+\mathbf{q},\mathbf{k}',\mathbf{k}-\mathbf{q}}^{eh'e'h}\Big)\ . \end{aligned} \tag{13.102}$$

The homogeneous part of Eq. (13.98) contains the kinetic energies of electrons and holes plus their Coulomb attraction. This term is diagonal in the basis of exciton eigenstates. The contributions denoted with the subscript *inhom* in Eq. (13.98) are the different inhomogeneous *driving* terms, i.e., they are the sources for the microscopic polarizations. The direct coupling of the carrier system to the electromagnetic field is represented by the terms proportional to $\mathbf{d}\cdot\mathbf{E}$, see Eq. (13.100). These terms include the linear optical coupling ($\mathbf{d}\cdot\mathbf{E}$) and the phase-space filling contributions ($\mathbf{d}\cdot\mathbf{E}\ P^{*}P$).

As a consequence of the many-body Coulomb interaction, Eq. (13.98) contains further optical nonlinearities. The contributions that are of first-order in the Coulomb interaction, which are proportional to $VPP^{*}P$, are given by Eq. (13.101). Those, together with the phase-space filling terms, correspond to the Hartree–Fock limit of Eq. (13.98). The *correlation contributions* to the polarization equation, see Eq. (13.102), consist of four terms of the structure $VP^{*}\bar{B}$, where $\bar{B}$ is the genuine four-particle correlation function defined in Eq. (13.97). Hence, as a consequence of the many-body Coulomb interaction, the two-particle electron–hole amplitude P is coupled to higher-order correlation functions $\bar{B}$.

If the calculation of the coherent nonlinear optical response is limited to

a finite order in the applied field, the many-particle hierarchy is truncated automatically and one is left with a finite number of correlation functions. This truncation occurs since one considers here purely optical excitation where only the optical field exists as linear source which in first-order induces a linear polarization, in second order leads to carrier occupations, and so on. In the more general situation, where incoherent populations may be present, as, e.g., by pumping via carrier injection or in the presence of relaxed occupations, a classification of the nonlinear optical response in terms of powers of a field is no longer meaningful. For such cases, one can use a cluster expansion or nonequilibrium Green's functions to obtain systematic approximation schemes to the many-body hierarchy.

Equation (13.98) has been derived within the coherent $\chi^{(3)}$-limit, i.e., by keeping all contributions up to third-order in the electromagnetic field. If this condition is fulfilled, the nonlinear optical response is fully determined by the dynamics of single and two electron–hole–pair excitations, P and $\bar{B}$, respectively. The equation for $\bar{B}$'s is obtained as

$$\frac{\partial}{\partial t}\bar{B}^{eh'e'h}_{\mathbf{k},\mathbf{k}',\mathbf{k}'',\mathbf{k}'''} = \frac{\partial}{\partial t}\bar{B}^{eh'e'h}_{\mathbf{k},\mathbf{k}',\mathbf{k}'',\mathbf{k}'''}|_{hom} + \frac{\partial}{\partial t}\bar{B}^{eh'e'h}_{\mathbf{k},\mathbf{k}',\mathbf{k}'',\mathbf{k}'''}|_{inhom} \ , \quad (13.103)$$

with

$$\begin{aligned} i\hbar\frac{\partial}{\partial t}\bar{B}^{eh'e'h}_{\mathbf{k},\mathbf{k}',\mathbf{k}'',\mathbf{k}'''}|_{hom} &= -\left(E^{e}_{\mathbf{k}} + E^{h'}_{\mathbf{k}'} + E^{e'}_{\mathbf{k}''} + E^{h}_{\mathbf{k}'''}\right)\bar{B}^{eh'e'h}_{\mathbf{k},\mathbf{k}',\mathbf{k}'',\mathbf{k}'''} \\ &+ \sum_{\mathbf{q}'} V_{q'}\Big(\bar{B}^{eh'e'h}_{\mathbf{k}+\mathbf{q}',\mathbf{k}'+\mathbf{q}',\mathbf{k}'',\mathbf{k}'''} - \bar{B}^{eh'e'h}_{\mathbf{k}+\mathbf{q}',\mathbf{k}',\mathbf{k}''-\mathbf{q}',\mathbf{k}'''} \\ &+ \bar{B}^{eh'e'h}_{\mathbf{k}+\mathbf{q}',\mathbf{k}',\mathbf{k}'',\mathbf{k}'''+\mathbf{q}'} + \bar{B}^{eh'e'h}_{\mathbf{k},\mathbf{k}'+\mathbf{q}',\mathbf{k}''+\mathbf{q}',\mathbf{k}'''} \\ &- \bar{B}^{eh'e'h}_{\mathbf{k},\mathbf{k}'+\mathbf{q}',\mathbf{k}'',\mathbf{k}'''-\mathbf{q}'} + \bar{B}^{eh'e'h}_{\mathbf{k},\mathbf{k}',\mathbf{k}''+\mathbf{q}',\mathbf{k}'''+\mathbf{q}'}\Big) \ , \quad (13.104) \\ i\hbar\frac{\partial}{\partial t}\bar{B}^{eh'e'h}_{\mathbf{k},\mathbf{k}',\mathbf{k}'',\mathbf{k}'''}|_{inhom} &= -V_{|\mathbf{k}-\mathbf{k}'''|}\left(P^{eh}_{\mathbf{k}'''} - P^{eh}_{\mathbf{k}}\right)\left(P^{e'h'}_{\mathbf{k}'} - P^{e'h'}_{\mathbf{k}''}\right) \\ &+ V_{|\mathbf{k}-\mathbf{k}'|}\left(P^{eh'}_{\mathbf{k}'} - P^{eh'}_{\mathbf{k}}\right)\left(P^{e'h}_{\mathbf{k}'''} - P^{e'h}_{\mathbf{k}''}\right) \ . \quad (13.105) \end{aligned}$$

The homogeneous part of the equation for $\bar{B}$ contains the kinetic energies as well as the attractive and repulsive interactions between two electrons and two holes, i.e., the *biexciton problem*. The sources of Eq. (13.103) consist of the Coulomb interaction potential times nonlinear polarization terms, VPP.

Since the equations of motion in the coherent $\chi^{(3)}$-limit are quite lengthy, in order to see the structure of the many-body couplings, it is

useful to reduce the notation and to consider a schematical set of equations of motion. These can be obtained from Eqs. (13.98) and (13.103) by neglecting all indices and superscripts,

$$i\hbar \frac{\partial}{\partial t} P = -E_P P + (d - b P^* P) E - V_{HF} P^* P P + V_{corr} P^* \bar{B} \tag{13.106}$$

and

$$i\hbar \frac{\partial}{\partial t} \bar{B} = -E_B \bar{B} - \bar{V}_{corr} P P \ . \tag{13.107}$$

Here, E_P and E_B are the energies of single- and biexciton states, and b denotes the Pauli blocking, V_{HF} the first-order (Hartree–Fock) Coulomb terms, and V_{corr} as well as $\bar{V}_{corr}$ Coulomb correlation contributions.

Formal integration of Eq. (13.107) yields

$$\bar{B}(t) = \frac{i}{\hbar} V \int_{-\infty}^{t} dt' e^{iE(t-t')/\hbar} P(t') P(t') \ . \tag{13.108}$$

Inserting this expression for $\bar{B}(t)$ into Eq. (13.106) shows that $P(t)$ depends on contributions $P(t')$ with $t' < t$, i.e., on terms with earlier time arguments. Such Coulombic memory effects would be neglected if one solved the coupled equations adiabatically within the Markov approximation.

As an application, we use the coherent $\chi^{(3)}$-equations to compute differential absorption spectra for different circular polarizations of the pump and probe pulses assuming excitation of the semiconductor energetically below the exciton resonance. Numerical results for the polarization-dependent excitonic optical Stark effect, are displayed in Fig. 13.7. In the upper right panel in Fig. 13.7, we see the computed differential absorption spectrum for co-circularly polarized pulses. This spectrum corresponds to the usual blueshift of the exciton resonance discussed in the previous sections of this chapter. The detailed analysis reveals that the phase-space filling nonlinearity and the first-order Coulomb terms, i.e., the Hartree–Fock contributions induce a blueshift, whereas the correlations alone would yield a redshift. However, for the $\sigma^+\sigma^+$ configuration the magnitude of the correlation-induced contribution is relatively small and in turn, the total signal is dominated by the blueshift of the Hartree–Fock terms.

The situation is, however, very different if opposite circularly polarized ($\sigma^+\sigma^-$) pump and probe pulses are considered, see the lower right panel in Fig. 13.7. For this configuration, the Hartree–Fock contributions for heavy-hole transitions vanish and the response is completely determined by

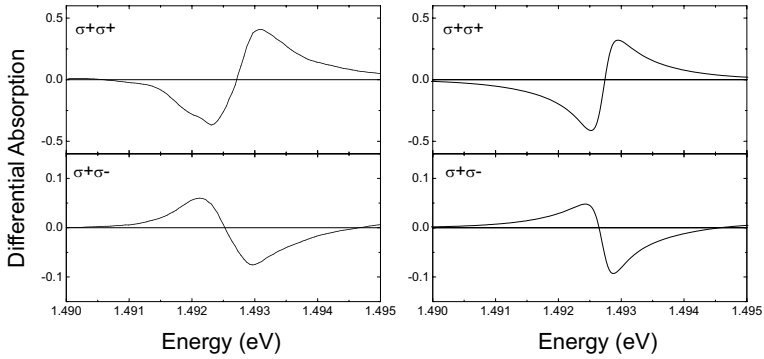

Fig. 13.7 Experimental (left column) and computed (right column) differential absorption spectra for a InGaAs/GaAs quantum-well sample. The pump pulses were detuned to 4.5 meV below the exciton resonance and the shown spectra were obtained at zero time delay. The usual blueshift is obtained for equal polarization (top row) and a redshift is obtained for opposite circular polarizations of the pump and probe pulses. [After Sieh *et al.* (1999).]

correlations. These correlations yield a redshift which is not compensated by other terms and thus survives. As Sieh *et al.* (1999) have shown, the occurrence of this redshift is not directly related to the existence of a bound biexciton that can be excited with $\sigma^+\sigma^-$ polarized pulses. This can be seen already from the analysis of the $\sigma^+\sigma^+$ excitation configuration, where no bound biexciton can be excited but still the correlation term alone amounts to a redshift of the exciton resonance.

Experimental measurements of the excitonic optical Stark effect for different pump–probe polarization configurations are displayed in the left column of Fig. 13.7. These measurements nicely confirm the predictions of the third-order theory.

REFERENCES

The first reports on the observation of the nonresonant optical Stark effect are:

A. Mysyrowicz, D. Hulin, A. Antonetti, A. Migus, W.T. Masselink, and H. Morkoc, Phys. Rev. Lett. **55**, 1335 (1985)

A. von Lehmen, J.E. Zucker, J.P. Heritage, and D.S. Chemla, Optics Lett. **11**, 609 (1986)

The Stark effect theory presented in this chapter has been developed in:

S. Schmitt-Rink, D.S. Chemla and H. Haug, Phys. Rev. **B37**, 941 (1988)
S.W. Koch, N. Peyghambarian, and M. Lindberg, J. Phys. **C21**, 5229 (1988)
C. Ell, J.F. Müller, K. El Sayed, and H. Haug, Phys. Rev. Lett. **62**, 306 (1989)

The polarization dependence and memory effects in the excitonic optical Stark effect have been presented in:

C. Sieh, T. Meier, A. Knorr, S.W. Koch, P. Brick, M. Hübner, C. Ell, J. Prineas, G. Khitrova, and H.M. Gibbs, Phys. Rev. Lett. **82**, 3112 (1999)

The systematic truncation of the equation hierarchy under coherent excitation conditions has been derived in:

V.M. Axt and A. Stahl, Z. Phys. **B 93**, 195 and 205 (1994)
M. Lindberg, Y.Z. Hu, R. Binder, and S. W. Koch, Phys. Rev. **B 50**, 18060 (1994)

see also:

W. Schäfer and M. Wegener, *Semiconductor Optics and Transport Phenomena*, Springer Verlag, Berlin (2002)

The expansion of optical nonlinearities in terms of nonlinear susceptibilities is summarized in:

N. Bloembergen, Nonlinear Optics, Benjamin Inc., New York (1965)

PROBLEMS

Problem 13.1: Show for a two-level system that $(1-2n)^2 + 4|P|^2$ is a conserved quantity.

Problem 13.2: Use Eqs. (13.2) – (13.5) to derive the optical Stark shift

results of Sec. 2-3 for the two-level atom.

Problem 13.3: Show that $\delta p_k^+ >> \delta p_k^-$ and derive the linearized Eq. (13.19).

Problem 13.4: Calculate the enhancement factors (13.40) using the exciton wave functions in $2D$ and $3D$.

Problem 13.5: Use the Heisenberg equation for the four-operator terms to derive Eq. (13.103) in the coherent $\chi^{(3)}$ limit.

This page intentionally left blank

Chapter 14

Wave-Mixing Spectroscopy

In extension of the optical Stark effect pump–probe experiments discussed in the previous chapter, we now want to present a more general analysis of two-pulse wave-mixing experiments. The model configuration is shown schematically in Fig. 14.1.

In general, one cannot consider all systems as spatially homogeneous because the light fields will be absorbed most strongly at the crystal surface where the beams enter and the two beams will in general propagate in different directions. The induced polarization will act in a spatially inhomogeneous way as a source term for Maxwell's equations describing the fields. Thus in general one has to determine a two-point density matrix of

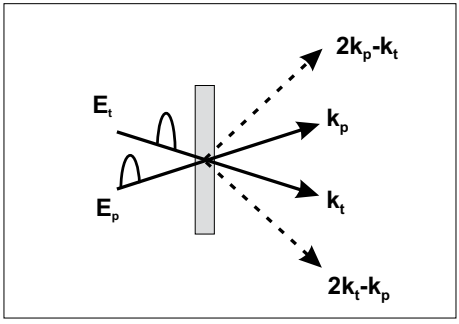

Fig. 14.1 Schematics of two-pulse experiments: Two successive pulses called pump and probe pulse with a delay time τ propagate in the directions $\mathbf{k_p}$ and $\mathbf{k_t}$ through the sample. The DTS is measured in the direction $\mathbf{k_t}$ of the test pulse, the FWM is measured in the direction $2\mathbf{k}_p - \mathbf{k}_t$ of the beam diffracted from the lattice induced by the two pulses.

the form

$$\rho_{ij}(\mathbf{r}_p, \mathbf{r}_t, t) = \langle \psi_j^\dagger(\mathbf{r}_t, t)\psi_i(\mathbf{r}_p, t)\rangle \ . \tag{14.1}$$

Introducing center-of-mass and relative coordinates $\mathbf{R} = (m_i\mathbf{r}_p + m_j\mathbf{r}_t)/(m_i + m_j)$ and $\mathbf{r} = \mathbf{r}_p - \mathbf{r}_t$ and a Fourier transformation with respect to the relative coordinate $\mathbf{r}$, one gets the Wigner distribution

$$\rho_{ij}(\mathbf{R}, \mathbf{k}, t) = \frac{1}{V}\int d^3 r e^{i\mathbf{k}\cdot\mathbf{r}}\rho_{ij}(\mathbf{R}, \mathbf{r}, t) \ . \tag{14.2}$$

With these distributions one can calculate the optically induced polarization,

$$P(\mathbf{R}, t) = \sum_{\mathbf{k}} d_{vc}\rho_{cv}(\mathbf{R}, \mathbf{k}, t) + c.c. \ . \tag{14.3}$$

This polarization enters into Maxwell's equations describing the dynamics of the light field as it propagates through the sample. Obviously, the determination of the Wigner functions and the resulting electromagnetic fields is considerably more involved in comparison with calculations of the density matrices in spatially homogeneous situations. As an alternative to the Wigner functions, one can also use density matrices which depend on two momenta

$$\rho_{ij}(\mathbf{k}_p, \mathbf{k}_t, t) = \langle a^\dagger_{j,\mathbf{k}_t}(t)a_{i,\mathbf{k}_t}(t)\rangle \ , \tag{14.4}$$

from which the information about the spatial variation can be obtained. In a single band, e.g., the distribution function at the spatial coordinate $\mathbf{R}$ is

$$n(\mathbf{R}, \mathbf{k}, t) = \sum_{\mathbf{K}} \rho(\frac{1}{2}\mathbf{K} + \mathbf{k}, -\frac{1}{2}\mathbf{K} + \mathbf{k}, t)e^{i\mathbf{R}\cdot\mathbf{K}} \ . \tag{14.5}$$

The advantage is that it is often much easier to formulate the equations of motion in momentum space than in real space. So far, these off-diagonal density matrices in K-space have been used successfully mainly for quantum wires, where the complications due to the angles between the two momenta do not exist. In thin samples however, where propagation effects and spatial inhomogeneities are of minor importance, one can calculate the resulting electromagnetic field which propagates in a certain direction by adiabatic approximations from the calculations for spatially homogeneous fields.

14.1 Thin Samples

In order to understand why the transmitted light in thin samples is proportional to the polarization field, we consider Maxwell's wave equation

$$\frac{\partial^2 \mathcal{E}}{\partial t^2} - \frac{c^2}{n_0^2}\Delta\mathcal{E} = -4\pi\frac{\partial^2 P}{\partial t^2} \simeq 4\pi\omega^2 P \ , \tag{14.6}$$

where n_0 is the refractive index of the unexcited crystal. The polarization formally constitutes an inhomogeneity. The field $\mathcal{E}$ can be calculated by a solution of the homogeneous equation plus an integral over the Green's function of the homogeneous field equation folded with the inhomogeneous polarization term. As for the calculations of the retarded Liénhard-Wiechert potentials in electrodynamics, this term reduces to the retarded polarization integral, in which the actual time is replaced by the retarded time $t - Rn/c$, where R is the distance between the coordinate of the polarization and that of the resulting field. In thin samples, these retardation effects are very small, the integral reduces to a weighted spatial average of the polarization term over the sample. In other words, the field caused by the polarization in the medium is proportional to the spatially homogeneous polarization.

For optically thin samples, we generalize the considered two-pulse laser light field which excites the sample by introducing the two propagation directions by means of two wave vectors $\mathbf{k}_p$ and $\mathbf{k}_t$. A spatial variation of the amplitudes is not considered. This way, we can write

$$\begin{aligned}\mathcal{E}(t) &= \mathcal{E}_p(t)e^{-i\left(\omega_p t - \mathbf{k}_p\cdot\mathbf{r}\right)} + \mathcal{E}_t(t-\tau)e^{-i\left[\omega_t(t-\tau) - \mathbf{k}_t\cdot\mathbf{r}\right]} \\ &= e^{i\mathbf{k}_p\cdot\mathbf{r}}\left[\mathcal{E}_p(t)e^{-i\omega_p t} + \mathcal{E}_t(t-\tau)e^{-i\omega_t(t-\tau)}e^{i\phi}\right] \ ,\end{aligned} \tag{14.7}$$

where we introduced the phase $\phi = (\mathbf{k}_t - \mathbf{k}_p)\cdot\mathbf{r}$. With such an excitation field the calculated induced polarization will also depend on the phase

$$P(t,\tau,\phi) = \sum_{\mathbf{k}} d_{vc}\rho_{cv,k}(\phi) + c.c. \propto E_{transm} \ . \tag{14.8}$$

The polarizations induced by the two delayed parts of the field (14.7) form a transient lattice with the lattice vector $\mathbf{k}_p - \mathbf{k}_t$. The field will be diffracted from this lattice into multiple orders determined by the factor $e^{i\mathbf{k}_p\cdot\mathbf{r}}e^{in\phi}$. For $n = 1$, one gets the propagation vector $\mathbf{k}_t$, that is in the direction of the delayed test pulse (see Fig. 14.1). This is the pump–probe situation analyzed for the excitonic optical Stark effect in Chap. 13. For $n = 2$, one

gets the propagation vector $2\mathbf{k}_t - \mathbf{k}_p$, etc. This is the direction of the first diffracted order in a degenerate *four-wave mixing* configuration.

The name *four-wave mixing* originates from the fact, that one generally has to consider a total of four different $\mathcal{E}$-fields, three incident and a scattered field. Here, we discuss only the so-called degenerate case where two fields are combined into the pump beam. Hence, the pump counts twice, whereas probe and transmitted fields count only once.

We numerically evaluate the resulting polarization for various values of the phase. In actual calculations, the polarization has to be obtained for only a few phase values. Because of the periodicity in ϕ, we extract from this knowledge the n-th order Fourier transform of the polarization

$$P_n(t,\tau) = \int_0^{2\pi} \frac{d\phi}{2\pi} P(t,\tau,\phi) e^{in\phi} \quad . \tag{14.9}$$

This evaluation of the polarization in various directions without treating the spatial inhomogeneity explicitly is called an adiabatic approximation. Alternatively, one can expand the density matrix $\rho = \sum_n \rho_n e^{i\phi n}$ and calculate the equations of motion for the various components successively.

To discuss pump-probe experiments, we have to calculate $P_1(t,\tau)$. The spectrum of the transmitted light is given by $|P_1(\omega,\tau)|^2$. Because the transmitted field in the test pulse direction $\mathbf{k}_t$ is not background-free, one often measures a differential signal by subtracting the spectrum $|P_t^0(\omega)|^2$ for the test field alone.

In Chap. 13, we already discussed the example of the excitonic optical Stark effect. Here, we now show a case where the modifications of the interband continuum are studied. Specifically, we discuss the results of a low-intensity experiment according to Leitenstorfer et pal. on GaAs with a two color titanium sapphire laser. The pump pulse was tuned to 150 meV above the band edge and had a duration of 120 fs. In the differential transmission spectrum of the delayed probe pulse with a duration of 25 fs tuned 120 meV above the gap, one sees, at negative time delays an increased transition probability around the spectral position of the pump pulse due to Pauli blocking.

Due to excitonic enhancement above the populated states and to a minor degree due to band-gap shrinkage, an induced absorption is observed above the spectral position of the pump pulse. A remarkably sharp feature is present in the earliest probe spectrum which seems to contradict the time–energy uncertainty relation. Above a delay of 100 fs the build up of the first LO-phonon cascade structure is seen clearly followed by a struc-

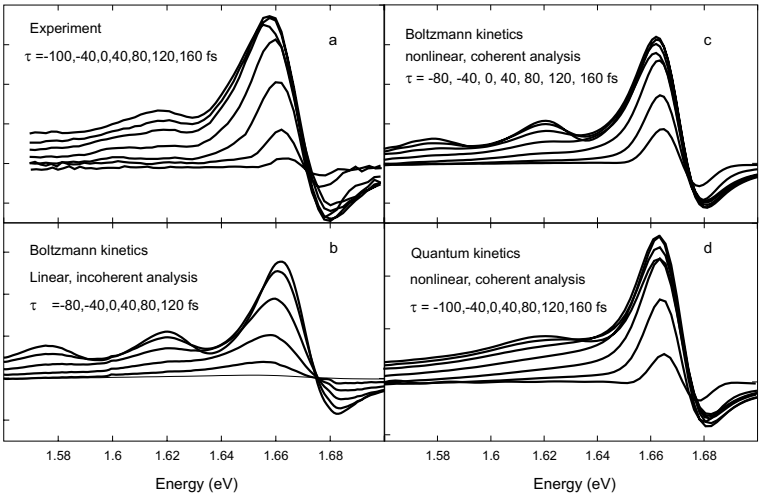

Fig. 14.2 Measured (a) and calculated DTS spectra in various approximations for delay times ranging from −100 fs to 160 fs. (b) Incoherent analysis with Markovian scattering kinetics, (c) Coherent analysis with Markovian scattering kinetics, (d) Coherent analysis with non-Markovian quantum kinetics. [The measured spectra are according to Fürst *et al.* (1996), the calculated spectra are according to Schmenkel *et al.* (1998).]

ture due to two successive phonon emission processes at still later times. In these experiments, only $8 \cdot 10^{14}\mathrm{cm}^{-3}$ carriers have been excited, so that the relaxation kinetics was dominated by LO-phonon scattering. We present in Fig. 14.2 the calculated differential transmission spectra for three approximations to the relaxation kinetics. In the second figure, the test spectra have been calculated in the Markovian limit of the LO-phonon relaxation kinetics by inserting the population distributions calculated for the pump pulse into the Bloch equations for the test pulse. This incoherent analysis fails to explain the sharp spectral features at the high energy cross-over from reduced to induced absorption at early time delays. We note further that the build-up of the first and particularly the second peak of the phonon cascade occurs in this theoretical formulation faster than in the experiment. If one replaces the incoherent analysis by a coherent one, i.e., if one treats only one set of Bloch equations for the two pulses together and determines the polarization in the $\mathbf{k_t}$ direction at the end, one sees that the sharp spectral features at the cross-over point and at earliest delays are now present as

in the experimental spectra. If one uses finally the delayed non-Markovian quantum kinetics of the phonon scattering, the time scale of the build-up of the phonon peaks now also agrees with the experiment. Thus, the analysis of this experiment shows clearly the need for the coherent determination of the test-beam polarization and for the non-Markovian quantum relaxation kinetics.

Next, we discuss a femtosecond four-wave mixing experiment of Wegener et pal. on GaAs in which for the first time the LO-phonon quantum beats have been seen superimposed on the exponentially decaying time-integrated four-wave mixing signal. The time-integrated four-wave mixing signal is theoretically determined by $\int_{-\infty}^{+\infty} dt|P_2(t,\tau)|^2$. There is also the possibility to measure instead the time-resolved signal $|P_2(t,\tau)|^2$, both as a function of the real time t and the delay time τ, or the frequency-resolved signal $|P_2(\omega,\tau)|^2$. The quantum beats, which are clearly seen in the experimental and theoretical time-integrated four-wave mixing signals, are due to the phonon oscillations in the integral kernel of the non-Markovian scattering integrals. The two pulses had a duration of 14 fs and had the form of a hyperbolic secans

$$\mathcal{E}_0(t) = E_0 \frac{1}{\cosh(t/\Delta t)} \quad . \tag{14.10}$$

As a residual Coulomb scattering was also present under the experimental conditions, we use, in addition to the dephasing by phonon scattering, an excitation-induced phenomenological damping in the form $\gamma = \gamma_0 + \gamma_1 n(t)$, where $n(t)$ is the number of carriers at time t. The carrier frequency of the two pulses was degenerate and was tuned to the exciton resonance.
As Fig. 14.3 shows, one gets a nearly perfect agreement between the experiment and the quantum kinetic calculations. Naturally, the oscillations are only present in a non-Markovian version of the dephasing kinetics. The time-integrated four-wave mixing signals show on the exponential decay an oscillation with the frequency $(1 + m_e/m_h)\omega_0$, which can be understood as the beating frequency of two interband polarization components coupled by the coherent exchange of an LO-phonon between conduction-band states. These observed phonon beats are a clear manifestation of the delayed quantum kinetics.

Finally, we want to mention that the quantum kinetics used to analyze originally the two described experiments has been derived by nonequilibrium Green's functions. In the weak coupling theory, the integral kernel of the resulting scattering integrals is expressed in terms of retarded and

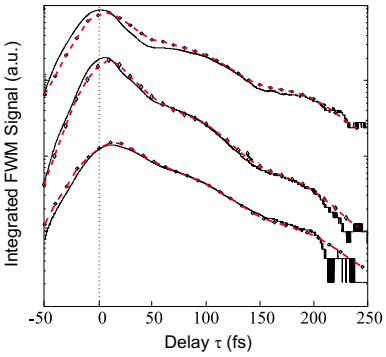

Fig. 14.3 Measured (solid lines) and calculated (dashed lines) time-integrated four-wave mixing signals for three excitation densities (1.2×10^{16} cm^{-3} (top curve), 1.9×10^{16} cm^{-3} (middle curve) and 6.3×10^{16} cm^{-3} (bottom curve)) with LO-phonon scattering. [After Bányai *et al.* (1995).]

advanced electron Green's functions of the state $\mathbf{k}$ and $\mathbf{k}+\mathbf{q}$ coupled by the exchange of a phonon. These spectral functions are again determined in the mean-field approximation like the time- evolution function $T_{ij,k,q}(t,t')$ for the phonon-assisted density matrices. As the mean-field terms do not couple the states $\mathbf{k}$ and $\mathbf{k}+\mathbf{q}$, the result of both theories on this level is identical.

14.2 Semiconductor Photon Echo

The photon echo is a special example of a four-wave mixing experiment; it is the optical analogon of Hahn's (1950) famous spin echo in nuclear magnetic resonance. For the experimental observation of the photon echo, the system is excited by a sequence of two pulses that are separated in time by τ. At the time 2τ the system spontaneously emits a light pulse in the four-wave mixing direction, the photon echo. This phenomenon is known from atoms, where it occurs in systems with sufficient inhomogeneous broadening.

In semiconductors, photon echoes can be obtained, e.g., at excitonic resonances if the system is inhomogeneously broadened. This case is very similar to the atomic system and can be understood accordingly. More interesting is the situation of the intrinsic semiconductor photon echo that also occurs in systems without any inhomogeneous broadening relying on

the specific properties of interband continuum of the electron–hole excitations.

To analyze the intrinsic photon echo in semiconductors, we start from the coherent semiconductor Bloch equations (13.6) – (13.7). In order to obtain analytic results, we want to solve the Bloch equations in first order of the weak pulse E_t and in second order of the strong pulse E_p, to compute the leading contribution to the signal in the direction $2\mathbf{k}_p - \mathbf{k}_t$. To keep our analytical analysis as simple as possible, we ignore all dissipative contributions in the semiconductor Bloch equations. These contributions could be included, but they would make our equations more complicated. To eliminate the population n_k, we use the conservation law, Eq. (13.9). Since we restrict our overall result to be of third order in the field amplitude, we expand Eq. (13.9) as in Eq. (13.18) and keep only the lowest-order term. The resulting equation for the interband polarization is

$$\begin{aligned} i\hbar\frac{d}{dt}P_k = \hbar\epsilon_k\, P_k - \sum_{k'} V_{k'}\, P_{k+k'} - 2\sum_{k'} V_{k'}\, |P_{k+k'}|^2 P_k \\ +2\sum_{k'} V_{k'}\, P_{k+k'}\, |P_k|^2 - d_{cv}\, E(1-2|P_k|^2) \ . \end{aligned} \tag{14.11}$$

This equation can be simplified, making again use of the known solutions of the Wannier equation (10.35)

$$\hbar\epsilon_k\, \psi_{\lambda,k} - \sum_{k'} V_{k'} \psi_{\lambda,k+k'} = \hbar\epsilon_\lambda\, \psi_{\lambda,k} \ . \tag{14.12}$$

Expanding the interband polarization,

$$\begin{aligned} P_k &= \sum_\lambda \psi_{\lambda,k}\, P^\lambda \\ P^\lambda &= \sum_k \psi^*_{\lambda,k}\, P_k \ , \end{aligned} \tag{14.13}$$

inserting into Eq. (14.11), multiplying by $\psi^*_{\lambda',k}$ and summing over k, we obtain

$$i\hbar\frac{d}{dt}P^{\lambda} = \hbar\epsilon_{\lambda}P^{\lambda} - 2\sum_{k,k'}V_{k'}\sum_{\lambda'\lambda''\lambda'''}\psi^{*}_{\lambda,k}\left(\psi^{*}_{\lambda',k+k'}\psi_{\lambda'',k+k'}\right.$$
$$\left.-\psi^{*}_{\lambda',k}\,\psi_{\lambda'',k+k'}\right)\psi_{\lambda''',k}(P^{\lambda'})^{*}P^{\lambda''}\,P^{\lambda'''}$$
$$-d_{cv}\,E\,\psi^{*}_{\lambda}(0) + 2\,d_{cv}\,E\sum_{k}\sum_{\lambda'\lambda''}\psi^{*}_{\lambda,k}\,\psi^{*}_{\lambda',k}\,\psi_{\lambda'',k}(P^{\lambda'})^{*}P^{\lambda''}\ . \qquad (14.14)$$

Here, we used

$$\sum_{k}\psi^{*}_{\lambda,k} = \psi^{*}_{\lambda}(r=0) = \psi^{*}_{\lambda}(0)\ . \qquad (14.15)$$

We solve Eq. (14.14) using perturbation theory, keeping the results which are first-order in E_t and second order in E_p. For simplicity, we assume that no temporal overlap exists between the two pulses. Hence, we can choose a time t_0 so that the first pulse is gone and the second one has not come yet. Since the explicit form of Eq. (14.14) is somewhat lengthy, we show our solution procedure for the simpler equation

$$i\frac{dP}{dt} = \epsilon\,P + E + a|P|^2E + b|P|^2\,P\ , \qquad (14.16)$$

which has the same basic structure as Eq. (14.14). To obtain the solution in first order of E_t, we drop all nonlinearities and solve

$$i\,\frac{dP}{dt} = \epsilon\,P + E_t\ , \qquad (14.17)$$

with the initial condition that P vanishes before the pulse E_t arrives. For the time t_0 after the first pulse E_t is gone and the second pulse E_p has not yet arrived, we obtain by integrating Eq. (14.17)

$$P(t_0) = -i\,e^{-i\epsilon t_0}\,E_t(\epsilon)\ . \qquad (14.18)$$

Here,

$$E_t(\epsilon) = \int_{-\infty}^{t_0}dt\,E_t(t)\,e^{i\epsilon t}\ , \qquad (14.19)$$

which is the Fourier transform of E_t at the frequency ϵ since $E_\tau(t) = 0$ for $t > t_0$.

For the integration over the second pulse, we use the polarization (14.18) as an initial condition. To obtain a result, which is of second order in E_p, we solve the equation iteratively. First, we use again Eq. (14.17) to get

$$P^{(0)}(t) = -i\, e^{-i\epsilon t} \left[E_t(\epsilon) + \int_{t_0}^{t} dt'\, E_p(t')\, e^{i\epsilon t'} \right] \quad , \tag{14.20}$$

and then we iterate the Eq. (14.18) once:

$$i\,\frac{dP^{(1)}}{dt} = \epsilon\, P^{(1)} + E_p + a|P^{(0)}|^2 E_p + b|P^{(0)}|^2 P^{(0)} \quad . \tag{14.21}$$

Since the pulses propagate in different directions,

$$E_{t/p} \propto \exp(i\mathbf{k}_{t/p} \cdot \mathbf{r}) \quad , \tag{14.22}$$

and we are interested only in the contribution which propagates in the direction $2\mathbf{k}_p - \mathbf{k}_t$, we pick out from Eq. (14.21) only those terms which are proportional to $E_p\, E_p\, E_t^*$, before we perform the final integration.

Following this procedure with the full equation (14.14), we obtain

$$\begin{aligned} P(t)\frac{\hbar^3}{|d_{cv}|^2 d_{cv}} &= -2i \sum_k \sum_{\lambda\lambda'\lambda''} \psi_\lambda(0)\, \psi^*_{\lambda,k}\, \psi_{\lambda'}(0)\, \psi^*_{\lambda',k}\, \psi^*_{\lambda''}(0)\, \psi_{\lambda'',k}\, E_t^*(\lambda') \\ &\times \int_{t_0}^{t} dt'\, e^{-i\epsilon_\lambda(t-t')+i\epsilon_\lambda{}'t'}\, E_p(t') \int_{t_0}^{t'} dt''\, e^{-i\epsilon_{\lambda''}(t'-t'')}\, E_p(t'') \\ &- 2 \sum_{kk'} \sum_{\lambda\lambda'\lambda''\lambda'''} V_{k-k'} \psi_\lambda(0)\, \psi^*_{\lambda,k}\, \psi^*_{\lambda''}(0)\, \psi_{\lambda'',k'}\, \psi^*_{\lambda'''}(0)\, \psi_{\lambda''',k} \\ &\times \left[\psi_{\lambda'}(0)\, \psi^*_{\lambda',k'} - \psi_{\lambda'}(0) \psi^*_{\lambda',k} \right] E_t^*(\lambda') \int_{t_0}^{t} dt'\, e^{-i\epsilon_\lambda(t-t')+i\epsilon_{\lambda'}t'} \\ &\times \int_{t_0}^{t'} dt''\, e^{-i\epsilon_{\lambda''}(t'-t'')} E_p(t'') \int_{t_0}^{t'} dt'''\, e^{-i\epsilon_{\lambda'''}(t'-t''')} E_p(t''') \quad , \end{aligned} \tag{14.23}$$

where $E(\lambda) = E(\epsilon_\lambda)$. The first term in Eq. (14.23), which does not vanish when the Coulomb matrix element V_k is set to 0, describes the response of an inhomogeneous set of independent oscillators. The last term in Eq. (14.23) is due to the exchange terms in the semiconductor Bloch equations. It has been shown by Lindberg *et al.* (1992), that these exchange terms contribute considerably to the excitonic part of the semiconductor photon echo. Since these considerations are beyond the scope of this book, we

refer the interested reader to the original literature listed at the end of this chapter.

For our analytical evaluations, we concentrate on the much simpler case when the excitation frequency is above the band gap, well within the interband absorption continuum. In this case, we treat the Coulomb interaction perturbatively. We neglect the Coulomb interaction in the wave functions and keep it only in the exchange contributions as multiplying matrix element in the sums, so that

$$\psi_{\lambda,k} \simeq \delta_{k\lambda} \text{ and } \psi_\lambda(0) \simeq 1 \ . \tag{14.24}$$

The states are essentially free particle states and consequently the eigenvalues ϵ_λ are basically

$$\hbar\epsilon_\lambda \simeq E_g + \frac{\hbar^2}{2m}\lambda^2 \ . \tag{14.25}$$

The signal (14.23) takes the form

$$\begin{aligned} P(t)\frac{\hbar^3}{|d_{cv}|^2 d_{cv}} &= -2i \sum_\lambda E_t^*(\lambda)\, e^{-i\epsilon_\lambda t} \left[\int_{t_0}^{t} dt'\, E_p(t')\, e^{i\epsilon_\lambda t'}\right]^2 \\ &\quad - 2\sum_{\lambda\lambda'} V_{\lambda-\lambda'}\, E_t^*(\lambda')\, e^{-i\epsilon_\lambda t} \int_{t_0}^{t} dt' \left[1 - e^{i(\epsilon_\lambda - \epsilon_{\lambda'})(t-t')}\right] \\ &\quad \times \int_{t_0}^{t'} dt''\, E_p(t'')\, e^{i\epsilon_\lambda t''} \int_{t_0}^{t'} dt'''\, E_p(t''') e^{i\epsilon_{\lambda'} t'''} \ . \end{aligned} \tag{14.26}$$

If we assume simple δ-function pulses,

$$\begin{aligned} E_t(t) &= E_t\, \delta(t+\tau) \\ E_p(t) &= E_p\, \delta(t) \ , \end{aligned} \tag{14.27}$$

then

$$E_t(\lambda) = E_t\, e^{-i\epsilon_\lambda \tau} \ , \tag{14.28}$$

and, for $t > t_0$, we obtain for the first term in Eq. (14.26):

$$P_{(1)}(t) \propto E_t^* E_p^2 \sum_\lambda e^{-i\epsilon_\lambda (t-\tau)} \propto E_t^*\, E_p^2\, \delta(t-\tau) \ . \tag{14.29}$$

Hence, the polarization and therefore also the field emitted in the direction $2\mathbf{k}_p - \mathbf{k}_t$ peaks at a delayed time τ, which is equal to the temporal separation of the two pulses. This is the signature of the photon echo. Thus, the first term of Eq. (14.26) describes the photon echo of the semiconductor continuum states. The second term in Eq. (14.26) gives a nonecho contribution, which is caused by the exchange terms in the semiconductor Bloch equations. We do not analyze this term any further in this chapter and refer the interested reader to Lindberg *et al.* (1992) for more details.

At the end of this section, we show an example of the numerical evaluations of the full semiconductor Bloch equations for the photon echo configuration discussed here (Koch *et al.* 1992). These numerical evaluations were done for 120 fs (FWHM) pulses which excite a CdSe sample at the 1s-exciton resonance. Since the short pulses are spectrally broad they excite also the higher exciton states, as well as the lower part of the ionization continuum. The 1s-exciton is, however, dominant and contributes to the total signal like a single oscillator. Additionally, many-body effects like the band-gap renormalization can also become important since they may completely modify the resonance conditions.

In Fig. 14.4, we show the numerically computed time resolved signal in photon echo direction for two 100 fs (FWHM) pulses with 400 fs delay

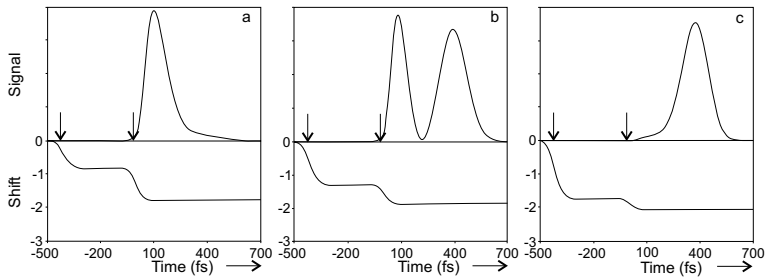

Fig. 14.4 Time-resolved signal in photon echo direction for excitation at the exciton resonance. The dephasing time is 200 fs, the time delay is 400 fs, and the pulse FWHM is 100 fs for both pulses. The peak value of the dipole coupling energy of the second pulse is $d_{cv}\,E_2 = 0.1\,E_R$, where the exciton binding energy $E_R = 16$ meV in CdSe. The peaks of the pulses are marked by arrows. The lower parts of the figures show the renormalized band edge $(E_G - E_G^0)/E_R$ as function of time. Here, E_G^0 is the unrenormalized band edge. In Figs. (a) – (c), the peak amplitude of the first pulse is changed: (a) $d_{cv}\,E_1 = 0.03\,E_R$, (b) $d_{cv}\,E_1 = 0.06\,E_R$, and (c) $d_{cv}\,E_1 = 0.1\,E_R$. [From Koch *et al.* (1992)]

between the pulses. We see in Fig. 14.4a (upper part), that for the case of a weak first pulse, only an almost instantaneous signal and no photon echo at +400 fs occurs. This signal is solely due to the exchange correlation between the excited excitons. For higher pulse intensities (Figs. 14.4b and 14.4c), we see the gradual development of an echo signal, which coexists with the instantaneous signal for intermediate intensities.

To analyze the origin of this scenario, we plot the time dependence of the renormalized band gap in the bottom part of the figures. Comparison of the top and bottom parts of Fig. 14.4a – 14.4c reveals that the echo contribution in the time-resolved signal occurs as soon as the continuum states are shifted into resonance during the presence of the first pulse (band-gap shift below — $1E_R$ in Fig. 14.4b). Consequently, direct continuum excitation is possible, which yields a photon echo signal at 400 fs because of the intrinsic inhomogeneous broadening of the electron–hole continuum states. Intermediate field strengths result in a characteristic double peak structure in the signal.

REFERENCES

The theory-experiment comparison for the differential transmission spectra with LO-phonon scattering has been presented in:

C. Fürst, A. Leitenstorfer, A. Laubereau, and R. Zimmermann, Phys. Rev. Lett. 78, 1545 (1996)
A. Schmekel, L. Bányai, and H. Haug, J. Lumminesc. 76/77, 134 (1998)

The femtosecond four-wave mixing with LO-phonon scattering has been published in:

L. Bányai, D.B. Tran Thoai, E. Reitsamer, H. Haug, D. Steinbach, M.U. Wehner, M. Wegener, T. Marschner, and W. Stolz, Phys. Rev. Lett. 75, 2188 (1995)

The prototype of an echo phenomenon is the spin echo first presented by:

E.L. Hahn, Phys. Rev. **80**, 580 (1950)

The analysis of the semiconductor photon echo follows:

M. Lindberg, R. Binder, and S.W. Koch, Phys. Rev. **A45**, 1865 (1992)

S.W. Koch, A. Knorr, R. Binder, and M. Lindberg, phys. stat. sol. **b173**, 177 (1992)

PROBLEMS:

Problem 14.1: Derive Eq. (14.11) using a third-order expansion of the coherent semiconductor Bloch equations.

Problem 14.2: Perform the analysis described in Eqs. (14.16) – (14.22) to derive Eq. (14.23).

Chapter 15

Optical Properties of a Quasi-Equilibrium Electron–Hole Plasma

In situations where either the width of a single pulse or the delay between the pump and probe pulse are longer than the intraband relaxation time, the electron and hole distributions have already relaxed to thermal Fermi distributions.

$$f_{i,k} = \frac{1}{e^{\beta(\frac{\hbar^2 k^2}{2m_i} - \mu_i)} + 1} \quad . \tag{15.1}$$

Here, the chemical potentials μ_i are measured with respect to the actual band edge, that is in an interacting system with respect to the renormalized band edge. The configuration is quasi-stationary, which is meant to imply that the chemical potentials and the temperatures of the distributions may vary slowly in time.

For such a situation, the treatment of the semiconductor Bloch equations is simplified by the fact that the equations for the electron and hole distributions do not have to be evaluated for all momenta as they are known to be Fermi distributions. Summing the equations for the electron and hole distributions over all momenta, one obtains a rate equation for the total number of electrons or holes. All intraband scattering processes drop out by this procedure, because they do not change the total number of electrons or holes. From the resulting total carrier numbers at a given time one can calculate the corresponding chemical potentials $\mu_i(t)$. Most often one can assume charge neutrality so that $N_e(t) = N_h(t)$. If the temperatures $T_i(t)$ of the electron and hole gases also have to be calculated, one multiplies the equations for the electron–hole distributions with the kinetic energy of the corresponding carriers. After summation, one obtains, at least for weakly interacting carrier gases, two energy rate equations from which the variation of the electron and hole temperatures with time can be calculated. Here,

we assume for simplicity that the temperature and chemical potentials of the distributions are known or can be obtained by fitting the calculated to the measured spectra.

The main remaining task is then the solution of the equations for the interband polarization components. In this regime of slowly varying or even stationary fields, the screening of the particle–particle Coulomb interaction by the carriers is fully developed and can be described by its equilibrium form. The more complex problem of the temporal build-up of the screening from the Coulomb scattering terms can be avoided in this situation. A common approximation for the treatment of the influence of screening on the optical properties is to use a screened Hartree–Fock approximation with an RPA screening which is particularly simple in the plasmon–pole approximation (see Chap. 8). Here, the bare Coulomb potential is replaced by the statically screened potential both in the renormalized single-particle energies and in the renormalized Rabi frequencies. As an improvement, one can use quasi-static screening in which the frequency is given by the change of the single-particle frequency, $e_{i,k'} - e_{i,k}$.

The renormalized single-particle energies in a quasi-equilibrium system are

$$\hbar e_{i,k} = \hbar \epsilon_{i,k} - \sum_{\mathbf{k}'} V_{s,|\mathbf{k}-\mathbf{k}'|} f_{i,k'} \quad , \tag{15.2}$$

and the renormalized Rabi frequency is

$$\hbar \omega_{\mathrm{R,k}} = d_{cv} \mathcal{E}_0 + \sum_{\mathbf{k}'} V_{s,|\mathbf{k}-\mathbf{k}'|} P_{\mathbf{k}'} \quad , \tag{15.3}$$

where

$$V_{s,q} = \frac{V_q}{\varepsilon(q, \omega = 0)} \tag{15.4}$$

is the statically screened potential. Thus, attractive (electron–hole) and repulsive (electron–electron and hole–hole) interactions are treated in the same way. This is important because a considerable cancellation occurs between these two interactions as will be discussed below. To simplify the problem further, we will use a phenomenological Markovian approximation, $\propto -\gamma P_k(t)$, for the dephasing rate. γ is either constant or linearly dependent on the excitation density $N_i(t)$, in order to include the effects of induced dephasing. As shown below, this approximation for the damping together with the quasi-equilibrium approximation needs to be done consistently.

In Chap. 10, we solved the interband polarization equation for an unexcited crystal and found an absorption spectrum consisting of sharp absorption lines due to the bound states and a broad absorption band due to the ionization continuum. Now, we analyze the changes of this band-edge spectrum when a quasi-equilibrium electron–hole plasma exists in the crystal. The spectrum of a pure plasma has already been calculated and discussed in Chap. 5 in the free-carrier approximation. In this chapter, we calculate how an excitonic spectrum with sharp bound-state resonances gradually changes into a plasma spectrum with increasing electron-hole-pair population.

For a constant light field, the stationary equation for the interband polarization component in the rotating wave approximation is

$$\hbar(\omega - e_{e,k} - e_{h,k} + i\gamma)P_{\mathbf{k}} = -(1 - f_{e,k} - f_{h,k})\left(d_{cv}\mathcal{E} + \sum_{\mathbf{k}'} V_{s|\mathbf{k}-\mathbf{k}'|}P_{\mathbf{k}'}\right) . \tag{15.5}$$

polarization equation in quasi-equilibrium

The coupled equations for the polarizations in the different momentum states form a set of linear, inhomogeneous algebraic equations, which can be solved, e.g., by numerical matrix inversion. As already discussed in Chap. 5, absorption and gain occur depending on the sign of the inversion factor

$$(1 - f_{e,k} - f_{h,k}) \ . \tag{15.6}$$

The cross-over from absorption to gain occurs where the inversion is zero. This condition can also be written as

$$\frac{1}{e^{-\beta(\frac{\hbar^2k^2}{2m_h} - \mu_h)} + 1} = \frac{1}{e^{\beta(\frac{\hbar^2k^2}{2m_e} - \mu_e)} + 1} \ . \tag{15.7}$$

which implies (see problem 15.1)

$$e^{-\beta(\frac{\hbar^2k^2}{2m_h} - \mu_h)} = e^{\beta(\frac{\hbar^2k^2}{2m_e} - \mu_e)} \ . \tag{15.8}$$

Taking the logarithm on both sides, one finds for the cross-over energy

$$\frac{\hbar^2k^2}{2m_e} + \frac{\hbar^2k^2}{2m_h} = \mu_e + \mu_h \ . \tag{15.9}$$

In the limit of vanishing damping, the imaginary part of the free-carrier interband polarization components implies energy conservation

$$\hbar\omega = E_g' + \frac{\hbar^2 k^2}{2m_e} + \frac{\hbar^2 k^2}{2m_h} \ . \tag{15.10}$$

From this law for the optical transition and the cross-over condition (15.9), one finds the cross-over energy between gain and absorption

$$\hbar\omega - E_g' = \mu_e + \mu_h \ , \tag{15.11}$$

i.e., optical gain in the spectral region above the renormalized band gap and the total chemical potential, and optical absorption for higher energies. Besides the band filling and band-gap renormalization another important influence of the plasma is the screening of the Coulomb potential. The attractive electron–hole potential is weakened by the plasma screening causing a reduction of the excitonic effects in the spectra. Actually, at a critical plasma density, the combined effects of the screening and of the occupation of k-states by the plasma result in a vanishing exciton binding energy. Above this critical density, also called Mott density, only ionized states exist. However, as we will see, the attractive potential still modifies the plasma spectrum considerably.

The screening of the Coulomb potential and the Fermi exchange effects contribute to the renormalization of the single-particle energies which results in the band gap shrinkage $\Delta E_g = E_g' - E_g$. The band-gap shrinkage and the reduction of the exciton binding energy are of similar size, so that normally no shift of the exciton resonance occurs as the plasma density is increased. The influence of the plasma is only seen in a reduction of the exciton oscillator strength due to the increasing exciton Bohr radius with increasing plasma density, until the band edge reaches the exciton level at the Mott density. Above the Mott density the exciton resonance no longer exists. However, the attractive Coulomb potential still increases the probability to find the electron and hole at the same position, which causes an excitonic enhancement (Coulomb enhancement) of the plasma absorption or gain spectrum.

The fact that the inversion factor (15.6) can change its sign complicates the solution of Eq. (15.5) since it implies that the corresponding homogeneous eigenvalue equation is non-Hermitian. In the following, we describe first a numerical method for obtaining rather accurate solutions by a matrix inversion, and then two approximate solutions which are considerably simpler and can be used above the Mott density, i.e., in the high-density

regime. In the final section of this chapter, we discuss the so-called plasma theory, which provides a simple analytical approximation scheme for $3D$ semiconductors.

15.1 Numerical Matrix Inversion

Because the screened Coulomb potential $V_{s,\mathbf{k}-\mathbf{k}'}$ depends not only on $|\mathbf{k}'|$ but also on the angle between $\mathbf{k}$ and $\mathbf{k}'$, we want to simplify the problem by introducing an angle-averaged potential by

$$\sum_{\mathbf{k}'} V_{s,|\mathbf{k}-\mathbf{k}'|} P_{\mathbf{k}'} \rightarrow \sum_{k'} \bar{V}_{s,k,k'} P_{k'} \quad , \tag{15.12}$$

where the angle-averaged potential is given by

$$\bar{V}_{s,k,k'} = \frac{1}{2} \int_{-1}^{+1} d(cos\theta) V_{s,[k^2+k'^2-2kk'cos(\theta)]^{1/2}} \quad \text{in } 3D \tag{15.13}$$

and

$$\bar{V}_{s,k,k'} = \frac{1}{2\pi} \int_{0}^{2\pi} d\phi V_{s,[k^2+k'^2-2kk'cos(\phi)]^{1/2}} \quad \text{in } 2D \ . \tag{15.14}$$

With this approximation we take only s-wave scattering into account and the integral equation becomes one-dimensional. Because Eq. (15.5) is linear in the field (the polarization becomes nonlinear only via the plasma density, which is a function of the light intensity), we can introduce a susceptibility function χ_k by

$$P_k = \chi_k \, \mathcal{E} \ . \tag{15.15}$$

The susceptibility function obeys the integral equation

$$\boldsymbol{\chi_k = \chi^0_k \left(1 + \frac{1}{d_{cv,k}} \sum_{k'} \bar{V}_{s,k,k'} \chi_{k'} \right)} \ , \tag{15.16}$$

susceptibility integral equation

where χ^0_k is the free-carrier susceptibility function of Chap. 5:

$$\chi^0_k = -d_{cv,k} \frac{1 - f_{e,k} - f_{h,k}}{\hbar(\omega + i\gamma - e_{e,k} - e_{h,k})} \ . \tag{15.17}$$

More realistic optical line shapes are obtained by taking into account the finite damping γ (dephasing) of the interband polarization. As discussed in the previous chapter, the dephasing for high-density situations is dominated by carrier–carrier scattering. At lower densities, carrier–phonon and carrier–impurity scattering are the main sources of dissipation. For the purposes of the present discussion, the detailed mechanism of damping and dephasing is assumed to be not relevant. We therefore simply replace the infinitesimal damping in χ_0 by the inverse dephasing time γ. If one uses a finite damping γ, the energy conservation is smeared out and as a consequence the cross-over from absorption to gain at the total chemical potential would no longer be guaranteed. According to Green's function theory under these conditions a spectral representation has to be used

$$\chi^0_k = d_{cv,k} \int_{-\infty}^{+\infty} \frac{d\omega'}{2\pi} \frac{2\gamma/\hbar}{(\omega' - e_{e,k} - e_{h,k})^2 + \gamma^2} \frac{1 - f_e(\hbar\omega' - e_{h,k}) - f_h(e_{h,k})}{\omega - \omega' + i\delta} \ . \tag{15.18}$$

Instead of using a constant γ, a better description of the band-tail absorption can be obtained with a frequency-dependent $\gamma_k(\omega)$. Such a dynamical damping results naturally if it is calculated as the imaginary part of a frequency-dependent self-energy. Here, we take it in the form

$$\gamma_k(\omega) = \gamma^0 \frac{1}{e^{(E_k - \hbar\omega)/E_\alpha} + 1}$$

in order to describe the exponential absorption tail. The energy E_k is given by $E_k = \hbar^2 k^2 / 2m$ and E_α is a numerical constant.

Even though Eq. (15.17) has the same form as the free-carrier susceptibility in Chap. 5, the single-particle energies in Eq. (15.17) are the renormalized energies calculated in the quasi-static approximation of Chap. 9. Hence, Eq. (15.17) includes the band-gap renormalization effects due to the electron–hole plasma. Next, we introduce a vertex function Γ_k which describes the deviations of the full susceptibility χ from χ^0:

$$\chi_k = \Gamma_k \chi_k^0 \ . \tag{15.19}$$

The vertex function obeys the equation

$$\boldsymbol{\Gamma_k = 1 + \frac{1}{d_{cv,k}} \sum_{k'} \chi^0_{k'} \bar{V}_{s,k,k'} \Gamma_{k'}} \ . \tag{15.20}$$

vertex integral equation

The integral equation (15.20) will now be solved by various methods.

The integral over k' is approximated by a discrete sum

$$\sum_{k'} \to \int \frac{dk'}{2\pi} \to \sum_i \frac{\Delta k_i'}{2\pi} \ . \tag{15.21}$$

In numerical evaluations, one typically obtains converging solutions if around 100 terms are included in the summation. Here, the k_i can be taken equidistantly, however, better accuracy is obtained if the k_i are taken as the points of support of a Gaussian quadrature. At low densities the angle-averaged potential becomes singular for $k' = k$. This singularity has to be removed before the numerical matrix inversion is performed. One adds and subtracts a term

$$\left(\sum_{k'} F_{k,k'} \bar{V}_{s,k,k'} \right) \Gamma_k \chi_k^0 + \sum_{k'} \bar{V}_{s,k,k'} \left(\chi^0_{k'} \Gamma_{k'} - F_{k,k'} \chi^0_k \Gamma_k \right) \ , \tag{15.22}$$

where $F_{k,k'}$ is chosen so that $F_{k,k} = 1$ and that the sum in the first bracket can be evaluated analytically, e.g., in $3D$

$$F_{k,k'} = \frac{2k^4}{k'^2(k'^2 + k^2)} \ . \tag{15.23}$$

The bracket of the difference term in (15.22) vanishes at $k = k'$ where $\bar{V}_{s,k,k'}$ is singular, so that the total term is a smooth function at $k = k'$. With

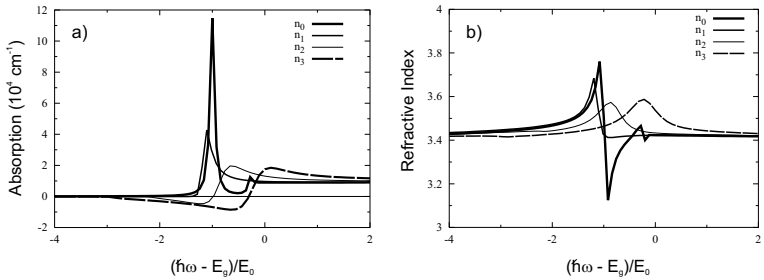

Fig. 15.1 Computed absorption (a) and refractive index spectra (b) for bulk GaAs at $T = 10$ K using the matrix-inversion procedure. The used parameters are: $m_e = 0.0665$, $m_h = 0.457$, $\epsilon_o = 13.74$, $\epsilon_\infty = 10.9$, $a_0 = 125$ Å, $E_0 = 4.2$ meV, and the densities are 0 (1), $5 \cdot 10^{15}\text{cm}^{-3}$ (2), $3 \cdot 10^{16}\text{cm}^{-3}$ (3), and $8 \cdot 10^{16}\text{cm}^{-3}$ (4), respectively. The damping is $\hbar\gamma = 0.05E_0$

such a procedure, compensation terms can be found for the plasmon–pole approximation both in $3D$ and $2D$.

Fig. 15.1 and Fig. 15.2 show the optical spectra which are obtained by numerical matrix inversion for the examples of bulk GaAs and bulk InSb for various plasma densities. The resulting complex susceptibility

$$\chi(\omega) = \frac{1}{L^3} \sum_{\mathbf{k}} d_{cv}^* \chi_k \tag{15.24}$$

defines the complex optical dielectric function $\epsilon(\omega) = 1 + 4\pi\chi(\omega)$ which in turn determines the spectra of absorption $\alpha(\omega)$, Eq. (1.51) and refraction $n(\omega)$, Eq. (1.50).

At low plasma densities the absorption spectra in Fig. 15.1-a shows well-resolved $1s$ and $2s$ exciton resonances, followed by an ionization continuum enhanced by excitonic effects. A plasma density of 10^{16} cm^{-3} is close to the Mott density where the exciton bound states cease to exist. The excitonic enhancement still causes the appearance of a maximum around the original exciton ground-state position. At still higher densities a band-gap reduction far below the position of the original exciton ground state is seen, and simultaneously a build-up of optical gain occurs. The vanishing of the exciton resonance in the absorption spectrum also causes considerable changes in the refractive index, as shown in Fig. 15.1-b. Particularly, if the laser beam is tuned below the exciton resonance, where the absorption is relatively weak, the index of refraction decreases with increasing plasma

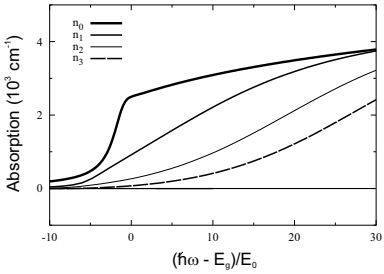

Fig. 15.2 Computed absorption spectra for bulk InSb at $T = 77$ K using the matrix-inversion procedure. The used parameters are: $m_e = 0.0145$, $m_h = 0.4$, $\epsilon_0 = 17.05$, $\epsilon_\infty = 15.7$, $a_0 = 644.8$ Å, $E_0 = 0.665$ meV, and the densities N are 0 (1), $8 \cdot 10^{15}\mathrm{cm}^{-3}$ (2), $2 \cdot 10^{16}\mathrm{cm}^{-3}$ (3), and $3 \cdot 10^{16}\mathrm{cm}^{-3}$ (4), respectively.

density. This effect is often exploited in optical switching devices which are based on dispersive optical bistability, see Chap. 16.

The bulk InSb spectra of Fig. 15.2 have been calculated with a damping $\hbar\gamma = 2E_0 = 1$ meV, which is twice as large as the exciton Rydberg. This case is typical for narrow band-gap semiconductors. Here, the exciton is not resolved in the unexcited medium and causes only a step-like absorption edge.

The corresponding absorption spectra for ideal $2D$ GaAs are shown in Fig. 15.3. Only one hole band was taken into account. Experimentally

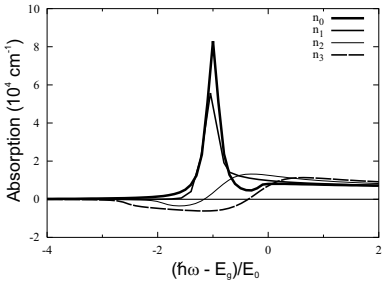

Fig. 15.3 Computed absorption spectra for $2D$ GaAs at $T = 77$ K using the matrix-inversion procedure. The used parameters are: $a_0 = 62,5$ Å, and $E_0 = 16,8$ meV, all the other parameters are the same as in Fig. 15.1. The densities N are 0 (1), $1 \cdot 10^{11}\mathrm{cm}^{-2}$ (2), $5 \cdot 10^{11}\mathrm{cm}^{-2}$ (3), and $1 \cdot 10^{12}\mathrm{cm}^{-2}$ (4), respectively.

in quantum-well structures, one often sees superimposed the contributions of more than one band, e.g. of the heavy- and the light-hole bands in GaAs-based materials.

Finally, we discuss the plasma density-dependent absorption spectra of a quantum wire. As already mentioned in Chap. 8, the screening of the Coulomb potential by the confined plasma is expected to be of little importance in a quantum wire, because the field lines passing through the barrier material cannot be screened. Fig. 15.4-a shows the calculated absorption spectra for a cylindrical GaAs quantum-well wire and Fig. 15.4-b shows the corresponding refractive index spectra. The q1D Coulomb potential of a cylindrical quantum wire, Eq. (7.78), is used in the calculations. The spectra have been obtained by matrix inversion and have been calculated without screening. The spectra calculated with screening (Benner and Haug, 1991) do not differ substantially, showing that for q1D systems the effect of state filling is the most important source of the optical nonlinearities.

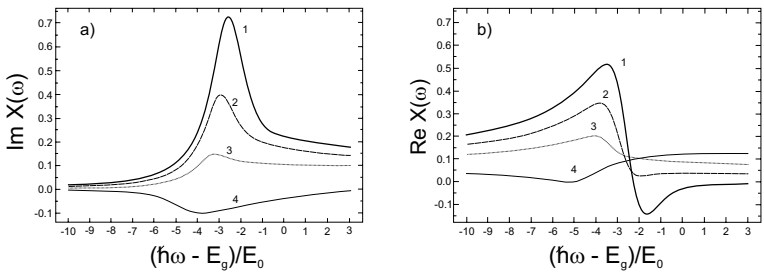

Fig. 15.4 Computed absorption (a) and infractive index spectra (b) for a cylindrical q1D GaAs quantum wire at $T = 300$ K using the matrix-inversion procedure. The parameters are the same as in Fig. 15.1. The 1D-densities are $na_0 = 0$ (1), $na_0 = 0.5$ (2), $na_0 = 1$ (3), and $na_0 = 2$ (4), respectively. Ω is the energy spacing between subbands, and E_0 and a_0 are the bulk exciton binding energy and Bohr radius, respectively.

Studying the absorption spectra in Fig. 15.4-a, one might conclude that the band-gap reduction is not very strong in quantum wires. Actually, however, the opposite is true. The band-gap shrinkage in q1D is larger than in higher dimensional materials, as can be seen in Fig. 15.5.

For the density $na_o = 2$, ΔE_g reaches already five exciton binding energies. The fact, that the absorption peak in Fig. 15.4-a shows only a slight red shift is thus again a result of the compensation between reduction of the exciton binding energy and gap shift.

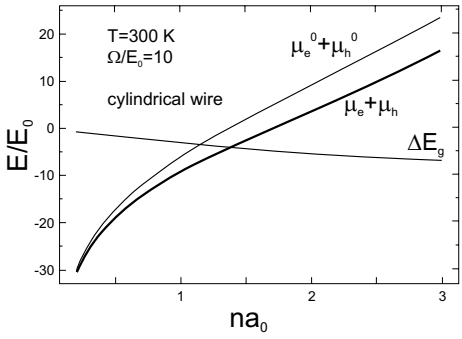

Fig. 15.5 Band-gap reduction, ΔE_g, and chemical potentials as functions of carrier density for the quantum wire of Fig. 15.4

We conclude, that with the reduction of the dimension in mesoscopic semiconductor microstructures the influence of screening on the quasi-equilibrium nonlinearities decreases, while the influence of state filling increases.

15.2 High-Density Approximations

The integral equation (15.20) can be solved approximately if the attractive electron–hole potential is not too strong, i.e., in the high-density limit, where plasma screening and phase-space occupation have reduced the strength of the Coulomb potential sufficiently. We rewrite Eq. (15.20) by introducing a formal interaction parameter σ, which will be assumed to be small

$$\Gamma_k = 1 + \frac{\sigma}{d_{cv}} \sum_{k'} \bar{V}_{s,k,k'} \chi^0_{k'} \Gamma_{k'} \quad . \tag{15.25}$$

A power expansion of Γ in terms of σ yields

$$\Gamma_k = \sum_n q_n \sigma^n \quad , \tag{15.26}$$

where the first coefficient is determined by

$$q_1 = \frac{1}{d_{cv}} \sum_{k'} \bar{V}_{s,k,k'} \chi^0_{k'} \quad . \tag{15.27}$$

In general, one can express Eq. (15.26) as the ratio of two polynomials

$$P_k^{(N,M)} = \frac{\sum_{n=0}^{N} r_n \sigma^n}{\sum_{m=0}^{M} s_m \sigma^m} \ , \tag{15.28}$$

which represents the (N, M)-Padé approximation. The coefficients r_n and s_n can be obtained by a comparison with the original expansion (15.26). We use the simplest nontrivial (0,1)-Padé approximation

$$\Gamma_k = P_k^{(0,1)} = \frac{1}{1 - q_{1k}} \ , \tag{15.29}$$

which results in an optical susceptibility of the form

$$\boldsymbol{\chi(\omega) = \frac{1}{L^3} \sum_{k} \frac{d_{cv}^* \chi_k^0}{1 - q_{1k}}} \ . \tag{15.30}$$

Padé approximation

The denominator in Eq. (15.30) expresses the influence of the multiple electron–hole scattering due to their attractive interaction potential V_s, which causes the excitonic enhancement.

Another approximation for the integral equation (15.20) is obtained by inserting a dominant momentum, which we take as the Fermi momentum, into the angle-averaged screened Coulomb potential. The Fermi momentum is

$$k_F = (3\pi^2 n)^{1/3} \quad \text{in } 3D \tag{15.31}$$

$$k_F = (2\pi n)^{1/2} \quad \text{in } 2D \ , \tag{15.32}$$

see Chaps. 6 and 7. Then the susceptibility integral equation (15.16) becomes

$$\chi_k = \chi_k^0 \left(1 + \frac{1}{d_{cv}} \sum_{k'} \chi_{k'} \bar{V}_{s,k_F,k'} \right) = \chi_k^0 [1 + S(\omega)] \ , \tag{15.33}$$

and for

$$S(\omega) = \frac{1}{d_{cv}} \sum_{k'} \chi_{k'} \bar{V}_{s,k_F,k'} \tag{15.34}$$

we get the self-consistency equation

$$S(\omega) = \frac{1}{d_{cv}} \sum_k \chi_k^0 \bar{V}_{s,k_F,k} \big[1 + S(\omega)\big] \tag{15.35}$$

with the solution

$$1 + S(\omega) = \frac{1}{1 - \frac{1}{d_{cv}} \sum \chi_k^0 \bar{V}_{s,k_F,k}} \quad . \tag{15.36}$$

Eq. (15.36) yields the optical susceptibility

$$\chi(\omega) = \frac{\sum d_{cv} \chi_k^0}{L^3 - \frac{1}{d_{cv}} \sum_k \chi_k^0 \bar{V}_{s,k_F,k}} \tag{15.37}$$

expressing again, in a different approximation, the effect of the excitonic enhancement, however, with a simple momentum-independent enhancement factor $1 + S(\omega)$.

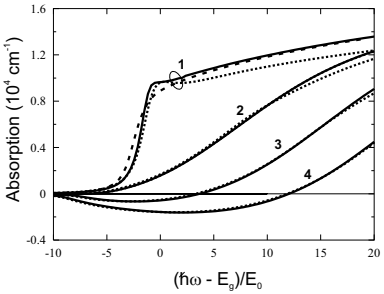

Fig. 15.6 $3D$ absorption spectra for GaAs at 300 K for the densities $1 \cdot 10^{16}\mathrm{cm}^{-3}$ (1), $1{\cdot}10^{18}\mathrm{cm}^{-3}$ (2), $2{\cdot}10^{18}\mathrm{cm}^{-3}$ (3), and $3{\cdot}10^{18}\mathrm{cm}^{-3}$ (4), respectively. Matrix inversion (full lines), Padé approximation (dashed lines), high-density approximation (dotted lines).

Taking the spectral representation, Eq. (15.18), only for the imaginary part, we compare absorption spectra for $3D$ and $2D$ semiconductors in Figs. 15.6 and 15.7 for the different levels of approximations. We show the results obtained *a*) by solving Eq. (15.20) by numerical matrix inversion (full curves), *b*) by using the (0,1)-Padé approximation (15.30) (dashed curves) and *c*) using the high-density approximation (15.37) (dotted curves).

The agreement of both approximations *b*) and *c*) with the numerical solution *a*) becomes very good, if a pronounced optical gain exists. At lower plasma-densities, where the gain vanishes, but where the densities are still above the Mott density, the (0,1)-Padé approximation yields a slightly better description of the excitonic enhancement than the high-density approximation, particularly in the $2D$ case. At low densities, where bound states of the exciton exist, both approximations are unable to give a reliable description of the bound-state resonances in the absorption spectra.

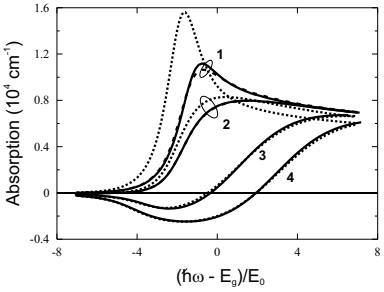

Fig. 15.7 $2D$ absorption and gain spectra for GaAs at 300 K for the densities $1 \cdot 10^{10}\mathrm{cm}^{-2}$ (1), $1 \cdot 10^{11}\mathrm{cm}^{-2}$ (2), $2 \cdot 10^{12}\mathrm{cm}^{-2}$ (3), and $3 \cdot 10^{12}\mathrm{cm}^{-2}$ (4), respectively. The full lines are the result of the matrix inversion, the dashed line is the Padé approximation and the dotted line represents the high-density approximation.

15.3 Effective Pair-Equation Approximation

For many practical applications, it is very useful to have an approximate analytical solution for the full density regime, which can then be used in further studies, e.g., of optical bistability (see Chap. 16) or nonlinear optical devices. Such an approximation scheme (plasma theory) for $3D$ systems has been developed by Banyai and Koch (1986) in terms of an effective electron–hole–pair equation. The main approximation of this theory is that it ignores the reduction of the attractive electron–hole Coulomb interaction via occupation of k-states by the plasma, assuming that the dominant weakening comes through the plasma screening. This assumption is reasonable in $3D$ systems at elevated temperatures, but it fails in $2D$ and q1D where state filling is more important.

We start from the Fourier-transformed polarization equation in the form

$$\big[\hbar(\omega + i\gamma) - \mathcal{H}\big]P = -(1 - f_{e,k} - f_{h.k})d_{cv}\mathcal{E} \ , \tag{15.38}$$

where the eigenvalue equation of the hermitian Hamilton operator is

$$\mathcal{H}\phi_{\nu,k} = (\epsilon_{e,k} + \epsilon_{h,k})\phi_{\nu,k} - \sum_{k'} V_{s,k-k'}\phi_{\nu,k'} = E_\nu \phi_{\nu,k} \ . \tag{15.39}$$

Expanding the polarization components into the eigenfunctions

$$P_k = \sum_n a_\nu \phi_{\nu,k} \ , \tag{15.40}$$

the solution of Eq. (15.38) can be written in the form

$$P_k = -\sum_\nu \phi_{\nu,k} \frac{\tanh\left[\frac{\beta}{2}(\hbar\omega - E_g - \mu)\right]}{\hbar(\omega + i\gamma) - E_\nu} d_{cv}\mathcal{E} \sum_{k'} \phi^*_{\nu,k'} \ , \tag{15.41}$$

where we approximate

$$1 - f_{e,k} - f_{h,k} \simeq \tanh\left[\frac{\beta}{2}(\hbar\omega - E_g - \mu)\right] \ .$$

The resulting absorption coefficient is then

$$\alpha(\omega) = \frac{4\pi^2\omega}{n_b c}|d_{cv}|^2 \tanh\left[\frac{\beta}{2}(\hbar\omega - E_g - \mu)\right] \sum_\nu |\psi_\nu(\mathbf{r} = 0)|^2 \delta(E_\nu - \hbar\omega) \ . \tag{15.42}$$

The remaining problem for the analytic evaluation is to obtain the eigenfunctions ψ_ν and the corresponding eigenvalues for the screened Coulomb potential. Unfortunately, we do not know an analytic solution for the Wannier equation with the Yukawa potential. However, there is a reasonably good approximation to the screened Coulomb potential, which is the so-called Hulthén potential

$$V_H(r) = -\frac{2e^2\kappa/\epsilon_0}{e^{2\kappa r} - 1} \ , \tag{15.43}$$

for which one can solve the Wannier equation (10.35). As in Chap. 10, we make the ansatz

$$\psi_\nu(\mathbf{r}) = f_{nl}(r)Y_{lm}(\theta, \phi) \ , \tag{15.44}$$

where $\nu = n, l, m$ represents the relevant set of quantum numbers. We obtain the radial equation

$$-\frac{\partial^2 f_{nl}}{\partial r^2} - \frac{2}{r}\frac{\partial f_{nl}}{\partial r} + \left[\frac{l(l+1)}{r^2} - \frac{g\lambda^2}{e^{\lambda r}-1}\right] f_{nl} = \epsilon_{nl} f_{nl} \tag{15.45}$$

with

$$\lambda = 2\kappa, \quad g = \frac{1}{a_0\kappa}, \quad \text{and} \quad \epsilon_{nl} = \frac{E_{nl}}{E_0 a_0^2} \ .$$

Since we are only interested in those solutions which do not vanish at the origin,

$$f_{nl}(r=0) \neq 0 \ ,$$

we restrict the analysis of Eq. (15.45) to $l = 0$ and drop the index of f and ϵ. For this case, we obtain from Eq. (15.45)

$$-\frac{\partial^2 u}{\partial r^2} - \frac{g\lambda^2 u}{e^{\lambda r}-1} = \epsilon u \ , \tag{15.46}$$

where we introduced

$$u(r) = r f(r) \ . \tag{15.47}$$

Defining

$$z = 1 - e^{-\lambda r} \, , \, w(r) = u(r)/z(1-z)^{\beta} \tag{15.48}$$

with

$$\beta = \sqrt{-\epsilon/\lambda^2} \tag{15.49}$$

and inserting these definitions into Eq. (15.46) yields

$$z(1-z)\frac{\partial^2 w}{\partial z^2} + [2 - (2\beta+3)z]\frac{\partial w}{\partial z} - (2\beta + 1 - g)w = 0 \ . \tag{15.50}$$

This is the hypergeometric differential equation, which has the convergent solution

$$F(\mathrm{a}, b, c; z) = 1 + \frac{ab}{c}\frac{z}{1!} + \frac{a(a+1)b(b+1)}{c(c+1)}\frac{z^2}{2!} + \ldots \ , \tag{15.51}$$

where it is required that $c \neq 0, -1, -2, \ldots$. In our case, we have

$$a = 1 + \beta + \sqrt{g + \beta^2}$$
$$b = 1 + \beta - \sqrt{g + \beta^2}$$
$$c = 2 \ . \tag{15.52}$$

15.3.1 *Bound states*

For the bound-state solutions, we have $\epsilon_\nu < 0$. Since f must be a normalizable function, we request

$$f(r \to \infty) \to 0 \ , \tag{15.53}$$

which yields the condition that

$$b = 1 - n \, , \quad n = 1, 2, 3, \ldots$$

and therefore,

$$\beta = \frac{1}{2n}(g - n^2) \equiv \beta_n \ \text{and} \ \epsilon_n = -\lambda^2 \beta_n^2 \, ; \quad n = 1, 2, \ldots \ . \tag{15.54}$$

The energetically lowest bound state ($1s$-exciton) is ionized for

$$g \to 1 \, , \text{ i.e., } a_0 \kappa \to 1 \ ,$$

which is the Mott criterion for the Hulthén potential, Eq. (15.43). Inverting the transformations (15.47), (15.48), and using Eq. (15.51), we obtain the bound-state wave functions as

$$\psi_\nu(r) = N_n \frac{z(1-z)^{\beta_n}}{r} F(1 - n, \, 1 + g/n, \, 2; z) Y_{lm} \ , \tag{15.55}$$

where the normalization constant is

$$N_n = \sqrt{\frac{1}{8\pi} g^3 \frac{1}{n} \left(\frac{1}{n^2} - \frac{n^2}{g^2} \right)} \ . \tag{15.56}$$

The relevant factor for the optical response is therefore

$$|\psi_n(r = 0)|^2 = \frac{\lambda^3}{32\pi^2} g^3 \frac{1}{n} \left(\frac{1}{n^2} - \frac{n^2}{g^2} \right) \ , \tag{15.57}$$

where a factor $1/4\pi$ comes from the spherical harmonics.

15.3.2 *Continuum states*

For the unbound solutions of Eq. (15.45), we have $\epsilon_\nu > 0$ and

$$\beta_\nu = i\sqrt{\epsilon_\nu}/\lambda \ . \tag{15.58}$$

Inserting (15.58) into Eqs. (15.51) and (15.52) and normalizing the resulting wave function in a sphere of radius R, i.e.,

$$4\pi \int_0^R dr|u_\nu(r)|^2 = 1 \ , \tag{15.59}$$

we obtain $\epsilon_\nu = \nu^2\pi^2/R^2$ and

$$f_\nu = N_\nu \frac{z}{r}(1-z)^{\beta_\nu} F\left(1+\beta_\nu+\sqrt{g-|\beta_\nu|^2}, 1+\beta_\nu- \sqrt{g-|\beta_\nu|^2}, 2; z\right) \tag{15.60}$$

with

$$N_\nu = \frac{1}{\sqrt{R}}\left[\frac{|\beta_\nu|\sinh(2\pi|\beta_\nu|)g}{\cosh(2\pi|\beta_\nu|) - \cos\left(2\pi\sqrt{g-|\beta_\nu|^2}\right)}\right]^{1/2} \ , \tag{15.61}$$

where $\cos(ix) = \cosh(x)$. Finally, for the optical response, we need

$$\sum_\nu |\psi_\nu(r=0)|^2 f(\beta_\nu) = \frac{1}{E_0 2\pi^2 a_0^3} \times \int_0^\infty dx \frac{\sinh(\pi g\sqrt{x})}{\cosh(\pi g\sqrt{x}) - \cos(\pi\sqrt{4g-xg^2})} f(x) \ , \tag{15.62}$$

where the spin summation together with the spherical harmonics contribute a factor $1/2\pi$.

15.3.3 *Optical spectra*

Combining Eqs. (15.57) and (15.62) with Eq. (15.42) yields

$$\alpha(\omega) = \alpha_0 \tanh\left[\frac{\beta}{2}(\hbar\omega - E_g - \mu)\right] \frac{\hbar\omega}{E_0}\left[\sum_n \frac{1}{n}\left(\frac{1}{n^2} - \frac{n^2}{g^2}\right)\delta_\Gamma\left(\Delta - \frac{E_n}{E_0}\right) + \int_0^\infty dx \frac{\sinh(\pi g\sqrt{x})}{\cosh(\pi g\sqrt{x}) - \cos(\pi\sqrt{4g-xg^2})}\delta_\Gamma(\Delta - x)\right] \ , \tag{15.63}$$

where α_0 and Δ are defined in Eqs. (5.81) and (10.106), respectively, the n-summation runs over all bound states,

$$\delta_\Gamma(x) = \frac{2}{\pi\Gamma\cosh(x/\Gamma)} \ , \tag{15.64}$$

and a factor 2 in the exciton part results from the spin summation. Eq. (15.63) yields semiconductor absorption spectra that vary with carrier density $N = \Sigma f(k)$. The theoretical results agree very well with experimental observations for many different semiconductor materials. An example of such a comparison with experiments is shown in Fig. 15.8. From the

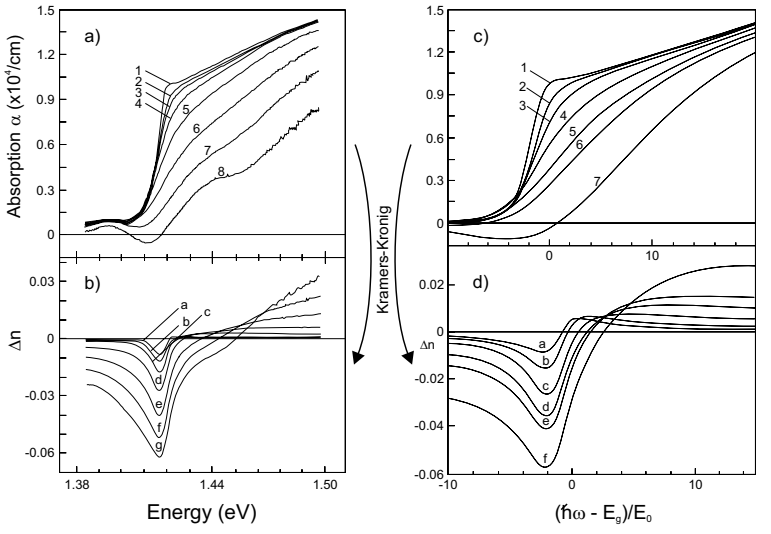

Fig. 15.8 Experimental and theoretical absorption and refractive index spectra are compared for room temperature GaAs. [After Lee *et al.* (1986).] (*a*) The experimental absorption spectra are obtained for different excitation intensities I *(mW)*: 1) 0; 2) 0.2; 3) 0.5; 4) 1.3; 5) 3.2; 6) 8; 7) 20; 8) 50 using quasi-*cw* excitation directly into the band and a 15 μm excitation spot size. The oscillations in curve 8) are a consequence of imperfect antireflection coating. (*b*) The dispersive changes Δn are obtained through a Kramers–Kronig transformation of the absorptive changes $\alpha(I = 0) - \alpha(I)$ (*a*). The agreement with direct measurements of dispersive changes has been tested for the same conditions using a 299-Å multiple-quantum-well sample. (*c*) Calculated absorption spectra using the plasma theory for the densities N (cm^{-3}): 1) 10^{15} (linear spectrum); 2) $8 \cdot 10^{16}$; 3) $2 \cdot 10^{17}$; 4) $5 \cdot 10^{17}$; 5) $8 \cdot 10^{17}$; 6) $1 \cdot 10^{18}$; 7) $1.5 \cdot 10^{18}$. (*d*) Kramers–Kronig transformation of the calculated absorption spectra.

absorptive changes

$$\Delta\alpha(\omega) = \alpha(\omega, N_2) - \alpha(\omega, N_1) \ , \tag{15.65}$$

one obtains the corresponding dispersive changes

$$\Delta n(\omega) = n(\omega, N_2) - n(\omega, N_1) \tag{15.66}$$

through the Kramers–Kronig transformation

$$\Delta n(\omega) = \frac{c}{\pi} P \int_0^\infty d\omega' \frac{\Delta\alpha(\omega')}{\omega'^2 - \omega^2} \ , \tag{15.67}$$

where P again indicates the principle value. Examples of the dispersive changes in bulk GaAs are shown in Figs. 15.8-b and 15.8-d.

It is worthwhile to note at this point that the Kramers–Kronig transformation (15.67) is valid even though we are dealing with a nonlinear system, as long as $\Delta\alpha$ depends only on parameters that are temporally constant. We have to be sure that the carrier density N does not vary in time, or that N varies sufficiently slowly so that it is justified to treat its time-dependence adiabatically.

REFERENCES

For details on the matrix-inversion technique see:

H. Haug and S. Schmitt-Rink, Progr. Quantum Electron. **9**, 3 (1984) and the given references
S. Schmitt-Rink, C. Ell, and H. Haug, Phys. Rev. **B33**, 1183 (1986)

The Padé and high-density approximations are discussed in:

C. Ell, R. Blank, S. Benner, and H. Haug, Journ. Opt. Soc. Am. **B6**, 2006 (1989)
H. Haug and S. W. Koch, Phys. Rev. **A39**, 1887 (1989)

For the quantum-wire calculations see:

S. Benner and H. Haug, Europhys. Lett. **16**, 579 (1991)

The effective pair-equation approximation (plasma theory) is derived and applied in:

L. Bányai and S.W. Koch, Z. Physik **B63**, 283 (1986)
S.W. Koch, N. Peyghambarian, and H. M. Gibbs, Appl. Phys. (Reviews) **63**, R1 (1988)
Y.H. Lee, A. Chavez-Pirson, S.W. Koch, H.M. Gibbs, S.H. Park, J. Morhange, N. Peyghambarian, L. Bányai, A.C. Gossard, and W. Wiegmann, Phys. Rev. Lett. **57**, 2446 (1986)

PROBLEMS

Problem 15.1: Show that the vanishing of the inversion occurs at the photon energy $\hbar\omega - E_g' = \mu_e + \mu_h$.

Problem 15.2: Derive the expression for the optical susceptibility using the (1,2) Padé approximation.

Problem 15.3: Derive the self-consistency equation (15.35).

Problem 15.4: Discuss the Hulthén potential for small and large radii and compare it to the Yukawa potential.

Problem 15.5: Verify that Eq. (15.63) yields the correct free-particle result for $a_0 \to \infty$ and the Wannier result for $\kappa \to 0$.

This page intentionally left blank

Chapter 16

Optical Bistability

Optical instabilities in semiconductors can occur if one combines the strong material nonlinearities with additional feedback. The simplest example of such an instability is *optical bistability*, in which one has situations with two (meta-) stable values for the light intensity transmitted through a nonlinear material for one value of the input intensity I_0. Which transmitted intensity the output settles down to, depends on the excitation history. A different state is reached, if one either decreases the incident intensity I_0 from a sufficiently high original level, or if one increases I_0 from zero. The possibility to switch a bistable optical device between its two states allows the use of such a device as binary optical memory.

A proper analysis of the optical instabilities in semiconductors requires a combination of the microscopic theory for the material nonlinearities with Maxwell's equations for the light field, including the appropriate boundary conditions. The polarization relaxes in very short times, determined by the carrier–carrier and carrier–phonon scattering, to its quasi-equilibrium value which is governed by the momentary values of the field and the carrier density. Therefore, we can use the quasi-equilibrium results of Chap. 15 for the optical susceptibility as the material equation, which implies that the polarization dynamics has been eliminated adiabatically.

The process of carrier generation through light absorption couples the electron–hole–pair density to the electromagnetic field. The electromagnetic field in turn is described by the macroscopic Maxwell equations, in which the polarization field depends on the value of the electron–hole–pair density through the equation for the susceptibility. This set of equations, i.e., the microscopic equation for the susceptibility together with the macroscopic equations for the carrier density and for the light field, constitutes the combined microscopic and macroscopic approach to consistently describe

semiconductor nonlinearities.

16.1 The Light Field Equation

Before we discuss two examples of optical bistability in semiconductors, we present a systematic derivation of the relevant equations. Wave propagation in dielectric media is described by

$$\left(\nabla^2 - \text{grad}\,\text{div} - \frac{1}{c^2}\frac{\partial^2}{\partial t^2}\right)\mathcal{E} = \frac{4\pi}{c^2}\frac{\partial^2 \mathcal{P}}{\partial t^2} \ , \tag{16.1}$$

where Maxwell's equations request div $\mathbf{D} = 0$, since we assume no external charges. However, div $\mathcal{E} = -\mathcal{E}\frac{\nabla\epsilon}{\epsilon} = -\mathcal{E}\cdot\nabla\ln(\epsilon)$, where ϵ is the medium dielectric constant, is generally not zero. Therefore, the electromagnetic field is no longer purely transverse but also has a longitudinal component.

To obtain the equations for the longitudinal and transverse variations of the field amplitudes, we assume a Gaussian incident light beam

$$\mathcal{E} = \mathcal{E}_0\, e^{-r^2/w_0^2}, \quad r^2 = x^2 + y^2 \ ,$$

with a characteristic (transverse) width w_0 which propagates in z direction. Using the ansatz

$$\begin{aligned}
\nabla &= \mathbf{e}_T\nabla_T + \mathbf{e}_z\frac{\partial}{\partial z} \\
\mathcal{E} &= e^{-i(\omega t - kz)}(\mathbf{e}_T\,\mathcal{E}_T + \mathbf{e}_z\,\mathcal{E}_z) \\
\mathcal{P} &= e^{-i(\omega t - kz)}(\mathbf{e}_T\,\mathcal{P}_T + \mathbf{e}_z\,\mathcal{P}_z) \ ,
\end{aligned} \tag{16.2}$$

we subdivide the wave equation (16.1) into a longitudinal and a transverse part. $\mathbf{e}_z$ and $\mathbf{e}_T$ in Eq. (16.2) are the unit vectors in z-direction and in the transverse directions, respectively. The transverse equation is

$$\begin{aligned}
&\nabla_T\left[\nabla_T\mathcal{E}_T + \left(ik + \frac{\partial}{\partial z}\right)\mathcal{E}_z\right] - \left(-k^2 + 2ik\frac{\partial}{\partial z} + \frac{\partial^2}{\partial z^2} + \nabla_T^2\right)\mathcal{E}_T \\
&= \frac{1}{c^2}\left(\omega^2 + 2i\omega\frac{\partial}{\partial t} - \frac{\partial^2}{\partial t^2}\right)\left(\mathcal{E}_T + 4\pi\mathcal{P}_T\right) \ ,
\end{aligned} \tag{16.3}$$

and the longitudinal equation is

$$\left(ik + \frac{\partial}{\partial z}\right) \nabla_T \mathcal{E}_T - \nabla_T^2 \mathcal{E}_z = \frac{1}{c^2}\left(\omega^2 + i2\omega\frac{\partial}{\partial t} - \frac{\partial^2}{\partial t^2}\right)\left(\mathcal{E}_z + 4\pi\mathcal{P}_z\right) \ . \quad (16.4)$$

As usual, the polarization is related to the optical susceptibility or the dielectric function via

$$\mathcal{P}_{z,T} = \chi\mathcal{E}_{z,T} = \frac{\epsilon - 1}{4\pi}\mathcal{E}_{z,T} \ . \quad (16.5)$$

It is now convenient to split the susceptibility into the linear part χ_0 and the nonlinear, density-dependent part χ_{nl}

$$\chi = \chi_0 + \chi_{nl}(N) = \frac{\epsilon_0 - 1}{4\pi} + \frac{\epsilon_{nl}(N)}{4\pi} \ . \quad (16.6)$$

Even though we explicitly deal with a density-dependent nonlinearity, this treatment can easily be generalized to also include, e.g., thermal and other nonlinearities. To derive the coupled equations for the longitudinal and transverse field components from Eqs. (16.3) and (16.4), we use the so-called paraxial approximation, see Lax *et al.* (1975). Scaled variables are introduced as

$$x = \bar{\mathrm{x}}\, w_0 \,; \quad y = \bar{\mathrm{y}}\, w_0 \,; \quad z = \bar{\mathrm{z}}\, l \,; \quad t = \bar{\mathrm{t}}\, \tau_R \ , \quad (16.7)$$

where

$$l = k w_0^2 \quad (16.8)$$

is the diffraction length of the beam in z direction, $\tau_R = l\, n_b/c$ is the characteristic propagation time over that distance, $n_b = \sqrt{\epsilon_0}$ and $\omega = ck/n_b$. The dimensionless number

$$f = \frac{w_0}{l} << 1 \quad (16.9)$$

serves as small parameter allowing us to expand all quantities in powers of f. Consistent equations are obtained using

$$\begin{aligned} \mathcal{E}_T &= \mathcal{E}_T^{[0]} + f^2\mathcal{E}_T^{[2]} + \cdots \ , \\ \mathcal{E}_z &= f\mathcal{E}_z^{[1]} + f^3\mathcal{E}_z^{[3]} + \cdots \ , \\ \chi_{nl} &= f^2\chi_{nl}^{[2]} + f^4\chi_{nl}^{[4]} + \cdots \ . \end{aligned} \quad (16.10)$$

Inserting Eqs. (16.9) and (16.10) into Eqs. (16.3) and (16.4) yields a set of coupled equations in the orders $\mathcal{O}(f)$, $\mathcal{O}(f^3), \cdots$. Restricting ourselves to $\mathcal{O}(f)$, we obtain

$$k\mathcal{E}_z^{[1]} = i\,\nabla_T\,\mathcal{E}_T^{[0]} \tag{16.11}$$

and

$$\left[\frac{\boldsymbol{c}}{\boldsymbol{n_b}}\frac{\boldsymbol{\partial}}{\boldsymbol{\partial_z}} - \boldsymbol{i}\frac{\boldsymbol{c}}{\boldsymbol{2kn_b}}\boldsymbol{\nabla_T^2} + \frac{\boldsymbol{\partial}}{\boldsymbol{\partial t}} + \frac{\boldsymbol{c\alpha(\omega,N)}}{\boldsymbol{2n_b}} - \boldsymbol{i}\frac{\boldsymbol{\omega\Delta n(\omega,N)}}{\boldsymbol{n_b}}\right]\boldsymbol{\mathcal{E}_T^{[0]}} = \boldsymbol{0}\ , \tag{16.12}$$

transverse field equation

where we used Eqs. (1.51), (1.50) to introduce absorption and refractive-index change,

$$\alpha(\omega,N) = \frac{4\pi\omega}{n_b c}\chi''(\omega,N) \quad \text{and} \quad \Delta n(\omega) \simeq \frac{2\pi\chi'_{nl}(\omega,N)}{n_b}\ , \tag{16.13}$$

respectively. Eq. (16.10) shows that the electromagnetic field is purely transverse in lowest order, but it may nevertheless depend on the transverse coordinate. Only in next order, there is a small longitudinal component whose size depends on f.

For simplicity of notation, we now replace $\mathbf{e}_T\,\mathcal{E}_T^{[0]}$ by $\mathcal{E}$. Through $\alpha(\omega,N)$ and $\Delta n(\omega,N)$, the field amplitude $\mathcal{E}$ is nonlinearly coupled to the electron–hole–pair density

$$N = \frac{1}{L^3}\sum_{\mathbf{k}} n_{e,\mathbf{k}} = \frac{1}{L^3}\sum_{\mathbf{k}} n_{h,\mathbf{k}}\ . \tag{16.14}$$

Note, that we use N for the electron–hole–pair density in this chapter to distinguish it clearly from the refractive index n.

16.2 The Carrier Equation

To obtain a dynamic equation for the total carrier density, we sum the equation for the carrier distribution, see Eq. (12.19)

$$\frac{dN}{dt} = -2\,\mathrm{Im}\frac{1}{L^3}\sum_{\mathbf{k}}\left\{\frac{1}{\hbar}\Big[d_{cv}\mathcal{E}(t) + \sum_{\mathbf{q}\neq\mathbf{k}} V_{|\mathbf{k}-\mathbf{q}|}P_{\mathbf{q}}(t)\Big]P^*_{\mathbf{k}}(t)\right\} \ , \qquad (16.15)$$

where we used the explicit expression (12.18) for the generalized Rabi frequency. We can convince ourselves that the Coulomb term in Eq. (16.15) does not contribute. To show this, we write

$$2\,\mathrm{Im}\sum_{\mathbf{k},\mathbf{q}} V_{|\mathbf{k}-\mathbf{q}|}P_{\mathbf{q}}P^*_{\mathbf{k}} = \mathrm{Im}\sum_{\mathbf{k},\mathbf{q}}\Big(V_{|\mathbf{k}-\mathbf{q}|}P_{\mathbf{q}}P^*_{\mathbf{k}} + V_{|\mathbf{q}-\mathbf{k}|}P_{\mathbf{k}}P^*_{\mathbf{q}}\Big) \ , \qquad (16.16)$$

where we interchanged $\mathbf{q} \longleftrightarrow \mathbf{k}$ in the second half of the sum. The RHS of this equation has the structure

$$\mathrm{Im}(A + A^*) = \mathrm{Im}(2\,\mathrm{Re}\,A) \equiv 0 \ . \qquad (16.17)$$

Hence, Eq. (16.15) simplifies to

$$\frac{dN}{dt} = -\frac{2}{\hbar}\,\mathrm{Im}\,\frac{1}{L^3}\sum_{\mathbf{k}} d_{cv}\mathcal{E}(t)P^*_{\mathbf{k}}(t) \ . \qquad (16.18)$$

Now, we express the time-dependent polarization through its Fourier transform, which we write as product of susceptibility and field,

$$\frac{dN}{dt} = -\frac{2}{\hbar}\,\mathrm{Im}\,\frac{1}{L^3}\sum_{\mathbf{k}} d_{cv}\mathcal{E}(t)\int\frac{d\omega}{2\pi}\chi^*_{\mathbf{k}}(\omega)\mathcal{E}^*(\omega)e^{i\omega t} \ , \qquad (16.19)$$

where we should remember, that the susceptibility function contains only the resonant term, since $P_{\mathbf{k}} = P_{he}(\mathbf{k})$, Eq. (12.9). For a monochromatic field of the form

$$\mathcal{E}(t) = \mathcal{E}_0 e^{-i\omega_0 t} \ , \qquad (16.20)$$

$$\mathcal{E}(\omega) = 2\pi\mathcal{E}_0\delta(\omega - \omega_0) \ , \qquad (16.21)$$

Eq. (16.19) yields

$$\frac{dN}{dt} = -\frac{1}{\hbar}\,\mathrm{Im}\,\mathcal{E}(t)\,\mathcal{E}_0\,\frac{1}{L^3}\sum_{\mathbf{k}} d_{cv}\,\chi^*_{\mathbf{k}}(\omega_0)\,e^{i\omega_0 t} \ . \qquad (16.22)$$

To take the imaginary part, we write

$$\mathrm{Im}\,\mathcal{E}(t)\,\mathcal{E}^*(t)\frac{1}{L^3}\sum_k d_{cv}\,\chi_k^*(\omega_0) = |\mathcal{E}(t)|^2\,\mathrm{Im}\,\frac{1}{L^3}\sum_k d_{cv}\,\chi_k^*(\omega_0)\ . \quad (16.23)$$

Hence, Eq. (16.22) becomes

$$\frac{dN}{dt} = \frac{1}{\hbar}|\mathcal{E}(t)|^2\chi''(\omega_0)\ , \quad (16.24)$$

where we evaluated the **k**-summation. Expressing the imaginary part of the susceptibility in terms of the intensity absorption coefficient, we get

$$\frac{dN}{dt} = |\mathcal{E}(t)|^2\frac{n_b c}{4\pi}\frac{\alpha(\omega_0)}{\hbar\omega_0} = \frac{\alpha(\omega_0)}{\hbar\omega_0}I\ , \quad (16.25)$$

where we introduced the intensity

$$I = |\mathcal{E}(t)|^2\frac{n_b c}{4\pi}\ . \quad (16.26)$$

Note, that in the spirit of the quasi-equilibrium approximation, the field amplitude and therefore also the intensity can be slow functions of time. Replacing ω_0 by ω and phenomenologically adding carrier recombination and diffusion, we write the rate equation for the carrier density N as

$$\boldsymbol{\frac{\partial N}{\partial t} = -\frac{N}{\tau} + \frac{\alpha(\omega, N)}{\hbar\omega}I + \nabla D\nabla N}\ . \quad (16.27)$$

electron–hole–pair rate equation

Here, τ is the carrier life time and D is the electron–hole–pair diffusion coefficient, also called the ambi-polar diffusion coefficient.

Eqs. (16.12) and (16.27), together with an expression for the nonlinear susceptibility determine the quasi-equilibrium nonlinear optical response of semiconductors. Note, that this approach involves the adiabatic elimination of the polarization dynamics, which is often justified if the field variations are slow compared to the fast phase destroying processes.

16.3 Bistability in Semiconductor Resonators

Dispersive optical bistability or bistability through decreasing absorption may be obtained if a semiconductor is brought into an optical resonator, which introduces the required feedback for the light field. In the following, we consider a Fabry–Perot resonator (Fig. 16.1) consisting of two lossless mirrors of reflectivity R and transmissivity $T = 1 - R$. The nonlinear semiconductor material fills the space between the mirrors. In many practical applications, the mirrors are actually the end faces of the semiconductor crystal itself, and R is just the natural reflectivity, or R is increased through additional high reflectivity coatings evaporated onto the semiconductor surfaces.

As shown schematically in Fig. 16.1, it is useful to decompose the complex transverse field amplitude $\mathcal{E}$ into the forward and backward propagating parts to treat the feedback introduced by the mirrors. We write

$$\mathcal{E} = \mathcal{E}_F + \mathcal{E}_B = \xi_F e^{-i\phi_F} + \xi_B e^{i\phi_B} \quad , \tag{16.28}$$

where the amplitudes ξ and the phases ϕ are real quantities. Depending on the phase relation between $\mathcal{E}_F$ and $\mathcal{E}_B$, there can be either constructive or destructive interference, leading to a maximum or minimum of the light intensity transmitted through the etalon.

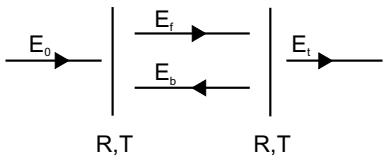

Fig. 16.1 Schematic drawing of a Fabry-Perot etalon. The mirrors have reflectivity R, transmissivity $T = 1 - R$, and E_o, E_f, E_b, E_t are incident, forward traveling, backward traveling, and transmitted field, respectively.

Dominantly dispersive nonlinearities can be observed in semiconductors, since the refractive index of the medium changes via the carrier density with the light intensity, causing the optical path between the mirrors of the etalon to change with intensity. These intensity-induced changes tune the etalon in or out of resonance with light of a fixed frequency. In reality, absorptive and dispersive changes occur simultaneously, but either one may

be dominant in a particular frequency regime.

The boundary conditions of the Fabry-Perot resonator can be written as

$$\mathcal{E}_F(z=0) = \sqrt{T}\,\mathcal{E}_0 + \sqrt{R}\,\mathcal{E}_B(z=0) \tag{16.29}$$

$$\mathcal{E}_B(z=0) = \sqrt{R}\,\mathcal{E}_F(z=L)e^{i\beta/2-\alpha_{tot}L/2} \tag{16.30}$$

$$\mathcal{E}_F(z=L) = \frac{\mathcal{E}_t}{\sqrt{T}} = \mathcal{E}_F(z=0)e^{i\beta/2-\alpha_{tot}L/2} \ , \tag{16.31}$$

yielding

$$\left|\frac{\mathcal{E}_t}{\mathcal{E}_0}\right|^2 = \frac{T^2}{(e^{\alpha_{tot}L/2} - Re^{-\alpha_{tot}L/2})^2 + 4R\sin^2(\beta/2)} \ , \tag{16.32}$$

where we used

$$\cos(\beta) = 1 - 2\sin^2(\beta/2) \ .$$

The effective absorption α_{tot}, as well as the phase shift β still have to be computed. The total phase shift of the light after passing through the resonator can be written as

$$\beta = \phi_F(z=L) - \phi_B(z=L) - 2\delta \ , \tag{16.33}$$

where 2δ contains all carrier-density-independent phase shifts of the linear medium and of the mirrors. If we ignore transverse variations, and insert Eq. (16.28) into Eq. (16.12), we obtain for the field amplitudes

$$\left(\frac{\partial}{\partial t} + \frac{n_b}{c}\frac{\partial}{\partial t} + \frac{\alpha(\omega,N)}{2}\right)\xi_{F,B} = 0 \ , \tag{16.34}$$

and for the phases

$$\left(\frac{\partial}{\partial z} + \frac{n_b}{c}\frac{\partial}{\partial t}\right)\phi_{F,B} = \mp\frac{\omega\Delta n(\omega,N)}{c} \ , \tag{16.35}$$

where the minus sign is for ϕ_F.

Most semiconductor bistability experiments are done for resonator lengths $L \simeq 0.5 - 2\mu m$. Under these conditions, the round-trip time for the light in the resonator is substantially shorter than the carrier relaxation

time τ and it is justified to adiabatically eliminate the dynamics of the light field (bad cavity limit),

$$\frac{\partial \xi}{\partial t} \simeq 0 \text{ and } \frac{\partial \phi}{\partial t} \simeq 0 \ . \tag{16.36}$$

Solving Eqs. (16.34) and (16.35) for these conditions yields

$$\xi_{F,B}(z) = \xi_{F,B}(0) \exp\left\{-\frac{1}{2}\int_0^z dz'\, \alpha\big[N(z')\big]\right\} \tag{16.37}$$

and

$$\phi_{F,B}(z) = \mp\frac{\omega}{c}\int_0^z dz' \Delta n\big[N(z')\big] \ , \tag{16.38}$$

showing that α_{tot} and β in Eq. (16.32) are given by

$$\alpha_{tot} = \frac{1}{L}\int_0^L dz\, \alpha[N(z)] \tag{16.39}$$

and

$$\frac{\beta}{2} = -\left\{\delta + \frac{\omega}{c}\int_0^L dz\, \Delta n\big[N(z)\big]\right\} \ . \tag{16.40}$$

The spatial carrier distribution $N(z)$ has to be computed from Eq. (16.27).

To describe typical semiconductor etalons, it is often a good approximation to neglect all spatial density variations (diffusion dominated case). Then one can trivially evaluate the integrals in Eqs. (16.39) and (16.40), and Eq. (16.32) becomes

$$\boldsymbol{I_t = \frac{T^2 I_0}{\left[e^{\alpha(\omega,N)\frac{L}{2}} - Re^{-\alpha(\omega,N)\frac{L}{2}}\right]^2 + 4R\,\sin^2\left[\delta + \omega\Delta n(\omega,N)\frac{L}{c}\right]}} \ . \tag{16.41}$$

transmission through a resonator

Eq. (16.41) is the well-known equation for the transmission of a Fabry-Perot etalon. This transmission exhibits peaks whenever the argument of the $\sin^2$-term equals integer multiples of π.

Through α and Δn, Eq. (16.41) is coupled to the spatially averaged rate equation (16.27)

$$\frac{dN}{dt} = -\frac{N}{\tau} + \frac{\alpha(\omega, N)}{\hbar\omega} I \ , \tag{16.42}$$

where I has to be taken as the average intensity inside the resonator

$$I \simeq I_t \frac{1+R}{T} \ . \tag{16.43}$$

Note, that the incident intensity I_0 in Eq. (16.41) may still be time-dependent, but all variations have to be slow on the time scale of the resonator round-trip time (adiabatic approximation).

To explicitly solve Eqs. (16.41) – (16.43) for an example of practical interest, we use the band-edge nonlinearities of room-temperature GaAs (Fig. 15.8) as obtained from the theory in Sec. 15.3. Inserting the computed $\alpha(N)$ and $\Delta n(N)$ into Eqs. (16.41) – (16.43) allows us to directly study nonlinear optical device performance. We obtain bistable hysteresis curves by plotting transmitted intensity versus input intensity. In Fig. 16.2, we show some typical results for slightly different resonator lengths L, i.e., for different detunings of the excitation frequency ω with respect to the nearest resonator eigenfrequency $\omega_R < \omega$, where

$$\omega_R = m\frac{\pi c}{L n_b} \, , \, m = 0, 1, 2, \cdots \ . \tag{16.44}$$

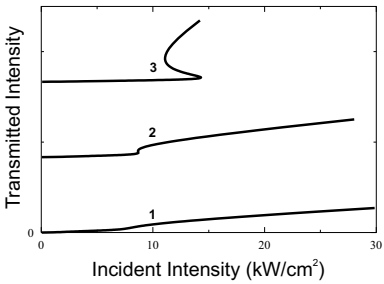

Fig. 16.2 Optical bistability for GaAs at $T = 300$ K, as computed from Eq. (16.41) using the absorption and refractive index data shown in Fig. 15.8. The mirror reflectivity $R = 0.9$, the resonator lengths are 2.0168 μm (1), 2.0188 μm (2), and 2.0233 μm (3), respectively, and the operating frequency ω is chosen such that $(\hbar\omega - E_g)/E_0 = -4$.

Curve 2 in Fig. 16.2 shows marginal and curve 3 shows well developed optical bistability for some range of input intensities, whereas curve 1 exhibits only nonlinear transmission.

For a situation similar to the one in curve 3 of Fig. 16.2, a stability analysis shows that the intermediate branch with the negative slope is unstable and therefore not realized under usual experimental conditions. Hence, increasing the incident intensity I_0 from 0 leads to a transmitted intensity I_t that follows the lower bistable branch until I_0 reaches the switch-up intensity, denoted by B in Fig. 16.3, then I_t follows the upper branch. On the other hand, lowering I_0 from an original value $I_0 > B$ leads to a transmission following the upper branch, until I_0 reaches the switch-down intensity, denoted by A in Fig. 16.3.

Optically nonlinear or bistable semiconductor etalons may be used as all-optical logic or switching devices, see Gibbs (1985). Since the bistable etalon maintains one of two discrete output states for some range of input intensity, it is possible to use it in the so-called *latched mode*. In that case, one divides the total input beam into several beams, which may serve as *holding beam* or *switching beam(s)*. The holding beam has an intensity positioned between the switch points of the bistable loop (A and B in Fig. 16.3) and is used to bias the device. The switching beam — which actually is the input logic beam — then only has to be sufficiently large for the total incident intensity to exceed the switch-up threshold B. The device, once switched, would remain in a high transmission state even if the switching beam is removed. It has to be turned off by interrupting its bias power or by some other mechanism.

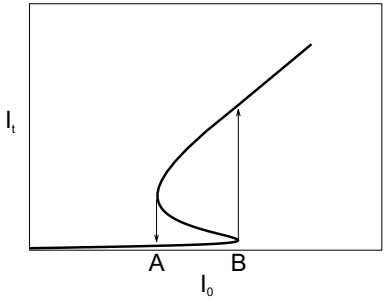

Fig. 16.3 Optical bistability for GaAs at $T = 300$ K, where B, A denote the switch-up and switch-down intensities.

In this latched mode of operation, one can obtain signal amplification. When a nonlinear etalon is operated as a passive device, it obviously has no overall gain relative to the total incident power. However, it is possible to achieve differential gain, in which case the device is able to transmit a larger signal than the signal used to switch it. Differential gain makes it possible to use the output of one device as input (switching beam) for one or more other devices. This process is called *cascading* and the number of devices that can be switched with the output of a single device is usually referred to as *fan-out*. Using two beams as input in addition to the proper bias beam makes it possible to realize all-optical gates which perform logic functions, such as AND, OR, or NOR.

16.4 Intrinsic Optical Bistability

From a conceptual point of view, the simplest example of optical bistability is obtained, if one considers a medium whose absorption increases with increasing excitation density. Bistability in such a system may occur without any external feedback since the system provides its own internal feedback. Increasing the carrier density leads to an increasing absorption that causes the generation of even more carriers, etc.. There are numerous mechanisms which may cause such an induced absorption in semiconductors and other systems. Here, we concentrate on the induced absorption which is observed in semiconductors like CdS at low temperatures, as a consequence of the band-gap reduction (Koch *et al.*, 1985). However, most of the macroscopic features discussed below are quite general and may very well also occur in other systems.

In Fig. 16.4, we show the absorption spectra for CdS, which have been computed using the theory of Sec. 15.3. For some frequencies below the exciton resonance, we see that the absorption increases with increasing carrier density. Assuming now that the semiconductor is excited at such a frequency below the exciton, one has only weak absorption for low intensities. Nevertheless, if the exciting laser is sufficiently strong, even this weak absorption generates a density of electron–hole pairs which causes a reduction of the semiconductor band gap. Eventually, the band edge shifts below the frequency of the exciting laser giving rise to a substantially increased one-photon absorption coefficient. Consequently, the absorption increases with increasing carrier density.

Since we want to emphasize here the general aspects of increasing ab-

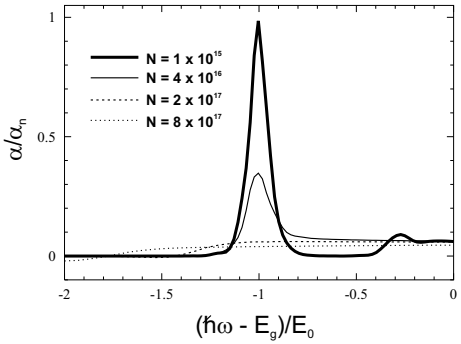

Fig. 16.4 Computed absorption spectra for CdS at $T = 30$ K. These results have been obtained using the theory of Sec. 15.3, with the parameters: $m_e = 0.235$, $m_h = 1,35$, $\epsilon_0 = 8.87$, $a_0 = 30.1$ Å, $E_0 = 27$meV, $\Gamma = 0.04E_0$, and $\alpha_n = 10^6/$cm.

sorption optical bistability, we do not use the original CdS data, but a simple generic model:

$$\alpha(N) = \begin{cases} \alpha_L\,, & N < N_1 \\ \alpha_L + (\alpha_H - \alpha_L)\,\sin\left[\frac{\pi(N-N_1)}{2(N_2-N_1)}\right]\,, & N_1 < N < N_2 \\ \alpha_H\,, & N_2 < N \end{cases} \tag{16.45}$$

Here, α_L and α_H denote the low and high absorption values.

The coupling between carrier density N and light intensity I is described by Eq. (16.27), which in the stationary, spatially homogeneous case leads to

$$\alpha(N) = \frac{N}{I}\frac{\hbar\omega}{\tau}\ . \tag{16.46}$$

This relation can be bistable, as indicated in Fig. 16.5, where we plot $\alpha(N)$, Eq. (16.45), and the straight line, which is the RHS of Eq. (16.46). The slope of this straight line is inversely proportional to I. The intersection points with the curve $\alpha(N)$ are the graphical solutions of Eq. (16.46), clearly showing the occurrence of three simultaneous solutions indicating intrinsic optical bistability without resonator feedback (see Fig. 16.6). It is worthwhile to stress at this point that for such an induced absorption bistability only a single pass of the light beam through the medium is required. Hence, one has no superposition of forward and backward traveling waves as, e.g.,

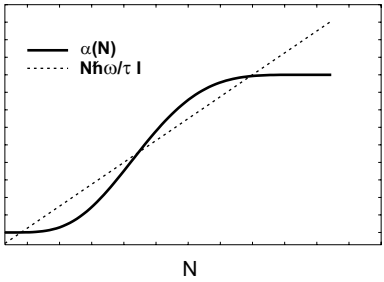

Fig. 16.5 Graphical solution of Eq. (16.46) using $\alpha(N)$ given by Eq. (16.45).

in the Fabry-Perot resonator. Therefore, one may neglect nonlinear dispersive effects as long as one is only interested in the characteristic variation of the transmitted intensity and not in transverse beam-profile variations or in diffraction effects.

To obtain an equation for the light intensity, we multiply Eq. (16.12) by $\mathcal{E}^*$ and add the complex conjugate equation

$$\left[\frac{\partial}{\partial t} + \frac{c}{n_b}\frac{\partial}{\partial z} + \frac{c}{n_b}\alpha(N)\right]\mathcal{E}\,\mathcal{E}^* = -\frac{ic}{2kn_b}\left(\mathcal{E}\nabla_T^2\mathcal{E}^* - \text{c.c.}\right) \ . \tag{16.47}$$

The RHS of Eq. (16.47) describes beam diffraction. This effect can be neglected if the length over which the light propagates is much smaller

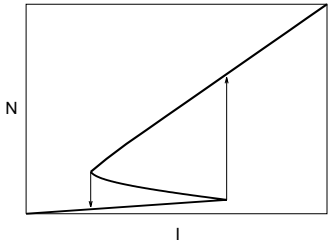

Fig. 16.6 Bistability of the carrier density N as function of intensity I, obtained as solution of Eq. (16.46). The lines with the arrows indicate switch-up of carrier density N when I is increased from 0, and switch-down when I is decreased from a sufficiently high value.

than the characteristic diffraction length. For a sufficiently thin sample, we can therefore approximate Eq. (16.47) as

$$\left[\frac{\partial}{\partial t} + \frac{c}{n_b}\frac{\partial}{\partial z} + \frac{c}{n_b}\alpha(N)\right] I = 0 \ . \tag{16.48}$$

If N is constant, the steady state solution of Eq. (16.48) is Beer's law

$$I(z) = I(z=0)e^{-\alpha(N)z} \ , \tag{16.49}$$

where $z = 0, L$ are the sample front and end faces, respectively. Eq. (16.49) shows that the transmitted intensity $I_t = I(z = L)$ is high (low) if $\alpha(N)$ is low (high).

If the carrier density exhibits optical bistability, as shown in Fig. 16.6, the corresponding transmitted intensity shows the hysteresis loop plotted in Fig. 16.7. We see that the transmitted intensity follows the input intensity I_0 for low I_0. When I_0 exceeds the value at which the carrier density switches to its high value, the sample absorption also switches up and the transmitted intensity switches down.

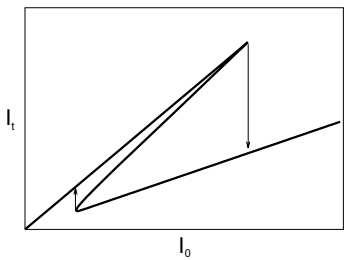

Fig. 16.7 Transmitted intensity versus input intensity for the carrier bistability shown in Fig. 16.6. The lines with the arrows indicate switch-down of the transmitted intensity I_t when the incident intensity $I_0 = I(z = 0)$ is increased from 0, and switch-up when I_0 is decreased from a sufficiently high value.

The described situation is experimentally relevant, if $D\tau/L^2 >> 1$, i.e., in the diffusion dominated case or for very thin semiconductor samples at the center of the input beam. Induced absorption bistability in CdS for these conditions has indeed been observed experimentally, and the experimental results are properly described by the outlined theory. In addition, there exist interesting longitudinal, transverse, and dynamic instabilities

in such induced absorbers. However, the discussion of these effects goes beyond the scope of this book.

REFERENCES

For the paraxial approximation in two-level systems see:

M. Lax, W.H. Louisell, and W.N. McKnight, Phys. Rev. **A11**, 1365 (1975)

The theory of Lax *et al.* (1975) has been generalized for the case of semiconductor nonlinearities in:

S.W. Koch and E.M. Wright, Phys. Rev. **A35**, 2542 (1987)

For reviews of optical bistability and its applications to optical logic see:

H.M. Gibbs. *Optical Bistability: Controlling Light with Light*, Academic Press (1985)
M. Warren, S.W. Koch, and H.M. Gibbs, in the special issue on integrated optical computing of IEEE *Computer*, Vol **20**, No. 12, *p.* 68 (1987)
From Optical Bistability Towards Optical Computing, eds. P. Mandel, S.D. Smith, and B.S. Wherrett, North Holland, Amsterdam (1987)

The theory of intrinsic optical bistability through band-gap reduction is discussed in:

S.W. Koch, H.E. Schmidt, and H. Haug, J. Luminescence **30**, 232 (1985)

PROBLEMS

Prolem 16.1: Derive Eqs. (16.11), (16.12) and the corrections of $O(f^2)$ applying the procedure outlined in the text.

Problem 16.2: Show that the resonator formula (16.32) satisfies all the boundary conditions specified in Eqs. (16.29) – (16.31).

Problem 16.3: Discuss dispersive optical bistability for the case of a Kerr medium with linear losses $\alpha = \alpha_0$ and $\Delta n = n_2 N$. Solve the coupled Eqs. (16.41) and (16.42) graphically and analyze the conditions for optical bistability.

Chapter 17

Semiconductor Laser

From a technological point of view, semiconductor light-emitting diodes are probably the most important electro-optical semiconductor devices. Whereas the majority of these diodes is used at relatively low power levels under spontaneous light emission conditions, suitably designed devices can operate as semiconductor lasers. These lasers are used for many applications in data communication with optical fibers, for data recording and processing (CD players, laser printers), and for optical control and display devices. Today, low-power semiconductor laser diodes have become relatively cheap mass products. Modern crystal growth techniques are used to engineer lasers with well specified device properties. Most of the presently available diodes are made from binary, ternary or quarternary III-V compounds to get an active material with the desired band gap and laser frequency. Microstructures with low optical losses have been developed and quantum confinement effects can be exploited to obtain low-threshold laser diodes. In addition to III-V compound lasers, narrow-gap semiconductor lasers, such as lead salt laser diodes, are used in the far infrared. Successful operation of quantum-well laser diodes in large parts of the visible region of the optical spectrum has been reported and quantum-dot laser structures are under active investigation for a wide variety of emission frequencies.

In this chapter, we discuss the physical principles and the quantum mechanical equations which govern the action of semiconductor lasers. For the rich spectrum of different device designs, we have to refer to special books on semiconductor lasers [e.g. Thompson (1980) or Agrawal and Dutta (1986)]. As in the description of passive bistable semiconductor devices in Chap. 16, we need the equations for the electrons in the semiconductor in combination with Maxwell's equations for the laser light. A classical treatment of the light field, if necessary supplemented with stochastic noise sources, is

sufficient as long as we are not interested in the photon statistics and other quantum mechanical aspects of the laser light. The electric field $E(t)$ is driven by the dielectric polarization $P(t)$ which in turn is determined by the inversion of the electrons, i.e., the electron–hole plasma density $N(t)$. The main difference compared to passive devices is that the field is generated by the laser itself, and the energy is supplied by a pump source, usually in form of an injection current. The resulting negative absorption provides the optical gain so that the spontaneously emitted light can grow into coherent laser light.

17.1 Material Equations

In laser diodes, one has a relatively dense quasi-thermal electron–hole plasma, in which the relaxation times are of the order of 100 fs, while the spontaneous lifetime in a direct-gap semiconductor is typically of the order of ns. The relaxation rate of the light field in the laser cavity is of the order of the cavity round-trip time, $\simeq 10$ ps, so that the polarization follows more or less instantaneously all changes of the electron-hole density and of the light field. Under these conditions the polarization dynamics can be eliminated adiabatically, and we can base our discussion on the equations derived in the previous chapter. However, we have to include additional terms into the equations for the field and the carrier density, in order to properly model the semiconductor laser configuration.

Instead of discussing the complex susceptibility χ in laser theory, one sometimes prefers to deal with gain, $g(\omega)$, and refractive index, $n(\omega)$, which are defined as

$$g(\omega) + 2ik_0\, n(\omega) = \frac{4\pi\omega}{n_b c}\Big[i\chi'(\omega) - \chi''(\omega)\Big] \ . \tag{17.1}$$

The gain function, $g(\omega)$, is the negative of the absorption coefficient, Eq. (1.53).

To keep the present analysis as simple as possible, we ignore all effects which lead to deviations from the quasi-equilibrium assumption, such as spectral, spatial, or kinetic hole burning. Hence, it is sufficient to use the electron–hole–pair rate equation (16.27) supplemented by laser specific terms. For the present purposes, we write this rate equation as

$$\frac{dN}{dt} = r_p - r_{st} - r_{sp} - r_{nr} \ , \tag{17.2}$$

where the different rates on the RHS describe injection pumping of carriers (r_p), stimulated emission (r_{st}), spontaneous emission (r_{sp}), and the nonradiative transitions (r_{nr}), respectively. Note, that the adiabatic elimination of the polarization and the local equilibrium assumption can only be justified if one is interested in time scales that are long in comparison to the inter-particle collision times.

The pump rate due to an injection current density j can be written as

$$r_p = \frac{j\eta}{ed} \ , \tag{17.3}$$

where η is the quantum efficiency and d the transverse dimension of the active region in the laser. The loss rate due to stimulated emission has been derived in the previous chapter, where it was discussed as generation rate due to light absorption:

$$r_{st} = \frac{g(\omega)}{\hbar\omega}\mathcal{E}_0^2\frac{n_b c}{8\pi} = -\frac{1}{2\hbar}\chi''(\omega)\mathcal{E}_0^2 \ . \tag{17.4}$$

Since the quasi-equilibrium susceptibility contains the factor

$$(1 - f_{e,k} - f_{h,k}) = (1 - f_{e,k})(1 - f_{h,k}) - f_{e,k}f_{h,k} \ , \tag{17.5}$$

we can always write its imaginary part as

$$\chi''(\omega) = \chi''_a(\omega) - \chi''_e(\omega) \ , \tag{17.6}$$

where the emission part

$$\chi_e \propto f_e f_h \ , \tag{17.7}$$

and the absorption part,

$$\chi_a \propto (1 - f_e)(1 - f_h) \ , \tag{17.8}$$

respectively. Eq. (17.7) shows that the probability for light emission out of a state is proportional to the joint probability to have an electron and hole in this state, whereas absorption, Eq. (17.8), requires that both states are unoccupied. For the *Padé* approximation of Chap. 15, this part is

$$\chi_e(\omega) = -\sum_{\mathbf{k}} \frac{|d_{cv,k}|^2 f_{e,k} f_{h,k}}{1 - q_1} \frac{1}{\hbar(\omega + i\delta - e_{e,k} - e_{h,k})} \ . \tag{17.9}$$

Using the subdivision of the susceptibility in Eq. (17.6), we can also divide the gain coefficient as

$$g(\omega) = -\frac{4\pi\omega}{cn_b}(\chi_a'' - \chi_e'') \equiv g_a - g_e \ , \tag{17.10}$$

where g_a and g_e are the probabilities per unit length for absorbing and emitting a photon, respectively. Thus $-g_e c/n_b$ is the emission probability of a photon per unit time.

The spontaneous emission rate into the continuum of all photon modes is with $\omega = \omega_{\mathbf{q},\lambda}$, where $\mathbf{q}$, λ label the photon wave vector and polarization,

$$r_{sp} = -\frac{1}{L^3}\sum_{\mathbf{q},\lambda}\frac{c}{n_b}g_e(\omega_{\mathbf{q},\lambda}) = 2\frac{4\pi}{(2\pi)^3}\int dq\, q^2 \frac{4\pi\omega}{\epsilon_0}\chi_e''(\omega_{\mathbf{q}}) \tag{17.11}$$

or

$$r_{sp} = \int_0^\infty \frac{d\omega}{2\pi\epsilon_0}\left(\frac{2\omega n_b}{c}\right)^3 \chi_e''(\omega) \ , \tag{17.12}$$

where we have used $n_b \simeq (\epsilon_0)^{1/2}$. The weight factor ω^3 shows that it is difficult for higher laser frequencies to overcome the losses due to spontaneous emission. This is one of the major problems in the development of an x-ray laser.

The nonradiative recombination rate has a linear term describing recombination under multi-phonon emission at deep traps levels. Additionally, in narrow-gap semiconductors and at high plasma densities, one often also has to consider Auger recombination processes. These processes are proportional to the third power of the plasma density, so that the total nonradiative recombination rate can be written as

$$r_{nr} = \frac{N}{\tau} + CN^3 \, . \tag{17.13}$$

The influence of the Auger recombination rates increase with decreasing gap energy. In infrared semiconductor lasers, this is often the dominant loss term.

17.2 Field Equations

In the semiclassical description for the semiconductor laser, we use the wave equation (16.1) and include an additional term proportional to the

conductivity σ to model the losses of the laser cavity:

$$\left(\nabla^2 - \text{grad div} - \frac{1}{c^2}\frac{\partial^2}{\partial t^2} - \frac{4\pi\sigma}{c^2}\frac{\partial}{\partial t}\right)\mathcal{E} = \frac{4\pi}{c^2}\frac{\partial^2 \mathcal{P}}{\partial t^2} \ . \tag{17.14}$$

In the simplest case, the cavity of a semiconductor laser is the resonator formed by the two parallel cleaved end faces of the crystal. To treat the space dependence of the electromagnetic field, we use an expansion in terms of orthonormal cavity eigenmodes $u_n(\mathbf{r})$:

$$\mathcal{E}(r,t) = \sum_n \mathcal{E}_n(t) u_n(\mathbf{r}) \ ,$$

and

$$\mathcal{P}(r,t) = \sum_n \mathcal{P}_n(t) u_n(\mathbf{r}) \ , \tag{17.15}$$

and equivalently for the polarization. The spatial eigenmodes fulfill the condition

$$(\nabla^2 - \text{grad div}) u_n(\mathbf{r}) = -\frac{\omega_n^2 \epsilon_0}{c^2} u_n(\mathbf{r}) \ , \tag{17.16}$$

where ω_n is the eigenfrequency of the nth resonator mode.

Expressing the polarization through the carrier-density-dependent susceptibility and the field,

$$\mathcal{P}_n = \frac{\epsilon_0 - 1}{4\pi}\mathcal{E}_n + \chi(N)\mathcal{E}_n \ , \tag{17.17}$$

we obtain, see problem (17.2),

$$\frac{d^2}{dt^2}\left\{\left[1 + \frac{4\pi}{\epsilon_0}\chi(N)\right]\mathcal{E}_n\right\} + \frac{\kappa c}{n_b}\frac{d\mathcal{E}_n}{dt} + \omega_n^2 \mathcal{E}_n = 0 \ , \tag{17.18}$$

where we introduced $\kappa c/n_b = 4\pi\sigma/\epsilon_0$ as the cavity loss rate.

Equation (17.18) for the field amplitude, together with the carrier rate equation (17.2) establish a simple model for the average properties of a semiconductor laser. To gain some insight into the laser action, we look for steady state solutions of Eqs. (17.18) and (17.2). For this purpose, we make the ansatz

$$\mathcal{E}_n = E_0\, e^{-i\omega_m t} \quad \text{and} \quad N = N_0 \ . \tag{17.19}$$

Inserting (17.19) into Eqs. (17.18) and (17.2) yields

$$\left[\omega_m^2 - \omega_n^2 + i\omega_m \frac{\kappa c}{n_b} + \frac{4\pi\omega_m^2}{\epsilon_0}\chi(N_0)\right] E_0 = 0 \ , \tag{17.20}$$

and

$$\frac{\chi''(N_0)}{2\hbar} E_0^2 - \frac{N_0}{\tau} + r_p = 0 \ , \tag{17.21}$$

where, for simplicity, we omitted the spontaneous emission and the nonlinear nonradiative recombination term CN^3 in Eq. (17.2). Separating real and imaginary parts of Eq. (17.20), we obtain the following coupled equations

$$\left[\kappa - g(N_0, \omega_m)\right] E_0 = 0 \ , \tag{17.22}$$

$$\left\{\omega_m^2 \left[1 + \frac{4\pi\chi'(N_0)}{\epsilon_0}\right] - \omega_n^2\right\} E_0 = 0 \ , \tag{17.23}$$

and

$$N_0 = \tau \left[r_p + \frac{\chi''(N_0)}{2\hbar} E_0^2\right] \ , \tag{17.24}$$

where Eq. (17.1) has been used to express the imaginary part of the susceptibility in Eq. (17.22) through the real part of the gain.

We see that Eqs. (17.22) – (17.24) have two regimes of solutions:

i) for $g(N_0, \omega_m) < \kappa$

$$E_0 = 0 \quad \text{and} \quad \frac{N_0}{\tau} = r_p \ , \tag{17.25}$$

ii) for $\kappa = g(N_0, \omega_m)$, the field $E_0 \neq 0$, and the solutions are

$$\kappa = g(N_0, \omega_m) \ , \tag{17.26}$$

$$\omega_m^2 = \frac{\omega_n^2}{1 + 4\pi\chi'(N_0)/\epsilon_0} \ , \tag{17.27}$$

and

$$E_0^2 = \left(\frac{N_0}{\tau} - r_p\right) \frac{2\hbar}{\chi''(N_0)} = \left(r_p - \frac{N_0}{\tau}\right) \frac{8\pi\hbar\omega_m}{c n_b g(N_0, \omega_m)} \ . \tag{17.28}$$

Eq. (17.25) yields a carrier density which increases linearly with the pump rate r_p, as long as the laser light field vanishes. If the carrier density is high enough, so that the gain $g(N_0, \omega_m)$ compensates the losses κ, the laser field E_0 begins to grow. The condition (17.26) describes the laser threshold, and Eq. (17.27) determines the operating frequency of the laser, which is pulled away from the cold cavity frequency ω_n. This *mode pulling* is caused by the refractive index changes due to the increased carrier density.

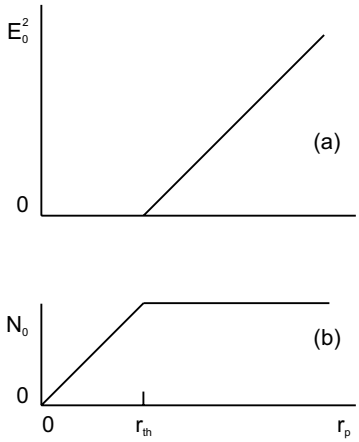

Fig. 17.1 (a) Intensity E_0^2 versus pump r_p showing the linear dependence of Eq. (17.28) above the threshold pump value r_{th}. (b) Carrier density N_0 versus r_p showing how N_0 is clamped at its threshold value according to the steady-state saturated-gain equals loss condition, Eq. (17.26).

Fig. 17.1 schematically shows the solutions (17.25) – (17.28). Assuming an originally unexcited system without electrons or holes, we increase the plasma density by increasing the pump rate r_p. The increasing plasma density then leads to growing gain g, until the gain equals the losses and the laser threshold is reached. Clearly the condition (17.26) is fulfilled first at that frequency which corresponds to the gain maximum. However, since the cavity modes ω_n are discretely spaced, one may not have an eigenmode directly at the gain maximum. In this case, the mode closest to the gain maximum starts to lase. The actual laser frequency ω_m is determined from

Eq. (17.27).

In our simple spatially homogeneous model, in which spectral hole burning is impossible due to the rapid carrier–carrier scattering, the plasma can support only one stable laser mode. Once the threshold of the first laser mode is reached, increased pumping does not increase the plasma density, but rather leads to an increase of the intensity of the lasing mode. At this point it should be noted that the laser equations derived in this chapter are valid only if the field is not too strong, since we did not include any high-field effects. Intensive laser beams may very well contribute to the energy renormalization for the electrons and holes. These radiative self-energy corrections describe the spectral hole burning, which for lasers gives rise to an extra gain saturation at high fields.

A sharp laser threshold as in Fig. (17.1) is usually not realized in experiments. The observed lasing transition is typically somewhat more gradual, due to the unavoidable presence of spontaneous emission into the laser mode and due to other noise sources in the laser. To include such effects, we have to extend our simple treatment to include dissipation and fluctuation contributions.

17.3 Quantum Mechanical Langevin Equations

In a more complete laser theory, we have to include the fluctuations, which are necessarily linked with dissipative processes. In the following, we discuss quantum mechanical *Langevin equations*, which provide a method that allows us to incorporate, at least approximately, dissipative processes and the connected fluctuations into the Heisenberg equations for a given quantum mechanical operator. With this method we obtain noise terms in the dynamic equations for the laser field and the reduced density matrix of the electronic excitations.

As an example, we first show for the harmonic oscillator that it is quantum mechanically inconsistent to have only dissipative terms in addition to the usual Heisenberg equation. The equation of motion for the Boson annihilation operator of the harmonic oscillator is

$$\frac{db}{dt} = \frac{i}{\hbar}[\mathcal{H}, b] = -i\omega b \ . \tag{17.29}$$

To include damping in the traditional way, we write

$$\frac{db}{dt} = \left(-i\omega - \frac{\kappa}{2}\right) b \ . \tag{17.30}$$

The solution of this equation is $b(t) = b(0)\exp[-i\omega + \kappa/2)t]$, and it is a simple exercise (see problem 17.1) to show that the commutator $[b(t), b^\dagger(t)]$ is not equal to one for all times. The damping term causes a decay of the commutator. We can correct this inconsistency by adding a fluctuation operator $f(t)$ to the equation of motion

$$\boldsymbol{\frac{db}{dt} = \left(-i\omega - \frac{\kappa}{2}\right) b(t) + f(t)} \ . \tag{17.31}$$

Langevin equation

For simplicity, we always assume in this book that the fluctuation operators can be described as Markovian noise sources. This means that the stochastic fluctuations at different times are uncorrelated (no memory)

$$\boldsymbol{\langle f(t) f^\dagger(s)\rangle = 2D\,\delta(t-s)} \ . \tag{17.32}$$

Markovian fluctuations

The average in Eq. (17.32) is taken over a reservoir to which the system must be coupled in order to introduce irreversible behavior. D is called the diffusion constant, which is related via the dissipation–fluctuation theorem to the damping constant κ.

To obtain an explicit form for the fluctuation operator and the dissipation rate, let us discuss the coupling of the harmonic oscillator to a reservoir (also called a bath), which consists of a large set of harmonic oscillators B_λ with a continuous energy spectrum $\hbar\Omega_\lambda$. We assume that the bath oscillators are all in thermal equilibrium and are not disturbed by the coupling to the harmonic oscillator which represents our system. In other words, we assume that the bath is infinitely large in comparison to the system of interest.

The total system-bath Hamiltonian is

$$\frac{\mathcal{H}}{\hbar} = \omega b^\dagger b + \sum_\lambda \Omega_\lambda \, B_\lambda^\dagger B_\lambda + \sum_\lambda g_\lambda \left(b B_\lambda^\dagger + B_\lambda b^\dagger \right) \ . \tag{17.33}$$

The equations of motion for the oscillators of the system and bath are

$$\frac{db}{dt} = -i\omega b - i \sum_\lambda g_\lambda B_\lambda$$

and

$$\frac{dB_\lambda}{dt} = -i\Omega_\lambda B_\lambda - i g_\lambda b \ . \tag{17.34}$$

Formally integrating the equation for the bath operator, we obtain

$$B_\lambda(t) = B_\lambda(0) e^{-i\Omega_\lambda t} - i g_\lambda \int_0^t d\tau \, b(\tau) \, e^{-i\Omega_\lambda (t-\tau)} \ . \tag{17.35}$$

Inserting this result into the equation for the system operator yields

$$\frac{db}{dt} = -i\omega b - i \sum_\lambda g_\lambda \left[B_\lambda(0) e^{-i\Omega_\lambda t} - i g_\lambda \int_0^t d\tau \, b(\tau) \, e^{-i\Omega_\lambda (t-\tau)} \right] \ , \tag{17.36}$$

which we write in the form

$$\frac{db}{dt} = -i\omega b + f(t) - \frac{\kappa}{2} b(t) \ . \tag{17.37}$$

Now, we identify

$$\frac{\kappa}{2} b(t) \simeq \sum_\lambda g_\lambda^2 b(0) e^{-i\Omega_\lambda t} \int_0^t d\tau \, e^{i(\Omega_\lambda - \omega)\tau} \simeq \left[\sum_\lambda g_\lambda^2 \, \pi \, \delta(\Omega_\lambda - \omega) \right] b(t) \ , \tag{17.38}$$

where we approximated $b(t) \simeq b(0) \exp(-i\omega t)$. In Eq. (17.38), we recognize Fermi's golden rule for the transition rate per unit time of an energy quantum $\hbar\omega$ into the continuous spectrum of the bath. Using the density of states $\rho(\omega) \simeq \rho$, assuming $g(\omega) \simeq g$, and integrating over all bath energies, we get the damping constant

$$\kappa = g^2 2\pi\rho \ . \tag{17.39}$$

The fluctuation operator $f(t)$ is given by the second term in Eq. (17.36) as

$$f(t) = -i \sum_{\lambda} g_\lambda B_\lambda(0) e^{-i\Omega_\lambda t} \ . \tag{17.40}$$

Obviously, if we average $f(t)$ over the bath $< \cdots >= tr\, \rho_B \ldots$, with

$$\rho_B = \frac{e^{-\beta H_B}}{tr\, e^{-\beta H_B}} \ , \tag{17.41}$$

we find $\langle f(t) \rangle = 0$. For the second moments, we get

$$\langle f^\dagger(t) f(s) \rangle = \sum_{\lambda} g_\lambda^2 \, \langle B_\lambda^\dagger(0) B_\lambda(0) \rangle \, e^{i\Omega_\lambda (t-s)} \simeq g^2 g_0(\omega) \rho 2\pi \delta(t-s) \ ,$$

or

$$\begin{aligned}
&\boldsymbol{\langle f^\dagger(t) f(s) \rangle = \kappa\, g_0(\omega) \delta(t-s)} \ , \\
&\boldsymbol{\langle f(t) f^\dagger(s) \rangle = \kappa \left[g_0(\omega) + 1 \right] \delta(t-s)} \ , \\
&\boldsymbol{\langle f(t) f(s) \rangle = 0} \text{ and } \boldsymbol{\langle f^\dagger(t) f^\dagger(s) \rangle = 0} \ .
\end{aligned} \tag{17.42}$$

dissipation-fluctuation theorem for harmonic oscillator

Here, $g_0(\omega) = \left[\exp(\beta\hbar\omega) - 1 \right]^{-1}$ is the thermal Bose distribution for the bath quanta. Eqs. (17.42) are called dissipation-fluctuation relations because they link the correlations of the fluctuations and the damping constant κ, which describes the dissipation rate. We see that our simple model yields, at least approximately, Markovian correlations for the fluctuations.

For the discussion of noise sources in the electron–hole system of the semiconductor laser, one needs a more general formulation of the quantum mechanical dissipation–fluctuation theorem. Following Lax (1966), we therefore write the general Langevin equation for a set of quantum mechanical variables O_μ as

$$\frac{d}{dt} O_\mu = A_\mu(\{O_\mu\}, t) + F_\mu(\{O_\mu\}, t) \ , \tag{17.43}$$

where the dissipation rates A_μ are calculated in second-order perturbation theory in the interaction of the system with its reservoirs, as shown above for the example of the harmonic oscillator. The Markov assumptions for the fluctuations are then:

$$
\begin{aligned}
&F_\mu(t) \text{ is independent of all } O_\mu(s) \text{ for } t > s \ ; \\
&\langle F_\mu(t) \rangle = 0 \ ; \\
&\langle F_\mu(t) F_\nu(s) \rangle = 2 D_{\mu\nu}\, \delta(t-s) \ . \qquad (17.44)
\end{aligned}
$$

In order to determine the generalized diffusion coefficients $D_{\mu\nu}$, we use the Langevin equation (17.43). We obtain $O_\mu(t+\Delta t)$, where Δt is a small time interval, from $O_\mu(t)$ as

$$
O_\mu(t+\Delta t) - O_\mu(t) = \int_t^{t+\Delta t} ds\, A_\mu(\{O_\mu\}, s) + \int_t^{t+\Delta t} ds\, F_\mu(\{O_\mu\}, s)
$$

or

$$
\Delta O_\mu \simeq A_\mu\, \Delta t + \int_t^{t+\Delta t} ds\, F_\mu(s) \ . \qquad (17.45)
$$

For the time derivative of the bilinear expression $\langle O_\mu(t) O_\nu(t) \rangle$, we find

$$
\begin{aligned}
\frac{d}{dt}\langle O_\mu(t) O_\nu(t)\rangle \simeq & \frac{1}{\Delta t}\Big[\langle O_\mu(t+\Delta t) O_\nu(t+\Delta t)\rangle - \langle O_\mu(t) O_\nu(t)\rangle\Big] \\
\simeq & \frac{1}{\Delta t}\Big[\langle (O_\mu(t)+\Delta O_\mu)(O_\nu(t)+\Delta O_\nu)\rangle - \langle O_\mu(t) O_\nu(t)\rangle\Big] \\
\simeq & \frac{1}{\Delta t}\Big[\langle O_\mu(t) \Delta O_\nu\rangle + \langle \Delta O_\mu\, O_\nu\,(t)\rangle + \langle \Delta O_\mu \Delta O_\nu\rangle\Big] \ .
\end{aligned}
$$

Using Eq. (17.45) we get

$$
\begin{aligned}
\frac{d}{dt}\langle O_\mu(t) O_\nu(t)\rangle \simeq & \langle O_\mu A_\nu\rangle + \langle A_\mu O_\nu\rangle \\
& + \frac{1}{\Delta t}\left[\langle O_\mu(t) \int_t^{t+\Delta t} ds\, F_\nu(s)\rangle + \langle \int_t^{t+\Delta t} ds\, F_\mu(s) O_\nu(t)\rangle\right] \\
& + \langle A_\mu(t) \int_t^{t+\Delta t} ds\, F_\nu(s)\rangle + \langle \int_t^{t+\Delta t} ds\, F_\mu(s) A_\nu(t)\rangle \\
& + \frac{1}{\Delta t}\langle \int_t^{t+\Delta t} ds\, F_\mu(s) \int_t^{t+\Delta t} ds'\, F_\nu(s')\rangle \ . \qquad (17.46)
\end{aligned}
$$

The terms in the second line of Eq. (17.46) do not contribute because $O_\mu(t)$ is not correlated with the fluctuations $F_\nu(s)$ for $t < s < t+\Delta t$ (see Eq. (17.44)). The terms in the third line are of third order in the

system-bath interaction and are neglected. Inserting the Markov assumption, Eq. (17.44), into the last line of Eq. (17.46), we get the result

$$\boldsymbol{2D_{\mu\nu} = \frac{d}{dt}\langle O_\mu O_\nu\rangle - \langle A_\mu O_\nu\rangle - \langle O_\mu A_\nu\rangle} \ . \tag{17.47}$$

dissipation–fluctuation theorem

According to Eq. (17.47), one has to calculate the time-derivative of the bath-averaged term $\langle O_\mu O_\nu\rangle$ and subtract the expressions which contain the linear dissipation rate A_μ in order to get the diffusion coefficients $D_{\mu\nu}$.

As an application of Eq. (17.47), we now use the example of spontaneous emission to calculate the diffusion coefficient for $n_{i,\mathbf{k}}$ and $P_{\mathbf{k}}$. Note, that we do not adiabatically eliminate the interband polarization dynamics in this example. For more details, see Haug and Haken (1967). The interaction Hamiltonian with the bath of photons is

$$\mathcal{H}_I = \sum \hbar d_{cv}\left(a^\dagger_{c,\mathbf{k}} a_{v,\mathbf{k}} B_\lambda + B^\dagger_\lambda a^\dagger_{v,\mathbf{k}} a_{c,\mathbf{k}}\right) \ , \tag{17.48}$$

where the index λ runs over the continuum of all photon modes. We assume that the bath is in the vacuum state $|0_\lambda\rangle$ without photons, so that only spontaneous emission and no absorption is possible. The change of the population density in the state $c, \mathbf{k}$ calculated in second-order perturbation theory is

$$\frac{d}{dt}\langle n_{c,\mathbf{k}}\rangle = -d_{cv}^2 \sum_\lambda \langle n_{c,\mathbf{k}}(1-n_{v,\mathbf{k}})\rangle\, \pi\delta(\epsilon_{ck} - \epsilon_{vk} - \Omega_\lambda) = \langle A_{n_{c,\mathbf{k}}}\rangle \ , \tag{17.49}$$

in agreement with Fermi's golden rule. In order to calculate the diffusion coefficient $D_{n_{c,\mathbf{k}},n_{c,\mathbf{k}}}$, we have to evaluate

$$\frac{d}{dt}\langle n_{c,\mathbf{k}} n_{c,\mathbf{k}}\rangle = \frac{d}{dt}\langle n_{c,\mathbf{k}}\rangle = \langle A_{n_{c,\mathbf{k}}}\rangle \ ,$$

so that

$$2D_{n_{c\mathbf{k}},n_{c\mathbf{k}}} = d_{cv}^2 \sum_\lambda \langle n_{c,\mathbf{k}}(1-n_{v,\mathbf{k}})\rangle\, \pi\delta(\epsilon_{ck} - \epsilon_{vk} - \Omega_\lambda) \ , \tag{17.50}$$

which describes the typical shot noise for population variables. In general, shot noise consists of the sum of all transition rates in and out of the considered state. Because we assume that no photons are present in the bath,

only emission processes, i.e., transitions out of the state $c, \mathbf{k}$ are possible. In local equilibrium, where $\langle n_{i\mathbf{k}} \rangle = f_{ik}$, we have to consider only the total number of electrons in one band. Because the optical transition probabilities at different $\mathbf{k}$-values are not correlated, one gets for the fluctuations of the total electron density N_c the result

$$2D_{N_c,N_c} = d_{cv}^2 \sum_{\lambda,\mathbf{k}} f_{ck}(1 - f_{vk})\, \pi\delta(\epsilon_{ck} - \epsilon_{vk} - \Omega_\lambda) \ , \tag{17.51}$$

which is just the total spontaneous transition rate. Similarly, one calculates the auto-correlation of the fluctuations of the polarization P_k

$$2D_{P_\mathbf{k},P_\mathbf{k}^\dagger} + 2D_{P_\mathbf{k}^\dagger,P_\mathbf{k}} = 2\gamma_k \big[f_{ck}(1 - f_{vk}) + f_{vk}(1 - f_{ck}) \big] \ . \tag{17.52}$$

These polarization fluctuations determine mainly the coherence properties of the semiconductor laser light.

The different dissipative contributions to the carrier rate equation (17.2) can be modeled by a coupling to a suitable bath. The resulting noise sources all have shot noise character (see e.g. Haug, 1967, 1969)

$$\frac{dN}{dt} = r_p - r_{st} - r_{sp} - r_{nr} + F_p + F_{st} + F_{sp} + F_{nr} \ . \tag{17.53}$$

The correlations of the fluctuations are discussed below.

Diode lasers are pumped by an injection current, which is driven by a voltage source via a serial resistor R_s. If the serial resistor is larger than the differential resistance of the diode, R_s suppresses the current fluctuations in the diode. The resulting pump noise is, as Yamamoto and Machida (1987) have shown, simply the Nyquist noise in the serial resistor

$$\langle F_p(t) F_p(s) \rangle = \frac{4k_B T}{e^2 L^3 R_s}\, \delta(t - s) \ . \tag{17.54}$$

Obviously, by increasing R_s one can essentially suppress the pump noise.

For the stimulated emission, we obtain from the generalized dissipation fluctuation theorem, Eq. (17.54),

$$\langle F_{st}(t) F_{st}(s) \rangle = \frac{|\mathcal{E}_0(t)|^2}{2L^3} \Big[\chi_a''(\omega) + \chi_e''(\omega) \Big]\, \delta(t - s) \ , \tag{17.55}$$

where we used Eqs. (17.1) and (17.6). In the evaluation of the various terms in Eq. (17.55), we had to take the expression for χ before the expectation

values were taken, i.e.,

$$f_{e,k} \rightarrow a^{\dagger}_{c,\mathbf{k}} a_{c,\mathbf{k}} \tag{17.56}$$

and correspondingly for the other population terms. A close inspection of Eq. (17.55) shows that $\langle F_{st}(t) F_{st}(s) \rangle$ is proportional to

$$f_e f_h + (1 - f_e)(1 - f_h) \ ,$$

which describes the sum of the interband transition rates due to the laser action.

The noise terms due to spontaneous emission have the correlation

$$\langle F_{sp}(t) F_{sp}(s) \rangle = \frac{r_{sp}}{L^3} \, \delta(t - s) \ , \tag{17.57}$$

and the nonradiative transition noise yields

$$\langle F_{nr}(t) F_{nr}(s) \rangle = \frac{r_{nr}}{L^3} \, \delta(t - s) \ . \tag{17.58}$$

17.4 Stochastic Laser Theory

The basic equations for our stochastic laser theory are (17.53) and (17.18) with an added noise term. To get a feeling for the solutions of these equations, we analyze the situation, where we have small fluctuations around the steady state values of Eqs. (17.26) – (17.28), which are now the mean (bath averaged) values. Following Vahala and Yariv (1983), we express all quantities in terms of their mean values and slowly varying amplitude and phase perturbations, i.e.,

$$\mathcal{E}_n = [E_0 + E(t)] e^{-i\left[\omega_m t - \phi(t)\right]} \ ,$$

$$N = N_0 + n(t) \ ,$$

and

$$\chi(N) = \chi(N_0) + \frac{\partial \chi}{\partial N_0} n(t) \ , \tag{17.59}$$

where the first-order Taylor coefficient is

$$\frac{\partial \chi}{\partial N_0} = \left. \frac{\partial \chi}{\partial N} \right|_{N = N_0} \ .$$

We insert (17.59) into Eq. (17.18) and linearize the resulting equation in terms of the perturbations $E(t)$, $\phi(t)$ and $n(t)$. As described in problem (17.4), we obtain

$$i2\omega_m \left(\frac{dE}{dt} + iE_0 \frac{d\phi}{dt} \right) + i\,\omega_m\, E_0 \frac{8\pi}{\epsilon_0} \frac{\partial \chi}{\partial N_0} \frac{dn}{dt} + \omega_m^2 \frac{4\pi}{\epsilon_0} \frac{\partial \chi}{\partial N_0} E_0\, n$$

$$+ \left[\omega_m^2 - \omega_n^2 + i\omega_m \frac{\kappa c}{n_b} + \frac{4\pi\omega_m^2}{\epsilon_0} \chi(N_0) \right] E_0 = F(t) \ . \tag{17.60}$$

On the RHS of Eq. (17.60) we added the classical Markovian noise term $F(t) = F'(t) + i\,F''(t)$ with

$$\langle F(t) \rangle = 0 \ ,$$

$$\langle F'(t) F'(t') \rangle = \langle F''(t) F''(t') \rangle = W \delta(t - t') \ ,$$

and

$$\langle F'(t) F''(t) \rangle = 0 \ , \tag{17.61}$$

where W is given by the rate of spontaneous emission into the laser mode. The expression for W can be determined from the quantum mechanical theory of Sec. 17-3.

Eq. (17.60) describes the field and phase perturbations which are coupled to the carrier density perturbations $n(t)$. Introducing the expansion (17.59) into the Langevin equation (17.53) for the carrier density yields

$$\frac{dn}{dt} + \frac{\partial \chi''}{\partial N_0} \frac{1}{2\hbar} E_0^2 n - \frac{\chi''(N_0) E_0 E}{\hbar} + \frac{n}{\tau} - \frac{\chi''(N_0)}{2\hbar} E_0^2 + \frac{N_0}{\tau} - r_p = F_n \ , \tag{17.62}$$

where, as in Sec. 17.2, we again omitted the spontaneous emission and the nonlinear nonradiative recombination term CN^3. F_n is the sum of the relevant noise contributions.

The perturbations of the carrier density and the field amplitude and phase have zero mean values. Therefore, taking the bath average of the coupled Eqs. (17.60) and (17.62), yields the steady state laser equations (17.22) – (17.24). Using these equations in Eqs. (17.60) and (17.62) gives

three coupled equations which link the amplitude, phase and carrier-density perturbations to the Langevin noise terms

$$\frac{dE}{dt} + E_0 \frac{4\pi}{\epsilon_0} \frac{\partial \chi'}{\partial N_0} \frac{dn}{dt} + E_0 \omega_m \frac{2\pi}{\epsilon_0} \frac{\partial \chi''}{\partial N_0} n = \frac{F''}{\omega_m} \ , \tag{17.63}$$

$$\frac{d\phi}{dt} + \frac{4\pi}{\epsilon_0} \frac{\partial \chi''}{\partial N_0} \frac{dn}{dt} - \omega_m \frac{2\pi}{\epsilon_0} \frac{\partial \chi'}{\partial N_0} n = -\frac{F'}{\omega_m E_0} \ , \tag{17.64}$$

and

$$\frac{dn}{dt} + \frac{n}{\tau_r} - \frac{\omega_r^2 \epsilon_0}{E_0 \omega_m 2\pi \partial \chi''/\partial N_0} E = F_n \ . \tag{17.65}$$

Here, we defined

$$\frac{1}{\tau_r} = \frac{1}{\tau} + E_0^2 \frac{\partial \chi''}{\partial N_0} \frac{1}{2\hbar} \ ,$$

$$\omega_r^2 = E_0^2 \omega_m \frac{2\pi}{\hbar \epsilon_0} \frac{\partial \chi''}{\partial N_0} \chi''(N_0) = -I_0 \kappa \frac{4\pi}{\hbar \epsilon_0} \frac{\partial \chi''}{\partial N_0} \ , \tag{17.66}$$

and

$$I_0 = E_0^2 \frac{c n_b}{8\pi} \ . \tag{17.67}$$

To appreciate these definitions, let us take the time derivative of the deterministic part of Eq. (17.65):

$$\frac{d^2 n}{dt^2} + \frac{dn}{dt} \frac{1}{\tau_r'} - \frac{\omega_r^2 \epsilon_0}{E_0 \omega_m 2\pi \partial \chi''/\partial N_0} \frac{dE}{dt} = 0 \ , \tag{17.68}$$

and eliminate $\frac{dE}{dt}$ using the deterministic part of Eq. (17.63). We obtain

$$\frac{d^2 n}{dt^2} + \frac{dn}{dt} \frac{1}{\tau_r'} + \omega_r^2 n = 0 \ , \tag{17.69}$$

where

$$\frac{1}{\tau_r'} = \frac{1}{\tau_r} + \frac{2\omega_r^2}{\omega_m} \frac{\partial \chi'/\partial N_0}{\partial \chi''/\partial N_0} \ . \tag{17.70}$$

Eq. (17.69) shows that the density exhibits damped oscillations, the so-called *relaxation oscillations*. The parameter combinations ω_r and τ_r' are the frequency and damping time of these relaxation oscillations for $\omega_R >> 1/\tau_r'$.

Eqs. (17.63) – (17.65) are coupled first-order differential equations which can be solved by Laplace transformation. From the resulting expressions for $E(t)$, $\phi(t)$, and $n(t)$ we can compute the autocorrelation functions, such as $\langle E(t+\tau)E(t)\rangle$. We obtain for the phase autocorrelation function, see problem (17.6),

$$\begin{aligned}\langle\phi(t+\tau)\phi(t)\rangle &= \frac{W}{4\omega_m^2 E_0^2}(1+\alpha^2)t \\ &\quad + [B_1\cos(\beta\tau) + B_2\sin(\beta|\tau|)]e^{-|\tau|/2\tau_r} \quad , \end{aligned} \tag{17.71}$$

where B_1 and B_2 are combinations of the constants entering Eqs. (17.63) – (17.65),

$$\beta^2 = \left(\omega_r^2 - \frac{1}{4\tau_r^2}\right)$$

and

$$\alpha = \frac{\partial\chi'/\partial N_0}{\partial\chi''/\partial N_0} \quad . \tag{17.72}$$

is the so-called *line-width enhancement factor.*

The laser line width is obtained from

$$\begin{aligned}\langle\mathcal{E}^*(t+\tau)\mathcal{E}(t)\rangle &\simeq E_0^2 e^{i\omega_m\tau} i\langle e^{i\left[\phi(t+\tau)-\phi(t)\right]}\rangle \\ &\simeq E_0^2 e^{i\omega_m\tau} e^{-\frac{1}{2}\langle\left[\phi(t+\tau)-\phi(t)\right]^2\rangle} \\ &\simeq E_0^2 e^{i\omega_m\tau} exp\Bigg\{-\frac{W}{8\omega_m^2 E_0^2}(1+\alpha^2)|\tau| \\ &\quad + e^{-|\tau|/\tau_r}\Big[B_1\cos(\beta\tau) + B_2\sin(\beta|\tau|)\Big] - B_1\Bigg\} \quad . \end{aligned} \tag{17.73}$$

Assuming for the moment $|\tau| >> \tau_r$, we obtain from Eq. (17.73)

$$\langle\mathcal{E}^*(t+\tau)\mathcal{E}(t)\rangle \simeq E_0^2 e^{i\omega_m\tau} e^{-\frac{W}{8\omega_m^2 E_0^2}(1+\alpha^2)|\tau|} \quad . \tag{17.74}$$

Fourier transformation of Eq. (17.74) yields the field spectrum

$$S_E(\omega) = \int_{-\infty}^{\infty} d\tau\, e^{-i\omega\tau} \langle \mathcal{E}^*(\tau)\mathcal{E}(0)\rangle$$
$$= E_0^2 \frac{\Delta\omega}{(\omega-\omega_m)^2 + (\Delta\omega/2)^2} \ , \tag{17.75}$$

where

$$\Delta\omega = \frac{W}{4\omega_m^2 E_0^2}(1+\alpha^2) \ . \tag{17.76}$$

Eq. (17.76) is the Schawlow–Townes line-width formula, except for the additional term α^2. Since α^2 is often larger than one in semiconductor gain media, the laser line width usually exceeds the Schawlow–Townes limit. Hence, the expression *line-width enhancement factor* for α. The expression (17.76) for the semiconductor laser line width has been derived first by Haug and Haken (1967), but only later has it been recognized that the line width enhancement factor α in semiconductors can be much larger than unity, because generally the density-dependent refractive changes of the complex gain function are quite large in semiconductors as compared to atomic systems.

Fourier transformation of the full correlation function (17.73) is not possible analytically. In order to show the basic features, we ignore the term proportional B_2 and approximate $\exp(-|\tau|/\tau_r) \simeq 1$, $\beta \simeq \omega_r$, assuming weakly damped relaxation oscillations. We use the associated series (Abramowitz and Stegun, 1972) for the modified Bessel functions I_n to write

$$e^{B_1[cos(\omega_r\tau)-1]} = I_0(B_1) + 2\sum_{n=1}^{\infty} I_n(B_1)\cos(n\omega_r\tau) \ . \tag{17.77}$$

Inserting our approximations and Eq. (17.77) into Eq. (17.73), and evaluating Eq. (17.75) yields

$$S_E(\omega) = E_0^2 \Delta\omega \sum_{n=-\infty}^{\infty} \frac{e^{-B_1} I_n(B_1)}{(\omega-\omega_m-n\omega_r)^2 + (\Delta\omega/2)^2} \ , \tag{17.78}$$

showing that the laser spectrum consists of a series of lines at $\omega = \omega_m + n\omega_r$.

An example of the spectrum is shown in Fig. 17.2. The main peak is at ω_m and the sidebands occur at multiples of the carrier relaxation oscillation

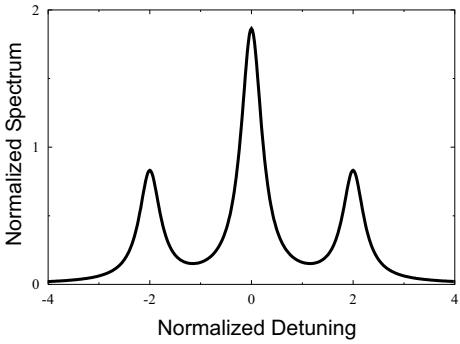

Fig. 17.2 Plot of the main mode and the first two sidemodes of the normalized laser spectrum, Eq. (17.75). For illustration, we choose the frequency of the relaxation oscillations $\omega_r = 2$, $B_1 = 1$, $\Delta\omega/\omega_r = 0.25$.

frequency. Such spectra, usually with stronger damped sidemodes, are indeed observed in semiconductor lasers above threshold, see, e.g., Thompson (1980) or Agrawal and Dutta (1986).

17.5 Nonlinear Dynamics with Delayed Feedback

A single-mode semiconductor laser diode displays a rich scenario of nonlinear dynamical effects with bistable, quasi-periodic and chaotic behavior, if one provides an optical feedback which couples a part of the emitted light field $E(t-\tau)$ with an appropriate delay τ back into the resonator. In order to get these instabilities, the delay-time has to be of the order of an inverse relaxation oscillation frequency, i.e. $\tau\omega_r \simeq 1$. Because the relaxation oscillation frequencies are typically in the MHZ-region, experimental realizations typically use the field from a distant optical reflector.

In the presence of delayed feedback, the appropriate field equation in the slowly varying amplitude approximation is

$$\left(\frac{d}{dt} - i\omega_0\right) E_0(t) = \frac{1}{2}\left[G(N) - \frac{1}{T_p}\right] E_0(t) + \eta E_0(t-\tau) \ , \qquad (17.79)$$

where η is the strength of the feedback. The intensity gain G differs by a factor of 2 from the amplitude gain g defined in (17.1). It is considered here

as a complex gain function, i.e. $G' = 2g$, while the imaginary part describes the dispersive influence. In terms of the complex dielectric function, the complex gain is $G = 8\pi i\omega\chi/(n_b c)$. Similarly, the inverse photon lifetime T_p is related to the cavity loss κ by $T_p^{-1} = 2\kappa$. The material equation is according to (17.2)

$$\begin{aligned}\frac{dN}{dt} &= r_p - r_{st} - r_{sp} - r_{nr} \\ &= r_p - G'I(t) - \frac{N}{T_N} \ .\end{aligned} \tag{17.80}$$

Writing the field $E_0 = \sqrt{I}e^{i(\omega_0 t+\Phi)}$ in terms of the intensity $I(t)$ and a phase $\Phi(t)$, the field equation yields

$$\frac{dI}{dt} = \left(G' - \frac{1}{T_p}\right) I(t) + 2\eta\sqrt{I(t)I(t-\tau)}\cos\big[\omega_0\tau + \Phi(t) - \Phi(t-\tau)\big] \ , \tag{17.81}$$

and

$$\frac{d\Phi}{dt} = \frac{1}{2}G''(N) - \eta\sqrt{\frac{I(t-\tau)}{I(t)}}\sin\big[\omega_0\tau + \Phi(t) - \Phi(t-\tau)\big] \, . \tag{17.82}$$

Next, we simplify the gain by linearizing it around its value at threshold. With $\Delta N = N - N_{thr}$, we get for the real part of the gain

$$G'(\Delta N) = G'(N_{thr}) + \frac{\partial G'(N)}{\partial N}\Delta N = \frac{1}{T_p} + A\Delta N \ , \tag{17.83}$$

where we used the fact that at threshold the gain equals the losses $\frac{1}{T_p}$. For the imaginary part, we introduce the line-width enhancement factor in the form

$$\alpha = -\frac{\partial G''/\partial N}{\partial G'/\partial N} \ , \tag{17.84}$$

compare (17.72) and write

$$G''(\Delta N) = G''(N_{thr}) + \frac{\partial G''}{\partial N}\Delta N = G''(N_{thr}) - \alpha A\Delta N \ . \tag{17.85}$$

For sufficiently strong laser fields, it may happen that the gain is spectrally deformed since the stimulated emission predominantly removes carriers that are in states energetically close to the laser resonance. This *spectral hole*

burning is often treated phenomenologically by introducing an intensity-dependent gain in the form

$$G'(\Delta N, I) = \frac{G'(\Delta N)}{1 + \epsilon I(t)} \simeq G'(\Delta N)\big[1 - \epsilon I(t)\big] \ , \tag{17.86}$$

where the expanded form can be used for weak saturation. This approximation can indeed be motivated by detailed studies of the scattering kinetics (see Schuster and Haug (1996)). Ignoring a constant phase shift, we obtain the following equations for the intensity, phase, and the deviations of the total carrier number from its threshold value

$$\frac{dI}{dt} = \left[G'(\Delta N, I) - \frac{1}{T_p}\right] I(t) + \eta\sqrt{I(t)I(t-\tau)}\cos\big[\omega_0\tau + \Phi(t) - \Phi(t-\tau)\big] \ , \tag{17.87}$$

$$\frac{d\Phi}{dt} = -\frac{\alpha}{2}A\Delta N(t) - \eta\sqrt{\frac{I(t-\tau)}{I(t)}}\sin\big[\omega_0\tau + \Phi(t) - \Phi(t-\tau)\big] \ , \tag{17.88}$$

and

$$\frac{d\Delta N}{dt} = \Delta r_p - G'(\Delta N, I)I(t) - \frac{\Delta N}{T_N} \ . \tag{17.89}$$

These equations are know as the Lang–Kobayashi equations.

As an application, we now analyze under which conditions a weak level of feedback can transform the relaxation oscillations of a semiconductor laser into self-sustained oscillations. In the relaxation oscillations, the carrier and photon numbers oscillate out of phase about their mean value. Because the oscillations are damped, they are usually present only after fast switching processes or as a consequence of noise. The delayed external feedback, however, can counteract the damping leading to stable oscillations. In terms of the parameters of the Lang-Kobayashi, (17.87) – (17.89), the relaxation oscillation frequency (17.66) becomes

$$\omega_r^2 = \frac{\partial G'}{\partial N}\Delta r_p \ . \tag{17.90}$$

This form shows that the relaxation oscillation frequency varies as the square root of the pump rate above threshold. Decomposing the phase into a part linear in time and an oscillating one, we get

$$\Phi(t) = \Delta\omega_0 t + \phi(t) \ . \tag{17.91}$$

The time average $< d\Phi(t)/dt >= \Delta\omega_0 t$ describes the shift of the laser frequency by the feedback. For external laser modes, which obey the condition

$$\omega_L = \omega_0 + \Delta\omega_0 = \frac{(2M - 1/2)\pi}{\tau} \ , \tag{17.92}$$

where M is a positive integer, the trigonometric functions simplify to

$$\cos\big[\omega_0\tau + \Phi(t) - \Phi(t-\tau)\big] = \sin\big[\phi(t) - \phi(t-\tau)\big] \ , \tag{17.93}$$

and

$$\sin\big[\omega_0\tau + \Phi(t) - \Phi(t-\tau)\big] = -\cos\big[\phi(t) - \phi(t-\tau)\big] \ . \tag{17.94}$$

The cos term can be replaced by its temporal average. Without this replacement, one would get additionally the contributions of the higher harmonics $2m\omega$ with $m = 1, 2, \ldots$. A detailed analysis shows further that under the chosen conditions one can use the following simplifications

$$\sqrt{I(t)I(t-\tau)} \simeq I_0 \quad \text{and} \quad \sqrt{I(t-\tau)/I(t)} \simeq 1 \ , \tag{17.95}$$

where I_0 is the stationary mean intensity value. As only oscillations with small amplitudes will be considered, one can linearize the product $G'(t)I(t)$ around its stationary value. Denoting the stationary values as I_0 and N_0, we define the oscillatory deviations $p(t)$ and $n(t)$ via

$$I(t) = I_0\big[1 + p(t)\big] \quad \text{and} \quad N(t) = N_0 + \frac{T_p n(t)}{\partial G'/\partial N} \ . \tag{17.96}$$

The mean photon number is

$$I_0 = \Delta r_p T_p' \ , \quad \text{where} \quad T_p' = \frac{T_p}{1 + \epsilon/(AT_n)} \simeq T_p \ . \tag{17.97}$$

The mean shift of the laser frequency is

$$\langle\dot{\Phi}\rangle = \eta\langle\cos\big[\phi(t) - \phi(t-\tau)\big]\rangle \ , \tag{17.98}$$

and the stationary carrier density is

$$N_0 = N_{thr} - \frac{\partial G'/\partial I}{\partial G'/\partial N} I_0 \ . \tag{17.99}$$

The equations of motion for $p(t), \phi(t),$ and $m(t)$ are

$$\frac{dp}{dt} = -2\Gamma_p p(t) + \frac{n(t)}{T_p} + 2\eta\sin\big[\phi(t) - \phi(t-\tau)\big] \ , \tag{17.100}$$

$$\frac{d\phi}{dt} = \frac{\alpha}{2T_p} n(t) \ , \tag{17.101}$$

and

$$\frac{dn}{dt} = -2\Gamma_n n(t) - \tilde{\Omega}^2 T_p p(t) \ . \tag{17.102}$$

Here, $\tilde{\Omega}$ is the relaxation oscillation frequency of the solitary laser $\tilde{\Omega}^2 = \omega_r^2 - (\Gamma_p + \Gamma_n)^2 \simeq \omega_r^2$. The damping rates Γ_p and Γ_n are given by

$$2\Gamma_p = -\frac{\partial G/\partial I}{\partial G/\partial N}\omega_r^2 T_p \quad \text{and} \quad 2\Gamma_n = \frac{1}{T_N} + \omega_r^2 T_p \ . \tag{17.103}$$

An approximative solution of these equations is obtained in the form of simple harmonic oscillations

$$\phi(t) = \frac{1}{2} a_\phi \cos(\omega t) \ , \tag{17.104}$$

$$p(t) = a_p \cos(\omega t - \mu_0), \ a_p = \frac{(\omega/\omega_r)^2 a_\phi}{\alpha \cos(\mu_0)}, \ \mu_0 = \arctan(\frac{2\Gamma_n}{\omega}) \ , \tag{17.105}$$

and

$$n(t) = -a_n \sin(\omega t) \quad \text{with} \quad a_n = \frac{\omega T_p}{\alpha} a_\phi \ . \tag{17.106}$$

The amplitude and period of the limit cycle is obtained from the equations of motion using the expansion $\sin(b\sin(x)) \simeq 2J_1(b)\sin(x)$, where $J_1(b)$ is the first order Bessel function. With $b = a_\phi \sin(\frac{\omega\tau}{2})$ one gets the implicit equation

$$\frac{b}{2J_1(b)} = \frac{\eta}{\eta_c} \ , \tag{17.107}$$

where the critical feedback strength η_c for the formation of the limit cycle with the period ω is given by

$$\eta_c = \left(\frac{\omega}{\omega_r}\right)^2 \frac{\Gamma_p + \Gamma_n}{\alpha \sin^2(\omega\tau/2)} \ . \tag{17.108}$$

Using a quadratic expansion of the Bessel function $2J_1(b)/b \simeq 1 - b^2/8$ one gets a square root law of the form

$$b = 2\sqrt{2}\sqrt{1 - \frac{\eta_c}{\eta}} \ , \tag{17.109}$$

which is typical for a so-called Hopf bifurcation. The frequency of the limit cycle is found from

$$\frac{\omega}{\omega_r} - \frac{\omega_r}{\omega} = \frac{2(\Gamma_n + \Gamma_p)}{\omega_r \tan(\omega\tau/2)} \quad . \tag{17.110}$$

This equation has in principle an infinite series of solutions. As an example, we consider feedback levels $\eta \geq \eta_c$, where only two solutions ω_i with $i = 1, 2$ are possible. In Fig. 17.3, we compare the analytical results to numerical solutions of the full equations. Fig. 17.3a shows the dominant characteristic frequencies of the two solutions and Fig. 17.3b displays the amplitudes of the intensity oscillations which are marked by the arrows in Fig. 17.3a. In Fig. 17.3c, we plot the parameter ranges in which the different stationary, single frequency (monostable) and bistable solutions appear.

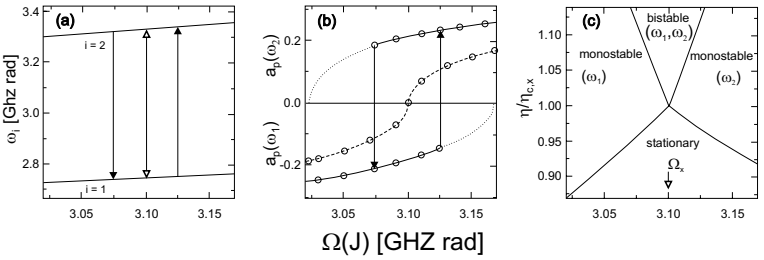

Fig. 17.3 Two bistable limit cycles as a function of the relaxation frequency $\Omega(J) = \omega_r(r_p)$, where $J = r_p$ is the pump current. (a) Frequencies of the two limit cycles. (b) Amplitudes of the oscillating photon density. The circles give the results of the numerical integration. (c) Critical feedback rates for the various types of solutions. The parameters are $\alpha = 6$, $T_p = 2\,\mathrm{ps}$, $T_n = 2\,\mathrm{ns}$, $\tau = 1\,\mathrm{ns}$, $(\partial \mathrm{G}'/\partial \mathrm{I})/(\partial \mathrm{G}'/\partial \mathrm{N}) = -4.6$. [According to Ritter and Haug (1993).]

The numerical solutions of the Lang-Kobayashi equations and the experimental findings of Mørk *et al.* (1990) confirm the calculated scenario for small feedback levels quite well. At higher feedback levels frequency doubling of the oscillations and quasi-periodic solutions arise, which finally go over into chaotic solutions. These chaotic solutions are characterized by strange attractors, which can be generated, e.g., by plotting the successive intensity maxima I_{n+1}^{max} versus I_n^{max} of the oscillations.

REFERENCES

M. Abramowitz and I.A. Stegun, *Handbook of Mathematical Functions* (Dover Publ., 1972)

For the general laser theory see:

H. Haken, *Laser Theory*, Handbuch der Physik Vol. *XXV/2c*, Springer, Berlin 1970
M. Lax, in 1966 Brandeis University Summer Institute of Theoretical Physics Vol. II, eds. M. Chretien, E.P. Gross, and S. Deser, Gordon and Breach, New York 1968
M. Sargent, M.O. Scully, and W. Lamb, *Laser Physics*, Addison-Wesley, Reading M. A. 1974

For the description of semiconductor lasers see:

A. Yariv, *Optical Electronics*, 3rd *ed.*, Holt, Rinehart and Winston, New York 1985
G.H.B. Thompson, *Physics of Semiconductor Laser Devices*, Wiley, Chichester 1980
G.P. Agrawal and N.K. Dutta, *Long-Wavelength Semiconductor Lasers*, Van Norstrand Reinhold, New York 1986
W.W. Chow and S.W. Koch, *Semiconductor-Laser Fundamentals*, Springer, Berlin, 1999

For semiconductor laser noise theory see:

H. Haug, Z. Physik **200**, 57 (1967); Phys. Rev. **184**, 338 (1969)
H. Haug and H. Haken, Z. Physik **204**, 262 (1967)
K. Vahala and A. Yariv, IEEE Journ. Quantum Electron. **QE-19**, 1096 and 1102 (1983)
Y. Yamamoto and S. Machida, Phys. Rev. **A35**, 5114 (1987)
H. Haug and S.W. Koch, Phys. Rev. **A39**, 1887 (1989)

For an analysis of the gain saturation see e.g.:

S. Schuster and H. Haug, JOSA B 13, 1605 (1996)

For a treatment of the nonlinear dynamics of semiconductor lasers with weak optical feedback see e.g.:

R. Lang and K. Kobayashi, IEEE JQE-16, 347 (1980)
A. Ritter and H. Haug, JOSA B 10, 130 and 145 (1993); and IEEE JQE-29, 1064 (1993)
J. Mørk, J. Mark, and B. Tromborg, Phys. Rev. Lett. 65, 1999 (1990)

PROBLEMS

Problem 17.1: Show that the commutator relation of the harmonic oscillator is violated if one includes only dissipation in the Heisenberg equation for b and $b^\dagger$.

Problem 17.2: Derive Eq. (17.18) for the field amplitudes from the wave equation (17.14). Use the eigenmode expansion (17.15) and $\chi(N=0)=0$, since the background susceptibility has been included in ϵ_0.

Problem 17.3: Use the general fluctuation–dissipation theorem, Eq. (17.47), to derive the diffusion coefficients, Eqs. (17.50) – (17.52).

Problem 17.4: Use the expansion (17.59) to derive Eq. (17.60) from Maxwell's wave equation (17.18). Hint: Neglect all second-order derivatives of the perturbations, all products of perturbations, terms proportional to $(\omega_m^2-\omega_n^2)E$, σE, $\sigma\phi$, and use

$$\left[1+\frac{4\pi\chi(N_0)}{\epsilon_0}\right]\begin{pmatrix}E\\ \phi\end{pmatrix}\simeq\begin{pmatrix}E\\ \phi\end{pmatrix}\ .$$

Problem 17.5: Solve Eqs. (17.63) – (17.65) using Laplace transformations.

Problem 17.6: Use the solutions of problem 17.5 to compute $\langle\phi(t+\tau)\phi(t)\rangle$. Hint: Keep decaying terms $\propto\exp(-\omega|\tau|)$, but neglect all terms proportional $\exp(-\omega t)$, for and $\omega>0$.

This page intentionally left blank

Chapter 18

Electroabsorption

An important tool in solid-state spectroscopy is the application of static electric or magnetic fields. These fields give rise to characteristic changes in the optical spectra yielding valuable information about the nature of the optical transitions. In this chapter, we discuss the effects of dc-electric fields on the absorption of bulk ($3D$) and quantum-well (quasi-$2D$) semiconductors showing that the field effects in the respective absorption spectra are remarkably different.

Applying an electric field to atomic systems causes a reduction of the overall symmetry, which leads to the splitting of degenerate levels and to field-dependent level shifts. This effect is called the (dc) Stark effect. If one applies an external electric field to a semiconductor, this field has a pronounced influence on the optically active electron–hole pairs. In comparison to these effects, it is often justified to disregard field-induced changes in the atomic orbits. Following this philosophy, we therefore describe the atomic orbits by the unperturbed Bloch functions and study the influence of the field on the relative motion of the electron–hole pair using effective mass approximation.

18.1 Bulk Semiconductors

In Chap. 10, we compute the semiconductor band-edge absorption spectrum for directly allowed optical transitions. The result can be written as

$$\alpha(\omega) = \alpha_b \sum_n |\psi_n(\mathbf{r}=0)|^2 \delta(E_n - \hbar\omega) \ , \tag{18.1}$$

where

$$\alpha_b = \frac{8\pi^2 |d_{cv}|^2 \omega}{n_b c} \ , \tag{18.2}$$

including a factor 2 from the spin summation. In Eq. (18.1), ψ_n and E_n are the eigenfunctions and energy eigenvalues of the electron–hole pair, respectively, where E_n includes the band-gap energy E_g.

If we disregard the Coulomb effects altogether, the stationary Schrödinger equation of the relative motion of the electron–hole pair in the presence of an electric field F (parallel to the z-axis) can be written as

$$\left(-\frac{\hbar^2 \Delta}{2m_r} - ezF - E_n \right) \psi_n(\mathbf{r}) = 0 \ . \tag{18.3}$$

To solve this equation, we make the ansatz

$$\psi_n(\mathbf{r}) = \frac{1}{L} e^{i(k_x x + k_y y)} \psi_n(z) \ , \tag{18.4}$$

where $L = V^{1/3}$ is the linear extension of the system. We write the energy eigenvalue as

$$E_n = \frac{\hbar^2}{2m_r} (k_{||}^2 + \kappa_n^2) \equiv E_{n,k_{||}} \ , \tag{18.5}$$

with $k_{||}^2 = k_x^2 + k_y^2$. Inserting Eqs. (18.4) and (18.5) into Eq. (18.3), we find

$$\left(\frac{d^2}{dz^2} + fz + \kappa_n^2 \right) \psi_n(z) = 0 \ , \tag{18.6}$$

where

$$f = eF \frac{2m_r}{\hbar^2} = \frac{eF}{E_0 a_0^2} \ , \tag{18.7}$$

and E_0 and a_0 are the usual excitonic units, defined in Chap. 10. Eq. (18.7) shows that $f a_0^3$ is the ratio between the dipole energy in the field and the exciton Rydberg energy, $ea_0 F/E_0$. Introducing the dimensionless variable Z by

$$Z = f^{1/3} z \tag{18.8}$$

and substituting

$$\zeta_n = Z + \kappa_n^2 f^{-2/3} = Z + (a_0\kappa_n)^2 \left(\frac{E_0}{a_0 eF}\right)^{2/3} \quad , \tag{18.9}$$

we find

$$\psi_n''(\zeta_n) = -\zeta_n \psi_n(\zeta_n) \ , \tag{18.10}$$

where $\psi_n''(\zeta) = d^2\psi_n/d\zeta^2$. The solution of Eq. (18.10) is

$$\psi_n(z) = a_n \, Ai(-\zeta_n) \ , \tag{18.11}$$

where $Ai(x)$ is the Airy function (Abramowitz and Stegun, 1972),

$$Ai(x) = \frac{1}{\pi}\int_0^\infty du \, \cos\left(\frac{u^3}{3} + ux\right) \ , \tag{18.12}$$

and a_n is a normalization constant. The Airy function decays exponentially for positive arguments

$$\lim_{x\to\infty} Ai(x) = \frac{1}{2\sqrt{\pi}x^{1/4}} \, e^{-\frac{2}{3}x^{3/2}} \left(1 - \frac{3c_1}{2x^{3/2}}\right) \ , \tag{18.13}$$

with $c_1 = 15/216$. For negative arguments, the Airy function oscillates,

$$\lim_{x\to\infty} Ai(-x) = \frac{1}{\sqrt{\pi}x^{1/4}} \sin\left(\frac{2}{3}x^{3/2} + \frac{\pi}{4}\right) \ , \tag{18.14}$$

expressing the accelerating action of the field. The normalization constant a_n is determined by

$$a_n^{-2} = \int_{-\infty}^{\infty} dz |Ai(-\zeta_n)|^2 = \lim_{L\to\infty} \int_{-L}^{L} dz |Ai(-\zeta_n)|^2 \ , \tag{18.15}$$

or, using Eqs. (18.8) and (18.9),

$$\frac{f^{1/3}}{a_n^2} = \lim_{L\to\infty} \int_{-Lf^{1/3}}^{Lf^{1/3}} dx \, |Ai(x)|^2 \ . \tag{18.16}$$

With partial integration we obtain

$$\int_{-Lf^{1/3}}^{Lf^{1/3}} dx |Ai(x)|^2 = xAi^2(x)|_{-Lf^{1/3}}^{Lf^{1/3}} - \int_{-Lf^{1/3}}^{Lf^{1/3}} dx 2x Ai(x) Ai'(x) \ . \tag{18.17}$$

Because $Ai(x)$ satisfies the differential equation

$$Ai''(x) = xAi(x) \ , \tag{18.18}$$

we get

$$\begin{aligned}\int_{-Lf^{1/3}}^{Lf^{1/3}} dx\,|Ai(x)|^2 &= xAi^2(x)|_{-Lf^{1/3}}^{Lf^{1/3}} - \int_{-Lf^{1/3}}^{Lf^{1/3}} dx\,2\,Ai''(x)\,Ai'(x) \\ &= xAi^2(x)|_{-Lf^{1/3}}^{Lf^{1/3}} - \int_{-Lf^{1/3}}^{Lf^{1/3}} dx\,\frac{d\big[Ai'(x)\big]^2}{dx} \\ &= \Big\{xAi^2(x) - \big[Ai'(x)\big]^2\Big\}|_{-Lf^{1/3}}^{Lf^{1/3}} \ . \end{aligned} \tag{18.19}$$

Inserting Eq. (18.19) into Eq. (18.16) yields

$$a_n^{-2} = \lim_{L\to\infty} \sqrt{\frac{L}{f^{1/3}}}\frac{1}{\pi} \ , \tag{18.20}$$

where we used the fact that $Ai(x)$ and $Ai'(x)$ vanish for $x \to \infty$. For $Ai(-x)$ and $Ai'(-x)$, we inserted the asymptotic expressions given by Eq. (18.14) and by

$$\lim_{x\to\infty} Ai'(-x) = \frac{x^{1/4}}{\sqrt{\pi}} \cos\left(\frac{2}{3}x^{3/2} + \frac{\pi}{4}\right) \ . \tag{18.21}$$

The energy eigenvalues are computed from the boundary condition

$$\psi_n(z = L) = 0 \tag{18.22}$$

as

$$\frac{2}{3}\sqrt{f}\left(L + \frac{\kappa_n^2}{f}\right)^{3/2} = \left(n - \frac{1}{4}\right)\pi \ . \tag{18.23}$$

Solving Eq. (18.23) for κ_n and inserting the result into Eq. (18.5) yields

$$E_{n,k_{||}} = \frac{\hbar^2}{2m_r}\left\{k_{||}^2 - Lf + \left[\frac{3\pi f}{2}(n - 1/4)\right]^{2/3}\right\} \ . \tag{18.24}$$

Now, we have all the ingredients needed to evaluate Eq. (18.1), which we write as

$$\alpha(\omega) = \alpha_b \int_{-\infty}^{\infty} \frac{dk_x}{2\pi} \int_{-\infty}^{+\infty} \frac{dk_y}{2\pi} \sum_n \frac{\pi f^{1/3}}{\sqrt{L}} \delta(E_{n,k_{||}} + E_g - \hbar\omega)$$
$$\times \left| Ai\left[f^{-2/3} \left(k_{||}^2 - \frac{2m_r E_{n,k_{||}}}{\hbar^2} \right) \right] \right|^2 \quad . \tag{18.25}$$

We change the sum over n to an integral over E

$$\sum_n \rightarrow \int_0^{\infty} dE \, \frac{dn}{dE} \tag{18.26}$$

and evaluate the density of states using Eq. (18.23)

$$\frac{dn}{dE} = \frac{2m_r}{\hbar^2 \pi \sqrt{f}} \left(L + \frac{\kappa_n^2}{f} \right)^{1/2} \simeq \frac{2m_r}{\hbar^2 \pi \sqrt{f}} \sqrt{L} \quad . \tag{18.27}$$

We dropped the additive term in $L + \kappa_n/f$, since we are finally interested in the limit $L \rightarrow \infty$, see above. Inserting Eq. (18.26) and (18.27) into Eq. (18.25) yields

$$\alpha(\omega) = \alpha_b \int_0^{\infty} \frac{dk_{||}^2}{(2\pi)^2} \frac{2m_r}{\hbar^2 f^{1/3}} \left| Ai\left\{ f^{-2/3} \left[k_{||}^2 + \frac{2m_r(E_g - \hbar\omega)}{\hbar^2} \right] \right\} \right|^2$$
$$= \frac{\alpha_b}{2\pi} \frac{m_r f^{1/3}}{\hbar^2} \int_{\epsilon}^{\infty} dx \, |Ai(x)|^2 \quad , \tag{18.28}$$

where

$$\epsilon = \frac{2m_r(E_g - \hbar\omega)}{\hbar^2 f^{2/3}} = \frac{E_g - \hbar\omega}{E_0} \left(\frac{E_0}{e a_0 F} \right)^{2/3} \quad . \tag{18.29}$$

Again, we evaluate the integral in Eq. (18.28) by partial integration, following the steps in Eqs. (18.16) – (18.19). The result is

$$\int_{\epsilon}^{\infty} dx \, |Ai(x)|^2 = -\epsilon Ai^2(\epsilon) + [Ai'(\epsilon)]^2 \quad . \tag{18.30}$$

The total absorption spectrum is thus

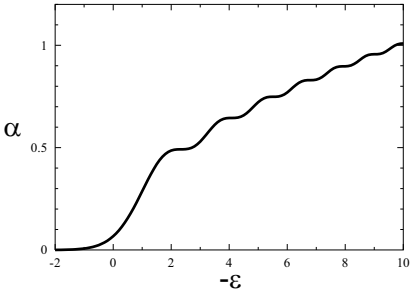

Fig. 18.1 Absorption spectrum for free carriers in an electric field according to Eq. (18.31). The absorption α is given in units of $\alpha' = \alpha_b m_r f^{1/3}/(2\pi\hbar^2)$ and ϵ is given by Eq. (18.29)

$$\boldsymbol{\alpha(\omega) = \frac{\alpha_b}{2\pi}\frac{m_r f^{1/3}}{\hbar^2}\{-\epsilon Ai^2(\epsilon) + [Ai'(\epsilon)]^2\}} \ . \tag{18.31}$$

electroabsorption for free carriers

Fig. 18.1 shows the resulting absorption as function of ϵ. The oscillatory character of the Airy functions for negative arguments leads to oscillations in the absorption spectrum above the band gap. The amplitude of these oscillations decreases with increasing energy. We can also see from Fig. 18.1 that the absorption has a tail below the gap, i.e., for $\hbar\omega < E_g$ or $\epsilon > 0$.

Using the asymptotic form (18.13) and

$$\lim_{x\to\infty} Ai'(x) = \frac{x^{1/4}}{2\sqrt{\pi}}\, e^{-\frac{2}{3}x^{3/2}} \left(1 + \frac{21c_1}{10x^{3/2}}\right) \ , \tag{18.32}$$

we obtain the below-gap absorption as

$$\boldsymbol{\alpha(\omega) \simeq \frac{\alpha_b}{32\pi^2} \frac{f}{E_g - \hbar\omega} \exp\left\{ -\frac{4}{3f} \left[\frac{2m_r(E_g - \hbar\omega)}{\hbar^2} \right]^{3/2} \right\}} \quad . \quad (18.33)$$

Franz-Keldysh effect

Eq. (18.33) describes the exponential low energy absorption tail which is caused by the electric field f. The frequency range of this tail increases with f. One may understand the appearance of the absorption tail as a photon-assisted field-induced tunneling of an electron from the valence band into the conduction band.

The absorption spectrum far above the band edge, $\hbar\omega >> E_g$ or $\epsilon << 0$, can be estimated using Eqs. (18.14) and (18.21) with the result

$$\alpha(\omega) = \frac{\alpha_b}{(2\pi)^2} \left(\frac{2m_r}{\hbar^2} \right)^{3/2} \sqrt{\hbar\omega - E_g} \quad . \quad (18.34)$$

Eq. (18.34) is nothing but the free-carrier absorption result of Chap. 5 for a $3d$-system.

18.2 Quantum Wells

If one applies the electric field perpendicular to the layer of a quantum well, the situation is quantitatively different from that in bulk material. Because of the opposite charges, the field pushes electron and hole toward the opposite walls of the well. Hence, the overlap between the corresponding particle-in-a-box wave functions is drastically modified. To discuss this effect, we again disregard for the time being the modifications caused by the electron–hole Coulomb interaction.

In a spatially inhomogeneous situation, such as in a quantum well, one has to use a two-point susceptibility function in real space representation $\chi(\mathbf{R}, \mathbf{R}', \omega)$, which connects nonlocally the polarization and the field according to

$$P(\mathbf{R}, \omega) = \int d^3R' \, \chi(\mathbf{R}, \mathbf{R}', \omega) E(\mathbf{R}', \omega) \quad . \quad (18.35)$$

The optical susceptibility is given by a generalization of Eq. (18.1) as

$$\chi(\mathbf{R},\mathbf{R}',\omega) = \chi_0 \sum_{\mu} \frac{\psi_\mu^*(\mathbf{R},\mathbf{r}=0)\psi_\mu(\mathbf{R}',\mathbf{r}'=0)}{\hbar(\omega+i\delta)-E_\mu} \ . \tag{18.36}$$

Here, $\psi_\mu(\mathbf{R},\mathbf{r})$ is the wave function of an electron–hole pair, and $\mathbf{R}$, $\mathbf{r}$ are the center-of-mass and relative coordinates, respectively. In spatially homogeneous situations, χ depends only on $\mathbf{R}-\mathbf{R}'$. The Fourier transform with respect to the difference of the center-of-mass coordinates yields the spatial dispersion, i.e., the wave-vector dependence of the susceptibility discussed in Chap. 11. However, due to the spatially inhomogeneous situation in a quantum well one has

$$\chi(\mathbf{R},\mathbf{R}',\omega) \neq \chi(\mathbf{R}-\mathbf{R}',\omega) \ .$$

The light wave length in the visible range is of the order of 10^{-4}cm. This is much larger than the typical quantum-well width, which for GaAs is around 10^{-6}cm. Therefore, it is useful to introduce a susceptibility which is averaged over the quantum-well volume,

$$\bar{\chi} = \frac{1}{V}\int d^3R \int d^3R' \chi(\mathbf{R},\mathbf{R}',\omega) \ . \tag{18.37}$$

This averaged susceptibility locally connects the optical polarization and the electromagnetic field.

Let us consider, for simplicity, a potential well of infinite depth extending over $-L/2 \leq z \leq L/2$. The pair wave function of a narrow quantum well can be taken as the product of particle-in-a-box wave functions for the electron and hole times the function describing the relative motion in the plane of the layer

$$\psi_\mu(\mathbf{R},\mathbf{r}) = \psi_{n_e}(z_e)\psi_{n_h}(z_h)\phi_{k_{||}}(\mathbf{r}_{||}) \ . \tag{18.38}$$

Electron and hole wave functions in the z direction obey the equation

$$\left(-\frac{\hbar^2}{2m_i}\frac{d^2}{dz_i^2} \pm eEz_i\right)\psi_{n_i}(z_i) = E_{n_i}\,\psi_{n_i}(z_i) \ , \tag{18.39}$$

where the $+(-)$ sign is linked to $i = e(h)$. The boundary conditions are

$$\psi_{n_i}(z=\pm L/2) = 0 \ . \tag{18.40}$$

Without the field the wave functions are just the simple trigonometric functions with even and odd parity

$$\psi_n^0(z) = \begin{Bmatrix}\cos(k_n z)\\ \sin(k_n z)\end{Bmatrix} \text{ with } k_n = \frac{\pi}{L}\begin{Bmatrix}2n+1\\ 2n\end{Bmatrix} \text{ for } n = 0, 1, 2, \ldots \ . \quad (18.41)$$

The absorption spectrum resulting from Eqs. (18.36) – (18.41) is

$$\alpha(\omega) = \frac{\alpha_b}{L} \sum_{\mathbf{k}_{||}, n_e, n_k} \frac{\delta(\hbar\omega - E_g - E_{k_{||}} - E_{n_e} - E_{n_h})}{A_{n_e} A_{n_h}} \times \left| \int_{-L/2}^{+L/2} dz\, \psi_{n_e}(z)\, \psi_{n_h}(z) \right|^2 \ , \quad (18.42)$$

quantum confined Franz-Keldysh spectrum

with $E_{k_{||}} = \frac{\hbar^2 k_{||}^2}{2m}$ and the normalization

$$A_{n_i} = \int_{-L/2}^{+L/2} dz\, |\psi_{n_i}(z)|^2 \ .$$

The overlap integral in Eq. (18.42) results from the spatial average, Eq. (18.37), over $R_z = z_e = z_h = z$, because $r_z = z_e - z_h = 0$ according to (18.36), and in the same way over R_z'.

Eq. (18.39) is again solved in terms of Airy functions. However, in order to fulfill the boundary conditions, we have to use a linear combination of the two independent types of Airy functions $Ai(\zeta)$ and $Bi(\zeta)$, where

$$Bi(x) = \frac{1}{\pi} \int_0^\infty du \left[e^{-\frac{u^3}{3} + ux} + \sin\left(\frac{u^3}{3} + ux\right)\right] \ , \quad (18.43)$$

see Abramowitz and Stegun (1972). The solution of Eq. (18.39) is thus

$$\psi_{n_i}(z_i) = a_i Ai(\zeta_i) + b_i Bi(\zeta_i) \ , \quad (18.44)$$

with

$$\zeta_{n_i} = \pm f^{1/3} z_i - \kappa_{n_i}^2 f^{-2/3} \ . \quad (18.45)$$

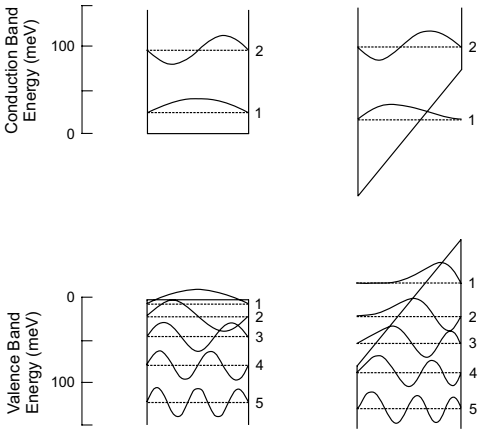

Fig. 18.2 Calculated wave functions and energy levels for a 150 Å thick GaAs-like quantum well at 0 and 10^5 Vcm^{-1}. [After Schmitt-Rink *et al.* (1989).]

The boundary condition yields the requirement for the existence of solutions

$$Ai(\zeta_{i+})Bi(\zeta_{i-}) = Ai(\zeta_{i-})Bi(\zeta_{i+}) \tag{18.46}$$

and

$$\frac{b_i}{a_i} = -\frac{Ai(\zeta_{i+})}{Bi(\zeta_{i+})} \ , \tag{18.47}$$

where $\zeta_{i\pm}$ corresponds to $z_i = \pm L/2$. Eq. (18.46) determines the energies $\kappa_{n_i}^2$ and Eq. (18.47) yields the relative weight of the Airy functions Bi and Ai. The summations over n_e and n_h in Eq. (18.42) are now replaced by integrations over the energies E_e and E_h

$$\alpha(\omega) = \frac{\alpha_b}{L} \sum_{\mathbf{k}_{||}} \int_{-eEL/2}^{\infty} dE_e \int_{-eEL/2}^{\infty} dE_h \frac{dn_e}{dE_e} \frac{dn_e}{dE_e} \times \delta(\hbar\omega - E_g - E_{k_{||}} - E_e - E_h)\, I_{eh} \ , \tag{18.48}$$

where I_{eh} is again the square of the normalized overlap integral between the electron and hole wave functions

$$I_{eh} = \frac{\left| \int_{-L/2}^{+L/2} dz\, \psi_{n_e}(z) \psi_{n_h}(z) \right|^2}{A_{n_e} A_{n_h}} \quad . \tag{18.49}$$

Fig. 18.2 shows the calculated wave functions in the potential well with and without an electric field. The picture of the wave functions gives immediately the information how the overlap integral I_{eh} changes due to the field for the various inter-subband transitions.

In Fig. 18.3, we plot the calculated absorption spectrum for a GaAs quantum well with L= 150 Å width in the presence of an electric field of 10^5 Vcm^{-1}. We see, e.g., that the transition between the second valence subband and the first conduction subband, which was forbidden without field, obtains a large oscillator strength in the field. For the limit $L \to \infty$, the inter-subband transitions approach the modulation of the bulk Franz-Keldysh spectrum.

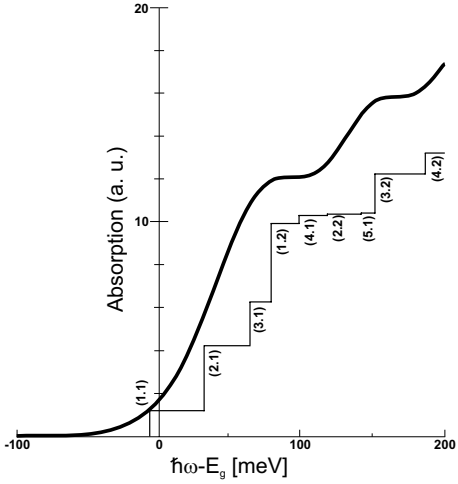

Fig. 18.3 Calculated absorption of a 150 Å thick GaAs-like quantum well at 10^5 Vcm^{-1}. The individual transitions are labeled (n_v, n_c) where n_v (n_c) is the valence (conduction) subband number. The smooth line is the calculated Franz-Keldysh effect for bulk material, see Fig. 18.1. [After Schmitt-Rink *et al.* (1989).]

18.3 Exciton Electroabsorption

In this section, we extend the treatment to include the attractive electron–hole Coulomb potential. Instead of Eq. (18.3), we then have to solve the basic pair equation

$$\left(-\frac{\hbar^2\Delta}{2m_r} - ezF - \frac{e^2}{\epsilon_0 r} - E_\mu\right)\psi_\mu = 0 \ . \tag{18.50}$$

Again, we discuss the solution of this equation and the resulting optical spectra both for bulk and quantum-well semiconductors.

18.3.1 *Bulk Semiconductors*

The exciton in a bulk semiconductor loses its stability in the presence of an electric field, as can be seen easily by inspecting the total electron–hole potential in Eq. (18.50). Plotting this potential along the z direction, Fig. 18.4, we see immediately that the exciton can be ionized if one of the carriers tunnel from z_1 to z_2 through the potential barrier. The tunneling causes a lifetime broadening of the exciton resonance. For example, for GaAs the exciton resonance vanishes completely for fields larger than 10^3V/cm. In addition to the broadening, there is also a shift of the exciton resonance, the so-called (dc) Stark shift. Second-order perturbation shows immediately that the shift of the ground state is quadratic in the field and negative

$$\Delta E_0 \simeq -\frac{(ea_0F)^2}{E_0} \equiv -\mathcal{F}^2 E_0 \ , \tag{18.51}$$

which holds as long as the perturbation is sufficiently small, i.e., $\mathcal{F} << 1$. But still more interesting is the question how the Franz-Keldysh absorption tail will be modified by excitonic effects. To study the region of the exciton absorption tail, we use the quasi-classical approximation introduced into quantum mechanics by Wentzel, Kramers and Brillouin, and often called the WKB method. This approach has been applied by Dow and Redfield (1970) to the present problem, we follow here the analytical approximations by Merkulov and Perel (1973) and Merkulov (1974).

In excitonic units, Eq. (18.50) becomes

$$\left(\Delta + \mathcal{F}z + \frac{2}{r} - \epsilon\right)\psi = 0 \ , \tag{18.52}$$

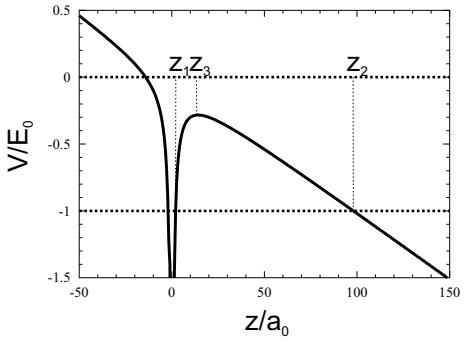

Fig. 18.4 Exciton potential in z-direction with an applied electric field ($\mathcal{F} = 0.01$).

where all coordinates are scaled with the Bohr radius and all energies with the exciton Rydberg energy, respectively. Since the scaled pair energy is always negative in the tail region, we introduced the positive energy scale

$$\epsilon \equiv -\frac{E_\mu}{E_0} \equiv \frac{E_g - \hbar\omega}{E_0} > 1 \ . \tag{18.53}$$

Here, the energy $\hbar\omega$ of the exciting photon is assumed to be below the band-gap energy, so that ϵ is always positive and larger than unity.

The maximum of the potential (point z_3 in Fig. 18.4) has an energy of $-2\sqrt{2\mathcal{F}}$ in z direction. For simplicity, we assume that the applied field is not too strong so that we always have potential barrier even for the lowest exciton state, i.e.,

$$2\sqrt{2\mathcal{F}} < \epsilon_{min} = 1 \ . \tag{18.54}$$

Under this condition, the exciton still exists as a quasi-bound state and we can essentially divide the solution of the problem into three steps: i) For the regime far away from the center of the exciton, we make a quasiclassical approximation and use $\hbar$ as formal expansion parameter. ii) For $z < z_1$, i.e., inside the Coulomb well, we neglect the electric field in comparison to the Coulomb potential and use the quantum mechanical solution (Chap. 10) for the exciton problem. iii) We match the solutions in the regime $z_1 < z < z_3$, where the quasiclassical approximation is still reasonably good and where the electric field is still small in comparison to the Coulomb potential.

First, we derive the quasiclassical solution for $z > z_2$. In cylindrical coordinates, the Laplace differential operator is given by

$$\Delta = \frac{1}{\rho}\frac{\partial}{\partial\rho}\rho\frac{\partial}{\partial\rho} + \frac{\partial^2}{\partial z^2} + \frac{1}{\rho^2}\frac{\partial^2}{\partial\phi^2} \quad , \tag{18.55}$$

where ρ is the radius perpendicular to z. Because only the wave functions with the angular-momentum quantum number $m = 0$ are finite in the origin and thus contribute to the absorption spectrum, we drop the dependence on the angle ϕ,

$$\left(\frac{1}{\rho}\frac{\partial}{\partial\rho}\rho\frac{\partial}{\partial\rho} + \frac{\partial^2}{\partial z^2} + \mathcal{F}z + \frac{2}{\sqrt{\rho^2+z^2}} - \epsilon\right)\psi_{sc} = 0 \quad . \tag{18.56}$$

The force $\mathbf{K}$ linked with the potential

$$V(\rho, z) = -\mathcal{F}z - 2/\sqrt{\rho^2+z^2} \tag{18.57}$$

is given as

$$\mathbf{K} = -\nabla V = \mathcal{F}\mathbf{e}_z - \frac{2z\mathbf{e}_z + 2\rho\mathbf{e}_\rho}{r^3} \quad , \tag{18.58}$$

where $\mathbf{e}_z$ and $\mathbf{e}_\rho$ are the unit vectors in z and ρ direction, respectively. The ratio of the two force components

$$\frac{K_\rho}{K_z} = -\frac{2\rho}{\mathcal{F}r^3 - 2z} \tag{18.59}$$

is always small for $r^2 >> \mathcal{F}^{-1}$. At the maximum of the potential barrier

$$z_3^2 = \frac{2}{\mathcal{F}} \quad ,$$

so that one can approximately neglect K_ρ in the region $z > z_3$. It is therefore a good approximation in the whole quasiclassical region to use only a one-dimensional potential

$$V(z) = -\mathcal{F}z - \frac{2}{z} \tag{18.60}$$

instead of the full potential, Eq. (18.57). In this case, Eq. (18.56) simplifies to

$$\left[\frac{1}{\rho}\frac{\partial}{\partial\rho}\rho\frac{\partial}{\partial\rho} + \frac{\partial^2}{\partial z^2} - V(z) - \epsilon\right]\psi_{sc} = 0 \quad . \tag{18.61}$$

Using the ansatz

$$\psi_{sc}(\rho, z) = \chi(\rho)\Psi(z) \ , \tag{18.62}$$

we can separate Eq. (18.61) into

$$\left[\frac{1}{\rho}\frac{\partial}{\partial\rho}\rho\frac{\partial}{\partial\rho} + p_\rho^2\right)\chi = 0 \tag{18.63}$$

and

$$\left[\frac{\partial^2}{\partial z^2} - V(z) - \epsilon - p_\rho^2\right]\Psi = 0 \ , \tag{18.64}$$

where p_ρ is the quasimomentum perpendicular to the z-axis.

Eq. (18.63) is a version of Bessel's differential equation and the solutions are the cylindrical Bessel functions

$$\chi(\rho) = J_0(p_\rho\rho) \ . \tag{18.65}$$

To solve Eq. (18.64), we make the quasiclassical approximation. For this purpose, we introduce again formally the $\hbar$-dependence of the kinetic energy operator, use $\hbar$ as a formal expansion parameter, and put it equal to unity at the end. We write Eq. (18.64) as

$$\left[\hbar^2\frac{\partial^2}{\partial z^2} + p^2(z)\right]\Psi = 0 \ , \tag{18.66}$$

where we introduce the quasimomentum $p(z)$ through the relation

$$p^2(z) = -\epsilon - V(z) - p_\rho^2 \ . \tag{18.67}$$

Inserting the ansatz

$$\Psi(z) = e^{\frac{i}{\hbar}\sigma(z)} \tag{18.68}$$

into Eq. (18.66) results in

$$i\hbar\sigma'' - (\sigma')^2 + p^2 = 0 \ . \tag{18.69}$$

Now, we expand the phase function $\sigma(z)$ formally in powers of $\hbar/i$

$$\sigma(z) = \sigma_0(z) + (\hbar/i)\sigma_1(z) + (\hbar/i)^2\sigma_2(z) + \cdots \tag{18.70}$$

and compare the various orders of $\hbar$. In the order $\mathcal{O}(\hbar^0)$, we obtain

$$\sigma_0'(z) = \pm p(z) \ , \tag{18.71}$$

with the solution

$$\sigma_0(z) = \pm \int_{z_2}^{z} d\zeta \, p(\zeta) \ . \tag{18.72}$$

The first-order equation is

$$i\sigma_0'' + 2i\sigma_0'\sigma_1' = 0 \ , \tag{18.73}$$

so that

$$\sigma_1(z) = -\ln \sqrt{p(z)} + \ln \, C \ , \tag{18.74}$$

where $\ln \, C$ is a normalization constant. Summarizing the results, we obtain

$$\Psi(z) = \frac{C}{\sqrt{|p(z)|}} \exp\left(\pm i \int_{z_2}^{z} d\zeta \, p(\zeta) \right) \ , \tag{18.75}$$

where we put the formal expansion parameter $\hbar \to 1$.

Because a classical particle cannot penetrate into regions in which the potential energy exceeds the total energy, we define the classical turning points by $p^2(z_{1,2}) = 0$ and find

$$z_{2,1} = \frac{1}{2\mathcal{F}} \left[(\epsilon + p_\rho^2) \pm \sqrt{(\epsilon + p_\rho^2)^2 - 8\mathcal{F}} \right] \ . \tag{18.76}$$

The quasimomentum $p(z)$ is real in the region, $z > z_2$ and the wave function (18.75) describes oscillatory solutions.

In the region of the potential barrier, $z_1 < z < z_2$, $\epsilon > 1$ and $-V(z) < 1$, so that $p^2(z) < 0$ and $p(z)$ is purely imaginary. Eq. (18.75) describes an exponentially increasing or decaying solution in the classically forbidden region. The exponentially increasing solution is clearly unphysical and has to be discarded, so that we have in the classically forbidden region

$$\Psi(z) = \frac{C}{\sqrt{|p(z)|}} \exp\left(- \int_{z_2}^{z} d\zeta \, |p(\zeta)| \right) \ . \tag{18.77}$$

Now, we can approximate

$$|p(z)| = \sqrt{\epsilon + V(z) + p_\rho^2} \simeq p_0(z) + \frac{p_\rho^2}{2p_0(z)} \tag{18.78}$$

with $p_0(z) = [\epsilon + V(z)]^{1/2}$ and the integral in Eq. (18.77) can be simplified by considering that z deviates only slightly from r, i.e.,

$$z = r\cos(\theta) \simeq r\left(1 - \frac{1}{2}\theta^2\right) \quad , \tag{18.79}$$

so that

$$\begin{aligned}\Psi(z) &\simeq \frac{C}{\sqrt{|p(z)|}} \exp\left[\int_{z_2}^{r} d\zeta \left(p_0 + \frac{p_\rho^2}{2p_0}\right) + \int_r^z d\zeta\, p_0\right] \\ &\simeq \frac{C}{\sqrt{|p(z)|}} \exp\left[-\int_r^{z_2} d\zeta \left(p_0 + \frac{p_\rho^2}{2p_0}\right)\right] \exp\left(-\frac{r\theta^2}{2}\sqrt{\epsilon}\right) \quad . \end{aligned} \tag{18.80}$$

Here, z_2 can be evaluated for $p_\rho \simeq 0$. Furthermore, in the vicinity of the z-axis the argument of the Bessel function can be put equal to zero $J_0(p_\rho\rho) \simeq J_0(0) = 1$, so that the semiclassical form of the wave function (18.62) becomes $\psi_{sc} = \Psi$.

Now, we turn to the solution of the exciton problem for the core region, $z < z_3$, in which we may neglect approximately the field. Using Eq. (10.70), we may write the exciton wave functions with $l = 0$ and $m = 0$, which are finite at the origin, as

$$\Psi_x(\mathbf{r}) = \Psi(0)\, e^{-r\sqrt{\epsilon}}\, F\left(1 - \frac{1}{\sqrt{\epsilon}}; 2; 2\sqrt{\epsilon}\, r\right) \quad , \tag{18.81}$$

where we used the relations

$$L_{n+l}^{2l+1}\left(\frac{2r}{na_0}\right) = \frac{(n+l)!(n+l)!}{(n-l-1)!(2l+1)!} F\left(-n+l+1; 2l+2; \frac{2r}{na_0}\right) \tag{18.82}$$

and

$$n = \frac{E_0}{E_n} = \frac{1}{\sqrt{\epsilon}} \ . \tag{18.83}$$

For $r >> \epsilon^{-1/2}$, one may use the asymptotic form of the confluent hypergeometric function,

$$F(a; b; z) \to \frac{e^z \Gamma(b) z^{a-b}}{\Gamma(a)} \tag{18.84}$$

which yields

$$\Psi_x(r) = \frac{\Psi(0)\exp[(-r\epsilon^{1/2})]}{\Gamma\left(1-\frac{1}{\sqrt{\epsilon}}\right)(2\sqrt{\epsilon}\,r)^{1+\frac{1}{\epsilon^{1/2}}}} \quad . \tag{18.85}$$

This function has to be matched with the spherical part of the semiclassical wave function (18.80) which is obtained by averaging the angle-dependent part of (18.80) over the angles

$$\begin{aligned}\bar{\Psi}_{sc}(r) &= \int \frac{d\Omega}{4\pi}\Psi(\mathbf{r}) = \int_0^{2\pi}\frac{d\phi}{2\pi}\int_0^{\pi}\frac{d\theta}{2}\sin\theta f(r)\exp\left(-\frac{1}{2}r\sqrt{\epsilon}\,\theta^2\right)\\ &\simeq \frac{1}{2}\int_0^{\pi} d\theta\,\theta\, f(r)\exp\left(-\frac{1}{2}r\sqrt{\epsilon}\,\theta^2\right)\\ &\simeq \frac{1}{4}\int_0^{\infty} dx f(r)\exp\left(-\frac{1}{2}r\sqrt{\epsilon}x\right) = f(r)\frac{1}{2r\sqrt{\epsilon}} \quad ,\end{aligned}$$

where $f(r)$ stands for the angle-independent parts. The total spherical part of the semiclassical wave function can therefore be written as

$$\bar{\Psi}_{sc}(r) \simeq \frac{C}{\epsilon^{1/4}(2\sqrt{\epsilon}r)^{1+\frac{1}{\sqrt{\epsilon}}}}\exp\left(-\int_{z_1}^{z_2}d\zeta\left(p_0+\frac{p_\rho^2}{2p_0}\right)-\frac{\ln\sqrt{\epsilon}}{\sqrt{\epsilon}}-\frac{1}{\sqrt{\epsilon}}-\sqrt{\epsilon}r\right) . \tag{18.86}$$

Here, we introduced the tunnel integral ranging from z_1 to z_2. The integral from z_1 to r has been evaluated approximately. The semiclassical wave function $\bar{\Psi}_{sc}$, Eq. (18.86), and the asymptotic exciton wave function Ψ_x, Eq. (18.85), have approximately the same r-dependence. We used $\epsilon^{-1/2}\ln 2r \simeq \epsilon^{-1/2}$, which holds approximately for the matching region. A comparison of the coefficients yields

$$\psi(0) = \frac{\Gamma\left(1-\frac{1}{\sqrt{\epsilon}}\right)C}{\epsilon^{1/4}}\exp\left(-T_t-\frac{p_\rho^2}{2}\alpha_t\right) \quad , \tag{18.87}$$

where

$$T_t = \int_{z_1}^{z_2} d\zeta\, p_0(\zeta) + \frac{\ln\sqrt{\epsilon}}{\sqrt{\epsilon}} + \frac{1}{\sqrt{\epsilon}} \tag{18.88}$$

and

$$\alpha_t = \int_{z_1}^{z_2} d\zeta \frac{1}{p_0(\zeta)} \quad . \tag{18.89}$$

The α_t correction term becomes unimportant, because the summation over all p_ρ values brings the correction down from the exponent, so that it enters into the result as an unimportant prefactor. The evaluation of the tunnel integral yields

$$T_t = \frac{2\epsilon^{2/3}}{3\mathcal{F}} - \frac{1}{\sqrt{\epsilon}} \ln\left(\frac{8\epsilon^{3/2}}{\mathcal{F}}\right) \quad . \tag{18.90}$$

The first term in Eq. (18.90) gives rise to the Franz-Keldysh result, while the second term describes the quite significant modification due to the Coulomb potential. The only unknown coefficient in the result is the normalization constant C. The existence of the exciton has little influence on the normalization which is determined by the asymptotic form of the wave function, see Chap. 10. Thus the normalization is the same as for free carriers.
The resulting absorption spectrum is

$$\boldsymbol{\alpha(\omega) = \alpha_{FK}(\omega)} \left\{ \boldsymbol{\Gamma}\left(\mathbf{1} - \frac{\mathbf{1}}{\sqrt{\boldsymbol{\epsilon}}}\right) \mathbf{exp}\left[\frac{\mathbf{1}}{\sqrt{\boldsymbol{\epsilon}}} \mathbf{ln}\left(\frac{\mathbf{8\epsilon^{3/2}}}{\boldsymbol{\mathcal{F}}}\right)\right]\right\}^{\mathbf{2}} \quad , \tag{18.91}$$

bulk exciton electroabsorption

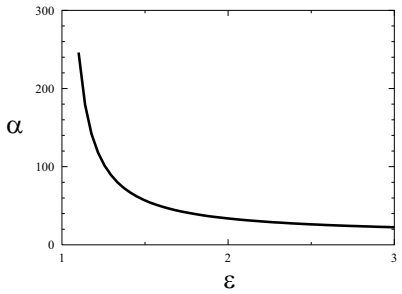

Fig. 18.5 Exciton enhancement of the electroabsorption according to Eq. (18.91). α is in units of α_{FK} and $\epsilon = (E_g - \hbar\omega)/E_0$.

where $\epsilon = (E_g - \hbar\omega)/E_0$ and $\alpha_{FK}(\omega)$ is the Franz-Keldysh absorption coefficient given in Eq. (18.33). An example of the absorption spectrum according to Eq. (18.91) is shown in Fig. 18.5. Depending on the detuning ϵ and the field strength $\mathcal{F}$, the exciton electroabsorption coefficient can be up to 10^3 times larger than the Franz-Keldysh absorption coefficient. The absorption approaches the Franz-Keldysh spectrum asymptotically only for very large detunings.

18.3.2 *Quantum Wells*

The spatial confinement in a quantum well prevents field ionization of the exciton up to very large field strengths. As a consequence, one can observe very large Stark shifts of, e.g., the lowest exciton resonance in a field perpendicular to the layer of the quantum well (Miller *et al.*, 1985).

In order to treat the problem, we decompose it into that of the one-dimensional motion of the noninteracting electron and hole in the quantum-well potential $V_i(z_i)$ and the field, and into that of the relative electron–hole motion in the layer under the influence of the Coulomb interaction. We write the total Hamiltonian as

$$\mathcal{H} = \mathcal{H}_{ez} + \mathcal{H}_{hz} + \mathcal{H}_{eh} \ , \tag{18.92}$$

where

$$\mathcal{H}_{iz} = -\frac{\hbar^2}{2m_i}\frac{\partial^2}{\partial z_i^2} + V_i(z_i) \pm eEz_i \, , \; i = e, h \tag{18.93}$$

and

$$\mathcal{H}_{eh} = -\frac{\hbar^2}{2m}\frac{\partial^2}{\partial r^2} - \frac{e^2}{\epsilon_0\sqrt{r^2 + (z_e - z_h)^2}} \ . \tag{18.94}$$

For the wave function, we use a product ansatz

$$\psi = \psi_e(z_e)\psi_h(z_h)\Psi_{eh}(r) \ , \tag{18.95}$$

where the wave functions $\psi_i(z_i)$ are the eigenfunctions of the Hamiltonian (18.93). Assuming infinitely high potential wells, the functions $\psi_i(z_i)$ are given by Eq. (18.44) in terms of Airy functions. The effect of a finite potential well and the resulting leaking of the wave functions into the embedding material can approximately be accounted for by introducing an effective well width L_{eff} which is slightly larger than the actual width L.

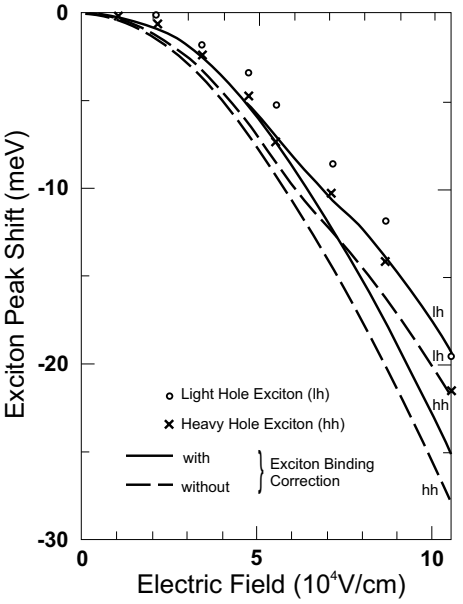

Fig. 18.6 Shift of the exciton peak position in a 95-Å multiple-quantum well as function of the electric field. [From Miller *et al.* (1985).]

For the wave function $\Psi_{eh}(r)$, a $1s$-like function is assumed with a radius λ, which is determined variationally

$$\Psi_{eh}(r) = \sqrt{\frac{2}{\pi}}\,\frac{e^{-\frac{r}{\lambda}}}{\lambda} \quad . \tag{18.96}$$

The total pair energy

$$E_{eh} = E_{ez} + E_{hz} + \langle \Psi^* | \mathcal{H}_{eh} | \Psi \rangle \tag{18.97}$$

is minimized with respect to λ for a given field F. The resulting energy shifts are shown in Fig. 18.6, together with the experimentally observed Stark shifts for the heavy and light hole (hh and lh) exciton of a GaAs quantum well with a width of 95 Å. One sees that Stark shifts up to 20 meV are obtained with an electric field of about 10^5 V/cm. Only above this large value of the electric field, field-induced tunneling sets in and broadens the exciton resonance. The quantum confined Stark shift of $\simeq$ 20meV is more

than twice the exciton binding energy of $\simeq$ 9meV in this quantum well.

REFERENCES

M. Abramowitz and I.A. Stegun, *Handbook of Mathematical Functions* (Dover Publ., 1972)
J.D. Dow and D. Redfield, Phys. Rev. **B1**, 3358 (1970)
I.A. Merkulov and V.I. Perel, Phys. Lett. **45A**, 83 (1973)
I.A. Merkulov, Sov. Phys. JETP **39**, 1140 (1974)
D.A.B. Miller, D.S. Chemla, T.C. Damen, A.C. Gossard, W. Wiegmann, T.H. Wood, and C.A. Burrus, Phys. Rev. **B32**, 1043 (1985)
S. Schmitt-Rink, D.S. Chemla, and D.A.B. Miller, Adv. in Phys. **38**, 89 (1989)

PROBLEMS

Problem 18.1: (a) Use first-order perturbation theory in the applied field to evaluate the absorption spectrum, Eq. (18.42), for the quantum-confined Franz-Keldysh effect. Use the basis functions (18.41) to show the reduction in oscillator strength for the transition between the lowest electron–hole subband, $0,\mathrm{h} \rightarrow 0,\mathrm{e}$. This transition is fully allowed without field, and it is reduced in the presence of the field. (b) Use the same method as in (a) to show that the field makes the transition $0,\mathrm{h} \rightarrow 1\mathrm{e}$ dipole allowed.

Problem 18.2: Show that the tunnel integral, first term of Eq. (18.88), can be transformed into the expression

$$T_1 = \mathcal{F}^{1/2} \int_{z_1}^{z_2} \frac{dz}{\sqrt{z}} \sqrt{(z_2 - z)(z - z_1)} \tag{18.98}$$

and further into the form

$$T_1 = \frac{\epsilon^{3/2}}{2^{3/2}\mathcal{F}}\, s^2 \int_{-1}^{+1} dt \sqrt{\frac{1-t^2}{1+st}} = \frac{\epsilon^{3/2}}{2^{3/2}\mathcal{F}}\, s^2\, I(s) \ , \tag{18.99}$$

where $s = \sqrt{1 - \frac{8\mathcal{F}}{\epsilon^2}} = \sqrt{1 - y^2}$.

Problem 18.3: Show that the evaluation of the integral $I(s)$, defined in Eq. (18.99), for $s = 1$ gives the Franz-Keldysh result $I(1) = \frac{4}{3}\sqrt{2}$.

Chapter 19

Magneto-Optics

The application of magnetic fields in solid state physics and particularly also in semiconductor optics has always been an extremely versatile tool, particularly for the identification of the symmetry of electronic states. Therefore, magneto-optics has become a very large field in its own right. In this chapter, we discuss only some basic aspects of the influence of the magnetic fields on the free electron motion, which are of particular interest for the intrinsic linear and nonlinear optical properties of semiconductors and semiconductor microstructures. We focus on the optical properties of magneto-excitons and magneto-plasmas in quantum confined structures.

The Lorentz force of a constant magnetic field constrains a free electron on a cyclotron orbit perpendicular to the magnetic field. An especially well-defined problem arises, if one applies a magnetic field perpendicularly to a quantum well which suppresses the electron motion in the field direction. In this configuration, interesting physical phenomena, such as the quantized Hall effect and the crystallization of the electrons into a Wigner crystal occur.

It has been shown that the Hartree-Fock theory becomes exact for a two-dimensional electron gas in the limit of low temperatures and high magnetic fields. Therefore, we limit our discussion in this chapter to the Hartree-Fock theory of magneto-excitons and magneto-plasmas in $2D$ quantum wells and $1D$ quantum wires. Modeling the wire configuration as an additional weak harmonic lateral confinement allows us to study the smooth transition between effectively $1D$ and $2D$ systems. In this treatment, we follow the theoretical work presented in Bayer *et al.* (1997) and show a comparison with experimental results.

First, we discuss the single-particle problem, which can be treated exactly for a harmonic lateral confinement potential in terms of modified

Landau eigenfunctions. Expanding the density matrix in the Landau basis, we derive the Bloch equations of the magneto-plasma. Only the Coulomb exchange terms are kept. Assuming quasi-equilibrium carrier distributions, we then use the polarization equation to calculate the linear absorption, gain and luminescence spectra, which can be compared most directly to experimental observations in quantum wires.

19.1 Single Electron in a Magnetic Field

We consider an electron in a quantum well ($x-y$ plane) that experiences an additional smooth lateral quantum-wire confinement potential in the x-direction. The electron moves under the influence of a constant magnetic field in the z-direction. For realistic quantum wires, the confinement potential can be assumed to have a Gaussian shape, which for the lower-lying states can be approximated by a harmonic oscillator potential.

We assume the validity of the effective mass approximation and neglect all band-mixing effects taking into account only those states that are formed out of the lowest quantum-well electron and heavy-hole subbands. The single-particle Hamiltonian for an electron ($j=e$) or a hole ($j=h$) moving in the $x-y$ plane with the wire axis in the y direction can be written as

$$\mathcal{H}_j^0 = \frac{\hbar^2}{2m_j}\left[\mathbf{p}_j - e_j\mathbf{A}(\mathbf{r}_j)\right]^2 + \frac{1}{2}m_j\Omega_j^2\mathbf{x}_j^2 + \frac{E_g}{2} \ . \tag{19.1}$$

Here, the band gap E_g of the underlying quantum well is split symmetrically between the electrons ($-|e|$) and holes ($|e|$). The term $\frac{1}{2}m_j\Omega_j^2\mathbf{x}_j^2$ models the lateral confinement potential characterized by the intersubband frequencies Ω_j.

The vector potential $\mathbf{A}$ describes the constant magnetic field $\mathbf{B}=\mathbf{e}_z B$ in z-direction. The vector potential is not uniquely defined. Two gauges are commonly used:
(i) the symmetric gauge with

$$\mathbf{A}(\mathbf{r}) = \frac{1}{2}\mathbf{B}\times\mathbf{r} = \frac{B}{2}(-y\mathbf{e}_x + x\mathbf{e}_y) \ , \tag{19.2}$$

(ii) the asymmetric Landau gauge

$$\mathbf{A}(\mathbf{r}) = xB\mathbf{e}_y \ . \tag{19.3}$$

One can easily verify that in both cases

$$\mathbf{B} = \text{curl } \mathbf{A} = \begin{vmatrix} \mathbf{e}_x & \mathbf{e}_y & \mathbf{e}_z \\ \partial/\partial x & \partial/\partial_y & 0 \\ A_x & A_y & 0 \end{vmatrix} = B\,\mathbf{e}_z \ . \tag{19.4}$$

For practical purposes, it is often advantageous to use the asymmetric Landau gauge (ii) which depends only on the x-coordinate. In this frame, the magnetic field produces together with the confinement potential (characterized by the oscillator frequency Ω_j) a harmonic oscillator potential in the x-direction, while one has a free motion in the y-direction.

In the Landau gauge, the single-particle Hamiltonian (19.1) can be written as

$$\begin{aligned} \mathcal{H}_j^0 &= \frac{\hbar^2}{2m_j}\left[\mathbf{p}_j - e_j B x_j \mathbf{e}_\mathbf{y})\right]^2 + \frac{1}{2}m_j\Omega_j^2 x_j^2 + \frac{E_g}{2} \qquad (19.5)\\ &= -\frac{\hbar^2}{2m_j}\frac{\partial^2}{\partial x_j^2} - \frac{\hbar^2}{2m_j}\frac{\partial^2}{\partial y_j^2} - \hbar\omega_{c,j}\frac{x_j}{i}\frac{\partial}{\partial y_j} + \frac{1}{2}m_j(\Omega_j^2+\omega_{c,j}^2)\mathbf{x}_j^2 + \frac{E_g}{2} \ , \end{aligned}$$

where

$$\boldsymbol{\omega_{c,j}} = \frac{\boldsymbol{e_j B}}{\boldsymbol{m_j}} \tag{19.6}$$

cyclotron frequency

is the cyclotron frequency of the carriers j.

For the total wave function, we make the ansatz

$$\psi_j(x_j, y_j) = \frac{e^{iky_j}}{\sqrt{L_y}}\phi_j(x_j) \ , \tag{19.7}$$

where the plane wave contribution results from the absence of a confining potential in y-direction. Inserting this ansatz into Schrödinger's equation and using a quadratic completion, we obtain the x-dependent Hamiltonian

$$\mathcal{H}^0(x_j) = -\frac{\hbar^2}{2m_j}\frac{\partial^2}{\partial x_j^2} + \frac{1}{2}m_j\omega_{eff,j}^2(x_j - \Delta x_j)^2 + \frac{\hbar^2 k^2}{2m_{eff,j}} + \frac{E_g}{2} \ . \tag{19.8}$$

Here, the effective oscillator frequency is given by

$$\omega_{eff,j} = \sqrt{\Omega_j^2 + \omega_{c,j}^2} \ . \tag{19.9}$$

The origin of the oscillator potential is shifted by

$$\Delta x_j = k\delta_j = k\frac{\hbar}{m_j}\frac{\omega_{c,j}}{\omega_{eff,j}^2} \quad . \tag{19.10}$$

Furthermore, we introduced the translational effective mass for the quantum-wire electron in a magnetic field

$$m_{eff,j} = m_j \left(\frac{\omega_{eff,j}}{\Omega_j}\right)^2 \quad . \tag{19.11}$$

This effective mass increases quadratically with the magnetic field once the cyclotron frequency exceeds the spectral difference between the wire subbands. Writing the oscillator potential term in the Hamiltonian (19.8) as

$$\frac{m_j^2}{\hbar^2}\omega_{eff,j}^2(x_j - k\delta_j)^2 \ = \frac{(x_j - k\delta_j)^2}{(l_{eff,j})^4} \quad , \tag{19.12}$$

we identify the characteristic length

$$l_{eff,j} = \sqrt{\frac{\hbar}{m_j\omega_{eff,j}}} \quad , \tag{19.13}$$

which is the amplitude of the electron's zero point fluctuations. This length is a generalization of the so-called Landau length, which determines the cyclotron radius. With $l_{eff,i}$, the shift Δx_i becomes $\Delta x_i = kl_{eff,i}^2(\omega_{c,i}/\omega_{eff,i})$. It is interesting to note that this shift of the origin depends on the momentum along the wire. This can be understood as the action of the Lorentz force on the moving carrier.

The eigenfunctions of (19.8) are shifted harmonic oscillator functions $\phi_\nu(x_j - \Delta x_j)$, also called modified Landau states. Hence, the complete

single-particle eigenfunctions are

$$\psi^j_{k,\nu}(x_j, y_j) = \frac{e^{iky_j}}{\sqrt{L_x}}\phi^j_\nu(x_j)$$
$$= \frac{e^{iky_j}}{\sqrt{L_x}}\phi_\nu(x_j - \Delta x_j) \text{ with } \nu = 0, 1, 2, \cdots \ . \tag{19.14}$$

modified Landau eigenfunctions

The corresponding single-particle energies are

$$\boldsymbol{E^j_{k,\nu}} = \frac{\hbar^2 \boldsymbol{k^2}}{\boldsymbol{2m_{eff,j}}} + \frac{\boldsymbol{E_g}}{\boldsymbol{2}} + \hbar\boldsymbol{\omega_{eff,j}}\left(\boldsymbol{\nu} + \frac{\boldsymbol{1}}{\boldsymbol{2}}\right) \ . \tag{19.15}$$

modified Landau ladder

The effective mass increases with increasing magnetic field showing how the field hinders the translational motion along the wire. The characteristic frequency of the Landau ladder with parabolic confinement potential and magnetic field is $\omega_{eff,j} = \sqrt{\Omega_j^2 + \omega_{c,j}^2}$. Thus, the magnetic field increases the lateral subband spacing.

Finally, we note that the electron and hole wave functions are the time-reversal counterparts of each other

$$\psi^e_{k,\nu} = \left(\psi^h_{-k,\nu}\right)^* \ . \tag{19.16}$$

19.2 Bloch Equations for a Magneto-Plasma

In order to study the optical properties of the quantum confined magneto-plasma, we derive the Bloch equations for this system by expanding the electron–hole density matrix into the modified Landau base (19.14), which diagonalizes the single-particle problem. The Coulomb interactions between the optically excited carriers are taken into account in the mean-field approximation. As mentioned above, this approximation becomes very good for strong effective quantum confinement through the combined influence of barriers and magnetic field.

For simplicity, we analyze a configuration with equal effective electron

and hole masses, so that

$$m_e\Omega_e = m_h\Omega_h = m\Omega \ , \tag{19.17}$$

where Ω is the total inter-subband spacing. This approximation assures local charge neutrality. While the values of the axial momentum k are unrestricted for $B = 0$, they are restricted in the presence of a magnetic field by the condition that the center of the carrier wave function $\Delta_j x$ must lie inside the quantum wire. This condition imposes

$$\Delta x_j = k\delta_j \leq \frac{L_x}{2} \tag{19.18}$$

as condition for the harmonic confinement potential.

If we fit the lateral subband splitting Ω with the energy splitting between the two lowest subbands of a rectangular square well

$$\hbar\Omega = \left(\frac{2\pi}{L_x}\right)^2 \frac{\hbar^2}{2m} - \left(\frac{\pi}{L_x}\right)^2 \frac{\hbar^2}{2m} = \frac{3\pi^2\hbar^2}{2mL_x^2} \tag{19.19}$$

we obtain for the largest allowed wave number k_m

$$L_x k_m = \frac{3\pi^2}{4}\frac{\omega_{eff}^2}{\omega_c\Omega} = \kappa_m \ . \tag{19.20}$$

Here, ω_c and ω_{eff} are also calculated with the reduced mass m. Now the density of states can be calculated:

$$\begin{aligned} D(E) &= tr\delta(E-\mathcal{H}) \ = \sum_{\nu,k} \delta(E - E_{k,\nu}) \\ &= \frac{L_y}{2\pi}\int_{-\kappa_m}^{\kappa_m} dk \sum_\nu \delta\left(\frac{\hbar^2k^2}{2m_{eff}} + E_{k=0,\nu} - E\right) \\ &= \frac{L_y}{L_x 2\pi\tilde{E}_0}\int_{-\kappa_m}^{\kappa_m} d\kappa \sum_\nu \delta\left(\kappa^2 - \frac{E - E_{k=0,\nu}}{\tilde{E}_0}\right) \ , \end{aligned} \tag{19.21}$$

where we used Eq. (4.6) for $D = 1$ with $\Delta k = \frac{L_y}{2\pi}$. Furthermore, we introduced $\kappa = kL_x$ as integration variable and $\tilde{E}_0 = \hbar^2/(2m_{eff}L_x^2)$ as characteristic energy. The integral over the delta function yields

$$D(E) = \frac{L_y}{L_x 2\pi\tilde{E}_0}\sum_\nu \Theta\left(\kappa_m^2 - \frac{E - E_{k=0,\nu}}{\tilde{E}_0}\right)\sqrt{\frac{\tilde{E}_0}{E - E_{k=0,\nu}}} \ . \tag{19.22}$$

With increasing magnetic field the single-particle density of states changes from the $1/\sqrt{E}$-like behavior of a $1D$ system to the δ-function-like behavior

of a totally confined system. Calculating now the total number of states g in a quasi-1D subband with index ν, one finds the relation

$$g \propto \frac{\omega_{eff}}{\Omega} \ . \tag{19.23}$$

In contrast to a quantum well in a normal magnetic field, for which the number of states in a Landau level depends linearly on the magnetic field, the number of states in a quantum wire is nearly constant for weak fields, and approaches the linear dependence only in the high-field limit.

The matrix elements of the Coulomb potential (see also Problem 19.2) can be written as

$$V^{j,j'}_{\nu,\nu';\nu',\nu}(q) = \sum_{q_x} \frac{2\pi e_j e_{j'}}{\epsilon_0 \sqrt{q^2+q_x^2}} \left| \int dx \phi^*_\nu(x+\delta q) e^{iq_x x} \phi_{\nu'}(x) \right|^2 = V^{j,j'}_{\nu,\nu'} \ , \tag{19.24}$$

where ϵ_0 is the background dielectric function. Using the modified Landau states (19.14), one can evaluate the Coulomb matrix elements analytically in terms of modified Bessel functions of zeroth and first order (see the evaluations in Wu and Haug). As defined in Sec. 12.2, the single-particle density matrix is

$$\rho_{i,\nu;i',\nu}(k,t) = \langle a^\dagger_{i,k,\nu}(t) a_{i',k,\nu}(t) \rangle \ , \text{where } \{i,i'\} = \{c,v\} \ . \tag{19.25}$$

Here, we consider only diagonal elements in ν because the optical transitions in our model connect only states with the same Landau subband quantum number. Switching to the electron–hole representation, the relevant carrier densities are

$$\rho^{ee}_{\nu,\nu}(k) = \langle \alpha^\dagger_{k,\nu} \alpha_{k,\nu} \rangle = n^e_{k,\nu} \tag{19.26}$$

and

$$\rho^{hh}_{\nu,\nu}(k) = \langle \beta^\dagger_{k,\nu} \beta_{k,\nu} \rangle = n^h_{k,\nu} \ , \tag{19.27}$$

with the electron and hole operators $\alpha, \alpha^\dagger$ and $\beta, \beta^\dagger$, respectively. Following the derivation in Chap. 12, we find for the optical interband polarization

$$\rho^{eh}_{\nu,\nu}(k,t) = \langle \beta_{-k,\nu} \alpha_{k,\nu} \rangle = P_{k,\nu} \tag{19.28}$$

the dynamic equation

$$\left(i\frac{\partial}{\partial t} - e^e_{k,\nu} - e^h_{k,\nu}\right) P_{k,\nu} = \left(n^e_{k,\nu} + n^h_{k,\nu} - 1\right)\omega_{R,k,\nu}(t) + i\left.\frac{\partial P_{k,\nu}}{\partial t}\right|_{scatt} . \tag{19.29}$$

Here, the carrier energies $e^j_{k,\nu}$ are the exchange renormalized single-particle energies

$$\hbar e^j_{k,\nu} = E^j_{k,\nu} - \sum_{q,\nu',j} V^{jj'}_{\nu,\nu'}(q) n^{j'}_{k-q,\nu'}(t) \ , \tag{19.30}$$

with the Landau ladder energies $E^j_{k,\nu}$ (19.15). The sum j' extends only over the Landau subbands of the considered species.

The exchange renormalized Rabi frequency ω_R is given by

$$\hbar\omega_{R,k,\nu}(t) = d_{cv}\mathcal{E}(t) + \sum_{q,\nu'} V^{eh}_{\nu,\nu'}(q) P_{k-q,\nu'} \ . \tag{19.31}$$

The equations for the carrier densities are

$$\frac{\partial}{\partial t} n^j_{k,\nu} = -2\mathrm{Im}\left[\omega_{R,k,\nu}(t) P^*_{k,\nu}\right] + \left.\frac{\partial n^j_{k,\nu}}{\partial t}\right|_{scatt} , \tag{19.32}$$

copmpare Eqs. (12.19).

Because in quantum wires the luminescence emerging from the end of the wires can be measured most easily, we limit our analysis to the calculation of the wire luminescence. In the experiments, the carriers are excited by a a *cw* pump field and have enough time to thermalize before their radiative decay. Therefore, we have to calculate only the polarization equation with quasi-equilibrium Fermi distributions of the carriers. The density and the temperature of the carrier distributions are used as fitting parameters in the comparison with corresponding measured spectra.

19.3 Magneto-Luminescence of Quantum Wires

In this section, we follow the procedure discussed in Chap. 15 to compute the quasi-equilibrium optical nonlinearities. We slightly generalize the treatment by including the summations over the Landau subband states.

Again, we start by calculating the stationary optical interband polarization components which are linear in the field $\mathcal{E}(t) = E_0 e^{-i\omega t}$. The sta-

tionary polarization equation is in the rotating wave approximation

$$\hbar\Big(\omega - e^e_{k,\nu} - e^h_{k,\nu} + i\gamma\Big) p_{k,\nu} = \left(f^e_{k,\nu} + f^h_{k,\nu} - 1\right)\Big[d_c v\mathcal{E}_0 + \sum_{q,\nu'} V^{eh}_{\nu\nu'}(q) p_{k-q,\nu'}\Big] \,, \tag{19.33}$$

where $p_{k,\nu} = P_{k,\nu} e^{-i\omega t}$. From the scattering term, we took only a phenomenological dephasing or damping rate γ into account. The electron and hole distributions are thermal Fermi functions, e.g.,

$$f^e_{k,\nu} = \frac{1}{e^{\left(\hbar\omega_{eff}\left(\nu+\frac{1}{2}\right) + \frac{\hbar^2 k^2}{2m^e_{eff}} - \mu^e\right)\beta} + 1} \,. \tag{19.34}$$

With this ansatz, we not only assume that the electrons of a given Landau subband are in thermal equilibrium, but that all electron subbands are in equilibrium among each other.

It is advantageous to eliminate the amplitude of the light field by introducing a susceptibility component

$$\chi_{k,\nu}(\omega) = \frac{P_{k,\nu}(t)}{\mathcal{E}(t)} \,, \tag{19.35}$$

which depends on the carrier frequency of the light. The total susceptibility is then obtained as

$$\chi(\omega) = d_{cv} \sum_{k,\nu} P_{k,\nu}(\omega) \,. \tag{19.36}$$

The equation for the susceptibility component can be written in the form

$$\boldsymbol{\chi_{k,\nu}(\omega) = \chi^0_{nk}(\omega) - \chi^0_{nk}(\omega) \frac{1}{d_{cv}} \sum_{k',\nu'} V^{eh}_{\nu\nu'}(k-k') \chi^0_{nk}(\omega)} \,, \tag{19.37}$$

susceptibility integral equation

where we again used the spectral representation according to Eq. (15.18). From the susceptibility, one gets the luminescence spectrum using the equi-

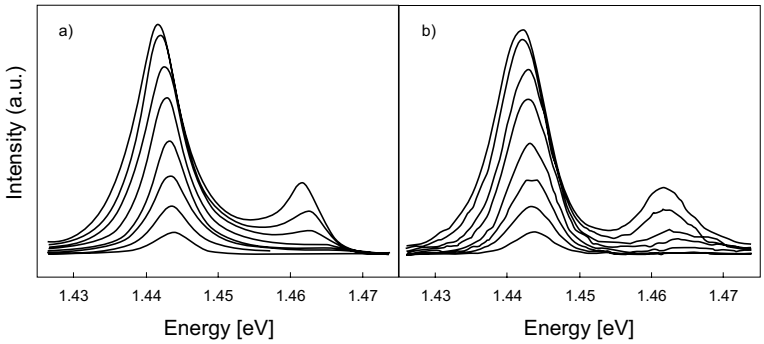

Fig. 19.1 (a) Calculated and (b) measured luminescence spectra. The experiments were done using a modulated barrier $In_{0.13}Ga_{0.87}As/GaAs$ quantum wire at $B = 10.5$ T. The plasma densities and temperatures used in the theoretical spectra have been determined to fit the experimental spectra with increasing excitation power. [After M. Bayer *et al.* (1997).]

librium relation

$$I(\omega) \propto \frac{\mathrm{Im}\{\chi(\omega)\}}{e^{\beta(\hbar\omega-\mu)}-1} \ , \tag{19.38}$$

where $\mu = \mu_e + \mu_h$ is the electron-hole chemical potential with respect to the band gap.

As an example of the resulting spectra, we show in Fig. 19.1 calculated luminescence spectra for a field $B = 10.5$ T, where the magnetic confinement dominates already over the lateral barrier confinement (see problem 19.3). In this situation, the wire resembles already in some respects a $2D$ system in a strong magnetic field. The spectra are calculated for various carrier densities n and plasma temperatures T. The densities and the temperatures are chosen to give the best fit to the corresponding experimental spectra shown in the same figure. The investigated sample is based on a $In_{0.13}Ga_{0.87}As/GaAs$ quantum well. The top $GaAs$ layer has been removed by selective etching, except for a 29 nm wide stripe. This remaining stripe modulates the ground-state energy of the quantum well and causes a lateral confinement. The resulting quantum wire had a width of $L_x = 29\,\mathrm{nm}$. The electron–hole concentration has been generated by a *cw* Ar^+ laser ($\lambda = 514.5$ nm) with power densities of up to $3\,\mathrm{kWcm}^{-2}$. The sample has been immersed in liquid He ($T = 1.8$ K). The appropriate material parameters are: the subband spacing $\Omega \simeq 2E_0 \simeq 8.4\,\mathrm{meV}$, where

E_0 is the $3D$ exciton Rydberg of GaAs. The broadening has been taken to be $\gamma = 1E_0$. At the lowest density of $n = 0.12 \times 10^6\,\mathrm{cm}^{-1}$ and the corresponding lowest excitation power, only the emission from the lowest wire subband is seen. Note that the excess energy of the exciting laser causes heating of the plasma (but not of the lattice), so that the plasma temperature increases with the excitation power from 43 K at the lowest excitation power to 117 K at the highest power. At higher powers the $n = 2$ wire subband starts to be filled so that also luminescence from this next higher level takes place, while the $n = 1$ line saturates. In the excitation region, where also the $n = 2$ subband line is present, both peaks of the two luminescence lines show a slight shift to lower energies at higher excitation powers, which is more pronounced for the $n = 2$ transitions.

In particular, one can see that the $n = 1$ line does not shift at all as long as the the $n = 2$ subband is not filled (the three lowest densities). The calculations show that here already a strong band-gap shift exists, but it is completely compensated by the reduction of the exciton correlations. It is known that for a $2D$ system the compensation is exact in the limit of a strong magnetic field essentially due to the neutrality of the electron–hole pair, which explains the absence of any shift with only one occupied subband. Due to the interaction between carriers in two different subbands, the energy renormalization becomes stronger than the effect of the attractive interactions.

REFERENCES

For the literature of the $2D$ electron in a perpendicular magnetic field see:

L.D. Landau and L.M. Lifshitz, *Quantum Mechanics*, Pergamon, New York 1958
I.V. Lerner and Yu.E. Lozovik, Sov. Phys. JETP **53**, 763 (1981)
D. Paquet, T.M. Rice, and K. Ueda, Phys. Rev. **B32**, 5208 (1985)

$2D$ magneto excitons are treated in:

O. Akimoto and H. Hasegawa, J. Phys. Soc. Jpn. **22**, 181 (1967)
A.H. McDonald and D.S. Ritchie, Phys. Rev. **B33**, 8336 (1986)
C. Stafford, S. Schmitt-Rink, and W. Schäfer, Phys. Rev. **B41**, 10000 (1990)
G.E.W. Bauer, in *Optics of Excitons in Confined Systems*, eds.

A. D'Andrea, R. Del Sole R. Girlanda, and A. Quattropani, Inst. of Phys. Conf. Series No. 123, 283 (1992)

$2D$ magneto-plasmas are treated in:

T. Uenoyama and L.J. Sham, Phys. Rev. **B39**, 11044 (1989)
G.E.W. Bauer, Phys. Rev. Lett. **64**, 60 (1990) and Phys. Rev. **B45**, 9153 (1992)
M. Bayer, Ch. Schlier, Ch. Gréus, S. Benner, and H. Haug, Phys. Rev. **B55**, 13180 (1997)
M.W. Wu and H. Haug, Phys. Rev. **B58**, 13060 (1998)

PROBLEMS

Problem 19.1: Derive the single-particle Hamiltonian (19.8) for the states $\phi_{k,\nu}$.

Problem 19.2: Show that the Coulomb matrix element can be written in the form (19.24), by calculating the integral

$$\int dxdy \int dx'y' \psi^*_{k'n'}(x,y)\psi^*_{k,\nu}(x',y')V(x-x',y-y')\psi_{k',\nu'}(x'y')\psi_{k,\nu}(x,y) \ .$$

Use the Fourier transform of the $2D$ Coulomb potential

$$V(x-x',y-y') = \sum_{q,q_x} \frac{2\pi e^2}{\epsilon_0 \sqrt{q^2+q_x^2}} e^{iq(y-y')} e^{iq_x(x-x')} \ ,$$

and the eigenfunctions (19.14).

Problem 19.3: (a)Calculate the cyclotron energy $\hbar\omega_c = eB/m$ for $B =$ 10.5 T in the $InGaAs/Ga$ quantum wire in units of meV. Use a reduced electron–hole mass of $m = 0.06m_0$, where m_0 is the free electron mass. In SI units, the specific electron charge $e/m_0 = 1.759 \times 10^{11}$A s kg^{-1}, while a Tesla is T = kg s^{-2} A^{-1}. Here, A denotes Ampere.
(b) Calculate for comparison the energy of the subband spacing $\hbar\Omega$ in meV with the same reduced mass.

Chapter 20

Quantum Dots

The ultimate quantum-confinement effects occur in very small semiconductor structures, called *quantum dots*, which confine the laser-excited electron–hole pairs in all three space dimensions. Such systems can be realized in many different ways, including glasses doped with semiconductor microcrystallites, microstructures fabricated by lithographic techniques, interface fluctuations in quantum wells, strain-induced quantum dots and many more. A common aspect of all of these systems is that their geometry provides a confinement potential with a spatial extension comparable to the exciton Bohr radius in the respective semiconductor material. The detailed shape of the potential depends on the respective system, including more or less spherical confinement in microcrystallites, parabolic confinement in interface dots, or more complicated shapes in other systems. For more detailed discussion of experimental realizations of quantum dots and of the resulting confinement potentials, we refer the interested reader to the literature cited at the end of this chapter. Here, we only want to discuss the basic principles of optical excitations in quantum-dot systems.

20.1 Effective Mass Approximation

For most of the discussion in this chapter, we consider a spherical hard wall confinement potential. More precisely, we assume a sphere of radius R and background dielectric constant ϵ_2 embedded in another material with background dielectric constant ϵ_1. It is reasonably straightforward to modify the results for other (simple) geometries, such as microcubes, boxes, or parabolic confinement potentials. We concentrate on systems where

$$R \leq a_0 \ , \tag{20.1}$$

but still much larger than the semiconductor lattice constant. Hence, these quantum dots are mesoscopic structures in the sense of Chap. 4.

Using the envelope function approximation, we assume again that the electron wave function can be written as

$$\psi(\mathbf{r}) = \zeta(\mathbf{r})\, \mathbf{u}_\lambda(\mathbf{k} \simeq \mathbf{0}, \mathbf{r}) \ , \tag{20.2}$$

compare Eq. (4.1). Here, $u_\lambda(\mathbf{k} \simeq \mathbf{0}, \mathbf{r})$ is the Bloch function of the bulk material, and $\zeta(\mathbf{r})$ is the envelope function. The wave function $\psi(\mathbf{r})$ has to satisfy the boundary conditions of the quantum dot. For simplicity, we analyze the case of ideal quantum confinement, i.e.,

$$\psi(r \geq R) = 0 \ . \tag{20.3}$$

Furthermore, we assume that the energy eigenvalues of the electron in the periodic lattice, i.e., the energy bands, are not appreciably modified through the quantum confinement. Therefore, we use the effective mass approximation to describe the free motion of electrons and holes.

The Hamiltonian for one electron–hole pair is

$$\mathcal{H} = \mathcal{H}_e + \mathcal{H}_h + V_{ee} + V_{hh} + V_{eh} \ , \tag{20.4}$$

where the kinetic terms are

$$\mathcal{H}_e = -\frac{\hbar^2}{2m_e} \int d^3r\, \hat{\psi}_e^\dagger(\mathbf{r})\, \nabla^2 \hat{\psi}_e(\mathbf{r}) + E_g \int d^3r\, \hat{\psi}_e^\dagger(\mathbf{r})\, \hat{\psi}_e(\mathbf{r}) \ , \tag{20.5}$$

and

$$\mathcal{H}_h = -\frac{\hbar^2}{2m_h} \int d^3r\, \hat{\psi}_h^\dagger(\mathbf{r}) \nabla^2 \hat{\psi}_h(\mathbf{r}) \ , \tag{20.6}$$

and the Coulomb interaction is described by

$$V_{ee} = \frac{1}{2} \int\int d^3r\, d^3r'\, \hat{\psi}_e^\dagger(\mathbf{r})\, \hat{\psi}_e^\dagger(\mathbf{r}')\, V(\mathbf{r}, \mathbf{r}')\, \hat{\psi}_e(\mathbf{r}')\, \hat{\psi}_e(\mathbf{r}) \ , \tag{20.7}$$

$$V_{eh} = -\int\int d^3r\, d^3r'\, \hat{\psi}_e^\dagger(\mathbf{r})\, \hat{\psi}_h^\dagger(\mathbf{r}')\, V(\mathbf{r}, \mathbf{r}')\, \hat{\psi}_h(\mathbf{r}')\, \hat{\psi}_e(\mathbf{r}) \ , \tag{20.8}$$

and

$$V_{hh} = V_{ee}(e \to h) \ , \tag{20.9}$$

where $V(r)$ is the effective Coulomb interaction potential inside the quantum dot.

The Coulomb interaction between two point charges in a spherical dot, which is embedded in a material with different background dielectric constant, is

$$V(\mathbf{r_1},\mathbf{r_2})|_R = V(\mathbf{r_1},\mathbf{r_2})|_{R=\infty} + \delta V(\mathbf{r_1},\mathbf{r_2}) \ , \tag{20.10}$$

where $V(\mathbf{r_1},\mathbf{r_2})|_{R=\infty}$ is the usual bulk Coulomb interaction, and the additional term is caused by the induced surface charge of the sphere,

$$\delta V(\mathbf{r_1},\mathbf{r_2}) = Q_1(\mathbf{r_1}) + Q_1(\mathbf{r_2}) \mp Q_2(\mathbf{r_1},\mathbf{r_2}) \ , \tag{20.11}$$

with -(+) for charges with opposite (equal) sign, respectively (Brus, 1984). The different contributions in Eq. (20.11) are

$$Q_1(\mathbf{r}) = \sum_{n=0}^{\infty} Q_{1,n}(r) \ , \tag{20.12}$$

with

$$Q_{1,n}(r) = \frac{e^2}{2R}\,\alpha_n\,(r/R)^{2n} \ , \tag{20.13}$$

and

$$Q_2(\mathbf{r_1},\mathbf{r_2}) = \sum_{n=0}^{\infty} Q_{2,n}(\mathbf{r_1},\mathbf{r_2}) \ , \tag{20.14}$$

with

$$Q_{2,n}(\mathbf{r_1},\mathbf{r_2}) = \alpha_n\,\frac{e^2}{R}\left(\frac{r_1 r_2}{R^2}\right)^n\, P_n\big[\cos(\theta)\big] \ , \tag{20.15}$$

where θ is the angle between $\mathbf{r}_1$ and $\mathbf{r}_2$, P_n is the n-th order Legendre polynomial and

$$\alpha_n = \frac{(\epsilon_2/\epsilon_1 - 1)(n+1)}{\epsilon_2(n\,\epsilon_2/\epsilon_1 + n + 1)} \ . \tag{20.16}$$

Obviously, the surface polarization term δV vanishes for $\epsilon_1 = \epsilon_2$.

20.2 Single Particle Properties

The eigenstates and energy eigenvalues for a single electron in the quantum dot are determined by the Schrödinger equation

$$\mathcal{H}|\psi_e\rangle = E_e\,|\psi_e\rangle \ . \tag{20.17}$$

The eigenstate is of the form

$$|\psi_e\rangle = \int d^3r\,\zeta_e(\mathbf{r})\hat{\psi}_e^\dagger(\mathbf{r})\,|0\rangle \ , \tag{20.18}$$

where $|0\rangle$ is the crystal ground state, i.e., the state without excited electrons or holes. The coefficients $\zeta(\mathbf{r})$ in Eq. (20.18) have to be determined from Eq. (20.17). Using the Hamiltonians (20.6) – (20.9) in Eq. (20.17), we find

$$V_{ee}\,|\psi_e\rangle = V_{eh}\,|\psi_e\rangle = V_{hh}\,|\psi_e\rangle = \mathcal{H}_h\,|\psi_e\rangle = 0 \ . \tag{20.19}$$

However, we have

$$\begin{aligned}\mathcal{H}_e\,|\psi_e\rangle = & -\frac{\hbar^2}{2m_e}\int d^3r'[\nabla^2\hat{\psi}_e^\dagger(\mathbf{r}')]\,\hat{\psi}_e(\mathbf{r}')\int d^3r\,\zeta_e(\mathbf{r})\,\hat{\psi}_e^\dagger(\mathbf{r})\,|0\rangle \\ & +E_g\int d^3r'\int d^3r\,\hat{\psi}_e^\dagger(\mathbf{r}')\,\psi_e(\mathbf{r}')\,\zeta_e(\mathbf{r})\,\hat{\psi}_e^\dagger(\mathbf{r})\,|0\rangle \ ,\end{aligned}$$

which can be written as

$$\begin{aligned}\mathcal{H}_e\,|\psi_e\rangle &= -\frac{\hbar^2}{2m_e}\int d^3r'\int d^3r\,\zeta_e(\mathbf{r})\,\delta(\mathbf{r}-\mathbf{r}')\,[\nabla^2\hat{\psi}_e^\dagger(\mathbf{r}')]\,|0\rangle \\ &\quad +E_g\int d^3r'\int d^3r\,\zeta_e(\mathbf{r})\,\hat{\psi}_e^\dagger(\mathbf{r})\,\delta(\mathbf{r}-\mathbf{r}')\,|0\rangle \\ &= -\frac{\hbar^2}{2m_e}\int d^3r\,[\nabla^2\zeta_e(\mathbf{r})]\,\hat{\psi}_e^\dagger(\mathbf{r})|0\rangle + E_g\int d^3r\,\zeta_e(\mathbf{r})\,\hat{\psi}_e^\dagger(\mathbf{r})\,|0\rangle \\ &= E_e\int d^3r\,\zeta_e(\mathbf{r})\,\hat{\psi}_e^\dagger(\mathbf{r})\,|0\rangle \ .\end{aligned} \tag{20.20}$$

This equation is satisfied if

$$-\frac{\hbar^2}{2m_e}\,\nabla^2\zeta_e(\mathbf{r}) = (E_e - E_g)\,\zeta_e(\mathbf{r}) \ , \tag{20.21}$$

which is the one-electron eigenvalue equation. Similarly, we find for the one-hole state

$$-\frac{\hbar^2}{2m_h}\,\nabla^2\zeta_h(\mathbf{r}) = E_h\,\zeta_h(\mathbf{r}) \ . \tag{20.22}$$

The problem is completely defined with the boundary conditions

$$\zeta_e(\mathbf{r}) = \zeta_h(\mathbf{r}) = 0 \quad \text{for} \quad |\mathbf{r}| \geq R \ . \tag{20.23}$$

The solution is

$$\boldsymbol{\zeta_{e,nlm}(\mathbf{r}) = \sqrt{\frac{2}{R^3}}\,\frac{j_l(\alpha_{nl}r/R)}{j_{l+1}(\alpha_{nl})}\,Y_{l,m}(\Omega)} \ , \tag{20.24}$$

single-particle wave function in quantum dot

where j_l is the spherical Bessel function of order l and $Y_{l,m}$ denotes the spherical harmonics. The boundary condition (20.23) is satisfied if

$$j_l(\alpha_{nl}) = 0 \quad \text{for} \quad n = 1, 2, \cdots \tag{20.25}$$

and

$$\begin{aligned} &\alpha_{10} = \pi,\ \alpha_{11} = 4.4934,\ \alpha_{12} = 5.7635,\ \alpha_{20} = 6.2832 \ , \\ &\alpha_{21} = 7.7253,\ \alpha_{22} = 9.0950,\ \alpha_{30} = 9.4248 \cdots \ . \end{aligned} \tag{20.26}$$

Since the wave function (20.24) depends only on R and not on any physical parameters which are specific for the electron, the corresponding wave function for the hole must have the same form, and we can drop the index e/h of the functions $\zeta(\mathbf{r})$ from now on. Inserting (20.24) into Eq. (20.22), we obtain the discrete energies

$$E_{e,nlm} = E_g + \frac{\hbar^2}{2m_e}\,\frac{\alpha_{nl}^2}{R^2} \tag{20.27}$$

and

$$E_{h,nlm} = \frac{\hbar^2}{2m_h}\,\frac{\alpha_{nl}^2}{R^2} \ . \tag{20.28}$$

The nl eigenstates are usually referred to as $1s$, $1p$, etc. The lowest two energy levels given by Eqs. (20.27) and (20.28) are shown schematically in Fig. 20.1. In practice, however, the single-particle spectrum is rather

uninteresting since it is not observed in optical absorption measurements. As discussed before, the absorption is always given by the electron–hole–pair excitation spectrum.

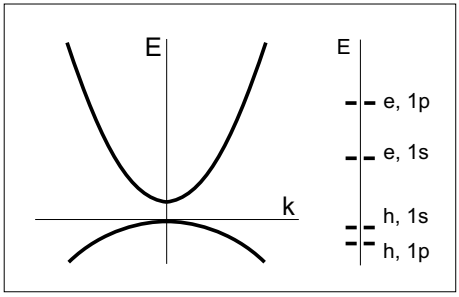

Fig. 20.1 Schematic plot of the single-particle energy spectrum in bulk semiconductors (left). The single-particle energies for electrons (e) and holes (h) in small quantum dots are shown in the right part of the figure.

20.3 Pair States

For the electron-hole-pair eigenstates, we make the ansatz

$$|\psi_{eh}\rangle = \int\int d^3r_e\, d^3r_h\, \psi_{eh}(\mathbf{r}_e, \mathbf{r}_h)\hat{\psi}_e^\dagger(\mathbf{r}_e)\hat{\psi}_h^\dagger(\mathbf{r}_h)\,|0\rangle \tag{20.29}$$

and obtain the Schrödinger equation for the pair

$$\left[-\frac{\hbar^2}{2m_e}\nabla_e^2 - \frac{\hbar^2}{2m_h}\nabla_h^2 - V(\mathbf{r_e}, \mathbf{r_h})\right]\psi_{eh}(\mathbf{r_e}, \mathbf{r_h}) = (E - E_g)\psi_{eh}(\mathbf{r_e}, \mathbf{r_h}) \ . \tag{20.30}$$

Because of the boundary conditions

$$\psi_{eh}(\mathbf{r_e}, \mathbf{r_h}) = 0 \text{ if } |\mathbf{r}_e| > R \quad \text{or} \quad |\mathbf{r}_h| > R \ , \tag{20.31}$$

it is not useful to introduce relative and center-of-mass coordinates in contrast to the case of bulk or quantum-well semiconductor materials.

If the quantum dot radius is smaller than the bulk-exciton Bohr radius, $R < a_0$, electron and hole are closer together than they would be in

the corresponding bulk material. This leads to a dramatic increase of the pair energy with decreasing quantum-dot size. As function of quantum-dot radius, the kinetic part of the energy varies like

$$\langle \mathcal{H}_e + \mathcal{H}_h \rangle \propto \frac{1}{R^2} \ , \tag{20.32}$$

whereas the interaction part behaves like

$$\langle V_{ij} \rangle \propto \frac{1}{R} \ . \tag{20.33}$$

To obtain an estimate of the pair energy for small dot radii, $R << a_0$, it is a reasonable first-order approximation to consider the electrons and the holes essentially as noninteracting and ignore the Coulomb energy in comparison to the kinetic energy. This yields

$$E_{eh,nlm} = E_{e,nlm} + E_{h,nlm} \ , \tag{20.34}$$

i.e., an energy variation proportional to R^{-2}. Experimentally, this increasing pair energy is observed as a pronounced blueshift of the onset of absorption with decreasing dot size.

It is not analytically possible to solve the pair Schrödinger equation (20.30) including the Coulomb interaction. Therefore, one has to use numerical or approximation methods. One method consists of expanding the full pair-state into the eigenstates of the system without Coulomb interactions,

$$|\psi_{eh,lm}\rangle = \sum_{\substack{n_1, n_2 \\ l_1, l_2}} C_{n_1,n_2,l_1,l_2} \, |n_1 n_2 l_1 l_2; lm\rangle \ . \tag{20.35}$$

For such an expansion, it is important to note that the total angular momentum operator $\hat{L}$ commutes with the Hamiltonian, i.e., the angular momentum is a good quantum number and the eigenstates of the Hamiltonian are also eigenstates of $\hat{L}^2$ and $\hat{L}_z$. A convenient choice of the one-pair-state basis functions is

$$|n_1 n_2 l_1 l_2; lm\rangle = \sum_{m_1 m_2} \langle l_1 m_1 l_2 m_2 | lm \rangle \, |n_1 l_1 m_1\rangle_e \, |n_2 l_2 m_2\rangle_h \ , \tag{20.36}$$

where $\langle l_1 m_1 l_2 m_2 | lm \rangle$ is the Clebsch-Gordan coefficient and l and m the angular momentum quantum numbers of the pair state.

Using the expansion (20.36), we compute the expectation value of the Hamiltonian truncating the expansion at finite values of n, l and m. This transforms the Hamiltonian into a matrix. Eqs. (20.32) – (20.33) show that for the regime of sufficiently small quantum dots, the single-particle energies are much larger than the Coulomb contributions. Therefore, the off-diagonal elements in the Hamiltonian matrix are small in comparison to the diagonal elements and the truncation of the expansion introduces only small errors. The magnitude of these errors can be checked by using increasingly large $n_i l_i m_i$ values. Numerical diagonalization of the resulting matrix yields the energy eigenvalues and the expansion coefficients of the pair wave function (Hu *et al.*, 1990). Examples of the results are shown in Fig. 20.2, where we plot the ground-state energy E_{1s} for one electron–hole pair as function of the quantum-dot radius. This figure clearly shows the sharp energy increase for smaller dots expected from Eq. (20.34).

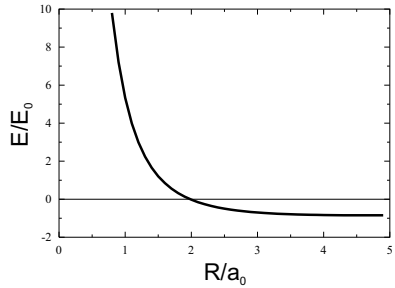

Fig. 20.2 Plot of the ground-state energy of one electron–hole pair in a quantum dot. Energy and radius are in units of the bulk–exciton Rydberg E_0 and Bohr radius a_0, respectively. The electron–hole mass ratio has been chosen as $m_e/m_h = 0.1$.

For convenience, we also use the notation $1s$, $1p$, etc. for the situation with Coulomb interaction. This notation indicates that the leading term in the wave function expansion is the product of the $1s$ single-particle functions,

$$\psi_{eh}(r_e, r_h) \simeq \zeta_{100}(r_e)\,\zeta_{100}(r_h) + \text{other states} \ . \tag{20.37}$$

Note, however, that if one keeps only this product state and neglects the rest, one may get completely wrong answers for quantities like binding energies or transition dipoles.

In Fig. 20.3, we show an example of the radial distributions, which is defined as

$$\mathbf{Pr} = r_e^2 \int d\Omega_e \, d^3 r_h \, r_h^2 \, |\psi_{eh}(\mathbf{r_e}, \mathbf{r_h})|^2 \tag{20.38}$$

for the electron and correspondingly for the hole in the quantum dot. Fig. 20.3 shows that, as a consequence of the electron–hole Coulomb interaction, the heavier particle, i.e., the hole, is pushed toward the center of the sphere.

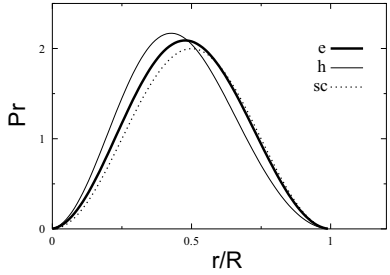

Fig. 20.3 Plot of the distribution, Eq. (20.38), of an electron (e) and a hole (h) in a quantum dot with $R/a_0 = 1$. The lowest curve (sc) shows the distribution if one neglects the Coulomb interaction.

In addition to the numerical solution, one can also find an approximate analytical solution for the state with one electron–hole pair in quantum dots if the electron–hole mass ratio, m_e/m_h, is very small. In this case, the motion of the particles may be approximately decoupled, as in the hydrogen-atom problem, and

$$a_0 \simeq \frac{\hbar^2}{m_e \, e^2} \quad . \tag{20.39}$$

Since the electron states are well separated in energy, we may concentrate on the lowest single electron states. The single-particle hole states are closer in energy and correlations between the states are more important. Therefore, we use the ansatz for the pair wave function

$$\psi_{eh,nlm}\,(\mathbf{r}_e, \mathbf{r}_h) \simeq \zeta_{nlm}(\mathbf{r}_e)\, \psi_h(\mathbf{r}_h) \quad . \tag{20.40}$$

Inserting (20.40) into Eq. (20.30) and projecting with $\zeta^*_{nlm}(\mathbf{r}_e)$, we obtain

$$\left[-\frac{\hbar^2}{2m_e}\,\nabla_h^2 - \int d^3r_e\,|\zeta_{nlm}(\mathbf{r}_e)|^2\,V(\mathbf{r}_e,\mathbf{r}_h)\right]\,\psi_h(\mathbf{r}_h)$$
$$= \left(E_{eh} - E_g - \frac{\hbar^2}{2m_e}\,\frac{\alpha_{nl}^2}{R^2}\right)\,\psi_h(\mathbf{r}_h)\ . \tag{20.41}$$

Eq. (20.41) describes the motion of the hole in the average potential induced by the electron. The potential is attractive and if we take $(nlm) = (100)$ it is spherically symmetrical. This effective potential is responsible for pushing the hole toward the center of the sphere, as shown in Fig. 20.3.

20.4 Dipole Transitions

In order to compute the optical response of semiconductor quantum dots, we need the dipole transition matrix elements between the different electron–hole–pair states. The interaction Hamiltonian is written as

$$\hat{\mathcal{H}}_{int} = -\hat{\boldsymbol{P}}\cdot\boldsymbol{\mathcal{E}}(t)\ , \tag{20.42}$$

where $\hat{\boldsymbol{P}}$ is the polarization operator and $\boldsymbol{\mathcal{E}}(t)$ is the light field. The polarization is a single-particle operator, which can be written as

$$\hat{\boldsymbol{P}} = \int d^3r \sum_{i,j=e,h} \hat{\psi}_i^\dagger(\mathbf{r})\,e\mathbf{r}\,\hat{\psi}_j(\mathbf{r})$$

or, evaluating the summation,

$$\hat{\boldsymbol{P}} = \int d^3r e\mathbf{r}\Big[\hat{\psi}_e^\dagger(\mathbf{r})\hat{\psi}_e(\mathbf{r}) + \hat{\psi}_h(\mathbf{r})\hat{\psi}_h^\dagger(\mathbf{r}) + \hat{\psi}_e^\dagger(\mathbf{r})\hat{\psi}_h^\dagger(\mathbf{r}) + \hat{\psi}_h(\mathbf{r})\hat{\psi}_e(\mathbf{r})\Big]\ . \tag{20.43}$$

The field operators are expanded as

$$\hat{\psi}_e(\mathbf{r}) = \sum_{nlm} \psi_{nlm}^e(\mathbf{r})\,a_{nlm} \tag{20.44}$$

and

$$\hat{\psi}_h(\mathbf{r}) = \sum_{nlm} \psi_{nlm}^h(\mathbf{r})\,b_{nlm}\ , \tag{20.45}$$

where $\psi(\mathbf{r})$ is the single-particle wave function (20.2) with $\zeta(\mathbf{r})$ given by (20.24), and a_{nlm} and b_{nlm} are the annihilation operators for an electron or hole in the state nlm, respectively. Inserting the expansions (20.44) and (20.45) into (20.43) yields an explicit expression for the polarization operator. In the evaluation, we basically follow the line of argumentation explained in Sec. 10.1. This way, we obtain for the first term in Eq. (20.43)

$$\int d^3r e\mathbf{r}\hat{\psi}_e^\dagger(\mathbf{r})\hat{\psi}_e(\mathbf{r}) \simeq \sum_{\substack{nlm \\ n'l'm'}} a_{nlm}^\dagger a_{n'l'm'} \sum_{\substack{unit \\ cells}} e\mathbf{R}\zeta_{nlm}^*(\mathbf{R})\zeta_{n'l'm'}(\mathbf{R}) \ . \tag{20.46}$$

Replacing the sum over the unit cells by an integral yields

$$\begin{aligned} \int d^3r\, e\mathbf{r}\, \hat{\psi}_e^\dagger(\mathbf{r})\, \hat{\psi}_e(\mathbf{r}) &= \sum_{\substack{nlm \\ n'l'm'}} a_{nlm}^\dagger\, a_{n'l'm'} \int d^3R\, e\mathbf{R}\, \zeta_{nlm}^*(\mathbf{R})\, \zeta_{n'l'm'}(\mathbf{R}) \\ &\equiv \sum_{\substack{nlm \\ n'l'm'}} \mathbf{p}_{nlm;n'l'm'}\, a_{nlm}^\dagger\, a_{n'l'm'} \ . \end{aligned} \tag{20.47}$$

Using the symmetries of the functions ζ_{nlm}, Eq. (20.24), one can verify that

$$\mathbf{p}_{nlm;nlm} = 0 \,,$$

and

$$\mathbf{p}_{nlm;n'l'm'} \neq 0 \quad \text{for} \quad n \neq n' \,; \quad l - l' = 0 \ , \pm 1 \,; \quad m - m' = 0 \,, \pm 1 \ . \tag{20.48}$$

The second term of Eq. (20.30) is evaluated by making the appropriate $e \to h$ replacements in Eqs. (20.46) and (20.47). The result shows that these two terms do not involve creation or destruction of electron–hole pairs. Their only effect is to change the state of either the electron or the hole, leaving the respective state of the other particle unchanged. These terms therefore describe *"intraband" transitions*.

The last two terms in Eq. (20.43) involve creation and annihilation of electron–hole pairs, i.e., *"interband" transitions*. For these terms, we get

$$\int d^3r\, e\mathbf{r}\, \hat{\psi}_e^\dagger(\mathbf{r})\, \hat{\psi}_h^\dagger(\mathbf{r}) = \mathbf{d}_{c\nu} \sum_{\substack{nlm \\ n'l'm'}} a_{nlm}^\dagger\, b_{n'l'm'}^\dagger \int d^3R\, \zeta_{nlm}^*(\mathbf{R})\, \zeta_{n'l'm'}(\mathbf{R})$$

$$= \mathbf{d}_{c\nu} \sum_{nlm} a_{nlm}^\dagger\, b_{nlm}^\dagger \quad , \tag{20.49}$$

where

$$\mathbf{d}_{c\nu} = \int d^3r\, e\mathbf{r}\, u_c^*(\mathbf{r}) u_v(\mathbf{r}) \quad . \tag{20.50}$$

Hence, we see that this term introduced transitions between states in different bands, creating pairs of electrons and holes with the same quantum numbers.

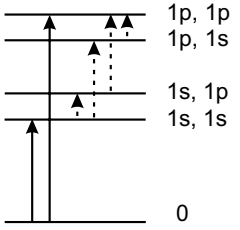

Fig. 20.4 Energy level scheme for the states with zero or one electron–hole pair. The "interband transitions" are indicated by the arrows connecting the ground state to the $1s, 1s$ and the $1p, 1p$ state. The "intraband transitions" are shown as dashed arrows.

In Fig. 20.4, we plot schematically the energy spectrum of the energetically lowest one-electron–hole–pair states with total angular momentum $\mathrm{l} = 0,\ \mathrm{l} = 1$. The solid lines indicate the most important dipole-allowed interband transitions. The dashed lines show the intraband transitions involving a change of the state of the electron or the hole.

20.5 Bloch Equations

In this section, we derive the optical Bloch equations for quantum dots using density matrix theory (compare Chap. 4). The reversible part of the dynamic equation for the density matrix is given by the Liouville equation

$$i\hbar \frac{\partial}{\partial t} \rho = [\mathcal{H} + \mathcal{H}_I, \rho] \ , \tag{20.51}$$

where $\mathcal{H}$ is the total Hamiltonian of the electronic excitations in the quantum dot, and $\mathcal{H}_I$ describes the dipole coupling to the light field. Damping can be modeled microscopically by explicitly introducing the respective interactions, however, for our purposes it is sufficient to simply use the appropriate phenomenological damping constants in the final equations.

After the diagonalization, the quantum-dot Hamiltonian can be written in the form

$$\mathcal{H} = \sum_e \hbar\omega_e \, P_{ee} + \sum_b \hbar\omega_b \, P_{bb} \ , \tag{20.52}$$

where the indices e and b refer to the one-pair and two-pair states, and $\hbar\omega_e$ and $\hbar\omega_b$ are the numerically computed energy eigenvalues, respectively. The operators P_{ij} are projectors which in the bracket formalism have the form $|i\rangle\langle j|$. The interaction Hamiltonian is then

$$\mathcal{H}_I = -\sum_e \mu_{eo} \ P_{eo} - \sum_{eb} \mu_{be} \ P_{be} + \text{h.c.} \ , \tag{20.53}$$

where

$$\mu_{ij} = \mathbf{d}_{ij} \cdot \boldsymbol{\mathcal{E}}(t) \tag{20.54}$$

and the index o refers to the ground state without any electron–hole pairs.

The density matrix is the sum of all diagonal and off-diagonal contributions

$$\begin{aligned} \rho = \rho_{oo}|o><o| + \sum_{ee'} \rho_{ee'}|e><e'| + \sum_{bb'} \rho_{bb'}|b><b'| \\ + \sum_e (\rho_{eo}|e><o| + h.c) + \sum_{be} (\rho_{be}|b><e| + h.c) \\ + \sum_b (|b><o| + h.c.) \ . \end{aligned} \tag{20.55}$$

Inserting Eq.(20.55) into Eq.(20.51) and projecting the resulting equation onto the different states, one obtains for the matrix elements the equations of motion

$$
\begin{aligned}
i\hbar\frac{d\rho_{eo}}{dt} &= \hbar\omega_e\rho_{eo} + \sum_{e'}\mu_{e'o}\rho_{ee'} - \sum_{b}\mu_{eb}\rho_{bo} - \mu_{eo}\rho_{oo} \\
i\hbar\frac{d\rho_{be}}{dt} &= \hbar(\omega_b - \omega_e)\rho_{be} - \sum_{e'}\mu_{be'}\rho_{e'e} + \sum_{b'}\mu_{b'e}\rho_{bb'} + \mu_{oe}\rho_{bo} \\
i\hbar\frac{d\rho_{ee'}}{dt} &= \hbar(\omega_e - \omega_{e'})\rho_{ee'} + \mu_{oe'}\rho_{eo} - \mu_{eo}\rho_{oe'} - \sum_{b}(\mu_{eb}\rho_{be'} - \mu_{be'}\rho_{eb}) \\
i\hbar\frac{d\rho_{bb'}}{dt} &= \hbar(\omega_b - \omega_{b'})\rho_{bb'} + \sum_{e}(\mu_{eb'}\rho_{be} - \mu_{be}\rho_{eb'}) \\
i\hbar\frac{d\rho_{bo}}{dt} &= \hbar\omega_b\rho_{bo} - \sum_{e}(\mu_{be}\rho_{eo} - \mu_{eo}\rho_{be}) \\
\rho_{oo} &= 1 - \sum_{e}\rho_{ee} - \sum_{b}\rho_{bb} \ . \qquad (20.56)
\end{aligned}
$$

multilevel Bloch equations for quantum dots

If one wants to compute optical properties of semiconductor quantum dots, it is in general necessary to numerically evaluate Eqs. (20.56) for the relevant excitation conditions. Using these solutions the optical polarization is then obtained as

$$P(t) = \sum_{e} d_{oe}\rho_{eo}(t) + \sum_{eb} d_{eb}\rho_{be}(t) + \text{h.c.} \ , \qquad (20.57)$$

where $\mathbf{d}_{ij}$ is the dipole matrix element in field direction.

20.6 Optical Spectra

In the following, we calculate the steady-state optical properties for pump-probe excitation and different levels of the pump intensity. To gain some insights, we first analyze the linear absorption properties. For an unexcited system, only transitions between the ground state and the one-pair states

contribute. Hence, the linear polarization can be written as

$$P_l = \sum_e d_{oe}\,\rho_{eo} + \text{h.c.}\ , \tag{20.58}$$

where ρ_{eo} has to be evaluated linear in $\mathcal{E}_p$. The susceptibility is then obtained from

$$\chi_l(\omega) = \frac{P_l(\omega)}{\mathcal{E}_p(\omega)}\ , \tag{20.59}$$

where $\mathcal{E}_p(\omega)$ is the amplitude of the weak test beam.

Introducing a phenomenological damping constant γ_e and keeping only terms that are of first order in the field, we obtain from Eqs. (20.56),

$$\frac{\partial}{\partial t}\,\rho_{oe}^{(1)} = -(i\omega_e + \gamma_e)\rho_{oe}^{(1)} + i d_{oe}\,\frac{\mathcal{E}_p(t)}{\hbar}\ . \tag{20.60}$$

Solving Eq. (20.60) and inserting the result into Eq. (20.58), we obtain the linear susceptibility as

$$\chi_l(\omega) = \frac{i}{\hbar}\sum_e |d_{oe}|^2\,\left[\frac{1}{\gamma_e + i(\omega_e - \omega)} + \frac{1}{\gamma_e - i(\omega_e + \omega)}\right]\ . \tag{20.61}$$

The corresponding absorption coefficient is then

$$\boldsymbol{\alpha_l(\omega)\ =\ \frac{4\pi\omega}{\hbar c\sqrt{\epsilon_2}}\sum_e |d_{oe}|^2\,\frac{\gamma_e}{\gamma_e^2 + (\omega_e - \omega)^2}}\ , \tag{20.62}$$

linear absorption coefficient for quantum dots

where only the resonant part was taken into account.

Eq. (20.62) shows that the absorption spectrum of a single quantum dot consists of a series of Lorentzian peaks centered around the one-electron–hole–pair energies $\hbar\omega_e$. To compare the theoretical results with experimental measurements of real quantum dot systems, however, one has to take into account that there is always a certain distribution of dot sizes $f(R)$ around a mean value $\bar{\mathrm{R}}$. Since the single-particle energies depend strongly on R, the R-distribution introduces a pronounced inhomogeneous broadening of the observed spectra. Theoretically, this can be modeled easily by noting that α_l in Eq. (20.62) is actually $\alpha_l|_R$, i.e., the linear absorption

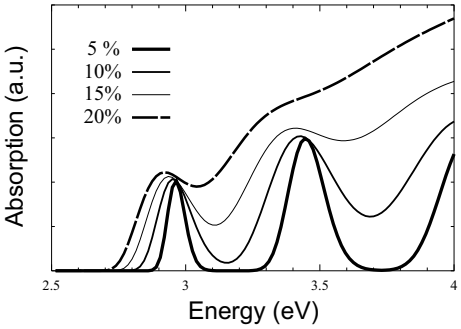

Fig. 20.5 Linear absorption for CdS quantum dots with a Gaussian size distribution around a mean radius of 20 Å. The different curves are for the widths of the Gaussian size distribution indicated in the figure.

spectrum for a given radius R. The average absorption is then computed as

$$\alpha_l(\omega)|_{a\nu} = \int_0^\infty dR\, f(R)\, \alpha_l(\omega)|_R \ . \tag{20.63}$$

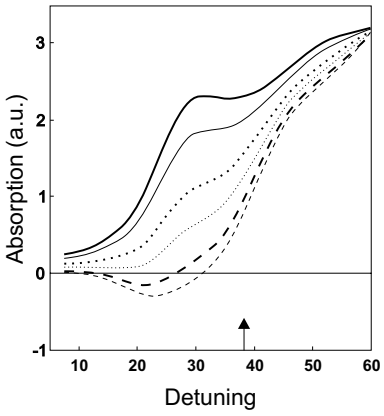

Fig. 20.6 Computed probe absorption spectra for increasing pump generated populations of the one- and two-pair states. The detuning is $(\hbar\omega - E_g)/E_0$. The arrow indicates the frequency of the pump laser. [From Hu *et al.* (1996).]

Using for $f(R)$ simply a Gaussian distribution around $\bar{R} = 20$ Å, we obtain for CdS quantum dots the results shown in Fig. 20.5. One clearly sees the energetically lowest one-pair resonances, which merge to a continuous structure with increasing width of the size distribution. Absorption spectra similar to those in Fig. 20.5 are experimentally observed in many quantum dot systems.

In the nonlinear regime, one has to solve the full set of Bloch equations (20.56). Assuming a pump–probe configuration, we obtain increasing levels of one- and two-pair-state populations with increasing intensities of the pump beam. For such a situation, Hu *et al.* (1996) computed the series of probe absorption spectra, shown in Fig. 20.6. We see a gradual bleaching of the energetically lowest transitions until, at sufficiently high excitation level, negative absorption, i.e., optical gain occurs. This gain can be used to produce semiconductor lasers with quantum dots as active material. For these lasers, one typically uses arrays of quantum dots based on III-V materials. More details can be found, e.g. in Bimberg *et al.* (1999).

REFERENCES

The "classical" papers introducing the theory of semiconductor quantum dots are:

L.E. Brus, J. Chem. Phys. **80**, 4403 (1984)
Al. L. Efros and A.L. Efros, Sov. Phys. Semicond., **16**, 772(1982)

Reference books on semiconductor quantum dots include:

L. Banyai and S.W. Koch, Semiconductor Quantum Dots, World Scientific Publ., Singapore (1993)
U. Woggon, Optical Properties of Semiconductor Quantum Dots, Springer Tracts in Modern Physics 136, Springer Verlag, Berlin (1997)
D. Bimberg, M. Grundmann, and N.N. Ledentsov, Quantum Dot Heterostructures, Wiley and Sons, New York (1999)

The work presented in this chapter is largely based on:

Y.Z. Hu, M. Lindberg, and S.W. Koch, Phys. Rev. **B42**, 1713 (1990)

see also:

Y.Z. Hu, H. Giessen, N. Peyghambarian, and S.W. Koch, Phys. Rev. **B53**, 4814 (1996)

PROBLEMS

Problem 20.1: Compute the effective Coulomb interaction potential between two point charges in a dielectric sphere of radius R and background dielectric constant ϵ_2 which is embedded in a medium with background dielectric constant ϵ_1.

Problem 20.2: Solve Eq. (20.21) for a quantum-box. Discuss the single-particle energy eigenvalues as function of box-length.

Problem 20.3: Evaluate the Liouville equation (20.51) for the density matrix given in Eq. (20.55). Show, that the density-matrix elements obey the multilevel Bloch equations (20.56).

Problem 20.4: Expand the multilevel Bloch equations (20.56) in third order in the pump field and derive the corresponding nonlinear optical susceptibility.

Chapter 21

Coulomb Quantum Kinetics

In this final chapter, we come back to the discussion of the scattering terms in the semiconductor Bloch equations (12.19). So far, we have treated only scattering of carriers with LO-phonons (see chapter 12). However, for the proper analysis of configurations with finite carrier densities, we have to include carrier–carrier scattering and the screening of the Coulomb potential.

Screening by optically generated carriers in a semiconductor can be treated quite naturally in the framework of nonequilibrium Green's functions, where the interaction is described by a dynamical two-time-dependent propagator. This allows us to investigate, e.g., the dynamical build-up of screening after ultrafast carrier excitation. This dynamics reflects the time it takes the generated carriers to rearrange themselves in order to optimally screen their mutual interaction potential.

Because nonequilibrium, or Keldysh Green's functions may be less familiar to the reader, we present a relatively simple introduction into this technique in Appendix B. For a more complete coverage, we refer to the books quoted at the end of the chapter.

We note at this point, that the theory of reduced density matrices also allows us to treat screening. Here, one has to include the equations of motion of all two-particle (or four-point) density matrices, as has been known in plasma physics for quite some time. Because this treatment is less explored and quite involved in a two-band semiconductor, we refer again to the literature quoted at the end of this chapter. Generally, it turns out that both methods have their own advantages and are particularly well suited for specific approximations, as will be shown below.

After presenting the general formulation of the problem, we proceed in this chapter by first treating the interaction as a given statically screened

object. This is a good assumption for time scales that are long compared to the inverse plasma frequency. We evaluate the scattering integral by including the direct and exchange contributions. This approximation is called the second Born approximation.

The quantum kinetics of the femtosecond build-up of screening is then treated in the last section of this chapter. The screening develops roughly within the period of a plasma oscillation. In a next step, we then treat the combined dynamical interactions by the exchange of longitudinal plasmons and optical phonons. In order to reduce the complexity, the exchange interaction is neglected in this discussion.

21.1 General Formulation

As derived in Appendix B, the scattering integral for the single-time density matrix $\rho(t)$ in a spatially homogeneous situation is given by

$$\left.\frac{\partial \rho_{\mathbf{k}}(t)}{\partial t}\right|_{scatt} = -\int_{-\infty}^{t} dt' \Big[\Sigma_{\mathbf{k}}^{>}(t,t')G_{\mathbf{k}}^{<}(t',t) - \Sigma_{\mathbf{k}}^{<}(t,t')G_{\mathbf{k}}^{>}(t',t) - G_{\mathbf{k}}^{>}(t,t')\Sigma_{\mathbf{k}}^{<}(t',t) + G_{\mathbf{k}}^{<}(t,t')\Sigma_{\mathbf{k}}^{>}(t',t)\Big] \quad . \tag{21.1}$$

quantum kinetic collision integral

Here, the density matrix, the particle propagators $G^{<}, G^{>}$ and the scattering self-energies $\Sigma^{<}, \Sigma^{>}$ are all matrices in the band indices. Eq. (21.1) shows that the dynamics of the single-time density matrix is coupled to two-time propagators, so that one does not have a closed equation for the density matrix. Without scattering, i.e., for free particles or particles which experience only a mean field interaction, one can show that the two-time propagators can be expressed in terms of single-time density matrices and a retarded or advanced Green's function which describes the correlation between the times t and t':

$$G^{<}(t,t') = i\langle a^{\dagger}(t')a(t)\rangle = -G^{r}(t,t')\rho(t') + \rho(t)G^{a}(t,t') \quad . \tag{21.2}$$

generalized Kadanoff–Baym ansatz

This equation is often called generalized Kadanoff–Baym ansatz. It holds

in systems where the interaction is weak. Once the scattering self-energies are also expressed in terms of the particle propagators, the generalized Kadanoff–Baym ansatz allows one to close the equation. Naturally, the retarded and advanced Green's functions have still to be evaluated self-consistently in the mean-field approximation. By self-consistently we mean that both quantities have to be computed jointly within the numerical integration of the coupled equations for ρ and the spectral functions. In this way, these spectral functions can still describe nontrivial renormalizations such as the Hartree–Fock band-edge renormalizations, excitonic effects, or the optical Stark effect.

Let us now turn to the evaluation of the scattering self-energy. Instead of formulating the perturbation theory in terms of unperturbed Green's functions and bare interaction potentials, we apply a self-consistent scheme in which the self-energies are expressed by the dressed particle propagators and screened interaction potentials. In Fig. 21.1, the Feynman diagrams are given for those terms that are included in this treatment. The first diagram, called the GW approximation, would actually be the exact one, if the full vertex correction was included. The second diagram of Fig. 21.1 is the first vertex correction or the exchange self-energy, as can be seen from the crossing particle lines.

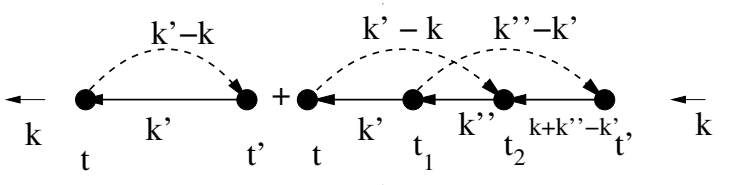

Fig. 21.1 Feynman diagrams for the scattering self-energy with the GW self-energy and the exchange self-energy, also called first vertex correction.

To show that the second diagram in Fig. 21.1 is indeed a vertex correction, we redraw it in the way shown in Fig. 21.2. This way, we obtain the same type of diagram as the first one in Fig. 21.1, however, the left vertex (or interaction point) is renormalized. Naturally, an infinite series of higher and higher vertex corrections should be included to make the self-energy exact. Unfortunately, such a procedure is not possible.

Not even the summation of a selected class of vertex corrections, called

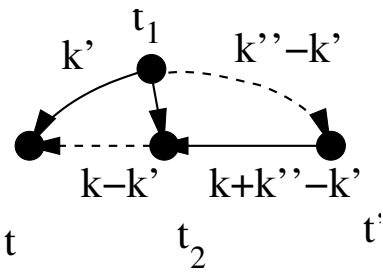

Fig. 21.2 The scattering exchange self-energy drawn as vertex correction of the GW self-energy.

the ladder diagrams shown in Fig. 21.3, have so far been evaluated in the nonequilibrium many-body theory, because of its complexity.

It is important to remember that all nonequilibrium Feynman diagrams have to be evaluated for times which are ordered on the Keldysh contour which runs from minus infinity — where the system was in equilibrium — through the two times of the Green's function back to minus infinity (see Appendix B). The first part of this contour is called the positive branch, the part running backwards the negative branch. In order to be sure that in a "lesser" function the first time argument is always earlier (less) than the second one, the first argument has to be on the positive and the second one on the negative branch of the Keldysh contour. The GW self-energy is thus

$$\Sigma^{<\ GW}_{\mathbf{k}}(t,t') = i\hbar \sum_{\mathbf{k}'} G^{<}_{\mathbf{k}-\mathbf{k}'}(t,t') W^{>}_{k'}(t',t) \ . \tag{21.3}$$

Here, the propagators always start at the vertex at the right time argument, and run to the vertex at the left time argument. Therefore, the time arguments of the interaction W are interchanged. Because $t > t'$ on the contour

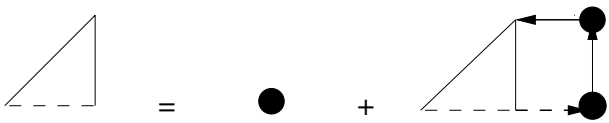

Fig. 21.3 The ladder approximation for the Coulomb vertex.

W is a "greater" function $W^{>}(t',t)$. In a next step, we want to express this "greater" potential in terms of the retarded and advanced interaction potential, $W^r(t,t')$ and $W^a(t,t')$, which determine the dielectric response.

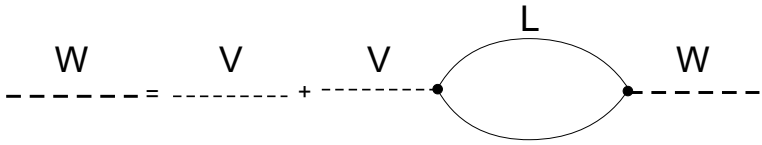

Fig. 21.4 Integral equation for the screened potential W.

The screened potential W obeys in contour time space an integral equation shown symbolically in Fig. 21.4. Similarly, the retarded potential obeys a simple Dyson equation in the form

$$W^r_{\mathbf{q}}(t,t') = V_{\mathbf{q}}\delta(t,t') + V_{\mathbf{q}}L^r_{\mathbf{q}}(t,t_1)W^r_{\mathbf{q}}(t_1,t') \ . \tag{21.4}$$

Here, a matrix notation for the real time arguments is used and it is implied that one has to integrate over repeated time arguments. $V_{\mathbf{q}}$ is the bare Coulomb potential, and $L^r(t,t')$ is the retarded irreducible polarization function.

If we write Eq. (21.4) for the lesser part of the potential, the first term $V_{\mathbf{q}}\delta(t,t')$ does not contribute, because the two time arguments are on different branches of the contour and therefore cannot be equal. In the random phase approximation (RPA), $L^r(t,t')$ is simply a bubble of Green's functions describing intraband scattering. The lesser part of the potential is then

$$W^<_{\mathbf{q}}(t,t') = V_{\mathbf{q}}[L_{\mathbf{q}}(t,t_1)W_{\mathbf{q}}(t_1,t')]^< \ , \tag{21.5}$$

where all times are considered still on the contour. With the Langreth theorem described in Appendix B, the product $(LW)^<$ can be evaluated and one finds

$$W^<_{\mathbf{q}}(t,t') = V_{\mathbf{q}}L^r_{\mathbf{q}}(t,t_1)W^<_{\mathbf{q}}(t_1,t') + V_{\mathbf{q}}L^<_{\mathbf{q}}(t,t_1)W^a_{\mathbf{q}}(t_1,t') \ , \tag{21.6}$$

where now all times are real times, i.e., no longer contour times.

If we now multiply Eq. (21.4) with V^{-1}, we find $(V^{-1}-L)W^r = 1$, so that $W^{r,-1} = V - L$. Similarly, Eq. (21.6) gives $(V^{-1}-L)W^< = L^<W^a = W^{r,-1}W^<$. Multiplying the last equation with W^r yields the result

$$\boldsymbol{W}_{\mathbf{q}}^{>,<}(t,t') = \boldsymbol{W}_{\mathbf{q}}^{r}(t,t_1)\boldsymbol{L}_{\mathbf{q}}^{>,<}(t_1,t_2)\boldsymbol{W}_{\mathbf{q}}^{a}(t_2,t') \quad . \tag{21.7}$$

optical theorem for the scattering potential

This relation is called *optical theorem*. Here, we have implied that the same relation can be derived for the greater function if the polarization L is also taken as a greater function (see also Problem 21.3). The relation (21.7) shows that the GW scattering self-energy is actually quadratic in the spectral functions W^r and W^a.

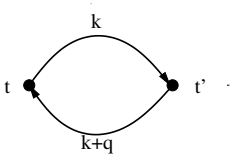

Fig. 21.5 Polarization bubble.

If we evaluate the polarization diagram of Fig. 21.5 in RPA we find

$$L_{\mathbf{q}}^{<}(t,t') = -i\hbar \sum_{\mathbf{k}} G_{\mathbf{k}+\mathbf{q}}^{<}(t,t')G_{\mathbf{k}}^{>}(t',t) \quad . \tag{21.8}$$

The GW scattering self-energy becomes

$$\begin{aligned}\Sigma_{\mathbf{k}}^{<\,GW}(t,t') = \hbar^2 \sum_{\mathbf{k}',\mathbf{k}''} \int dt_1 \int dt_2 G_{\mathbf{k}'+\mathbf{k}}^{<}(t,t')W_{\mathbf{k}'}^{r}(t',t_2) \\ \times\, G_{\mathbf{k}''}^{>}(t_1,t_2)G_{\mathbf{k}''+\mathbf{k}'}^{<}(t_2,t_1)W_{\mathbf{k}'}^{a}(t_1,t) \quad .\end{aligned} \tag{21.9}$$

The three propagators $G^{<,>}$ yield in the scattering rate the initial and final state occupation factors, if one expresses the functions $G^{<,>}$ by the density matrices via the generalized Kadanoff–Baym ansatz.

The evaluation of the exchange scattering self-energy is considerably more involved. Still in the contour time formalism, we get from the diagram

of Fig. 21.2

$$\Sigma^{ex}_{\mathbf{k}}(t,t') = -\hbar^2 \sum_{\mathbf{k}',\mathbf{k}''} G_{\mathbf{k}'}(t,t_1) W_{\mathbf{k}'-\mathbf{k}}(t_2,t) \times G_{\mathbf{k}''}(t_1,t_2) W_{\mathbf{k}''-\mathbf{k}'}(t',t_1) G_{\mathbf{k}-\mathbf{k}'+\mathbf{k}''}(t_2,t') \ . \tag{21.10}$$

In order to write this diagram in real time, the most efficient way is to sum for each contour time integral over its branch index α, which is $+$ for the positive branch and $-$ for the negative branch. In this notation, $\Sigma^{<}(t,t') = \Sigma^{+-}(t,t')$, showing that the time t is on the earlier positive branch while t' is on the later, negative branch. Symbolically written, the exchange self-energy yields four terms with the following combination of Keldysh indices:

$$\begin{aligned}
&\sum_{\alpha_1,\alpha_2} G^{+\alpha_1} W^{\alpha_2 +} G^{\alpha_1\alpha_2} W^{-\alpha_1} G^{\alpha_2 -} \\
&= \sum_{\alpha_2} (G^{++} W^{\alpha_2 +} G^{+\alpha_2} W^{-+} G^{\alpha_2 -} + G^{+-} W^{\alpha_2 +} G^{-\alpha_2} W^{--} G^{\alpha_2 -}) \\
&= G^{++} W^{++} G^{++} W^{-+} G^{+-} + G^{+-} W^{++} G^{-+} W^{--} G^{+-} \\
&+ G^{++} W^{-+} G^{+-} W^{-+} G^{--} + G^{+-} W^{++} G^{-+} W^{--} G^{--} \ .
\end{aligned} \tag{21.11}$$

The second term in the final result contains three $G^{<,>}$ propagators and the $++$ and $--$ components of the potential. With the relations

$$W^{++} = W^r - W^{+-} \ , \qquad W^{--} = W^a + W^{+-} \ , \tag{21.12}$$

we can transform this term into a scattering rate with two spectral functions of the potential and three particle propagators, which has again the structure of the GW term. This term is thus the exchange Coulomb scattering rate which belongs to the direct Coulomb scattering rate of the GW scattering self-energy. One sees, however, that generally the vertex correction contains also contributions of third and fourth order in the interaction potential, if one expresses the potential via the optical theorem by the retarded and advanced components of the potential. We will not consider these higher order terms any further.

The second-order vertex contribution to the scattering self-energy is

$$\Sigma^{<\ ex}_{\mathbf{k}}(t,t') = -\hbar^2 \sum_{\mathbf{k}',\mathbf{k}''} \int dt_1 \int dt_2 G^{<}_{\mathbf{k}'}(t,t_1) W^{r}_{\mathbf{k}'-\mathbf{k}}(t_2,t) \times G^{>}_{\mathbf{k}''}(t_1,t_2) W^{a}_{\mathbf{k}''-\mathbf{k}'}(t',t_1) G^{<}_{\mathbf{k}-\mathbf{k}'+\mathbf{k}''}(t_2,t') \ . \tag{21.13}$$

So far, in the literature, this exchange contribution has been considered mainly in the long-time regime, where a quasi-equilibrium screened potential can be assumed.

21.2 Second Born Approximation

We now explicitly derive the scattering rates as determined by the GW and exchange scattering self-energies in the long-time limit. The quantum kinetic study of the time-dependent build-up of screening will show that this approximation is reasonable on time scales that are large compared to the inverse electron–hole plasma frequency.

Under these, with respect to the screening dynamics, quasi-stationary conditions, the two-time retarded and advanced statically screened potential becomes singular in the time difference

$$W^{r,a}_{\mathbf{k}}(t_1,t_2) = W_{\mathbf{k}}(t_1)\delta(t_1-t_2) \ , \tag{21.14}$$

where $W_{\mathbf{k}}(t)$ is the quasi-equilibrium statically screened Coulomb potential, which still depends parametrically on the carrier densities. Note that the form (21.14) holds only for a statically screened potential, a frequency-dependent screening would result in a potential which depends on the difference time coordinate. With (21.14), all time integrals in the scattering self-energy vanish, and only the time-integral in the scattering rate (21.1) remains. Consistently with the above assumptions, we will make a Markov approximation for this last integration. Naturally, all particle propagators are still matrices in the band index. After applying the generalized Kadanoff–Baym ansatz (21.2) to all particle propagators in the self-energies and the scattering rates, only spectral, i.e., retarded and advanced, Green's functions and single-time density matrices remain.

Since we are in the long-time limit, we assume that the off-diagonal spectral functions have already decayed. As a further simplifying approximation, we take the diagonal elements of the spectral functions in the effective-particle approximation. With $G^a(t,t') = [G^r(t',t)]^*$ we get

$$\begin{aligned} G^r_{ii,k}(t,t') &= -\frac{i}{\hbar}\Theta(t-t')e^{-\frac{i}{\hbar}\left(\varepsilon_{i,k}-i\gamma\right)(t-t')} \\ G^a_{ii,k}(t,t') &= \frac{i}{\hbar}\Theta(t'-t)e^{-\frac{i}{\hbar}\left(\varepsilon_{i,k}-i\gamma\right)(t-t')} \ . \end{aligned} \tag{21.15}$$

Here, $\varepsilon_{i,k}$ are the mean-field renormalized single-particle energies and γ is a quasi-particle broadening. In the Markov approximation, the slowly

varying density matrix elements are pulled out of the time integral with the time argument taken at the upper boundary t. The remaining integral leads to a Lorentzian resonance denominator $g(\varepsilon)$

$$\int_{-\infty}^{t} dt'\; e^{\frac{i}{\hbar}(\varepsilon+i\Gamma)(t-t')} = \hbar g(\varepsilon) \simeq \hbar\left[\pi\delta(\varepsilon) + i\frac{\mathrm{P}}{\varepsilon}\right] \quad . \tag{21.16}$$

In the electron–hole picture with the quasi-equilibrium Fermi functions $f^e = f^c$ and $f^h = 1 - f^v$, we obtain the following equation of motion for the coherent interband polarization:

$$\begin{aligned}\left[i\hbar\frac{\partial}{\partial t} - \varepsilon^e_{\mathbf{k}}(t) - \varepsilon^h_{\mathbf{k}}(t)\right] P_{\mathbf{k}}(t) + \left[1 - f^e_{\mathbf{k}}(t) - f^h_{\mathbf{k}}(t)\right]\Omega_{\mathbf{k}}(t) \\ = i\Big[-S^D_{\mathbf{k}}(t) + S^{OD}_{\mathbf{k}}(t) + V^D_{\mathbf{k}}(t) - V^{OD}_{\mathbf{k}}(t)\Big] \quad .\end{aligned} \tag{21.17}$$

The LHS of Eqs. (21.17) is again the polarization equation of the semiconductor Bloch equations (12.19) with the Hartree–Fock renormalizations of the energies and the Rabi frequency

$$\varepsilon^a_{\mathbf{k}}(t) = \epsilon^a_{\mathbf{k}} - \sum_{k'} V_{\mathbf{k}-\mathbf{k}'}\, f^a_{\mathbf{k}'}(t), \tag{21.18}$$

$$\hbar\Omega_{\mathbf{k}}(t) = \mathbf{d}_{cv}\cdot\mathbf{E}(t) + \sum_{k'} V_{\mathbf{k}-\mathbf{k}'}\, P_{\mathbf{k}'}(t) \quad . \tag{21.19}$$

The terms on the RHS of Eq. (21.17) are derived from the scattering integral and describe dephasing of the macroscopic polarization due to carrier scattering and polarization interaction, as well as the corresponding renormalizations of the Hartree–Fock self-energies. Keeping all terms up to second order in the statically screened interaction potential, we get the scattering rates in the second Born approximation:

$$S^D_{\mathbf{k}} = \sum_{\mathbf{k}',\mathbf{k}''} \sum_{a,b} g\left(\varepsilon^a_{\mathbf{k}} + \varepsilon^b_{\mathbf{k}'+\mathbf{k}''} - \varepsilon^b_{\mathbf{k}''} - \varepsilon^a_{\mathbf{k}'+\mathbf{k}}\right)\left(2\,W^2_{\mathbf{k}'} - \delta_{ab}\,W_{\mathbf{k}'}W_{\mathbf{k}-\mathbf{k}''}\right)$$
$$\times P_{\mathbf{k}}\left[(1-f^b_{\mathbf{k}'+\mathbf{k}''})f^b_{\mathbf{k}''}f^a_{\mathbf{k}'+\mathbf{k}} + f^b_{\mathbf{k}'+\mathbf{k}''}(1-f^b_{\mathbf{k}''})(1-f^a_{\mathbf{k}'+\mathbf{k}}) - P_{\mathbf{k}'+\mathbf{k}''}P^*_{\mathbf{k}''}\right], \tag{21.20}$$

$$S^{OD}_{\mathbf{k}} = \sum_{\mathbf{k}',\mathbf{k}''} \sum_{a,b} g\left(-\varepsilon^a_{\mathbf{k}} - \varepsilon^b_{\mathbf{k}'+\mathbf{k}''} + \varepsilon^b_{\mathbf{k}''} + \varepsilon^a_{\mathbf{k}'+\mathbf{k}}\right)\left(2\,W^2_{\mathbf{k}'} - \delta_{ab}\,W_{\mathbf{k}'}W_{\mathbf{k}-\mathbf{k}''}\right)$$
$$\times P_{\mathbf{k}'+\mathbf{k}}\left[(1-f^a_{\mathbf{k}})(1-f^b_{\mathbf{k}'+\mathbf{k}''})f^b_{\mathbf{k}''} + f^a_{\mathbf{k}}f^b_{\mathbf{k}'+\mathbf{k}''}(1-f^b_{\mathbf{k}''}) - P^*_{\mathbf{k}'+\mathbf{k}''}P_{\mathbf{k}''}\right], \tag{21.21}$$

$$V^D_{\mathbf{k}} = \sum_{\mathbf{k}',\mathbf{k}''} \sum_{a} g\left(\varepsilon^a_{\mathbf{k}} - \varepsilon^{\bar{a}}_{\mathbf{k}'+\mathbf{k}''} + \varepsilon^{\bar{a}}_{\mathbf{k}''} - \varepsilon^a_{\mathbf{k}'+\mathbf{k}}\right) W_{\mathbf{k}'}W_{\mathbf{k}-\mathbf{k}''}$$
$$\times P_{\mathbf{k}}\left(P^*_{\mathbf{k}'+\mathbf{k}} - P^*_{\mathbf{k}'+\mathbf{k}''}\right)P_{\mathbf{k}''}\ , \tag{21.22}$$

$$V^{OD}_{\mathbf{k}} = \sum_{\mathbf{k}',\mathbf{k}''} \sum_{a} g\left(-\varepsilon^a_{\mathbf{k}} + \varepsilon^{\bar{a}}_{\mathbf{k}'+\mathbf{k}''} - \varepsilon^{\bar{a}}_{\mathbf{k}''} + \varepsilon^a_{\mathbf{k}'+\mathbf{k}}\right) W_{\mathbf{k}'}W_{\mathbf{k}-\mathbf{k}''}$$
$$\times\Big\{P_{\mathbf{k}'+\mathbf{k}}\Big[(1-f^a_{\mathbf{k}})f^{\bar{a}}_{\mathbf{k}'+\mathbf{k}''}(1-f^{\bar{a}}_{\mathbf{k}''}) + f^a_{\mathbf{k}}(1-f^{\bar{a}}_{\mathbf{k}'+\mathbf{k}''})f^{\bar{a}}_{\mathbf{k}''}\Big]$$
$$-P_{\mathbf{k}'+\mathbf{k}''}\Big[(1-f^a_{\mathbf{k}})(1-f^{\bar{a}}_{\mathbf{k}''})f^a_{\mathbf{k}'+\mathbf{k}} + f^a_{\mathbf{k}}f^{\bar{a}}_{\mathbf{k}''}(1-f^a_{\mathbf{k}'+\mathbf{k}})\Big]\Big\}\ , \tag{21.23}$$

where the distribution functions and the statically screened potential parametrically vary in time if the total number of carriers changes. The notation $\bar{a} = h(e)$ for $a = e(h)$ is used.

The scattering terms which originate from the direct and exchange interaction are called S. Scattering terms which are solely connected with the vertex correction are called V. Depending on whether these rates are diagonal (or off-diagonal) in the momentum variable of the polarization component $P_{\mathbf{k}}$ the terms are divided into V^D, S^D and V^{OD}, S^{OD}. In other words, the terms V^D, S^D are $\propto P_{\mathbf{k}}$, while the off-diagonal parts depend on other polarization components $P_{k'\neq k}$. In S^D and S^{OD}, we find direct (GW) contributions, $\propto W^2_{\mathbf{k}'}$, as well as exchange (vertex) contributions, $\propto W_{\mathbf{k}'}W_{\mathbf{k}-\mathbf{k}''}$.

Eqs. (21.20) and (21.22) can be formally divided into shift and damping terms:

$$i\left[-S^D_{\mathbf{k}}(t) + V^D_{\mathbf{k}}(t)\right] = \left[\Delta_{\mathbf{k}}(t) + i\Gamma_{\mathbf{k}}(t)\right]P_{\mathbf{k}}(t)\ . \tag{21.24}$$

$\Gamma_{\mathbf{k}}(t)$ describes a momentum-dependent diagonal damping rate that generalizes the T_2 time and $\Delta_{\mathbf{k}}(t)$ yields the corresponding corrections to the Hartree–Fock renormalizations of the free-particle energies in Eq. (21.17). Similarly, Eqs. (21.21) and (21.23) yield momentum-dependent off-diagonal damping and shift contributions:

$$i\left[S_{\mathbf{k}}^{OD}(t) - V_{\mathbf{k}}^{OD}(t)\right] = \sum_{\mathbf{k}'}\left[-\Delta_{\mathbf{k},\mathbf{k}'}(t) + i\Gamma_{\mathbf{k},\mathbf{k}'}(t)\right] P_{\mathbf{k}'}(t) \ , \tag{21.25}$$

which couple various $\mathbf{k}$-states of the interband polarization. Note, that the $\mathbf{k}$-sum of the RHS of Eq. (21.17) vanishes since $\sum_{\mathbf{k}}(S_{\mathbf{k}}^{D} - S_{\mathbf{k}}^{OD}) = \sum_{\mathbf{k}} V_{\mathbf{k}}^{D} = \sum_{\mathbf{k}} V_{\mathbf{k}}^{OD} = 0$. This clearly shows that dephasing of the coherently driven interband polarization is an interference effect, also known as *excitation-induced dephasing*.

On the other hand, correlation contributions combine with the unscreened Hartree–Fock renormalizations of the free particle energies and the Rabi energy to a momentum-dependent band-gap shift and a renormalized Rabi energy in second Born approximation. Correspondingly, the reduction of the exciton binding energy, the band-gap renormalization and the damping are computed including all first and second order terms in the screened Coulomb interaction. The fact that both, screening corrections to the Hartree–Fock contributions and scattering (damping) contributions originate from the same correlation terms underlines the common microscopic origin of scattering and screening.

In the limiting case of a weak field $\mathbf{E}$, the polarization $P_{\mathbf{k}}$ depends only linearly on the field, $f_{\mathbf{k}}^{a}$ becomes field-independent, and cubic polarization terms vanish. This situation is realized in the quasi-equilibrium limit when a weak test field probes the pre-excited system which contains thermalized carriers described by Fermi–Dirac distribution functions.

The polarization equation (21.17) together with the scattering terms in the second Born approximation has been used extensively to investigate dephasing and correlations in quasi-equilibrium electron–hole systems. As an example, we show in Fig. 21.6 the computed gradual saturation of the exciton resonance due to the increasing population density. This saturation due to excitation-induced dephasing occurs without loss of oscillator strength, i.e., the integral over the $1s$-exciton line remains basically constant during the saturation.

Excitonic saturation can be observed in a pump–probe configuration using resonant short pulse excitation, see Chaps. 13 – 15 for details. An example of a measured spectrum for a multiple quantum-well structure is

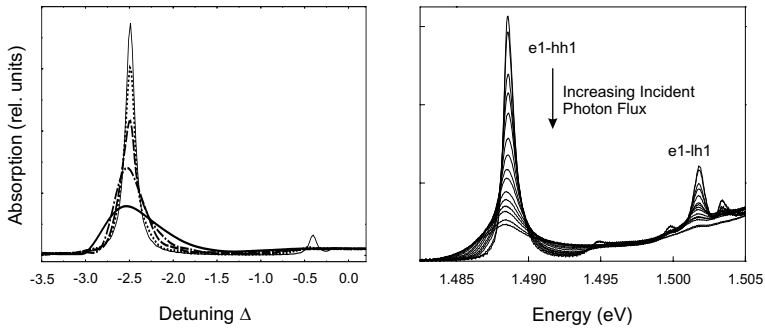

Fig. 21.6 Calculated (left figure) and measured (right figure) saturation of the exciton resonance of an InGaAs/GaAs quantum-well structure. According to Jahnke *et al.* (1996).

shown in the RHS part Fig. 21.6. The main qualitative features of the experimental results are in nice agreement with the microscopic theory. Especially, it has been verified that the 1*s*-exciton oscillator strength is well conserved.

From a slightly different perspective, the microscopic analysis of dephasing is nothing but a detailed line-shape theory. Hence, the results can also

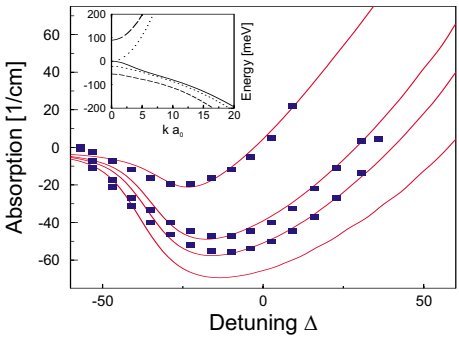

Fig. 21.7 Calculated (solid lines) and measured (dots) gain spectra for a InGaAs/AlGaAs quantum-well laser structure. The inset shows the band structure computed on the basis of the $\mathbf{k} \cdot \mathbf{p}$ theory discussed in Chap. 3. According to Hader *et al.* (1999).

be used to predict the optical spectra in systems with elevated electron–hole–plasma densities where part of the absorption becomes negative, i.e., optical gain is realized. These gain media are the basis for semiconductor laser operation (see Chap. 17). The calculation of the proper gain line shape has been a long standing problem since the use of a constant dephasing approximation leads to the prediction of unphysical absorption energetically below the gain region. As it turns out, the numerical solutions of the semiconductor Bloch equations, where dephasing is treated according to the second Born approximation, provide a solution of the laser line-shape problem yielding very good agreement with experimental results, as shown in Fig. 21.7. For more details of the microscopic semiconductor laser and gain theory see, e.g., Chow and Koch (1999).

21.3 Build-Up of Screening

If a sample is excited by a femtosecond pulse, some time is needed until the optically created carriers rearrange in order to screen their mutual Coulomb interaction. The characteristic time in this problem is the period of a plasma oscillation. For an electron-hole gas, e.g., in GaAs, with a density of about $10^{18}\mathrm{cm}^{-3}$, the energy of a plasmon is in the same order as that of a longitudinal optical phonon. Hence, the corresponding time scale is in the order of 100 fs. With modern femtosecond spectroscopy where the pulses can be as short as a few fs, the regime of the build-up of screening is accessible in experiments. As a test for the predictions of the quantum kinetic calculations of the build-up of screening, which we will discuss below, an optical pump and THz probe experiment is ideally suited to detect the delayed build-up of a plasma resonance. Other experiments which are performed within this build-up regime of screening are femtosecond FWM experiments with and without coherent control. In this ultrashort time regime, we have to give up the quasi-equilibrium assumptions used in the previous section and calculate the two-time-dependence of the screening and of the spectral functions self-consistently. In detail the following elements have to be included in the treatment:

- **Self-consistent calculation of the two-time-dependent screened Coulomb potential**
  The two-time-dependent retarded screened Coulomb potential $W^r_{\mathbf{q}}(t,t')$ (21.4) has to be calculated. We restrict ourselves to the RPA polarization function (21.8). This approximation is in general not sufficient

in the full two-time-dependent treatment of quantum kinetics, because it is not a conserving approximation. We refer, for a more detailed discussion of this subtle point, e.g., to the investigation of Gartner *et al.* (2000). Because RPA violates the charge neutrality one gets a long wave length divergence $q \to 0$ if one attempts to solve the integral equation (21.4) using only two-time-dependent Green's functions. Fortunately, if one uses the generalized Kadanoff–Baym ansatz (21.2) to eliminate the $G^{<,>}(t,t')$ in favor of the single-time density matrix and the spectral functions the divergence cancels. Therefore, we will use the reduction to the density matrix by the generalized Kadanoff–Baym ansatz. As an input for the solution of the integral equation, we need the density matrix and the spectral functions at each time step. Therefore, the integral equation can only be solved self-consistently together with the Bloch equations and the spectral functions. Note, that in the polarization loop we have at each vertex a summation over the band index. Therefore, the polarization diagram does not only include the electron and hole particle propagators, but also the off-diagonal elements connected with the interband polarization.

- **Self-consistent calculation of the spectral functions**
  We will calculate the matrix of the retarded and advanced Green's functions in the mean-field approximation. Due to the Hartree–Fock exchange term the mean-field Hamiltonian depends on the density matrix. In this way, the band-gap shrinkage due to the Hartree–Fock self-energy as well as excitonic correlations and the renormalizations due to the optical Stark effect are included. The mean-field Hamiltonian can be written as

$$\mathcal{H}^{mf} = \sum_{ij,\mathbf{k}} \mathcal{H}^{mf}_{ij,\mathbf{k}}(t) a^{\dagger}_{i,\mathbf{k}} a_{j,\mathbf{k}} \ , \tag{21.26}$$

  where i,j are band indices. The retarded Green's function is defined as

$$G^{r}_{ij,\mathbf{k}}(t,t') = -\frac{i}{\hbar}\Theta(t-t')\langle [a_{i,\mathbf{k}}(t), a^{\dagger}_{j,\mathbf{k}}(t')]_{+}\rangle \ . \tag{21.27}$$

  The equation of motion for the retarded Green's function under the mean-field Hamiltonian is

$$i\hbar \frac{\partial G^{r}_{ij,\mathbf{k}}(t,t')}{\partial t} = \delta(t-t')\delta_{ij} + \sum_{i'} \mathcal{H}^{mf}_{ii',\mathbf{k}}(t) G^{r}_{i'j,\mathbf{k}}(t,t') \ . \tag{21.28}$$

The initial value for the integration is

$$G^r_{ij,\mathbf{k}}(t',t') = -\frac{i}{\hbar}\delta_{ij} \ . \tag{21.29}$$

For the damping, we will use a phenomenological damping constant, which is compatible with the collision broadening of the considered situation. This ansatz can be improved by using a phenomenological non-Markovian damping which results not in an exponential decay, but in a decay in the form of an inverse hyperbolic cosine, which is Gaussian for short and exponential for long times.

- **Self-consistent solution of the Bloch equations in the GW approximation**
  Together with the integral equation of $W^r_{\mathbf{q}}(t,t')$ and the differential equation for the retarded Green's function $G^r_{\mathbf{k}}(t,t')$, we have to solve the semiconductor Bloch equations. Because the momentum integrations in the exchange terms in the scattering self-energy are too demanding for this program we use only the GW scattering self-energy (21.3), together with the optical theorem.
- **Self-consistent treatment of the screening of the LO-phonon and Coulomb interaction**
  One advantage of the described program is that one can include the screening of the interaction with LO-phonons relatively easily. This is necessary because the energies of LO-phonons and plasmons are comparable for a highly excited electron–hole gas. Indeed, the screening is determined by the LO-phonon and the plasmon pole. Formally, one only has to replace the inhomogeneous term $V_{\mathbf{q}}$ in the integral equation of $W_{\mathbf{q}}$ by the bare phonon and Coulomb interaction $W^0_{\mathbf{q}}(t,t')$:

$$W^0_{\mathbf{q}}(t,t') = g^2_{\mathbf{q}} D_{\mathbf{q}}(t,t') + V_{\mathbf{q}}\delta(t,t') \ , \tag{21.30}$$

  where $g^2_{\mathbf{q}} \propto q^{-2}$ is the Fröhlich interaction matrix element between electrons and LO-phonons, and $D_{\mathbf{q}}(t,t')$ is the propagator of the thermal phonon bath. Diagrammatically the integral equation for the effective particle–particle interaction is shown in Fig. 21.8. Only the deconvolution from the Keldysh contour times to the real times is more involved. For details we refer to Vu and Haug (2000).

In the following, we present some numerical results of such calculations for actual femtosecond experiments. Here, we have calculated the two-time-dependent screened effective interaction potential $W^r_{\mathbf{q}}(t,t')$ self-consistently for GaAs following an 11 fs pump pulse. We have taken an incomplete

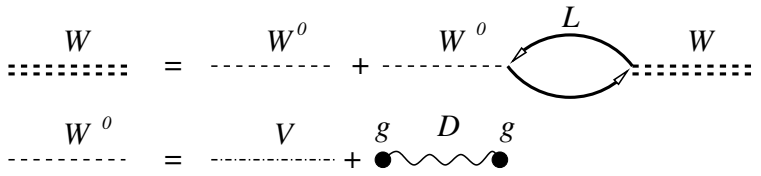

Fig. 21.8 Integral equation for the screened effective potential W for LO-phonon and Coulomb interaction.

Fourier transformation of the retarded potential which is compatible with the condition $t \geq t'$:

$$W^r_{\mathbf{q}}(\omega, t) = \int_{-\infty}^{t} dt' W^r_{\mathbf{q}}(t, t') e^{i\omega(t-t')} = \frac{V_{\mathbf{q}}}{\epsilon_{\mathbf{q}}(\omega, t)} \quad . \tag{21.31}$$

The imaginary part of the inverse dielectric function is plotted in Fig. 21.9 for various times for an excitation density of $n = 1.1 \cdot 10^{18}\mathrm{cm}^{-3}$. One sees the LO-phonon resonance at about 36 meV. At the chosen density, the plasmon pole evolves gradually on the high energy side of the LO-phonon. The plasmon pole is fully developed after a few hundred femtoseconds. The dispersion of the plasmon pole can be seen to be of quadratic form. It should be noted that it is quite demanding to calculate the Fourier transform of such a sharp structure as the LO-phonon pole. The slight shift from the transverse to the longitudinal frequency as the plasmon pole evolves it not resolved in these calculations. It should be noted that in the described experiment the THz field was focused strongly on the sample, so that it was no longer a purely transverse field and thus sensitive to longitudinal excitations (see Sec. 16.1).

Recent experiments with an optical femtosecond pump pulse and a single-cycle THz probe pulse of Leitenstorfer *et al.* confirm the calculated picture of a gradual build-up of screening. Particularly, in recent experiments on InP where both resonances lie well within the resolution of the experimental set-up, the mentioned shift of the phonon resonance and the complete build-up of the LO-phonon-plasmon mixed mode picture has been detected clearly.

Using two delayed 10 fs pulses, the above described model has been applied to a time-integrated FWM experiment of Wegener *et al.* In agreement with the experiment, we find from a fit to the calculated data a plasma-

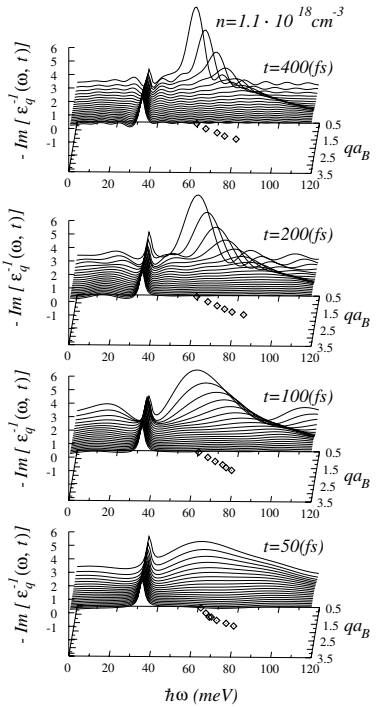

Fig. 21.9 The calculated imaginary part of the inverse dielectric function $\epsilon_{\mathbf{q}}(\omega, t)$ for GaAs after an 11 fs pulse which excited $n = 1.1 \cdot 10^{18}\text{cm}^{-3}$ for various delay times. According to Vu and Haug (2000).

density-dependent dephasing time τ with the following form

$$\frac{1}{\tau} = \gamma_0 + an^{\frac{1}{3}} \quad , \tag{21.32}$$

where a is a constant and the density-independent term is due to LO-phonon scattering. The calculated and measured dephasing times in this experiment on GaAs get as short as 10 fs.

In a FWM experiment again with 10 fs pulses, the pump pulse was split into a double pulse. The two pulses are coherent with respect to each other and the coherent control delay time can be varied with attosecond precision. Again the described theory and the experiment yield LO-phonon-plasmon oscillations on the decaying time-integrated FWM signal, which can be switched on and off by varying the coherent control delay time.

In this way, the plasmon oscillation can even be seen in real time. The resulting oscillation frequencies from the quantum kinetic calculations and the experiment are shown in Fig. 21.10. One sees clearly from the density-dependence of the oscillation period that the oscillations belong to the upper branch of the mixed phonon–plasmon mixed mode spectrum.

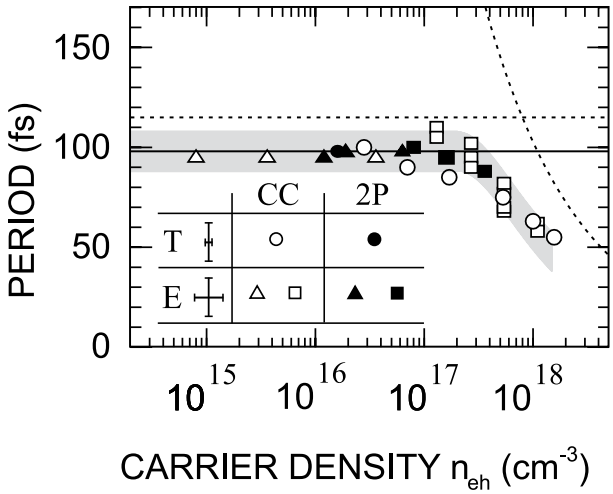

Fig. 21.10 Comparison of computed oscillation frequencies (T) and experimental results (E). The filled symbols are two-pulse photon echo experiments (2P) and the open symbols are coherent control experiments (CC). Triangles (squares) correspond to measurements at 77 (300) K. The two dashed curves correspond to the bare LO-phonon and the plasmon oscillation period. According to Vu *et al.* (2000).

REFERENCES

For the literature on the nonequilibrium Green's functions see

L. Keldysh, Sov. Phys. JETP **20**, 1018 (1965)
L.P. Kadanoff and G. Baym, *Quantum Statistical Mechanics*, Benjamin, New York (1962)

D.F. DuBois, in *Lectures in Theoretical Physics*, eds. W.E. Brittin, and A.O. Barut, and M. Guenin, Gordon and Breach, New York (1967)

For applications of the nonequilibrium Green's functions to ultrafast semiconductor spectroscopy see:

H. Haug and A.P. Jauho, *Quantum Kinetics in Transport and Optics of Semiconductors*, Springer, Berlin (1966)
M. Bonitz (ed), *Progress in Non-Equilibrium Green's Functions*, World Scientific, Singapore (2000)
W. Schäfer and M. Wegener, *Semiconductor Optics*, Springer, Berlin (2002)
R. Binder and S.W. Koch, Prog. Quant. Electr. **19**, 307 (1995)
F. Jahnke, M. Kira, and S.W. Koch, Z. Phys. **B104**, 559 (1997)

For applications of the second Born results to compute absorption and gain spectra see:

F. Jahnke, M. Kira, S.W. Koch, G. Khitrova, E. Lindmark, T. Nelson, D. Wick, J. Berger, O. Lyngnes, H.M. Gibbs, and K. Thai, Phys. Rev. Lett. **77**, 5257 (1996)
J. Hader, D. Bossert, J. Stohs, W.W. Chow, S.W. Koch, and J. Moloney, Appl. Phys. Lett. **74**, 2277 (1999)
W.W. Chow and S.W. Koch, *Semiconductor-Laser Fundamentals*, Springer, Berlin, 1999

For the treatment of the time-dependent screening in the density matrix theory see:

H.W. Wyld and B.D. Fried, Annals of Physics **23**, 374 (1963)
T. Woltering, V.M. Axt, and T. Kuhn, Phys. Rev. **B67**, 115311 (2003)

For the treatment of the time-dependent screening in terms of nonequilibrium Green's functions and the experimental measurement of the build-up of screening see:

L. Banyai, Q.T. Vu, B. Mieck, and H. Haug, Phys. Rev. Lett. **81**, 882 (1998)
Q.T. Vu and H. Haug, Phys. Rev. **B62**, 7179 (2000)
P. Gartner, L. Banyai, and H. Haug, Phys. Rev. **B62**, 7116 (2000)
W.A. Hügel, M.F. Heinrich, M. Wegener, Q.T. Vu, L. Banyai, and H. Haug, Phys. Rev. Lett. **83**, 3313 (1999)

Q.T.Vu, H. Haug, W.A. Hügel, S. Chatterjee, and M. Wegener, Phys. Rev. Lett. **85**, 3508 (2000)
R. Huber, F. Tauser, A. Brodschelm, M. Bichler, G. Abstreiter, and A. Leitenstorfer, Nature **414**, 286 (2001)
H. Haug, Nature **414**, 261 (2001)

PROBLEMS

Problem 21.1: Derive the generalized Kadanoff–Baym ansatz
(a) for free particles
(b) for particles governed by a mean-field Hamiltonian.

Problem 21.2: Show that the ladder integral equation of Fig 21.3 yields after the first iteration the vertex diagram of Fig. 21.2.

Problem 21.3: Proof the optical theorem (21.7) for the "greater" function explicitly.

Problem 21.4: Give the two by two matrix of the mean-field Hamiltonian (21.26) with coupling to the light field and Hartree–Fock Coulomb corrections explicitly.

Appendix A

Field Quantization

In this appendix, we review the general quantization procedure for a given classical field. As a result, we obtain a formulation of quantum mechanics in terms of generation and annihilation operators, which is well suited to describe many-body systems. In this language, the transition from state l to state m is described as annihilation of the respective quasi-particle in state l and simultaneous creation of that quasi-particle in state m.

Formally, one can also apply the quantization procedure to the one-particle Schrödinger field, which is the origin of the name *second quantization*, which is often used instead of *field quantization*. In this appendix, we discuss the general formalism of field quantization and illustrate it with three examples: i) the electromagnetic field, ii) the displacement field, iii) the Schrödinger field. In the process, we introduce the appropriate quanta, namely, *photons* for the electromagnetic field, *phonons* for the displacement field, and *electrons* for the Schrödinger field. Anticipating the introduction of these quanta, we use their names as headings for our subsections. For the electromagnetic and displacement fields, we use the ordinary commutator (with a minus sign), while for the electrons we use anti-commutators. These simple choices automatically yield the correct statistics, namely Bose-Einstein statistics for the electromagnetic and displacement fields and Fermi-Dirac statistics for the electrons.

A.1 Lagrange Functional

We denote by $\phi_j(\mathbf{r}, t)$ the general field variable, which may be the vector potential A_j, the displacement field ξ_j, or any other field. Generalizing Lagrangian and Hamiltonian point mechanics to the continuum case, we

introduce a Lagrange functional which depends on fields according to

$$L[\phi_j] = \int d^3r \mathcal{L}(\phi_j,\, \partial\phi_j/\partial t,\, \partial\phi_j/\partial x_i,\, \mathbf{r},\, t) \ . \tag{A.1}$$

The Euler–Lagrange equations (field equations) are obtained from Hamilton's principle

$$\delta \int_{t_0}^{t_1} L\, dt = 0 = \delta \int_{t_0}^{t_1} dt \int d^3r \mathcal{L}(\phi_j,\, \partial\phi_j/\partial t,\, \partial\phi_j/\partial x_i,\, \mathbf{r},\, t) \ . \tag{A.2}$$

In Eq. (A.2), the variation δ acts on the fields (not on the coordinates)

$$\delta\mathcal{L} = \sum_j \left(\frac{\delta\mathcal{L}}{\delta\phi_j}\delta\phi_j + \frac{\delta\mathcal{L}}{\delta\frac{\partial\phi_j}{\partial t}}\delta\dot{\phi}_j + \sum_i \frac{\delta\mathcal{L}}{\delta\phi_j^i}\delta\phi_j^i \right) \ , \tag{A.3}$$

where we introduced the abbreviations $\dot{\phi} = \partial\phi/\delta t$, $\phi_j^i = \partial\phi_j/\partial x_i$. $\delta\mathcal{L}/\delta\phi_j$ denotes the functional derivative of $\mathcal{L}$ with respect to the j-th component of the vector field ϕ. Assuming as usual that variations and derivatives commute, we can use partial integration. Since $\delta\phi(t_0) = \delta\phi(t_1) = 0$ and since $\delta\phi$ also vanishes at the boundaries of the system, we obtain

$$\delta\int_{t_0}^{t_1} dtL = \int_{t_0}^{t_1} dt \int d^3r \left(\frac{\delta\mathcal{L}}{\delta\phi_j} - \frac{\partial}{\partial t}\frac{\delta\mathcal{L}}{\delta\frac{\partial\phi_j}{\partial t}} - \sum_i \frac{\partial}{\partial x_i}\frac{\delta\mathcal{L}}{\delta\frac{\partial\phi_j}{\partial x_i}} \right) \delta\phi_j = 0 \ . \tag{A.4}$$

The variations $\delta\phi_j$ are arbitrary, so that Eq. (A.4) can be satisfied only if

$$\frac{\delta\mathcal{L}}{\delta\phi_j} - \frac{\partial}{\partial t}\frac{\delta\mathcal{L}}{\delta\frac{\partial\phi_j}{\partial t}} - \sum_i \frac{\partial}{\partial x_i}\frac{\delta\mathcal{L}}{\delta\frac{\partial\phi_j}{\partial x_i}} = 0 \ . \tag{A.5}$$

These equations are the Euler–Lagrange or field equations.

i) **photons**

Photons are the quanta of the electromagnetic field. To keep things as simple as possible, we restrict our discussion to the electromagnetic field in vacuum. For this, we have

$$\int dt\, L = \int dt \int d^3r \frac{1}{8\pi}(\mathcal{E}^2 - H^2) \ , \tag{A.6}$$

where

$$\mathbf{H} = \nabla \times \mathbf{A} = \mathrm{curl}\mathbf{A} \ , \tag{A.7}$$

A is the vector potential,

$$\mathcal{E} = -\nabla\phi - \frac{1}{c}\frac{\partial \mathbf{A}}{\partial t} \ , \tag{A.8}$$

and ϕ is the scalar potential. Using Eqs. (A.7) and (A.8) in Eq. (A.6), we write the Lagrangian density as

$$\mathcal{L} = \frac{1}{8\pi}\left[\left(\nabla\phi + \frac{1}{c}\frac{\partial \mathbf{A}}{\partial t}\right)^2 - (\mathrm{curl}\mathbf{A})^2\right] \ . \tag{A.9}$$

The components A_i of the vector potential and the scalar potential ϕ are the elements of the general field variable $\phi_i(\mathbf{r}, t)$ discussed above, i.e.,

$$\phi_i = A_i \text{ for } i = 1, 2, 3 \text{ and } \phi_4 = \phi \ . \tag{A.10}$$

To obtain the field equations, we need the results

$$\frac{\delta\mathcal{L}}{\delta A_j} = \frac{\delta\mathcal{L}}{\delta\phi} = \frac{\delta\mathcal{L}}{\delta\frac{\partial\phi}{\partial t}} = 0 \, , \tag{A.11}$$

$$\frac{\delta\mathcal{L}}{\delta\frac{\partial A_j}{\partial t}} = \frac{1}{4\pi c}\left(\frac{\partial\phi}{\partial x_j} + \frac{1}{c}\frac{\partial A_j}{\partial t}\right) \ , \tag{A.12}$$

$$\frac{\delta\mathcal{L}}{\delta\frac{\partial\phi}{\partial x_i}} = \frac{1}{4\pi}\left(\frac{\partial\phi}{\partial x_i} + \frac{1}{c}\frac{\partial A_i}{\partial t}\right) \ , \tag{A.13}$$

and

$$\begin{aligned}
\frac{\delta\mathcal{L}}{\delta\frac{\partial A_j}{\partial x_l}} &= -\frac{\delta}{\delta\frac{\partial A_j}{\partial x_l}} \sum \epsilon_{imk}\frac{\partial A_k}{\partial x_m}\epsilon_{iqn}\frac{\partial A_n}{\partial x_q}\frac{1}{8\pi} \\
&= -\frac{1}{8\pi}\sum \epsilon_{ilj}\,\epsilon_{iqn}\frac{\partial A_n}{\partial x_q} - \frac{1}{8\pi}\sum \epsilon_{imk}\frac{\partial A_k}{\partial x_m}\epsilon_{ilj} \\
&= -\frac{1}{4\pi}\sum \epsilon_{ilj}\,\epsilon_{iqn}\frac{\partial A_n}{\partial x_q} \\
&= -\frac{1}{4\pi}\left(\frac{\partial A_j}{\partial x_l} - \frac{\partial A_l}{\partial x_j}\right) \ .
\end{aligned} \tag{A.14}$$

In Eq. (A.14), we have used the so-called Levi–Civita tensor ϵ_{ijk}, which has the following properties

$$\epsilon_{123} = 1 \, , \ \epsilon_{213} = -1 \, , \ \epsilon_{iij} = 0 \ , \tag{A.15}$$

where *cyclic permutations* of the indices do not change the result, i.e., $\epsilon_{123} = \epsilon_{312} = \epsilon_{231}$, etc. For the product of the tensors, we have the rule

$$\sum_i \epsilon_{ijl}\epsilon_{imn} = \delta_{jm}\delta_{ln} - \delta_{jn}\delta_{lm} \ . \tag{A.16}$$

The Levi–Civita tensor is very useful when evaluating vector products, curls and the like. For example, the curl of a vector is

$$\mathrm{curl}\mathbf{A} = \sum \mathbf{e}_i \frac{\partial}{\partial x_j} A_l \, \epsilon_{ijl} \ . \tag{A.17}$$

Combining Eqs. (A.9) – (A.14) with the Euler–Lagrange equations, we get

$$\frac{1}{4\pi}\left[\sum \frac{\partial}{\partial x_i}\left(\frac{\partial A_j}{\partial x_i} - \frac{\partial A_i}{\partial x_j}\right) - \frac{1}{c}\frac{\partial}{\partial t}\left(\frac{\partial \phi}{\partial x_j} + \frac{1}{c}\frac{\partial A_j}{\partial t}\right)\right] = 0 \tag{A.18}$$

or, using Eqs. (A.7) and (A.8)

$$\mathrm{curl}\ \mathbf{H} = \frac{1}{c}\frac{\partial}{\partial t}\mathcal{E} \ , \tag{A.19}$$

which is one of Maxwell's equations. Analogously we obtain

$$\sum \frac{\partial}{\partial x_i}\left(\frac{\partial \phi}{\partial x_i} + \frac{1}{c}\frac{\partial A_i}{\partial t}\right) = 0 \ , \tag{A.20}$$

which is nothing but

$$\mathrm{div}\ \mathcal{E} = 0 \, . \tag{A.21}$$

The other two Maxwell equations are just the definitions of the potentials. Equation (A.8) yields

$$\mathrm{curl}\ \mathcal{E} = -\frac{1}{c}\frac{\partial \mathbf{H}}{\partial t} \ , \tag{A.22}$$

since

$$\nabla \times \mathcal{E} = \nabla \times \left(-\nabla\phi - \frac{1}{c}\frac{\nabla \mathbf{A}}{\partial t}\right) = -\frac{1}{c}\frac{\partial}{\partial t}\nabla \times \mathbf{A} \tag{A.23}$$

and from Eq. (A.7) we have

$$\mathrm{div}\ \mathbf{H} = 0 \tag{A.24}$$

since

$$\nabla \cdot (\nabla \times \mathbf{A}) = 0 \ . \tag{A.25}$$

Equations (A.19), (A.21), (A.22) and (A.24) are the complete Maxwell equations in vacuum, which occur here as our field equations.

ii) **phonons**

As second example, we treat waves in an elastic medium. The quanta of these waves are the phonons. We denote by $\xi_i(\mathbf{r}, t)$ the i-th component of the displacement field at point $\mathbf{r}$ and time t. The displacement field satisfies the classical wave equation

$$\frac{\partial^2}{\partial t^2}\xi_i - c^2\nabla^2\xi_i = 0 \ . \tag{A.26}$$

The corresponding Lagrangian is

$$\mathcal{L} = \frac{1}{2}\rho\left[\sum_i \left(\frac{\partial \xi_i}{\partial t}\right)^2 - \sum_{ij} c^2 \left(\frac{\partial \xi_i}{\partial x_j}\right)^2\right] \ , \tag{A.27}$$

where we have the density ρ as a prefactor so that $\mathcal{L}$ has the correct unit of an energy density. We arrived at Eq. (A.27) by an educated guess and by verifying that the field equations are indeed just Eq. (A.26).

iii) **electrons**

As we see below, the electrons appear through the quantization of the Schrödinger equation. This is the origin of the name *second quantization*, although the name *field quantization* is generally more appropriate. Here, we consider the single-particle Schrödinger equation as our classical wave equation

$$i\hbar\frac{\partial \psi}{\partial t} - \mathcal{H}_{sch}\,\psi = 0 \ , \tag{A.28}$$

where

$$\mathcal{H}_{sch} = -\frac{\hbar^2\nabla^2}{2m} + V(\mathbf{r}) \tag{A.29}$$

and ψ is the complex wave function. We treat ψ and ψ^* as the quantities that have to be varied independently. Our educated guess for the

Lagrangian is

$$\mathcal{L} = \psi^* \left(i\hbar\dot{\psi} - \mathcal{H}_{sch}\psi \right) \ , \tag{A.30}$$

which can be verified by evaluating Eq. (A.5). The variation with respect to ψ^* yields

$$\frac{\delta\mathcal{L}}{\delta\psi^*} - \frac{\partial}{\partial t}\frac{\delta\mathcal{L}}{\delta\frac{\partial\psi^*}{\partial t}} - \sum \frac{\partial}{\partial x_i}\frac{\delta\mathcal{L}}{\delta\frac{\partial\psi^*}{\partial x_i}} = 0 \ . \tag{A.31}$$

The last two terms on the LHS of this equation are identically zero and

$$\frac{\delta\mathcal{L}}{\delta\psi^*} = 0 = i\,\hbar\frac{\partial\psi}{\partial t} - \mathcal{H}_{sch}\psi \ , \tag{A.32}$$

which is the Schrödinger equation (A.28). The variation with respect to ψ is more lengthy, but it can be shown to yield the conjugate complex Schrödinger equation

$$-i\hbar\frac{\partial\psi^*}{\partial t} - \mathcal{H}_{sch}\psi^* = 0 \ . \tag{A.33}$$

A.2 Canonical Momentum and Hamilton Function

The next step in our general procedure is to introduce the canonical momentum and the Hamilton functional. As in point mechanics, the canonical momentum $\Pi_i(\mathbf{r},t)$ for $\phi_i(\mathbf{r},t)$ is defined as

$$\Pi_i = \frac{\delta\mathcal{L}}{\delta\frac{\partial\phi_i}{\partial t}} \tag{A.34}$$

and the Hamilton density is defined as

$$h = \sum_i \Pi_i\frac{\partial\phi_i}{\partial t} - \mathcal{L} \ , \tag{A.35}$$

where all variables have to be expressed in terms of Π and ϕ.

i) **photons**

Using the Lagrangian (A.9) in Eq. (A.34), we obtain

$$\Pi_i = \frac{\delta\mathcal{L}}{\delta\frac{\partial A_i}{\partial t}} = \frac{1}{4\pi c}\left(\frac{\partial\phi}{\partial x_i} + \frac{1}{c}\frac{\partial A_i}{\partial t}\right) \ , \tag{A.36}$$

so that $\Pi_i = -\mathcal{E}/4\pi c$. Solving (A.36) for $\partial A_i/\partial t$ yields

$$\frac{\partial A_i}{\partial t} = 4\pi c^2 \Pi_i - c\,\frac{\partial \phi}{\partial x_i} \quad . \tag{A.37}$$

The momentum density canonical to the scalar potential ϕ vanishes identically because $\mathcal{L}$ does not depend on $\partial\phi/\partial t$. Therefore, we cannot treat ϕ in the same way as $\mathbf{A}$. Actually, as we will show below, the Hamilton density is independent of ϕ. Therefore, we can completely eliminate ϕ from the discussion by choosing the gauge $\phi = 0$.

The Hamilton density is

$$\begin{aligned} h &= \sum \Pi_i \left(4\pi c^2 \Pi_i - c\frac{\partial \phi}{\partial x_i} \right) - \frac{1}{8\pi}[(4\pi c\Pi)^2 - (\text{curl } \mathbf{A})^2] \\ &= 2\pi c^2 \Pi^2 + \frac{1}{8\pi}(\text{curl } \mathbf{A})^2 \quad , \end{aligned} \tag{A.38}$$

since the term $c\Pi\cdot\nabla\phi$ vanishes. To prove this, we make a partial integration of the total Hamiltonian. This transforms $c\Pi \cdot \nabla\phi$ into $-c\phi\nabla \cdot \Pi$. We can drop this term if we limit the treatment to solutions for which $\nabla \cdot \Pi = \nabla \cdot \mathcal{E} = 0$. To see that this is possible, we consider the Hamilton equation for Π,

$$\frac{\partial \Pi}{\partial t} = -\frac{1}{4\pi}\nabla \times \nabla \times \mathbf{A} = 0 \quad . \tag{A.39}$$

This equation shows that $\nabla \cdot \Pi$ always remains zero if we choose it to be zero initially.

ii) **phonons**

Using the Lagrangian (A.27) in Eq. (A.34), we obtain the canonical momentum

$$\Pi_i = \frac{\delta \mathcal{L}}{\delta \frac{\partial \xi_i}{\partial t}} = \rho\,\frac{\partial \xi_i}{\partial t} \quad . \tag{A.40}$$

This result is the continuum version of the well-known relation from point mechanics, where $p = m\dot{x}$. The Hamiltonian is computed as

$$h = \frac{\Pi^2}{2\rho} + \frac{\rho c^2}{2} \sum_{ik} \left(\frac{\partial \xi_i}{\partial x_k} \right)^2 \quad , \tag{A.41}$$

where the first term on the RHS is the continuum version of $p^2/2m$ and the second term is the potential.

iii) **electrons**

Here we use the Lagrangian (A.30) to obtain

$$\Pi = i\hbar\psi^* \tag{A.42}$$

and

$$\begin{aligned} h &= \Pi\dot{\psi} - \frac{1}{i\hbar}\,\Pi i\hbar\dot{\psi} + \frac{1}{i\hbar}\Pi\,\mathcal{H}_{sch}\,\psi \\ &= \frac{1}{i\hbar}\,\Pi\,\mathcal{H}_{sch}\,\psi \ . \end{aligned} \tag{A.43}$$

A.3 Quantization of the Fields

Now, we have prepared everything to come to the crucial step of field quantization. First a reminder: the transition from classical mechanics to quantum mechanics can be done formally by replacing the classical variables $\mathbf{r}$ and $\mathbf{p}$ by operators $\hat{\mathbf{r}}$ and $\hat{\mathbf{p}}$ that fulfill the commutation relations

$$[\hat{r}_l\,,\,\hat{p}_j] = i\hbar\delta_{lj} \ ,$$

$$[\hat{r}_l\,,\,\hat{r}_j] = 0 \ ,$$

and

$$[\hat{p}_l\,,\,\hat{p}_j] = 0 \ , \tag{A.44}$$

where here and in the following a commutator without a subscript always denotes the *minus commutator*

$$[\hat{\mathrm{A}},\hat{\mathrm{B}}] \equiv [\hat{\mathrm{A}},\hat{\mathrm{B}}]_- = \hat{\mathrm{A}}\hat{\mathrm{B}} - \hat{\mathrm{B}}\hat{\mathrm{A}} \ . \tag{A.45}$$

In this appendix, we use hats on top of the variables to denote operators.

The field quantization is now done by replacing the fields $\phi_i \rightarrow \hat{\phi}_i$, $\Pi_i \rightarrow \hat{\Pi}_i$ and the Hamiltonian $\mathcal{H} \rightarrow \hat{\mathcal{H}}$. For the field operators, we demand the commutation relations

$$[\hat{\phi}_l(\mathbf{r},t),\,\hat{\Pi}_j(\mathbf{r}',t)]_\pm = i\hbar\delta_{lj}\,\delta(\mathbf{r}-\mathbf{r}') \ ,$$

$$[\hat{\phi}_l(\mathbf{r},t),\,\hat{\phi}_j(\mathbf{r}',t)]_\pm = 0 \ ,$$

and

$$[\hat{\Pi}_l(\mathbf{r},t),\, \hat{\Pi}_j(\mathbf{r}',t)]_{\pm} = 0 \ , \tag{A.46}$$

where

$$[\hat{\mathrm{A}},\hat{\mathrm{B}}]_{+} = \hat{\mathrm{A}}\hat{\mathrm{B}} + \hat{\mathrm{B}}\hat{\mathrm{A}} \tag{A.47}$$

and $[\hat{A},\hat{B}]_{-}$ is given by Eq. (A.45). Both commutators occur in nature, the minus commutator for Bosons like photons and phonons, and the plus-commutator, usually called the *anti-commutator*, for Fermions, e.g., electrons. By choosing the appropriate type of commutator, we automatically get the correct quantized field theory.

i) **photons**

In the $\phi = 0$ gauge, we have $\Pi_i(r,t) = (1/4\pi c^2)\,\partial A_i/\partial t$ and $A_i(\mathbf{r},t)$ as canonical variables. After quantization, the commutation relations are

$$[\hat{A}_l(\mathbf{r},t),\, \hat{\Pi}_j(\mathbf{r}',t)]_{-} = i\hbar\delta_{lj}\delta(\mathbf{r}-\mathbf{r}') \ , \tag{A.48}$$

and the Hamilton operator becomes

$$\hat{\mathcal{H}} = \int d^3r \left[2\pi c^2\hat{\Pi}^2 + \frac{1}{8\pi}(\ \mathrm{curl}\hat{\boldsymbol{A}})^2\right] \ . \tag{A.49}$$

For many applications, we want to work in the Coulomb gauge

$$\nabla\cdot\mathbf{A} = 0 \ , \tag{A.50}$$

where the electromagnetic field is transverse. In this gauge, the commutator between $\mathbf{A}$ and Π is no longer given by Eq. (A.48) because the individual components of these operators are connected by $\nabla\cdot\mathbf{A} = 0$ and $\nabla\cdot\Pi = 0$. In the Coulomb gauge, the commutator (A.48) has to be replaced by

$$[\hat{A}_l(\mathbf{r},t),\, \hat{\Pi}_j(\mathbf{r}',t)]_{-} = i\hbar\delta^t_{lj}(\mathbf{r}-\mathbf{r}') \ , \tag{A.51}$$

see Schiff (1968). Here, the transverse δ-function is defined as

$$\delta^t_{lj}(\mathbf{r}-\mathbf{r}') = \delta_{lj}\delta(\mathbf{r}-\mathbf{r}') - \frac{1}{4\pi}\frac{\partial}{\partial r_l}\frac{\partial}{\partial r_j}\frac{1}{|\mathbf{r}-\mathbf{r}'|} \ . \tag{A.52}$$

In order to introduce photon operators (in vacuum), we expand the field operators in terms of plane waves

$$\mathbf{u}_{\lambda\mathbf{k}} = \frac{e^{i\mathbf{k}\cdot\mathbf{r}}}{L^{3/2}}\mathbf{e}_{\lambda\mathbf{k}} \ , \tag{A.53}$$

where $\mathbf{e}_{\lambda\mathbf{k}}$ is the polarization unit vector, so that

$$\int d^3r \mathbf{u}^*_{\lambda\mathbf{k}}(\mathbf{r}) \cdot \mathbf{u}_{\lambda'\mathbf{k}'}(\mathbf{r}) = \delta_{\lambda\lambda'}\delta_{\mathbf{k},\mathbf{k}'} \tag{A.54}$$

and

$$\sum_{\lambda=1,2} e_{\lambda\mathbf{k},l}\, e_{\lambda\mathbf{k},j} + \frac{k_l k_j}{k^2} = \delta_{lj} \ . \tag{A.55}$$

If we wanted to quantize the electromagnetic field in a resonator or in some other geometry we would use the appropriate eigenmodes instead of plane waves.

Since the electromagnetic field in the Coulomb gauge is transverse, we know that $\mathbf{k}$ is perpendicular to $\mathbf{e}_{\lambda\mathbf{k}}$, implying that $\nabla\cdot\mathbf{u} = 0$. The expansion of the field operators is

$$\hat{\mathbf{A}}(\mathbf{r},t) = \sum_{\mathbf{k},\lambda}[\hat{b}_{\lambda\mathbf{k}}\,\mathbf{u}_{\lambda\mathbf{k}}(\mathbf{r}) + \hat{b}^\dagger_{\lambda\mathbf{k}}\,\mathbf{u}^*_{\lambda\mathbf{k}}(\mathbf{r})]B_{\lambda k} \tag{A.56}$$

and

$$\hat{\mathbf{\Pi}}(\mathbf{r},t) = \frac{1}{4\pi c^2}\frac{\partial\hat{\mathbf{A}}}{\partial t} = \sum_{\mathbf{k},\lambda}\left(\frac{\partial\hat{b}_{\mathbf{k}\lambda}}{\partial t}\mathbf{u}_{\lambda\mathbf{k}} + \frac{\partial\hat{b}^\dagger_{\mathbf{k}\lambda}}{\partial t}\mathbf{u}^*_{\lambda\mathbf{k}}\right)\frac{B_{\lambda k}}{4\pi c^2} \ , \tag{A.57}$$

where the expansion coefficients $\hat{b}$, $\hat{b}^\dagger$ are the photon operators. We determine the quantity $B_{\lambda k}$ so that the photon operators fulfill simple commutation relations.

To evaluate the time derivative of the photon operators, we make use of the fact that the vector potential $\mathbf{A}$ satisfies the wave equation

$$\left(\frac{\partial^2}{\partial t^2} - c^2\nabla^2\right)\hat{\mathbf{A}} = 0 \ . \tag{A.58}$$

Inserting the expansion (A.56), we obtain

$$\frac{\partial^2}{\partial t^2}\hat{b}_{\lambda\mathbf{k}} = -\omega_k^2\hat{b}_{\lambda\mathbf{k}}$$

and

$$\frac{\partial^2}{\partial t^2}\hat{b}^\dagger_{\lambda\mathbf{k}} = -\omega_k^2 \hat{b}^\dagger_{\lambda\mathbf{k}} \ , \tag{A.59}$$

where $\omega_k = ck$. Equation (A.59) is fulfilled if

$$\frac{\partial}{\partial t}\hat{b}_{\lambda\mathbf{k}} = -i\omega_k \hat{b}_{\lambda\mathbf{k}}$$

and

$$\frac{\partial}{\partial t}\hat{b}^\dagger_{\lambda\mathbf{k}} = i\omega_k \hat{b}^\dagger_{\lambda\mathbf{k}} \ . \tag{A.60}$$

Inserting Eq. (A.60) into Eq. (A.57) yields

$$\hat{\Pi}(\mathbf{r},t) = -\frac{1}{4\pi c^2}\sum i\omega_k \, B_{\lambda k}(\hat{b}_{\lambda\mathbf{k}}\,\mathbf{u}_{\lambda\mathbf{k}} - \hat{b}^\dagger_{\lambda\mathbf{k}}\,\mathbf{u}^*_{\lambda\mathbf{k}}) \ . \tag{A.61}$$

To determine the commutation relations of the photon operators, we insert the expansions (A.56) and (A.61) into the commutator (A.48) to obtain

$$\sum_{\substack{\lambda,\mathbf{k}\\ \lambda',\mathbf{k}'}} \frac{-iB_{\lambda k}B_{\lambda' k'}\omega_{k'}}{4\pi c^2}\Big[\Big(\hat{b}_{\lambda\mathbf{k}}u_{\lambda\mathbf{k},l}(\mathbf{r}) + \hat{b}^\dagger_{\lambda\mathbf{k}}u^*_{\lambda\mathbf{k},l}(\mathbf{r})\Big) \ , \\ \Big(\hat{b}_{\lambda'\mathbf{k}'}u_{\lambda'\mathbf{k}',j}(\mathbf{r}') - \hat{b}^\dagger_{\lambda'\mathbf{k}'}u^*_{\lambda' k',j}(\mathbf{r})\Big)\Big] = i\hbar\delta_{lj}\delta(\mathbf{r}-\mathbf{r}') \ . \tag{A.62}$$

This commutator is satisfied if

$$[\hat{b}_{\lambda\mathbf{k}} \, , \, \hat{b}^\dagger_{\lambda'\mathbf{k}'}] = \delta_{\lambda\lambda'}\delta_{\mathbf{k}\mathbf{k}'}$$

and

$$[\hat{b}_{\lambda\mathbf{k}} \, , \, \hat{b}_{\lambda'\mathbf{k}'}] = 0 = [\hat{b}^\dagger_{\lambda\mathbf{k}} \, , \, \hat{b}^\dagger_{\lambda'\mathbf{k}'}] \tag{A.63}$$

and the normalization constant is chosen as

$$B_{\lambda k} = \left[\frac{2\pi c^2\hbar}{\omega_k}\right]^{1/2} \ . \tag{A.64}$$

Summarizing these results, we have

$$\hat{\mathbf{A}}(\mathbf{r},t) = \sum_{\lambda\mathbf{k}} \sqrt{\frac{2\pi c^2\hbar}{\omega_k}}\big[\hat{b}_{\lambda\mathbf{k}}\,\mathbf{u}_{\lambda\mathbf{k}}(\mathbf{r}) + \hat{b}^\dagger_{\lambda\mathbf{k}}\,\mathbf{u}^*_{\lambda\mathbf{k}}(\mathbf{r})\big] \ , \tag{A.65}$$

$$\hat{\Pi}(\mathbf{r},t) = -i\sum_{\lambda\mathbf{k}}\sqrt{\frac{\hbar\omega_k}{8\pi c^2}}\left[\hat{b}_{\lambda\mathbf{k}}\,\mathbf{u}_{\lambda\mathbf{k}}(\mathbf{r}) - \hat{b}^{\dagger}_{\lambda\mathbf{k}}\,\mathbf{u}^{*}_{\lambda\mathbf{k}}(\mathbf{r})\right] \ , \tag{A.66}$$

and the Hamiltonian

$$\hat{\mathcal{H}} = \sum\frac{\hbar\omega_k}{2}(\hat{b}^{\dagger}_{\lambda\mathbf{k}}\hat{b}_{\lambda\mathbf{k}} + \hat{b}_{\lambda\mathbf{k}}\hat{b}^{\dagger}_{\lambda\mathbf{k}}) = \sum\hbar\omega_k(\hat{b}^{\dagger}_{\lambda\mathbf{k}}\hat{b}_{\lambda\mathbf{k}} + 1/2) \ . \tag{A.67}$$

ii) **phonons**

Here, we quantize the canonical variables into the field operators $\hat{\xi}_i(\mathbf{r},t)$ and $\hat{\Pi}_i(\mathbf{r},t) = \rho\,\partial\hat{\xi}_i/\partial t$ with the commutations relations

$$[\hat{\xi}_j(\mathbf{r},t)\,\hat{\Pi}_l(\mathbf{r}',t)]_- = i\hbar\delta_{jl}\delta(\mathbf{r}-\mathbf{r}') \ . \tag{A.68}$$

Again, we expand the field operators

$$\hat{\xi}(\mathbf{r},t) = \sum[\hat{b}_{\mathbf{k}}\mathbf{u}_{\mathbf{k}}(\mathbf{r}) + \hat{b}^{\dagger}_{\mathbf{k}}\mathbf{u}^{*}_{\mathbf{k}}(\mathbf{r})]B_k \tag{A.69}$$

and similarly for $\hat{\Pi}$. Choosing the functions $\mathbf{u}$ as plane waves

$$\mathbf{u}_{\mathbf{k}}(\mathbf{r}) = \mathbf{e}_{\mathbf{k}}\frac{e^{i\mathbf{k}\cdot\mathbf{r}}}{L^{3/2}} \ ,$$

where $\mathbf{e}_{\mathbf{k}} = \mathbf{k}/|\mathbf{k}|$ and the normalization constant as $B_k = \sqrt{\hbar/2\rho\omega_k}$, we find the commutation relation between the phonon operators

$$[\hat{b}_{\mathbf{k}},\,\hat{b}^{\dagger}_{\mathbf{k}'}] = \delta_{\mathbf{k},\mathbf{k}'} \ , \tag{A.70}$$

and the Hamilton operator becomes

$$\hat{\mathcal{H}} = \sum\hbar\omega_k(\hat{b}^{\dagger}_{\mathbf{k}}\hat{b}_{\mathbf{k}} + 1/2) \ . \tag{A.71}$$

iii) **electrons**

Here, we introduce the field operators $\hat{\psi}$ and $\hat{\Pi} = i\hbar\hat{\psi}^{\dagger}$ and we use the Fermi anti-commutation relations

$$[\hat{\psi},\,\hat{\psi}]_+ = 0 = [\hat{\psi}^{\dagger},\,\hat{\psi}^{\dagger}]_+ \tag{A.72}$$

and

$$[\hat{\psi}(\mathbf{r},t),\,\hat{\Pi}(\mathbf{r}',t)]_+ = i\hbar\delta(\mathbf{r}-\mathbf{r}') \ , \tag{A.73}$$

which is equivalent to

$$[\hat{\psi}(\mathbf{r},t),\, \hat{\psi}^\dagger(\mathbf{r}',t)]_+ = \delta(\mathbf{r}-\mathbf{r}') \ . \tag{A.74}$$

From the Hamilton density, Eq. (A.43), we obtain

$$\hat{h} = \frac{1}{i\hbar}\hat{\Pi}(\mathbf{r})\,\mathcal{H}_{sch}\hat{\psi}(\mathbf{r}) = \hat{\psi}^\dagger(\mathbf{r})\,\mathcal{H}_{sch}\hat{\psi}(\mathbf{r}) \ , \tag{A.75}$$

which yields the Hamilton operator of the noninteracting electron system as

$$\hat{\mathcal{H}} = \int d^3r\, \hat{\psi}^\dagger(\mathbf{r})\,\mathcal{H}_{sch}\hat{\psi}(\mathbf{r}) \ . \tag{A.76}$$

The derivation of the Hamiltonian for an interacting electron system is discussed, e.g., in the textbook of Davydov. Here, we only want to mention that one has to start from the N-particle Schrödinger Hamiltonian which is then transformed into the Fock representation. One finally obtains

$$\begin{aligned}\hat{\mathcal{H}} = &\int d^3r\, \hat{\psi}^\dagger(\mathbf{r})\,\mathcal{H}_{sch}\hat{\psi}(\mathbf{r}) \\ &+ \frac{1}{2}\int d^3r \int d^3r'\, \hat{\psi}^\dagger(\mathbf{r})\,\hat{\psi}^\dagger(\mathbf{r}')\,V(\mathbf{r},\mathbf{r}')\,\hat{\psi}(\mathbf{r}')\,\hat{\psi}(\mathbf{r}) \ .\end{aligned} \tag{A.77}$$

This expression shows that the interaction term has a similar structure as the single-particle term, but instead of $\mathcal{H}_{sch}$ the electron density operator $\hat{\psi}^\dagger(\mathbf{r})\,\hat{\psi}(\mathbf{r})$ times the potential V appears. The whole interaction term is thus the product of the density operators at $\mathbf{r}$ and $\mathbf{r}'$ multiplied by the pair interaction potential. The factor $1/2$ appears to avoid double counting.

We now expand the field operators into the eigenfunctions ϕ_n of the single-particle Schrödinger Hamiltonian.

$$\mathcal{H}_{sch}\,\phi_n = E_n\,\phi_n \ , \tag{A.78}$$

so that

$$\hat{\psi}(\mathbf{r},t) = \sum \hat{a}_n(t)\,\phi_n(\mathbf{r}) \ . \tag{A.79}$$

These eigenfunctions could be any complete set, such as the Bloch or Wannier functions. It is important to choose the appropriate set for the problem at hand. The electron operators obey the anti-commutation relation

$$[\hat{a}_m,\, \hat{a}_n^\dagger]_+ = \delta_{n,m} \ , \tag{A.80}$$

and we obtain the single-particle Hamilton operator

$$\hat{\mathcal{H}} = \sum_n E_n \, \hat{a}_n^\dagger \, \hat{a}_n \quad . \tag{A.81}$$

Similarly, from Eq. (A.77) we get the many-body Hamiltonian

$$\hat{\mathcal{H}} = \sum_n E_n \, \hat{a}_n^\dagger \hat{a}_n + \frac{1}{2} \sum V_{m'n'mn} \, \hat{a}_{m'}^\dagger \hat{a}_{n'}^\dagger \hat{a}_m \hat{a}_n \quad , \tag{A.82}$$

where

$$V_{m'n'mn} = \langle m'n'|V|nm\rangle$$

is the matrix element of the interaction potential.

REFERENCES

Field quantization is treated in most quantum mechanics textbooks. See, e.g.:

C. Cohen-Tannoudji, J. Dapont-Roc, and G. Grynberg, *Photons and Atoms*, Wiley, New York (1989)
A.S. Davydov, *Quantum Mechanics*, Pergamon, New York (1965)
L.I. Schiff, *Quantum Mechanics*, McGraw-Hill, New York (1968)

Appendix B

Contour-Ordered Green's Functions

In this appendix, we make the connection with the many-body techniques which are appropriate to describe a nonequilibrium system on an advanced level and which have been used in Chap. 21 to describe the quantum kinetics in an interacting electron–hole plasma. We present a short introduction to nonequilibrium Green's functions and show that this formalism yields quite naturally a method to determine the spectral and kinetic properties of a many-body system, which is driven away from equilibrium by time-dependent external fields. Naturally, we can only give a brief introduction here, for further extensions we refer the reader to the existing literature. We follow closely the introduction of the nonequilibrium functions by Haug and Jauho (1996).

The nonequilibrium problem is formulated as follows. We consider a system evolving under the Hamiltonian

$$\mathcal{H} = h + \mathcal{H}'(t) \ . \tag{B.1}$$

The time-independent part of the Hamiltonian h is split in two parts: $h = \mathcal{H}_0 + \mathcal{H}_i$, where $\mathcal{H}_0$ is a single-particle Hamiltonian and $\mathcal{H}_i$ contains many-body interactions. It is further assumed that the nonequilibrium part $\mathcal{H}'(t)$ vanishes for times $t < t_0$. (We will take $t_0 \ \rightarrow \ -\infty$ at a suitable point.) The nonequilibrium part is, in the context of the present book, the interaction of the carriers with a laser pulse.

Before the perturbation is turned on, the system is described by the thermal equilibrium density matrix,

$$\varrho(h) = \frac{\exp(-\beta h)}{\mathrm{tr}[\exp(-\beta h)]} \ . \tag{B.2}$$

The task is to calculate the expectation value of a given observable, to

which one associates a quantum mechanical operator O, for times $t \geq t_0$:

$$\langle O(t) \rangle = \mathrm{tr}[\varrho(h) O_H(t)] \ . \tag{B.3}$$

The subscript H indicates that the dependence is governed by the full Hamiltonian, i.e., O is written in the Heisenberg picture.

B.1 Interaction Representation

We transform the time-dependence of O_H with the full Hamiltonian to a simpler form, namely to that of O_h with the stationary part of the Hamiltonian. To eliminate the time-dependent external perturbation, we use the relation

$$O_H(t) = v_h^\dagger(t, t_0) O_h(t) v_h(t, t_0) \ . \tag{B.4}$$

Here,

$$v_h(t, t_0) = T\{\exp[-\frac{i}{\hbar} \int_{t_0}^{t} dt' \mathcal{H}'_h(t')]\} \ , \tag{B.5}$$

the quantity $\mathcal{H}'_h(t)$ is the interaction representation of the time-dependent perturbation $\mathcal{H}'(t)$

$$\mathcal{H}'_h(t) = \exp[\frac{i}{\hbar} h(t - t_0)] \mathcal{H}'(t) \exp[-\frac{i}{\hbar} h(t - t_0)] \ , \tag{B.6}$$

and T is the time-ordering operator which arranges the latest times to left.

We now introduce contour-ordered quantities. The expression (B.4) can be written in another, but equivalent, form:

$$O_H(t) = T_{C_t}\Big\{\exp\big[-\frac{i}{\hbar} \int_{C_t} d\tau \mathcal{H}'_h(\tau)\big] O_h(t)\Big\} \ , \tag{B.7}$$

where the contour C_t is depicted in Fig. B.1. Where possible, we employ the convention that time variables defined on a complex contour are denoted by Greek letters, while Roman letters are used for real time variables.

Fig. B.1 Contour C_t.

The contour extends from t_0 to t and back again. Here, the time arguments are on the real axis or slightly above it; if $\mathcal{H}'(t)$ can be analytically continued no problems can arise. The meaning of the contour-ordering operator T_{C_t} is the following: the operators with time labels that occur later on the contour have to stand to the left of operators with earlier time labels. The second part of the branch puts the exponential transformation operator to the left of the operator $O_h(t)$. For a formal proof, we refer to Haug and Jauho (1996). The contour-ordering operator is an important formal tool, which allows us to develop the nonequilibrium theory along lines parallel to the equilibrium theory.

We now define the contour-ordered Green's function:

$$G(1,1') \equiv -\frac{i}{\hbar}\langle T_C[\psi_H(1)\psi_H^\dagger(1')]\rangle \ , \tag{B.8}$$

where the contour C starts and ends at t_0; it runs along the real axis and passes through t_1 and t_1' once and just once (Fig. B.2).

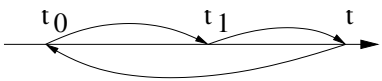

Fig. B.2 Contour C.

Here, ψ_H and $\psi_H^\dagger$ are the Fermion field operators in the Heisenberg picture. Finally, we employ the shorthand notation $(1) \equiv (\vec{x}_1, t_1)$ [or $(1) \equiv (\vec{x}_1, \tau_1)$, when appropriate].

The contour-ordered Green's function plays a similar role in nonequilibrium theory as the causal Green's function plays in equilibrium theory: it possesses a perturbation expansion based on Wick's theorem. However, since the time labels lie on the contour with two branches, one must keep track of which branch is in question. With two time labels, which can be located on either of the two branches of the contour of Fig. B.2, there are four distinct possibilities. Thus, (B.8) contains four different functions:

$$G(1,1') = \begin{cases} G_c(1,1') = G^{++}(1,1') & t_1, t_{1'} \in C_1 \\ G^{>}(1,1') = G^{-+}(1,1') & t_1 \in C_2, t_{1'} \in C_1 \\ G^{<}(1,1') = -G^{+-}(1,1') & t_1 \in C_1, t_{1'} \in C_2 \\ G_{\tilde{c}}(1,1') = -G^{--}(1,1') & t_1, t_{1'} \in C_2 \end{cases} . \tag{B.9}$$

The notation with the contour time indices, which is used, e.g., in the book by Schäfer and Wegener (2002), shows directly to which part of the contour the time argument belongs.

In Eq. (B.9), we introduced the *causal*, or *time-ordered* Green's function G_c,

$$\begin{aligned} G_c(1,1') &= -\frac{i}{\hbar}\langle T[\psi_H(1)\psi_H^\dagger(1')]\rangle \\ &= -\frac{i}{\hbar}\theta(t_1 - t_{1'})\langle\psi_H(1)\psi_H^\dagger(1')\rangle + \frac{i}{\hbar}\theta(t_{1'} - t_1)\langle\psi_H^\dagger(1')\psi_H(1)\rangle \ , \end{aligned} \tag{B.10}$$

the *"greater"* function $G^>$, also called hole propagator,

$$G^>(1,1') = -\frac{i}{\hbar}\langle\psi_H(1)\psi_H^\dagger(1')\rangle \ , \tag{B.11}$$

the *"lesser"* function $G^<$, also called particle propagator,

$$G^<(1,1') = +\frac{i}{\hbar}\langle\psi_H^\dagger(1')\psi_H(1)\rangle \ , \tag{B.12}$$

and the *antitime-ordered* Green's function $G_{\tilde{c}}$,

$$\begin{aligned} G_{\tilde{c}}(1,1') &= -\frac{i}{\hbar}\langle\tilde{T}[\psi_H(1)\psi_H^\dagger(1')]\rangle \\ &= -\frac{i}{\hbar}\theta(t_{1'} - t_1)\langle\psi_H(1)\psi_H^\dagger(1')\rangle + \frac{i}{\hbar}\theta(t_1 - t_{1'})\langle\psi_H^\dagger(1')\psi_H(1)\rangle \ . \end{aligned} \tag{B.13}$$

Since $G_c + G_{\tilde{c}} = G^< + G^>$, there are only three linearly independent functions. This freedom of choice is reflected in the literature, where a number of different conventions can be found. For our purposes, the most suitable functions are $G^{>,<}$ (which are often also denoted by a common name, "correlation function"), and the advanced and retarded functions defined as

$$\begin{aligned} G^a(1,1') &= \frac{i}{\hbar}\theta(t_{1'} - t_1)\langle[\psi_H(1), \psi_H^\dagger(1')]_+\rangle \\ &= \theta(t_{1'} - t_1)[G^<(1,1') - G^>(1,1')] \ , \end{aligned} \tag{B.14}$$

and

$$\begin{aligned} G^r(1,1') &= -\frac{i}{\hbar}\theta(t_1 - t_{1'})\langle[\psi_H(1), \psi_H^\dagger(1')]_+\rangle \\ &= \theta(t_1 - t_{1'})[G^>(1,1') - G^<(1,1')] \ . \end{aligned} \tag{B.15}$$

Obviously, $G^a(1,1') = G^r(1',1)^*$. We observe further that $G^r - G^a = G^> - G^<$. Actually, the knowledge of two nonequilibrium Green's functions is sufficient to calculate all of them. Because of their different physical

content, we prefer to work with the particle propagator $G^<$, which describes the kinetics of the system and the spectral Green's function G^r, which determines the time-dependent renormalizations in the system. One can show further that one can do perturbation expansions, apply Wick's and use Feynman diagrams just as one can for equilibrium systems.

For the practical use of the nonequilibrium Green's functions, one has to replace the contour integrals by real time integrals. This procedure is called the analytic continuation, and many different formulations exist in the literature, see Haug and Jauho (1996) for details.

The contour-ordered Green's function has the same perturbation expansion as the corresponding equilibrium time-ordered Green's function. Consequently, given that a self-energy functional can be defined, the contour-ordered Green's function has the same Dyson equation as the equilibrium function:

$$G(1,1') = G_0(1,1') + \int d^3x_2 \int_{C_v} d\tau_2 G_0(1,2)U(2)G(2,1') + \int d^3x_2 \int d^3x_3 \int_C d\tau_2 \int_C d\tau_3 G_0(1,2)\Sigma(2,3)G(3,1') \ . \quad \text{(B.16)}$$

Here, we assume that the nonequilibrium term in the Hamiltonian can be represented by a one-body external potential U. The interactions are contained in the (irreducible) self-energy $\Sigma[G]$.

B.2 Langreth Theorem

In considering the Dyson equation (B.16), we encounter terms with the structure $C = AB$, or, explicitly,

$$C(t_1, t_{1'}) = \int_C d\tau A(t_1,\tau)B(\tau, t_{1'}) \ , \quad \text{(B.17)}$$

and their generalizations involving products of three (or more) terms. Since we are presently only concerned with temporal variables, we suppress all other variables (spatial, spin, etc.), which have an obvious matrix structure. To evaluate (B.17), let us assume for definiteness that t_1 is on the first half, and that $t_{1'}$ is on the latter half of C (Fig B.3).
In view of our discussion in connection with (B.10) – (B.15), we are thus analyzing a "lesser" function.

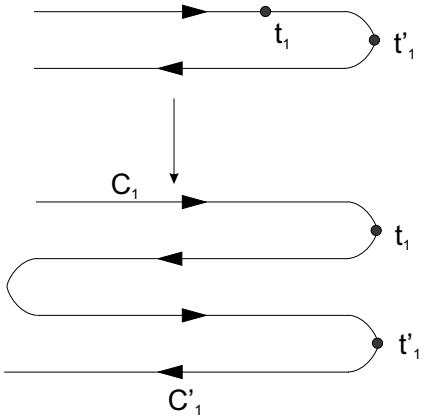

Fig. B.3 Deformation of contour C.

The next step is to deform the contour as indicated in Fig. B.3. Thus (B.17) becomes

$$C^<(t_1,t_{1'}) = \int_{C_1} d\tau A(t_1,\tau)B^<(\tau,t_{1'}) + \int_{C_1'} d\tau A^<(t_1,\tau)B(\tau,t_{1'}) \ . \tag{B.18}$$

Here, in appending the sign $<$ to the function B in the first term, we made use of the fact that as long as the integration variable τ is confined on the contour C_1 it is less than (in the contour sense) $t_{1'}$. A similar argument applies to the second term. Now, we consider the first term in (B.18), and split the integration into two parts:

$$\begin{aligned}\int_{C_1} d\tau A(t_1,\tau)B^<(\tau,t_{1'}) &= \int_{-\infty}^{t_1} dt\ A^>(t_1,t)B^<(t,t_{1'}) \\ &\quad + \int_{t_1}^{-\infty} dt\ A^<(t_1,t)B^<(t,t_{1'}) \\ &\equiv \int_{-\infty}^{\infty} dt\ A^r(t_1,t)B^<(t,t_{1'}) \ ,\end{aligned} \tag{B.19}$$

where we used the definition of the retarded function (B.15). A similar analysis can be applied to the second term involving contour C_1'; this time the advanced function is generated. Putting the two terms together, we

have the first of Langreth's results:

$$C^<(t_1,t_{1'}) = \int_{-\infty}^{\infty} dt\Big(A^r(t_1,t)B^<(t,t_{1'}) + A^<(t_1,t)B^a(t,t_{1'})\Big) \ . \quad \text{(B.20)}$$

The same result applies to the "greater" function: one just replaces all $<$'s by $>$'s. It is easy to generalize the result (B.20) for a (matrix) product of three functions: If $D = ABC$ on the contour, then, on the real axis, one has

$$D^< = A^rB^rC^< + A^rB^<C^a + A^<B^aC^a \ . \quad \text{(B.21)}$$

Once again a similar equation holds for the "greater" functions. One often needs the retarded (or advanced) component of a product of functions defined on the contour. The required expression is derived by repeated use of the definitions (B.10) – (B.15), and the result (B.20):

$$\begin{aligned} C^r(t_1,t_{1'}) &= \theta(t_1-t_{1'})[C^>(t_1,t_{1'}) - C^<(t_1,t_{1'})] \\ &= \theta(t_1-t_{1'})\int_{-\infty}^{\infty} dt[A^r(B^>-B^<) + (A^>-A^<)B^a] \\ &= \theta(t_1-t_{1'})\left[\int_{-\infty}^{t_1} dt(A^>-A^<)(B^>-B^<)\right. \\ &\qquad \left. + \int_{-\infty}^{t_{1'}} dt(A^>-A^<)(B^<-B^>)\right] \\ &= \int_{t_{1'}}^{t_1} dtA^r(t_1,t)B^r(t,t_{1'}) \ . \end{aligned} \quad \text{(B.22)}$$

In our compact notation, this relation is expressed as $C^r = A^rB^r$. When considering the various terms in the diagrammatic perturbation series, one may also encounter terms where two Green's function lines run (anti)parallel. For example, this can be the case in a polarization or self-energy diagram. In this case, one needs the "lesser" and/or retarded/advanced components of structures like

$$\begin{aligned} C(\tau,\tau') &= A(\tau,\tau')B(\tau,\tau') \ , \\ D(\tau,\tau') &= A(\tau,\tau')B(\tau',\tau) \ , \end{aligned} \quad \text{(B.23)}$$

where τ and τ' are contour variables. The derivation of the required formulae is similar to the analysis presented above. One finds

$$\begin{aligned} C^<(t,t') &= A^<(t,t')B^<(t,t') \ , \\ D^<(t,t') &= A^<(t,t')B^>(t',t) \ , \end{aligned} \quad \text{(B.24)}$$

and

$$\begin{aligned} C^r(t,t') &= A^<(t,t')B^r(t,t') + A^r(t,t')B^<(t,t') + A^r(t,t')B^r(t,t') \ , \\ D^r(t,t') &= A^r(t,t')B^<(t',t) + A^<(t,t')B^a(t',t) \\ &= A^<(t,t')B^a(t',t) + A^r(t,t')B^<(t',t) \ . \end{aligned} \tag{B.25}$$

As earlier, the relations (B.24) can immediately be generalized to "greater" functions. For a quick reference, we have collected the rules provided by the Langreth theorem in Table B.1.

contour	real axis
$C = \int_C AB$	$C^< = \int_t \left(A^r B^< + A^< B^a\right)$
	$C^r = \int_t \left(A^r B^r\right.$
$D = \int_C ABC$	$D^< = \int_t \left(A^r B^r C^< + A^r B^< C^a + A^< B^a C^a\right)$
	$D^r = \int_t A^r B^r C^r$
$C(\tau,\tau') = A(\tau,\tau')B(\tau,\tau')$	$C^<(t,t') = A^<(t,t')B^<(t,t')$
	$C^r = A^<(t,t')B^r(t,t') + A^r(t,t')B^<(t,t')$
	$+A^r(t,t')B^r(t,t')$
$D(\tau,\tau') = A(\tau,\tau')B(\tau',\tau)$	$D^<(t,t') = A^<(t,t')B^>(t',t)$
	$D^r = A^<(t,t')B^a(t',t) + A^r(t,t')B^<(t',t)$.

Table B.1 Rules for analytic continuation

B.3 Equilibrium Electron–Phonon Self-Energy

The retarded electron–phonon self-energy $\Sigma^r_{\rm ph}$ is a central object in the analysis of many physical properties of metals and semiconductors. At finite temperatures, one conventionally uses the Matsubara technique to perform the analytic continuation. The Langreth theorem can be used to give a very compact derivation of $\Sigma^r_{\rm ph}$. In lowest order in the electron–phonon matrix element M_q, we have

$$\Sigma_{\rm ph}(k,\tau,\tau') = i\sum_q |M_q|^2 G(k-q,\tau,\tau')D(q,\tau,\tau') \ . \tag{B.26}$$

Here, G is the free-electron Green's function while D is the free-phonon Green's function. Equation (B.26) is in a form where we can apply (B.25). In equilibrium, all quantities depend on time only through the difference of the two time labels, and it is advantageous to work in frequency space.

Performing the Fourier transform gives

$$\Sigma^r_{\rm ph}(k,\omega) = i\int \frac{d\varepsilon}{2\pi}\sum_q |M_q|^2 [G^<(k-q,\omega-\varepsilon)D^r(q,\varepsilon) + G^r(k-q,\omega-\varepsilon)D^<(q,\varepsilon) + G^r(k-q,\omega-\varepsilon)D^r(q,\varepsilon)] \,. \quad \text{(B.27)}$$

The expressions for the free equilibrium Green's functions are (the reader is urged to verify these relations!):

$$\begin{aligned} D^<(q,\omega) &= -2\pi i[(N_q+1)\delta(\omega+\omega_q) + N_q\delta(\omega-\omega_q)] \,, \\ D^r(q,\omega) &= \frac{1}{\omega-\omega_q+i\eta} - \frac{1}{\omega+\omega_q+i\eta} \,, \\ G^<(k,\omega) &= 2\pi i n_{\rm F}(\omega)\delta(\omega-\varepsilon_k) \,, \\ G^r(k,\omega) &= \frac{1}{\omega-\varepsilon_k+i\eta} \,. \end{aligned} \quad \text{(B.28)}$$

Substituting these expressions in (B.27), one finds after some straightforward algebra

$$\Sigma^r_{\rm ph}(k,\omega) = \sum_q M_q^2 \left[\frac{N_q - n_{\rm F}(\varepsilon_{k-q}) + 1}{\omega-\omega_q-\varepsilon_{k-q}+i\eta} + \frac{N_q + n_{\rm F}(\varepsilon_{k-q})}{\omega+\omega_q-\varepsilon_{k-q}+i\eta}\right] . \quad \text{(B.29)}$$

The shortness of this derivation, as compared to the standard one, nicely illustrates the formal power embedded in the Langreth theorem.

REFERENCES

L.P. Kadanoff and G. Baym, *Quantum Statistical Mechanics*, Benjamin, New York (1962)

D.C. Langreth, in *Linear and Nonlinear Electron Transport in Solids*, ed. J.T. Devreese and E. van Doren, Plenum, New York (1976)

H. Haug and A.P. Jauho, *Quantum Kinetics in Transport and Optics of Semiconductors*, Springer, Berlin (1996)

W. Schäfer and M. Wegener, *Semiconductor Optics and Transport Phenomena*, Springer, Berlin (2002)

This page intentionally left blank

Index